NASA Conference Publication 3058

Annihilation in Gases and Galaxies

Proceedings of a workshop held at
NASA Goddard Space Flight Center
Greenbelt, Maryland
July 19-21, 1989

NASA

NASA Conference Publication 3058

Annihilation in Gases and Galaxies

Edited by
Richard J. Drachman
Goddard Space Flight Center
Greenbelt, Maryland

Proceedings of a workshop held at
NASA Goddard Space Flight Center
Greenbelt, Maryland
July 19–21, 1989

National Aeronautics and
Space Administration
Office of Management
Scientific and Technical
Information Division

1990

II

ORGANIZING COMMITTEE

Edward Armour, University of Nottingham

Anand Bhatia, Goddard Space Flight Center

Karl Canter, Brandeis University

Richard Drachman, Goddard Space Flight Center

Arnab Ghosh, Indian Association for the Cultivation of Science

Alice Harding, Goddard Space Flight Center

Leonard Roellig, City University of New York

David Schrader, Marquette University

Guenther Sinapius, University of Bielefeld

PREFACE

It has become a tradition to hold a positron workshop as a satellite of the biennial meeting of the International Conference on the Physics of Electronic and Atomic Collisions (ICPEAC) at a location fairly convenient to the main meeting. To some extent this was a reaction to the fact that the large alternate-year conferences on positron annihilation had become dominated by the field of positron interactions in condensed matter. The organizers of the first of these workshops simply wished to re-emphasize the interesting problems involving "gaseous positronics." In addition, they wanted a gathering of a manageable size, where lively discussions and personal interactions would not be inhibited by sheer numbers of participants.

Each of the subsequent workshops has followed this pattern, aiming for an attendance of under 100. Several have also featured some unique variation on the theme of positrons in gases; one year the comparison of positrons with electrons was emphasized, and one year atomic physics with positrons was central. Because the fifth workshop in the series was to be held under the auspices of NASA's Goddard Space Flight Center it seemed appropriate to devote extra time to astrophysics and antimatter, along with the more traditional topics. The Workshop on Annihilation in Gases and Galaxies (July 19-21, 1989) was the result. The Organizing Committee had no difficulty in proposing a good list of invited speakers, and there was quite a large number of contributions as well.

The present volume contains most of the papers presented at the Workshop. They have been arranged roughly according to subject matter but without regard for whether they were invited or contributed papers, presented orally or as posters. The invited papers were, however, allowed up to 15 pages, while a limit of 3 pages was imposed on the contributed ones. Unfortunately, several of the most interesting contributions will not be found here; they are missing for a variety of good reasons. Nevertheless, all the topics discussed at the Workshop are well represented.

It was agreed that there is continuing interest in meetings like this one and that the field of positron physics is lively enough and developing rapidly enough that the series should be extended. The next Workshop will be held in Sydney, Australia in 1991.

Richard J. Drachman
November 8, 1989

TABLE OF CONTENTS

POSITRON–ALKALI ATOM SCATTERING

R. P. McEachran, M. Horbatsch, A. D. Stauffer and S. J. Ward†
Department of Physics, York University, Toronto, Canada, M3J 1P3

ABSRACT

Positron–alkali atom scattering has recently been investigated both theoretically and experimentally in the energy range from a few eV up to 100 eV. On the theoretical side calculations of the integrated elastic and excitation cross sections as well as total cross sections for Li, Na and K have been based upon either the close-coupling method or the modified Glauber approximation. These theoretical results are in good agreement with experimental measurements of the total cross section for both Na and K. Resonance structures have also been found in the $L = 0$, 1 and 2 partial waves for positron scattering from the alkalis. The structure of these resonances appears to be quite complex and, as expected, they occur in conjunction with the atomic excitation thresholds. Currently both theoretical and experimental work is in progress on e^+–Rb scattering in the same energy range.

INTRODUCTION

The study of positron–alkali scattering is of considerable interest since these atoms can be viewed as one-electron atoms with fixed cores, and hence the overall system can be considered as an effective three-body problem. The early theoretical work on e^+–alkali atom scattering was confined primarily to the simplest alkali, namely Li. Low-energy elastic scattering of positrons from Li in the energy range up to 7 eV was investigated using the polarized-orbital method by Bui and Stauffer;[1] they determined the elastic total and momentum transfer cross sections as well as Z_{eff}. This work was later extended to Na by Bui.[2]

On the other hand Sarkar *et al*[3] used the first Born approximation (FBA), the polarized FBA as well as the modified eikonal method to calculate the cross section for e^+–Li scattering for energies up to 500 eV. Borodonaro *et al*[4] and Ferrante *et al*[5] used the classical JWKB method to determine elastic cross sections for energies up to 7 eV for all the alkalis from Li to Cs. Except for the polarized-orbital method, all of the above methods are high-energy techniques and hence are unlikely to produce reliable results in the low-energy regime, say from 0 up to 50 eV.

In the past few years experimental measurements of the total cross section in the energy range from a few eV to nearly 100 eV have become available for e^+ scattering from K,[6,7] Na[8] and Rb[9]. Parallel to this development there have been several elaborate close-coupling calculations of the integrated elastic and excitation cross sections for Li,[10–14] Na[13–14] and K[12–15] as well as more recently for Rb.[16] The total integrated cross section for e^+ scattering from Li, Na and K has also been determined in a modified Glauber approximation[17,18] within the model potential approach and repeated recently for K in an improved modified Glauber approximation.[19] The overall agreement between theory and experiment is quite gratifying.

Resonance structures have also been found in the $L = 0$, 1 and 2 partial waves in the vicinity of the atomic excitation thresholds in Li, Na and K.[14,20,21] The widths of these resonances are quite narrow, varying between 0.2 and 130 meV. In addition some evidence has been found for the existence of positron–alkali bound states.

Besides excitation, two more inelastic channels need to be considered, namely ionization and positronium formation. The total ionization cross section for e^+–Li scattering has been found using both the FBA as well as by distorted-wave techniques.[22–23]

Positron–alkali scattering is also interesting both experimentally as well as theoretically since the rearrangement channel (positronium formation) is always open. This possibility should have a pronounced influence on the elastic and various excitation cross sections at very low energy. There have been several calculations[24–27] of the positronium formation cross section in the alkalis based upon either the FBA or various forms of the distorted-wave approximation. However, only the two-state calculation for Li of Guha and Ghosh,[28] which included polarization potentials in both channels and the distorted-wave approach of Mazumdar and Ghosh,[29] also for Li, which determined the incident wavefunction via a polarized-orbital method are liable to prove reliable in the low-energy regime.

This review will be concerned solely with the recent theoretical treatments used to determine the integrated elastic and differential cross sections, the various excitation cross sections and the total cross section for the alkalis. A brief discussion of the resonance structures will also be presented. Whenever possible a direct comparison with experiment will be made.

THEORY

The close-coupling method

The alkali atoms, to a good approximation, can be considered as one-electron systems where the valence electron moves outside a fixed or frozen core, consisting of the nucleus and the remaining electrons. Based upon this assumption the alkalis can be treated within the close-coupling framework in an analogous manner to that formulated by Percival and Seaton[30] for e^-–H scattering.

If the quantum numbers of the valence electron are denoted by $n_1 l_1 m_1 m_{s_1}$ and those of the incident positron by $kl_2 m_2 m_{s_2}$ then we can define the functions Ψ_γ according to

$$\Psi_\gamma(\mathbf{r}_c\sigma_c, \mathbf{r}_1\sigma_1, \hat{\mathbf{r}}_2\sigma_2) = \Phi(\mathbf{r}_c\sigma_c, \mathbf{r}_1\sigma_1)\, Y_{l_2 m_2}(\hat{\mathbf{r}}_2)\, \chi_{m_{s_2}}(\sigma_2) \quad (1)$$

where $Y_{l_2 m_2}(\hat{\mathbf{r}}_2)$ and $\chi_{m_{s_2}}(\sigma_2)$ represent the angular momentum and spin functions of the positron and $\mathbf{r}_c\sigma_c$ and $\mathbf{r}_1\sigma_1$ represent the space and spin coordinates of the core and valence electrons respectively. Here γ collectively represents the quantum numbers $n_1 l_1 m_1 m_{s_1}$ $kl_2 m_2 m_{s_2}$ and Φ denotes the bound state wavefunction of the atom. The latter, in turn, is represented by a single Slater determinant of the individual electron orbitals.

Since spin-orbit coupling is neglected, the total orbital and spin angular momentum quantum numbers $LSM_L M_S$ will be separately conserved during the collision. Consequently, calculations are simplified by using, instead of γ, the alternative representation $\Gamma = n_1 k l_1 l_2 L S M_L M_S$. These two representations are related by the unitary transformation

$$\langle\gamma|\Gamma'\rangle = \delta(n_1 l_1 l_2, n_1' l_1' l_2')\, C(l_1\, l_2\, L'; m_1'\, m_2'\, M') \times C(\tfrac{1}{2}\, \tfrac{1}{2}\, S'; m_{s_1}'\, m_{s_2}'\, M_S') \quad (2)$$

If we now define the so-called channel functions Ψ_Γ by

$$\Psi_\Gamma(\mathbf{r}_c\sigma_c, \mathbf{r}_1\sigma_1, \hat{\mathbf{r}}_2\sigma_2) = \sum_\gamma \langle\gamma|\Gamma\rangle\, \Psi_\gamma(\mathbf{r}_c\sigma_c, \mathbf{r}_1\sigma_1, \hat{\mathbf{r}}_2\sigma_2) \quad (3)$$

then the total wavefunction of the system takes the form

$$\Psi(\mathbf{r}_c\sigma_c, \mathbf{r}_1\sigma_1, \mathbf{r}_2\sigma_2) = \sum_\Gamma \Psi_\Gamma(\mathbf{r}_c\sigma_c, \mathbf{r}_1\sigma_1, \hat{\mathbf{r}}_2\sigma_2)\, \frac{1}{r_2}\, F_\Gamma(r_2) \quad (4)$$

The functions $F_\Gamma(r_2)$ describe the radial motion of the incident positron. The close-coupling equations are now obtained by projecting the Schrödinger equation for Ψ onto Ψ_Γ; one thus obtains

$$\left[\frac{\mathrm{d}^2}{\mathrm{d}r^2} - \frac{l_2(l_2+1)}{r^2} - 2V_c(r) + k_\nu^2\right] F_{\nu L S}(r) = -2\sum_{\nu'} V(\nu,\nu')_L\, F_{\nu' L S}(r) \quad (5)$$

where $\nu \equiv n_1 l_1 l_2$

$$V_c(r) = \frac{Z}{r} - \sum_{nl} 2(2l+1)\, y_0(nl, nl; r) \quad (6)$$

$$V(\nu,\nu')_L = \sum_\lambda f_\lambda(l_1 l_2, l_1' l_2'; L)\, y_\lambda(n_1 l_1, n_1' l_1'; r) \quad (7)$$

and

$$y_\lambda(n_1 l_1, n_1' l_1'; r) = r^{-\lambda-1}\int_0^r P_{n_1 l_1}(x)\, P_{n_1' l_1'}(x)\, x^\lambda\, \mathrm{d}x + r^\lambda \int_r^\infty P_{n_1 l_1}(x)\, P_{n_1' l_1'}(x)\, x^{-\lambda-1}\, \mathrm{d}x \quad (8)$$

In the above equations the P's are the radial atomic orbitals. The summation in equation (6) is over the core orbitals and the coefficients f_λ, given in equation (7), are defined in Percival and Seaton.[30]

If the $\nu' th$ linearly independent solution for $F_{\nu L S}(r)$ is now denoted by $F_{\nu L S}^{\nu'}(r)$ then the appropriate scattering boundary conditions are

$$F_{\nu L S}^{\nu'}(0) = 0 \quad (9)$$

and

$$F_{\nu L S}^{\nu'}(r)_{r\to\infty} \sim \frac{1}{\sqrt{k_\nu}}\left[\delta(\nu,\nu')\sin\left(k_\nu r - \frac{l\pi}{2}\right) + R_{\nu\nu'}^{LS}\cos\left(k_\nu r - \frac{l\pi}{2}\right)\right] \quad (10)$$

Here the coefficients $R_{\nu\nu'}^{LS}$ are the corresponding elements of the reactance matrix or $\mathbf{R}$ matrix which, in turn, is related to the scattering matrix $\mathbf{S}$ and the transition matrix $\mathbf{T}$ according to

$$\mathbf{S} = \frac{\mathbf{1} + i\mathbf{R}}{\mathbf{1} - i\mathbf{R}} \quad (11)$$

and

$$\mathbf{T} = \mathbf{S} - \mathbf{1} \quad (12)$$

The total cross section for the excitation of an alkali atom from the state $n_1' l_1'$ to $n_1 l_1$ is given (in units of πa_0^2) by

$$\sigma(n_1' l_1' \to n_1 l_1) = \sum_{LS}\sum_{l_2 l_2'} \frac{(2L+1)(2S+1)}{4k_{\nu'}^2(2l_1'+1)}\, |T_{\nu\nu'}^{LS}|^2 \quad (13)$$

and the corresponding elastic differential cross section is given by

$$\frac{d\sigma}{d\Omega}(n_i' l_i' \rightarrow n_i' l_i') = \sum_S \frac{(2S+1)}{16k_{v'}^2} \left| \sum_{L l_f'} (2L+1)\, P_L(\cos\theta)\, T_{v'v'}^{LS} \right|^2 \quad (14)$$

The modified Glauber approximation

While the conventional Glauber amplitude was found to work quite well for $e^{\pm}$–atom scattering at intermediate energies[31] it was nonetheless shown[32] that it could be improved by correcting its second-order eikonal term with the counterpart of the second-Born approximation. Thus, in the so-called modified Glauber approximation, we have

$$f_{MG} = f_G - f_{G2} + f_{B2} \quad (15)$$

The total cross section is then obtained by means of the optical theorem,

$$\sigma = \frac{4\pi}{k_i} \mathrm{Im}\, f(0) \quad (16)$$

where $f(0)$ is the scattering amplitude in the forward direction without change in energy.

In the case of a larger atom (such as Na or K) one encounters serious difficulties in an eikonal-type approximation, like the modified Glauber approximation, in the evaluation of the multiple-scattering terms in the scattering amplitude. These terms arise from the scattering of the incident projectile by the core electrons of the target. In order to overcome this difficulty a model potential approach was developed by Gien[33] for $e^{\pm}$–alkali scattering. Here the potential which describes the scattering of the incident projectile by the alkali atom is expressed as

$$V(\mathbf{r}, \mathbf{r}') = V_a(\mathbf{r}, \mathbf{r}') + V_c(r') \quad (17)$$

where, in the case of a positron

$$V_a(\mathbf{r}, \mathbf{r}') = -\left[\frac{1}{|\mathbf{r} - \mathbf{r}'|} - \frac{1}{r'}\right] \quad (18)$$

is the scattering potential of the projectile by the 'one-electron' atom and $V_c(r')$ is the core potential of the target atom. Here $\mathbf{r}$ and $\mathbf{r}'$ represent the coordinates of the valence electron and the incident positron respectively.

The core potential, V_c, of the alkali$^+$ ions is also used to generate the bound-state valence orbitals of the atoms.

In terms of the two-potential formalism[34] the scattering amplitude can be expressed as

$$f(\theta) = -\frac{1}{2\pi} \langle \Phi_f \exp i\mathbf{k}_f \cdot \mathbf{r}' \mid V_c(r') \mid \chi_i^{(+)} \rangle - \frac{1}{2\pi} \langle \chi_f^{(-)} \mid V_a(\mathbf{r}, \mathbf{r}') \mid \Psi_i^{(+)} \rangle \quad (19)$$

Here Φ_f is the final state atomic wavefunction and $\Psi_i^{(+)}$ is the solution of the full Schrödinger equation of the system consisting of the incident positron plus the alkali target. The functions $\chi_{i,f}^{(\pm)}$ are called distorted waves and, in principal, are solutions of the full Schrödinger equation with $V(\mathbf{r}, \mathbf{r}')$ replaced by just $V_c(r')$. The subscripts (i, f) refer to the initial and final states of the system and the superscripts $(\pm)$ refer to outgoing and incoming wave boundary conditions respectively.

If the scattering amplitude is now evaluated using the Glauber technique then the first term above represents the Glauber amplitude of the core-potential scattering and the second term represents the core-corrected Glauber amplitude of the projectile scattering by the 'one-electron' atom.

RESULTS

Lithium

Several close-coupling calculations for the elastic cross section as well as various excitation cross sections have been performed for e^+–Li scattering by Khan *et al*[10] in the energy range 2–10 eV, and extended by Sarkar *et al*[11] to the energy range 15–100 eV. More recently Ward *et al*[13] have reported similar calculations in the energy range 0.5–50 eV. In each case the most elaborate calculation carried out by the above authors respectively was based upon the inclusion of the 5 atomic states (2s–2p–3s–3p–3d) in the eigenfunction expansion for the total wavefunction. In the work of Khan *et al* and Sarkar *et al* the analytic Hartree-Fock wavefunctions of Weiss[35] were used for the bound state orbitals whereas Ward *et al* employed both frozen-core Hartree-Fock as well as model potential wavefunctions.[36]

On the other hand Gien[18] has given results for the total cross section for e^+–Li scattering based upon the core-corrected modified Glauber approximation in the energy range from 40 to 1000 eV. So far there are no experimental measurements with which to compare.

In table 1 we present the 5-state close-coupling results referred to above for the elastic, the resonance transition and the total cross section together with the total cross section determined in the core-corrected modified Glauber approximation. These results are also shown in figure 1.

TABLE 1. Elastic, resonant excitation and total integrated cross sections (πa_0^2) for e^+–Li scattering in the energy range 0.5–100 eV.

	Refs. 10, 11			Ref. 13			Ref. 18
Energy (eV)	2s–2s	2s–2p	Total	2s–2s	2s–2p	Total	Total
0.5				351.95		351.95	
1.0				212.15		212.15	
1.5				183.58		183.58	
2.0				169.49	21.24	190.72	
3.0				106.87	72.29	179.16	
4.0	67.79	78.07	151.10	71.86	79.09	160.36	
5.0	48.46	79.10	135.29	52.11	81.68	145.11	
7.0	29.14	73.99	112.80	31.19	77.61	121.04	
10.0	17.68	67.33	94.70	18.13	68.15	97.27	
15.0	9.93	56.43	74.89				
20.0	7.17	49.53	63.38	7.51	47.35	61.00	
30.0	4.97	38.90	48.16	5.14	36.54	45.56	
40.0	4.07	30.14	37.32	4.08	29.84	36.68	35.67
50.0	3.37	24.23	30.00	3.44	25.21	30.77	30.82
70.0							24.37
80.0	2.37	14.48	18.25				
100.0	1.99	10.63	13.69				18.71

The close-coupling results of Sarkar *et al* and Ward *et al* are in satisfactory agreement; the slight differences could be attributed to the use of different bound state wavefunctions as well as the different numerical procedures used to determine the cross sections. On the other hand, the differences between the cross sections of Khan *et al* and Ward *et al* are somewhat more than what might be expected from these causes.

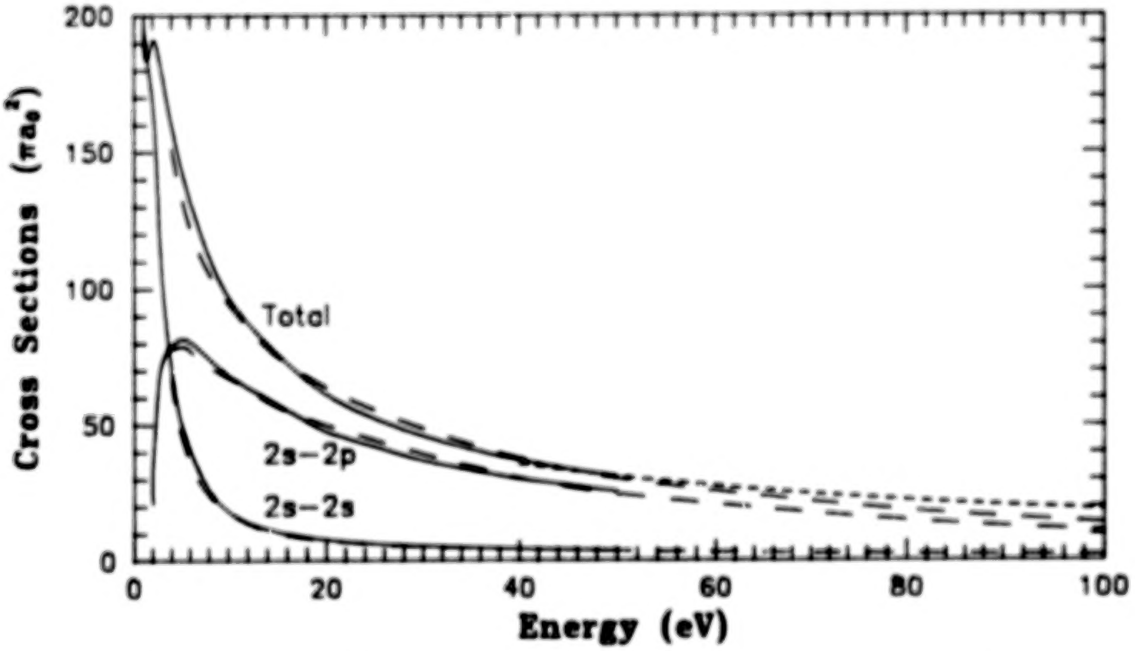

FIG. 1. The 5-state close-coupling elastic, resonance excitation and total cross section and the modified Glauber total cross section for e^+–Li scattering: (– – –), Khan *et al*[10] and Sarkar *et al*;[11] (——), Ward *et al*;[13] (· · ·), Glen.[18]

The total cross sections of the core-corrected modified Glauber approximation are either comparable to or lie above the close-coupling results with the difference increasing with increasing energy. However, it should be noted that the total cross sections in the close-coupling procedure include neither excitations to bound levels with principal quantum number $n \geq 4$ nor the ionization and positronium formation channels.

In the close-coupling calculations of positron–alkali collisions of Ward *et al*[14,20] and Horbatsch *et al*[21] a number of resonances in the $L = 0$, 1 and 2 channels have been found in the vicinity of the atomic excitation thresholds. The appearance of such resonances near thresholds is well established in electron scattering from atoms and in particular from the alkalis.[37,38] In positron–atom scattering, resonance structures have been calculated in detail only for the e^+–H system.[39] However, hydrogen is quite different from the alkalis in many ways. In particular, its energy levels are degenerate and a large contribution to its dipole polarizability can be attributed to the continuum P states. In the alkalis, whose polarizabilities are very large, over 98% of the dipole polarizability comes from just the resonant excitation transition. Also significant is the fact that in the alkalis the Ps formation channel is open at zero energy.

In the work of Ward *et al*[14] the R matrices obtained from 4-state (2s–2p–3s–3p) and 5-state close-coupling approximations were diagonalized and the eigenphase sum was computed according to

$$\sum_i \eta_{iL}(E) = \sum_i \tan^{-1}(\lambda_i) \tag{20}$$

where the λ_i are the eigenvalues of the respective R matrices. The resonances for which the eigenphase sum underwent a change of π rad were analyzed in terms of the single-resonance Breit-Wigner formula

$$\sum_i \eta_{iL}(E) = \eta_L^{(B)}(E) + \tan^{-1}\frac{\frac{1}{2}\Gamma_{BW}}{E_{BW} - E} \tag{21}$$

by means of a method described by Nesbet.[37] In figure 2 we show the eigenphase sum for $L = 0$ from both 4- and 5-state close-coupling calculations based upon model potential wavefunctions. We first note that the 4-state calculation yields different results in the vicinity of the 2p threshold (1.844 eV). Thus the presence of the 3d orbital, as a closed channel, in the eigenfunction expansion plays a key role in developing the discontinuity present in the 4-state calculation into the usual resonance shape. Nonetheless, the eigenphase sum changes by only 2 rad at $E_{res} = 1.86$ eV with a full width $\Gamma = 35$ meV.

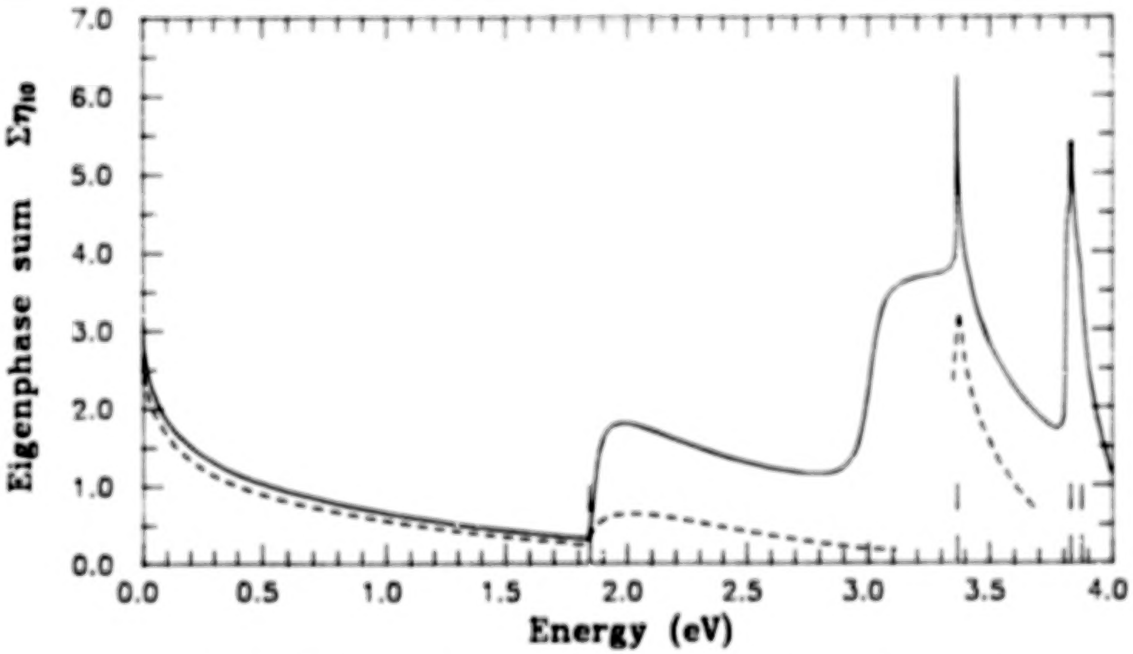

FIG. 2. The eigenphase sum for $L = 0$, e^+–Li scattering in a 5-state (——), and 4-state (– – –) close-coupling approximation. The dashes indicate the positions of the excitation thresholds in the model potential approximation at 1.844, 3.367, 3.829 and 3.874 eV.

As can also be seen from the figure there is a 5-state resonance below the 3s excitation thresold (3.367 eV) which is not present in the 4-state results. The resonance parameters here are $E_{res} = 3.01$ eV and $\Gamma = 40$ meV. A

narrow resonance, E_{res} = 3.365 eV, Γ = 1 meV occurs immediately below the 3s excitation threshold; it is present in both the 4- and 5-state eigenfunction expansions. The 5-state calculation also displays a further narrow resonance just below the 3p excitation threshold (3.829 eV) which is missing in the 4-state results. Ward *et al*[14,20] have shown that this general type behaviour in the $L = 0$ channel persists in the $L = 1$, and 2 channels as well, not only for Li but also for Na and K.

At zero energy Ward *et al*[14,20] point out that the s-wave ($L = 0$) phase shifts for Li, Na and K start at least at π rad since they begin with negative slopes (positive scattering lengths) and the polarization potential, which dominates at zero energy, is attractive. This implies the possible existence of at least one bound state in these e^+–alkali systems.

However, Ps formation is possible at zero energy and hence the shape, position and even the existence of resonances could be radically altered when this channel is properly taken into account in a calcualtion. The situation with respect to the existence of bound states in the e^+–alkali systems could also be altered.

Sodium

On the theoretical side the situation for e^+–Na scattering is somewhat the same as for lithium. Sarkar *et al*[11] have carried out close-coupling calculations of the elastic cross section as well as various excitation cross sections in the energy range 4–100 eV. Similar calculations have also been reported by Ward *et al*[13] in the energy range 0.5–50 eV. The most elaborate calculation by Sarkar *et al* was based upon the inclusion of 4 atomic states (3s-3p-3d-4p) in the eigenfunction expansion for the total wavefunction. On the other hand, the most accurate results of Ward *et al* were based upon the 5-state expansion (3s-3p-3d-4s-4p). In the work of Sarkar *et al* the analytic Hartree-Fock wavefunction of Clementi and Roetti[60] was used for the ground state and the wavefunctions of Kundu *et al*[61] and Kundu and Mukherjee[62] for the excited p- and d-states respectively. The frozen-core wavefunctions of Ward *et al* were determined from the model potential of Peach.[36] Ward *et al* also performed a 4-state calculation but based upon the atomic states (3s-3p-3d-4s) and hence a direct comparison of their results with those of Sarkar *et al* is not possible. Nonetheless, the overall agreement between these two sets of close-coupling results is satisfactory.

Glen[18] has also given results for the total cross section for e^+–Na scattering based upon the core-corrected modified Glauber approximation in the energy range from 40 to 1000 eV. In table 2 we present the 4-state (Sarkar *et al*[11]) and 5-state (Ward *et al*[13]) close-coupling values for the elastic, the resonance transition and the total cross section as well as the total cross section determined by Glen[18] in the core-corrected Glauber approximation.

TABLE 2. Elastic, resonant excitation and total integrated cross sections (πa_0^2) for e^+–Na scattering in the energy range 0.5–100 eV.

	Ref. 11			Ref. 13			Ref. 18
Energy (eV)	3s–3s	3s–3p	Total	3s–3s	3s–3p	Total	Total
0.5				341.24		341.24	
1.0				205.18		205.18	
1.5				175.53		175.53	
2.0				189.47		189.47	
2.5				130.92	48.23	179.15	
3.0				110.22	66.11	176.33	
3.5				87.52	67.47	165.75	
4.0	71.48	66.87	144.19	73.96	69.25	159.21	
5.0	54.24	72.37	137.78	54.13	69.99	144.71	
7.0				33.04	65.91	121.57	
7.5	30.54	72.80	120.87				
10.0	19.78	65.82	102.54	19.84	59.21	98.81	
15.0	11.82	54.56	74.89				
20.0	8.84	46.46	65.04	8.98	44.61	63.78	
30.0	6.56	38.67	51.13	6.49	35.83	48.50	
40.0	5.41	33.56	43.04	5.35	29.93	39.59	29.62
50.0	4.74	26.52	34.30	4.67	25.67	33.61	26.41
70.0							21.68
80.0	3.53	14.25	19.31				
100.0	3.04	11.04	15.30				17.18

However, it should be noted that, in contrast to Li, where only the elastic, and resonance transition cross sections are of significant magnitude, the other excitation cross sections in Na (i.e. 3s–3d, 3s–4s and 3s–4p) do contribute appreciably to the total cross section. When compared with the corresponding close-coupling values for the total cross section the core-corrected modified Glauber results appear to be too low at energies below 100 eV.

For Na there are the experimental data of Kwan *et al*[8] for the total cross section with which to compare. However, since experimentally it is not possible to discriminate against positrons scattered elastically through small angles about the forward direction, a knowledge of the elastic differential cross section enables one to estimate how much flux has been lost by means of this effect. Thus Ward *et al*[13] calculated an effective elastic cross section defined as

$$\sigma_{el}^{eff} = 2\pi \int_{\theta_0}^{\pi} \sin\theta \frac{d\sigma_{el}}{d\Omega} d\theta \qquad (<\theta_0^2) \qquad (22)$$

where θ_0 is the lower limit of the experimental angular discrimination. An estimate of this quantity has been made in the experimental measurements of Kwan *et al*[8] for several values of the energy of the incident positron. When this effective elastic cross section is added to the various excitation cross sections an effective total cross section is obtained which can, more meaningfully, be compared with the experimental data. In figure 3 we illustrate the various theoretical results referred to above for the total cross section for e^+–Na scattering together with the experimental data.

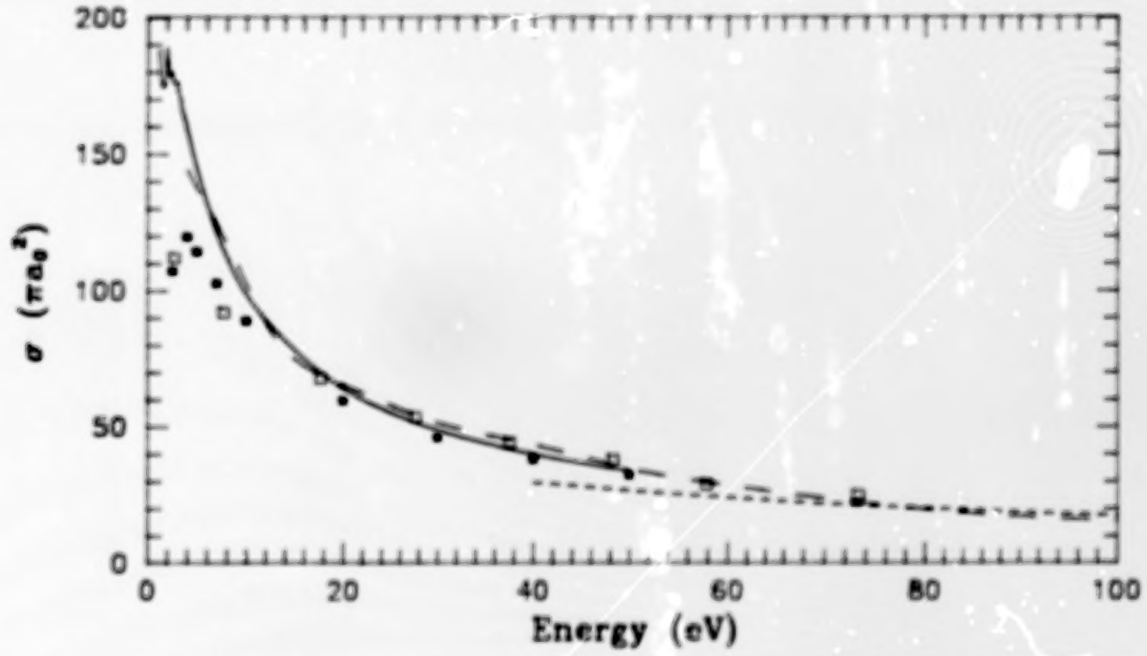

FIG. 3. The total cross section for e^+–Na scattering: (– – –), 4-state close-coupling approximation (CCA), Sarkar *et al*;[11] (——), 5-state CCA, Ward *et al*;[13] ■, effective 5-state CCA, Ward *et al*;[13] (· · ·), core-corrected modified Glauber approximation, Glen;[18] □, experimental data, Kwan *et al*.[8]

The overall agreement between the *effective* total cross section of Ward *et al*[13] and experiment is quite satisfactory over the entire energy range below 50 eV. It should be noted that below 20 eV it becomes very important to make allowance for the fact that experimentally there is a serious loss of flux from positrons elastically scattered through small angles. However, the effective cross section is highly sensitive at low energies to the particular value used in equation (22) for the cut-off angle θ_0. The value of θ_0 increases rapidly as the energy decreases and hence the apparent structure in the effective cross section may be artifical.

Above 20 eV the total cross sections of Sarkar *et al*[11] are also in quite satisfactory agreement with experiment. On the other hand the total cross section determined in the core-corrected modified Glauber approximation by Glen[18] appears to be slightly too low in this energy region.

Potassium

In the case of e^+–K scattering several close-coupling calculations of the elastic cross section as well as various excitation cross sections have been reported by Ward *et al.*[12–15] The most elaborate of these is a 5-state (4s–4p–5s–3d–5p) calculation, which employed model potential wavefunctions,[36] in the energy range 0.5 to 50 eV.

Once again Gien[18] has reported results for the total cross section for e^+–K scattering based upon the core-corrected modified Glauber approximation in the energy range from 40 to 1000 eV. However, more recently Gien[19] has repeated these calculations in an improved Glauber approximation in the energy range from 11 to 102.5 eV. In his original work[18] only the contribution from the 4s intermediate state to the second Born term for one-electron atom scattering was evaluated exactly; i.e. the remaining contributions were determined via closure. In his most recent work[19] the contributions from the 4p and 5s as well as the 4s intermediate states have been evaluated exactly.

In table 3 we present the 5-state close-coupling values of Ward *et al*[15] for the elastic, the resonance transition and the total cross section together with the total cross sections as determined by Gien[18,19] in the core-corrected modified Glauber approximation.

TABLE 3. Elastic, resonant excitation and total integrated cross sections (πa_0^2) for e^+–K scattering in the energy range 0.5–102.5 eV.

	Ref. 13			Refs. 18, 19	Ref. 19
Energy (eV)	4s–4s	4s–4p	Total	Total	Total
0.5	666.57		666.57		
1.0	510.78		510.78		
1.5	486.71		486.71		
2.0	322.75	79.60	402.35		
2.5	239.39	126.40	365.79		
3.0	184.65	125.42	329.17		
3.5	145.34	119.65	298.29		
4.0	117.83	112.33	273.44		
5.0	82.56	100.14	235.97		
7.0	48.96	87.57	189.72		
10.0	29.66	80.09	151.56		
11.0				38.07	105.85
20.0	14.27	64.65	97.60		
21.1				48.85	84.96
30.0	10.66	52.79	74.37		
31.2				46.15	70.75
40.0	9.01	44.11	60.44	42.04	61.28
41.4				41.38	59.99
50.0	8.02	37.67	51.33	37.49	52.92
70.0				30.37	
76.8				28.52	38.61
100.0				23.61	
102.5				23.19	30.76

We first note that, similar to Na, the other excitation cross sections in K (i.e. 4s–5s, 4s–3d and 4s–5p) make an appreciable contribution to the total cross section. Secondly we see that, when the contribution to the second Born term is evaluated more precisely, the core-corrected modified Glauber approximation agrees with the close-coupling results down to 30 eV.

For K there are the experimental data of Stein *et al*[6,7] for the total cross section with which to compare. In order to obtain satisfactory agreement with experiment at low energies Ward *et al*[13] again found it necessary to calculate, using equation (22), an effective elastic, and hence total cross section. In figure 4 we illustrate the above theoretical results for the total cross for e^+–K scattering together with the experimental data.

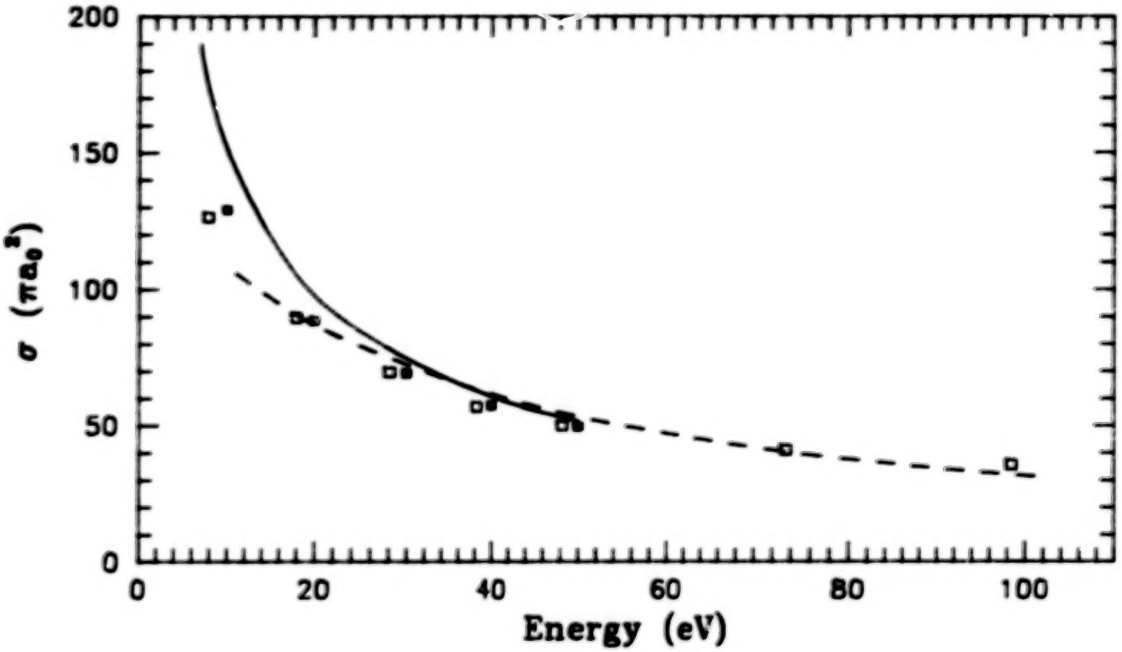

FIG. 4. The total cross section for e^+–K scattering: (——), 5-state close-coupling approximation (CCA), Ward *et al*;[13] ■, effective 5-state CCA, Ward *et al*;[13] (- - -), core-corrected modified Glauber approximation, Gien;[19] □, experimental data, Stein *et al*.[6,7]

Once again the overall agreement between the *effective* total cross section of Ward *et al*[13] and experiment is quite satisfactory over the entire energy range below 50 eV. The improved modified Glauber approximation is similarly in quite satisfactory agreement with experiment down to about 30 eV. It is worth noting that the K cross sections are, however, much larger in magnitude than the corresponding ones for Na. This is a reflection of the larger value of the static dipole polarizability of K, namely $293 \pm 6\ a_0^3$ versus $159 \pm 3\ a_0^3$ for Na.[43]

Rubidium

Quite recently work has began on the corresponding 5-state close-coupling calculation (5s–5p–4d–6s–6p) for e^+–Rb scattering.[16] In this case the bound-state wavefunctions of Rb were determined variationally by means of a polarized frozen-core Hartree-Fock technique which has previously proved to be quite successful in atomic structure calculations on Na.[44,45] This calculation is the only theoretical research which has been reported so far for this system.

In table 4 we present the results of this calculation for the elastic, resonance excitation and total cross section as well as the effective total cross section, as determined with the aid of equation (22), for e^+–Rb scattering.

TABLE 4. Elastic, resonant excitation and total integrated cross sections (πa_0^2) for e^+–Rb scattering in the energy range 3.7–28 eV.

	Ref. 16			
Energy (eV)	5s–5s	5s–5p	σ_{tot}	σ_{tot}^{eff}
3.7	124.23	92.20	289.66	209.28
5.8	62.76	76.18	219.07	170.83
7.8	42.16	77.68	185.58	151.47
17.8	17.64	73.12	114.98	102.69
28.0	12.79	60.27	86.12	80.31

Once again we observe that the other excitation cross sections in Rb (i.e. 5s–4d, 5s–6s and 5s–6p) make a significant contribution to the total cross section. We also note that at 3.7 eV nearly 2/3 of the elastic scattering flux will not be detected experimentally and that this fraction increases to 4/5 at 7.8 eV. Nonetheless, the effective total cross section as predicted by this 5-state close-coupling approximation is monotonically increasing as the energy of the incident positron decreases. This behaviour is in contrast to the experimental data of Stein *et al*[9] which has a maximum in the low energy regime. In figure 5 we present the corresponding elastic differential cross section at several energies. These cross sections are, as expected, highly peaked in the forward direction and possess a minimum between 35 and 40° which is then followed by one or more secondary maxima. This overall behaviour pattern of the differential cross section is typical of all the alkalis studied so far.[13,14,28,29]

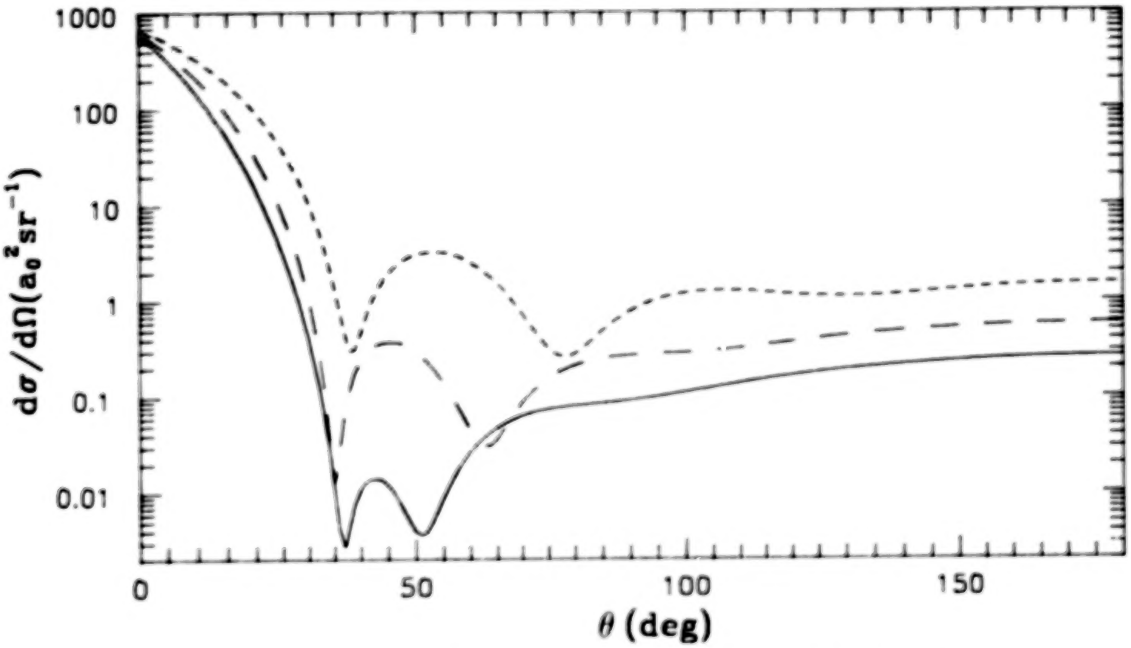

FIG. 5. The elastic differential cross section for e^+–Rb scattering in a 5-state close-coupling approximation: (- - -), 3.7 eV; (– – –), 5.8 eV; (——), 7.8 eV.

CONCLUSIONS

The effective total cross sections, as determined in a 5-state close-coupling procedure, are in quite satisfactory agreement with the experimental data for Na and K; the exception to this is Rb. When the second Born term in the core-corrected modified Glauber approximation is evaluated accurately this approach will also yield total cross sections in agreement with experiment down to relatively low energies. For the alkalis, Li, Na and K, the the close-coupling approximation predicts an extensive series of resonance structures associated with the atomic excitation thresholds and holds forth the possibility of true bound states in these e^+–alklai systems. The same situation will no doubt be true for the remaining alkalis.

However, the most important theoretical problem remaining in low-energy e^+–alkali scattering is the accurate inclusion of the positronium formation channel; ionization is, of course, also important. The incorporation of these two channels into, say, a close-coupling calculation, could have a major effect upon the resulting cross sections at lower energies and could seriously influence the various resonance structures as well as alter the situation with respect to the existence of bound states in the e^+–alkali systems

ACKNOWLEDGMENTS

We would like to thank Professors T. S. Stein and W. E. Kauppila for valuable discussions. This work was supported by the Natural Sciences and Engineering Research Council of Canada.

† Present address: Department of Physics and Astronomy, University of Tennessee, Knoxville, TN 37996-1501, U.S.A.

[1] T. D. Bui and A. D. Stauffer, Can. J. Phys. **49**, 2527, (1971).

[2] T. D. Bui, J. Phys. B. **8**, L153, (1975).

[3] K. Sarkar, B. C. Saha and A. S. Ghosh, Phys. Rev. A **8**, 236, (1973).
[4] G. Bordonaro, C. Ferrante, M. Zarcone and P. Cavaliere, Nuovo Cim. **35B**, 349, (1976).
[5] G. Ferrante, L. L. O. Cascio and M. Zarcone, Nuovo Cim. **44B**, 99, (1978).
[6] T. S. Stein, R. D. Gomez, Y.-F. Hsieh, W. E. Kauppila, C. K. Kwan and Y. J. Wan, Phys. Rev. Lett. **55**, 488, (1985).
[7] T. S. Stein, M. S. Dababneh, W. E. Kauppila, C. K. Kwan and Y. J. Wan, *Atomic Physics with Positrons*, ed. J. W. Humberston and E. A. G. Armour (London: Plenum) p. 251, (1988).
[8] C. K. Kwan, W. E. Kauppila, R. A. Likaszew, S. P. Parikh, T. S. Stein, Y. J. Wan and M. S. Dababneh, Phys. Rev. A, (1989), submitted.
[9] T. S. Stein, C. K. Kwan, W. E. Kauppila, R. A. Likaszew, S. P. Parikh, Y. J. Wan and M. S. Dababneh, *Proc. of the Workshop on Annihilation in Gases and Galaxies*, published in these Proceedings.
[10] P. Khan, S. Dutta and A. S. Ghosh, J. Phys. B. **20**, 2927, (1987).
[11] K. P. Sarkar, M. Basu and A. S. Ghosh, J. Phys. B. **21**, 1649, (1988).
[12] S. J. Ward, M. Horbatsch, R. P. McEachran and A. D. Stauffer, *Atomic Physics with Positrons*, ed. J. W. Humberston and E. A. G. Armour (London: Plenum) p. 265, (1988).
[13] ——, J. Phys. B. **22**, 1845, (1989).
[14] ——, Nucl. Instrum. Methods **B42**, 472, (1989).
[15] ——, J. Phys. B. **21**, L611, (1988).
[16] R. P. McEachran, M. Horbatsch and A. D. Stauffer, *Proc. of the Workshop on Annihilation in Gases and Galaxies*, published in these Proceedings.
[17] T. T. Gien, Phys. Rev. A **5**, 2020, (1987).
[18] ——, Chem. Phys. Lett. **139**, 23, (1987) (Erratum **142**, 575).
[19] ——, J. Phys. B. **22**, L129, (1989).
[20] S. J. Ward, M. Horbatsch, R. P. McEachran and A. D. Stauffer, J. Phys. B. **22**, (1989), accepted.
[21] M. Horbatsch, S. J. Ward, R. P. McEachran and A. D. Stauffer, *Proc. of the Workshop on Annihilation in Gases and Galaxies*, published in these Proceedings.
[22] M. Basu and A. S. Ghosh, J. Phys. B. **19**, 1249, (1986).
[23] K. K. Mukherjee and P. S. Mazumdar, J. Phys. B. **21**, 2327, (1988).
[24] S. Guha and B. C. Saha, Phys. Rev. A **21**, 564, (1980).
[25] S. Guha and P. J. Mandal, J. Phys. B. **13**, 1919, (1980).
[26] P. J. Mandal and S. Guha, J. Phys. B. **13**, 1937, (1980).
[27] S. N. Nahar and J. M. Wadehra, Phys. Rev. A **35**, 4533, (1987).
[28] S. Guha and A. S. Ghosh, Phys. Rev. A **23**, 743, (1981).
[29] P. S. Mazumdar and A. S. Ghosh, Phys. Rev. A **34**, 4433, (1986).
[30] I. C. Percival and M. J. Seaton, Proc. Camb. Phil. Soc. **53**, 654, (1957).
[31] E. Gerjuoy and B. K. Thomas, Rep. Prog. Phys. **37**, 1345, (1974).
[32] T. T. Gien, J. Phys. B. **9**, 3203, (1976).
[33] ——, Chem. Phys. Lett. **127**, 233, (1986).
[34] J. R. Taylor, *Scattering Theory*, New York: Wiley (1972).
[35] A. W. Weiss, Astrophys. J. **138**, 1262, (1963).
[36] G. Peach, Comment. At. Mol. Phys. **11**, 101, (1982) and private communication, (1986).
[37] R. K. Nesbet, *Variational Methods in Electron–Atom Scattering Theory*, New York: Plenum (1972).
[38] N. S. Scott, K. Bartschat, P. G. Burke, O. Nagy and W. B. Eissner, J. Phys. B. **17**, 3775, (1984).
[39] Y. K. Ho, Phys. Rep. **99**, 1, (1983) and references therein.
[40] E. Clementi and C. Roetti, At. Data Nucl. Data Tables **14**, 187, (1974).
[41] B. Kundu, D. Ray and P. K. Mukherjee, Phys. Rev. A **34**, 62, (1986).
[42] B. Kundu and P. K. Mukherjee, Phys. Rev. A **35**, 980, (1987).
[43] T. M. Miller and B. Berderson, Adv. At. Mol. Phys. **13**, 1, (1977).
[44] R. P. McEachran and M. Cohen, J. Phys. B. **16**, 3125, (1983).
[45] M. Cohen and R. P. McEachran, J. Phys. B. **17**, 2979, (1984).

SCATTERING OF POSITRONS AND ELECTRONS BY ALKALI ATOMS

T.S. Stein, W.E. Kauppila, C.K. Kwan, R.A. Lukaszew, S.P. Parikh,
Y.J. Wan*, S. Zhou, and M.S. Dababneh**
Department of Physics and Astronomy, Wayne State University
Detroit, Michigan 48202, USA

ABSTRACT

Absolute total scattering cross sections (Q_T's) have been measured for positrons and electrons colliding with sodium, potassium, and rubidium in the 1-102 eV range, using the same apparatus and experimental approach (a beam transmission technique) for both projectiles. The present results for positron-sodium and -rubidium collisions represent the first Q_T measurements reported for these collision systems. Features which distinguish the present comparisons between positron- and electron-alkali atom Q_T's from those for other atoms and molecules (room-temperature gases) which have been used as targets for positrons and electrons are (1) the proximity of the corresponding positron- and electron-alkali atom Q_T's over the entire energy range of overlap, with an indication of a merging or near-merging of the corresponding positron and electron Q_T's near (and above) the relatively low energy of about 40 eV, and (2) a general tendency for the positron-alkali atom Q_T's to be higher than the corresponding electron values as the projectile energy is decreased below about 40 eV.

INTRODUCTION

One of the incentives for making direct comparison measurements between positron- and electron-scattering from the same target gases is the potential that such comparisons have for providing deeper insight into atomic scattering phenomena than may be acquired by studying the scattering of only one type of projectile from various gases. Since positrons, being the antiparticles of electrons, have the same magnitudes for the mass, charge, and spin as the electron, but have the opposite sign of charge, comparison measurements of the scattering of positrons and electrons by atoms and molecules can reveal interesting differences and similarities that arise from the basic interactions which contribute to scattering. The exchange interaction contributes to electron scattering but does not play a role in positron scattering. The static interaction (associated with the interaction of the projectile with the Coulomb field of the undistorted atom) is attractive for the electron and repulsive for the positron, while the polarization interaction (resulting from the distortion of the atom by the charged projectile) is attractive for both projectiles. The net effect of the static and polarization interactions is that they add to each other in electron scattering whereas they tend to cancel each other in positron scattering. Thus, if one considers just the contributions from the static and polarization interactions, in general, Q_T's for positrons would be expected to be smaller than those for electrons at low energies. As the projectile energy is increased, the polarization and exchange interactions eventually become negligible compared with the static interaction, and the expected result is a merging of the corresponding positron and electron Q_T's at sufficiently high projectile energies. Two scattering channels that are open only to positrons are (1) annihilation, which is negligible for the positron energies (>0.2 eV) that have been used in positron-beam scattering experiments, and (2) positronium (Ps) formation, which has a threshold energy 6.8 eV

below the ionization threshold energy of the target atom.

The general trends observed in comparisons of the total scattering of positrons and electrons by the room-temperature gases that have been investigated appear to be consistent with predictions based on the simple interaction model described above. As illustrations of these general trends, comparison measurements[1-4] for the inert gases (Ne, Ar, and Kr) which correspond to the alkali metal atoms (Na, K, and Rb) discussed in this article, are shown in Figs. 1, 2, and 3 respectively. In these Figures, one can see (1) the tendency for the measured positron-inert gas Q_T's to be significantly lower than the corresponding electron Q_T's at low energies (except in the immediate vicinities of the deep Ramsauer-Townsend

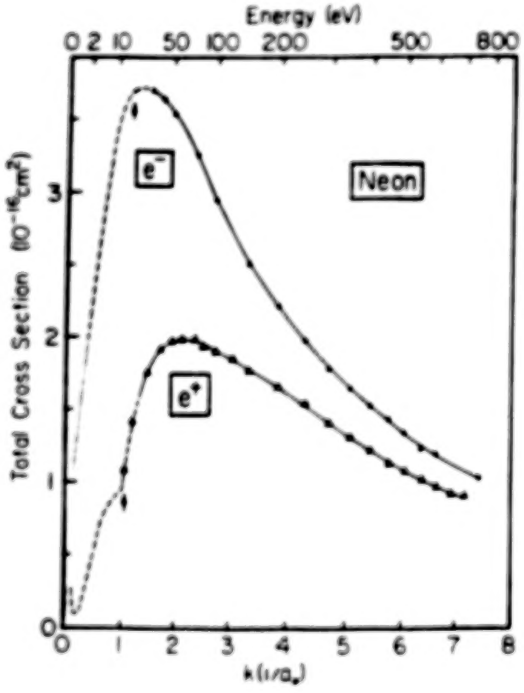

Fig. 1. Comparison of positron- and electron-Ne total cross sections. The lowest inelastic thresholds for each projectile are indicated by arrows. (From Kauppila et al., Ref. 1).

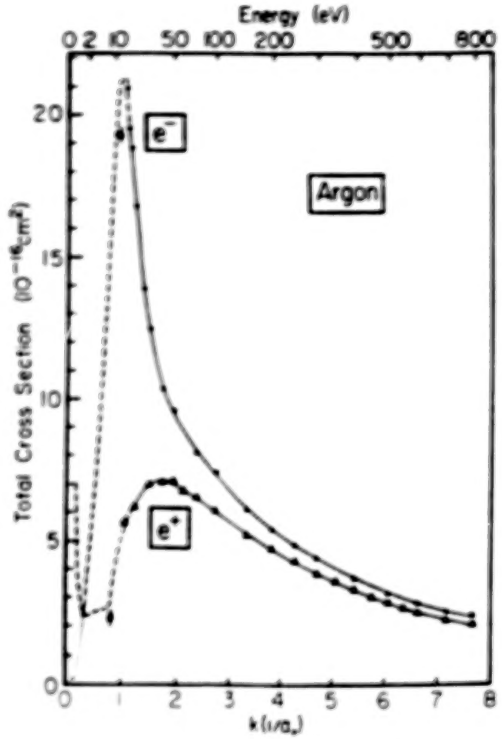

Fig. 2. Comparison of positron- and electron-Ar total cross sections. (From Kauppila et al., Ref. 1).

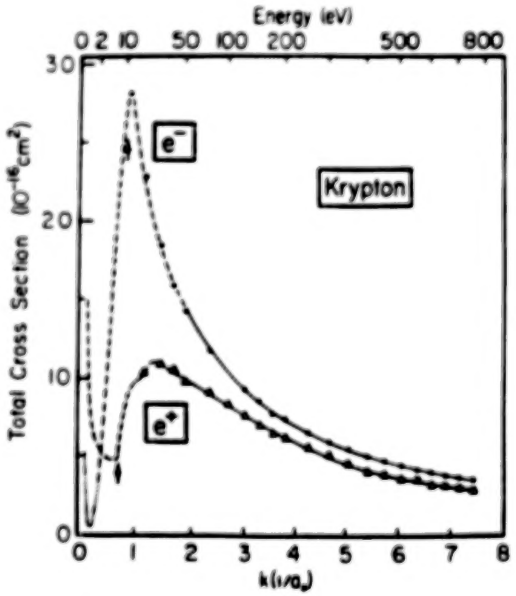

Fig. 3. Comparison of positron- and electron-Kr total cross sections. (From Dababneh et al., Ref. 3).

minima for the electron cases as shown in Figs. 2 and 3), (2) clear indications in the positron Q_T curves of the onset of Ps formation near the predicted Ps formation thresholds, and (3) the tendency for the positron and electron Q_T's to approach each other as the projectile energy is increased to sufficiently high energies. Mergings of positron and electron Q_T's have actually been observed for helium,[1] molecular hydrogen,[5] and water vapor[6] in the vicinity of about 200 eV.

It is of interest to consider whether all atoms and molecules would be expected to exhibit the same general tendencies for positron and electron scattering comparisons as those described above (and illustrated in Figs. 1-3). In order to investigate this matter further, we have been focusing our attention recently on positron-electron scattering comparisons for the alkali atoms. The alkali atoms have a relatively simple electronic structure with a single loosely bound valence electron moving outside a core of closed shells. Although there is some similarity between the single valence electron alkali atoms and atomic hydrogen, it has been pointed out[7] that the ground states of the alkali atoms have different characteristics than that of the H atom and that approximation schemes developed for the hydrogen atom will not necessarily be equally successful for the alkali atoms. One difference is associated with the atomic energy level separations. The energy separation between the ground state and first excited states of H is 10.2 eV whereas the largest corresponding separation for all of the alkali atoms is only 2.1 eV (which is for the case of sodium). The large coupling between the ground state and the first excited state of the alkali atoms influences significantly the behavior of both elastic and inelastic scattering.[7] Another feature of the alkali metal atoms is their very large polarizabilities relative to room-temperature gases. As examples, Na, K, and Rb have polarizabilities[8] of approximately 159, 293, and 319 a_o^3 (where a_o = Bohr radius), respectively, in comparison with the corresponding inert gas atoms, Ne, Ar, and Kr, with polarizabilities of 2.67, 11.1, and 16.7 a_o^3, respectively. Another unique feature of the alkali atoms is that since they all have ionization threshold energies less than the binding energy (6.8 eV) of Ps in its ground state, Ps can be formed by positrons of arbitrarily small incident energy, and thus the Ps formation channel is always open for these atoms. In contrast to this, the room temperature gases which have been used as targets for positrons and electrons all have Ps formation thresholds of at least several eV.

Our first report on the measurement of positron and electron-alkali atom Q_T's was on potassium[9], where we found that the corresponding positron and electron Q_T's were much closer to each other over the entire energy range studied (5 - 49 eV) than had been observed for any other target atoms and molecules investigated previously. In this paper, we report our present[10] positron- and electron-Na, K, and Rb results from 1 - 102 eV. The positron-Na and -Rb results represent the first reported Q_T measurements for these collision systems.

EXPERIMENTAL TECHNIQUE

We use a beam transmission technique to make absolute Q_T measurements for positrons and electrons colliding with alkali atoms in the same apparatus. Details of the apparatus and technique are provided elsewhere,[9,10] so only a brief description of our experimental approach is provided below. The positron source is ^{11}C produced on site by the $^{11}B(p,n)^{11}C$ reaction, generated by bombarding a boron target with protons from a Van de Graaff accelerator. The electron source is a thermionic cathode. A weak, curved axial magnetic field (produced by a curved solenoid) is used to guide the projectile beam from the source region to the scattering region, and to

discriminate against high energy positrons coming from the source. The measured full-width at half-maximum of the energy distribution of the detected positron beam is less than 0.10 eV, while that of the electron beam is between 0.15 and 0.20 eV.

A schematic diagram of the alkali-atom scattering system is shown in Fig. 4. The main component in this system is the scattering cell consisting of the main oven body, and a detachable cylinder which contains the alkali metal. The weak guiding axial magnetic field produced by the curved solenoid is extended into the scattering region by means of two coils located concentrically with the entrance and exit apertures of the scattering cell. A Channeltron electron multiplier (CEM) on the input side of the oven serves (when its front end is biased appropriately) as a detector for positrons or electrons about to enter the oven. When the cone (front end) of that detector is placed at ground potential, the projectile beam is permitted to pass through the oven and the transmitted beam is detected by another CEM at the output end of the oven. A retarding element (which becomes coated with the alkali metal effusing from the oven) located between the oven and the output CEM is used to measure the projectile energy as well as to provide additional discrimination (beyond geometrical considerations) against projectiles scattered through small angles in forward directions.

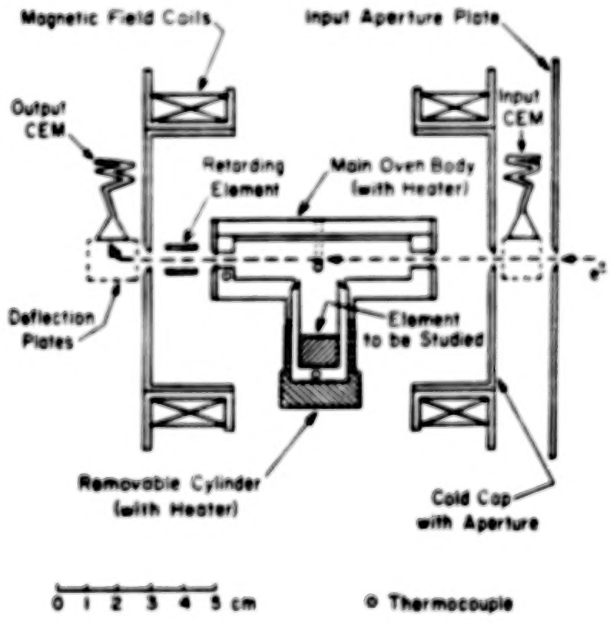

Fig. 4. Experimental setup for measuring total cross sections for alkali atoms. (From Stein et al., Ref. 9).

Our Q_T's are determined by measuring (1) the ratio, R_{cold}, of the output CEM to the input CEM counts per second when the oven is relatively cool so that there is a negligible vapor-pressure in the oven, and (2) the ratio, R_{hot} of the output CEM to the input CEM counts per second with the oven at an elevated temperature so that there is a high enough vapor-pressure in the oven to attenuate the projectile beam appreciably. The purpose of using the ratio of the output CEM to the input CEM counts per second is to normalize the transmitted beam intensity with respect to the incident beam intensity. Determinations of (1) the beam transmission ratio, R_{hot}/R_{cold}, (2) the number density, n, of the alkali atoms, which is determined by measuring the temperature of the oven and by using published vapor pressure data,[11] and (3) the beam path length, L of the projectiles thorough the oven, can be used with the relationship,

$$R_{hot} = R_{cold} \exp(-nLQ_T)$$

to obtain absolute positron- and electron-alkali atom Q_T's. It should be recognized that a major potential source of error in our Q_T measurements is related to the accuracy of the determination of n which is limited by the accuracy of our measurements of the scattering cell temperature, and by the accuracy of the vapor pressure data that we use. As a result of our continuing efforts to improve our determination of n (by improving the accuracy of our

measurements of the scattering cell temperature and by trying to identify the most reliable vapor pressure data in the literature), we feel that the present positron- and electron-K and electron-Na Q_T measurements[10] should be regarded as superseding our corresponding earlier measurements.[9,12]

RESULTS AND DISCUSSION

Electrons

Our present electron-Na, and -K, Q_T measurements (Kwan et al.[10]) are shown in Figs. 5 and 6 respectively along with prior measurements[13-19] and theoretical[20-22] results. The present electron results were obtained using the same apparatus and technique as was used for our positron measurements. Walters[20] has obtained Q_T's for electron-Na and -K collisions by adding the partial cross sections that he selected from existing theoretical and experimental results for the elastic (Q_E), resonance excitation (Q_R, which represents the 3s-3p transition for Na, and the 4s-4p transition for K), the sum of other discrete excitations (Q_D), and the ionization (Q_I) cross sections. Since Walters reported these Q_T values, Q_R and cross sections for numerous other discrete excitations have been measured by Phelps and Lin[16] for Na and by Phelps et al.[18] for K, and we have added these more recent excitation cross section results (rather than the Q_R and Q_D values used by Walters) to the values of Q_E and Q_I selected by Walters, to obtain the Q_T curves shown in Figs. 5 and 6 for Na and K, which we refer to as "Walters-Phelps curves". Our measured electron-Na Q_T values are in reasonable agreement with the shape and absolute values of the Walters-Phelps curves and in good agreement (averaging about 10% lower) with the theoretical values of Msezane[22] who added the elastic, resonance excitation, 3s-3d, 3s-4s, 3s-4p, and 3s-4d cross sections obtained from his 6 state close-coupling calculation to existing direct ionization cross sections obtained by others. Our measured electron-K Q_T

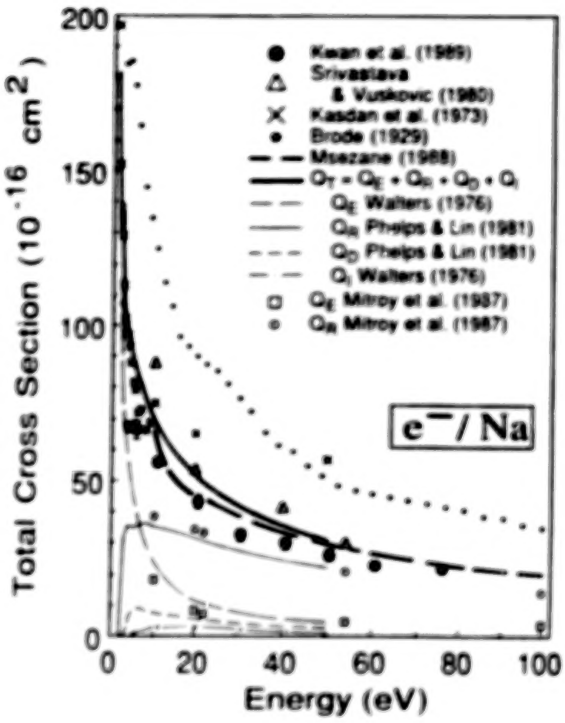

Fig. 5. Electron-Na cross sections.

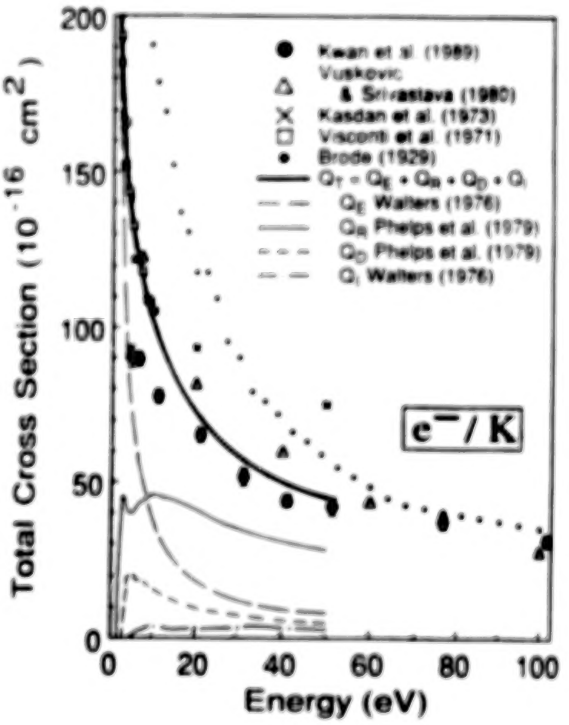

Fig. 6. Electron-K cross sections.

values are also in quite good agreement with the corresponding Walters-Phelps Q_T curve, averaging only about 10% lower from 20 to 50 eV. Of the prior measurements, the indirect determinations of Srivastava and Vuskovic[15] for Na, and of Vuskovic and Srivastava[19] for K, (who used their own crossed-beam measurements of differential cross sections for elastic scattering and for a number of different transitions from the ground state, and ionization cross sections measured by others) are in the closest overall agreement with the present corresponding measurements. As the energy is reduced below 10 to 20 eV, there is a tendency for our measured electron-Na and -K Q_T's to fall somewhat further below the corresponding curve of Msezane (for Na) and the Walters-Phelps curves. We feel that the explanation for this trend in Na and K may be as follows. The bias on the retarding element shown in Fig. 4 is always set within 1.25 V of the "cut-off" retarding voltage for the projectiles, and since the Na and K excitation thresholds are 2.10 eV and 1.61 eV respectively, there should be 100% discrimination against all inelastically scattered projectiles. In the vicinity of 20 eV for Na and K, the Walters-Phelps results in Figs. 5 and 6 show that the elastic scattering cross section (Q_E) is about 20% of Q_T for Na and about 25% of Q_T for K, and becomes an even smaller fraction of Q_T as the electron energy increases toward 50 eV. As the electron energy is reduced below 10 eV on the other hand, Q_E rapidly becomes a progressively larger fraction of Q_T, and at 5 eV, Q_E accounts for more than 50% of Q_T for both Na and K. In addition, the angular discrimination of our apparatus[9,10] against elastically scattered projectiles becomes poorer as the projectile energy decreases. For instance, the angular discrimination for electrons is estimated to be about 13° near 5 eV, 9° near 10 eV, 7° near 20 eV, and is about 5° or less from 30 eV to 100 eV. (The angular discrimination for elastically scattered positrons is somewhat poorer than that for electrons, but behaves in a similar way, being about 13° near 10 eV, 11° near 20 eV, 9° near 30 eV, and continuing to improve with increasing energy, reaching about 5° from 75 to 100 eV.) Our estimates of errors introduced into the electron-Na and -K Q_T's due to an inability to discriminate against projectiles elastically scattered through small angles in the forward direction suggest that as the electron energy is reduced below 10 to 20 eV, the increasing ratio of Q_E to Q_T, and the poorer angular discrimination may account for our measured Q_T's falling further below Msezane's results[22] and the Walters-Phelps curves. At 20 eV and above on the other hand, we estimate that the amount by which our measured Q_T's would be low due to our inability to discriminate against projectiles elastically scattered through small angles in the forward direction, should be of the order of 10% or less for electron-Na and -K collisions. Taking into consideration the uncertainty in our determination of the number density of atoms in our oven ($\pm$20%), and the potential errors in our measured Q_T's associated with the angular discrimination of our measurements, the closeness (and the consistency) of the close-coupling electron-Na Q_T results of Msezane[22] and the Walters-Phelps electron-Na and -K Q_T curves to our own corresponding measured values gives us some confidence that our experimental technique and apparatus for measuring electron-alkali atom Q_T's is basically sound. Since the same apparatus and technique is used for the positron measurements, we feel that they should not be greatly in error.

Positrons

The present measured positron-Na, -K (Kwan et al.[10]) and -Rb (preliminary) Q_T's are shown in Figs. 7-10 along with prior theoretical results.[23-33] Two separate Figures (Figs. 7 and 8) have been used for Na because of the abundance of theoretical results for this system. Ward et al.[25,32] have performed five-state close-coupling calculations of Q_T for positron-Na and

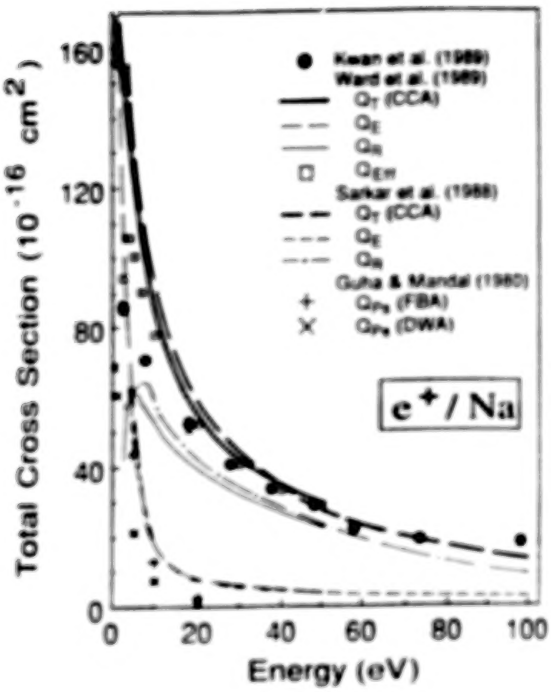

Fig. 7. Positron-Na cross sections.

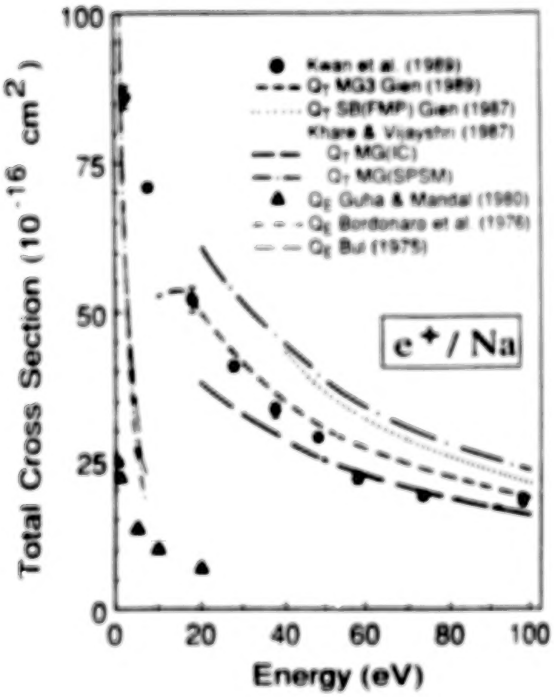

Fig. 8. Positron-Na cross sections.

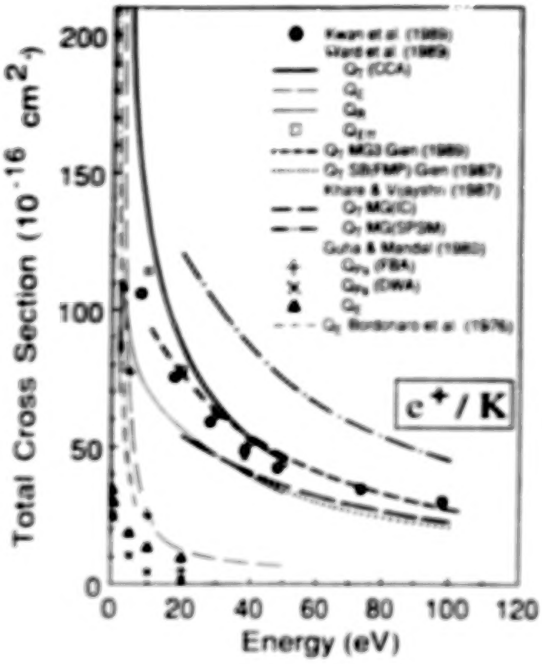

Fig. 9. Positron-K cross sections.

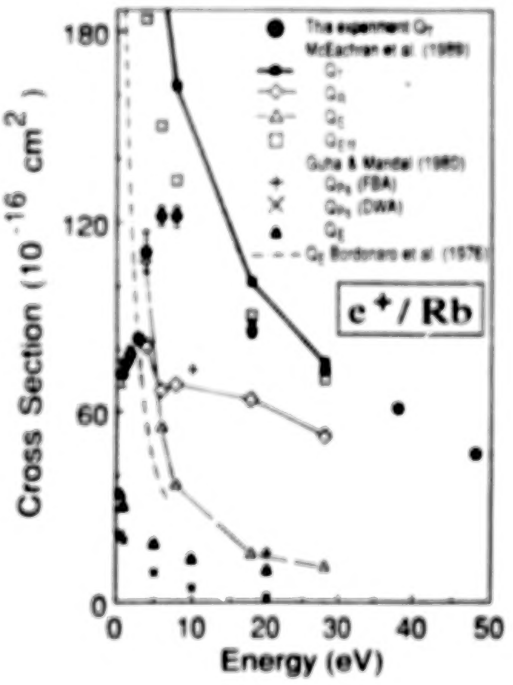

Fig. 10. Positron-Rb cross sections. The present Q_T measurements are preliminary values.

-K collisions that include the cross sections for elastic scattering, resonance excitation, and a few other discrete excitations (3s-4s, 3d, 4p for Na and 4s-5s, 3d, 5p for K) but do not include the cross sections for Ps formation and for ionization which are both expected to be relatively small[20,23] above 10 eV. McEachran et al.[33] have extended such Q_T calculations to Rb where they include the cross sections for elastic scattering, resonance excitation (5s-5p), and other discrete excitations (5s-4d, 6s, 6p) and do not include the cross sections for Ps formation and for ionization. In addition, Ward et al.[25,32] (for Na and K) and McEachran et al.[33] (for Rb) have used our estimates of our angular discrimination along with their differential elastic cross section results to calculate effective cross sections, Q_{Eff}, which represent their theoretical estimates of the Q_T's that we would be expected to obtain if the only error in our measurements were that associated with our inability to discriminate against projectiles elastically scattered through small angles in the forward direction. Our measured Q_T's are in reasonable agreement with their corresponding Q_T calculations for Na (Fig. 7) and K (Fig. 9) and are even closer to their Q_{Eff} values (within 10% over most of the energy range of overlap). For Rb (Fig. 10), our measured Q_T's are in good agreement with the theoretical Q_{Eff} values of McEachran et al.[33] for all energies of overlap above about 6 eV. However, as the positron energy is reduced below 4 eV, our measured Q_T values decrease sharply, whereas the theoretical Q_{Eff} values of McEachran et al. continue rising, and this gives rise to a significant discrepancy at the lowest energies of overlap. Aside from this puzzling discrepancy at the lowest energies in the positron-Rb case, there is good overall agreement between the close-coupling approximation Q_{Eff} results of Ward et al.[25,32] for positron-Na, -K and of McEachran et al.[33] for positron-Rb for most of the energy range of overlap. The positron-Na Q_T results of Ward et al.[25] are also quite close to the earlier four-state close-coupling approximation Q_T results of Sarkar et al.[24] (Fig. 7) which include their cross sections for elastic scattering, resonance excitation, 3s-3s and -4p excitations, and the Ps formation cross sections calculated by Guha and Mandal,[23] and first Born approximation values of ionization cross sections obtained by Walters[20]. The positron-Na and -K modified Glauber approximation ("MG3") Q_T results (Figs. 8 and 9) of Glen[30,31] are in reasonable agreement with the present results.

Positron and Electron Comparisons

In Figs. 11-13 our direct comparison measurements between positron- and electron-Na, -K, and -Rb Q_T's are shown along with selected experimental[13,16-18] and theoretical[20,25,32] results. It should be noted that even though, as mentioned earlier, a major potential source of error in our absolute Q_T determinations is associated with the determination of the number density of atoms in the scattering cell, our direct positron-electron comparison measurements should still be meaningful because essentially the same oven temperatures are used for each projectile for a given alkali atom. We find that Na, K, and Rb each exhibit remarkably similar Q_T's for positron and electron collisions over the entire energy range that has been studied. (The only indication of a substantial difference between the positron and electron Q_T's for these atoms so far is at the lowest energies studied for Rb, where the measured positron Q_T decreases abruptly as the positron energy is reduced below 4 eV.) We also find that our corresponding positron and electron Q_T's for Na, K, and Rb merge within the uncertainties of the measurements in the vicinity of 40 eV and remain essentially merged up to the highest energies studied thus far. In sharp contrast to the case for positron- and electron-room temperature gas Q_T's, the positron-Na,

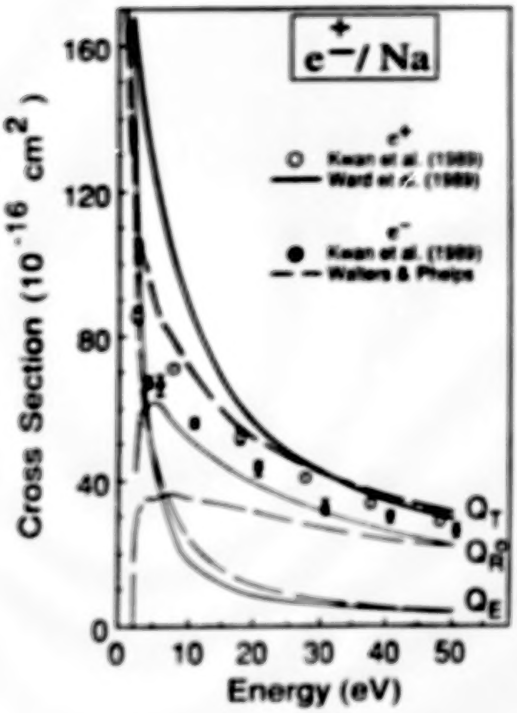

Fig. 11. Comparisons of positron- and electron-Na cross sections.

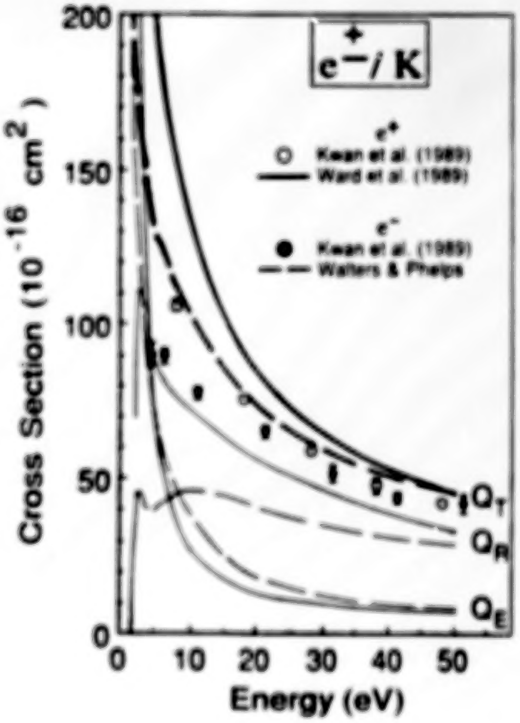

Fig. 12. Comparisons of positron- and electron-K cross sections.

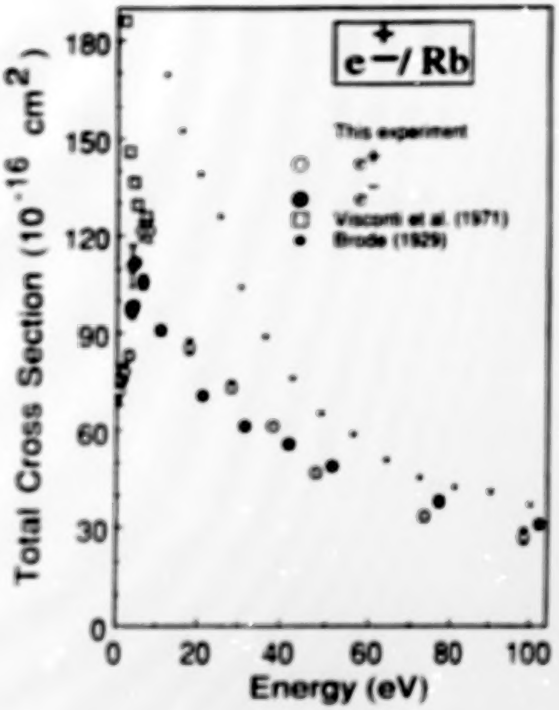

Fig. 13. Comparison of positron- and electron-Rb total cross sections. The present measurements are preliminary values.

-K, and -Rb Q_T's become increasingly higher than the corresponding Q_T's for electrons as the projectile energy is reduced from 40 eV down to the lowest energies studied in each case with the exception of the lowest energies for Rb shown in Fig. 13 (preliminary results).

It is interesting that when the Walters-Phelps electron-Na and -K Q_T curves are compared with the corresponding positron-Na and -K Q_T results obtained by Ward et al.[25,32] as shown in Figs. 11 and 12 respectively, mergings, or at least near-mergings of the positron and electron Q_T's are observed to occur in the vicinity of 30 to 50 eV, and as the projectile energy is reduced below this energy range, the positron Q_T's are observed to become increasingly larger than the corresponding electron values for each of these atoms. The close-coupling electron-Na Q_T results of Msezane[22] are

consistent with this picture since they are in good agreement with the Walters-Phelps curves shown in Fig. 11. Thus, the comparisons between the Walters-Phelps electron-Na, and -K Q_T curves (and the Msezane[22] curve for Na) and the close-coupling results of Ward et al.[25,32] for positrons colliding with Na and K tend to support our observations of a merging (or near-merging) of the positron and electron Q_T's near the relatively low energy of 40 to 50 eV, and also support our observations that the positron Q_T's are higher than the corresponding electron values below 40 eV (at least down to the lowest energies studied thus far). If these observations are correct, it is of interest to consider why the comparisons between positron and electron scattering from the alkali atoms indicate a dominance of the positron- over the electron-Q_T's at low energies whereas for the room-temperature gases, the situation is for the most part, reversed. Why do the room-temperature gases (illustrated by Figs. 1-3) all seem to fit, in general, the simple interaction model referred to in the Introduction which implies that the positron cross sections at low energies would be expected to be lower than the corresponding electron cross sections? That prediction was based upon the tendency toward cancellation of the static and polarization interactions in positron scattering, in contrast to the addition of these interactions in the electron case. Why do the alkali atoms appear to be showing the opposite behavior?

Perhaps the simple argument referred to in the Introduction concerning the relative roles of the static and polarization interactions is applicable to the total scattering cross section if the dominant contribution to it is elastic scattering for both positrons and electrons. However, perhaps when inelastic processes become dominant for either positrons or electrons (or both), this argument in its simple form no longer applies to a comparison of their total scattering cross sections. Theoretical investigations by Walters[20,34] of electron-alkali atom scattering indicate that with increasing energy beyond the first excitation thresholds (which are 2.10 eV or less for the alkali atoms) there is a change-over from a situation where polarization effects are dominant to one in which flux loss[34] becomes dominant. Figs. 11 and 12 indicate that the resonance excitation becomes the dominant contribution to positron and to electron scattering from Na and K near the relatively low energy of 10 eV. It can also be seen from Figs. 11 and 12 that while the elastic cross section (Q_E) is predicted to be somewhat larger for electrons than for positrons above 10 eV, it makes a relatively small contribution to Q_T as the projectile energy is increased above this energy. On the other hand, Figs. 11 and 12 indicate that the resonance excitation cross section (Q_R) is significantly larger for the positron than for the electron at low energies and is the main contribution to Q_T above 10 eV. We have chosen not to show a comparison of the sum of the other discrete excitations (Q_D) for positrons and electrons in Figs. 11 and 12 because Ward et al.[25,32] have only included cross sections for three such excitations for Na(3s-4s, 3d, 4p) and K(4s-5s, 3d, 5p) whereas the Q_D's used for the Walters-Phelps Q_T electron curves in Figs. 11 and 12 include 14 such excitations. However it is interesting to note that for the 3 corresponding excitation processes in Na and K which have been calculated for positrons[25,32] and measured for electrons,[16,18] the positron cross sections tend to be significantly larger than the corresponding electron cross sections at low energies, similar to the situation shown for the resonance excitation in Figs. 11 and 12. The positron- and electron-Na and -K ionization cross sections are expected to be small, and if the positron- and electron-He ionization cross section comparisons[35] can serve as a guide, one might expect Q_I for the positron-Na and K collisions to be larger than the corresponding electron values. In

addition to this, although the theoretical predictions of Q_{Ps} by Guha and Mandal[23] shown in Figs. 7 and 9 indicate that Q_{Ps} makes a relatively small contribution to Q_T for energies above 10 eV, this is still an additional inelastic contribution to Q_T which does not have a counterpart in electron-alkali atom collisions, and it appears (as seen in Figs. 7 and 9) to be playing an increasingly important role in Q_T as the positron energy decreases below 10 eV. The above information suggests that the positron-alkali atom Q_T's may rise above the corresponding electron values as the projectile energy is reduced below 40 eV mainly due to the relatively large contributions to Q_T by inelastic processes (especially excitation) which are predicted to have larger cross sections for positrons than for electrons at these low energies. Although the elastic cross section for alkali atoms is predicted to be slightly larger for electrons than for positrons at low energies (between 5 and 50 eV), it appears that Q_E contributes too little to Q_T to make Q_T larger for electrons than it is for positrons, as is the case for the room-temperature gases in this energy range.

It should be noted that although our observations indicate a merging of the positron- and electron-Na and -K Q_T's at the relatively low energy of about 40 eV, and a dominance of the positron Q_T's over the corresponding electron Q_T's at lower energies, and although this picture is supported by the comparisons of the Walters-Phelps Q_T curves (and the Msezane[22] curve) for electrons with the Ward et al.[25,32] close-coupling approximation results for positrons, modified Glauber (MG3) calculations by Gien[30,31] for positron- and electron-Na and -K collisions, shown in Figs. 14 and 15 predict a different behavior for the positron-electron comparisons. According to Gien's calculations,[30,31] the positron- and electron-Na and K Q_T's do not merge even up to energies as high as 1000 eV, and furthermore, the electron Q_T's are larger than the positron Q_T's over

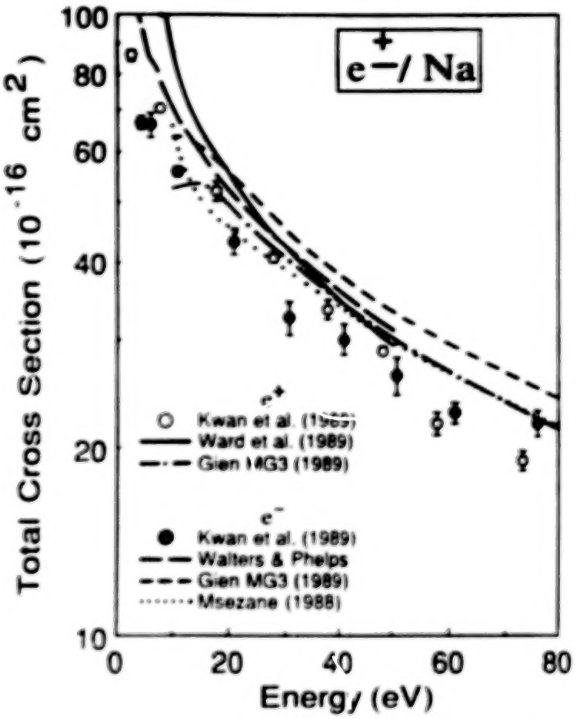

Fig. 14. Comparisons of positron- and electron-Na total cross sections.

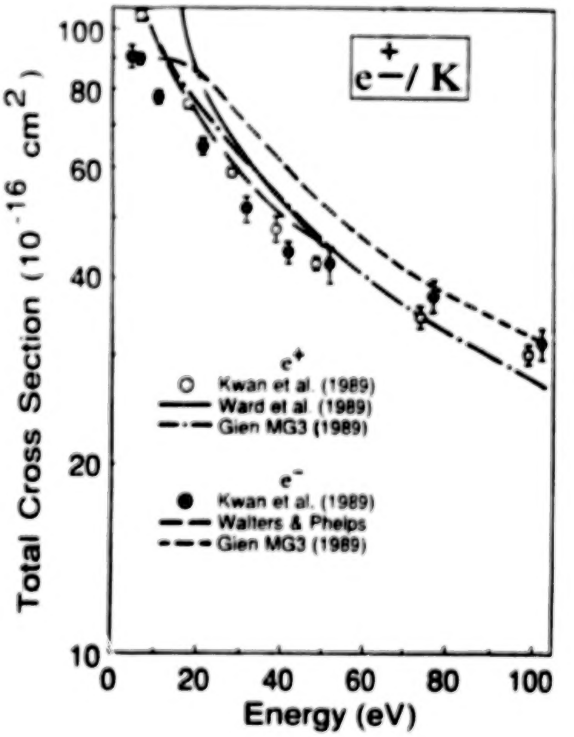

Fig. 15. Comparisons of positron- and electron-K total cross sections.

essentially his entire energy range. It should be noted however, that whereas Gien's positron-Na and -K Q_T's are in quite good agreement with those of Ward et al.[25,32] (and Sarkar et al.[24] for Na), his electron Q_T's are somewhat higher than those associated with the Walters-Phelps curves for Na and K and the results of Msezane[22] for Na. It is also of possible interest that Gien has not included the effects of exchange in his electron calculations.

FUTURE DIRECTIONS

Based upon our direct comparison measurements of Q_T's for positron- and electron-alkali atom collisions up to the present time, we feel that it would be of interest to address the following points in future research. (1) Is there actually a merging (or near-merging) of Q_T's for positron- and electron-Na, K, and Rb collisions in the vicinity of 40 eV, and are the positron Q_T's larger than the corresponding electron values below that energy as our observations (preliminary for Rb) indicate? As mentioned above, our observations tend to be supported by a comparison (Figs. 11 and 12) of the Walters-Phelps electron-Na and -K Q_T curves (and electron-Na Q_T's obtained by Msezane[22] using a close-coupling approximation) with the corresponding positron values obtained by Ward et al.[25,32] using a close-coupling approximation. However the modified Glauber approximation (MG3) results of Gien[22] for Na and K suggest a significantly different behavior for the positron and electron comparisons (Figs. 14 and 15). Up to the present time, theorists who have done close-coupling approximation calculations of Q_T for positron-alkali atom collisions have not done them for electron-alkali atom collisions and vice versa. In order to conduct a more stringent theoretical test of the validity of our observed low energy mergings and the reversal of the "normal" arrangement of positron and electron Q_T's at low energies, it could be helpful if theorists who have done a close-coupling approximation calculation for one of these projectiles colliding with an alkali atom would do a comparable close-coupling approximation calculation for the other projectile. In a certain sense, this could be considered to be the theoretical counterpart to our having measured Q_T's for the two projectiles in the identical apparatus using the same experimental technique as opposed to comparing our measured positron-alkali atom Q_T's to another experimental group's measured electron-alkali atom Q_T's. (2) Although the positron and electron elastic scattering cross sections predicted by Ward et al.[25,32] and Walters,[20] respectively, for Na and K collisions are in the usual order from about 5 to 50 eV (the electron Q_E's being higher than the corresponding positron values), it is curious that the the positron and electron Q_E's appear to cross each other (Figs. 11 and 12) in the vicinity of 5 eV, so that as the projectile energy is reduced below 5 eV, it appears that the positron Q_E's are larger than the corresponding electron values. Is this representative of the actual situation, or is it possible that the Ward et al. calculation of Q_E at these low energies is too large due to the neglect of Ps formation, which may be playing a more important role as the positron energy decreases. (3) If our observed low-energy mergings of positron- and electron-alkali atom Q_T's are valid, this may provide additional evidence that mergings of positron- and electron-atom Q_T's can occur at unexpectedly low energies. In this connection it should be noted that the first observation[1] of such a low energy merging was for He where the positron and electron Q_T's were found to merge (to within 2%) near 200 eV. The distorted wave second Born approximation (DWA) calculations of Dewangan and Walters[36] predict that a merging of the positron and electron-He Q_T's (to within 2%) does not occur until 2000 eV. These calculations also indicate that at 200 eV, where Kauppila et al.[1] have observed the merging of positron and electron Q_T's, the electron total elastic cross section is about 2.4 times as large as the corresponding positron cross

section. Thus at the energy (about 200 eV) where the positron and electron Q_T's have been observed[1] to merge, the partial contributions (such as Q_E) to Q_T are apparently behaving much differently for positrons than for electrons. A comparison[37] of a calculation of Q_T for 54.4-300 eV positron-atomic hydrogen collisions by Walters[37] (using a pseudostate close-coupling approximation that is supplemented by the second Born approximation) with similar calculations for electrons by Van Wyngaarden and Walters[38] indicates a situation similar to that just described for helium in the sense that the Q_T's for these projectiles remain very nearly merged down to the lowest energies studied (54.4 eV) whereas the cross section for elastic scattering is about 3 times as large for electrons as for positrons at 54.4 eV, while the cross sections for the 1s-2s and 1s-2p excitations are larger for positrons than for electrons. Our present observations[10] indicate that the alkali atom Q_T's may be merging at energies considerably lower than the asymptotic energies at which the first Born approximation is valid,[39] but based upon the information in Figs. 11 and 12, the partial elastic and inelastic contributions to Q_T may be at least close to separately merged where the Q_T's appear to be merging, in possible contrast to the He and atomic hydrogen situations. In relation to the question of mergings of positron and electron cross sections at unexpectedly low energies, it is of interest that a theoretical analysis by Dewangan[40] related to higher order Born amplitudes calculated in the closure approximation has been shown to imply[34,41] that if electron exchange can be ignored in the electron-scattering case, and if the closure approximation is valid, then a merging (or near-merging) of positron- and electron-atom Q_T's can occur at energies considerably lower than the asymptotic energies at which the first Born approximation is valid. (4) In light of the information (theoretical and experimental) that we have on positron and electron scattering comparisons up to the present time, it is interesting to consider the possibility that at low energies, in general, elastic scattering cross sections for electron-atom collisions may tend to be larger than those for positron-atom collisions (aside from complications like Ramsauer-Townsend effects), whereas inelastic scattering cross sections for positron-atom collisions may tend to be larger for positrons than they are for electrons. Perhaps the simple explanation given in the Introduction for why the electron Q_T's are larger than the corresponding positron values at low energy applies only to elastic scattering. Could there be a correspondingly simple explanation for why inelastic scattering cross sections may tend to be larger for positrons than for electrons in general (if this is indeed the case)? (5) In relation to item (4), it would be useful to have direct positron-electron comparison measurements (using the same apparatus and experimental technique) of resonance excitation cross sections for the alkali atoms to see if it is the case (as indicated by the comparisons shown in Figs. 11 and 12) that the resonance excitation cross section is so much larger for positrons than it is for electrons at low energies. This would be of particular interest in view of the indications shown in Figs. 11 and 12 that the resonance excitation becomes the main contribution to Q_T at energies above 10 eV or so. (6) What is the contribution of Ps formation to Q_T in positron-alkali atom scattering? The theoretical calculations of Q_{P_S} shown in Figs. 7,9, and 10 suggest that it plays a relatively unimportant role above 10 eV, but is increasing as the positron energy is reduced toward zero. As was mentioned above, it is possible to form Ps in collisions with alkali atoms at arbitrarily small positron energies. Does Q_{P_S} increase without limit as the positron energy approaches zero? It would be useful to have direct measurements of Q_{P_S} for positron-alkali atom collisions at low energies to investigate questions such as this.

ACKNOWLEDGEMENTS

We gratefully acknowledge the helpful assistance of James Klemic, and the support of the National Science Foundation for our research program.

REFERENCES

*Permanent address: Nanjing Institute of Technology, Nanjing, Jiangsu, The People's Republic of China
**Permanent address: Department of Physics, Yarmouk University, Irbid, Jordan.

1. W.E. Kauppila, T.S. Stein, J.H. Smart, M.S. Dababneh, Y.K. Ho, J.P. Downing, and V. Pol, Phys. Rev. A 24, 725 (1981).
2. T.S. Stein, W.E. Kauppila, V. Pol, J.H. Smart, and G. Jesion, Phys. Rev. A 17, 1600 (1978).
3. M.S. Dababneh, Y.-F. Hsieh, W.E. Kauppila, V. Pol, and T.S. Stein, Phys. Rev. A 26, 1252 (1982).
4. M.S. Dababneh, W.E. Kauppila, J.P. Downing, F. Laperriere, V. Pol., J.H. Smart, and T.S. Stein, Phys. Rev. A 22, 1872 (1980).
5. K.R. Hoffman, M.S. Dababneh, Y.-F. Hsieh, W.E. Kauppila, V. Pol, J.H. Smart, and T.S. Stein, Phys. Rev. A 25, 1393 (1982).
6. O. Sueoka, S. Mori, and Y. Katayama, J. Phys. B 19, L373 (1986).
7. B.H. Bransden and M.R.C. McDowell, Phys. Rep. 46, 249 (1978).
8. T.M. Miller and B. Bederson, Adv. At. Mol. Phys. 13, 1 (1977).
9. T.S. Stein, R.D. Gomez, Y.-F. Hsieh, W.E. Kauppila, C.K. Kwan, and Y.J. Wan, Phys. Rev. Lett. 55, 488 (1985).
10. C.K. Kwan, W.E. Kauppila, R.A. Lukaszew, S.P. Parikh, T.S. Stein, Y.J. Wan, S. Zhou, and M.S. Dababneh, to be published.
11. R.E. Honig and D.A. Kramer, RCA Rev. 30, 285 (1969).
12. T.S. Stein, M.S. Dababneh, W.E. Kauppila, C.K. Kwan, and Y.J. Wan, in "Atomic Physics with Positrons", edited by J.W. Humberston and E.A.G. Armour, NATO ASI Series B, Vol. 169, pp. 251-263 (Plenum, 1987).
13. R.B. Brode, Phys. Rev. 34, 673 (1929).
14. A. Kasdan, T.M. Miller, and B. Bederson, Phys. Rev. A 8, 1562 (1973).
15. S.K. Srivastava and L. Vuskovic, J. Phys. B 13, 2633 (1980).
16. J.O. Phelps and C.C. Lin, Phys. Rev. A 24, 1299 (1981).
17. P.J. Visconti, J.A. Slevin, and K. Rubin, Phys. Rev. A 3, 1310 (1971).
18. J.O. Phelps, J.E. Solomon, D.F. Korff, C.C. Lin, and E.T.P. Lee, Phys. Rev. A 20, 1418 (1979).
19. L. Vuskovic and S.K. Srivastava, J. Phys. B 13, 4849 (1980).
20. H.R.J. Walters, J. Phys. B 9, 227 (1976).
21. J. Mitroy, I.E. McCarthy, and A.T. Stelbovics, J. Phys. B 20, 4827 (1987).
22. A.Z. Msezane, Phys. Rev. A 37, 1787 (1988).
23. S. Guha and P. Mandal, J. Phys. B 13, 1919 (1980).
24. K.P. Sarkar, M. Basu, and A.S. Ghosh, J. Phys. B 21, 1649 (1988).
25. S.J. Ward, M. Horbatsch, R.P. McEachran, and A.D. Stauffer, J. Phys. B 22, 1845 (1989).
26. T.D. Bui, J. Phys. B 8, L153 (1975).
27. G. Bordonaro, G. Ferrante, M. Zarcone, and P. Cavaliere, Nuovo Cimento Soc. Ital. Fis. 35 B, 349 (1976).
28. S.P. Khare and Vijayshri, Indian J. Phys. 61B, 404 (1987).
29. T.T. Gien, Phys. Rev. A 35, 2026 (1987).
30. T.T. Gien, J. Phys. B 22, L463 (1989).
31. T.T. Gien, J. Phys. B 22, L129 (1989).
32. S.J. Ward, M. Horbatsch, R.P. McEachran, and A.D. Stauffer, J. Phys. B 21, L611 (1988).
33. R.P. McEachran, M. Horbatsch, A.D. Stauffer, and S.J. Ward, to appear in Proceedings of the "Workshop on

Annihilation in Gases and Galaxies", to be published as a NASA Conference Publication (NASA Goddard Space Flight Center, July, 1989).
34. H.R.J. Walters, Physics Reports 116, 1 (1984).
35. D. Fromme, G. Kruse, W. Raith, and G. Sinapius, Phys. Rev. Lett. 57, 3031 (1986).
36. D.P. Dewangan and H.R.J. Walters, J. Phys. B 10, 637 (1977).
37. H.R.J. Walters, J. Phys. B 21, 1893 (1988).
38. W.L. van Wyngaarden and H.R.J. Walters, J. Phys. B 19, 929 (1986).
39. H.R.J. Walters, private communication.
40. D. P. Dewangan, J. Phys. B 13, L595 (1980).
41. F.W. Byron, Jr, C.J. Joachain, and R.M. Potvliege, J. Phys. B 15, 3915 (1982).

ELASTIC SCATTERING OF e^- AND e^+ FROM Rb AND Cd

A W Pangantiwar** and Rajesh Srivastava*

* Physics Department, Roorkee University, Roorkee - 247 667 (India)

** Govt. College of Engineering, Aurangabad, Mahrashtra, (India)

ABSTRACT

Differential cross section results are calculated for the elastic scattering of electrons and positrons from the ground state of Rb and Cd atoms. An optical model potential approach is used for the calculation. Results are compared with the available electron impact experimental results.

I. INTRODUCTION

In the present workshop we wish to report our theoretical study of the elastic scattering of electrons and positrons by the ground state of Rb and Cd atoms. Since the differential cross sections (DCS) as compared to total cross sections provide more rigorous testing for theories and experiments we mainly evaluate the DCS results at various incident projectile energies, especially at energies for which electron impact experimental results are available. However, the direct measurements of the DCS for positrons elastically scattered from alkali and heavy atoms are also becoming available. In our study we describe elastic scattering of electrons and positrons from Rb and Cd atoms in the framework of an "optical model potential approach" (OMPA)[1]

II. THEORY

The choice of optical model potential used in our OMPA can be expressed as

$$V_{opt}(r) = V_{st}(r) + V_{ex}(r) + V_{pol}(r) \qquad ...(1)$$

The first three terms on the right hand side of equation (1) represent respectively the static, exchange and polarization potentials. Exchange potential is absent for positron scattering. We obtain static potential using multi-zeta type Hartree-Fock wavefunction[2] for Rb and Cd. For exchange potential following widely used form is used[3].

$$V_{ex}(r) = (k^2/2 - V_{st}(r) - [(k^2/2 - V_{st}(r))^2 + 8\pi\Gamma\rho(r)]^{1/2})/2 \qquad ...(2)$$

Here $\vec{k}$ is incident electron wavevector, $\rho(r)$ is atomic target charge density. For Cd, $\Gamma = 1$ and for Rb, $\Gamma = -1$ and $+1$ respectively for singlet and triplet modes of scattering. Following functional form of the polarization potential is chosen[4]

$$V_{pol}(r) = = (\alpha/2r^4)(1 - \exp[-(r/r_c g)^8]) \qquad ...(3)$$

α is dipole polarizability of target atom, r_c is cutoff parameter (see ref. 4) and g is energy dependent adjustable parameter chosen such that it provides best fit to electron impact exprimental DCS data. For positron scattering g is taken unity. From the known optical potential the Schrodinger equation is solved for phase shifts which

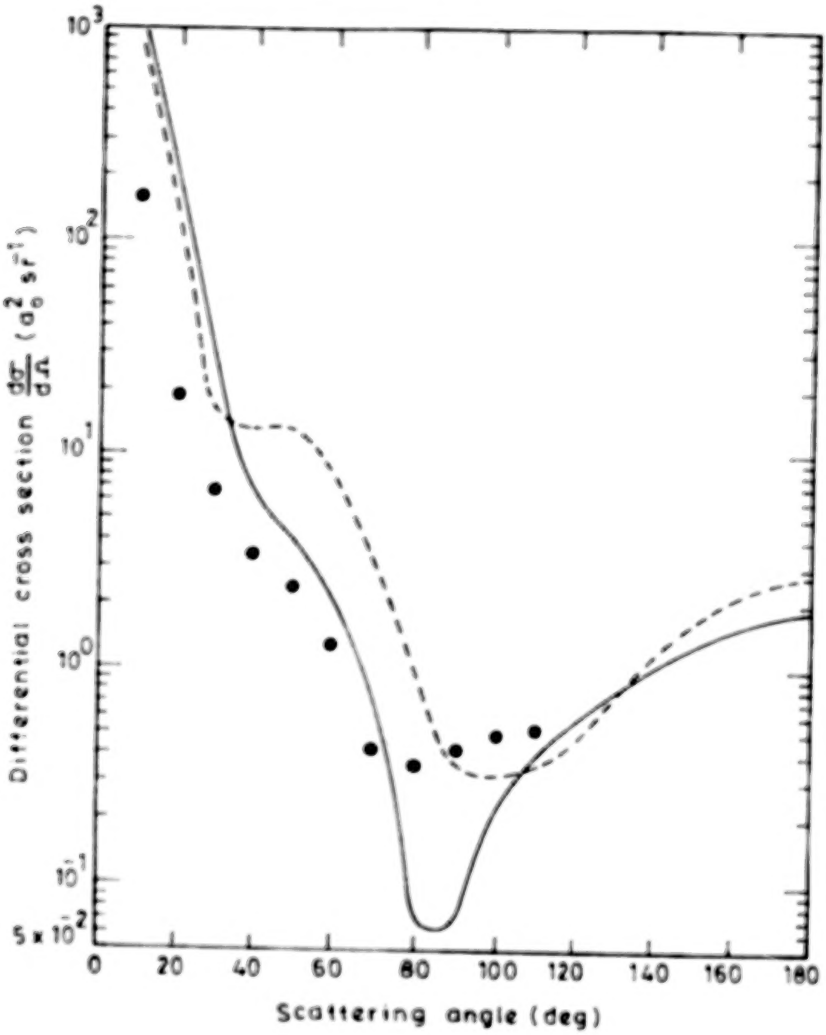

Fig. 1 : DCS results for $e^-(e^+)$-Rb elastic scattering at 10 eV.
—— present e^- results, --- present e^+ results, ● experiment[6].

Consequently define scattering amplitude and give DCS results in conventional manner[1].

III. RESULTS

The detail of the numerical calculation along with the DCS results for $e^-(e^+)$-Cd elastic scattering is being published elsewhere[5] and we briefly present here our $e^-(e^+)$-Rb elastic scattering DCS results. For Rb we take α = 319 and obtain[4] r_c = 3.576. The DCS results are calculated at 10 and 20 eV energies as displayed through figures 1 and 2. From these figures on comparing with experimental results[6] we find that our optical model potential describes the e^- - Rb elastic scattering reasonably well while for our positron scattering results future experiments can throw some light.

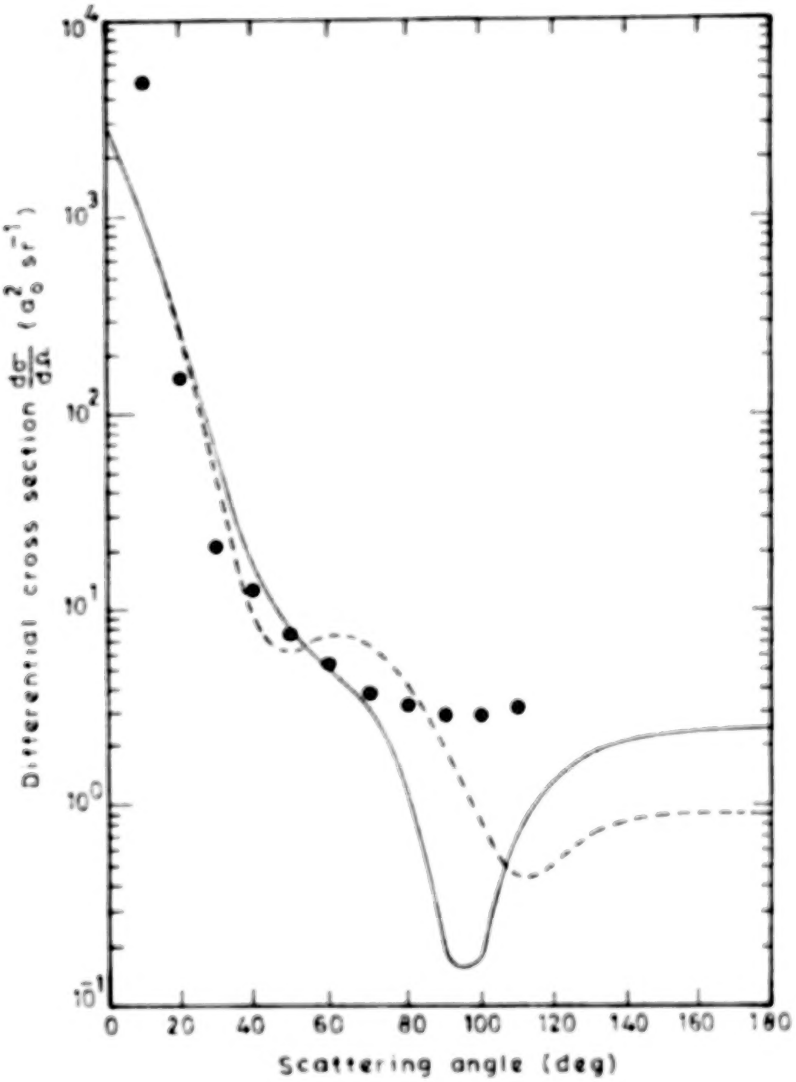

Fig. 2 : Same as Figure 1 at 20 eV.

REFERENCES

1. I Khurana, R Srivastava and A N Tripathi Phys.Rev.A 37 3720 (1988)
2. E Clementi and C Roetti At.Data,Nucl.Data Tables 14 177 (1974)
3. J B Furness and I E McCarthy, J.Phys.B 6 2280 (1973)
4. R Srivastava and W Williamson Jr Phys.Rev. A 35 103 (1987)
5. A W Pangantiwar and R Srivastava Phys.Rev. A (1989) In press.
6. L Vuskovic, L Malcki and S Trajmar J.Phys. B 17 2517 (1984).

Inelastic Scattering of Positrons with Sodium

S.P.Purohit and K.C.Mathur
Physics Department, University of Roorkee, Roorkee-247667, India

Abstract

The two potential approach is used to study the resonant 3s-3p excitation of sodium atom by positrons of energy 40 and 54.4ev.The angular variation of coherence and correlation parameters is presented. Comparison with the corresponding parameters in electron scattering is given to see the role of various interaction potentials in electron and positron scattering.

1 Introduction

The development of positron beams of well defined energy has led to several experimental studies on the scattering of positrons with atomic and molecular systems. Measurement of total and differential cross-sections for various excitation and ionization processes are in progress at several laboratories. In comparison to the total and differential cross-sections, the study of angular correlation parameters provides a much deeper insight into the dynamics of atomic and molecular collision process. Such studies have now become possible with electron beams. With the rapid development in positron beam technology it is expected that in near future angular correlation and polarization correlation measurements with positrons will become feasible. The positron scattering differs from electron scattering in many ways, such as the absence of exchange in positron scattering and absence of positronium formation in electron scattering. The nature of the static potential is different in the two cases. It is repulsive for positrons and attractive for electrons. This coupled with attractive polarization in both the cases leads to totally different distortion of the incident positron and electron wavefunctions. A relative comparison of electron and positron scattering therefore leads to significant information on the nature of the interaction potential.

Since sodium atomic targets are most suitable for experiments, we report here a theoretical study on the resonant 3s-3p excitation of sodium atom by positrons at intermediate energies of 40 and 54.4ev, where positronium formation cross-section would be negligible. The theoretical approach we follow is based on the two potential formalism[1], which has been found to yield reliable results at intermediate energies in our earlier work on electron scattering[1,2]. We present here the angular variation of the correlation parameters ($\lambda, \chi_-, < L_Y >$) and the polarization parameters ($P1, P2, P, \gamma$) for positron impact. Relative comparison with electron scattering is also given.

2 Theory

The T matrix for positron scattering, in the framework of the two potential approach, is given (to the first order) by[3],

$$T = < \phi_f \mid U \mid \chi_i^+ > + < \chi_f^- \mid W_f \mid \chi_i^+ > \quad (1)$$

where the total positron sodium interaction potential V in a channel j is divided as,

$$V = U_j + W_j \quad (2)$$

The distorted waves are the solution of Schroedinger equation,

$$(H_0 + U_{i,f})\chi^{+}_{i,f} = E\chi^{+}_{i,f} \quad (3)$$

The distorting potentials U_j are chosen as

$$U_j = V^j_S + V^j_P + V_C \quad (4)$$

where the static, polarization and core potentials for sodium are of the same form (except for the change of sign of static and core terms) as given in our earlier work[2] on electron sodium scattering. The differential cross-sections are given by.

$$\sigma = \sigma_0 + 2\sigma_1 \quad (5)$$

$$\sigma_m^{i\to f} = (1/4\pi^2)(k_f/k_i) \mid T_m^{i\to f} \mid^2 \quad (6)$$

The alignment and orientation parameters are defined as,

$$\lambda = \sigma_0/\sigma_1 \quad (7)$$

$$\chi = \arg(a_1/a_0) \quad (8)$$

$$< L_Y > = -2\sqrt{2} Im < a_0 a_1 > /\sigma \quad (9)$$

a_0 and a_1 are the excitation amplitudes for m=0 and m=1 magnetic substates. <> denotes spin average.

The polarization of radiation emitted perpendicular to the scattering plane is given by,

$$P1 = [I(0^0) - I(90^0)]/[I(0^0) + I(90^0)] \quad (10)$$

$$P2 = \frac{[I(45^0) - I(135^0)]}{[I(45^0) + I(135^0)]} \quad (11)$$

$$P3 = \frac{[I(RHC) - I(LHC)]}{[I(RHC) + I(LHC)]} \quad (12)$$

The alignment angle of the charge cloud with respect to the incident positron direction is given by,

$$\gamma = 0.5 \arg(P1 + iP2) \quad (13)$$

The coherence of excitation is determined by the reduced polarization vector $\mid P \mid$ (which takes into consideration the depolarizing influence of unresolved fine and hyperfine structure of excited state of sodium[4],

$$\mid P \mid = [\mid P1/c_1 \mid^2 + \mid P2/c_1 \mid^2 + \mid P3/c_2 \mid^2]^{1/2}, \quad (14)$$

where $c_1 = 0.141$ and $c_2 = 0.558$. The angular distribution of the above parameters provides information about the shape and rotation of the excited state.

3 Results

Figure 1 shows the differential cross-sections for positron (solid curve) and electron impact (dashed curve) excitation of sodium to the 3p state at 40 and 54.4ev energies. We find that in the low angle region the positron and electron cross-sections are nearly equal. This is expected also, since the low angle scattering is dominated by polarization potential which is identical in the two cases. In the large angle region the differences come primarily due to the absence of exchange in positron scattering, and due to the different nature of static interactions in the two cases.

Figure 2 gives the angular variation of the λ parameter for positron and electron scattering at the two energies. We find that for positron impact only one minima is obtained while for electron impact two minimas are obtained. The position of the first minimum in electron scattering nearly coincides with that of positron scattering.

Figure 3 gives the angular variation of the expectation value of the angular momentum transferred during the collision in perpendicular direction by positrons and electrons. We see that the positron and electron orientation is of opposite sign for low and intermediate angles while for large angles it is of the same sign. This behavior of orientation in positron and electron scattering is also found in our earlier work on lithium[3].

Figure 4 gives the angular variation of polarization and alignment in positron and electron scattering at the two energies. It is seen that

for positron scattering the alignment angle γ is negative in the whole angular range, thus showing that the charge cloud is always aligned away from the positron. The alignment in positron and electron scattering is nearly identical at low and at large angles.

The reduced polarization $|P|$ is almost unity in the entire angular region leading to coherent excitation by positrons.

We thank the Council of Scientific and Industrial Research, India for financial support for the above work. SPP thanks the University Grants Commission, India for a research fellowship.

4 References

1. S.Saxena and K.C.Mathur , J.Phys.B18, 509 (1985) .

2. K.C.Mathur and S.P.Purohit , J.Phys.B22, 4223 (1989) .

3. S.Saxena and K.C.Mathur , J.Phys.B19, 3181 (1986) .

4. N.Andersen, J.W.Gallagher, and I.V.Hertel , Phys.Rep.165, 1 (1988) .

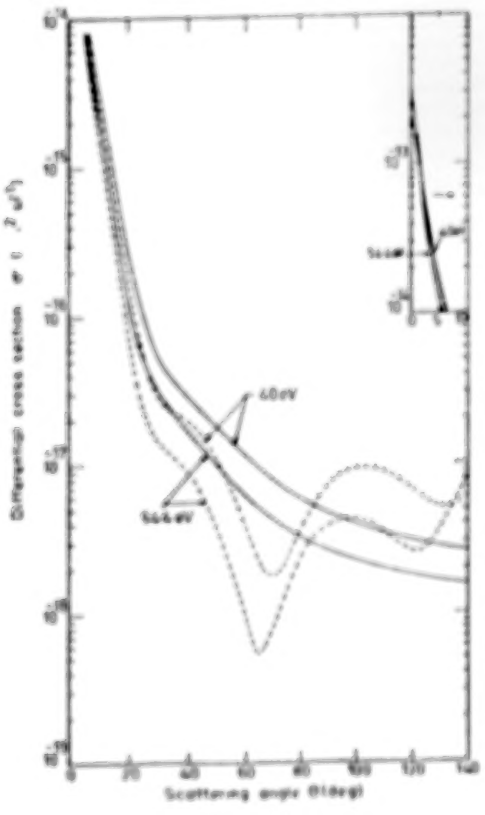

Figure 1

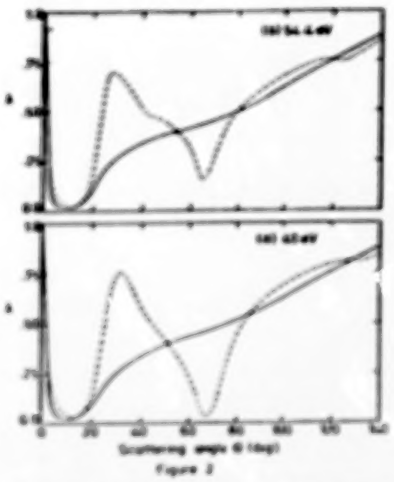

Figure 2

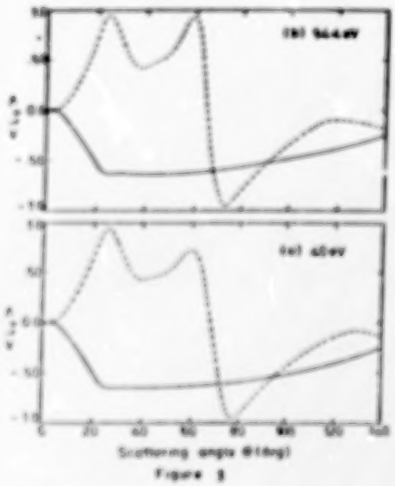

Figure 3

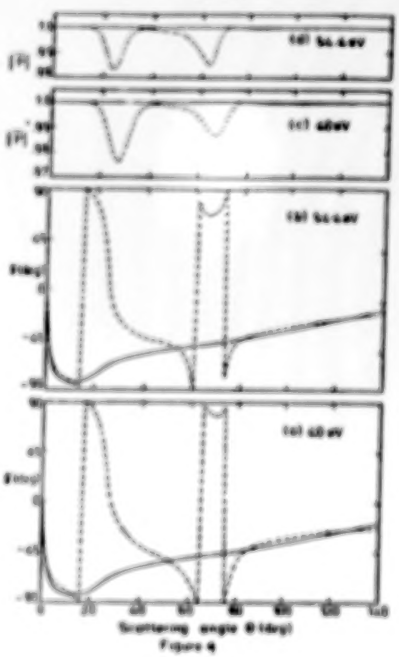

Figure 4

Positron collisions with alkali-metal atoms

T. T. Gien

Department of Physics, Memorial University of Newfoundland,
St. John's, Newfoundland, Canada A1B 3X7

The total cross sections for positron and electron collisions with potassium, sodium, lithium and rubidium are calculated, employing the modified Glauber approximation. The MG cross sections for positron collision with potassium and sodium at low intermediate energies are found to agree reasonably well with existing experimental data.

Measurements of total cross sections for collision of positron with potassium have been performed only very recently[1]. The experimental results of total cross sections for positron collision by sodium and rubidium have been reported only at this Workshop[2]. In view of the success of the modified Glauber approximation[3] in producing good agreement with experimental data of total cross section in the case of e^+-He, we have performed the calculation of total cross sections for positron (and electron) collisions with potassium, sodium and lithium, again employing the modified Glauber approximation (MG). The model-potential approach[4] will also be used in this calculation to enable the "exact" inclusion of the scattering effects of the core of the alkali atoms. The total cross sections are calculated via the optical theorem.

In alkali atoms, the energy of the first p states of the valence electron is only about 2 eV above its loosely bound s ground state. This results in a strong coupling between these two states and, thus, a very large dipole polarizability for the alkali atoms. Therefore, care must be taken in handling the effect of this particularly strong coupling between these s and p states. In the modified Glauber approximation, the effect of this strong coupling is seen to reflect in the large contribution to the second Born term of the valence-electron-atom scattering from the first p states, especially in the forward direction where the imaginary part of the scattering amplitude is used to calculate the total cross sections. To obtain a greater accuracy for our MG results, we feel that in this particular case of scattering by alkali-metal atoms, the contribution to the second Born term from the intermediate first p states should be evaluated exactly.

The MG total cross sections of positron (and electron) scattering from potassium, sodium and lithium were calculated for scattering energies ranging from about 10 eV to 1000 eV. The MG positron collision with potassium[5] are found to be in good agreement with experimental data available at low intermediate energies at present[1], if one takes into consideration the uncertainty existing in the experimental data due to the inability of discriminating against the elastically scattered

positrons (electrons) near the forward direction. At higher scattering energies (60 - 102.5 eV), the MG values tend to be somewhat smaller than the experimental values, while at lower energies, the MG values tend to be somewhat greater. We have also evaluated exactly the contribution to the second-Born term from the next higher intermediate state (5s for K, 4s for Na and 3s for Li) and we have found that the new values of total cross section only change minutely in comparison to the values obtained with the consideration of the closure approximation for this term. Therefore, we believe that the accuracy of the MG results will not be seriously affected by the employment of the closure approximation for the calculation of the contributions to the second-Born term from other higher excited intermediate states. The MG values of e^+-K collision are found to be consistent also with those obtained by Ward et al.[6] in the 5-state close-coupling calculation.

The MG values of total cross section for electron collision with potassium[5] are also in fair agreement with experimental data at energies higher than 50 eV. The MG electron cross sections are, however, found to be somewhat higher than the positron cross sections. The merging of the two sets of data above 30 eV, as was observed in experimental data[1], does not seem to materialize in our MG calculation. In our opinion, since the difference between the electron and positron MG cross sections above 30 eV is only within 15%, this non-merging of the theoretical data is still acceptable, in view of the possible uncertainty of the experimental data mentioned above. It is worth stressing that in the modified Glauber approximation, the non-merging of the electron and positron cross sections may be understood as to originate from the different contribution in positron and electron scattering to the cross sections from the core scattering.

For collision with sodium, we found that the positron total cross sections are also consistently lower than the electron cross sections for about 10 to 15 percent. The two cross sections did not merge with each other even at an energy as high as 1000 eV. The absolute difference between the electron and positron cross sections now seems to become smaller somewhat, because sodium is lighter than potassium, and therefore, the effect of its less "cumbersome" core would influence the cross sections somewhat less. For collision by lithium, whose core effect is much weaker, our calculation in the MG approximation does indeed provide a merging (within less than 1 to 3 per cent of difference) of the positron and electron cross sections at a rather low energy. It would, therefore, be interesting to also measure the total cross sections for collision by lithium, which have not been available in the literature. We also found that for all three of the alkali targets (K, Na, and Li), the total cross sections for positron and electron collisions, at least within the modified Glauber approximation, did not deviate from each other at some scattering energy above 100 eV and then re-merge at a much higher energy. The MG total cross sections for

positron (electron) scatterings from sodium[5] are found to be in reasonably good agreement with experimental data[1,2] in the range of 10 - 100 eV, and to be consistent with the results of close-coupling calculation[7] at energies lower than 50 eV. Our values of e^+ - Li collision are also consistent with the close-coupling values[7]. Our preliminary results of total cross section for e^+-Rb collision seem to also be consistent with those calculated in the close-coupling approximations[7] below 30 eV, and with experimental data[2] below 50 eV.

Table 1 MG total cross sections in πa_o^2 for e-K, e-Na and e-Li

K			Na			Li	
Energy (eV)	e^+	e^-	Energy (eV)	e^+	e^-	e^+	e^-
11.00	105.85	102.19	10.0	60.20	72.59	76.50	80.90
18.20	90.08	98.85	15.0	61.37	70.08	68.60	71.63
21.10	84.96	94.97	20.0	56.49	63.37	60.19	62.50
28.20	74.52	85.12	30.0	46.85	51.88	47.83	49.40
31.20	70.75	80.98	40.0	39.72	43.79	39.72	40.92
38.40	62.85	71.72	50.0	34.51	38.01	34.06	35.04
48.60	53.97	61.27	54.4	32.65	35.96	32.08	32.99
51.60	51.78	58.75	60.0	30.57	33.68	29.89	30.71
76.75	38.61	44.28	80.0	25.00	27.64	24.14	24.77
102.50	30.76	36.01	100.0	21.25	23.60	20.33	20.85
150.00	22.57	27.44	150.0	15.65	17.56	14.74	15.10
200.00	17.76	22.32	200.0	12.50	14.16	11.66	11.93
300.00	12.60	16.63	300.0	9.06	10.39	8.32	8.51
400.00	9.86	13.48	400.0	7.18	8.31	6.52	6.66
500.00	8.14	11.43	500.0	5.99	6.98	5.38	5.49
800.00	5.40	8.04	800.0	4.06	4.79	3.57	3.64
1000.00	4.45	6.78	1000.0	3.37	3.99	2.93	2.99

References

1) T. S. Stein, M. S. Dababneh, W. E. Kaupilla, C. K. Wan and Y. J. Yan, in Atomic Physics with Positrons ed J. W. Humbertson and E. A. Armour (New York: Plenum, 1988), p 251
2) T. S. Stein, Scattering of Positrons and Electrons by Alkali Atoms. Invited paper given at the Workshop (1989, this Proceedings).
3) T. T. Gien, Phys. Repts. 160, 123-87 (1988)
4) T. T. Gien, Chem. Phys. Lett. 127, 253 (1986)
5) T. T. Gien, J. Phys. B: At. Mol. Opt. Phys. 22, L129 (1989); J. Phys. B: At. Mol. Phys. 22 (1989, Letter section, in press)
6) S. J. Ward, M. Hortbatsch, R. P. McEachran and A. D. Stauffer, J. Phys. B: At. Mol. Phys. 21, L611 (1988).
7) R.P. McEachran, M. Horbatsch, A.D. Stauffer and S.J. Ward, Positron-Alkali Atom Scattering, Invited paper given at the Workshop (1989, this Proceedings); see also J. Phys. B: At. Mol. Phys. 22, 1845-1861 (1989).

INELASTIC COLLISIONS OF POSITRONS WITH ONE-VALENCE-ELECTRON TARGETS

MOHAMED ASSAD ABDEL-RAOUF

Chair for Theoretical Chemistry, Friedrich-Alexander University
Erlangen-Nürnberg, Egerlandstr. 3, 8520 Erlangen, FRG.

ABSTRACT

The total elastic and positronium formation cross sections of the inelastic collisions between positrons and various one-valence-electron atoms, (namely hydrogen, lithium, sodium, potassium and rubidium), and one-valence-electron ions, (namely hydrogen-like, lithium-like and alkaline-earth positive ions) are determined using an elaborate modified coupled-static approximation. Special attention is devoted to the behavior of the Ps cross sections at the energy regions lying above the Ps formation thresholds.

The interest of many authors in the collisions of positrons with one-valence-electron targets has been enormously increased in the last couple of years. In case of atomic targets (e.g. lithium, sodium, and potassium), various investigations have been carried out in order to calculate the elatsic and excitation cross sections under the assumption that the positronium formation channel, (which is open even at zero incident energy), has irrelevant contribution to the total inelastic cross sections. Particularly, the very recent results of Ward et al {1}, (for a review, see the references therein), have emphasized this argument at energies above 10 eV in comparison with the careful experimental results of the Detroit Group {2}.

For atomic targets (e.g. H, Li, Na, K and Rb) as well as ionic targets (e.g. hydrogen-like, lithium-like and alkaline-earth positive ions), the author has determined total elastic and positronium formation cross sections on a unified basis by virtue of a coupled-static formalism which allows for the switching on of the positronium polarisation potentials. He also employed a restricted coupled-static technique (with symmetrical reactance matrices) for the treatment of the positron collisions with alkali atoms and alkaline-earth positive ions. Tables 1 and 2 contain the results of this treatment. It is obvious that the role of the Ps channel increases with the size of the target and that interesting behaviors (resonances) show up in most cross sections of the problems considered. In table 3 we find the values of the elastic cross sections of the collisions of positrons with hydrogenlike ions determined at energies below the Ps threshold of e^+ - H scattering. Figs. 1 and 2 show the variation of the total elastic and Ps formation cross sections with a parameter δ, related to the incident energy (k_1^2) by $k_1^2 = 13.6\ (\sqrt{E_{ps}-E_T}+\delta)^2$ eV. From the first figure we realize that the elastic cross sec-

Table 1

Total cross sections (in a_0^2) of the inelastic collisions of positrons with alkali atoms calculated by the restricted coupled-static approximation.

k_1^2 (eV)	e^+ - Li		e^+ - Na		e^+ - K		e^+ - Rb	
	σ_{11}	σ_{12}	σ_{11}	σ_{12}	σ_{11}	σ_{12}	σ_{11}	σ_{12}
0.1	941.469	148.397	645.270	77.975	719.379	217.267	1412.455	1475.514
0.3	801.315	91.865	655.901	45.666	320.254	221.573	7949.010	3961.333
0.5	738.766	75.972	704.790	28.423	455.333	297.469	6953.694	1614.430
0.7	690.242	93.902	710.515	100.675	4204.943	124.410	4599.199	1087.248
0.9	645.286	88.222	964.165	460.303	622.312	102.141	4072.006	1145.076
1.0	636.696	90.263	691.374	99.349	2482.024	367.222	2522.331	1153.929
3.0	369.131	74.413	458.965	61.487	599.794	176.554	1316.109	52.054
5.0	230.472	58.970	258.300	47.046	399.824	109.816	437.963	60.365
7.0	152.337	47.781	144.570	51.064	253.556	102.289	269.108	77.717
9.0	103.806	32.341	107.874	58.372	149.309	115.816	313.231	75.563
10.0	85.049	25.222	55.260	59.524	129.054	100.086	282.141	122.521
20.0	27.835	3.558	4.402	4.933	32.591	36.379	76.223	39.655
30.0	17.929	1.080	2.198	1.459	12.713	8.080	129.475	4.456
40.0	13.760	0.426	2.044	0.574	11.357	0.624	43.668	14.395
50.0	11.362	0.191	1.419	0.253	10.137	0.249	43.061	13.132

Table 2

Total cross sections (in a_0^2) of the inelastic scattering of positrons by the alkaline-earth positive ions determined by the restricted coupled-static approximation. * denotes the switching on of the Ps polarisation potentials to the second channel.

k_1^2 (eV)	e^+ - Be^+ scattering			k_1^2 (eV)	e^+ - Mg^+ scattering		
	σ_{11}	σ_{12}	σ_{12}^*		σ_{11}	σ_{12}	σ_{12}^*
11.5	149.696	3.209	1.731	9.0	449.703	3.451	1.929
12.0	139.914	5.593	4.723	9.5	260.996	5.410	10.470
12.5	149.797	7.917	11.907	9.9	385.611	11.378	58.773
13.0	152.296	6.732	16.387	9.5	325.991	19.072	70.328
13.5	154.220	6.577	19.231	10.0	229.587	26.777	62.952
14.0	154.003	6.605	19.569	10.5	231.596	36.067	49.225
14.5	153.272	10.760	19.796	11.0	239.333	40.801	39.710
15.0	153.476	12.869	20.425	11.5	410.269	36.959	32.367
15.5	154.199	14.911	21.173	12.0	369.965	46.490	35.320
16.0	154.500	16.867	21.829	12.5	419.207	56.612	48.898
16.5	152.991	18.664	22.187	13.0	385.161	53.867	48.120
17.0	150.436	20.268	22.166	13.5	380.952	56.693	45.922
17.5	147.780	21.531	21.850	14.0	378.776	58.397	43.732
18.0	145.178	22.368	21.366	14.5	375.177	58.809	41.284
18.5	142.908	22.732	20.756	15.0	370.471	58.062	38.470
20.0	135.051	21.714	18.234	20.0	302.709	38.500	19.966
30.0	271.319	7.669	5.198	30.0	286.952	6.776	2.252
40.0	233.141	2.159	1.919	40.0	248.225	0.790	0.458
	e^+ - Ca^+ scattering				e^+ - Sr^+ scattering		
9.0	262.036	28.351	159.151	9.0	554.086	38.958	136.721
9.5	253.234	40.096	83.648	9.5	696.376	43.705	65.746
8.0	127.552	92.129	69.628	9.0	1076.246	48.218	99.283
8.5	489.814	90.324	83.999	9.5	948.641	45.395	197.243
7.0	232.229	129.693	99.102	8.0	662.269	39.488	204.168
7.5	526.695	118.759	134.058	8.5	526.357	166.585	116.357
8.0	514.025	130.868	107.796	7.0	644.866	136.062	206.023
8.5	395.009	117.036	151.287	7.5	369.897	119.481	109.986
9.0	306.418	118.065	127.981	8.0	420.388	137.162	111.782
9.5	578.466	132.536	131.192	8.5	461.677	160.096	73.996
10.0	308.068	153.083	112.717	9.0	318.432	98.997	110.089
10.5	508.376	99.159	75.772	9.5	525.656	82.690	48.696
11.0	376.539	111.713	108.039	10.0	585.142	68.910	104.221
11.5	472.790	90.852	84.591	10.5	569.770	61.807	38.790
20.0	325.448	23.483	19.897	11.0	539.961	110.756	49.981
30.0	287.861	1.999	4.383	20.0	412.929	17.725	22.572
40.0	254.766	5.278	4.217	30.0	353.386	4.776	8.106
50.0	190.221	5.232	4.140	40.0	259.269	2.721	3.143

tions of all ions decrease monotonically with the increase of ξ, while the Ps cross sections assume the opposite behavior and decrease (almost an order of magnitude) with the increase of Z.

In Figs. 3 and 4 we present two examples for our last investigation, namely the collisions of positrons with lithium-isoelectronic ions. There we plot the relation between the total Ps cross sections and the incident energy for $e^+ - C^{3+}$ and $e^+ - N^{4+}$, respectively, with and without switching on the Ps polarisation potentials. It is clear that these potentials shift the maxima of the pure coupled-static cross sections towards the Ps thresholds {3}. Finally, we hope that the present work would draw the attention of positron community to the field of positron-ion collisions and encourage the theorists to investigate the problems tackled here using more elaborate techniques.

ACKNOWLEDGMENT

I am extremely indebted to the Deutsche Forschungsgemeinschaft

TABLE 3 - *Total elastic cross sections (in a_0^2) of the collisions of positrons with different hydrogenlike targets at energies below the Ps formation threshold as e^+-H scattering.*

k_i(eV)	Targets					
	H	He^+	Li^{2+}	Be^{3+}	B^{4+}	Ne^{9+}
0.1	4.229	0.437	0.1110	0.0415	0.01520	0.001495
0.5	4.113	0.434	0.1106	0.0414	0.01917	0.001195
1.0	3.979	0.430	0.1100	0.0413	0.01914	0.001195
1.5	3.956	0.425	0.1095	0.0411	0.01910	0.001194
2.0	3.738	0.421	0.1090	0.0410	0.01907	0.001194
3.0	3.621	0.417	0.1085	0.0409	0.01903	0.001193
3.5	3.457	0.413	0.1080	0.0408	0.01900	0.001193
4.0	3.320	0.409	0.1075	0.0407	0.01898	0.001192
4.5	3.267	0.406	0.1070	0.0406	0.01893	0.001192
5.0	3.199	0.402	0.1065	0.0405	0.01889	0.001191
5.5	3.115	0.398	0.1060	0.0403	0.01885	0.001191
6.0	3.046	0.395	0.1055	0.0402	0.01882	0.001190
6.5	2.978	0.391	0.1050	0.0401	0.01879	0.001189

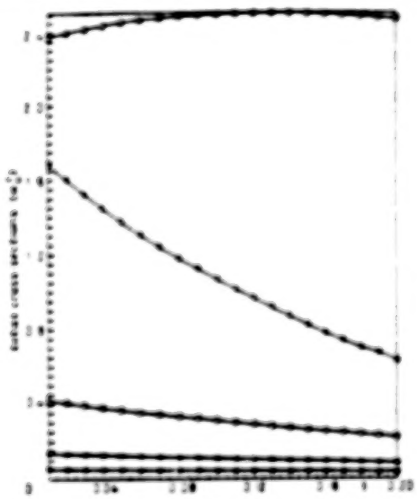

Fig. 1. - Comparison between the total elastic cross-sections on the inelastic collisions of positrons with different hydrogenlike targets. □ e^+-H, ○ e^+-He^+, ○ e^+-Li^{2+}, • e^+-Be^{3+}, ● e^+-B^{4+} scattering.

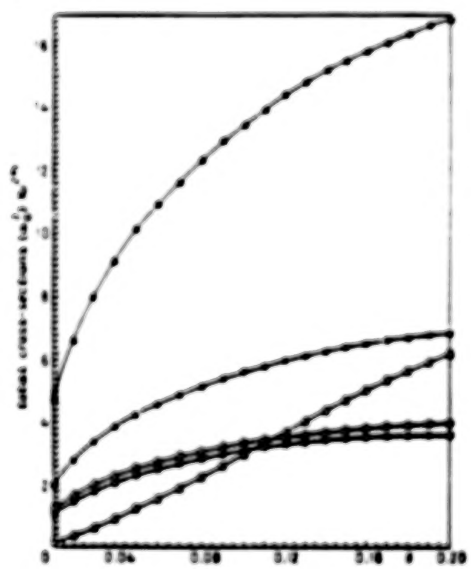

Fig. 2. - Comparison between the total positronium formation cross-sections of the inelastic collisions of positrons with different hydrogenlike targets. □ e^+-H, ○ e^+-He^+, ○ e^+-Li^{2+}, • e^+-Be^{3+}, ● e^+-B^{4+} scattering.

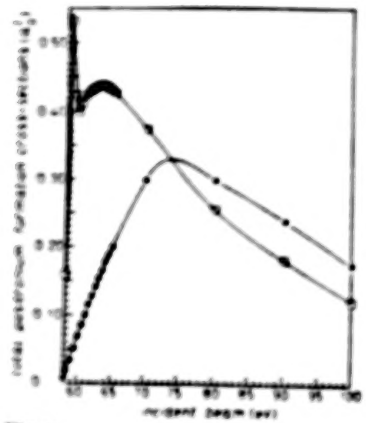

Fig 3.

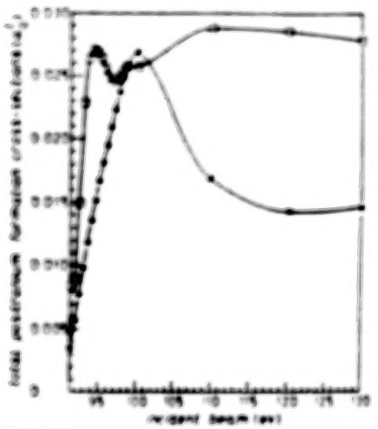

Fig. 4.

Fig 3 - Variation of the total positronium formation cross-section of e^+-C^{5+} inelastic scattering with the incident energy • pure coupled-static calculations. □ coupled-static with Ps polarization.

Fig 4 - Variation of the total positronium formation cross-section of e^+-N^{6+} inelastic scattering with the incident energy • pure coupled-static calculations. □ coupled-static with Ps polarization.

for providing me with the financial support required for visting this Workshop and the XVI. ICPEAC.

REFERENCES

(1) S.J. Ward, M. Horbatch, R.P. McEachran and A.D. Stauffer, J. Phys. B22, 1845, 1989.
(2) T. S. Stein et al, in Atomic Physics with Positrons, ed. J.W. Humberston and E.A.G. Armour, Plenum, 1987, p 251.
(3) See e.g. M. A. Abdel-Raouf, Nuovo Cim. 11D, 433, 1989.

POSITRON–RUBIDIUM SCATTERING

R. P. McEachran, M. Horbatsch, A. D. Stauffer
Department of Physics, York University, Toronto, Canada, M3J 1P3

ABSTRACT

A 5-state close-coupling calculation (5s-5p-4d-6s-6p) has been carried out for e^+–Rb scattering in the energy range 3.7–28.0 eV. In contrast to the results of similar close-coupling calculations for e^+–Na and e^+–K scattering the (effective) total integrated cross section has an energy dependence which is contrary to recent experimental measurements.

INTRODUCTION

During the past several years there have been a number of elaborate close-coupling calculations for e^+–Na[1–4] and e^+–K[2–5] scattering in the energy region from 0.5 to 100 eV. In addition, there have been other calculations for these two systems based upon the core-corrected modified Glauber approximation[6,7]. So far the total cross sections, as determined by both of these theoretical approaches, have been in satisfactory agreement with the corresponding experimental data for Na[8] and K[9,10] both with respect to the shape and magnitude of the cross sections.

In comparing theory with experiment it is necessary, particularly at the very low energies, to compensate for the fact that experimentally it is not possible to discriminate against positrons scattered *elastically* through small angles about the forward direction. Thus, in making their comparison with experiment, Ward *et al*[2–5] determined the elastic differential cross section and from this computed an effective elastic cross section and hence an effective total cross section.

We report here the first close-coupling calculation for e^+–Rb scattering and compare our results with the recent experimental measurements of Stein *et al.*[11]

THEORY

The close-coupling calculations for the alkalis have so far been based upon a one-electron model for the atom where the valence orbital, either in the ground or an excited state, moves in the central potential of a fixed (frozen) ion core.

This model can be most easily accommodated within the standard frozen-core Hartree-Fock approximation.[12] Here, the core orbitals of the closed-shell alkali ion are first computed via the standard fully-varied Hartree-Fock procedure and then, with these core orbitals held fixed, a single Hartree-Fock equation is solved in turn for each of valence orbitals (including the ground state) of the alkali atom. Although this simple model for the alkali atoms and alkali-like ions has met with some success in the determination of ionization energies and oscillator strengths for these systems[13–16] the overall accuracy of this model deteriorates with increasing size of the ion core.

However, this model can be significantly improved, and at the same time retain its one-electron character, if core polarization of the valence electron is encorporated into the model. Two different approaches to the inclusion of core polarization have so far proved quite successful. One method involves the use of a model potential which includes both the dipole and quadrupole polarizabilities of the alkali core.[17] The other method first determines a core polarization potential for the closed shell Hartree-Fock alkali ions via an adiabatic polarized-orbital procedure[18] and then solves variationally a single Hartree-Fock equation, which includes this core polarization potential, for the ground and excited valence states of the atom.[19,20]

In the close-coupling calculations of Ward *et al*[2–5] for positron scattering from Li, Na and K the model potentials of Peach[17] were primarily used to determine the atomic wavefunctions. In the present calculations for e^+–Rb scattering we have chosen to use polarized Hartree-Fock orbitals. Table 1 contains the ionization energies of the first few s-, p- and d-levels of Rb as obtained via the regular frozen-core Hartree-Fock procedure (FC-HF) and the polarized frozen-core Hartree-Fock method (PFC-HF). Also included are the corresponding experimental values for these ionization energies.[21]

TABLE 1. Ionization energies of Rb in atomic units.

Level	FC-HF	PFC-HF	Experiment
5s	0.137202	0.153621	0.153508
6s	0.058140	0.061719	0.061772
7s	0.032209	0.033591	0.033624
5p	0.090135	0.096921	0.095472
6p	0.043652	0.045643	0.045218
7p	0.025887	0.026760	0.026575
4d	0.060066	0.072899	0.065319
5d	0.033972	0.039773	0.036399
6d	0.021570	0.024397	0.022793

In the determination of the core polarization potential for Rb^+ only the 3d, 4s and 4p core Hartree-Fock orbitals were polarized. As can be seen from the table, the ionization energies for the s- and p-levels which were determined within the PFC-HF framework are in far better agreement with experiment than those obtained without core polarization. On the other hand neither model does

particularly well for the d-levels. This is most probably an indication that the 'one-electron' model is beginning to break down for an alkali the size of Rb.

The FC–HF model yields a dipole polarizability of 510 a_0^3; the PFC–HF procedure gives 353 a_0^3 which is approximately 10% higher than the experimental value of $319 \pm 6\ a_0^3$.[22]

The close-coupling equations can be written, in differential equation form, as

$$\left[\frac{d^2}{dr^2} - \frac{l_2(l_2+1)}{r^2} - 2V_c(r) + k_\nu^2\right] F_{\nu LS}(r) = -2\sum_{\nu'} V(\nu,\nu')_L\, F_{\nu' LS}(r) \tag{1}$$

where $\nu = n_1 l_1 l_2$

$$V_c(r) = \frac{Z}{r} - \sum_{nl} 2(2l+1)\, y_0(nl, nl; r) \tag{2}$$

$$V(\nu,\nu')_L = \sum_\lambda f_\lambda(l_1 l_2, l_1' l_2'; L)\, y_\lambda(n_1 l_1, n_1' l_1'; r) \tag{3}$$

and

$$y_\lambda(n_1 l_1, n_1' l_1'; r) = r^{-\lambda-1}\int_0^r P_{n_1 l_1}(x)\, P_{n_1' l_1'}(x)\, x^\lambda\, dx + r^\lambda \int_r^\infty P_{n_1 l_1}(x)\, P_{n_1' l_1'}(x)\, x^{-\lambda-1}\, dx \tag{4}$$

The functions $F_\Gamma(r)$ describe the radial motion of the incident positron and the P's are the radial atomic orbitals. The summation in equation (2) is over the core orbitals and the coefficients f_λ as well as the subscript Γ are defined in Percival and Seaton.[23]

In this work we have solved the equivalent integral equation formulation of the close-coupling equations by a technique which is similar to that used by McEachran and Fraser.[24] From the asymptotic form of the solutions to these equations one can obtain, with the help of asymptotic correction procedures,[25] the elements, $R^{LS}_{\nu\nu'}$, of the R matrix and hence the corresponding elements of the S and T matrices.

The total cross section for the excitation of an alkali atom from the state $n_1' l_1'$ to $n_1 l_1$ is given (in units of πa_0^2) by

$$\sigma(n_1' l_1' \to n_1 l_1) = \sum_{LS}\sum_{l_2 l_2'} \frac{(2L+1)(2S+1)}{4k_{\nu'}^2(2l_1'+1)} \left|T^{LS}_{\nu\nu'}\right|^2 \tag{5}$$

Experimentally it is impossible to discriminate against positrons scattered elastically through small angles about the forward direction. Thus a knowledge of the elastic differential cross section enables one to estimate how much flux has been lost by means of this effect. We have therefore calculated an effective elastic cross section defined as

$$\sigma_{el}^{eff} = 2\pi \int_{\theta_0}^{\pi} \sin\theta\, \frac{d\sigma_{el}}{d\Omega}\, d\theta \qquad (a_0^2) \tag{6}$$

where θ_0 is the lower limit of the experimental angular discrimination. An estimate of this quantity has been made in the experimental measurements of Stein *et al*[11] for each energy of the incident positron. This effective elastic cross section is then added to the various excitation cross sections to yield an effective total cross section which can, more meaningfully, be compared with the experimental data.

RESULTS

In table 2 we present our 5-state close-coupling results for the elastic, the various excitation cross sections and the total cross section for e^+–Rb scattering for energies between 3.7 and 28.0 eV. Also included in the table are results for the *effective* total cross section. The energies

TABLE 2. The elastic, excitation and total integrated cross sections (πa_0^2) for e^+–Rb scattering in the energy range 3.7–28.0 eV.

Energy (eV)	5s–5s	5s–5p	5s–4d	5s–6s	5s–6p	σ_{tot}	σ_{tot}^{eff}
3.7	124.23	92.20	67.65	4.67	0.91	289.66	209.28
5.8	62.76	76.18	75.12	2.50	2.51	219.07	170.83
7.8	42.16	77.68	61.02	1.58	3.14	185.58	151.47
17.8	17.64	73.12	20.52	0.98	2.72	114.98	102.69
28.0	12.79	60.27	10.23	0.88	1.95	86.12	80.31

chosen are such that they coincide with those given in the experimental data of Stein *et al.*[11]

We note that the elastic as well as the 5s–5p and 5s–4d excitation cross sections are the dominate contributors to the total cross section. By comparing the total cross section with the corresponding effective one it can be seen that at 3.7 eV almost 2/3 of the elastic scattering flux will not be detected experimentally; this fraction increases to nearly 4/5 at 7.8 eV. Nonetheless, our effective total cross section increases monotonically as the incident energy of the positron decreases. This behaviour of the effective total cross section, as predicted by our 5-state close coupling approximation, is in contrast to the experimental data of Stein *et al*[11] which has a maximum in the low energy region. Unfortunately we can not offer any explanation for this discrepancy as yet.

ACKNOWLEDGMENTS

We would like to thank Professors T. S. Stein and W. E. Kauppila for valuable discussions. This work was supported by the Natural Sciences and Engineering Research Council of Canada.

[1] K. P. Sarkar, M. Basu and A. S. Ghosh, J. Phys. B. **21**, 1649, (1988).

[2] S. J. Ward, M. Horbatsch, R. P. McEachran and A. D. Stauffer, *Atomic Physics with Positrons*, ed. J. W. Humberston and E. A. G. Armour (London: Plenum) p. 265, (1988).

[3] ——, J. Phys. B. **22**, 1845, (1989).

[4] ——, Nucl. Instrum. Methods (1989), in press.

[5] ——, J. Phys. B. **21**, L611, (1988).

[6] T. T. Gien, Chem. Phys. Lett. **139**, 23, (1987) (Erratum **142**, 575).

[7] ——, J. Phys. B. **22**, L129, (1989).

[8] C. K. Kwan, W. E. Kauppila, R. A. Lukaszew, S. P. Parikh, T. S. Stein, Y. J. Wan and M. S. Dababneh, Phys. Rev. A, (1989), submitted.

[9] T. S. Stein, R. D. Gomez, Y.-F. Hsieh, W. E. Kauppila, C. K. Kwan and Y. J. Wan, Phys. Rev. Lett. **55**, 488, (1985).

[10] T. S. Stein, M. S. Dababneh, W. E. Kauppila, C. K. Kwan and Y. J. Wan, *Atomic Physics with Positrons*, ed. J. W. Humberston and E. A. G. Armour (London: Plenum) p. 251, (1988).

[11] T. S. Stein, C. K. Kwan, W. E. Kauppila, R. A. Lukaszew, S. P. Parikh, Y. J. Wan and M. S. Dababneh, *Proc. of the Workshop on Annihilation in Gases and Galaxies*, published in these Proceedings.

[12] M. Cohen and R. P. McEachran, Adv. At. Mol. Phys. **16**, 1, (1984).

[13] R. P. McEachran, C. E. Tull and M. Cohen, Can. J. Phys. **47**, 835, (1969).

[14] ——, Astron. and Astrophys. **4**, 152, (1970).

[15] C. E. Tull, M. Jackson, R. P. McEachran and M. Cohen, Can. J. Phys. **50**, 1169, (1972).

[16] ——, J. Quant. Spectrosc. Radiat. Transfer **12**, 893, (1972).

[17] G. Peach, Comment. At. Mol. Phys. **11**, 101, (1982) and private communication, (1986).

[18] R. P. McEachran, D. L. Morgan, A. G. Ryman and A. D. Stauffer, J. Phys. B. **10**, 663, (1977).

[19] R. P. McEachran and M. Cohen, J. Phys. B. **16**, 3125, (1983).

[20] M. Cohen and R. P. McEachran, J. Phys. B. **17**, 2979, (1984).

[21] C. Moore, *Atomic Energy Levels*, Nat. Bur. Stand. Circ. No. 467, Vol I (Washington: U.S. Govt. Printing Office).

[22] T. M. Miller and B. Berderson, Adv. At. Mol. Phys. **13**, 1, (1977).

[23] I. C. Percival and M. J. Seaton, Proc. Camb. Phil. Soc. **53**, 654, (1957).

[24] R. P. McEachran and P. A. Fraser, Proc. Phys. Soc. **82**, 1038, (1963).

[25] L. A. Parcell, R. P. McEachran and A. D. Stauffer, J. Phys. B. **20**, 2307, (1987).

THEORETICAL SURVEY ON POSITRONIUM FORMATION AND IONISATION IN POSITRON ATOM SCATTERING

Madhumita Basu and A.S.Ghosh
Department of Theoretical Physics
Indian Association for the Cultivation of Science
Jadavpur, Calcutta 700032, INDIA

ABSTRACT

The present survey reports the recent theoretical studies on the formation of exotic atoms in positron-hydrogen, positron-helium and positron-lithium scattering specially at intermediate energy region. The ionisations of these targets by positron impact has also been considered. Theoretical predictions for both the processes are compared with existing measured values.

INTRODUCTION

In recent years, amazing developments in the studies of positron-atom scattering have been noticed. It has become possible due to the availability of intense and energy resolved positron beam and sensitive detectors. A large number of parallel theoretical studies, in recent years, also play a big role in it. The present survey concentrates on the recent theoretical developments in the studies of inelastic processes in e^+-atom scattering. In particular, we discuss on the following two inelastic processes.

i) Positronium formation in e^+-atom scattering;
ii) Ionisation of atoms by positron impact.

These two inelastic processes are not altogether different. Positronium atom may also be formed in the continuum. This has been first predicted by Brauner and Briggs[1] that the presence of (e^+-e^-) pair in the final state of positron impact ionisation results in a process known as 'positronium to the continuum'. This is due to the energy distribution of the secondary electron. The London group (Charlton et al[2]) reported the first experimental evidence for a peak in the energy distribution of the secondary electrons from positron impact ionisation.

In the last conference on Positron in Gases in 1987, the topic has been discussed in details. It is of no use to repeat this.

In the last workshop on Positron in Gases, there are little discussion about the theoretical models employed to investigate these two important inelastic processes, although, results are quo-

ted many times by different speakers. However, theoretical models are covered by Ghosh[3] in our national conference. In this resume, we discuss the theoretical models developed or employed to investigate these two inelastic processes after 1986.

Due to the limited time, we will consider H, He and Li atoms as targets. We start with Positronium formation in e^+-atom scattering.

Positronium Formation

Positronium (Ps), the decaying bound state of the electron and its antiparticle has presented an alluring challenge to experimentalists and theoretical physicists for over 35 years. Milestones in positronium research includes the observation of its ground state in 1951, observation of its excited state in 1975 and recent dramatic discovery of positronium negative ion (Ps^-) in 1981. Positronium atom, in its ground and excited states may be formed in e^+-atom and e^+-molecule collisions. A large number of theoretical studies have been carried out to predict capture cross sections using different theoretical models depending on the energy range considered. For earlier works one may go through a series of excellent reviews (Ghosh et al[4], Humberston[5], Ghosh[3] and Joachain[6]).

We start with Ps-formation in e^+-He scattering. This is due to the fact that maximum number of experiments have been carried out for this system (Fornari et al[7], Charlton et al[2], Fromme et al[8], Diana et al[9]). A large number of theoretical investigations have also been made during the same period. Mandal et al[10] have carried out a distorted wave model to predict ground state capture whereas Khan and Ghosh[11] and Khan et al[12] have reported ground and excited state capture cross section respectively using distorted wave polarized orbital method. McDowell and Peach[13] have also investigated the same process using classical theory of charge transfer. To have an idea about the agreement between the theoretical predictions and measured values, we compare the Ps formation cross sections (σ_{Ps}) in Fig.1. It is evident from Fig.1 that all experimental results except those of Charlton et al are in fair agreement with one another. Here, measured

$$\sigma_{Ps} = \sigma_{Ps}^{(1s)} + \sigma_{Ps} \text{ (all excited states)} \quad (1)$$

whereas theoretically

$$\sigma_{Ps} = \sigma_{Ps}^{(1s)} + \sigma_{Ps}^{(2s)} + \sigma_{Ps}^{(2p)} \quad (2)$$

as calculated by Khan et al.
At higher energies, theoretical results seem to underestimate σ_{Ps}

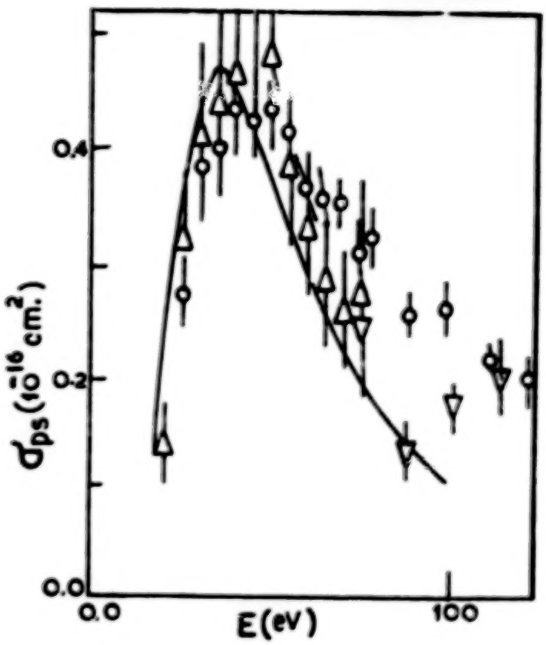

Fig.1. σ_{Ps} in e^+-He scattering: measured values - I, Charlton et al[2]; Δ, Fornari[7] et al ; ▽, Diana et al[9]; ♦, Fromme et al[3]; Theoretical results: —, Khan et al[10].

whereas at low energies the agreement is good. Moreover, experimental values are higher than first Born predictions (FBA) even at 300.0 eV. The situation demands a more elaborate calculation to investigate the problem at higher energies.

Ps formation in an e^--atom collision can be compared with electron transfer in a proton-atom collision. It is well known that in ion-atom scattering, the second Born term is of vital importance in determining the asymptotic behaviour of the capture cross section. Considering these facts, we have used a model in which the second-order effects are included in a realistic way. We have employed two second order models to calculate ground state capture cross sections. These models may be represented by the following two equations

$$g^{SBA} = g^{B1} + g^{B2} \qquad (3)$$

$$g^{BG} = g^{CS} + \tilde{g}^{B2} \qquad (4)$$

where g^{B1} is the first Born capture amplitude and g^{CS} is the capture amplitude obtained by solving coupled static equations. g^{B2} is the conventional second Born term. $\tilde{g}^{B2}$ is given by

$$\tilde{g}^{B2}_{\nu',\nu}(k',k) =$$

$$\frac{1}{2\pi^2} \sum_{\nu''=1s} \int \frac{d\vec{k}''}{(k''^2 - k^2_{\nu''} - i\varepsilon)}$$

$$\times g^{B1}_{\nu',\nu''}(k',k'') f^{B1}_{\nu'',\nu}(k'',k) \qquad (5)$$

where $g^{B1}_{\nu',\nu}(k',k)$ and $f^{B1}_{\nu',\nu}(k',k)$ are the first Born amplitudes in the direct and rearrangement channel respectively. In other words, in calculating $\tilde{g}^{B2}$, the summation over the ground state is omitted. Closure relation is found to be unsuitable in evaluating the second Born capture amplitude. The second Born terms g^{B2} and $\tilde{g}^{B2}$ are evaluated by retaining suitably chosen target states.

a) Hydrogen Atom

We have started the investigations with hydrogen atom (Basu and Ghosh[14]) as this is the trial horse for the theoreticians as

most accurate results are available or may be performed only in case of hydrogen atom. To have reliable results, convergence of the second Born term with the addition of the target state is required. We have retained two eigenstates (1s, 2s) and three pseudo-states (2p̄, 3s̄ and 3d̄). The pseudo states 2p̄ and 3d̄ are taken from Damburg and Karule[15] and 3s̄ from Burke and Webb[16]. To justify our choice of pseudo-states, we have evaluated the direct second Born amplitudes using these states. Table 1 gives the forward second Born amplitude for elastic e^--H scattering along with those of Holt[17] and Prasad[18].

Table 1. Forward second Born amplitude for elastic e^--H scattering (atomic unit).

E (eV)	50	100	300
Real			
Exact*	1.96	1.35	0.74
BG	1.73	1.25	0.65
Imaginary			
Exact*	1.60	1.31	1.15
BG	1.76	1.54	1.14

*Holt 10, Prasad 11.

Present results are in reasonably good agreement with those of exact predictions as given by Holt and Prasad. This is the reason behind our choice of Pseudo-state in the calculation.

We have calculated the differential cross section (DCS) for ground state capture in the energy range 50-360 eV using conventional second Born approximation (SBA) and in the energy range 50-300 eV by using model (2) (denoted by BG). Figs. 2 and 3 shows our DCS using BG

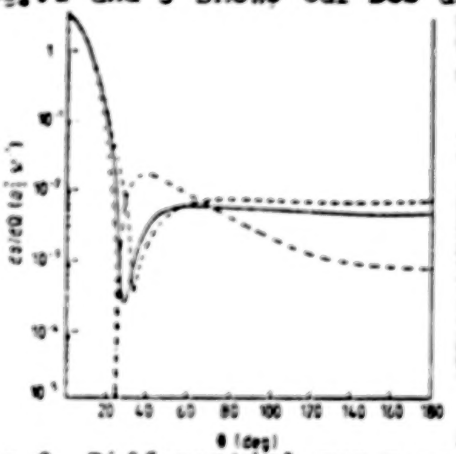

Fig. 2. Differential cross sections (DCS) (a_0^2 sr^{-1}) for ground state capture in e^+-H scattering at 80 eV; —, BG; --, SBA; – –, FBA

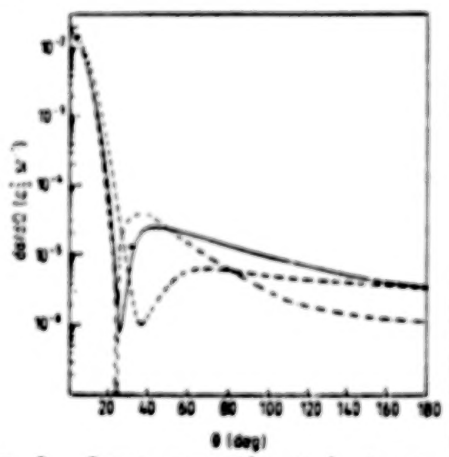

Fig. 3. Same as Fig. 2 but at 300 eV.

and SBA at the energies 80.0 and 300.0 eV. The results of the first Born approximation (FBA) have also been included. The FBA results attain a zero value around the scatte-

ring angle 25°, whereas the SBA and BG have structures near 45°. The FBA predicts zero cross section as the two parts of the amplitude are of opposite sign. The second order term prevents the total cancellation in the DCS and the residual structure is due to the destructive interference of the amplitudes. The Thomas peak for electron capture by heavier atoms is well known. For the p^+-H system, there are two peaks. In case of positron capture, the two peaks approach at about 45°. These features have been noticed by us at all energies.

Recently, Deb et al[19] have applied a second Born approximation in which Green's function is evaluated approximately to investigate the problem. In Fig.4, we

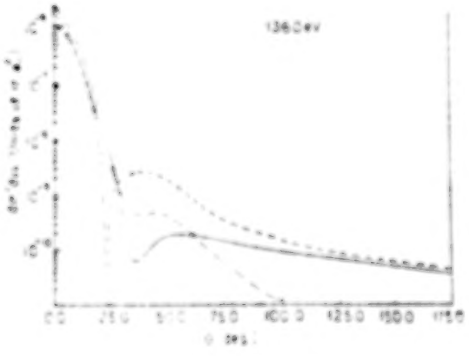

Fig.4. DCS (πa_0^2 sr_+^{-1}) for ground state capture in e^+-H scattering at 1360 eV, ——, SBA; – –, DWS (Deb et al[19]); ---, FBA.

compare our SBA results with those of Deb et al[19] (DWS) at the incident energy 1360 eV. Our SBA structure near 45° is more prominent than that of DWS. DWS results fall faster than ours after the scattering angle 50°. There is no reason to prefer one result over other. The results await experimental confirmation or more elaborate calculations.

Integrated cross sections for ground-state capture using SBA and BG are given in Table 2 along with FBA and coupled static results (CSA). The BG and SBA results are always greater than that of the FBA and the present values (BG) lies between those of FBA and SBA except at the lowest energy considered here (50 eV). From the table

Table 2. Integrated cross section (πa_0^2) for ground-state Ps-formation in e^+-H scattering.

Energy (eV)	FBA	CSA	SBA	BG
50	0.46	0.55	0.62	0.56
80	0.10	0.13	0.13	0.12
100	0.46^{-1}	0.51^{-1}	0.53^{-1}	0.46^{-1}
200	0.25^{-2}	0.28^{-2}	0.31^{-2}	0.26^{-1}
300	0.37^{-3}	0.40^{-3}	0.49^{-3}	0.39^{-3}
500	0.26^{-4}	-	0.38^{-4}	-

it is evident that the BG results are always less than the CSA results. It may be mentioned that the DWS results of Deb et al and DWPO results of Khan and Ghosh (not shown in the table) are always less than the present SBA and FBA results respectively.

We have extended our SBA to calculate n=2 excited state cap-

ture in e^+-H scattering. Second Born term is evaluated by retaining three eigenstates (1s, 2s, 2p) of the target atom. Tripathi, Sinha and Sil[20] have also predicted excited state (n=2) capture cross section using eikonal approximation. Fig.5 shows the DCS for 2s state

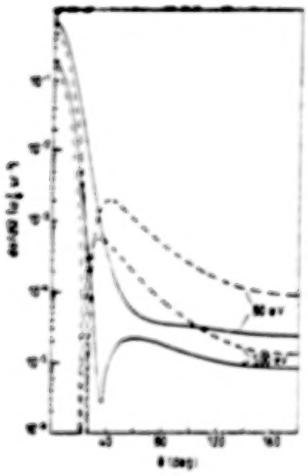

Fig.5. DCS (a_o^2 sr^{-1}) for 2s state capture in e^+-H scattering. The results at 500 eV are multiplied by 10^3. —, SBA; – –, FBA.

capture at the incident energies 80.0 and 500.0 eV. The FBA, as usual, predicts the zero cross section at all the energies. No structure is obtained in the DCS using the SBA upto the incident energy 100 eV. As the energy increases, the structure is more prominent and the position of the structure is around 45^o. We show only the results at 500.0 eV. The contribution of the second order terms is dominant around the zero values of the FBA at low energies. At high energies, these terms prevent total cancellation and we get the residual structure. However Khan et al using their distorted wave method have obtained structure for the same processes even at 13.6 eV.

Our DCS for the 2p-state capture process at 80 and 500 eV are shown in Fig.6. As in the case of

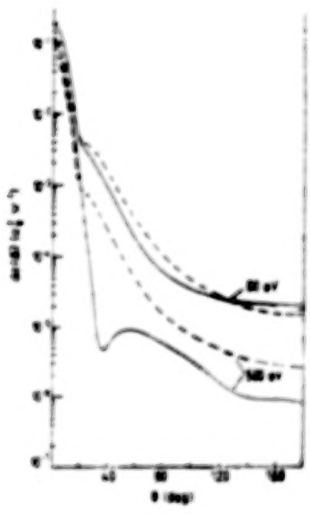

Fig.6. Same as Fig.5 but for 2p state capture.

the 2s state, we do not find any structure upto the incident energy 500 eV. Tripathi, Sinha and Sil have also obtained the structure above 500 eV. Here also, the structure is more prominent with the increase of energy and the position of the structure is around the scattering angle 45^o. It may be mentioned that the FBA does not predict any minimum in the energy range considered. Instead of being cancelled, the two terms of the FBA

amplitudes are combined. The second Born term is totally responsible for the structure at high energies. In fact, the destructive interference of the FBA and the SBA amplitudes at high energies provides the structure. We hasten to add that Thomas mechanism is valid only at high energies. Therefore, it is not surprising that we have not obtained Thomas peak for excited state capture at low energies.

Table 3 presents the integrated excited state capture cross sections.

Table 3. Integrated SBA cross section (πa_0^2) for excited (2s and 2p) state capture in e^+-H scattering.

E (eV)	2s	2p
50.0	0.165	0.366^{-1}
80.0	0.252^{-1}	0.601^{-2}
100.0	0.124^{-1}	0.219^{-2}
200.0	0.507^{-3}	0.620^{-4}
300.0	0.699^{-4}	0.663^{-5}
500.0	0.534^{-5}	0.348^{-6}

The present second Born results are always greater than those of the FBA. These results are of importance to obtain the total Ps-formation cross section. The present excited state capture cross section are not negligible when compared with ground state capture cross sections. It may be noted that 2s and 2p state capture cross sections differ by one order of magnitude, 2s state capture cross section being higher.

To find the validity of our methods, our group has carried out investigations using close coupling approximation (CCA) with two coupling schemes

1) H(1s), H(2s), H(2p), Ps(1s)
2) H(1s), H(2s), H(2$\bar{p}$), Ps(1s)

Instead of solving the conventional coupled integro-differential equations, we recast the Schrodinger equation into a coupled integral equation in the momentum space. The final one dimensional coupled integral equations have been solved by matrix inversion method. The details of the numerical method have been discussed in our paper (Basu, Mukherjee and Ghosh[21]).

At low incident energies (in the pre-gap region) very reliable s-, p- and d-wave ground state capture cross sections for e^+-H are available (Humberston and his co-workers[22-24]) using variational methods. In practice, it is not possible to perform such elaborate calculation at intermediate and high energies and also for complex systems. We compare two sets of s, p and d-wave phase shifts obtained using CCA with variational results in Tables 4 - 6.

It is well known that the s-wave Ps-formation cross section is very sensitive to the method employed. In Table 1, we have shown pre-

'sent two sets of results along with

Table 4. s-wave positronium formation cross sections (πa_o^2).

k	1s-2s-2p-Ps	1s-2s-2$\bar{p}$-Ps	H^{22}
0.71	.608(-2)	.558(-3)	.41(-2)
0.75	.418(-2)	.282(-3)	.44(-2)
0.8	.244(-2)	.113(-2)	.49(-2)
0.85	.156(-2)	-	.58(-2)

the variational prediction (Humberston[22].)

Table 5. p-wave positronium formation cross section (πa_o^2).

	1s-2s-2p-Ps	1s-2s-2$\bar{p}$-Ps	BH^{23}
0.71	.121(-1)	.803(-2)	.27(-1)
0.75	.278	.218	.37
0.8	.411	.344	.48
0.85	.470	.401	.56

In Tables 5 and 6 we have tabulated our present two sets of p- and d-wave capture cross sections. The

Table 6. d-wave positronium formation cross section (πa_o^2).

k	1s-2s-2p-Ps	1s-2s-2$\bar{p}$-Ps	BH^{24}
0.71	.286(-3)	.351(-3)	.62(-3)
0.75	.144	.170	.34
0.78	.465	.578	.81
0.85	.684	.897	.11(+1)

variational results (Brown and Humberston[23]) have also been included for comparison. Our p- and d-wave cross sections are in fair agreement with variational numbers the present numbers being lower.

The polarizability of Ps atom is eight times that of hydrogen. It is expected that the inclusion of long range force of the Ps atom will affect the results significantly.

Being encouraged by the above results, we have carried out our CCA calculations upto the incident energy (200 eV) (Mukherjee et al[25])

Fig. 7 shows the present differential cross section at 100 eV using ou- second order results (BG)

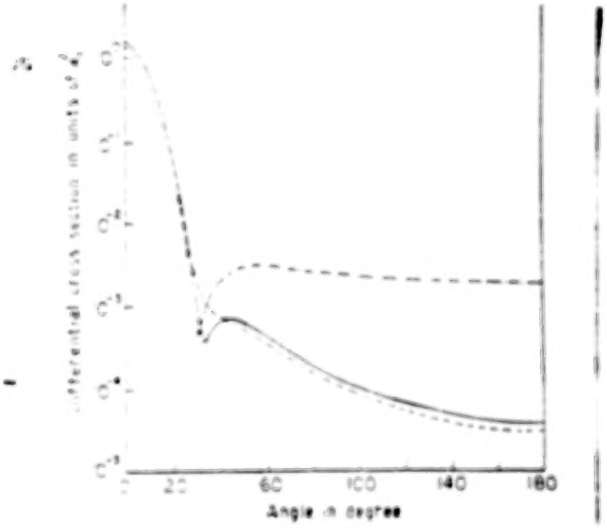

Fig. 7. DCS (a_o^2 sr^{-1}) for ground state capture in e^+-H scattering at 100.0 eV. —, eigenstate CCA; ---, pseudo-state CCA; – –, BG.

along with our two models of CCA at 100 eV. The position of the Thomas peak as obtained using eigen state CCA and BG are nearly identical whereas pseudo-state CCA fails to predict the Thomas peak. However, we may skip the minimum. At large scattering angles, the two sets if CCA results differ appreciably from BG. The contribution to the scattering amplitude upto the second order may not be sufficient for

convergent results at large scattering amplitude upto the second order may not be sufficient for convergent results at large scattering angles. This may be the reason of discrepancy.

Table 7 presents the ground state capture cross sections ob-

Table 7. Ground state capture cross section (in units of πa_o^2).

E (eV)	50	100	200	300
Pseudo	0.37*	0.46^{-1}	0.27^{-2}	-
SBA	0.62	0.33^{-1}	0.31^{-2}	0.49^{-3}
BG	0.56	0.46^{-1}	0.26^{-2}	0.39^{-3}
FBA	0.46	0.46^{-1}	0.25^{-2}	0.37^{-3}

*54.4 eV results.

tained by different methods. BG and SBA are the two second order results. Our pseudo-state CCA and the FBA results are also included for comparison. For incident energies E 100 eV, our CCA and BG results are in good agreement. It is interesting to note, even at 300 eV, the second order results BG and SBA are greater than the FBA results.

b) Helium Atom

Deb et al[26] have calculated ground state capture cross section using similar method as applied to the case of hydrogen atom in the high energy region. Here also, they have obtained the structure in the DCS around 50° as expected. Their ground state capture cross sections in the very high energies are also greater than the corresponding BK results. We are now investigating the same process using our FBA to calculate σ^{Ps}. Till now, we are able to include three eigenstates ($1s^2$, 2^1s, 2^1P) as intermediate one. Our preliminary result shows that cross section is increased by about 10 pct. over FBA at the incident energy 300 eV. Below this incident energy, results, may not be be reliable. Fig.8 shows the diffe

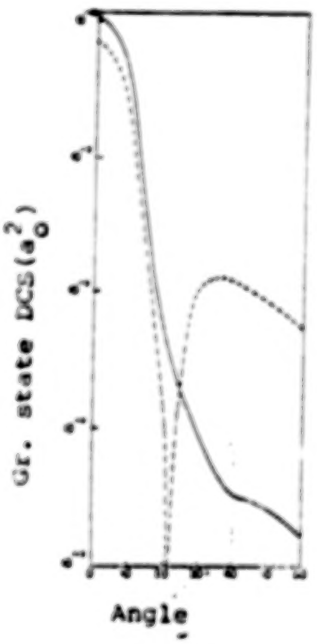

Fig.8. DCS in e^+-He ground state capture (a_o^2 sr^{-1}). —, SBA. --, FBA.

rential cross section at 300.0 eV using FBA and SBA for ground state capture in e^+-He scattering.

c) Lithium Atom

Recently, Abdel-Rauf[27] has employed a frozen-core coupled static method to investigate e^+-Li

and e^+-Na scattering. The effect of the inner shell is taken by introducing a core potential. Moreover, the exchange effect of the valence electron with those of core is included via local exchange potential. He has reported the results upto the incident energy 1000.0 eV. Using the wavefunction of Clementi and Roetti[28].

In the present conference, Ghosh and Basu[29] also report the coupled static calculations using the wavefunction of Weiss[30]. In our calculation, we assume that the valence electron is the only active electron. As the valence electron lies well outside the core, this, we expect, introduces marginal error. At low incident energies (5 eV) results differ appreciably from those of Abdel-Rauf (Table 8). We believe,

Table 8. Total ground state capture cross section (πa_0^2) using coupled static approximation.

E(eV)	Ghosh et al[29]	Abdel Raouf[27]
0.1	137.8	140.9
0.5	87.2	47.3
1.0	51.94	51.48
3.0	35.35	16.9
5.0	24.5	14.3

the difference between these two results are due to the use of different wavefunctions as well as with and without inclusion of exchange core potential. We also report our preliminary results using 2s,2p,ps CCA in this conference. It may be mentioned that we have also calculated the ground and n=2 state capture cross sections for e^+-Li scattering (Sarkar et al[31,32]) using the second order method of Basu and Ghosh[14] at intermediate energies.

ii) Ionisation

a) Helium Atom

We concentrate mainly on total ionisation cross section (σ_{ion}) in e^+-He scattering as three groups (Fromme et al[8], Diana et al[9], Sueoka[33]) have measured σ_{ion} for this system in this decade. The first quantum mechanical calculation for e^+-He ionisation including the positron signature has been carried out by us (Basu et al[34]). The choice of the effective charges are as follows :

	Z_A	Z_B
i)	1	1
ii)	0	1

A distorted wave method in which the wavefunction of the incoming positron F(X) satisfies the adiabatic Schrodinger equation given by

$$(\nabla_x^2 + k_i^2 + V_s(x) + V_p(x))F(\vec{x}) = 0 \qquad (5)$$

has been employed to investigate the problem. Here V_S and V_P are the static and polarization potentials respectively. The Hylleraas wavefunction has been used for computational

ease. The distortion in the initial channel is found to be insignificant. Campeanu et al[35] have repeated the calculation using Hartree-Fock wavefunction from Clementi and Roetti for e^+-He ionisation with certain modifications and using different distorted wave models. They have considered following different choices of effective charges

	Z_A	Z_B
i)	1	1
ii)	0	0
iii)	0	1
iv)	0	1

They argued that model (ii) of Basu et al[34] is not physically correct because when the ejected electron is faster than the scattered positron, it cannot screen the residual ion. In other words, they have taken the maximum value of the energy of the ejected electron to be E/2. Moreover, they have taken the distortion in the final channel.

In Fig.9, the theoretical predictions for total ionisation cross section (σ^+_{ion}) in e^+-He scattering are compared with the measured values of Fromme et al[33]. The agreement between the theoretical results and measured values is good.

b) Hydrogen Atom

Very recently, Spicher et al[36] have measured σ_{ion} for e^+-H

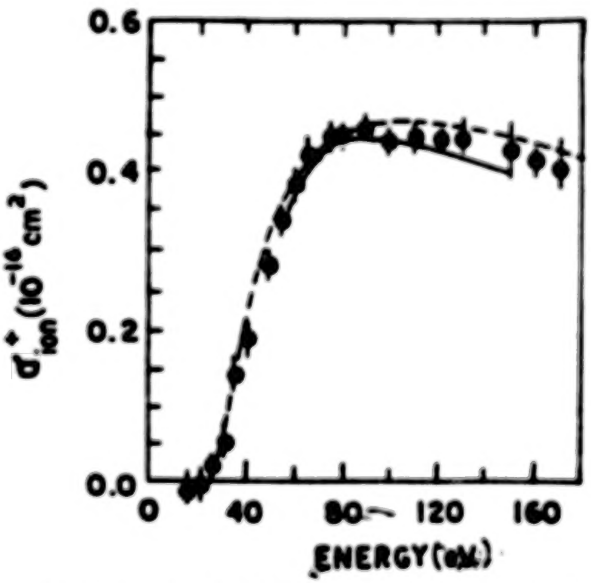

Fig.9. Ionisation cross section σ_{ion} (πa_0^2) in e^+-He scattering. —, Campeanu et al[35]; --, Basu et al[34]; ϕ, measured values of Fromme et al[3].

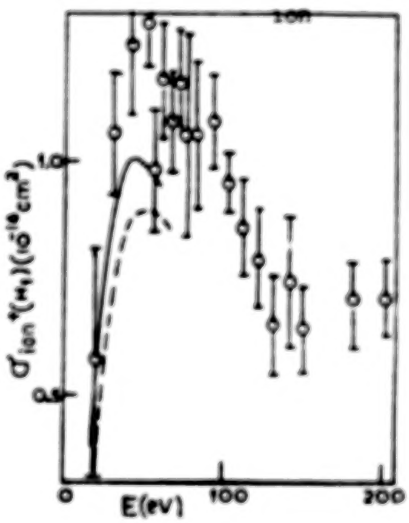

Fig.10. σ_{ion} in e^+-H ionisation: ϕ, Spicher et al[36]; —, Ghosh et al[37]; ---, Mukherjee et al[38].

scattering. It may be mentioned that we (Ghosh et al[37]) have performed the calculations for e^+-H ionisation using the same method

as applied e^+-He ionisation. Recently Mukherjee et al[38] have also investigated e^+-H ionisation following Campeanu et al. Theoretical results are compared with measured values in Fig.10. It is found that results of Ghosh et al are in good agreement with the measured values Results of Ghosh et al are in good agreement with the measured values Results of Mukherjee et al are lower than those of Ghosh et al and are in fair agreement with the experimental values.

c) Lithium atom

Basu and Ghosh[39] have calculated σ_{ion} in e^+-Li collision using distorted wave method. The ionisation cross section is found to be very small when compared to elastic or other inelastic processes. In absence of any elaborate work or experimental measurements, there is no scope for comparison

However, we like to point out certain salient features of ionisation process.

Theory of ionisation of atoms by electron and positron impact is complicated due to the role of Coulomb correlation in the asymptotic behaviour of ionised electron Peterhop-Rudge-Seaton theory of ionisation offers the prescription for the final state wavefunction and their relation between the effective charges Z_A and Z_B in the final state wavefunction is given by

$$\frac{Z_A}{k_A} + \frac{Z_B}{k_B} = \frac{1}{k_B} - \frac{1}{|k_A - k_B|} \qquad (5)$$

In the literature, we have found different choices for the effective charges satisfying the above relation but otherwise arbitrary. It is not possible to find an unique relation between the charges. The ionisation cross section is extrasensitive to the choice of the final state wavefunction (Ghosh et al[40]) This is apparent from Fig.11. Here

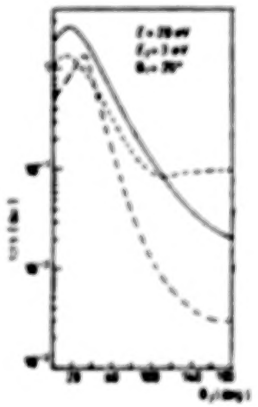

Fig.11. Triple differential cross section (TDCS) at e^+-H ionisation at E = 20 eV (E_2 = 3 eV, θ_1 = 20°): --, Z_B, -·-, choice (ii) of Ghosh et al[40]; —, DCA (multiplied by a factor of 10^3).

The results of triple differential cross section (TDCS) using double Coulomb approximation (DCA) differ from those of the Born results by a factor of 1000. The results using the other choices are also found to differ dramatically.

To study the ionisation process, one, we believe, has to be very careful regarding the asymptotic condition prescribed by Peterhop-

Rudge-Seaton. Moreover, the effective charges should fulfil the following limiting conditions which must be satisfied physically.

i) $k_A \to \infty$ or $k_B \to 0$ and $k_A > k_B$, the effective charges must behave as $Z_A \to 0$ and $Z_B \to 1$

ii) In the symmetric case i.e. $|k_A| = |k_B|$, the effective charges must be equal i.e. $Z_A = Z_B$.

Recently, Faisal and his coworkers[41] have initiated studies to investigate ionisation process in this light. They tried to get the values of the effective charges by exploiting Peterkop-Rudge-Seaton prescription and above two limiting conditions. Amongst their six unknown parameters, they have been able to solve five in terms of one. They tuned the unknown parameter with the triple differential cross section at one incident energy and at one angle. This is a limitation in their approach which of course authors are aware of. Moreover, this is not an unique way to solve the problem. We advocate one should study the ionisation process removing the arbitrary character in the choice of effective charges as far as practicable.

Acknowledgement : One of us, N. Basu, is thankful to CSIR and IUSA, Govt. of India for getting foreign travel support to attend the workshop. The authors are also thankful to Prof. Raith for giving their results of e^+-H ionisation prior to reporting anywhere else.

References :

1 M. Brauner and J. S. Briggs, J. Phys. B19 (1986) L325

2 M. Charlton, G. Laricchia, N. Zafar and F. M. Jacobsen in Atomic Physics with Positrons (eds. J. W. Humberston and E. A. G. Armour, Plenum, New York), p. 15 (1988).

3 A. S. Ghosh, in Atomic and Molecular Physics (ed. D. K. Rai and D. N. Tripathi, World Scientific Singapur, p. 344 (1988).

4 A. S. Ghosh, N. C. Sil and P. Mandal, Phys. Rep. C87 (1982) 313.

5 J. W. Humberston in Positron (Electron)-Gas Scattering, ed. W. E. Kauppila, T. S. Stein and J. M. Wadhera (Singapore: World Scientific) p. 35 (1986).

6 C. J. Joachain, Same as in Ref. 2, p. 71.

7 L. S. Fornari, L. M. Diana and P. G. Coleman, Phys. Rev. Lett. 51 (1983) 2276

8 D. Fromme, G. Kruse, W. Raith and G. Sinapius, Phys. Rev. Lett. 57 (1986) 3031.

9 L. M. Diana, P. G. Coleman, D. L. Brooks, P. K. Pendleton and D. M. Norman, Phys. Rev. A34 (1986) 2731.

10 P. Mandal, S. Guha and N. C. Sil, J. Phys. B12 (1979) 2913.

[11] P.Khan and A.S.Ghosh, Phys. Rev. A28 (1983) 2181.
[12] P.Khan, P.S.Majumdar and A.S. Ghosh, Phys. Rev. A31 (1985) 1405.
[13] G.Peach and M.R.C.McDowell, (1986) as quoted in ref.8.
[14] M.Basu and A.S.Ghosh, J. Phys. B21 (1988) 3439.
[15] R.J.Damburg and E.Karule, Proc. Phys. Soc. 90 (1967) 637.
[16] P.G.Burke and T.G.Webb, J. Phys. B3 (1970) L131.
[17] A.R.Holt, J. Phys. B5 (1972) L6.
[18] K.Prasad, Ph.D. thesis Queen's University of Belfast (1964).
[19] N.C.Deb, J.H.McGuire and N.C. Sil, Phys. Rev. A36 (1987) 3707.
[20] S.Tripathi, C.Sinha and N.C.Sil Phys. Rev. A 39 (1989) 2924
[21] M.Basu, M.Mukherjee and A.S. Ghosh, J. Phys. B22 (1989) 2195
[22] J.W.Humberston, J. Phys. B17 (1984) 2353.
[23] C.J.Brown and J.W.Humberston, J. Phys. B17 (1984) L423.
[24] C.J.Brown and J.W.Humberston, J. Phys. B18 (1985) L401.
[25] M.Mukherjee, M.Basu and A.S. Ghosh, (1989) Communicated.
[26] N.C.Deb, J.H.McGuire and N.C. Sil, Phys. Rev. A 36 (1987) 1062
[27] M.A.Abdel Rauf, J. Phys. B21 (1988) 2331.
[28] E.Clementi and C.Roetti, At. Data Nucl Data Tables 14, 177 (1974).
[29] A.S.Ghosh and M.Basu, in Poster of Workshop on Annihilation in Gases and Galaxies (1989).
[30] A.W.Weiss, Astrophys. J 138 (1963) 1262.
[31] K.P.Sarkar, D.Basu, M.Basu and A.S.Ghosh, Abs. XVI ICPEAC, New York, U.S.A., 1989.
[32] K.P.Sarkar, D.Basu, M.Basu and A.S.Ghosh, see as Ref.18.
[33] S.Sueoka, J. Phys. Soc. Jpn. 51 (1982) 3757.
[34] M.Basu, P.S.Mazumdar and A.S. Ghosh, J. Phys. B18 (1985) 369.
[35] R.I.Campeanu, R.P.McEachran and A.D.Stauffer, J. Phys. B20 (1987) 1635.
[36] G.Spicher, B.Clasen, W.Raith, G.Sinapius and W.Sperber, in Proc. of Workshop on Annihilation in Gases and Galaxies (1989)
[37] A.S.Ghosh, P.S.Mazumdar and M. Basu, Can. J. Phys. 63 (1985) 621.
[38] K.K.Mukherjee, N.R.Singh and P.S.Mazumdar, J. Phys. B22 (1989) 99.
[39] M.Basu and A.S.Ghosh, J. Phys. B19 (1986) 12449.
[40] A.S.Ghosh, P.S.Mazumdar and M.Basu, J. Phys. B18 (1985) 1881.
[41] S.Jetzke, J.Zaremba and F.A.M. Faisal, Z. Phys. D11 (1989) 63.

POSITRON SCATTERING BY ATOMIC HYDROGEN USING OPTICAL POTENTIALS AND WITH POSITRONIUM FORMATION

H. R. J. Walters
Department of Applied Mathematics,
Queen's University, Belfast,
Northern Ireland.

INTRODUCTION

We consider the scattering of positrons by H(1s) in a two-state model which incorporates optical potentials. The model explicitly describes elastic scattering, i.e.,

$$e^+ + H(1s) \rightarrow e^+ + H(1s) \qquad (1)$$

and Ps(1s) formation, i.e.,

$$e^+ + H(1s) \rightarrow Ps(1s) + p. \qquad (2)$$

The inelastic processes

$$e^+ + H(1s) \rightarrow e^+ + H^* \qquad (3)$$

$$Ps(1s) + p \rightarrow Ps^* + p \qquad (4)$$

where * stands for a state other than 1s, are implicitly taken into account through the optical potentials, which also allow for polarization of H(1s) and Ps(1s).

APPROXIMATIONS

Three levels of approximation are investigated which serve to illustrate the effects of polarization, absorption and positronium formation.

(i) Full Approximation (ELV2 + PSV2)

We start from the coupled static approximation. The wave function for the system in this approximation is

$$\Psi(\underline{r}_p, \underline{r}_e) = F(\underline{r}_p)\phi_{1s}(\underline{r}_e) + G(\underline{R})\phi_{1s}(\underline{r}) \qquad (5)$$

Here $\underline{r}_p$ and $\underline{r}_e$ are the coordinates of the positron and the electron relative to the proton as origin, $\underline{R} = (\underline{r}_p + \underline{r}_e)/2$, $\underline{r} = \underline{r}_p - \underline{r}_e$, ϕ_{1s} is the 1s wave function of atomic hydrogen, and ϕ_{1s} is that of ground state positronium.[1] The approximation (5) leads, in the usual manner, to the pair of coupled equations (in atomic units)

$$(\nabla_p^2 + k_o^2)\, F(\underline{r}_p) = 2\, V_{oo}(r_p) F(\underline{r}_p) + 2 \int K(\underline{r}_p, \underline{R})\, G(\underline{R})\, d\underline{R} \qquad (6a)$$

$$(\nabla_R^2 + p_o^2)\, G(\underline{R}) = 4 \int K(\underline{r}_p, \underline{R})\, F(\underline{r}_p)\, d\underline{r}_p \qquad (6b)$$

where V_{oo} is the static potential of H(1s), $K(\underline{r}_p, \underline{R})$ is the positronium formation coupling kernel, k_o is the momentum of the incident positron, and p_o is the momentum of the positronium.

Our full approximation is obtained by adding second order optical potentials[1] $V_{oo}^{(2)}$ and $V_{pp}^{(2)}$ to the H(1s) and Ps(1s) channels of (6), i.e.,

$$(\nabla_p^2 + k_o^2)\, F(\underline{r}_p) = 2\, V_{oo}(r_p)\, F(\underline{r}_p) + 2\, V_{oo}^{(2)}\, F(\underline{r}_p) + 2 \int K(\underline{r}_p, \underline{R})\, G(\underline{R})\, d\underline{R} \qquad (7a)$$

$$(\nabla_R^2 + p_o^2)\, G(\underline{R}) = 4\, V_{pp}^{(2)}\, G(\underline{R}) + 4 \int K(\underline{r}_p, \underline{R})\, F(\underline{r}_p)\, d\underline{r}_p \,. \qquad (7b)$$

The real part of the potential $V_{oo}^{(2)}$ contains the polarizability of H(1s) while the imaginary part allows for the direct excitations (3). Similarly, $V_{pp}^{(2)}$ contains the polarizability of Ps(1s) in its real part while representing the inelastic processes (4) through its imaginary part. The construction of these potentials is described later. Thus, in the approximation (7) both H(1s) and Ps(1s) can be polarized and excited through the direct collisions (3) and (4).

(ii) Simpler Approximation (ELV2 + PS)

In this approximation $V_{pp}^{(2)}$ is dropped from (7b) but $V_{oo}^{(2)}$ is retained in (7a).

Thus the Ps(1s) cannot be polarized or excited by the proton. Only H(1s) can be polarized and excited by the positron.

(iii) Simplest Approximation (ELV2)

Here we drop positronium formation completely and first look at the elastic scattering channel, i.e., we solve

$$(\nabla_p^2 + k_o^2)\, F(\underline{r}_p) = 2\, V_{oo}(r_p)\, F(\underline{r}_p) + 2\, V_{oo}^{(2)} F(\underline{r}_p) \qquad (8)$$

Construction of Optical Potentials[1]

The exact second order optical potentials $V_{oo}^{(2)}(\underline{r}_p,\underline{r}_p')$ and $V_{pp}^{(2)}(\underline{R},\underline{R}')$ are non-local and energy dependent. Their plane wave matrix elements

$$-\frac{1}{2\pi}\int e^{-i\underline{k}_f\cdot\underline{r}_p}\, V_{oo}^{(2)}(\underline{r}_p,\underline{r}_p')\, e^{i\underline{k}_o\cdot\underline{r}_p'}\, d\underline{r}_p\, d\underline{r}_p' \qquad (9a)$$

and

$$-\frac{1}{\pi}\int e^{-i\underline{p}_f\cdot\underline{R}}\, V_{pp}^{(2)}(\underline{R},\underline{R}')\, e^{i\underline{p}_o\cdot\underline{R}'}\, d\underline{R}\, d\underline{R}' \qquad (9b)$$

are equal to the second Born terms

$$f_{oo}^{B2}(k_o,q) \equiv -\frac{1}{8\pi^4}\sum_{n\neq 1s}\int d\underline{k}\, \langle \underline{k}_f\psi_{1s}|V|\underline{k}\psi_n\rangle \times \frac{\langle \underline{k}\psi_n|V|\underline{k}_o\psi_{1s}\rangle}{k_o^2 + 2(\varepsilon_o-\varepsilon_n) - k^2 + i\eta} \qquad (10a)$$

$$f_{pp}^{B2}(p_o,Q) \equiv -\frac{1}{2\pi^4}\sum_{n\neq 1s}\int d\underline{p}\, \langle \underline{p}_f\phi_{1s}|W|\underline{p}\phi_n\rangle \times \frac{\langle \underline{p}\phi_n|W|\underline{p}_o\phi_{1s}\rangle}{p_o^2 + 4(E_o - E_n) - p^2 + i\eta} \qquad (10b)$$

which describe elastic $e^+ + H(1s)$ and $Ps(1s) + p$ scattering respectively. In (10) $\underline{q} \equiv \underline{k}_o - \underline{k}_f$, $\underline{Q} \equiv \underline{p}_o - \underline{p}_f$, $\psi_n(\phi_n)$ is a hydrogen (positronium) eigenstate with energy $\varepsilon_n(E_n)$, $|\underline{k}\rangle \equiv e^{i\underline{k}\cdot\underline{r}_p}$, $|\underline{p}\rangle \equiv e^{i\underline{p}\cdot\underline{R}}$, $V \equiv \frac{1}{r_p} - \frac{1}{|\underline{r}_p - \underline{r}_e|}$, $W \equiv -\frac{1}{r_e} + \frac{1}{r_p}$ and the limit $\eta \to 0+$ is to be understood.

We use energy dependent local approximations[1] $V_{oo}^{(2)}(r_p)$ and $V_{pp}^{(2)}(R)$ which have the same on-energy-shell plane wave matrix elements as the exact potentials:

$$-\frac{1}{2\pi}\int e^{-i\underline{k}_f\cdot\underline{r}_p}\, V_{oo}^{(2)}(r_p)\, e^{i\underline{k}_o\cdot\underline{r}_p}\, d\underline{r}_p = f_{oo}^{B2}(k_o,q) \qquad (11)$$

where $|\underline{k}_f| = |\underline{k}_o|$. Then by simple Fourier inversion

$$V_{oo}^{(2)}(r_p) = -\frac{1}{\pi}\int_o^\infty \frac{\sin qr_p}{qr_p}\, f_{oo}^{B2}(k_o,q)\, q^2\, dq \qquad (12)$$

Expressions similar to (11) and (12) hold for $V_{pp}^{(2)}(R)$.

The second Born amplitude f_{oo}^{B2} is calculated using an orthonormal pseudostate basis $\bar{\psi}_n$ of 1s, 2s $\overline{3s}$, $\overline{4s}$, 2p, $\overline{3p}$, $\overline{4p}$, $\overline{3d}$ and $\overline{4d}$ states. Normally this is the basis of Fon et al[2], but a similar second basis is also employed to avoid problems with pseudostate thresholds. The pseudostates diagonalize the atomic Hamiltonian:

$$\langle \bar{\psi}_n|H_{atom}|\bar{\psi}_m\rangle = \bar{\varepsilon}_n\,\delta_{nm} \quad . \qquad (13)$$

The pseudostate approximation to f_{oo}^{B2} is given by the same formula (10a) but with ψ_n and ε_n replaced by $\bar{\psi}_n$ and $\bar{\varepsilon}_n$.

A positronium pseudostate basis $\bar{\phi}_n$ is similarly used to evaluate f_{pp}^{B2}. This basis is derived from the $\bar{\psi}_n$ basis by taking

$$\bar{\phi}_n(\underline{r}) = \frac{1}{2\sqrt{2}}\,\bar{\psi}_n(\underline{r}/2) \quad . \qquad (14)$$

It immediately follows that

$$\langle \bar{\phi}_n|H_{positronium}|\bar{\phi}_m\rangle = \tfrac{1}{2}\,\bar{\varepsilon}_n\,\delta_{nm} \qquad (15)$$

Because of symmetry only the p pseudostates, i.e., 2p, $\overline{3p}$, $\overline{4p}$, give a non-zero contribution to f_{pp}^{B2}.

RESULTS

Our results for e^+ + H(1s) elastic scattering, Ps(1s) formation, and the total and total inelastic e^+ + H(1s) cross sections are shown in figures 1 to 4. Comparison is made with the accurate variational calculations of Brown and Humberston[3] in the Ore gap (our ELV2 + PSV2 approximation has been used to extend their partial cross sections beyond the d-wave), with a new double-continuum R-matrix calculation[4] in the intermediate energy region 13 eV to 50 eV, and with the coupled pseudostate results of Walters[5] at higher energies. Also shown are corresponding electron scattering cross sections[6].

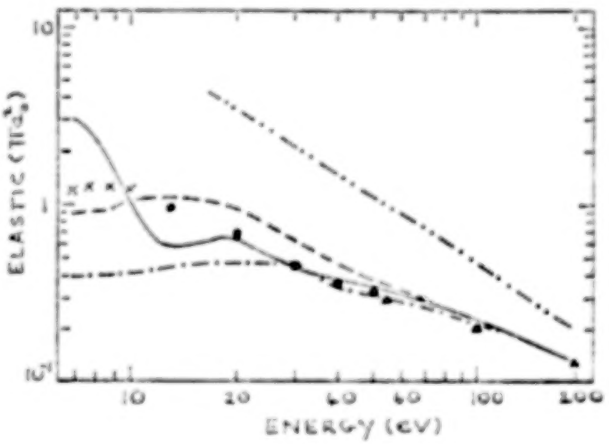

Figure 1. e^+ + H(1s) elastic cross section. Symbols: ——— Full Approximation ELV2 + PSV2; - - - -, Simpler Approximation ELV2 + PS; —·—·—, Simplest Approximation ELV2; —·· —·· —, electron cross section; X, variational results of Brown and Humberston[3]; ● , double-continuum R-matrix[4]; ▲ , coupled pseudostates[5].

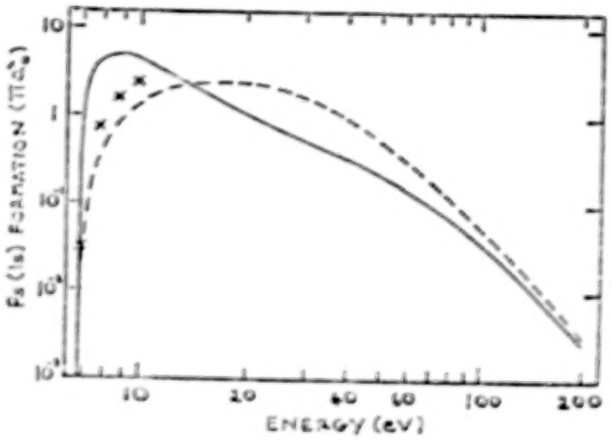

Figure 2. Ps(1s) formation cross section. Symbols as in figure 1.

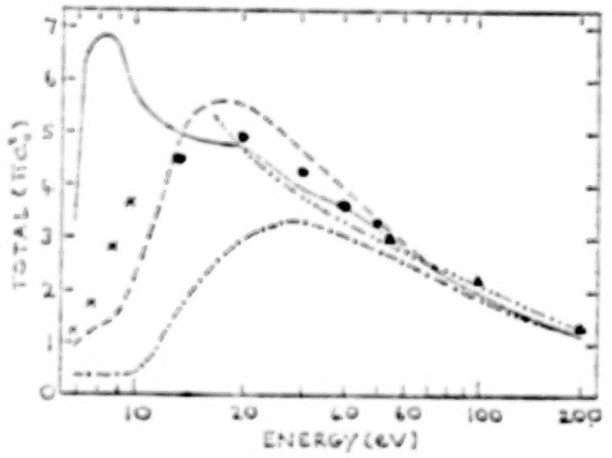

Figure 3. Total cross section. Symbols as in figure 1.

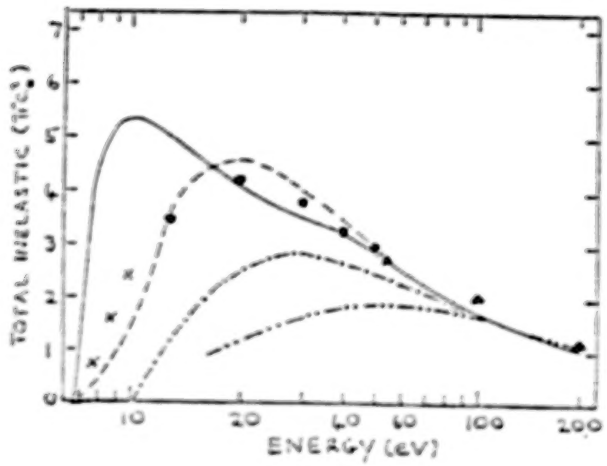

Figure 4. Total inelastic cross section. Symbols as in figure 1.

The following points are worth highlighting:

(i) At 20 eV and above the Full Approximation ELV2 + PSV2 appears to be performing well.

(ii) Polarization and absorption effects in the Ps(1s) channel can reduce the Ps(1s) formation cross section by a factor of three at intermediate energies.

(iii) Except at high energies: the elastic cross section for electron scattering substantially exceeds that for positron scattering; the total inelastic cross section for electron scattering is substantially lower than that for positron scattering; yet the (best) total cross sections for positron and electron scattering are in good agreement above 20 eV.

(iv) The simpler ELV2 + PS approximation gives cross sections which are generally too large at intermediate energies.

(v) Except for elastic scattering above 30 eV the simplest approximation ELV2 tends to produce cross sections which are too small.

References

1. H.R.J. Walters, Physics Reports 116, 1 (1984).

2. W. C. Fon, K. A. Berrington, P. G. Burke and A. E. Kingston, J. Phys. B 14, 1041 (1981).

3. C. J. Brown and J. W. Humberston, J. Phys. B 18, L401 (1985).

4. K. Higgins, P. G. Burke and H.R.J. Walters, J. Phys. B, to be published.

5. H.R.J. Walters, J. Phys. B 21, 1893 (1988).

6. M. P. Scott, T. T. Scholz, H.R.J. Walters and P. G. Burke, J. Phys. B, to be published.

POSITRONIUM FORMATION IN 2s STATE IN e^+-Li SCATTERING

K.P.Sarkar
Department of Physics, Gurudas College, Calcutta 700054, INDIA

and

D.Basu and Madhumita Basu
Department of Theoretical Physics
Indian Association for the Cultivation of Science
Jadavpur, Calcutta 700032, INDIA

There are ample theoretical reasons to investigate e^+-alkali atom scattering. Moreover, recent measurement on e^+-alkali atom system by Detroit group[1] has renewed much interest for investigating these processes. Here we study positronium (Ps) formation in excited 2s state in e^+-Li scattering at intermediate and high energies including second order effects following Basu and Ghosh[2]. Guha and Saha[3] have calculated the excited ns state capture cross sections using PBA at several incident energies ranging from 10-500 eV. It is well-known that PBA or any other first order approximation is not suitable to describe a rearrangement process at high energies since it is the second Born approximation to which the cross section converges. To our knowledge, no other work has yet been performed to predict excited state positronium formation cross sections in e^+-Li scattering.

In the conventional perturbative approach, the capture amplitude retaining upto the second order term, from the ground state $\langle\nu|$ of Li atom with momentum K to the excited state $|\nu'\rangle$ of the Ps atom with momentum K' is given by

$$g_{\nu',\nu}(\mathbf{K}',\mathbf{K}) = g^{B}_{\nu',\nu}(\mathbf{K}',\mathbf{K}) + g^{B2}_{\nu',\nu}(\mathbf{K}',\mathbf{K}) \quad (1)$$

where, ν stands for 2s state of Li atom and ν', 2s state of Ps atom. Here $g^{B}_{\nu',\nu}(\mathbf{K}',\mathbf{K})$ is the first Born excited state capture amplitude and $g^{B2}_{\nu',\nu}(\mathbf{K}',\mathbf{K})$ is the second order amplitude and is given by

$$g^{B2}_{\nu',\nu}(\mathbf{K}',\mathbf{K}) = \frac{1}{2\pi^2}\sum_{\nu''}\int \frac{d\mathbf{K}''}{K''^2 - K^2_{\nu''} - i\varepsilon} \times g^{B}_{\nu',\nu''}(\mathbf{K}',\mathbf{K}'')\, f^{B}_{\nu'',\nu}(\mathbf{K}'',\mathbf{K}) \quad (2)$$

f^B being the first Born scattering amplitude. The summation over ν'' runs over the discrete eigenstates of the target atom.

The use of closure relation in evaluating the rearrangement second order term is unsatisfactory. In the present calculation we assume that the valence electron is the active electron i.e. Ps atom is formed with the valence

electron only. We retain two target eigenstates, 2s and 2p, as intermediate ones. We have used the reliable Hartree-Fock wavefunction of Weiss[4] for ground and excited states of Li atom.

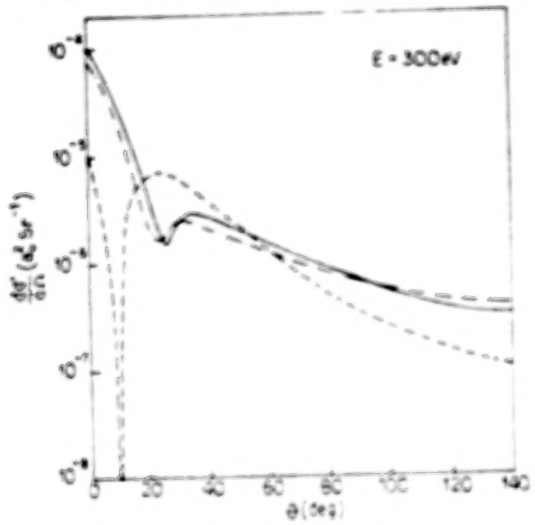

Fig.1. DCS (a_o^2) for excited 2s state capture in e^+-Li scattering at 300 eV. --, FBA; -·-, SBA (with 2s intermediate); —, SBA (with 2s 2p intermediate)

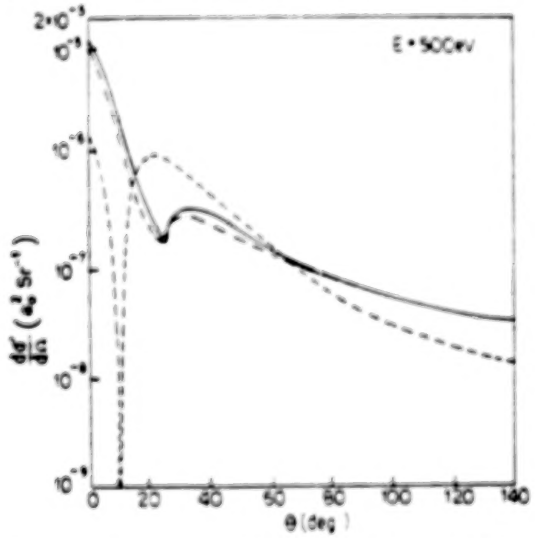

Fig.2. Same as in Fig.1 at 500 eV.

In Figs.1 and 2, we report our differential cross sections at two incident energies, 300 and 500 eV respectively. It is known that the second Born term is of vital importance in determining the asymptotic behaviour of the capture cross section. The contribution of the second Born term is found to be appreciable at 300 eV. With the increase of energy, the contribution decreases. The first Born DCS attains zero value around 10^o at both the energies as the two parts of the amplitude are of opposite sign and cancel each. Contribution of the second order term prevents the total cancellation in the DCS and the residual structure is due to the destructive interference of the amplitudes. The SBA structure is found around 30^o. These features have also been obtained by Basu and Ghosh.

The convergence of g^{B2} is of key importance. We could not test the convergence by increasing the higher target states as intermediate ones. The detailed results will be reported in the near future.

References :

1 T.S.Stein, M.S.Debabneh, W.E. Kauppila, C.K.Kwan and Y.Y.Wan, Atomic Physics with Positrons, eds. J.W.Humberston and E.A.G. Armour (Plenum Press) pp.251 (1987)

2 M.Basu and A.S.Ghosh, J. Phys B21, 3439 (1988).

[3] S.Guha and B.C.Saha, Phys. Rev. A21, 564 (1980)

[4] A.W.Weiss, Astrophysics J 138 1262 (1963).

Acknowledgement

The authors are thankful to Dr. A.S.Ghosh, I.A.C.S., Calcutta, India, for continuous help.

NEW PARAMETER-FREE POLARIZATION POTENTIALS IN LOW-ENERGY POSITRON COLLISIONS

Ashok Jain

Physics Department, Florida A & M University, Tallahassee, Florida--32307 (USA)

ABSTRACT

The polarization potential plays a decisive role in shaping up the cross sections in low-energy positron collisions with atoms and molecules. However, its inclusion without involving any adjustable parameter, is still a challange. Here we summarise various other techniques employed so far for positron collisions and discuss a new, nonadjustable and very simple form of the polarization potential for positron-atom (molecule) collisions below the threshold of positronium formation. This new potential, recently proposed by us, is based on the correlation energy (ϵ_{corr}) of a single positron in a homogeneous electron gas. The ϵ_{corr} has been calculated by solving the Schrödinger equation of the positron-electron system and fitted to an analytical form in various ranges of the density parameter. In the outside region, the ϵ_{corr} is joined smoothly with the correct asymptotic form ($-\frac{\alpha_0}{2r^4}$, where α_0 is the polarisibility of the target). We tested this new positron correlation polarization (PCOP) potential on several atomic and molecular targets such as the Ar, CO, and CH_4. The results on the total and differential cross sections on these targets are shown here alongwith the experimental data where ever they are available.

I. Introduction

In the positron(e^-) scattering with multi-electron atom (or molecule), a true e^- polarization potential is very difficult to incorporate without involving any adjustable parameter. Two simple stratagems have been quite popular: one, to use the electron polarization potential as such for the corresponding positron collisions and two, to employ a phenomenological form under the tuning procedure. However, both approaches are unsatisfactory and usually fail at the differential cross section (DCS) and annihilation parameter (Z_{eff}) level; although one may be succesful in getting good agreement for the integral quantities.

It is only recently that several theoretical attempts have been made to consider the polarization of the target atom (or molecule) by the e^- at the *ab initio* level[1-8]; however, these rigorous calculations are not totally parameter-free and suffer from including near-the-target nonadiabatic effects and also the correct values in the asymptotic region. Although, the question of nonadiabaticity may not as crucial for the positron projectile as it is for the electron case (see later). The polarization effects dominate the scattering process at very low energies (below about 5 eV). At somewhat higher energies (roughly above 5 eV), the DCS's are still quite sensitive to such charge distortion effects. Here we are concerned only at low energies, particularly below the positronium formation and/or any electronic excitation thresholds. For the one-electron positron-hydrogen case, the issue of polarization potential has recently been discussed by Abdel -Raouf[9]. A very recent and comprehensive review[10] on the e^--molecule scattering gives details on various approaches used so far to include polarization effects in positron scattering.

It is, therefore, always desirable to find some kind of simple form of the polarization force without involving any fitting parameter. At low impact energies, where the impinging positron is moving very slowly relative to the target electron, the distortion of the electronic charge cloud is quite different than the corresponding electron impact case. Asymptotically, the polarization potential can be assumed to be the same for both the projectiles (which is true up to the second-order perturbative theory only); however, at near-the-target encounters, both the charged projectiles interact differently with the charge cloud of the target. In this talk, we discuss a new parameter-free form of an approximate e^+ polarization potential which is simply a function of the target charge density and in addition is energy-independent.

A summary of earlier usage of various models for polarization potential in positron-molecule collisions is given by Morrison and coworkers[1-2]. Recently, Elza et al[8] have investigated various aspects of polarization/correlation effects in low-energy positron-N_2 collisions via a two-parameter model. Tennyson[3] and Tennyson and Morgan[4] have applied the R-matrix technique to positron-molecule (H_2, N_2 and CO) collisions. However, the inclusion of polarization force in all these the so called *ab initio* methods is not either satisfactory nor complete. From numerical point of view, these procedures are not easy to apply for a general positron-molecule system. The collision of positrons with polyatomic targets is even more complicated. We[11-12] have reviewed the situation on the polyatomic molecules with respective to the polarization effects and the comparison with the experimental data.

In the next section, we describe the new positron polarization potential and in section III, the numerical techniques are summarised. In order to demonstrate the success of the new positron correlation polarization (PCOP) potential, in section IV, we present some calculations on the differential and integral elastic cross sections for the atomic (Ar) and molecular (CO and CH_4) targets below the positronium (Ps) formation threshold (i.e. $E \leq 10$ eV). Concluding remarks are given in the last section.

II. The New Positron-Correlation-Polarization (PCOP) Potential

Asymptotically, for a general e^+-molecule collision system, the polarization potential behaves as

$$V_{pol}(r,\theta,\phi) = \frac{-1}{2r^4}\left[\alpha_0(4\pi)^{\frac{1}{2}} S_0^{01} + \alpha_2\left(\frac{4}{5}\pi\right)^{\frac{1}{2}} S_2^{01} + \alpha_2^1\left(\frac{4}{15}\pi\right)^{\frac{1}{2}} S_2^{21}\right], \qquad (1)$$

where the $S_\ell^{m\eta}$ is a real spherical harmonic (see Ref. 13 for its definition and various properties), (r,θ,ϕ) are the coordinates of the projectile referring to the center of the target and the spherical (α_0) and nonspherical (α_2 and α_2^1) polarisibilities are expressed in terms of the polarisibility tensor α_{ii} of the target, namely,

$$\alpha_0 = \frac{1}{3}(\alpha_{11} + \alpha_{22} + \alpha_{33});\ \alpha_2 = \frac{2}{3}(\alpha_{33} - \frac{1}{2}\alpha_{11} - \frac{1}{2}\alpha_{22});\ \alpha_2^1 = \alpha_{11} - \alpha_{22}.$$

The above form (Eq. 1) of the polarization potential is accurate at large r values up to the second-order perturbation theory. The problem arises when the projectile is near the target. A simple way to remedy this difficulty has been to multiply Eq. (1) by a cut-off function depending upon some adjustable parameter; however, this approach is unsatisfactory , although the results may be forced to agree with observations (see for example, Darewych[14], Horbatsch and Darewych[15]). For positron collisions, most of the calculations prior to 1984 used an electron polarization potential (EPP) assuming that such polarization effects are not sensitive to the sign of the charge of the projectile. Morrison and his group (Morrison et al[1]; Morrison[2]; Elza et al[8]) strongly advocated

for a need to generate a true positron polarization potential (PPP) rather than employing the EPP; they strengthened their point by presenting detailed calculations on the positron-H_2 and N_2 systems and comparing them with experimental data. Although earlier calculations on the positron collisions using the EPP gave good results as compared to experimental σ_t values, however, these theoretical results are generally poor at low energies and not qualitatively good at all for differential cross sections at any energy[16-17]. Unfortunately, the more rigorous calculations based on the variational polarised-orbital theories are not satisfactory either; Elza et al[8] have to introduce a cut-off function in both the short and long ranges and adjust two parameters to make theory and measurement in close agreement. Even in a more sophisticated R-matrix approach, an accurate inclusion of polarization effects has not been achieved yet[2-5].

Here, our goal is to look for a computationally simple form of the positron polarization potential which is different from the corresponding electron potential and virtually free from any adjustable parameter. The basic philosophy of the present approach is similar to the method of O'Connel and Lane[18] for the case of electron scattering based on the correlation energy of the target in the presence of an incoming electron. The present positron polarization potential is also based on the correlation energy of a localized positron in an electron gas and its hybridization with the correct asymptotic form. Here, we think the incoming e^+ as a charged impurity at a fixed distance in an homogeneous electron-gas. In positron annihilation experiments, a fundamental question to be asked is how the electron-positron interaction distorts the electronic structure of the system under investigation.

The e^+ correlation energy ϵ_{corr} in an electron gas has been evaluated phenomenologically[19-20] as well as using the Bethe-Goldstone type approach[21]. Recently, Arponen and Pajanne[22] have applied a completely new approach to the problem of a light impurity in an electron gas. In their method[22] the electron gas is described by a set of interacting bosons representing the collective excitations of the random-phase-approximation (RPA). Very recently, Boronski and Nieminen[23] have described the density functional theory of the electron-positron system and presented the results on the positron-electron correlation energy as a function of the density parameter r_s (see later) for different $n_+(\mathbf{r})/n_-(\mathbf{r})$ ratios including the case of one positron in a homogeneous electron gas. Here n_+ and n_- denote the densities of positrons and electrons respectively.

The physical picture of the positron correlation in an electron gas is as follows. When the incoming positron enters the target electronic charge cloud, we can assume the positron as localized instantaneously and correlating with the surrounding electrons of a given density, $n_-(\mathbf{r})$. The wave function of the positrons in such an electron-positron plasma, can be written as[23]

$$-\frac{1}{2}\nabla^2\psi_i^+(\mathbf{r}) + \mu_{xc}(n_+(\mathbf{r})) - \phi(\mathbf{r}) - \frac{\delta E_c^{e-p}(n_+,n_-)}{\delta n_+(\mathbf{r})}\psi_i^+(\mathbf{r}) = \epsilon_i^+\psi_i^+(\mathbf{r}), \qquad (2)$$

here μ_{xc} is the exchange-correlation potential (which is zero in the present one-positron case), $\phi(\mathbf{r})$ is the Hartree-Coulomb potential and E_c^{e-p} is the positron-electron correlation energy functional. The Eq. (2) has been solved numerically in a self-consistent manner[23]. Based on the paper of Arponen and Pajanne[22], Boronski and Nieminen[23] have given explicit expressions for the positron-electron correlation energy, $\epsilon_{corr}(r_s)$ interpolating it for the whole radial region. These expressions are obtained without giving any divergence problems in the calculations of annihilation rates over the entire range of the density parameter r_s (Kallio et al[24]). In their work, Arponen and Pajanne[22] have developed a new approach to solve the problem of a charged impurity in an electron gas. The correlation energy, ϵ_{corr}, is calculated from the ground-state expectation value of the Hamiltonian which describes the electron gas plus the incoming positron fixed at a distance. In the evaluation of ϵ_{corr}, the positron-electron interaction has also been considered (see Eq. 2). The analytic interpolated expressions for the ϵ_{corr} in the whole range of the density parameter r_s ($\frac{4}{3}\pi r_s^3\rho(\mathbf{r}) = 1$, where $\rho(\mathbf{r})$ is the undistorted electronic density of the target) are given as follows:

$$2\epsilon_{corr}(r_s) = -\frac{1.56}{\sqrt{r_s}} + (0.051 \ln r_s - 0.081)\ln r_s + 1.14; \qquad r_s \leq 0.302. \tag{3a}$$

$$2\epsilon_{corr}(r_s) = -0.92305 - \frac{0.05459}{r_s^2}; \qquad 0.302 \leq r_s \leq 0.56. \tag{3b}$$

$$2\epsilon_{corr}(r_s) = \frac{13.15111}{(r_s + 2.5)^2} + \frac{2.8655}{(r_s + 2.5)} - 0.6298; \qquad 0.56 \leq r_s \leq 8.0. \tag{3c}$$

and finally,

$$2\epsilon_{corr}(n(r_s)) = -179856.2768n^2 + 186.4207n - 0.524; \qquad 8.0 \leq r_s \leq \infty, \tag{3d}$$

where $n(r_s)$ is the electronic density corresponding to the density parameter r_s.

The PCOP potential, defined as a functional derivative of the correlation energy with respect to $\rho(\mathbf{r})$, can be derived conveniently from the following equation in terms of functional derivative of the density parameter[24].

$$V^{+}_{corr}(\mathbf{r}) = \left(1 - \frac{1}{3} r_s \frac{d}{dr_s}\right) \epsilon_{corr}(r_s). \tag{4}$$

Finally, we obtain the following form of the $V^{+}_{corr}(\mathbf{r})$ (in atomic units) from Eqs. (3)-(4): for $r_s \leq 0.302$,

$$2V^{+}_{corr}(\mathbf{r}) = \frac{-1.30}{\sqrt{r_s}} + (0.051 \ln(r_s) - 0.115)\ln(r_s) - 1.167; \tag{5a}$$

for $0.302 \leq r_s \leq 0.56$,

$$2V^{+}_{corr}(\mathbf{r}) = -0.92305 - \frac{0.09098}{r_s^2}; \tag{5b}$$

and for $0.56 \leq r_s \leq 8.0$,

$$2V^{+}_{corr}(\mathbf{r}) = -\frac{8.7674 r_s}{(r_s - 2.5)^3} + \frac{-13.151 + 0.9552 r_s}{(r_s + 2.5)^2} + \frac{2.8655}{(r_s + 2.5)} - 0.6298. \tag{5c}$$

Note that for molecular systems the short-range $\epsilon_{corr}(r_s)$ is to be divided by a factor of $(2\ell + 1)/\sqrt{4\pi}$ to account for molecular orientation not considered by Arponen and Pajanne[22]. Here we do not worry about the $8.0 \leq r_s \leq \infty$ region, as this range is beyond the crossing point where the polarization potential is accurately described by the asymptotic term (Eq. 1). It is to be noted that the interpolation formulae for the correlation energy (Eqs. (3)) were formulated in such a way that for the limit $r_s \to \infty$, the ϵ_{corr} reaches the value of Ps^- ion energy, i.e., -0.262 a.u.. In the present positron scattering case, we realize that in the $r_s \to \infty$ limit, the correlation energy approaches the correct asymptotic form of the polarization potential (the same prescription as suggested by O'Connel and Lane[18]).

Thus, the PCOP interaction potential, $V^{PCOP}_{pol}(\mathbf{r})$, for the e^+-molecule/atom system is given by,

$$V^{PCOP}_{pol}(\mathbf{r}) = V^{+}_{corr}(\mathbf{r}). \qquad r \leq r_c, \tag{6a}$$

and by Eq. (1) for the $r \geq r_c$ range. Here r_c is the radius where the V_{corr} and $-\alpha_0/2r^4$ (or $\alpha_2/2r^4$) terms cross each other for the first time. In addition, we will also report the similar cross sections under the ECOP potential, which has recently been employed for positron-molecule scattering (Jain[26-27], Gianturco et al[28]). Even though the EPP results are encouraging for some molecular targets (Jain and Thompson[29]), we feel that it is more appropriate to find a true positron polarization interaction.

The new PCOP potential (Eq. 6) has several favourable points worth mentioning here: first, it involves a true correlation of the incoming positron with the target electrons at short distance encounters and exihibits correct behavior in the asymptotic region; second, it is very easy to calculate and convenient to incorporate into any model potential approach; third, it is quite different from the corresponding EPP and finally, (see later), it gives qualitative good results for the total cross sections for several atomic and molecular targets as compared with experimental data.

III. Scattering Parameters

In fact, the numerical techniques to solve the scattering equation for the e^+ wave function are standard as employed for the electron scattering case. For the atomic target (Ar), we use the variable-phase-approach (VPA)[30] in order to determine phase-shifts at each energy; more details of the VPA approach are given in Ref. 31. The optical potential of the e^+-Ar system is determined very accurately from the numerical Hartree-Fock wave functions of the target[32]. In order to preserve numerical accuracy, convergence tests were carried out with respect to radial integration and number of partial waves retained in the evaluation of various cross sections[16].

For the diatomic molecule (CO) case, the scattering equations are set up in the single center formalism under the body-fixed (BF) adiabatic-nuclei-approximation (ANA). The final coupled scheme is formulated in the integral equation method[33]. More details for the positron-CO calculations can be found in our earlier[26-27] and recent[17] papers.

Assuming the CO molecule in its ground electronic ($1\sigma^2 2\sigma^2 3\sigma^2 4\sigma^2 1\pi^4$; $^1\Sigma$) and vibrational states, the equation of the continuum positron wave function, $P(\mathbf{r})$ in the single center formalism under the BF ANA can be written as,

$$[\nabla^2 + k^2 - 2V(\mathbf{r})]P(\mathbf{r}) = 0, \tag{7}$$

where k^2 is the positron energy in Rydbergs and the interaction potential $V(\mathbf{r})$ includes the repulsive static and attractive polarization forces. Expanding the $V(\mathbf{r})$ in terms of Legendre projections, v_λ,

$$V(\mathbf{r}) = V_{st}(\mathbf{r}) + V_{pol}(\mathbf{r}) = \sum_{\lambda=0}^{\lambda_{max}} [v_\lambda^{ST}(r) + v_\lambda^{POL}(r)]P_\lambda(\cos\theta), \tag{8}$$

we obtain the following set of coupled differential equations for the continuum function $P(\mathbf{r})$ for a given symmetry Λ,

$$[\frac{d^2}{dr^2} - \frac{\ell(\ell+1)}{r^2} + k^2]P^\Lambda_{\ell l_0}(r) = \sum_{\ell'} V_{\ell\ell'}(r)P^\Lambda_{\ell' l_0}(r), \tag{9}$$

where the potential matrix $V_{\ell\ell'}$ is determined as usual[34]. Here Λ corresponds to $\Sigma(\Lambda = 0)$, $\Pi(\Lambda = 1)$, $\Delta(\Lambda = 2)$, $\Phi(\Lambda = 3)$ etc. symmetries. There are several methods to solve equation (9), but we

adopt an integral-equation technique by converting the differential equation (9) into an integral equation[33].

$$P^{\lambda}_{\ell\ell_0}(r) = j_\ell(kr)\delta_{\ell\ell_0} - \sum_{\ell'} \int_0^r G_\ell(r,r') V_{\ell\ell'}(r') P^{\lambda}_{\ell'\ell_0}(r') dr', \tag{10}$$

where the Green's function is defined by

$$G_\ell(r,r') = k^{-1} [\eta_\ell(kr) j_\ell(kr') - j_\ell(kr) \eta_\ell(kr')], \tag{11}$$

in which $j_\ell(kr)$ and $\eta_\ell(kr)$ are Riccati-Bessel functions. Note that in the expansion (Eq. 8) of polarization term, we have only $\lambda = 0$ and 2 terms.

The CO molecule is a polar molecule which needs special attention in a BF adiabatic-nuclei theory where the forward DCS and σ_t are undefined[35]. In this respect, we employ the multipole-extracted-adiabatic-nuclei (MEAN) scheme of Norcross and Padial[36], in which the DCS for the $J \rightarrow J'$ rotational transition are given as

$$\frac{d\sigma}{d\Omega}(JJ') = \frac{d\sigma^{FBA}}{d\Omega}(JJ') + \frac{k_{J'}}{4k_J} \sum_{l_t} C(Jl_t J';00)^2 \frac{1}{k^2} \sum_{\lambda=0}^{\lambda_{max}} (B_{\lambda,l_t} - B^{FBA}_{\lambda,l_t}) P_\lambda(\cos\theta), \tag{12}$$

where the first term is the usual closed form for the (JJ') rotational excitation DCS in the space-fixed first-Born-approximation (FBA); k_J and $k_{J'}$ are respectively the wavevectors in the initial and the final channels; C (...) is a Clebsch-Gordan coefficient; l_t is the angular momentum transferred during the collision; B_{λ,l_t} are the DCS expansion coefficients and B^{FBA}_{λ,l_t} are the corresponding quantities in the FBA evaluated in the BF frame of reference. The channel vectors are related by the relation,

$$k^2_{J'} - k^2_J = B\,J'(J'+1) - J(J+1), \tag{13}$$

where B is the rotational constant of the CO molecule. Finally, the expressions for total ($\sigma_t^{JJ'}$) and the momentum transfer ($\sigma_m^{JJ'}$) cross sections are evaluated from equation (11) for any (JJ') transition. Total (summed over all final rotational states J') integrated (σ_t) and momentum transfer (σ_m) cross sections can easily be obtained from

$$\sigma_{t\ or\ m} = \sum_{J'} \sigma^{JJ'}_{t\ or\ m}. \tag{14}$$

However, for a proper comparison with experiment, we average the σ_t and σ_m over the Boltzmann distribution of rotational states at 300 K (represented as $\langle\sigma_t\rangle$ and $\langle\sigma_m\rangle$). This is quite easy since in the present energy region the sum over J' in equaton (14) is insensitive to J.

Finally, for a polyatomic molecule, we employ totally a different set of computer codes to obtain scattering parameters. The details are given elsewhere[13,37]. For a polyatomic target, it is again convenient to make use of the ANA and set up the scattering equations in the single-center-expansion scheme under the close-coupling formalism. The equation for the scattered positron function $P(\mathbf{r})$ is the same as given in Eq. (7), however, now the single-center-expansion scheme is quite different. The angular basis functions belong to the irreducible representation (IR) of the molecular point group. The $P(\mathbf{r})$, V_{st} and V_{pol} are expanded around the center-of-mass (COM) of the molecule in question. For example, the $P(\mathbf{r})$ is expanded as[13],

$$P(\mathbf{r}) = \sum_{\ell\lambda p\alpha} r^{-1} G^{(p\alpha)}_{\ell\lambda}(r) X^{(p\alpha)}_{\ell\lambda}(\hat{\mathbf{r}}), \tag{15}$$

where the $X_{\ell h}^{p\mu}$ are symmetry-adapted angular functions belonging to a particular irreducible representation $p\mu$ of the molecular point group. The static potential V_{st} is given by

$$V_{st}(\mathbf{r}) = \int |\psi_0|^2 \sum_{j=1}^{N} |\mathbf{r} - \mathbf{r}_j|^{-1} d\mathbf{r}_1 d\mathbf{r}_2 \cdots d\mathbf{r}_N - \sum_{i=1}^{M} Z_i |\mathbf{r} - \mathbf{R}_i|^{-1}, \tag{16}$$

where ψ_0 is the target ground state wavefunction given as a single Slater determinant of one-electron spin orbitals $\phi_n(\mathbf{r})$, N is the total number of electrons and M the number of nuclei in the molecule.

Finally, the scattering amplitude for e^+ with initial direction $\hat{\mathbf{k}}$ and the final direction $\hat{\mathbf{r}}$ is

$$f(\hat{\mathbf{k}}.\hat{\mathbf{r}}) = \frac{2\pi}{ik} \sum X_{\ell h}^{p\mu}(\hat{\mathbf{k}}) X_{\ell' h'}^{p\mu}(\hat{\mathbf{r}}) i^{\ell - \ell'} (\mathbf{S}_{\ell h, \ell' h'}^{p\mu} - \delta_{\ell\ell'}\delta_{hh'}), \tag{17}$$

where the sum being over ℓ, h, ℓ', h', p and μ. The $\mathbf{S}$ matrix is related with the $\mathbf{K}$ matrix in the usual fashion. The amplitude (Eq. 17) is defined in the BF frame of reference. In order to transform it into the space-fixed (SF) or the laboratory frame coordinate system, we employ the standard technique in terms of rotation matrices[13]. $\mathfrak{D}(\alpha, \beta, \gamma)$ (the $(\alpha\beta\gamma)$ are the three Euler's angles). If $\mathbf{r}'$ represents the coordinates of the positron with respect to SF coordinate system, the transformed amplitude, $f(\hat{\mathbf{k}}.\hat{\mathbf{r}}')$, is employed to determine the rotationally inelastic transition amplitude under the ANA theory, i.e.,

$$f(\mathbf{i} \to \mathbf{f}) = \langle \mathbf{i} | f(\hat{\mathbf{k}}.\hat{\mathbf{r}}'; \alpha\beta\gamma) | \mathbf{f} \rangle,$$

where $|\mathbf{i}\rangle$ and $|\mathbf{f}\rangle$ are respectively the initial and final rotational eigenfunctions. The total elastic cross sections are obtained by summing over all final rotational states and averaging over all initial states. The expressions for the differential, integral and momentum transfer cross sections are given for general non-linear polyatomic molecules in Ref. 13.

In the present CH_4 case, we do not face any convergence problem in the summation over various angular momentum quantum numbers. In fact, even the DCS's can be obtained easily with proper convergence within a reasonable size of the scattering matrix. For more details about the actual numerical parameters we recommend our previous paper[29]. In the present results on the positron-CH_4 collisions, we have kept the same single-center expansion and K-matrix parameters as described in Ref. 29.

Jain and Thompson[29] used three different approximations for the polarization interaction; all the three models were exactly the same as employed for electron scattering[38-40]. However, the most successful was the one based on the second-order perturbation theory under the Pople Shofield method[41] in which the distortion in each molecular orbital is the same. The non-adiabatic effects were included via the non-penetration criterion of Temkin[42]. This electron polarization potential[40] (to be denoted by JT) has so far been quite successful in positron-CH_4 collisions. Unfortunately, the JT potential has never been employed for any atomic system; however, it has been employed for the e^+-N_2 case[43] with fair success. The other two EPP used by Jain and Thompson[29] were based on the asymptotic form multiplied by the cut-off function. Although the use of non-penetrating scheme for the positron case may be questionable, however, we argue here that the non-adiabatic effects in e^+ case are not much effective due to relatively smaller local kinetic energy of the impinging positron in the vicinity of the target. Therefore, we emphasize here that in any polarised-orbital variational approach, the non-adiabatic correction may not be taken very seriously. In the findings of Elza et al[8], these non-adiabatic effects seem to change the results; however, it is hard to draw any conclusion since they introduce fitting parameters which makes physics less clear.

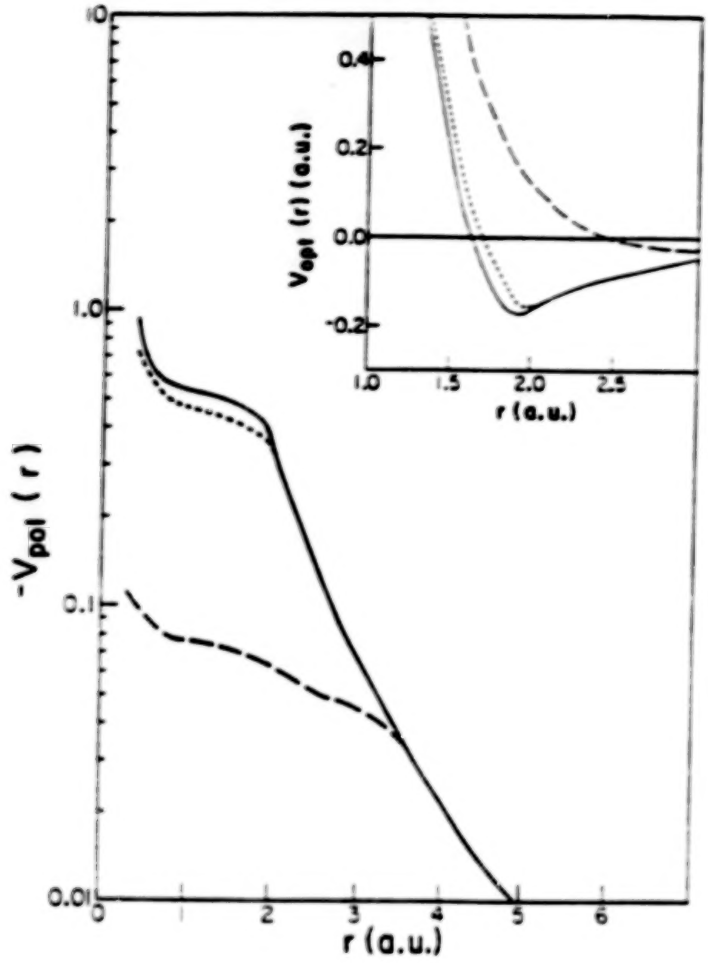

Fig. 1. Various polarization potentials for the e^-–Ar system. The potentials PCOP1, PCOP2 and ECOP are shown, respectively, by solid, dashed and long-dashed lines. The various notations are explained in the text. In the inset are shown the total optical potentials (sum of repulsive static and attractive polarization potentials) with various models: solid line. $V_{st} - V_{pol}^{PCOP2}$; dashed line. $V_{st} - V_{pol}^{PCOP1}$; long-dashed line. $V_{st} - V_{pol}^{ECOP}$.

IV. **Results and Discussion**

First, we display the new PCOP terms in Fig. 1 for the e^-–Ar system. We have considered two forms of the PCOP model: one, the correlation potential defined by Eq. (6) (to be denoted by PCOP2) and two, the correlation energy itself (Eq. 3, to be denoted by PCOP1). Both the PCOP1 and PCOP2 terms are plotted in Fig. 1. Also shown in this figure is the corresponding ECOP potential. We see a significant difference between the ECOP and PCOP curves. In general, the PCOP is stronger then the ECOP approximation. This simply means that the $e^- - e^-$ correlation energy is stronger, thus giving rise to a more attractive polarization potential. It seems realistic since the e^- is expected to distort the target charge cloud deeper due to strong correlation of electron and positron particles. A similar situation exists for molecular targets (CO and CH_4) (not shown).

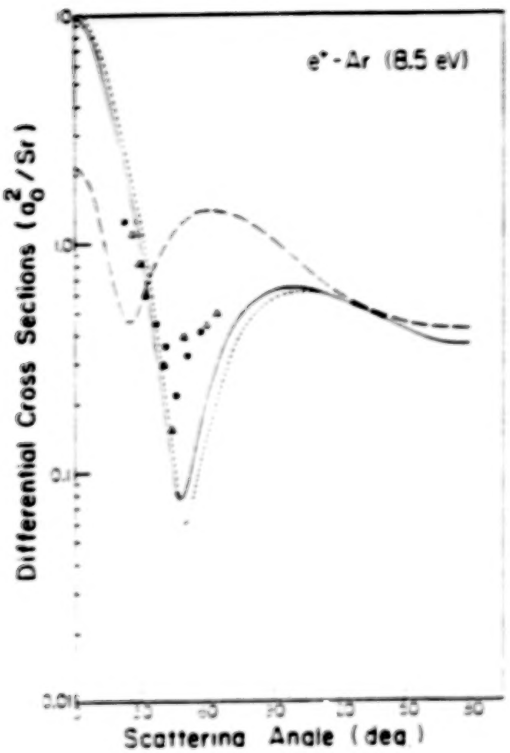

Fig. 2 Differential cross sections for the e^-–Ar elastic collision at 8.5 eV. Present theory: solid curve, PCOP2 model: dashed curve, PCOP1 model: long-dashed curve, ECOP model. The experimental points are taken from Refs. 44 and 45.

The total optical potential shown in the inset of Fig. 1 is a sum of repulsive static and attractive polarization terms; thus there is a zero–potential point and an attractive well. The position of the zero–point potential and the shape of the attractive well decide the penetration and sign of various partial waves. Here the role of polarization interaction is important and the low–energy scattering is strongly influenced by these cancellation effects not present in the electron scattering case. Thus the form of the polarization potential in the zero–potential and the attractive well region is very crucial to determine the scattering process.

Fig. 2 illustrates the DCS for the e^-–Ar system at 8.5 eV alongwith the ECOP results and the measurements of Refs. 44–45. We see a significant qualitative improvement represented by these PCOP curves. The dip in the experimental DCS around 50^0 is neatly reproduced by the new model, while the ECOP dip occurs at smaller angle (30^0). We have not shown other calculations[46–49] due to their semi-empirical nature. We have seen similar agreement between theory and experiment at other energies (lower and higher than 8.5 eV) also[16]. In order to further see the success of the PCOP model at lower energies, we have calculated the scattering length in the zero energy limit. The value of the PCOP scattering length is −4.89 (au), which compares very well with the experimental value[50] of -4.4 ± 0.5 (au); the ECOP model gives this value only 1.7 (au). It is thus quite clear that in this low energy limit a true positron polarization interaction makes big difference in the scattering parameters.

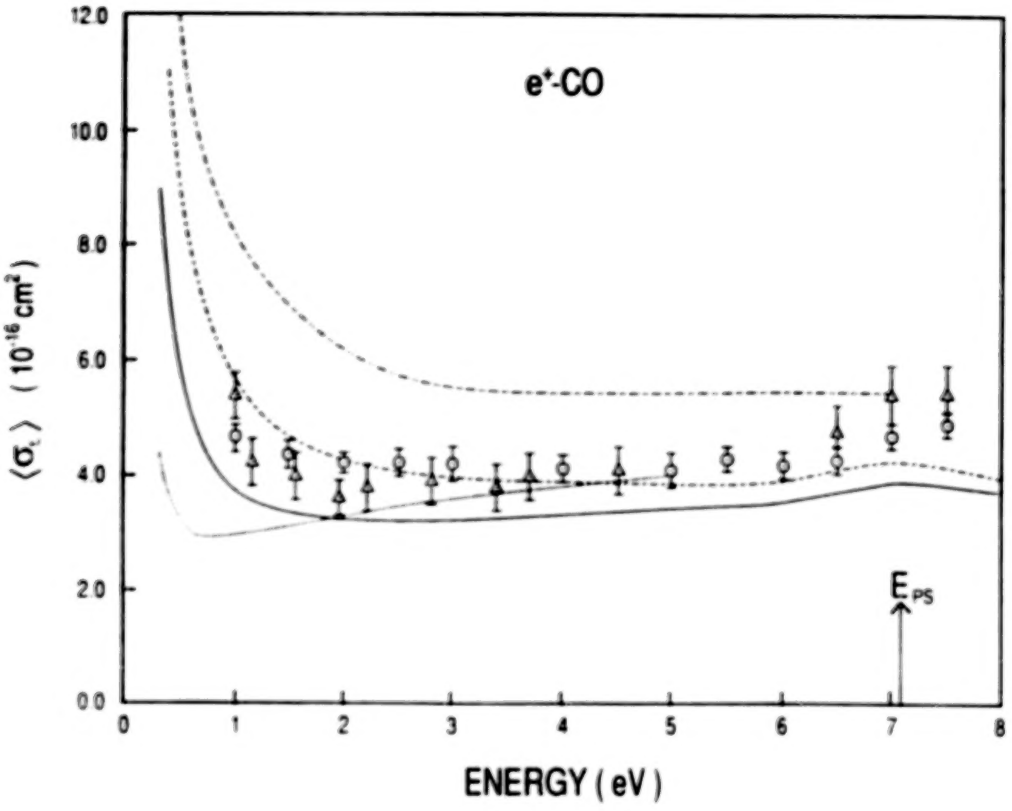

Fig. 3. Positron-CO (σ_t) cross sections in various theoretical models (including the R-matrix results[3], shown as dash-dot-dot curve) and experimental observations (circles, Kwan et al[51]: triangle, Sueoka and Mori[52]). Our PCOP results are shown using experimental value of the dipole moment (solid curve) and also the theoretical value of the dipole moment (dashed curve). The ECOP data[16] are plotted as the dotted curve.

We now discuss our e^+-CO calculations on the (σ_t) parameter. Fig. 3 shows the present PCOP (σ_t) alongwith the ECOP[28], R-matrix[4] and the experimental[51-52] results. We have shown two versions of the present PCOP (Eq. 6) model: one, with the present theoretical value of the dipole moment (D=0.099 a.u.), shown as dashed curve in Fig. 3 and two, by using the experimental value (D=0.044 au), shown as a solid line. Below 4 eV, the use of theoretical value of the dipole moment makes large changes in the (σ_t). The R-matrix results do not compare well with the measurements: one reason being that they employ their theoretical dipole moment value in the MEAN approximation and the second reason is related with their polarization force which still needs to be improved[53]. The inclusion of the polarization force makes large changes (about a factor of two or more) in the pure static results. It seems that the ECOP approximation is better at higher ($E \geq 2$ eV) energies; however, this conclusion may not be true as the two sets of DCS's differ significantly and we expect that the PCOP DCS's are better than the cooresponding ECOP cross sections [17].

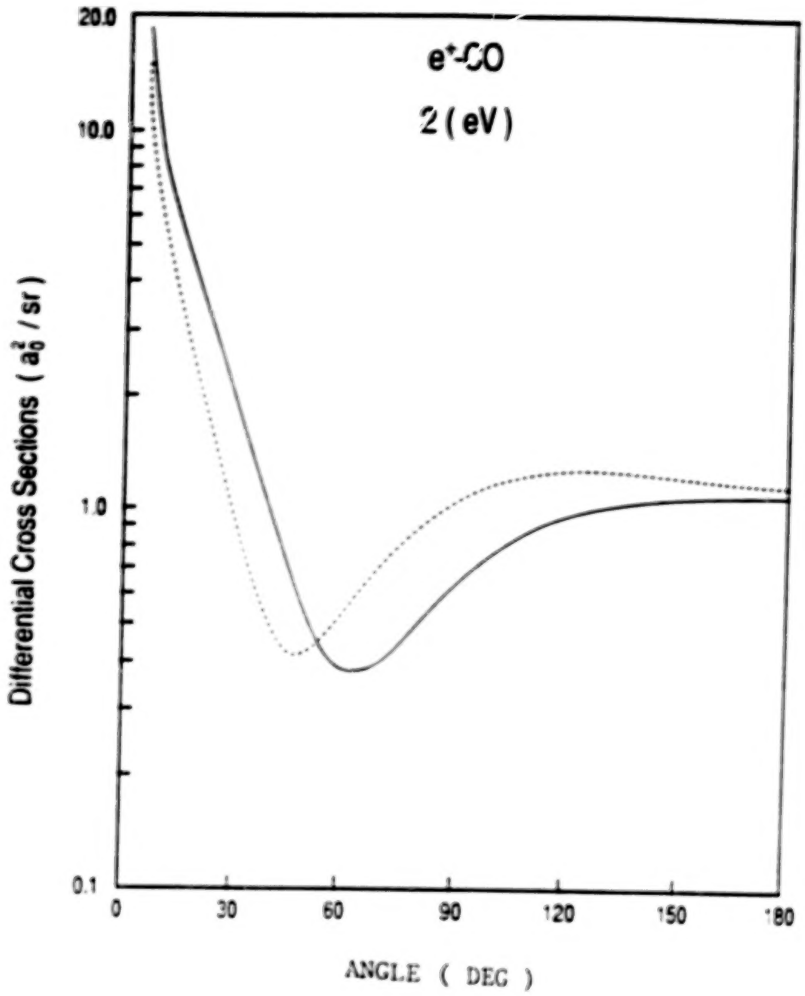

Fig. 4. Positron–CO DCS at 2 eV in the PCOP (solid curve) and ECOP (dashed curve)[26] polarization models.

In order to see the qualitative differences between the ECOP and PCOP models for the positron collisions with CO molecules, we have shown in Fig. 4, the differential cross sections at 2 eV. We see a qualitative difference between the two curves of Fig. 4 . The dip in the ECOP approximation occurs at lower angles while the PCOP dip in the DCS's curve occurs at somewhat larger angles; the difference between the positions of the two dips is about 20^0. The disagreement between these two polarization model is seen at all angles (Fig. 4). It is interesting to note that the total cross sections at this energy is almost same in both the PCOP and ECOP approximations. Thus, the integral cross sections are sometimes confusing and therefore a theoretical model should be judged from the angular functions which are more sensitive to model potential results. It would be very interesting to see the position of the dip in an experimental investigation. So far, we believe that the PCOP dip is more realistic.

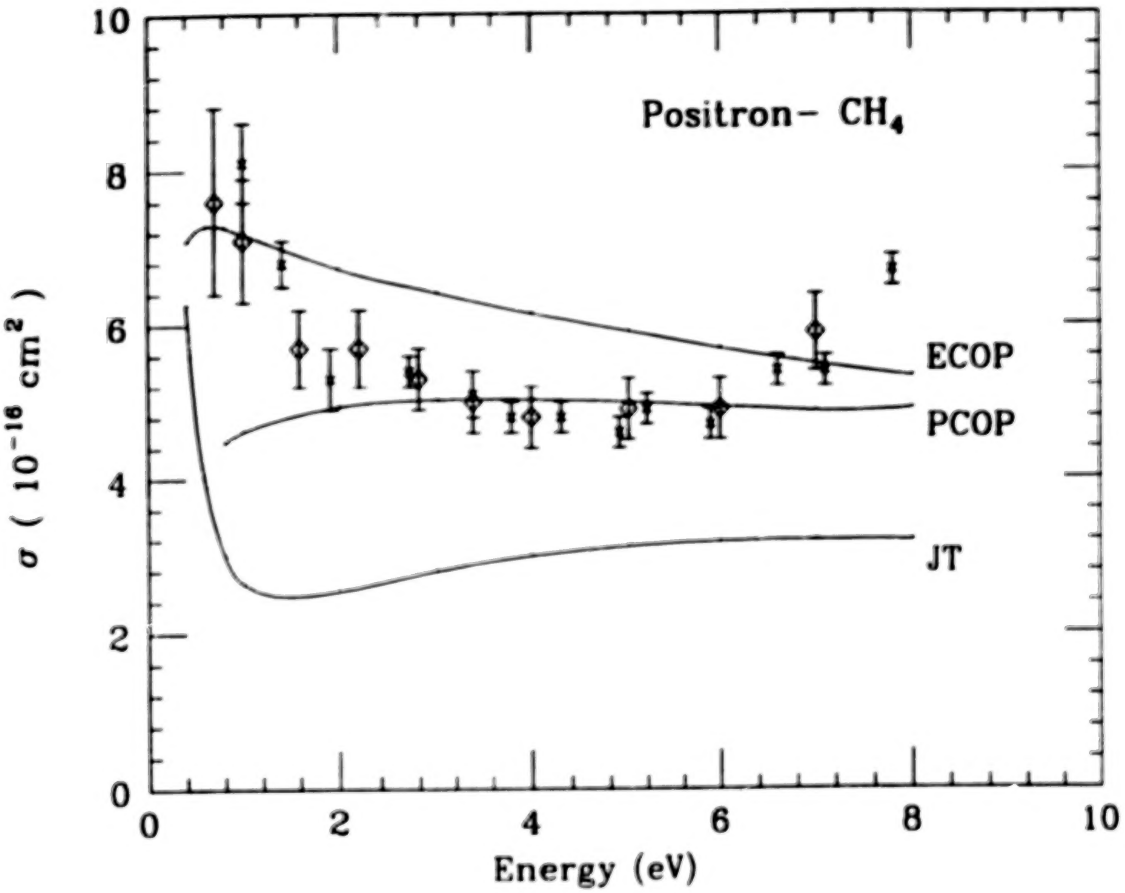

Fig. 5. The positron–CH_4 σ_t cross sections using the PCOP , ECOP[28] and JT[29] theoretical models. All the curves are labelled with respect to all these approximations. The experimental data are taken from Refs. 54 and 55.

From Fig. 3, we thus see that the PCOP model is quite successful in reproducing the experimental data, particularly at low energies where the ECOP calculations totally fail. At higher energies (above 3 eV) where the ECOP approximation seems to work well, the difference between the two sets of DCS is significant (see Fig. 4); for example, at 2 eV, the positions of the dips in the ECOP and PCOP curves occur at 40^0 and 50^0 angles respectively.

Right now there are no other DCS's (theoretical or experimental) available for comparison for the positron–CO elastic collisions. It would have been interesting to have a comparison between the PCOP and the R-matrix angular functions. It is possible that the DCS's for the positron–CO system be measured in the laboratory in future. Only then one can conclude finally about the usefulness of the PCOP model in the e^+–CO case. In passing, we would like to mention that at further lower energies (below 1 eV) the difference between various DCS calculations may be dramatic due to a stronger dependence of the collision dynamics on the polarization/correlation effects.

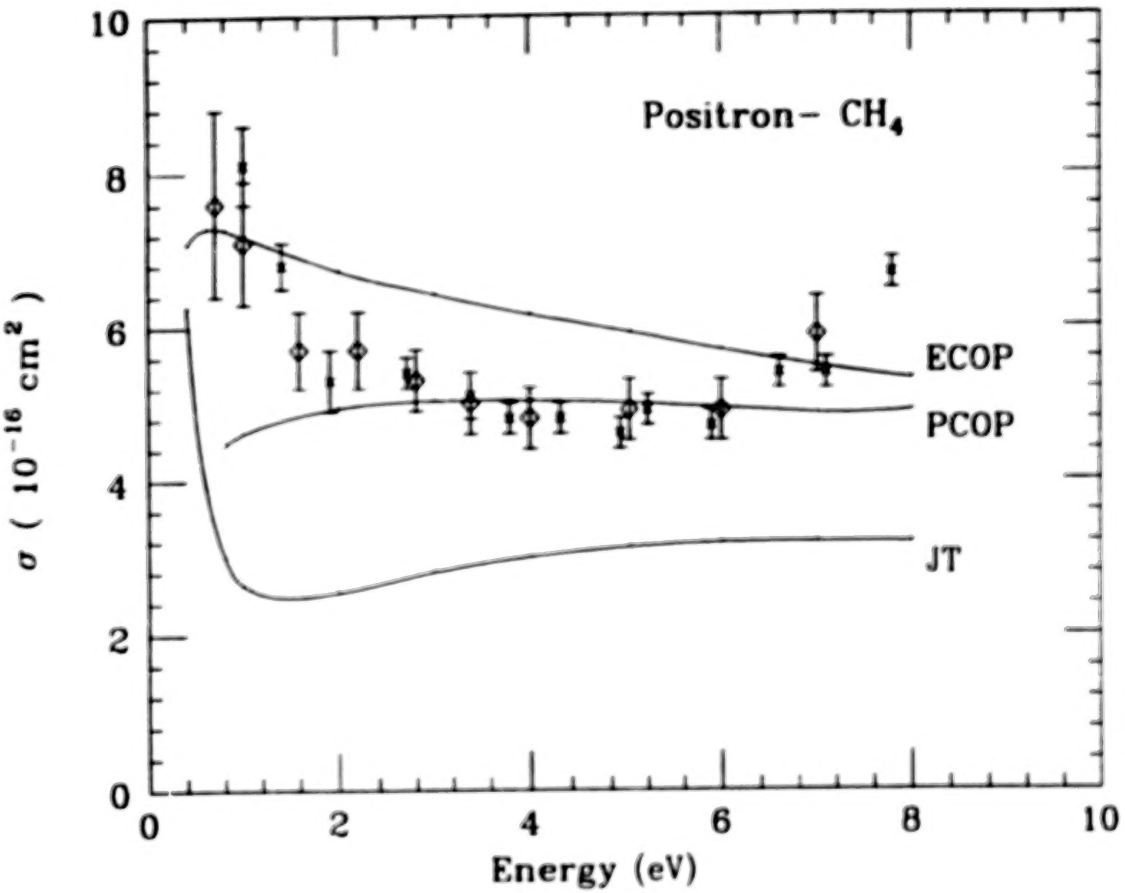

Fig. 5. The positron-CH_4 σ_t cross sections using the PCOP , ECOP[28] and JT[29] theoretical models. All the curves are labelled with respect to all these approximations. The experimental data are taken from Refs. 54 and 55.

From Fig. 3, we thus see that the PCOP model is quite successful in reproducing the experimental data, particularly at low energies where the ECOP calculations totally fail. At higher energies (above 3 eV) where the ECOP approximation seems to work well, the difference between the two sets of DCS is significant (see Fig. 4); for example, at 2 eV, the positions of the dips in the ECOP and PCOP curves occur at 40^0 and 50^0 angles respectively.

Right now there are no other DCS's (theoretical or experimental) available for comparison for the positron–CO elastic collisions. It would have been interesting to have a comparison between the PCOP and the R-matrix angular functions. It is possible that the DCS's for the positron–CO system be measured in the laboratory in future. Only then one can conclude finally about the usefulness of the PCOP model in the e^+–CO case. In passing, we would like to mention that at further lower energies (below 1 eV) the difference between various DCS calculations may be dramatic due to a stronger dependence of the collision dynamics on the polarization/correlation effects.

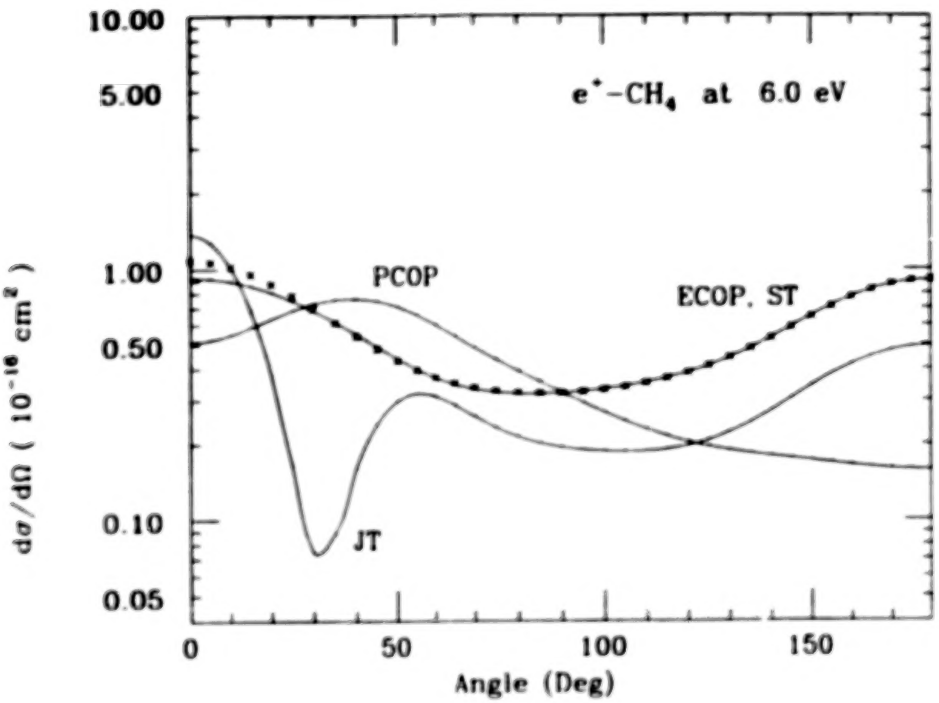

Fig. 6. DCS's for the e^+–CH_4 collisions at 6 eV using the PCOP, ECOP and JT[29] models for the polarization potential. The points (–) are the static only results.

Finally, in Fig. 5, we demonstrate our e^+–CH_4 σ_t values along with experimental points. Also shown in this Fig. 4 are the calculations using EPP models of Jain and Thompson[29] and Gianturco et al[28]. The measured data are taken from Dababneh et al[54] and Sueoka and Mori[55]. Again we see that the new PCOP gives very encouraging results as compared to other theoretical models based on the EPP. However, if we look into the corresponding DCS (Fig. 6) at 6 eV, the three models give totally different type of results. We need experimental data on the DCS in order to see which polarization approximation describes the collision properly. It is clear from Fig. 6 that even if there is some agreement in the total cross sections, the DCS's may be quite different both in quality and quantity.

V. Conclusions

We conclude that a true positron polarization approximation is essential to investigate the low–energy positron collisions with atoms and molecules. Even if the EPP and PCOP total cross sections are identical, the DCS differ significantly. We are in the process to test the sensitivity of the Z_{eff} parameter with respect to EPP and PCOP polarization models. We mention here that in the positron scattering, the question of nonadiabaticity may not be as serious as in the case of

electron collisions: the reason being that the positron being repelled by the nucleus of the target is not speeded up in the vicinity of the target; thus reducing the non-adiabatic effects.

In this article, we have discussed a new parameter-free positron polarization potential which is obtained by short range $\epsilon^+ - \epsilon^-$ correlation energy and the correct long range behaviour of the polarization potential. It should be realized that the inclusion of correlation/polarization effects in positron collisions is a very hard problem. In model approaches, such as the one discussed here, one has to compromise with the local and energy-dependent form of the polarization against its non-local and non-adiabatic nature. The use of model polarization potentials will still continue due to their simplicity and significant success even at the DCS level. We emphasize that all the positron polarization models should be tested with respect to differential cross sections and the very low energy parameters such as the scattering length and the annihilation paremeter.

Acknowledgement

Some useful discussion with Jonathan Tennyson about his R-matrix calculation is thankfully acknowledged. We thank the Florida State University Computing Center for providing supercomputer time. We acknowledge the support by the Florida State University Supercomputer Computations Research Institute which is partially funded by the U.S. Department of Energy through Contract No. DE-FC05-85ER250000.

REFERENCES

1. Morrison M A, Gibson T L and Austin D, J. Phys.B: At. Mol. Phys. **17**, 2725 (1984)
2. Morrison M A, *Proc 3rd Int. Conf. on Positron(Electron) Gas scattering* eds. Kauppila et al (World Scientific, Singapore, 1986) p. 100
3. Tennyson J, J. Phys. B: AT. Mol. Phys., **19**, 4255 (1986)
4. Tennyson J and Morgan L, J. Phys. B: At. Mol. Phys. **20**, L641 (1987)
5. Tennyson J and Danby G , *Atomic Physics with Positrons* eds. J. W. Humberston (Plenum, New York 1987) p. 111
6. Armour E A G , Phys. Rep. **169**, 1-98 (1988)
7. Barschat K, McEachran R P and Stauffer A D, J. Phys. **B21**, 2789 (1988)
8. Elza B K, Gibson T L, Morrison M A and Saha B C , J. Phys. **B22**: At. Mol. Phys., 113 (1988)
9. Abdel - Raouf M A, Acta Phys. Hungarica, **63**, 21 (1988)
10. Armour E A G, Phys. Rep., **169** , 1 (1988)
11. Jain A, Proc. 3rd. Int. Conf. on " Positron (Electron)-Gas Scattering ", Eds. Kauppila et al (World Scientific, Singapore 1986)
12. Jain A, Proc. 4th Int. Conf. on " Atomic Physics with Positrons ", Eds Humberston and Armour (Plenum, NY 1987)
13. Gianturco F A and Jain A, Phys. Rep., **143**, 347 (1986)
14. Darewych J W, J. Phys. B: At. Mol. Phys. **15**, L415 (1982)
15. Horbatsch M and Darewych J W, J. Phys. B: At. Mol. Phys. **16**, 4059 (1983)
16. Jain A, Phys. Rev. **A39** (in press, August 1989)
17. Jain A, J. Phys. B: At. Mol. Phys., (in press, 1989)
18. O'Connel J O and Lane N F, Phys. Rev. **A27**, 1893 (1983)

19. Sjolander S and Scott M J,Solid State Comm. **8**, 1881 (1970)
20. Sjolander S and Scott M J, Phys. Rev **B5**, 2109 (1972)
21. Hodges C H and Scott M J, Phys. Rev. **B7**, 73 (1973)
22. Arponen J and Pajanne E, Ann. Phys. **121**, 343 (1979)
23. Boronski E and Nieminen R M, Phys. Rev. **B34**, 3820 (1986)
24. Kallio A, Pietilanen P and Lantto L J, Phys. Scr. **25**, 943 (1982)
25. Kohn W and Sham L J, Phys. Rev. **140**, A1133 (1965)
26. Jain A, J. Phys. B: At. Mol. Phys. **B19**, L105–L110 (1986)
27. Jain A, J. Phys. B: At. Mol. Phys. **B19**, L379–L384 (1986)
28. Gianturco F A, Jain A and Pantano L C, Phys. Rev. **A36**, 4637 (1987)
29. Jain A and Thompson D G, J. Phys. B: At. Mol. Phys. **16** 1113 (1983)
30. Calogero F, " Variable Phase Approach to Potential Scattering", (New York, 1973)
31. Jain A, Phys. Rev. **A34**, 3707 (1986)
32. Karim K R and Jain A, Phys. Scripta, **39**, 238 (1989)
33. Morrison M A, Lane N F and Collins L A, Phys. Rev. **A15**, 2186 (1977)
34. Burke P G, Chandra N and Gianturco F A, J. Phys. **B3** 641 (1974)
35. Collins L A and Norcross D W, Phys. Rev. **A18**, 478 (1978)
36. Norcross D W and Padial N T, Phys. Rev. **A25**, 226 (1982)
37. Jain A, Ph.D thesis, The Queen's University, Belfast (1983)
38. Gianturco F A and Thompson D G, J. Phys. **B9**, L383 (1976)
39. Gianturco F A and Thompson D G, J. Phys. **B13**, 613 (1980)
40. Jain A and Thompson D G, J. Phys. **B15**, L631 (1982)
41. Pople J A and Shofield P, Phil. Mag., **2**, 591, (1957)
42. Temkin A, Phys. Rev. **107**, 1004 (1957)
43. Gillespie E S and Thompson D G, J. Phys. **B8**, 2858 (1975)
44. Coleman P G, McNutt J D, Phys. Rev. Lett. **42**, 1130 (1979)
45. Floeder K, Honer P, Raith W, Schwab A, Sinapius G and Spicher G, Phys. Rev. Lett. **23**, 2363 (1987)
46. Nakanishi H and Schrader D M, Phys. Rev. **A34**, 1823 (1986)
47. McEachran R P, Ryman A G and Stauffer A D, J. Phys. **B12**, 1031(1979)
48. Schrader D M, Phys. Rev. **A20**, 918 (1979)
49. Datta S K, Mandal S K, Khan P and Ghosh A S, Phys. Rev. **A32**, 633 (1985)
50. Lee G F and Jones G, Cand. J. Phys. **52**, 17 (1974)
51. Kwan Ch K, Hsieh Y F, Kauppila W E, Smith S J, Stein T S , Uddin M N and Dababneh M S 1983, Phys. Rev. **A27**, 1328
52. Sueoka O and Mori S, J. Phys. Soc. Japan **53**, 2491 (1984)
53. Tennyson J, private communication
54. Dababneh M S, Hseih Y -F, Kauppila W E, Kwan C K, Smith S J Stein T S and Uddin M N, Phys. Rev. **A38**, 1207 (1988)
55. Sueoka O and Mori J, J. Phys. **B19**, 4035 (1986)

THE CALCULATION OF THE CONTRIBUTIONS TO LOW ENERGY e^+H_2 SCATTERING FROM Σ_u^+ and Π_u SYMMETRIES USING THE KOHN VARIATIONAL METHOD

E. A. G. Armour, D. J. Baker† and M. Plummer
Mathematics Department, University of Nottingham, Nottingham NG7 2RD, England
†Rutherford Appleton Laboratory, Chilton, Didcot, Oxfordshire OX11 0QX, England

Abstract

Above incident energies of about 2 eV, the contribution to the total cross section in e^+H_2 scattering from the Σ_g^+ symmetry is insufficient to account for the experimental value. We describe calculations we have carried out of the lowest partial waves of Σ_u^+ symmetry and Π_u symmetry using the Kohn variational method. The contributions to the total cross section from the two equivalent partial waves of Π_u symmetry significantly reduce the discrepancy with experiment up to incident energies of 4–5 eV. Comparisions are made with recent *R*-matrix calculations performed by Danby and Tennyson[1].

Introduction

For incident energies up to about 2 eV, the contribution to the total cross section in e^+H_2 scattering from the lowest partial wave of Σ_g^+ symmetry is sufficient to account for the experimental value provided Hylleraas-type functions, containing the positron-electron distance as a linear factor, are included in the Kohn trial function[2]. The lowest partial wave of Σ_g^+ symmetry is the analogue of the s-wave in positron or electron-atom scattering. The next symmetries from which significant contributions may be expected as the energy increases above 2 eV are the Σ_u^+ and Π_u symmetries. The lowest partial waves of these symmetries are the analogue of the p-wave in positron or electron-atom scattering. The decrease in symmetry in changing from an atomic target such as H or He to H_2 splits the p-wave between the two symmetries: the $m = 0$ component is included in the Σ_u^+ symmetry, whereas the $m = \pm 1$ component is included in the Π_u symmetry.

The asymptotic effective potential between the target hydrogen molecule and an incident positron is of the form

$$V(\boldsymbol{r}) \underset{r\to\infty}{\sim} \frac{QP_2(\cos\theta)}{r^3} - \frac{\alpha_0}{2r^4} - \frac{\alpha_2 P_2(\cos\theta)}{2r^4} \qquad (1)$$

r and θ are spherical coordinates of the positron measured from the nuclear centre of mass, with the z-axis along the nuclear axis. Q is the quadrupole moment of the hydrogen molecule. The first term in (1) is the asymptotic form of the static potential, first order in the interaction between the positron and the target. The other terms are of second order. α_0 and α_2 are respectively the spherical and non-spherical dipole polarisabilities of the hydrogen molecule, and are linear combinations of $\alpha_\parallel$ and $\alpha_\perp$, the dipole polarisabilities parallel and perpendicular to the nuclear axis. In second order perturbation theory, the expressions for $\alpha_\parallel$ and $\alpha_\perp$ are made up of contributions from virtual excitations to states of Σ_u^+ and Π_u electronic symmetry respectively[3].

The Σ_g^+ partial wave trial function used in reference 2 did not include functions with the correct asymptotic form to deal with the long-range polarisation of the molecule. However, there is evidence from Kohn calculations of e^+H and e^+He scattering that short-range exponentially decaying trial functions are adequate in the case of the s-wave except in the vicinity of zero energy[4,5]. It is reasonable to expect that this will be the case for Kohn calculations of the lowest partial wave of Σ_g^+ symmetry in e^+H_2 scattering. There is no centrifugal barrier[6] and the phase shift is determined by the positron–molecule interaction at all separations and not just when the positron is far from the molecule.

This is not the case for higher partial waves which experience centrifugal barriers. For sufficiently low incident energies long-range behaviour dominates and the phase shifts for these partial waves may be obtained from the first Born approximation[7] using the asymptotic potential (1). Armour and Plummer[8] show for e^+H_2 scattering that the correct behaviour of the phase shifts at very low energies follows naturally from the Kohn equations if the trial function includes long-range polarisation functions of the correct form.

Several authors[5,9,10] have reported poor convergence of p-wave phase shifts at low incident energies (incident wave number $k = 0.1\,a_0^{-1}, 0.2\,a_0^{-1}$) in Kohn calculations of e^+H and e^+He scattering that did not include long-range polarisation functions in the trial function. Armour[11] found similar behaviour at low energies in a Kohn

calculation of the lowest partial wave of Σ_u^+ symmetry in e^+H_2 scattering that took no account of long-range polarisation. The trial functions for the present calculations of the lowest partial waves of Σ_u^+ and Π_u symmetries include long-range polarisation functions, separable correlation functions of Σ_g^+, Σ_u^+, Π_u and Π_g electronic symmetries, and Hylleraas-type functions, important at higher energies ($k > 0.1\,a_0^{-1}$) for taking into account short-range interactions between the positron and the target electrons.

The Calculations

The calculations are extensions of the earlier calculations[2,11]. Prolate spheroidal coordinates are employed in the fixed nuclei model and the open channel functions are made up of solutions to the free-particle equation in this coordinate system appropriate to the lowest partial waves of Σ_u^+ symmetry and Π_u symmetry, respectively. With Ψ_G the model H_2 ground-state wave function, the correlation functions are of the form

$$N(\lambda_1^{a_i}\lambda_2^{b_i}\mu_1^{c_i}\mu_2^{d_i}[M_1\cos(\phi_1-\phi_3)]^{p_i}[M_1\cos\phi_1]^{q_i}r_{13}^{t_i} + \lambda_2^{a_i}\lambda_1^{b_i}\mu_2^{c_i}\mu_1^{d_i}[M_2\cos(\phi_2-\phi_3)]^{p_i}[M_2\cos\phi_2]^{q_i}r_{23}^{t_i})e^{-\beta(\lambda_1+\lambda_2)}f_i(3)\Psi_G. \qquad (2)$$

Coordinates 1 and 2 represent the electrons and coordinates 3 represent the positron, and

$$f_i(3) = \begin{cases} \lambda_3^{r_i}\mu_3^{s_i}e^{-\alpha\lambda_3}M_3^{p_i}[M_3\cos\phi_3]^{w_i} & \text{(separable and Hylleraas functions),} \\ \left.\begin{matrix}\sin c\lambda_3 \\ \text{or} \\ \cos c\lambda_3\end{matrix}\right\} \frac{}{\lambda_3^{r_i}}(1-e^{-\gamma(\lambda_3-1)})^{w_i}\mu_3^{v_i}(M_3)^{p_i}\left[\frac{M_3\cos\phi_3}{\lambda_3}\right]^{w_i} & \text{(polarisation functions).} \end{cases}$$

$$M_i = [(\lambda_i^2-1)(1-\mu_i^2)]^{\frac{1}{2}}.$$

a_i, b_i, c_i, d_i, p_i, q_i, r_i, s_i, t_i, u_i, v_i and w_i are non-negative integers and α, β, γ and N are constants. $c = \frac{1}{2}kR$, with R the nuclear separation. r_{13} is the separation between electron 1 and the positron.

For overall Σ_u^+ symmetry, $c_i + d_i + s_i$ is odd and $q_i = u_i = 0$. The Hylleraas functions have $p_i = 0$, $t_i = 1$ and the separable and polarisation functions have $t_i = 0$, $w_i = 1$, $v_i = 2$, $p_i = 0$ or 1. For the Π_u calculation $c_i + d_i + s_i$ is even. The Hylleraas functions have $p_i = q_i = 0$, $t_i = u_i = 1$, the separable and polarisation functions have $t_i = 0$, $w_i = 2$, $v_i = 1$. For the separable functions, three sets of values are used for p_i, q_i and u_i: $p_i = 0$, $q_i = 0$, $u_i = 1$, $p_i = 1$, $q_i = 0$, $u_i = 1$ and $p_i = 0$, $q_i = 1$, $u_i = 0$. The two sets of values with $q_i = 0$ are used for the polarisation functions. In both calculations the polarisation functions have either Σ_u^+ or Π_u electronic symmetry.

Discussion of Results

The Σ_u^+ wave calculation is described elsewhere[12]. We find that the low-energy ($k \leq 0.1\,a_0^{-1}$) behaviour is dominated by the polarisation functions: the Born approximation is approximately obeyed in this region although the phase shifts fall off slightly as k approaches $0.1\,a_0^{-1}$. For higher incident energies up to $k = 1.0\,a_0^{-1}$ the Hylleraas functions contribute most to the phase shifts, although the polarisation functions remain important. There is good agreement with eigenphase sums for the Σ_u^+ symmetry obtained by Danby and Tennyson[1] using the R-matrix method with a systematic treatment of intermediate and long-range polarisation using polarised pseudostates. Towards the top of the energy range the R-matrix eigenphase sums become increasingly larger than the Kohn phase shifts; this may be due to the fact that the Kohn calculation does not allow for mixing of partial waves. Both calculations predict that the contribution to the total scattering cross section from this symmetry is much too small to reduce significantly the discrepancy with experiment above 2 eV.

For the Π_u wave, the polarisation functions again dominate low energy behaviour and the Born approximation is followed for $k < 0.1\,a_0^{-1}$. Above $k = 0.1\,a_0^{-1}$ the polarisation functions have less influence. The phase shifts using separable and separable plus polarisation functions are slightly larger than the corresponding R-matrix eigenphase sums for the Π_u symmetry[1]. As in the case of the Σ_g^+ wave[2], the inclusion of the Hylleraas functions substantially boosts the calculated phase shifts. The discrepancy with the experimental total cross section is significantly reduced; adding together the contributions from the Σ_g^+, Σ_u^+ and the two equivalent Π_u partial waves gives totals that are comparable with the results of Hoffman et al[13] up to 4–5 eV.

AB INITIO R-MATRIX CALCULATIONS OF e^+ – MOLECULE SCATTERING

Grahame Danby and Jonathan Tennyson,
Department of Physics and Astronomy, University College London,
Gower St., London WC1E 6BT, England

ABSTRACT

The adaptation of the molecular R-matrix method, originally developed for electron–molecule collision studies, to positron scattering is discussed. *Ab initio* R-matrix calculations are presented for collisions of low-energy positrons with a number of diatomic systems including H_2, HF and N_2. Differential elastic cross-sections for e^+–H_2 show a minimum at about 45° for collision energies between 0.3 and 0.5 Ryd. Our calculations predict a bound state of e^+HF. Calculations on inelastic processes in N_2 and O_2 are also discussed.

INTRODUCTION

The first principles calculation of low-energy positron molecule collision parameters is an active area which has recently been reviewed by Armour[1]. The most accurate calculations have largely been confined to hydrogenic targets. Over the past few years we have been studying positron collisions from a variety of diatomic targets[2–7]. As we will show, these calculations have now reached the stage where they not only aim to reproduce experiment but have made a number of experimentally testable predictions.

METHOD

The R-matrix method has been successfully used for a number of years by Burke, Noble and coworkers to study low-energy electron molecule collisions, see Gillan *et al* [8] for a recent presentation of the theory. These calculations have been able to reproduce even subtle features of observed electron-molecule collisions.

The basis of the R-matrix method is the division of space into two regions. The internal region is contained in a sphere centred on the target molecule centre-of-mass. This sphere is assumed to entirely enclose the target charge distribution. Typically, and for all calculations discussed below, the sphere has a radius of 10 a_0.

For positron–molecule collisions, the potential in the internal region comprises the repulsive positron – nuclei terms and the attractive, multicentre positron–electron interaction. The latter is particularly difficult to represent accurately. In the external region, the potential has a simple multipolar form representing the static moments of charge distribution and the dipole polarisability of the target.

An advantage of the R-matrix method is that computations on the difficult internal region are performed independent of scattering energy. This is done because the finite sphere has the effect of discretising the continuum which is then represented by numerical functions. These functions in principle form a complete set but in practice are truncated at some collision energy 2–3 times the highest energy of interest. The numerical functions augment L^2 functions, Slater Type Orbitals, which are used represent the target and to carry short range polarisation effects.

The R-matrix method of electron–molecule scattering has been extended to allow parallel studies for positron impact. Modifications consists of altering the signs of the relevant Coulomb integrals, neglecting exchange with target electrons and allowing the positron to occupy filled electron spinorbitals. In the internal region short and intermediate range polarisation effects are treated, respectively, by allowing single electron excitations of the target and by the introduction of polarised pseudostates. The asymptotic form of the polarisation potential is adopted for the outer region. Details of the implementation

of the R-matrix method for positron scattering calculations can be found in refs. 2 and 6.

RESULTS

Hydrogen molecule

Positron–H_2 calculations have been the subject of a series of studies by Armour and co-workers[1]. The best of these calculations are of high accuracy using explicit functions of the $e^- - e^+$ coordinates, so called Hylleraas functions, to give a good representation of electron–positron correlation, usually described as target polarisation effects. These calculations form a benchmark against which other methods can be tested.

We have recently completed a study of low-energy e^+–H_2 collisions[6]. These calculations tested several target representations, the best being one which recovered about 90% of the H_2 correlation energy. Methods of including short-, long- and intermediate-range polarisation effects were studied. These calculations showed that our short-range polarisation was not sufficient for the lowest Σ_g^+ symmetry but gave a good representation of higher symmetries. This enabled us to calculate differential cross sections for elastic e^+-H_2 collisions, an example of which is given below.

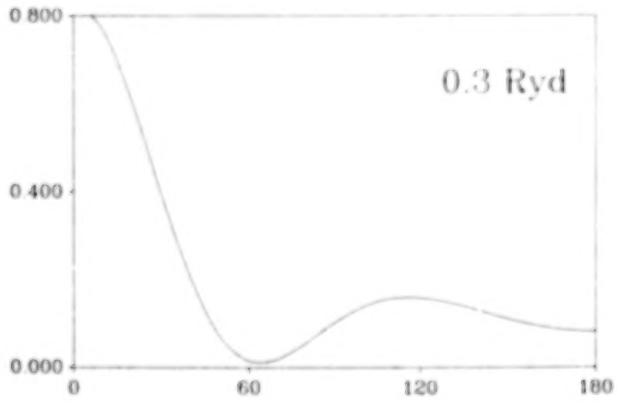

Fig. 1 Differential cross section, in a_0^2 sr^{-1}, for e^+–H_2 collisions[6].

These differential cross sections are of interest because they show a pronounced structure with a minimum in the cross section for all but the lowest energies. For scattering energies above 0.3 Ryd and below the positronium formation threshold this minimum is in the 40° – 60° region. Such minima have been predicted for e^+ - Noble gas systems but have yet to be confirmed experimentally.

Hydrogen fluoride

The collisions of low-energy electrons with polar molecules have caused considerable recent interest because of the observation of sharp spikes, particularly in vibrational excitation cross sections, for a number of these systems. It is now generally accepted that these spikes are caused by resonances associated with ro-vibrationally excited states of a very weakly bound negative ion of the system in question. A well studied[9] example of such systems is e^-–HF.

Of course for positron scattering any corresponding series of resonances would have immediate consequences for positron annihilation rates. A number of systems have been observed to have unusually high values of Z_{eff} [10], several of which are molecules with a large dipole moment. R-matrix positron scattering calculations on HF do indeed reveal the presence of a weakly bound state[5].

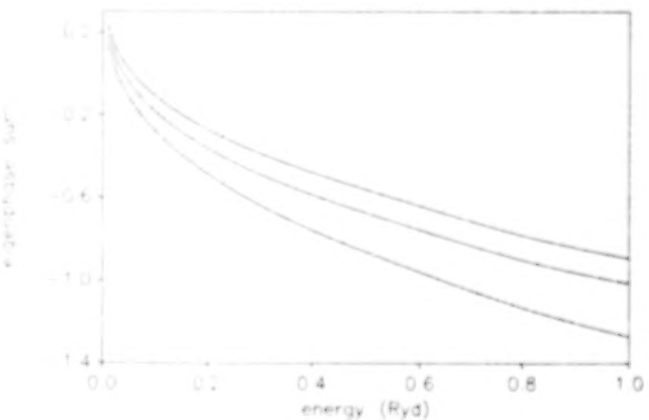

Fig. 2 Eigenphase sums for e^+-HF scattering with Σ_g^+ symmetry as a function of the degree of polarisation included in the calculation.

Since the publication of these calculations a programming error in our code has come to light[6]. This error only affects the inclusion of short range polarisation in our calculations and does not alter our conclusion that the e^+HF system supports a bound state. Above we give corrected eigenphase sums for scattering at the equilibrium HF geometry of 1.733 a_0. These eigenphase sums are, in order of increasing value, for static, static plus Σ polarisation and static plus Σ and Π polarisation models. These models are

analogous to those of Danby and Tennyson (1988).

For all models the HF eigenphase sums show a pronounced threshold peak characteristic of the presence of a bound state. Confirmation of a bound state can be obtained by searching the complex k plane to find a pole in the S-matrix (Morgan and Burke 1988). This analysis showed e^+HF to be bound by 1.4 $\times 10^{-9}$ Ryd in the static model and 3.1 $\times 10^{-9}$ Ryd in the $\Sigma + \Pi$ polarisation model. Adding further polarisation increases the binding energy to 3.3 $\times 10^{-9}$ Ryd.

Other systems

Calculations have been performed for scattering off a number of other diatomic targets such CO[3,4], N_2 [2,4,7] and F_2. These calculations have explored not only elastic effects, such as those discussed above, but also inelastic processes. The e^+ – CO calculations considered rotational excitation. Studies of vibrational excitation of N_2, of importance for the thermalisation of positrons in air, are nearing completion. Finally we have embarked on a study of electronic excitation effects in e^+ – O_2 collisions, a system for which unusual phenomena have already been observed experimentally[11].

CONCLUSIONS

Several positron – diatom collision systems have now been studied using the R-matrix method. These calculations have been shown to be capable of making firm predictions that are experimentally verifiable. It is clear that the calculations suffer from a weakness in that they uniformly underestimate the contribution due to the correlated positron – electron motions. This short range polarisation effect is most important at very low energies and for the penetrating s wave. Comparisons with H_2 calculations suggest that our calculations on symmetries higher than Σ_g^+ are not sensitive to this omission.

None of the calculations presented here made allowance for a positronium exit channel. This means that their range of validity is restricted to below the positronium formation threshold which occurs at a few eV for most molecules. Extension of our calculations into this region presents a formidable challenge, but one which is ripe for a concerted attempt to tackle.

Acknowledgements

We wish to thank Lesley Morgan and Charles Gillan for much practical advice during the course of this work. Stimulating discussions with Edward Armour and Martin Plummer are also gratefully acknowledged.

References

[1] E.A.G. Armour, Phys. Rep. **169**, 1 (1988).

[2] J. Tennyson, J. Phys. B **19**, 4255 (1986).

[3] J. Tennyson and L.A. Morgan, J. Phys. B **20**, L641 (1987).

[4] J. Tennyson and G. Danby, in *"Atomic Physics with Positrons"*, edited by E.A.G. Armour and J.W. Humberston, NATO Advanced Study Institutes Series B, Vol. 169 (Plenum, New York, 1988), p111.

[5] G. Danby and J. Tennyson, Phys. Rev. Lett. **61**, 2737 (1988).

[6] G. Danby and J. Tennyson, J. Phys. B (submitted).

[7] G. Danby and J. Tennyson, J. Phys. B (to be submitted).

[8] C. Gillan, O. Nagy, P.G. Burke, L.A. Morgan and C.J. Noble, J. Phys. B **20**, 4585 (1987).

[9] L.A. Morgan and P.G. Burke, J. Phys. B **21**, 2091 (1988).

[10] G.R. Heyland, M. Charlton, T.C. Griffith and G.L. Wright, Can. J. Phys. **60**, 503 (1982).

[11] Y. Katayama, O. Sueoka and S. Mori, J. Phys. B **20**, 1645 (1987).

NUMERICAL GREEN'S FUNCTIONS IN OPTICAL POTENTIAL CALCULATIONS FOR POSITRON SCATTERING FROM ARGON AND NEON

K. Bartschat†, R. P. McEachran‡ and A. D. Stauffer‡
†Department of Physics and Astronomy, Drake University,
Des Moines, Iowa 50311, U.S.A.
‡Physics Department, York University, Toronto, Canada M3J 1P3

ABSTRACT

We have applied an optical potential method to the calculation of positron scattering from the noble gases in order to determine the effect of open excitation channels on the shape of differential scattering cross sections.

THEORY

In positron–atom scattering the usual close-coupling expansion for the total wavefunction in terms of the sum of products of the bound-state wavefunctions of the target atom and the one-projectile scattering wavefunctions leads to the following set of integro-differential equations for the radial parts F_i of the scattering wavefunctions:

$$\left(\frac{\mathrm{d}^2}{\mathrm{d}r^2} - \frac{l_i(l_i+1)}{r^2} + k^2\right) F_i(r) = 2 \sum_j V_{ij}(r)\, F_j(r) \qquad (1)$$

Here the potential terms V_{ij} are given by

$$V_{ij}(r) = \frac{Z}{r}\,\delta_{ij} - \sum_{k=1}^{N} \left\langle \Phi_i \left| \frac{1}{|\mathbf{r}_k - \mathbf{r}|} \right| \Phi_j \right\rangle \qquad (2)$$

and the Φ_i are the bound-state wavefunctions of the N-electron target.

In practice only a finite number of bound target states can be included in the close-coupling expansion. Hence, we approximate the effect of the higher discrete target states as well as the ionization continuum by means of an optical potential. We divide the space of scattering functions into P- and Q-spaces. We choose for the P-space the elastic channel only and thus the Q-space contains all inelastic channels. In the Q-space we neglect all couplings between different channels but retain the couplings between the P- and Q-spaces. Thus our method requires the solution of the inhomogeneous differential equation

$$\left(\frac{\mathrm{d}^2}{\mathrm{d}r^2} - \frac{l_i(l_i+1)}{r^2} - 2\,V_{ii}(r) + k_i^2\right) F_i(r) = 2\,V_{i0}(r)\,F_0(r) \qquad (3)$$

for the radial functions F_i belonging to the Q-space. Here F_0 is the P-space (elastic) channel wavefunction. In our previous work[1] we ignored the diagonal term V_{ii} above and solved equation (3) by means of the free-particle Green's function involving the standard Riccati-Bessel functions.

In either case the solution to equation (3) can be written as

$$F_i(r) = -2 \int_0^\infty \mathrm{d}r'\, G_i(r,r')\, V_{i0}(r')\, F_0(r') \qquad (4)$$

where the Green's function $G_i(r,r')$ is given by

$$G_i(r,r') = \frac{1}{k_i}\, f_{l_i}(k_i r_<)\, [g_{l_i}(k_i r_>) + i\, f_{l_i}(k_i r_>)] \qquad (5)$$

The functions f_l and g_l are the regular and irregular solutions of equation (3) with the right-hand-side put to zero.

Upon substitution of equation (4) into the P-space form of equation (1) we obtain

$$\left(\frac{\mathrm{d}^2}{\mathrm{d}r^2} - \frac{l(l+1)}{r^2} - 2\,V_{00}(r) + k^2\right) F_0(r) = -\,U_{00}^{\mathrm{opt}}(r)\,F_0(r) \qquad (6)$$

where the optical potential is given by

$$U_{00}^{\mathrm{opt}}(r)\,F_0(r) = 4 \sum_{i \neq 0} \int_0^\infty \mathrm{d}r' V_{0i}(r)\, G_i(r,r')\, V_{i0}(r')\, F_0(r') \qquad (7)$$

The real part of the optical potential represents polarization while the imaginary part represents absorption due to the inelastic channels.

When the V_{ii} are ignored, f_l and g_l are the Riccati-Bessel functions.[1] However, if we retain the diagonal potentials in equation (3), then f_l and g_l have to be found by a numerical solution of the homogeneous differential equation.

RESULTS

We have extended our previous work on argon[1] by using the numerical Green's functions in the optical potential. We have also carried out similar calculations for positron scattering from neon.

The overall effect of retaining the diagonal potentials and hence using numerical Green's functions is quite small, i.e. of the order of a few percent of the differential cross sections at all angles.

The results of using optical potentials for positron–neon scattering yields cross sections whose behaviour is very similar to that of argon. In particular, the distinct minimum in the differential cross section which we obtained in our previous polarized-orbital calculations[2] is no longer present when the optical potential is used. Below we present some typical results for positron scattering from argon and neon.

Figure 1 illustrates the differential cross section for positron scattering from argon at 30 eV. The polarized-orbital calculation[2] shows a deep minimum at 21° while the two optical potential calculations, which differ only slightly, do not exhibit any such behaviour. The normalized experimental data[3] clearly favour the latter calculations.

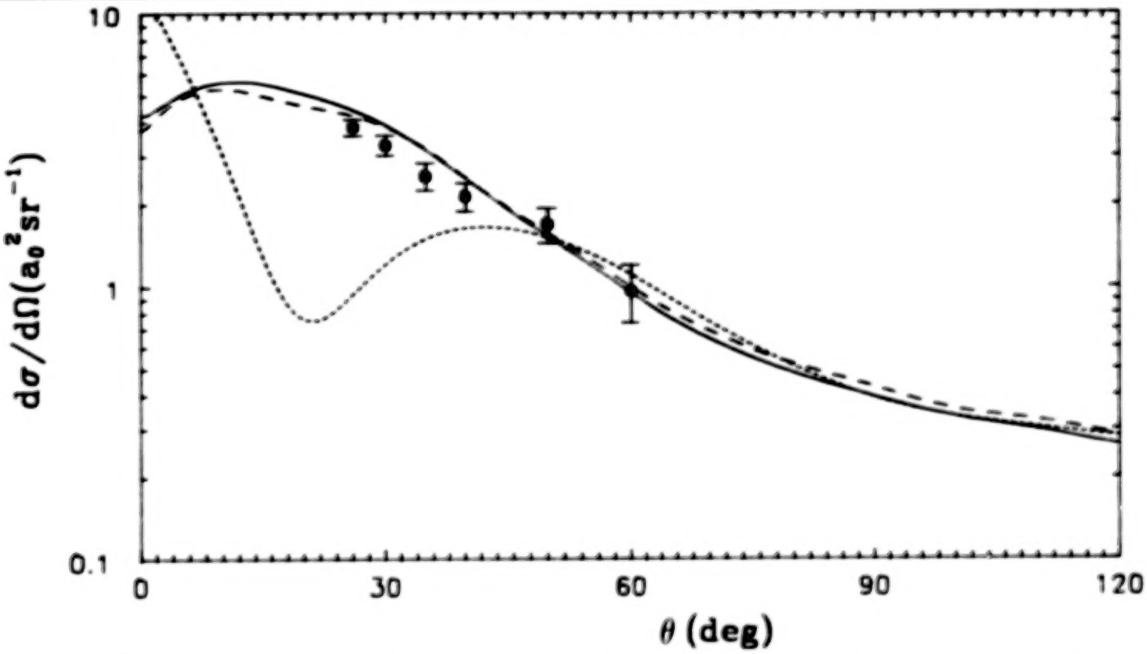

FIG. 1. Positron scattering from argon at 30 eV. (——), ten-state optical potential using free-wave Green's functions[1]; (– – –), ten-state optical potential using numerical Green's functions; (- - -), polarized-orbital approximation[2]; •, experimental data normalized at 60°.[3]

Figure 2 illustrates similar results for positron scattering from neon at 20 eV. Finally in figure 3 we show positron scattering from argon at 8.5 eV. At this energy only the elastic channel is open. Here the experimental data clearly show a minimum and agree well with the shape of the polarized-orbital calculations.[2]

ACKNOWLEDGMENTS

This research was supported by the Natural Sciences and Engineering Research Council of Canada and by the Deutsche Forschungsgemeinschaft.

[1] K. Bartschat, R. P. McEachran and A. D. Stauffer, J. Phys. B. **21**, 2789, 1988.

[2] R. P. McEachran and A. D. Stauffer, *Proc. of the Third Int. Workshop on Positron (Electron)–Gas Scattering*, ed. W. E. Kauppila, T. S. Stein and J. W. Wadehra (Singapore: World Scientific) p. 122, (1986).

[3] K. Floeder, P. Höner, W. Raith, A. Schwab, G. Sinapius and G. Spicher, Phys. Rev. Lett. **60**, 2363, 1988.

[4] W. E. Kauppila, S. J. Smith, C. K. Kwan and T. S. Stein, *Proc. of the Workshop on Annihilation in Gases and Galaxies*, to be published.

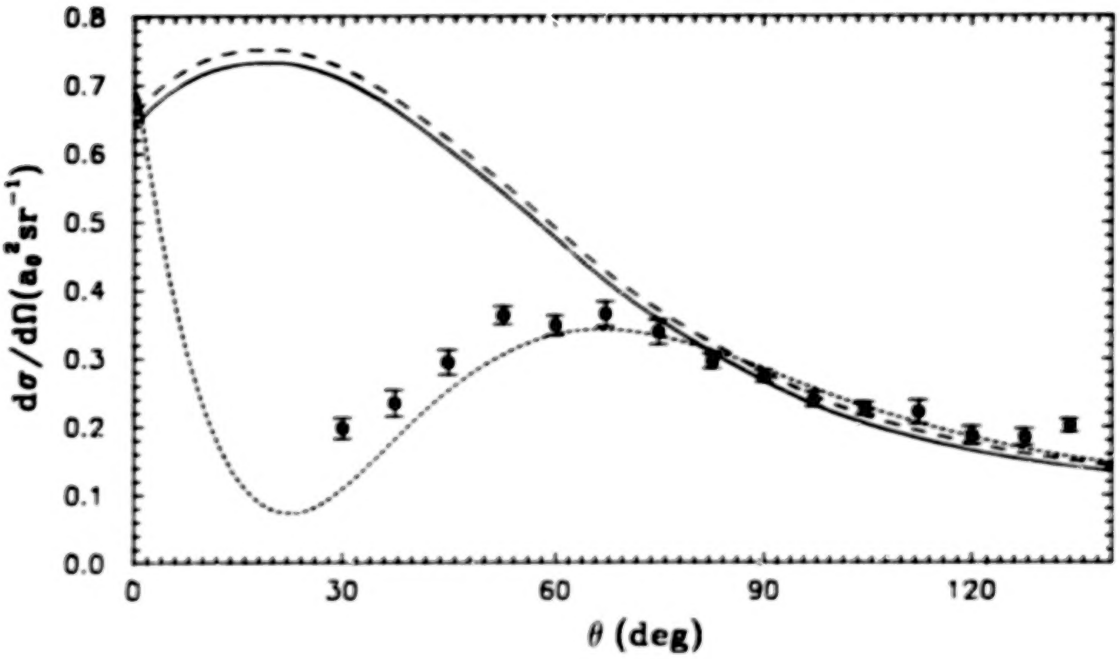

FIG. 2. Positron scattering from neon at 20 eV. (——), fourteen-state optical potential using free-wave Green's functions; (– – –), fourteen-state optical potential using numerical Green's functions; (- - -), polarized-orbital approximation[2]; •, experimental data normalized at 90°.[4]

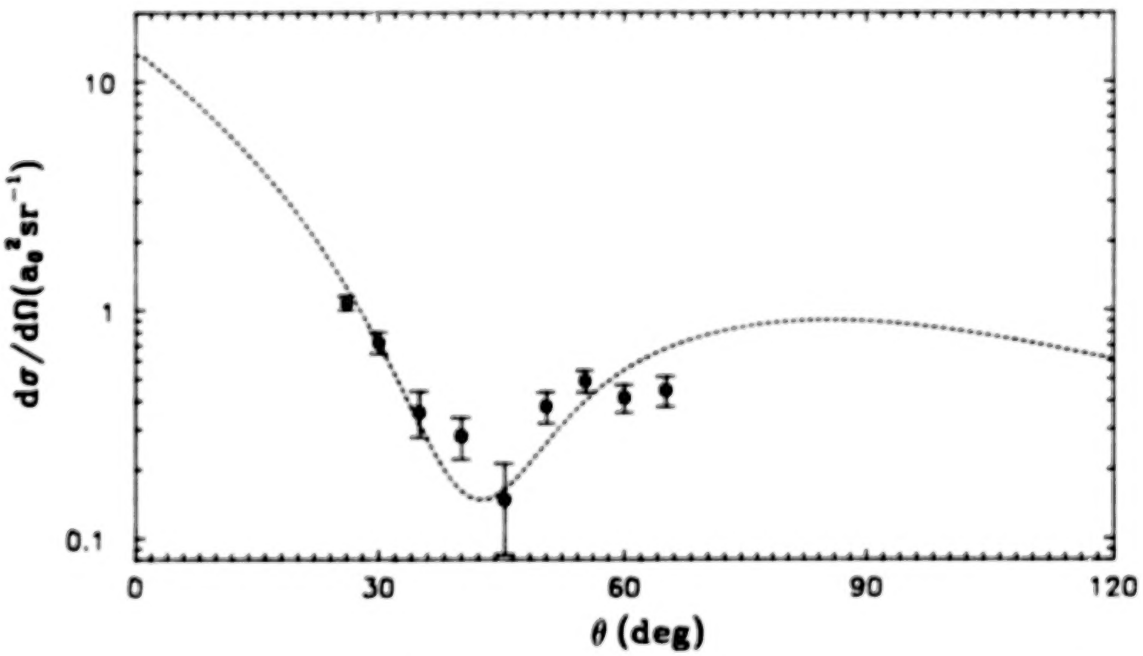

FIG. 3. Positron scattering from argon at 8.5 eV. (- - -), polarized-orbital approximation[2]; •, experimental data normalized at 45°.[3]

ANGULAR CORRELATION STUDIES IN NOBLE GASES

P G Coleman
School of Physics, University of East Anglia
Norwich NR4 7TJ, U.K.

ABSTRACT

There has been a recent revival of interest in the measurement of angular correlation of annihilation photons from the decay of positrons and positronium in gases. This revival has been stimulated by the possibility offered by the technique (a) to shed new light on the apparently low positronium formation fraction in the heavier noble gases: and (b) to provide information on positronium quenching processes in gases such as oxygen. There is also the potential for learning about positronium slowing down in gases.

This review will focus on experimental noble gas work conducted in the U.K. and Japan, and considers what new information has been, and may be, gained from these studies.

INTRODUCTION

Correct description of the angular correlation between gamma photons emitted upon the annihilation of positrons by atomic electrons, $I(\theta)$ has long been recognised as a stringent test of theories describing positron-atom interactions. For this reason many theoretical papers report calculations of scattering cross sections also include $I(\theta)$ and the annihilation cross sections resulting from the formalism employed.[1-5] Some results for $I(\theta)$ for the noble gases are depicted in figure 1. However, experimental studies of $I(\theta)$ have been literally few and far between, although the technique has been widely used for condensed matter research. Page and coworkers published a short

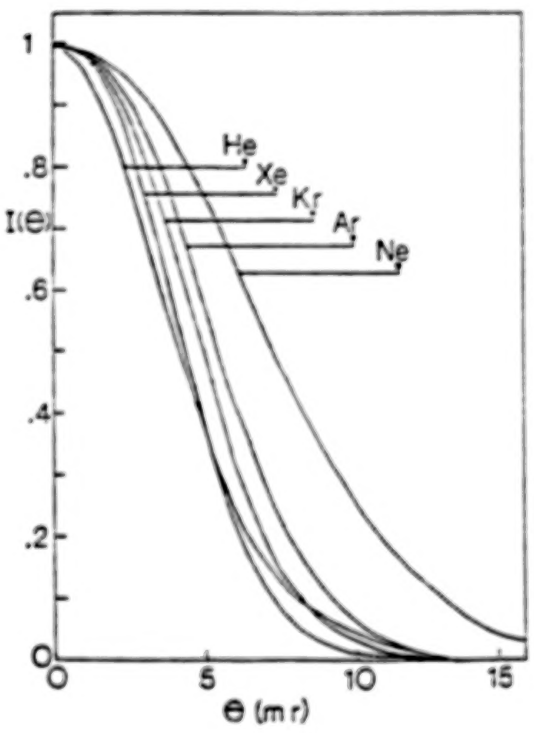

Figure 1
Theoretical angular correlation results from refs 1-5. Humberston's model H5 is plotted for He; the calculations of Drachman and McEachran et al for Ne lie between the plots for Ar and Xe.

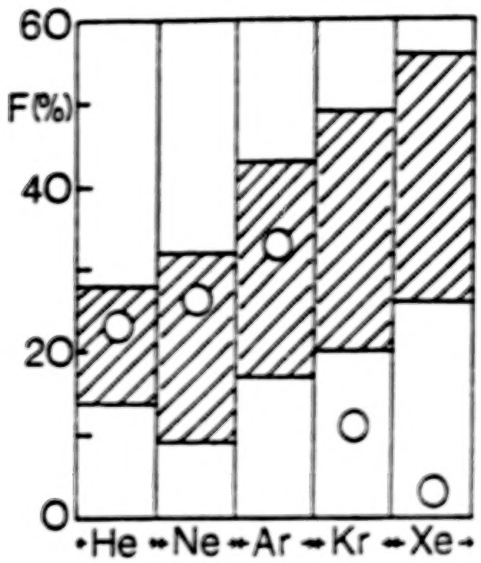

Figure 2
Measured Ps formation fractions for the noble gases (from lifetime measurements[10,11]). Shaded areas depict the range of values predicted by the Ore model.

series of papers in the late 1950's in which the angular correlation technique was used to study positronium quenching and the effects of high electric fields on positronium formation[9], but their work in noble gases was restricted to argon. Until recently the only other work in gases has focussed on positronium chemistry in molecular gases[9-11], and measurements in liquid noble gases which were used in comparisons with the theoretical calculations referred to above.[13]

The recent, albeit small, revival in experimental work in this area has been in part stimulated by the intriguing results from positron lifetime measurements in the noble gases that the amount of ortho-positronium (o-Ps) formed in krypton and xenon appears to be much lower than is expected from the Ore model predictions. The results, summarised in figure 2, were originally reported by Coleman et al[14] and Wright et al[15], and have been discussed in review papers including those of Charlton[16] and Griffith.[17] They were pursued further by Wright et al,[18] who reported the observation of fast lifetime components in spectra for both Kr and Xe. An example is shown in figure 3. Wright et al attributed the fast components to resonant capture of o-Ps into short-lived bound states by the Kr and Xe atoms, the measured fast lifetimes representing the capture rather than the annihilation rates. An alternative picture proposed by Jacobsen involves the spin conversion of fast o-Ps into p-Ps, whose decay is responsible for the fast components. Wright et al suggested that the models describing the mechanism for Ps formation and decay in the heavy noble gases could be tested by angular correlation measurements, and experiments were later performed on the two-dimensional angular correlation spectrometer at the University of East Anglia.[19] The hope here was that the p-Ps component - difficult to identify

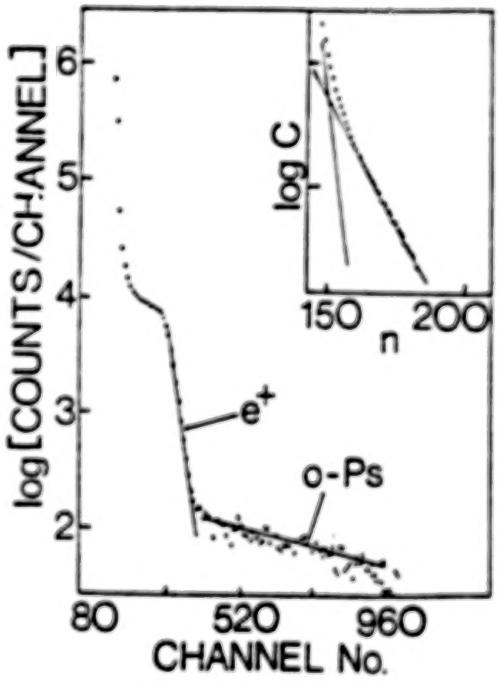

Figure 3
Lifetime spectrum for Xe at 9.64 amagat and 297K.[18] The inset shows two fast components attributed by Wright et al to resonant capture of o-Ps into atomic bound states.

directly in lifetime spectra - could be seen in I(θ) measurements, and thus provide alternative information on the amount of positronium formed.

During the same period Hyodo and coworkers have also used the (one-dimensional) angular correlation technique to study positron-gas annihilation, using silica aerogel to stop enough positrons in a thin region to allow high-resolution angular correlation measurements to be made with good statistics, irrespective of gas pressure. In addition to a number of measurements of positronium quenching in molecular gases[23], these researchers have also attacked the problem of Ps formation in xenon[24,25] and have obtained angular correlation data for He, Ne, Ar, Kr and Xe.[25]

We shall now consider in more detail the experimental results for the noble gases. Their contributions to date to the understanding of positronium formation and slowing down in noble gases will be assessed, in addition to any new information they provide on the basic positron-atom annihilation process.

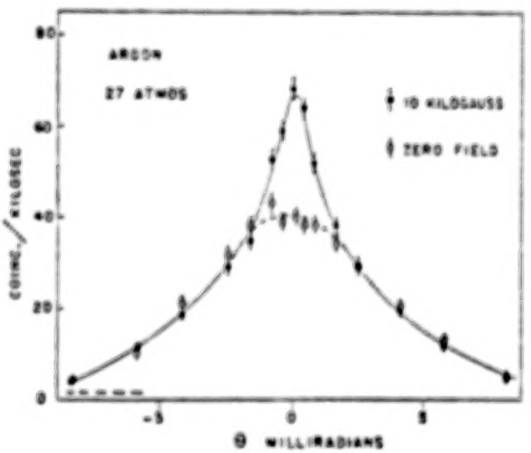

Figure 4
1D angular correlation spectra measured by Heinberg and Page.*

EARLY MEASUREMENTS

Figure 4 shows the result of Heinberg and Page* for argon. The gas was at high pressure - 27 atmospheres - and measurements (one-dimensional angular correlation) were taken with and without a 1 T magnetic field present. The results are interesting because they show the appearance of a narrow component with the application of the magnetic field. This the authors correctly assigned to "thermalised" positronium, the relatively long-lived m=0 o-Ps/p-Ps mixed state. Before proceeding further, then, it may be useful to consider briefly the observables in the angular correlation measurements with which we are concerned here.

OBSERVABLES

1. Free positron-atom annihilation.

Here the positron is assumed to be thermalised; widths (FWHM) of I(θ) curves range from about 5 to 12 mrad, reflecting the mean momenta of electrons available for annihilation.

2. Mixed-state positronium decay.

Angular correlation measurements are often performed with the sample in a high magnetic field, usually used to transport positrons over a few cm from the radioactive source to the sample, so that the source is out of sight of the detectors placed at either side.

In a magnetic field B, the m=0 triplet substate of positronium mixes with the singlet state. The decay rates of the mixed states, λ_1 and λ_2, are given by the expressions

$$\lambda_1 = (1 - x^2)\lambda_S + x^2\lambda_T$$

and

$$\lambda_2 = x^2\lambda_S + (1 - x^2)\lambda_T$$

where λ_S and λ_T are the annihilation rates for singlet and triplet decay, respectively (at low gas pressures - 8×10^9 and 7.1×10^6 s^{-1}, respectively) and $x = 2\omega_0/\omega_{hfs}$.

At B = 0.3T, the field used in the UEA experiments described later, $x^2 = 0.012$ and $\lambda_1 = 7.9 \times 10^9 s^{-1}$ (τ_1) and $\lambda_2^{-1} = 9.7$ns. There is ~ 9% mixing at 0.3T and the states decay via two-gamma emission, so that the annihilation photons contribute to I(θ) spectra.

State 1 is almost identical to unmixed p-Ps. Let us assume that no positronium formed above the upper limit of the Ore Gap - the atomic ionisation threshold - i.e., having kinetic energy greater than its binding energy (6.8eV) -survives its next collision. Then we can say that at time zero we have a p-Ps energy distribution ranging from 0 to 6.8eV. Because the mean life of p-Ps in the gas is ≥1.2ps significant slowing down prior to annihilation is unlikely, and component peaks of similar width (~10mrad) should be present in spectra for all the noble gases, of intensity corresponding to one quarter of the total positronium decays.

State 2 is relatively very long-lived positronium, and as such can lose much of its energy in elastic collisions with gas atoms prior to annihilation. This results in a narrower component on the measured spectra, such as that of Heinberg and Paget the lighter the gas atoms the more efficient the slowing down and the narrower the component. (The gas density is so high in figure 4 that almost total thermalisation is likely.) One can arrive at a crude estimate the degree of slowing down by assuming that the mixed-state positronium atoms lose 2m/M of their energy on each elastic collision. Then, one can show that after one mean lifetime (say 1ons) a 6.8eV Ps atom will have slowed to $[6.8 \cdot e^{-2/Z}]^{-4}$ eV in one atmosphere of a noble gas of atomic number Z and elastic scattering cross section of $5 \times 10^{-16} cm^2$. For helium this yields 3.27eV (so thermalisation is almost certain), whereas in Xenon the energy after 1ons is only 5.4eV - almost no slowing down at all.

Note that the three-gamma decay of o-Ps atoms is not detected,as the technique relies on the detection of two almost anticollinear gamma rays; therefore in a strong magnetic field only half of the positronium formed can contribute to an angular correlation spectrum (i.e, that in states 1 and 2 above).

SILICA AEROGEL MEASUREMENTS

Hyodo and coworkers have performed a series of experiments on noble and molecular gases with a high-resolution long-slit one-dimensional angular correlation apparatus described in reference 20. The annihilation signal rate was increased significantly, for gas pressures of one atmosphere or less,

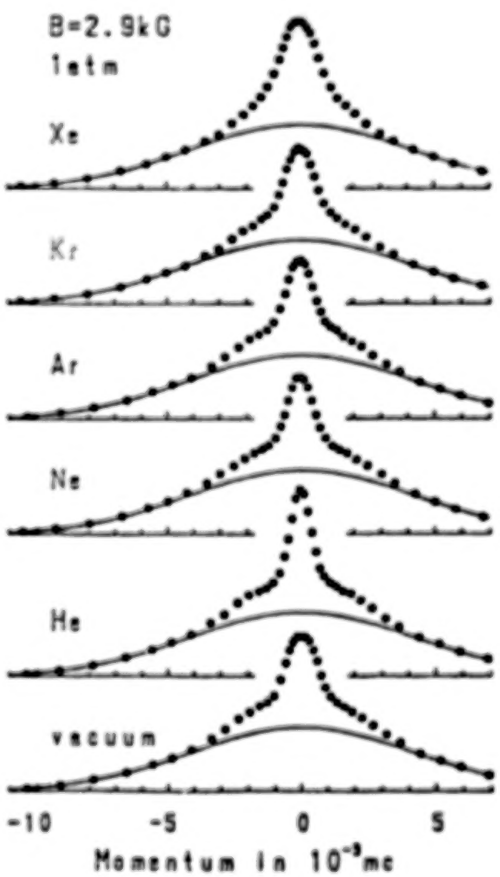

Figure 5
1D spectra of Kakimoto et al[21] for noble gases (with Aerogel moderator), exhibiting narrow components corresponding to the decay of mixed-state Ps.

by stopping the positrons in silica aerogel (an aggregate of amorphous SiO_2 fine particle grains). This, naturally, gives rise to signal arising from interactions with the aerogel, which is measured separately and subtracted from the data.

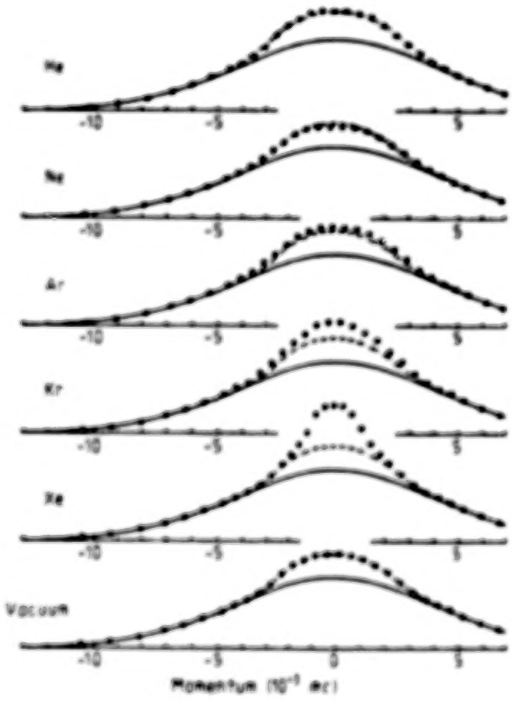

Figure 6

1D spectra of Kakimoto and Hyodo[21] for noble gases, demonstrating the increasing *Ps* formation probabilities as Z increases, in contradiction with the results shown in Fig.4 from lifetime measurements.

Slowing down of positronium

Figure 5, taken from reference 22, exhibits narrow peaks attributed to the long-lived ("state 2") *Ps* referred to above. The broadening of the peak as Z increases is consistent with the decreasing slowing-down efficiencies discussed earlier. The peak in vacuum is due to Ps formed in the grains.

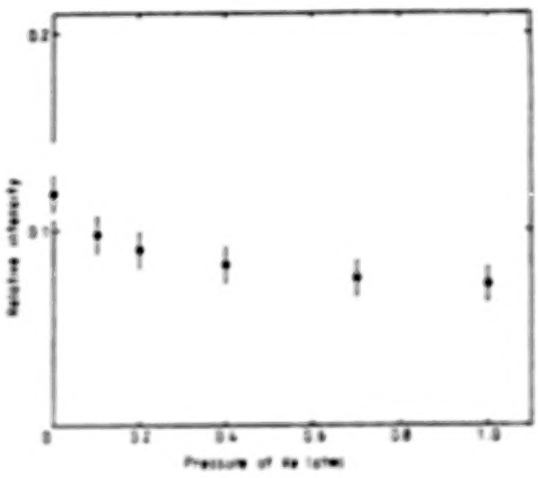

Figure 7

Relative intensity of mixed-state Ps in Xe as a function of gas pressure (from ref.22). The decrease in intensity is interpreted as evidence of strong o-Ps quenching in Xe.

Positronium formation in xenon

The same authors have concluded from their measurements in the noble gases and in xenon at different pressures and in a magnetic field (ref.21) that (a) there is substantial Ps formation in Kr and Xe (see, for example, figure 6), and that (b) part of the long-lived Ps is quenched by xenon (figure 7). This latter observation, say the authors, substantiates the model proposed by Wright et al. based on the formation of *Ps*-xenon resonance states during Ps slowing down.

TWO-DIMENSIONAL ANGULAR CORRELATION MEASUREMENTS

Measurements of two-dimensional angular correlation spectra for positrons and positronium annihilating in pure He, Ne, Ar, Kr and Xe, and in He-Xe mixtures, have been performed using the Anger-camera based system developed and built at the University of East Anglia.[23] This work was in collaboration with the positron group at University College London.

The spectrometer, used for many years to study electron momentum densities in metals and alloys, was adapted for the study of gases by (a) removing the existing sample holder, (b) installing a needle valve for the introduction of gases, and (c) using redesigned lead collimators which reduced the probability for detecting scattered gamma rays and defined well the viewed gas volume (25mmx5mmx5mm). No inner gas cell was used; it was found from early trials that premature annihilations from the cell walls and windows, especially of energetic Ps, could distort the measured spectra. Thus, only annihilation events in the gases were recorded; the probability of o-Ps reaching and be annihilated at the side walls of the entire sample chamber, within sight of the cameras, was found to be negligible. A constant magnetic field of 0.8T is used to transport positrons from the source to the viewed target volume, and so the mixed state Ps atoms discussed above are present.

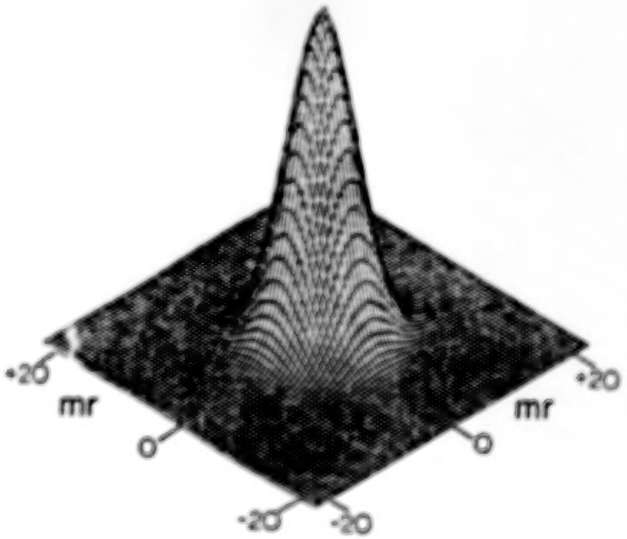

Figure 8

2D angular correlation result for argon at 1 atm, typical of those collected with the UEA spectrometer. The spectra are cylindrically symmetrical but a central cut (or angular average) allows better definition of component peaks than the equivalent 1D spectrum.

Unlike Hyodo et al, these measurements do not have the benefit of aerogel to stop positrons and increase statistics; by the same token, however, there is no aerogel background signal. Each run took several days (the lower the stopping power of the gas, the longer the run needed) and the cameras were moved in to 5m either side of the source, with an unavoidable loss of resolution (measured by recording spectra for a sample of quartz of suitable size: $\Delta\theta$ = 3.4mr). A pressure of one atmosphere was maintained for each gas studied, this being the maximum allowable in the sample chamber. A typical two-dimensional result is shown in figure 8; as the spectra are cylindrically symmetrical there is strictly no need for two- (as opposed to one-) dimensional measurements. However, if a central cut through the 2D peak is taken - or, better still, a cylindrical average is derived - resolution of different components is more readily achieved than with a 1D spectrum. However, after extracting components from the peak, one then has to normalise intensities by first multiplying by the peak width. (For example, the ratio of the volume of revolution of a Gaussian distribution to its area is proportional to its standard deviation.)

Angularly-averaged results for helium and xenon are shown in figure 9. The most important difference is the presence of a separable narrow component in the He spectrum, again corresponding to "state 2" positronium reduced almost to thermal energies by collisions with the light He atoms. In xenon it is not possible to identify a narrow component, and - unfortunately - this means that without careful modelling the data cannot tell us directly whether there is a Ps component present or not. A possibility here is the interpretation of a series of He/Xe mixture results; as the Ore Gaps of the two gases do not overlap, and the scattering cross sections for Xe should swamp those for He, it is hoped that the He atoms act primarily as moderators for the Ps formed in the Xe. Indeed, a narrow component is seen in the mixture runs.

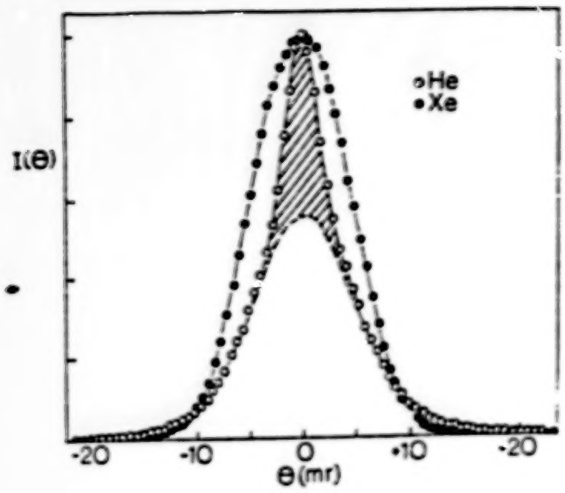

Figure 9

Central cuts through 2D spectra for He and Xe. The He spectrum is separated into positron/p-Ps and the narrower (shaded) "state 2" Ps components. The latter is of width close to the resolution of the spectrometer, and of intensity consistent with the Ps fraction shown in Fig.2. The width of the unshaded component is closer to the those calculated by Brachman and McEachran et al, Humberston's model DB, and the liquid He results of ref.13, than Humberston's HD calculation (which is plotted in Fig.1).

and future analysis may yield more information on Ps formation in xenon.

Figure 10 shows a three-Gaussian fit to the angularly-averaged argon spectrum. The positron component is computed to be 80% of the spectrum (rotated about the vertical through its centre) and of width 11.5 mr, the state 1 p-Ps-like component 10% (width 10.2mr) and the state 2 long-lived Ps component 10% (width 5.7mr). Remembering that only half of th Ps formed can be observed on the spectrum, the positron result is consistent with 3% Ps formation in argon; its shape can be compared with the I(θ) calculation of McEachran et al[3] and the liquid argon result of Briscoe et al.[13] (see figure 11). Clearly, very satisfactory agreement is obtained. Finally, the argon spectrum tells us that as the narrow component is still relatively wide, the state 2 Ps atoms are far from being thermalised through collisions with the argon atoms - perhaps still retaining, on average, ~4eV at annihilation. This figure is reasonably consistent with the first-order calculations discussed in the preceding section.

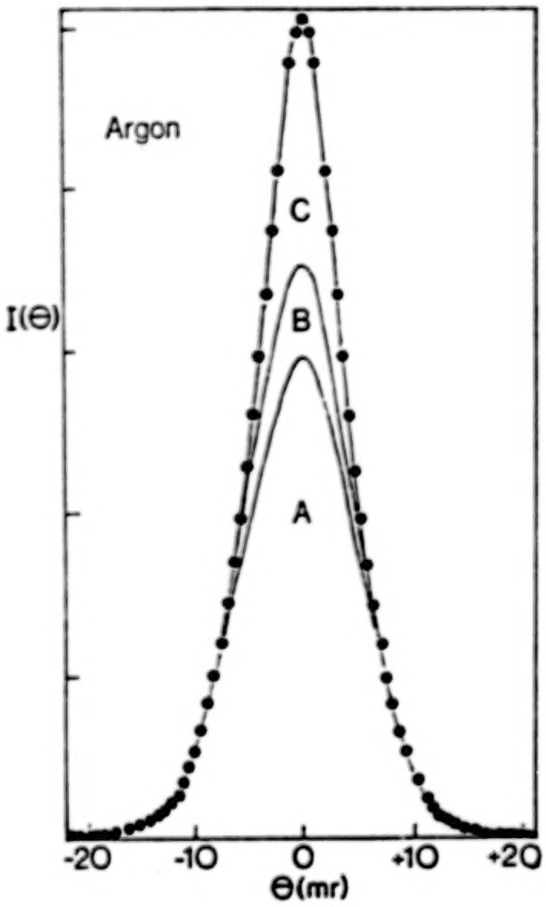

Figure 10

2D results for argon, cylindrically averaged. Gas pressure 1 atmosphere, B = 0.8T. Component A is due to free positron annihilation, B is p-Ps (state 1) and C is state 2 Ps.

CONCLUSIONS

Returning to the main motivations behind current activity in this field:

1. Positronium formation in xenon

Hyodo and coworkers claim that their results are consistent with the model of Wright et al, i.e. that positronium forms as expected (from Ore Gap considerations) but that o-Ps atoms are captured efficiently into an atomic bound state. Certainly positronium formation cross sections in Xe are large[2,5] and there is no reason to expect that positronium should not be formed in positron-xenon collisions. The 2D measurements at East Anglia, at the time of writing, do not provide us with clear evidence of Ps formation in Xe; hopes of unconstrained multicomponent fits to Xe spectra such as that illustrated in 9 must be considered to be remote if not impossible. It may be that measurements in pure Kr and Xe at much higher densities, such as those used by Heinberg and Page, would exhibit discernable features. However, there is some hope that the He-Xe mixture data may provide some relevant information, and we await further careful analyses of these data.

2. Positronium Slowing Down

Both Japanese and British groups appear to be able to provide information on positronium slowing down by elastic collisions with atoms, and with careful modelling one may even hope to gain some information on the order of magnitude of the Ps-atom scattering cross sections. The relative widths of the mixed-state Ps components should at least provide a comparison between those noble gases for which this component can be identified. Direct measurement of Ps-atom scattering cross sections is planned at University College London.

Angular correlation measurements in both ^{3}He and ^{4}He were performed as part of the UEA-UCL collaboration, in the hope that comparison of the widths of the state 2 positronium component would reflect only the mass difference between the helium atoms; this would then allow assignment of a mean Ps-atom cross section in the few-eV region. Unfortunately, however, both ^{3}He and ^{4}He are efficient Ps moderators; the widths of both state 2 Ps peaks are very close to the system resolution, implying near-thermalisation of Ps in both gases.

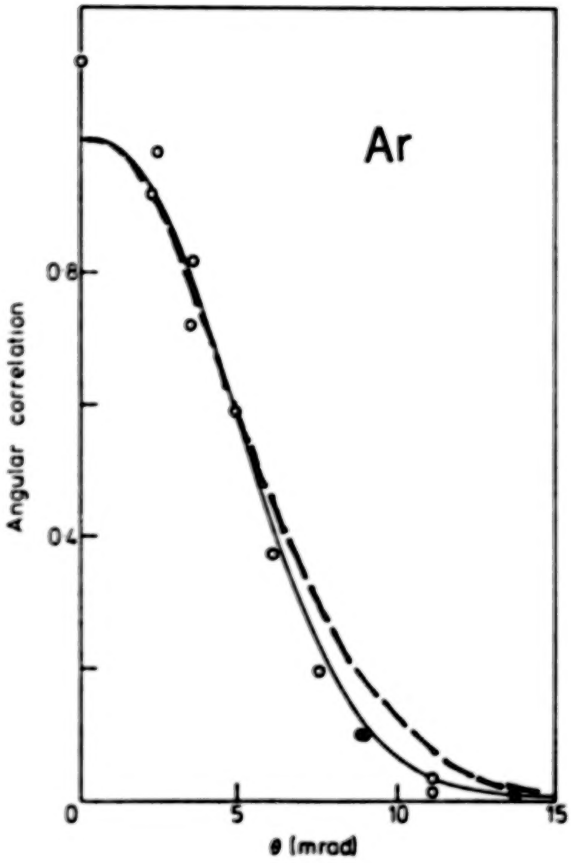

Figure 11

Calculated I(θ) from ref 4 (solid line) together with experimental results for liquid argon (ref 13) and the gaussian positron component from Fig.10 (broken line).

3. I(θ) for Positron-Atom Annihilation

There is now hope that new experimental values for annihilation in the gaseous state will be available for direct comparison with theoretical calculations. The UEA-UCL results for He, Ne and Ar will certainly provide I(θ) for positron annihilation, as figure 11 illustrates.

work is continuing in Japan and further analysis of the 2D pure gas and gas mixture data is being pursued.

ACKNOWLEDGEMENTS

The two-dimensional angular correlation work referred to in this review was performed with Roy West, Simon Rayner, Michael Charlton and Finn Jacobsen. I am particularly grateful to Finn Jacobsen for his hard work in analysing some of the data prior to this Workshop. I am also grateful to Toshio Hyodo for sending preprints, reprints and a list of references, of which I have made extensive use.

REFERENCES

1. Richard J Drachman
Phys.Rev. 173,237 (1969)
2. J W Humberston,
J.Phys.B. 7, L286 (1974)
3. R P McEachran, D L Morgan, A G Ryman and A D Stauffer
J.Phys.B. 11, 951 (1978)
4. R P McEachran, A G Ryman and A D Stauffer
J.Phys.B. 11, 551 (1978)
and 12, 1031 (1979)
5. R P McEachran, A D Stauffer and L E M Campbell
J.Phys.B. 13, 1281 (1980)
6. M Heinberg and L A Page
Phys.Rev. 107, 1589 (1957)
7. F E Obenshain and L A Page
Phys.Rev. 125, 573 (1962)
8. V I Goldanskii and A D Mokrushkin
High Energy Chemistry 2, 77 (1968)
9. A D Mokrushkin and V I Goldanskii
Sov.Phys.JETP 26, 314 (1968)
10. V I Goldanskii, A D Mokrushkin and A C Tatur
High Energy Chemistry 3, 22 (1969)
11. F R Stelat and P G Varlashkin
Phys.Rev.B 5, 4265 (1972)
12. R L Klobucnar and P J Karol
J.Phys.Chem. 84, 489 (1980)
13. C V Briscoe, S-I Choi & A T Stewart
Phys.Rev.Lett.20, 493 (1968)
14. P G Coleman, T C Griffith, G R Heyland and T L Killeen
J.Phys.B. 8, L165 (1975)
15. G L Wright, M Charlton, G Clark, T C Griffith and G R Heyland
J.Phys.B. 16, 4065 (1983)
16. M Charlton
Rep.Prog.Phys. 48, 737 (1985)
17. T C Griffith
Adv. Atomic and Mol.Phys. 22, 37 (1986)
18. G L Wright, M Charlton, T C Griffith and G R Heyland
J.Phys.B. 16, 4327 (1985)
19. P G Coleman, S Rayner, R N West, M Charlton and F Jacobsen
Atomic Physics with Positrons,
eds J W Humberston and E A G Armour (Plenum, 1987) p 305
20. M Kakimoto, T Hyodo, T Chiba, T Akahane and T S Chang
J.Phys.B. 20, L107 (1987)
21. M Kakimoto and T Hyodo
J.Phys.B. 21, 2977 (1988)
22. M Kakimoto and T Hyodo
Positron Annihilation,
eds L Dorikens-Vanpraet, M Dorikens and D Segers (World Scientific 1989) p 737
23. M Kakimoto, Y Nagashima, T Hyodo, K Fujiwara and T S Chang, ibid p 746
24. R N West, J Mayers, and P A Walters
J.Phys.E. 14, 478 (1981)
25. L N Diana, D L Brooks, P G Coleman, R L Chaplin and J P Howell
Positron Annihilation,
eds L Dorikens-Vanpraet, M Dorikens and D Segers (World Scientific 1989) p. 311

POSITRON EXCITATION OF NEON

L. A. Parcell[†], R. P. McEachran[‡] and A. D. Stauffer[‡]

[†] School of Mathematics, Physics, Computing and Electronics, Macquarie University, Sydney, N.S.W. 2109, Australia

[‡] Physics Department, York University, Toronto, Canada M3J 1P3

ABSTRACT

The differential and total cross section for the excitation of the $3s\,^1P_1^o$ and $3p\,^1P_1$ states of neon by positron impact have been calculated using a distorted-wave approximation. Our results agree well with experiment.

THEORY

We are continuing our earlier work on the positron excitation of the noble gases[1,2] by calculating cross sections for the excitation of the $2p^5\,(^2P_{1/2}^o)\,3s\,^1P_1^o$ as well as the $2p^5\,(^2P_{1/2}^o)\,3p\,^1P_1$ states of neon. We use a distorted wave approximation similar to our former calculations on helium.

In the incident channel the distortion potential consists of the static potential plus the polarized-orbital polarization potential used previously for elastic scattering.[3] In the excited channel the distortion potential consists of the appropriate static potential plus a polarization potential determined by an extension of Stone's method.[4]

In order to calculate this potential we construct the following polarized orbital:

$$\psi_{nlm}(\mathbf{r},\boldsymbol{x}) = \varphi_{nlm}(\mathbf{r}) + \sum_{\substack{n'l'm'\\ \lambda'\mu'}} \varphi_{n'l'm'}(\mathbf{r})\,\beta_{\lambda'}^{n'l'}(x)\,Y_{\lambda'\mu'}(\hat{\boldsymbol{x}})\,(l'm'\lambda'\mu' \mid l'\lambda' lm) \tag{1}$$

where the $\varphi_{nlm}(\mathbf{r})$ are the unperturbed states of the atom and $\mathbf{r}$ represents the coordinates of all the bound electrons. The positron coordinate is represented by $\boldsymbol{x}$ and the symbol $(l'm'\lambda'\mu' \mid l'\lambda' lm)$ is the usual vector-coupling coefficient.

We define the adiabatic hamiltonian $H_{\rm ad}$ as

$$H_{\rm ad} = H_{\rm atom} + V(\mathbf{r},\boldsymbol{x}) \tag{2}$$

where $H_{\rm atom}$ is the hamiltonian of the unperturbed atom and $V(\mathbf{r},\boldsymbol{x})$ represents the perturbation due to the incident positron. The unknown coefficients β_λ^{nl} are then determined from the set of equations

$$\langle \varphi_{nlm}(\mathbf{r}) \mid H_{\rm ad} - E(\boldsymbol{x}) \mid \psi_{nlm}(\mathbf{r},\boldsymbol{x}) \rangle = 0 \tag{3a}$$

and

$$\Big\langle \sum_{m''\mu''} \varphi_{n''l''m''}(\mathbf{r})\,Y_{\lambda''\mu''}(\boldsymbol{x})\,(l''m''\lambda''\mu'' \mid l''\lambda'' lm) \mid H_{\rm ad} - E(\boldsymbol{x}) \mid \psi_{nlm}(\mathbf{r},\boldsymbol{x}) \Big\rangle = 0 \tag{3b}$$

for all values of $n''l''$ and λ'' in the sum in (1). The angle brackets indicate integration over the electron coordinates only. The set of equations (3) are expanded in spherical harmonics and the various terms in the perturbed energy $E(\boldsymbol{x})$ are eliminated. Sufficient numbers of the lowest order equations from the set (3) are retained in order to solve for the unknown functions β_λ^{nl}. Note that these are *algebraic* equations for the unknown functions.

In the present work we restrict the sum in equation (1) to a single term by taking $\lambda' = 1$ and $\varphi_{n'l'm'}$ as the $3s\,^1P_1^o$ state when φ_{nlm} represents the $3p\,^1P_1$ state and vice versa. We note that the $2p^5 3p$ configuration gives rise to 3 possible multiplets, viz ^1D, ^1P and ^1S so that other choices for the polarized orbital are possible. With our particular choice the polarization potential becomes

$$V_{\rm p}(x) = -\frac{1}{4\sqrt{\pi}}\,\beta(x)\,\frac{1}{x}\,y_1(3s,3p;x) \tag{4}$$

for both states although the value for β differs in the two cases.

The distorted-wave T-matrix for the excitation is then given by

$$T(nlm \to n'l'm') = \langle \varphi_{n'l'm'}(\mathbf{r})\,\chi_f^-(\boldsymbol{x}) \mid V(\mathbf{r},\boldsymbol{x}) \mid \varphi_{nlm}(\mathbf{r})\,\chi_i^+(\boldsymbol{x}) \rangle \tag{5}$$

where χ_i^+ and χ_f^- are the distorted-waves in the incident and final channels respectively.

In the case of excitation to the $3p\,^1P_1$ state the cross section for the $m = 0$ magnetic sublevel is zero. This means that the differential cross section for this transition is zero for a scattering angle of 0° or 180°. The cross section also displays a dip near 90° at most energies. We show some typical results in figure 1.

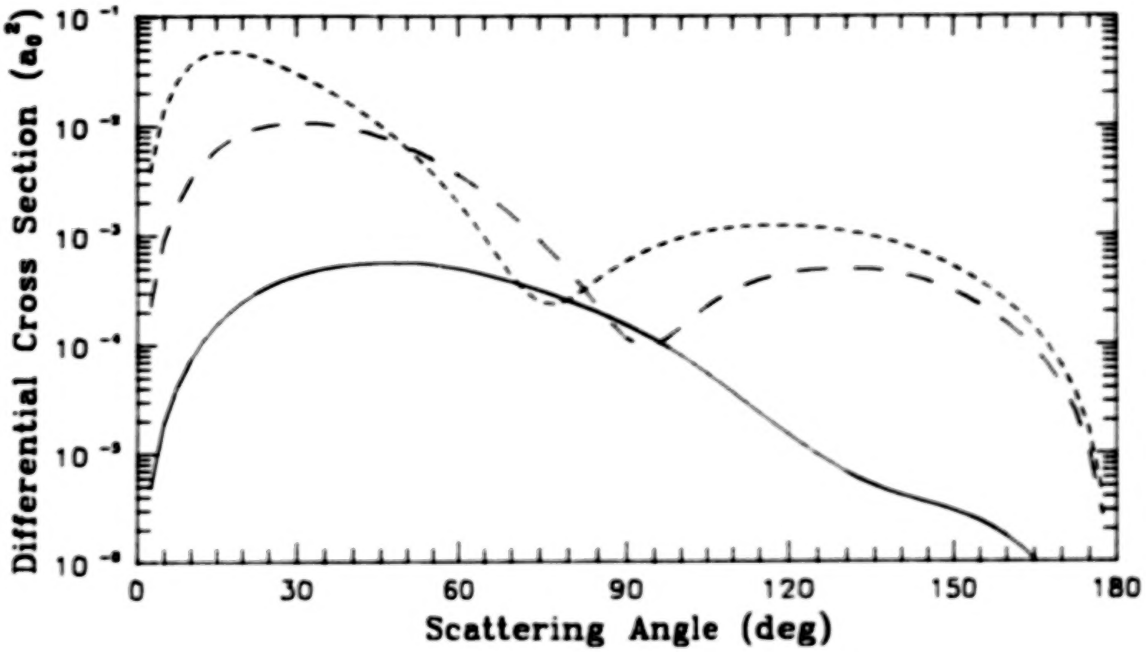

FIG. 1. Differential cross sections for the excitation of the $3p\,^1P_1$ state of neon by positron impact at 20 eV, (——); 25 eV, (– – –); and 40 eV, (- - -).

For the excitation of the $3s\,^1P_1^o$ state the differential cross sections decrease monotonically with angle.

The integrated cross sections for these two transitions are shown in figure 2 along with the experimental data.[5] The theoretical values for the excitation of the $3s\,^1P_1^o$ state are comparable in magnitude to the experiment results. The cross sections for the $3p\,^1P_1$ state are about a sixth of the magnitude of the ones for the $3s\,^1P_1^o$ state.

In comparing the theoretical and experimental results the following points should be noted. The experiment was based upon a time-of-flight technique which only measured scattering in the forward direction (approximately up to 60°). However, since the differential cross sections are peaked in the forward direction this does not introduce an appreciable error. It also measured all the positrons which arrived at the detector within the specified time period. Thus positrons exciting a variety of states were included and the measured cross section is a sum of these.

On the theoretical side, the cross sections for the excitation of the $3p\,^1D_1$ and $3p\,^1S_1$ states should also be taken into account when comparing with experiment. These latter cross sections are expected to be of the same order of magnitude as for the $3p\,^1P_1$ state. Excitation to higher states are not very important as the higher threshold energies for these states means a longer time-of-flight and hence a smaller proportion of the cross section was measured.

In conclusion, while the overall magnitude of our calculated cross sections agree quite well with the experimental data more detailed measurements will be necessary before more quantitative conclusions can be made.

ACKNOWLEDGMENTS

This work was supported by the Natural Sciences and Engineering Research Council of Canada and by a Macquarie University Research Grant.

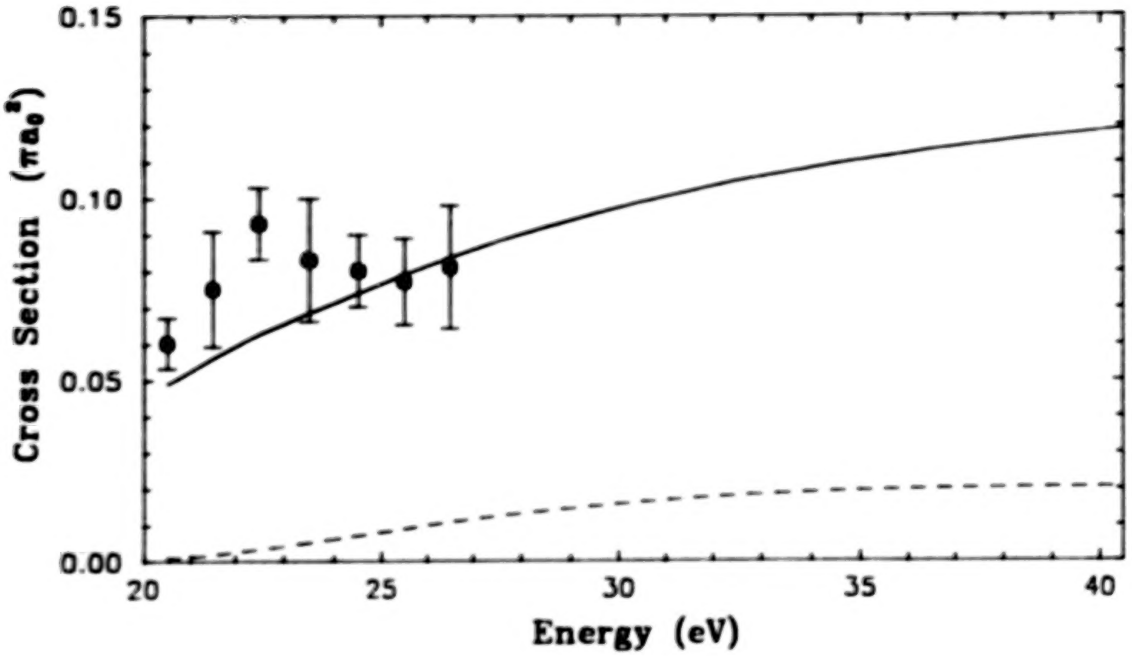

FIG. 2. Integrated cross sections for the excitation of neon by positron impact: (——), excitation of the $3s\,^1P_1^o$ state; (– – –), excitation of the $3p\,^1P_1$ state; (•), experiment.[5]

---

[1] L. A. Parcell, R. P. McEachran and A. D. Stauffer, J. Phys. B. **16**, 3125, 1983.

[2] ——, J. Phys. B. **20**, 2307, 1987.

[3] R. P. McEachran, A. G. Ryman and A. D. Stauffer, J. Phys. B. **11**, 551, 1978.

[4] P. M. Stone, Phys. Rev. **141**, 137, 1966.

[5] P. G. Colman, J. T. Hutton, D. R. Cook and C. A. Chandler, Can. J. Phys. **60**, 584, 1982.

POSITRON-INERT GAS DIFFERENTIAL ELASTIC SCATTERING

W.E. Kauppila, Steven J. Smith, C.K. Kwan, and T.S. Stein
Department of Physics and Astronomy, Wayne State University
Detroit, Michigan 48202 USA

ABSTRACT

Measurements are being made in a crossed-beam experiment of the relative elastic differential cross section (DCS) for 5-300 eV positrons scattering from inert gas atoms (He, Ne, Ar, Kr, and Xe) in the angular range from 30-134°. Results obtained at energies around the positronium (Ps) formation threshold provide evidence that Ps formation and possibly other inelastic channels have an effect on the elastic scattering channel.

INTRODUCTION

It is well known that DCS measurements provide a sensitive test of theoretical calculations. Furthermore, positron scattering by the inert gas atoms is particularly interesting because as the positron energy is increased above the lowest inelastic scattering threshold energy (for Ps formation) it is known[1] that the total cross sections increase rapidly and that Ps formation may quickly become as large or even larger than the elastic scattering cross section. As a result, measurements of positron elastic DCSs for the inert gases provide some good examples for investigating the effect of an inelastic scattering channel (e.g., Ps formation) on the elastic channel as the positron energy is increased through the Ps formation threshold.

EXPERIMENT

The basic experimental setup (shown in Fig. 1) and approach is the same as that used by Hyder et al.[2] Some modifications that have been made to improve the acquisition of data are the addition of (1) a second channeltron to detect scattered positrons, (2) a 150 millicurie sodium-22 positron source, and (3) a baffle between the primary beam path and channeltron #2. The origin of the

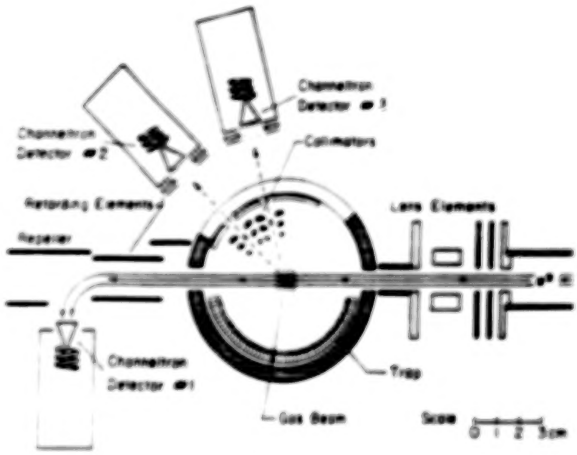

Figure 1

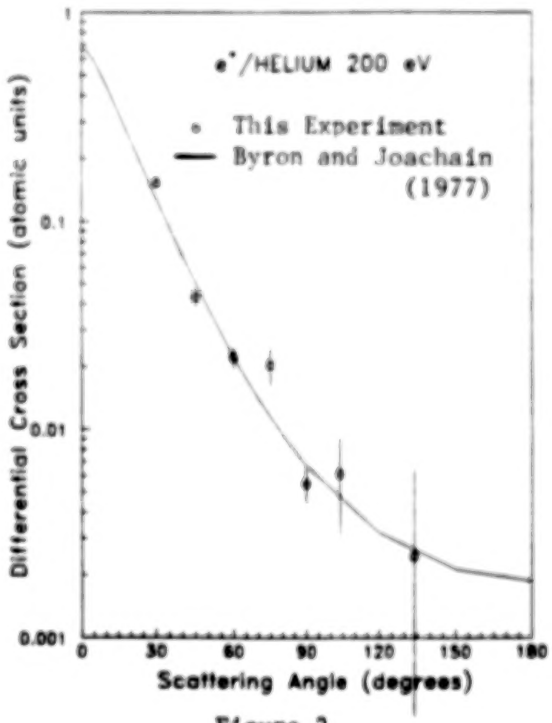

Figure 2

slow positron primary beam (intensity >100,000/sec at 100 eV with a FWHM of about 1.5 eV) is an annealed tungsten moderator placed in front of the sodium-22 source. Geometrical considerations and electron measurements made in the same system (and compared with prior experiments) indicate an overall angular resolution in the vicinity of $\pm 10^{\circ}$. The accuracy of our measurement angles is within a few degrees.

RESULTS

A sampling of our initial elastic DCS measurements (with statistical uncertainties) taken with our modified apparatus for the inert gases is shown in Figs. 2-6 where they are compared with various calculations[3-7] and some earlier measurements of Hyder et al.[1] In each case our results are normalized to a calculation at either 60 or 90°. We do not consider meaningful the few 134° values that seem out-of-line with the smaller angle values.

At high energies it is seen that our results are in good agreement with the eikonal Born series method calculation (within the framework of the optical model formalism) of Byron and Joachain[3] at 200 eV for He and the optical model calculations of Joachain et al.[6] for Ar at 300 eV. It is to be noted that the present measurements are about a factor of two lower at 30° than Hyder et al.[2], which we attribute to the addition of the above-mentioned baffle.

At positron energies just below the Ps formation thresholds we are finding quite good agreement with the polarized orbital calculations of McEachran et al.[4,7,8], as is seen in Fig. 6 at 5.9 eV for Xe and reported by Smith et al.[9] for Ne at 13.6 eV and Ar at 8.7 eV. For positron impact energies somewhat above the Ps formation thresholds we have been finding that our DCS measurements are appreciably different than the above polarized orbital calculations, as shown in Fig. 5 for Kr at 20 eV and by Smith et al. for Ar at 30 eV. It is to be noted that these polarized orbital calculations

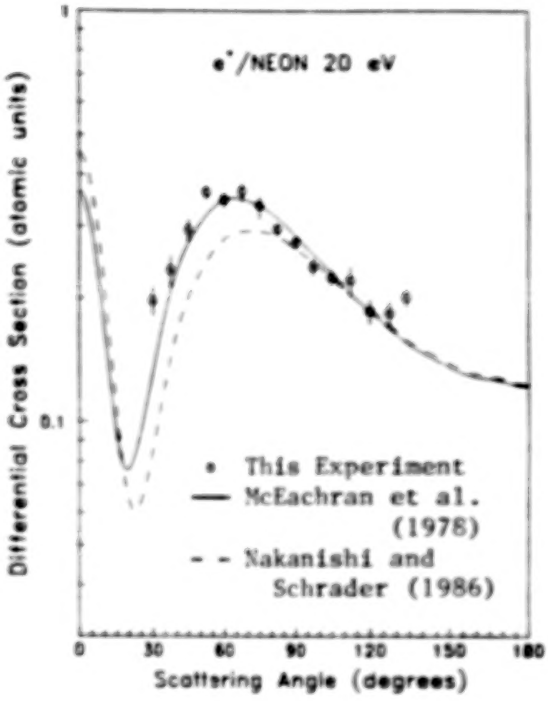

Figure 3

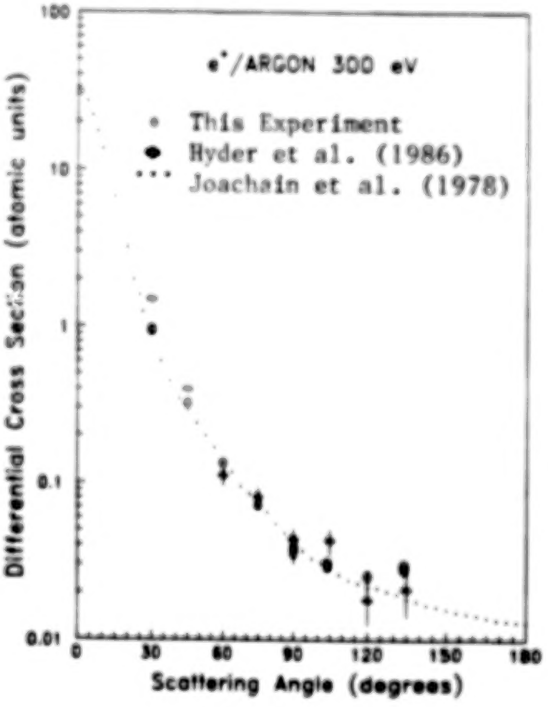

Figure 4

do not include any consideration for the effect of inelastic scattering channels on the elastic channel. Calculations have been made by Bartschat et al.[10] and Joachain and Potvliege[11] where the effect of inelastic channels on the elastic channel (referred to as absorption effects) have been considered and both of these groups have found that these absorption effects tend to remove the structure (minimum and maximum) in the DCS curves, which is somewhat consistent with what we observe for Kr at 20 eV (Fig. 5) and Ar at 30 eV (Smith et al.[9]). Our 20 eV Ne results in Fig. 3 are close to the calculation of McEachran et al.[4]

ACKNOWLEDGEMENTS

We acknowledge the helpful assistance of James Klemic. This work was supported by NSF Grant PHY-8706120.

REFERENCES

1. W.E. Kauppila and T.S. Stein, Adv. At. Mol. Phys. 26, 1 (1989/1990).
2. G.M.A. Hyder, M.S. Dababneh, Y.-F. Hsieh, W.E. Kauppila, C.K. Kwan, M. Mahdavi-Hezaveh, and T.S. Stein, Phys. Rev. Lett. 57, 2252 (1986).
3. F.W. Byron Jr. and C.J. Joachain, Phys. Rev. A 15, 128 (1977).
4. R.P. McEachran, A.G. Ryman, and A.D. Stauffer, J. Phys. B. 11, 551 (1978).
5. H. Nakanishi and D.M. Schrader, Phys. Rev. A 34, 1823 (1986).
6. C.J. Joachain, in Electronic and Atomic Collisions, edited by G. Watel (North-Holland, Amsterdam, 1978), p. 71; C.J. Joachain, R. Vanderpoorten, K.H. Winters, and F.W. Byron Jr., J. Phys. B 10, 227 (1977).
7. R.P. McEachran, A.D. Stauffer, and L.E.M. Campbell, J. Phys. B 13, 1281 (1980).
8. R.P. McEachran, A.G. Ryman, and A.D. Stauffer, J. Phys. B. 12, 1031 (1979).
9. S.J. Smith, W.E. Kauppila, C.K. Kwan, and T.S. Stein, Proc. ICPEAC XVI, Abstracts (1989). (to be published).
10. K. Bartschat, R.P. McEachran, and A.D. Stauffer, J. Phys. B 21, 2789 (1988).
11. C.J. Joachain and R.M. Potvliege, Phys. Rev. A 35, 4873 (1987).

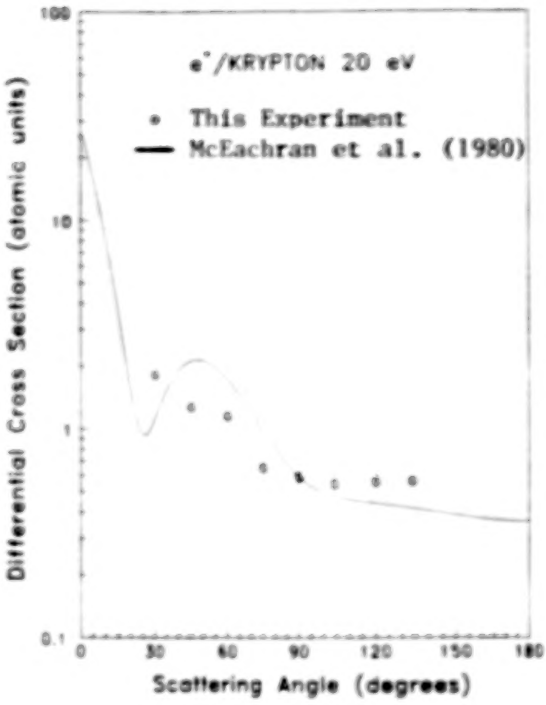

Figure 5

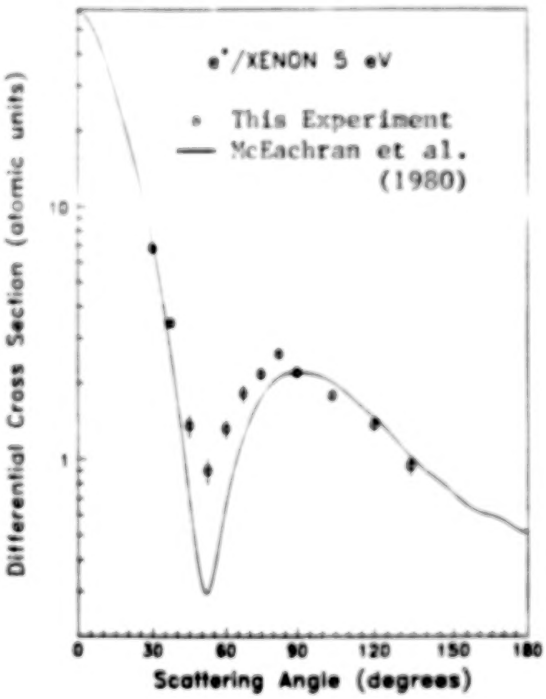

Figure 6

DIFFERENTIAL ELASTIC SCATTERING CROSS SECTIONS FOR 54.9eV POSITRONS INCIDENT ON HELIUM*

R. L. Chaplin, L. M. Diana, D. L. Brooks

The University of Texas at Arlington
Center for Positron Studies
Department of Physics
Arlington, TX, U.S.A.

ABSTRACT

We present absolute differential elastic scattering cross sections measured with our 3-m, high-resolution, time-of-flight spectrometer for 54.9eV positrons incident on He. Five point moving average differential cross sections are plotted against average scattering angles which range from 14° to 36°. Also the averages of five differential cross sections which have adjacent values of scattering angle are plotted versus the corresponding averages of the scattering angles. The curve fitted to these data is shaped like the theoretical curve but has its minimum and its maximum at scattering angles that are about 4° higher and 15° lower respectively than predicted by theory.

INTRODUCTION

The first measurements of differential elastic scattering cross sections for positrons were made in this laboratory on Ar (Ref. 1) with a 25cm spectrometer. Recently, relative values of differential elastic scattering cross sections, I(θ), for Ar obtained with crossed-beam apparatuses, have been reported.[2-4] The 3m time-of-flight (TOF) spectrometer with flight path 12 times that of the instrument that yielded the first I(θ) features vastly improved resolution. We present here preliminary values for I(θ) for 54.9eV positrons incident on He.

The 3m TOF spectrometer and its principles of operation are described in Ref. 5 and the calculation of I(θ) in Ref. 1.

RESULTS AND DISCUSSION

Two figures are used to present the results. In each of these the curve of short dashes is a polynomial fit to experimental data, and the curve of long dashes connects the I(θ) calculated by McEachran and Stauffer.[6]

The averages of five differential cross sections which occur at adjacent values of scattering angle are plotted against the corresponding averages of the scattering angles in Fig. 1. The polynomial fit to these points is shaped generally like the theoretical curve, but the minimum of the fit appears at a scattering angle that is larger by 4° and the secondary maximum at an angle that is 15° smaller than given by theory. Additionally, the experimental I(θ) are considerably larger than the theoretical values.

The five point moving averages of I(θ) plotted in Fig. 2 display two secondary maxima which are smoothed into one by the polynomial fit. It is possible that the apparent double secondary hump results from the superposition of scattering events in the foreward and

*It is a pleasure to note the important past and continuing contributions of Dr. P. G. Coleman.

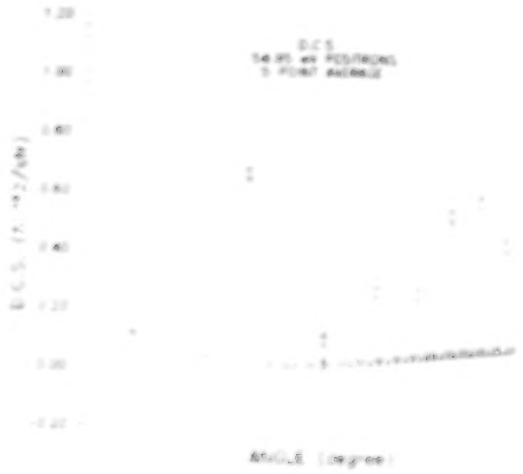

Fig. 1. Five point average differential elastic scattering cross sections. See text for explanations of curves.

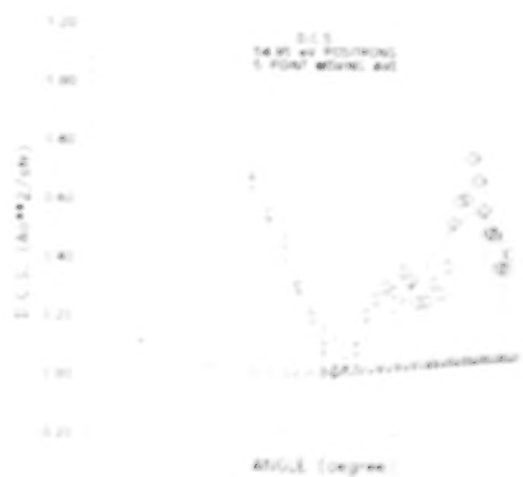

Fig. 2. Five point moving average differential elastic scattering cross sections. See text for explanation of curves.

backward directions, for back-scattered positions are reflected by the moderator and then appear in the TOF spectrum like positrons scattered into the forward supplementary angles with slightly longer flight paths. We will check this possibility by repeating the experiment with an appreciable spatial separation of moderator and scattering chamber to effect a significant relative shift of peaks on the TOF spectrum from forward and backward scattering events.

The TOF spectra for 54.9eV positrons yield $(0.47 \pm 0.04)\pi a_0^2$ for total cross section for impact ionization, Q_{ion}, $(0.083 \pm 0.011)\pi a_0^2$ for total excitation cross section, Q_{ex}, and $(0.16 \pm 0.06)\pi a_0^2$ for total elastic scattering cross section, Q_{el}. The Q_{ion} and Q_{ex} will be reduced slightly and the Q_{el} increased somewhat by application of corrections for double scattering. Even after correction for double scattering, the Q_{ion} will agree with the result obtained with our 2.3m spectrometer,[7] the Q_{ex} with the value of $0.079\pi a_0^2$ read from Sueoka's plot[8], and the Q_{el} will be reasonable, probably about $0.2\pi a_0^2$. However, the data in Ref. 7 suggest the possibility that Q_{el} at 54.9eV could be as high as $0.3\pi a_0^2$. This is one reason why our subsequent data acquisitions at 54.9eV will be made with stronger magnetic fields. The 145G used in obtaining the results reported here was ideal for the resolution of the excitation TOF peak from elastic scattering events but was too low to insure maximum possible detection of positrons scattered elastically between 36° and 144°. We estimate that 0.25% of the elastic events at 36° but that none at any of the other angles for which I(θ) are reported were lost in achieving elastic-excitation resolution.

ACKNOWLEDGMENTS

We wish to thank J. M. Wadehra for sharing the results of his Born approximation calculations of Q_{el} with us and R. P. McEachran and A. D. Stauffer for their polarized orbital results for Q_{el}. We wish to acknowledge, also, the support of the National Science Foundation through Grant PHY-8506933.

REFERENCES

1. P. G. Coleman and J. D. McNutt, Phys. Rev. Lett. 42, 1130 (1979).
2. G. M. A. Hyder, M. S. Dababneh, Y-F Hsieh, W. E. Kauppila, C. K. Kwan, M. Mahdavi-Hezaveh, and T. S. Stein, Phys. Rev. Lett. 57, 2252 (1986).
3. W. E. Kauppila and T. S. Stein, in Atomic Physics with Positrons, Proceedings of NATO Advanced Research Workshop on Atomic Physics with Positrons, London, England, edited

J. W. Humberston and E. A. G. Armour (Plenum Press, New York and London, 1987), p. 27.
4. K. Floeder, P. Honer, W. Raith, A. Schwab, G. Sinapius, and G. Spicher, Phys. Rev. Lett. 23, 2363 (1988).
5. L. M. Diana, R. L. Chaplin, D. L. Brooks, P. G. Coleman, and J. P. Howell, in Positron Annihilation, Proceedings of the Eighth International Conference on Positron Annihilation, Gent, Belgium, edited by L. Dorikens-Vanpraet, M. Dorikens, and D. Segers (World Scientific, Singapore, 1989), p. 308.
6. R. P. McEachran and A. D. Stauffer, in Proceedings of the Third International Workshop on Positron (Electron)-Gas Scattering, Detroit, Michigan, edited by W. E. Kauppila, T. S. Stein, and J. M. Wadehra (World Scientific, Singapore, 1986), p. 122 and personal communication.
7. L. M. Diana, R. L. Chaplin, D. L. Brooks, J. T. Adams, L. K. Reyna, and P. G. Coleman, contributed article in these proceedings.
8. O. Sueoka, J. Phys. Jpn. 51, 3757 (1982).

TOTAL CROSS SECTIONS FOR POSITRONS SCATTERED ELASTICALLY FROM HELIUM BASED ON NEW MEASUREMENTS OF TOTAL IONIZATION CROSS SECTIONS*

L. M. Diana, R. L. Chaplin, D. L. Brooks
J. T. Adams, L. K. Reyna

The University of Texas at Arlington
Center for Positron studies
Department of Physics
Arlington, TX, U.S.A.

ABSTRACT

We have applied an improved technique for employing our 2.3m spectrometer to measure total ionization cross sections, Q_{ion}, for positrons incident on He. The new Q_{ion} agree with the values we reported earlier. We present, also, estimates of total elastic scattering cross sections, Q_{el}, obtained by subtracting from total scattering cross sections, Q_{tot}, reported in the literature, our Q_{ion} and Q_{Ps} (total positronium formation cross sections) and total excitation cross sections, Q_{ex}, published by another researcher. The Q_{ion} and Q_{el} measured with our 3m high-resolution time-of-flight spectrometer for 54.9eV positrons are in accord with the results from the 2.3m spectrometer. The Q_{ion} are in fair agreement with theory tending for the most part to be higher, especially at 76.3 and 88.5eV. Our Q_{el} agree quite well with theory to the vicinity of 50eV, but at 60eV and above the experimental Q_{el} climb to and remain at about $0.30\pi a_o^2$ while the theoretical values steadily decrease.

INTRODUCTION

Our 2.3m spectrometer was put into its present form[1] to permit absolute, direct measurements of Q_{ion} and to simplify absolute determinations of Q_{Ps} for positrons incident on gases. We have applied an improved technique to extend the range of our first Q_{ion} measurements[2] in He. We compare these new preliminary results with theory and subtract them, our values for Q_{Ps} (Ref. 1), and Sueoka's results for Q_{ex} from Q_{tot} obtained from published values[4,5] to arrive at estimates of Q_{el}. A recent elaborate study of positron-helium partial cross sections has been published by Campeanu et al. (Ref. 12).

METHOD

We compute Q_{ion} from $Q_{ion}=fQ_{tot}/F$, where f is the fraction of incident positrons that produce ions by impact, F is the fraction that scatter into all channels, and Q_{tot} is obtained from the literature.

Reporting Q_{ion} in this way permits scaling the results to any set of Q_{tot}. We use those of Ref. 4 and 5 here because they are more recent than of our own. The apparatus used, the measurement of F, the calculation of the correction for double scattering, and possible sources of systematic error are fully discussed in Ref. 1. Counting the ionization electrons and the beam positrons equal periods of time allows the calculation of f. The current technique for couning ioniza-

*We thank Dr. P. G. Coleman for important past and continuing contributions.

tion electrons is to apply to the cone of the channel electron multiplier a voltage that is sufficiently low to prevent reflection of the beam positrons and consequent multiple passes through the target gas. This change of procedure enabled us to extend Q_{ion} determinations with this spectrometer to lower beam energies than were formerly tractable at a minor cost of applying a small correction for counting beam positrons together with the ionization electrons.

RESULTS AND DISCUSSION

The results are shown in Fig. 1. The open square shows a Q_{ion} obtained with our 3m high-resolution time-of-flight (TOF) spectrometer,[6] the solid line is drawn through the calculated points (+) of Mukherjee et al.[7] The Q_{ion} (o) are in fair agreement with theory, tending for the most part to be higher especially at 76.3 and 88.5 eV. The open stars depict Q_{el} that resulted from subtracting Q_{ion}, Q_{Ps} (Ref. 1 or 8) and Q_{ex} (Ref. 3) from Q_{tot} (Ref. 4 or 5). The x was determined by smoothly extrapolating Q_{tot} (Ref.4) from energies just below the positronium formation threshold energy to that energy. The two Q_{el} represented by triangles are for energies below the threshold for impact ionization and were calculated by subtracting Q_{Ps}[8] and Q_{ex}[9] from Q_{tot} (Ref. 4). The diamond resulted from employing in the subtractions the TOF Q_{ion}. The open cross shows a Q_{el} directly measured with the TOF spectrometer (Ref. 6) Its value will increase upon application of corrections.

The curve of mid-length dashes guides the eye through the experimental Q_{el} as their values dip just above the positronium formation threshold and climb to $0.30\pi a_0^2$ at 60eV. The curve of long dashes joins Q_{el} calculated by McEachran and Stauffer,[10] which agree well with the experimental values up to the vicinity of 50eV, after which they decline steadily.

The solid stars represent Q_{el} obtained by subtracting from Q_{tot} (Ref. 4 or 5), Q_{ex} (Ref. 3) and the Q_{Ps} and Q_{ion} from Ref. 11.

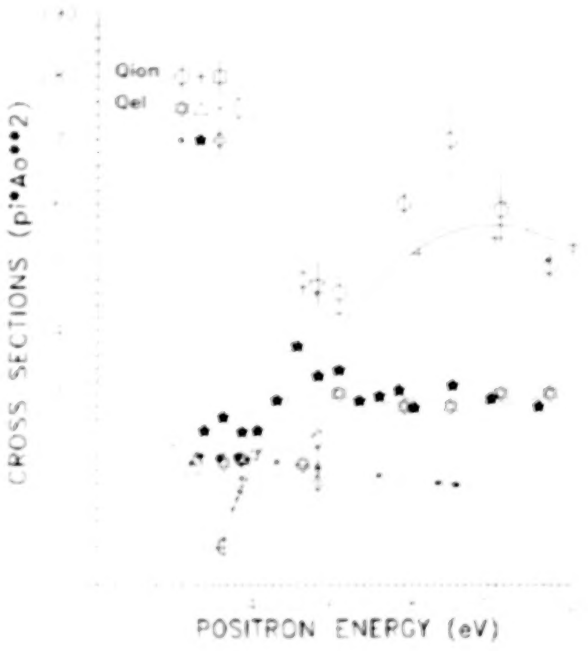

Fig 1. Total elastic and total impact ionization cross sections in He. See text for explanations of symbols.

ACKNOWLEDGMENTS

We wish to acknowledge the generosity of R. P. McEachran and A.D. Stauffer in supplying their calculated Q_{el}. We appreciate, also, the support of the National Science Foundation through Grant PHY-8506933.

REFERENCES

1. L. M. Diana, P. G. Coleman, D. L. Brooks, P. K. Pendleton, and D. M. Norman, Phys. Rev. A34, 2731 (1986).
2. L. M. Diana, L. S. Fornari, S. C. Sharma, P. K. Pendleton, and P. G. Coleman, in Positron Annihilation, Proceedings of the Seventh International Conference on Positron Annihilation, New Delhi, India, edited by P. C. Jain, R. M. Singru, and K. P. Gopinathan (World Scientific, Singapore, 1985), p. 342.
3. O. Sueoka, J. Phys. Soc. Jpn. 51, 3757 (1982).
4. T. S. Stein, W. E. Kauppila, V. Pol, J. H. Smart, and G. Jesion, Phys.

Rev. A17, 1600 (1978).
5. W. E. Kauppila, T. S. Stein, J. H. Smart, M. S. Dababneh, Y. K. Ho, J. P. Downing, and V. Pol, Phys. Rev. A24, 725 (1981).
6. L. M. Diana, R. L. Chaplin, D. L. Brooks, P. G. Coleman, and J. P. Howell, in Positron Annihilation, Proceedings of the Eighth International Conference on Positron Annihilation, Gent, Belgium, edited by L. Dorikens-Vanpraet, M. Dorikens, and D. Segers (World Scientific, Singapore, 1989) p. 308.
7. K. K. Mukherjee, P. S. Mazumdar, and S. Brajamani, Phys. Rev. A39, 756 (1989).
8. L. S. Fornari, L. M. Diana, and P. G. Coleman, Phys. Rev. Lett. 51, 2276 (1983).
9. P. G. Coleman, J. T. Hutton, D. R. Cook, and C. A. Chandler, Can. J. Phys. 60, 584 (1982).
10. R. P. McEachran, and A. D. Stauffer, in Proceedings of the Third International Workshop on Positron (Electron)-Gas Scattering, Detroit, Michigan, edited by W. E. Kauppila, T. S. Stein, and J. M. Wadehra (World Scientific, Singapore, 1986), p. 122 and personal communication.
11. D. Fromme, G. Kruse, W. Raith, and G. Sinapius, Phys. Rev. Lett. 57, 3031 (1986).
12. R. I. Campeanu, D. Fromme, G. Kruse, R. P. McEachran, L. A. Parcell, W. Raith, G. Sinapius, and A. D. Stauffer, J. Phys. B 20, 3557 (1987).

Ionisation of Atomic Hydrogen by Positron Impact

Gottfried Spicher, Björn Olsson, Wilhelm Raith, Günther Sinapius
and Wolfgang Sperber

Fakultät für Physik, Universität Bielefeld
D-4800 Bielefeld 1, Federal Republic of Germany

1 Experimental Setup

With our crossed beam apparatus [1] we measure the relative impact-ionisation cross section of atomic hydrogen by positron impact. A layout of the scattering region is given in fig. 1.

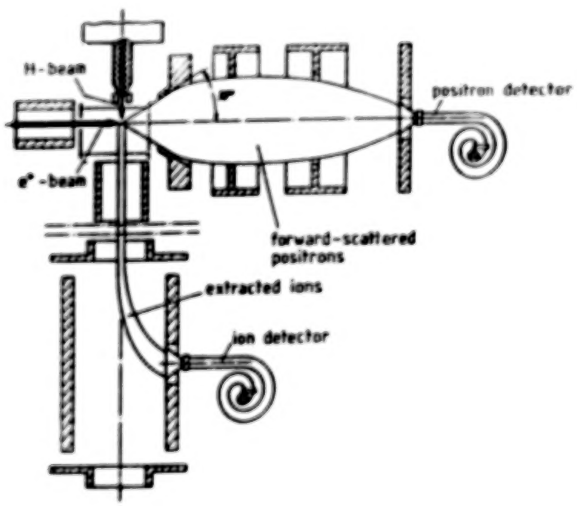

Figure 1: Layout of the experiment

2 Data Taking

Because of the H_2-molecules in the atomic beam and the residual gas both H_1^+ and H_2^+ ions are produced (see table 1). Positrons ionize atoms or molecules through two different processes: (a) impact ionisation: leaving an ion, a free electron and the projectile, or (b) positronium formation: leaving an ion and a positronium 'atom'. Impact ionisation leads to time-correlated signals on both detectors. The positron and the ion signals are processed by a time-to-pulse-height converter. If the ion follows the projectile in less than 4 μs this event is stored in a multichannel analyzer, H_1^+ and H_2^+ ions can be distinguished by there different flight times. Because of a relative high background on the ion-detector ($\sim 10\ s^{-1}$) produced by L_α-photons we analyze time-correlated signals only. In our set-up the detection of atomic ions produced via dissociative ionisation plays a minor role (less than 1% of the total ionisation signals). As long as the detection probabilities for the correlated positron-ion pairs and the overlapp of projectile and target beam are unknown we can only determine relative ion-formation probabilities. By switching the polarity of the optical elements for the primary beam transport we can also measure the respective values for electron impact. To obtain $\sigma^-_{Ion}(H_1)$ and $\sigma^-_{Ion}(H_2)$ the ion-formation probabilities are normalized at 100 eV to the data of Shah et al. [2] and Rapp, Englander-Golden [3], respectively. The same normalization factors are also used for the normalization of the positron impact ionisation data on H_1 and H_2, respectively. Fortunately we can check this procedure by comparing our e^+-H_2 results with those obtained in a different apparatus [4]. The energy of the projectiles can be variied between 10 eV and 600 eV; the intensities are in the order of 3000 s^{-1}. The observed ion-formation probabilities are rather low ($\leq 5 \times 10^{-6}$ ions/projectile), so automated around-the-clock measurements were performed for more than 100 days to obtain the presented data.

3 Results

In figure 2 the first measurements on the ionisation of atomic hydrogen by positron impact are shown.

Process	Cross Section	Threshold
$e^+ + H_1 \rightarrow Ps + H_1^+$	$\sigma_{Ps}(H_1)$	6.8 eV
$e^+ + H_1 \rightarrow e^+ + e^- + H_1^+$	$\sigma_{Ion}(H_1)$	13.6 eV
$e^+ + H_2 \rightarrow Ps + H_2^+$	$\sigma_{Ps}(H_2)$	8.6 eV
$e^+ + H_2 \rightarrow e^+ + e^- + H_2^+$	$\sigma_{Ion}(H_2)$	15.4 eV
$e^+ + H_2 \rightarrow Ps + H_1 + H_1^+$	$\sigma_{Ps,Diss}(H_2)$	11.1 eV
$e^+ + H_2 \rightarrow e^+ + e^- + H_1 + H_1^+$	$\sigma_{Ion,Diss}(H_2)$	17.9 eV

Table 1: The most important processes for the positron impact ionisation of atomic and molecular hydrogen

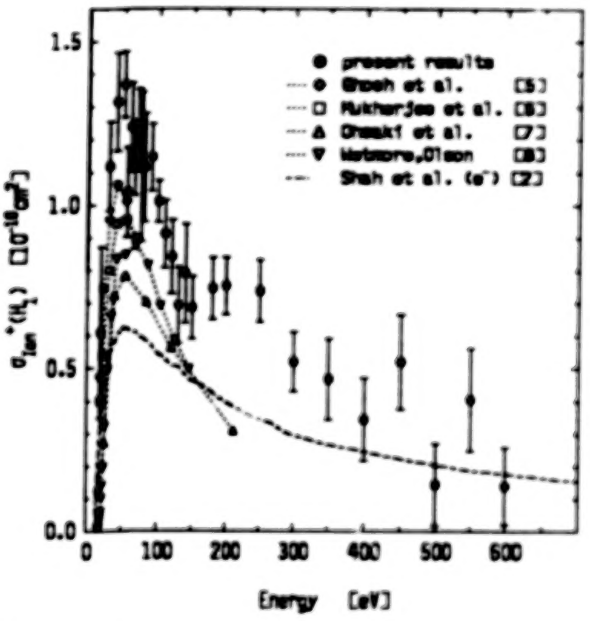

Figure 2: Positron impact ionisation cross sections: I. $\sigma^+_{Ion}(H_1)$.

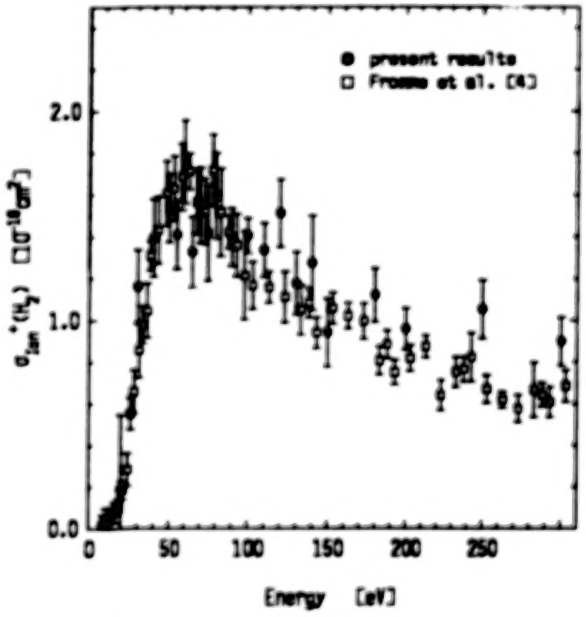

Figure 3: Positron impact ionisation cross sections: II. $\sigma^+_{Ion}(H_2)$.

Below 400 eV the e^+-H_1 impact ionisation cross section (fig. 2) is significantly higher than the respective e^- cross section, at 50 eV about a factor of two. Qualitatevely the cross section shows the shape predicted by the theoretical estimates, but at maximum all calculated values are too low. As mentioned above we measure the positron impact ionisation cross section for molecular hydrogen simultaneously (fig. 3). Our values agree excellently with those from Fromme et al. [4]. In order to check the performance of the apparatus we measure the number of time-correlated H_1^+- and H_2^+-ions for electron impact ionisation. The comparisons (fig. 4, 5) show a good agreement.

Note: We detect only those projectiles that are scattered into a angular sphere of $\pm$ 30^0. This may cause two errors in the detection of the correlated ion-projectile-pairs, depending on (a) the energy or, (b) the charge of the scattering projectile. To correct for the effect of error (a) we will form the ratio of the ion-formation probabilities produced by e^+ and e^- and multiplied them with the e^- cross sections from literature. So far there is only incomplete information on the effect of error (b).

4 Future / Acknowledgements

In a collaboration of members of the Brookhaven National Laboratory, the City College of CUNY and the University of Bielefeld this experiment will be continued at BNL. The apparatus will be modified and it will be possible to achieve more precise data with higher positron intensities, especially at ener-

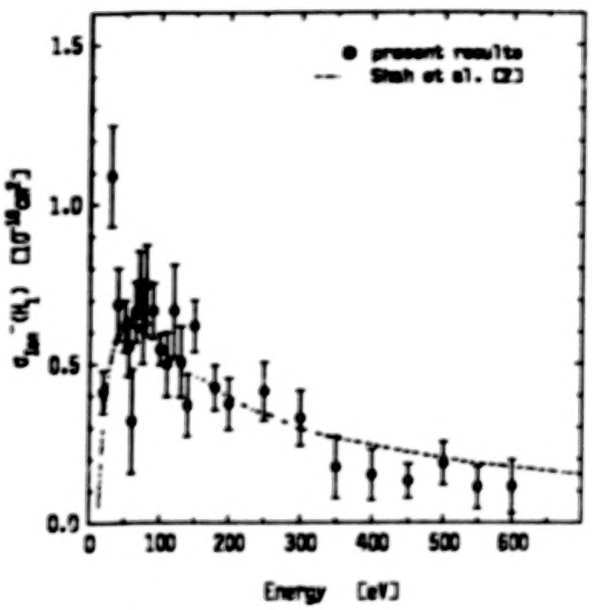

Figure 4: Electron impact ionisation cross sections: I. $\sigma^{-}_{Ion}(H_1)$.

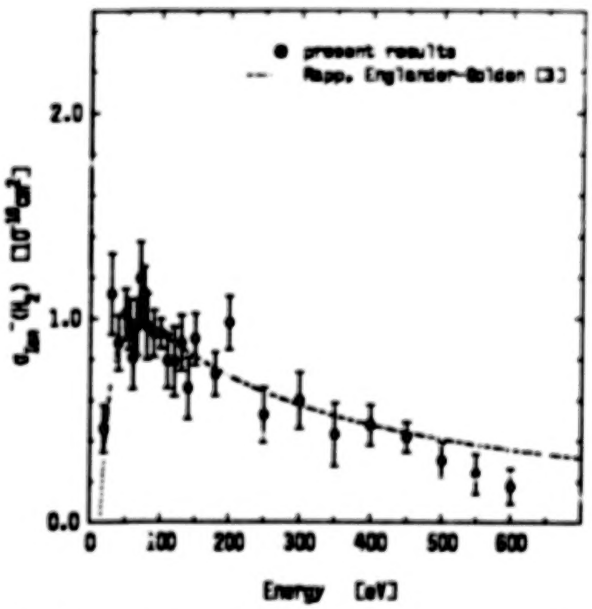

Figure 5: Electron impact ionisation cross sections: II. $\sigma^{-}_{Ion}(H_2)$.

gies near the threshold. The work at Bielefeld was supported by the Deutsche Forschungsgemeinschaft (DFG). Our Brookhaven project is being supported by the Bundesministerium für Forschung und Technologie (BMFT).

References

[1] Spicher, G., Gläsker, A., Raith, W., Sinapius, G., Sperber, W.

in: Humberston, J.W., Armour, E.A.G. [eds.]

Atomic Physics with Positrons

New York, 1987 (NATO ASI series. Series B, Physics; vol. 101)

[2] Shah, M.B., Elliot, D.S., Gilbody, H.B.

J. Phys. B: At. Mol. Phys. 20 (1987), 3501 - 3514

[3] Rapp, D., Englander-Golden, P.

J. Chem. Phys. 43 (1965), 1464 - 1479

[4] Fromme, D., Kruse, G., Raith, W., Sinapius, G.

J. Phys. B: At. Mol. Phys. 21 (1988), L261 - L265

[5] Ghosh, A.S., Majumdar, P.S., Basu, M.

Can. J. Phys. 63 (1985), 621 - 624

[6] Mukherjee, K.K., Singh, N.R., Mazumdar, P.S.

J. Phys. B: At. Mol. Phys. 22 (1989), 99 - 103

[7] Ohsaki, A., Watanabe, T., Nakanishi, K., Iguchi, K.

Phys. Rev. A 32 (1985), 2640 - 2644

[8] Wetmore, A.E., Olson, R.E.

Phys. Rev. 34 (1986), 2822 - 2829

MULTIPLE-IONIZATION OF XENON ATOMS BY POSITRON IMPACT

Georg Kruse, Andreas Quermann, Wilhelm Raith, Günter Sinapius

Fakultät für Physik, Universität Bielefeld, D-4800 Bielefeld 1
Federal Republic of Germany

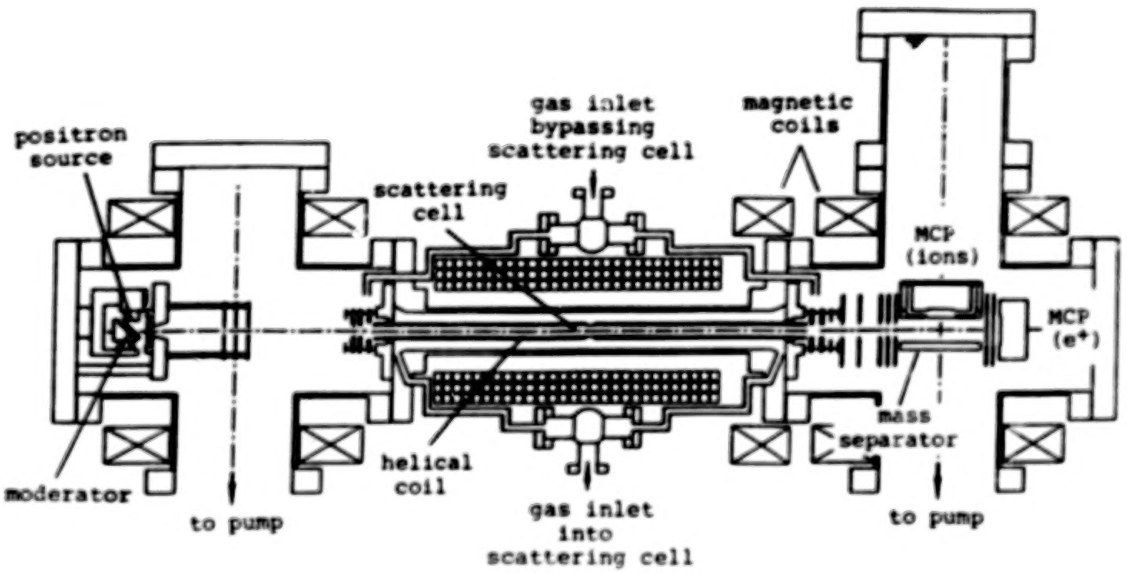

Figure 1 Cross section of the apparatus

Previously we measured the cross sections for positronium formation (σ_{Ps}) and single ionization by positron impact (σ_{ion}^{1+}) for He and H_2.[1,2] With the same apparatus, slightly modified, we are now investigating the single and multiple ionization of xenon. The principle of our method is the detection of ion and positron in time correlation which allows the discrimination of positronium formation (whereby the positron vanishes) and the destinction of single, double and triple impact ionization (which lead to different ion flight times from the gas target to the ion detector).

By using secondary electrons from the positron moderator we also perform similar measurements on electron impact ionization. By comparing with literature values for electron multiple ionization cross sections[3] we determine the detection-probability ratios for the differently charged ions.

Fig.1 shows a cross section through our apparatus. The main difference to the set-up used earlier[1,2] consists of a much stronger magnetic field (about 0.12 T in the center of the scattering cell), produced by a water-cooled coil. The higher field strength reduces the loss of ions due to wall collisions.

One of our goals is the measurement of the following ratios as functions of energy for positrons as well as electrons:

$$R_2 = \sigma_{1e2e}^{2+}/\sigma_{1e2e}^{1+}$$
$$R_3 = \sigma_{1e2e}^{3+}/\sigma_{1e2e}^{1+}$$

First results, demonstrated in Fig. 2, indicate that at 1 keV for positron impact both these ratios are considerably larger than for electron impact. For the ratio of double to single ionization cross section of helium above 200 eV Charlton et al.[4] found the opposite behavior.

References

1) Fromme D, Kruse G, Raith W, and Sinapius G 1986, Phys.Rev.Lett. 57, 3031-4

2) Fromme D, Kruse G, Raith W, and Sinapius G 1988, J.Phys.B: At.Mol.Opt.Phys. 21, L261-5

3) Krishnakumar E and Srivastava S K 1988, J.Phys.B: At.Mol.Opt.Phys. 21, 1055-82

4) Charlton M, Andersen L H, Brun-Nielsen L, Deutch B I, Hvelplund P, Jacobsen F M, Knudsen H, Laricchia G, Poulsen M R, and Pedersen J O 1988, J.Phys.B: At.Mol.Opt.Phys 21, L545-9

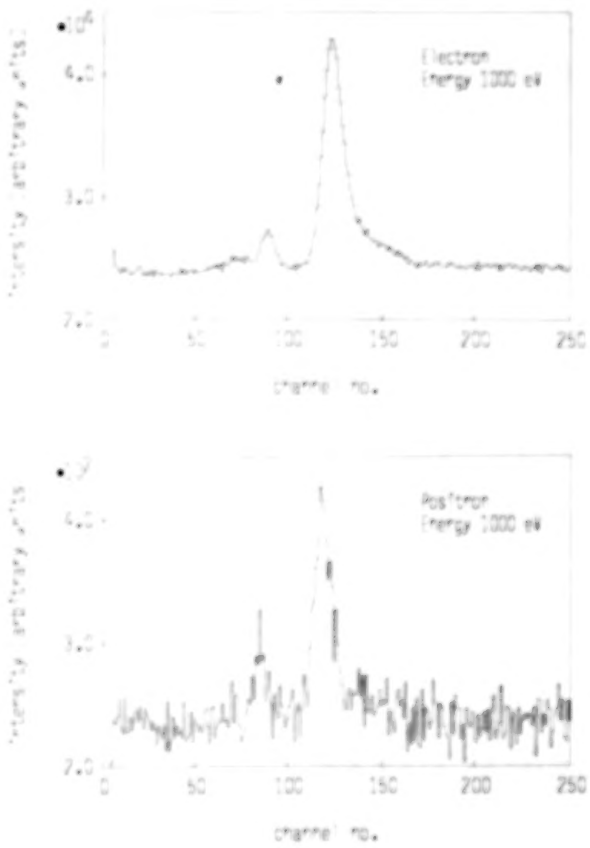

Figure 2 Time-correlation spectra obtained with 1000 eV electrons (top) and 1000 eV positrons (bottom).

DOUBLE IONIZATION OF HELIUM BY PARTICLE IMPACT.

Finn M. Jacobsen

Institute of Physics
Århus University
DK-8000 Århus, Denmark.

abstract

In this communication we review experimental results of the ratio, $R^{(2)}$, of double to single ionization of He by proton, antiproton, electron and positron impact in the energy range from 0.15 to about 10 MeV/amu. At high velocities (>1-2 Mev/amu) values of $R^{(2)}$ caused by electron impact merge with those for the antiproton while the positron results merge with those for the proton with the $\bar{p}$, e^- values being up to a factor of 2 greater than that for the p, e^+. At these velocities the single ionization cross sections caused by impact of any of these four particles are indistinguishable.

Double ionization by charged particle impact is a fundamental collision channel in which two electrons are removed from the target atom. Experimentally, this collision channel has been studied for a variaty of target atoms for different projectiles[1-10]. Since it was discovered that the cross section for double ionization, σ^{++}, of He by electron, e^-, impact exceeded that for the proton, p, by a factor of 2 at a velocity of 1-2 MeV/amu[1,6] much effort has been devoted to the study of this collision process. The question arose whether this difference in σ^{++} was due to a charge or a mass effect. A later experiment with antiprotons[6-7], $\bar{p}$, on He showed that the difference in σ^{++} for p and e^- was mainly a charge effect. In the latter experiment it was found that σ^{++} for $\bar{p}$ merge with that for e^- at a velocity of 1-2 MeV/amu. Recently, this picture was confirmed in a positron, e^+, experiment[8] where it was shown that σ^{++} for this projectile merge with that for p at around 1 MeV/amu.

In simple terms, we may consider three types of collisions which can cause double ionization of He. The first is the so-called shake off mechanism, SO, in which the projectile ionizes one electron and as a result of electron - electron correlation in the initial state the second electron is ionized. Secondly, the projectile may collide with one of the electrons which thereafter collides with the second one resulting in ionization of both electrons. This two step process we label TS-I, where I indicates a single projectile interaction. Finally, the direct process in which the projectile hits and ionizes both electrons, TS-II. Individually, the cross sections of these three mechanisms depend on the projectile charge, q, as q^2, q^2 and q^4 and as such give no hint that σ^{++} depends on the projectile charge. However, as was first pointed out by McGuire an interference in the final state between the direct channel (TS-II) and the shake-off process could lead to a term in σ^{++} proportional to q^3. A similar effect can also occur due to interference between TS-1 and TS-II.

Rather than measuring the values of σ^{++}, it is the ratio, $R^{(2)}$, of double to single ionization that is experimentally determined. At high

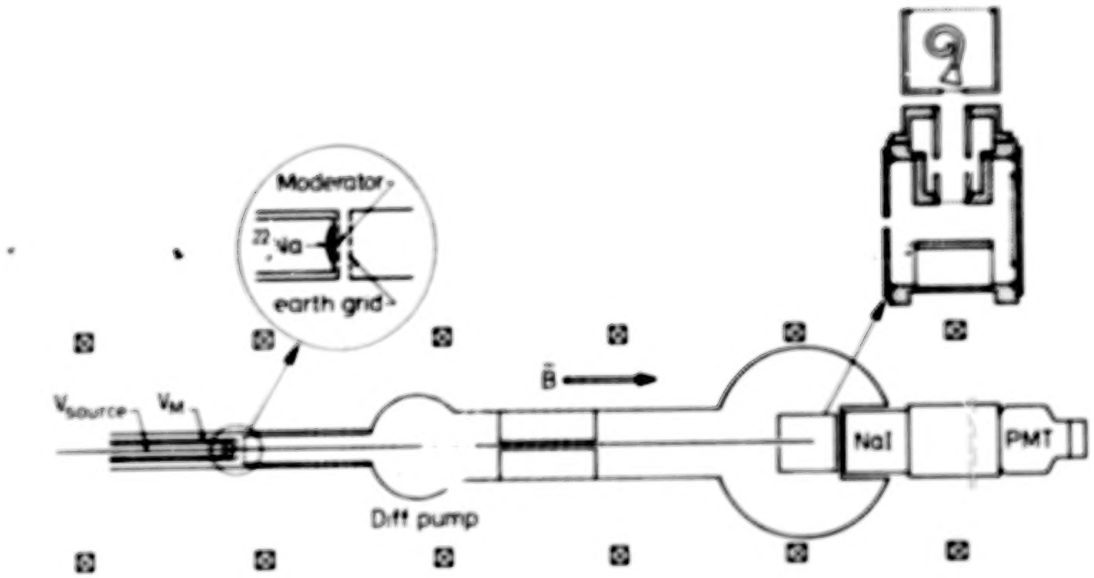

Fig. 1 The positron beam used for collision studies. The left insert shows the source - moderator configuration and the right one details of the scattering cell.

impact velocities it is well known that the single ionization cross sections of helium are indistinquishable for e^-, e^+, $\bar{p}$ and p with same velocities[1] and are well described within the Born approximation. Below, a brief description of the experimental proceduces in the determination of $R^{(2)}$ is given. This is followed by a review and discussion of the experimental results.

Fig. 1 shows the experimental setup used in the positron measurements. The e^+ beam with an intensity of 10^4 sec^{-1} and an energy spread of 2 - 3 eV is obtained from a 2 mCi ^{22}Na source and an annealed tungsten mesh as moderator. After acceleration to the desired energy the beam is transported to the gas cell by an axial magnetic field of 50 gauss. At the end of the gas cell the e^+ are further accelerated into an annihilation target of aluminium and then detected by a 125 mm x 100 mm NaI detector. The gas cell contained a pair of parallel plate electrodes 40 mm long and separated by 20 mm, which were electrically biased to provide an extraction field for the ions. One of the electrodes contained a 10 mm aperture covered with a high transmission grid. Some of the ions produced by positron impact were able to pass through this grid into a flight tube where they were further accelerated by a factor of 4.5 Q (Q being their charge state) and focussed onto the cone of a ceratron detector. Just prior to impact on the cone the ions were additional accelerated 3.9 Q keV. This impact energy resulted in unity detection efficiency for He^+ and He^{++} ions.

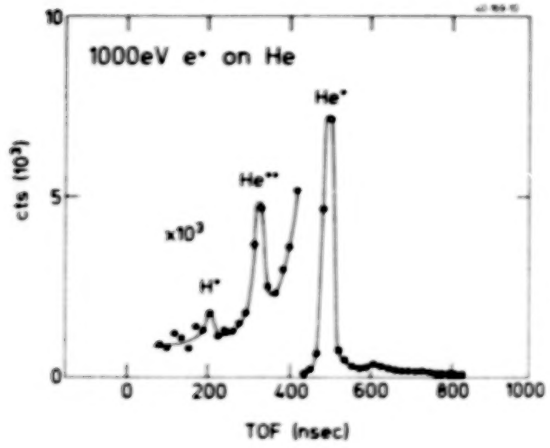

Fig. 2 shows a time of flight spectrum obtained for positrons colliding with the He target at an impact energy of 1 keV.

The extraction field for the ions was such that the total flight times were independent of their position of creation in the viewed portion of the gas cell. The ratio $R^{(2)}$ were determined by the Time Of Flight technique, TOF, in which the ceratron signal was used as a start in an inverted TOF coincidence setup with the stop signal supplied by the NaI detector. An example of a TOF spectrum is shown in Fig. 2. As observed, a tail appears on the single ionization peak due to delayed arrival of some of He^+ caused by resonant charge transfer reations in the gas. It was possible to account for all the single ionization events by including the tail when integrating over these events[8].

Basically, the experimental procedures followed in the e^-, $\bar{p}$ and p measurements were the same as that used for the e^+ with differences being: 1) the use of thin degrader foils to change the impact energy in the case of the $\bar{p}$ and in addition applying a TOF measurement for a more accurate determination of the $\bar{p}$ energies[7,10], 2) the use of a pulsed deflection system to provide a timing signal in the e^- case[8] and 3) applying a bunched beam delivered from a tandem accelerator in the p studies[7]. Furthermore, for the three latter particles the experiments were performed in a magnetic field free region. The effect of the magnetic field present in the e^+ case on the detection efficiency of the He ion were investigated and found unimportant for extraction fields greater than 100 V/cm[8]. For more detailed information on the experimental techniques employed in the e^-, e^+, $\bar{p}$ and p studies the reader is referred to the original papers.

Fig. 3 displays experimental results. The solid lines represent values for e^-, $\bar{p}$ and p with the latter results being average values as measured by several groups[1,5,7]. As observed the e^+ results merge with that of the p data and as such comfirm the results obtained by Andersen et.al.[7] that the large difference between the e^- and the p data is caused by a charge rather than a mass effect.

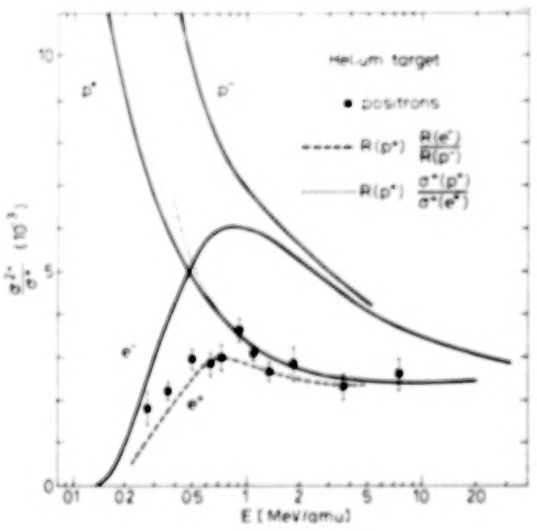

Fig. 3 shows the ratio of double to single ionization of He for protrons, antiprotons, electrons and positrons as a function of impact energy.

At lower energies the values of R for e^- and e^+ falls below that for $\bar{p}$ and p, respectively. This is probably mainly due to the much lower kinetic energy of the light particles resulting in fewer available final states for these projectiles compared to that of the much heavier $\bar{p}$ and p. A similar effect is observed when single ionization cross sections for e^+ and e^- are compared to that for the proton. To see whether this mass effect is similar for e^- and e^+ it has been suggested[8] to write $R^{(2)}(e^+)$ as:

$$R^{(2)}(e^+) = R^{(2)}(p)(R^{(2)}(e^-)/R^{(2)}(p))$$

and the result of this relation is shown as the dashed line in Fig. 3 and fits fairly well the positron results at impact energies in excess of 0.5 MeV/amu. This may indicate that the deviation between the e^- and $\bar{p}$ results (and correspondingly that for the e^+ and p) at energies between 0.5 and 2-5 MeV/amu is due to kinematic effects. At lower energies the results for the p and e^+ are influenced by electron capture resulting in the formation of H and Ps, respectively. In the e^+ experiment it was not possible to deduce the significance of double ionization of the He atom with Ps in the final state.

There have be a number of theoretical studies of double ionization of the He target since McGuire[12,13] suggested that the difference in σ^{++} for p and e^- was due to interference between the two different double ionization mechanisms SO and TS-II. Later Sørensen[7] argued that the observed difference of R for p and $\bar{p}$ could be explained by an interference between the two two-step mechanisms TS-I and TS-II. At impact energies greater than 1-2 MeV/amu of interest here one may question whether it is reasonable to speak about two distinct processes when considering the SO and TS-I mechanisms. In both of these cases the energy transfered by the projectile to the "first" e^- is generally low such that dynamic correlation between this e^- and the other target e^- should not be ignored. Double ionization by high energy photons results in the ejection of a fast electron and the subsequent electronic relaxation may result in ionization of the second e^-. The high energy limit of $R^{(2)}$ of He by photons is about one order of magnitude greater than that for particle impact[14].

In order to illustrate how interference in the final state may influence the values of $R^{(2)}$ differently for positive and negative projectiles we follow the ideas of Andersen et.al.[7]. In the SO and TS-I types of collisions the projectile interacts only with one electron through the perturbation $-Qe^2/r$, while the second e^- is ionized as a result of $e^- - e^-$ correlation. Consequently, we may write the total transition amplitude for these processes as

$$a_I = -QC_I \qquad (1)$$

where C_I is a constant. In the direct process, TS-II, where the projectile interacts with both electron we may write the total transition amplitude as

$$a_{II} = (-QC_1)(-QC_2) = Q^2 C_{II} \qquad (2)$$

with C_{II} being another constant. By ignoring any other processes which may lead to double ionization, we can express σ^{++} as

$$\begin{aligned}\sigma^{++} &= \Sigma |a_I + a_{II}|^2 \\ &= Q^2 \Sigma |C_I|^2 + Q^4 \Sigma |C_{II}|^2 \\ &\quad - Q^3 \Sigma |C_I C_{II}^* + C_I^* C_{II}| \\ &= Q^2 \sigma_I + Q^4 \sigma_{II} - Q^3 2\Sigma_{int} \qquad (3)\end{aligned}$$

where σ_I and σ_{II} are the cross sections for double ionization as a result of one and two projectile interactions and Σ indicates a summation over the final states. σ_{int} is the contribution due to interference between these two processes. Under the assumption that $\sigma^+(He^{++}) = 4\sigma^+(p)$ then we obtain from Eq. 3

$$R_I = R^{(2)}(p)+[R^{(2)}(\bar{p})-R^{(2)}(He^{++})]/3$$

$$R_{II} = -R^{(2)}(p)/2+R^{(2)}(\bar{p})/6+R^{(2)}(He^{++})/3$$

$$R_{int} = (R^{(2)}(\bar{p})-R^{(2)}(p))/4 \qquad (4)$$

By applying Eqs. 4 to the experimental results for $\bar{p}$, p and He^{++} Andersen et. al.[7] obtained the results displayed in Fig. 4. The dashed lines in Fig. 4 are obtained from theory/estimates detailed in ref. 7. As observed R_I is independent of the projectile energy in agreement with expectation as σ_I like σ^{++} is caused by a single projectile interaction. R_{II} is proportional to 1/E in rough agreement with the interpretation that σ_{II} is caused by two successive first Born types of collisions between the projectile and the target electrons. The interference term R_{int} is approximately proportional to $E^{-1/2}$ which is to be expected from the energy dependence of σ_I and σ_{II}.

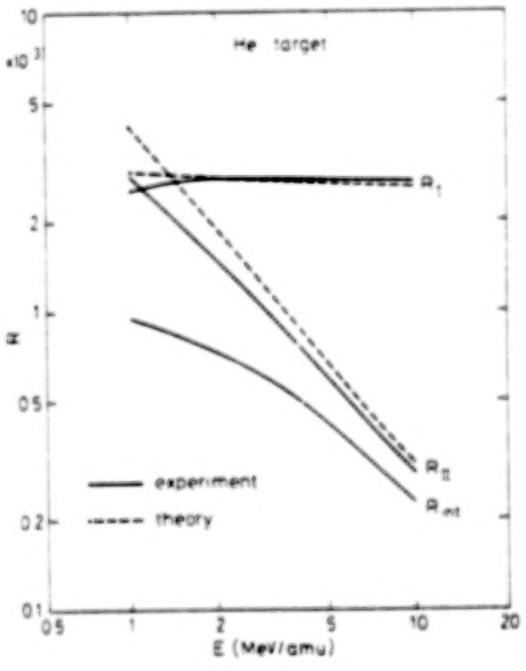

Fig. 4 shows the contributions of the various mechanisms involved in double ionization of the He target, see text for details.

Other theoretical interpretations of $R^{(2)}$ for the He target have been advanced, Reading and Ford[15], Olson[16] and Vegh[17] have all emphasized the role of e^- - e^- correlation in the postulated mechanisms by which this interaction may lead to a charge dependency of σ^{++}. Briefly, Reading and Ford[15] have suggested a model called interception in which they argue in the following way. A positive projectile outside the He atom will pull the nearest e^- away from the second one and thus reducing the probability of the TS-I mechanism while a negative projectile will push the two e^- toward each other. Reading and Ford[15] and Olsen[16] have also pointed out that in close collisions the screening of the nucleus depends on the projectile charge. For negative projectiles a transient decrease in the binding energy occurs which may result in an enhancement of σ^{++} over that for positively charged projectiles.

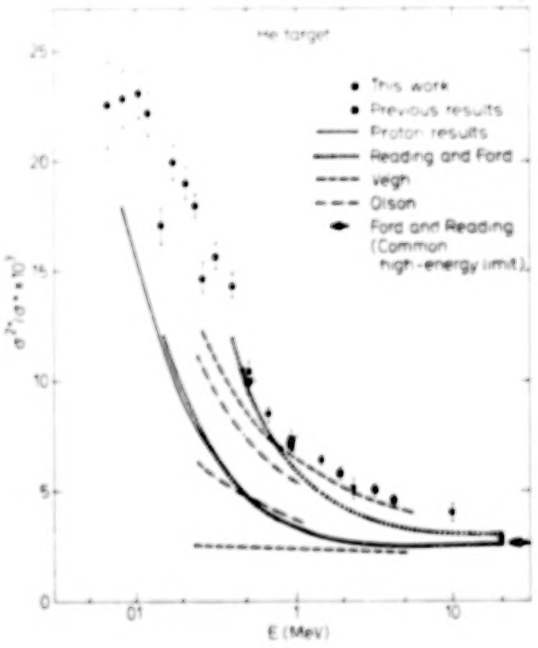

Fig. 5 compares theoretical and experimental results for the ratio of double to single ionization of He by p and $\bar{p}$ impact.

In ref.10 the experimental results of $R^{(2)}$ for p and $\bar{p}$ were compared to theoretical predictions[15-18] and their figure is reproduced in Fig. 5. The calculation of Reading and Ford[15] is based on the so-called forced-impulse methods, FIM, while that of Olson[16] results from a classical trajectory Monte Carlo, CTMC, study. Vegh[17] explains the difference in σ^{++} for p and $\bar{p}$ due to correlated motion of the target electrons during the collision. The results obtained by FIM seems most successful although at higher energies it only account for 50% of the measured effect. In a later calculation of the high energy limit of $R^{(2)}$ Reading and Ford[18] obtained excellent agreement with experiment by including d waves in their expansion.

In conclusion, it seems at present not possible experimentally to sort out which of the many effects in double ionization of He that are dominant for the difference in σ^{++} for positive and negative projectiles. However, what is established is the simularities of the e^+ and p results and correspondingly those of e^- and $\bar{p}$. Hence, further studies of correlation phenomena can be carried out using any of the two sets of projectiles.

References

[1] L.J. Puckett and D.W. Martin, Phys. Rev A1, 1432 (1970).
[2] T.D. Mark, J. Chem. Phys. 63, 3731 (1975);
[3] H.K. Haugen, L.H. Andersen, P. Hvelplund and H. Knudsen, Phys. Rev. A26, 1962 (1982).
[4] H. Knudsen, L.H. Andersen, P. Hvelplund, G. Astner, H. Cederquist, H. Danared, L. Liljeby and K.G. Rensfelt, J. Phys. B 17, 3545 (1984).
[5] M.B. Shah and H.B. Gilbody, J. Phys. B 18, 899 (1984);
[6] L.H. Andersen, P. Hvelplund, H. Knudsen, S.P. Møller, K. Elsener, K.G. Rensfelt and E. Uggerhøj, Phys. Rev. Lett. 57, 2147 (1986).
[7] L.H. Andersen, P. Hvelplund, H. Knudsen, S.P. Møller, A.H. Sørensen, K. Elsener, K.G. Rensfelt and E. Uggerhøj, Phys. Rev. A 36, 3612 (1987).
[8] M. Charlton, L.H. Andersen, L. Brun-Nielsen, B.I. Deutch, P. Hvelplund, F.M. Jacobsen, H. Knudsen, G. Laricchia, M.R. Poulsen and J.O. Pedersen, J. Phys. B 21, L545 (1988).
[9] M. Charlton, L. Brun-Nielsen, B.I. Deutch, P. Hvelplund, F.M. Jacobsen, H. Knudsen, G. Laricchia, and M.R. Poulsen, J. Phys. B in press.
[10] L.H. Andersen, P. Hvelplund, H. Knudsen, S.P. Møller, J.O.P. Pedersen, S. Tang-Petersen, E. Uggerhøj, K. Elsener and E. Morenzoni, to be published.
[11] D. Fromme, G, Kruse, W. Raith and G. Sinapius, Phys. Rev. Lett. 57, 3031 (1986).
[12] J.H. McGuire, Phys. Rev. Lett. 49, 1153 (1982).
[13] J.H. McGuire and J. Burgdofer, Phys. Rev. A 36, 4089 (1987).
[14] T.A. Carlson, Phys. Rev. 156, 142 (1967).
[15] J.F. Reading and A.L. Ford, J. Phys. B 20, 3747 (1987).
[16] R.E. Olson, Phys. Rev. A 36, 1519 (1987).
[17] L. Vegh, Phys. Rev. A 37, 992 (1988).
[18] J.F. Reading and A.L. Ford, J. Phys. B 21, L685 (1988).

POSITRONIUM REFLECTION AND POSITRONIUM BEAMS

M. Weber,[1] S. Tang,[1] R. Khatri,[1] S. Berko,[2] K.F. Canter,[2] K.G. Lynn,[3]
A.P. Mills, Jr.,[4] L.O. Roellig,[1] and A.J. Viescas[1]

[1] *City College of City University of New York*
[2] *Brandeis University*
[3] *Brookhaven National Laboratory*
[4] *A.T.&T. Bell Laboratories*

Abstract

We have observed specular reflection of positronium, Ps, and established that there is adequate intensity at higher energies to make further study worthwhile. The scattering appears to be restricted to the outermost surface with a mean free path of (0.75 ± 0.15)Å for Ps in LiF(100). With a greater intensity Ps beam one should see higher order diffraction beams as the result of the periodicity of the surface. Ps diffraction thus offers the possibility of being a novel and valuable probe to study the outermost surface and to study adsorbants on it. Two methods for producing Ps beams are described.

Introduction

At the Brookhaven National Laboratory we have initiated a program to study the interaction of positronium, Ps, with the surfaces of solids. An experimental investigation of the reflection of positronium (Ps) from solid surfaces is well warranted because of the fundamental nature of the electronic processes involved in Ps reflection and the possibility of developing a valuable new tool for surface structure determination. Our program of investigating Ps reflection was initiated as a result of the following reasoning. Since Ps can normally be expected to undergo elastic collisions from only the outer atomic layer of a solid, low energy Ps diffraction (LEPSD) could be a unique probe of ordered surface structures. This is somewhat similar to the situation for helium atom diffraction,[1] which is a powerful tool in surface structure determination because it is only sensitive to the outer surface layer. However, the savings in complexity of He atom diffraction by not having to treat multiple scattering from subsurface layers, as in the case of low energy electron diffraction[2-4] (LEED) is somewhat mitigated by having to deal with long range forces that dominate in the diffraction. The $\approx 0.02eV$ energies necessary for He atoms to have ≈ 1Å de Broglie wavelength results in the He atoms having classical turning radii far enough from the individual ion cores that the main scattering is due to the average potential presented by the surface.[1] This requires an accurate treatment of the atom-surface interaction potential which is difficult to obtain and is further complicated because the depth of the van der Waals attractive potential at the surface is approximately the same as the kinetic energy of the helium atom.[5] In order for Ps to have ≈ 1Å de Broglie wavelength, its energy must be on the order of $\approx 75eV$. At this energy, Ps "atoms" would be oblivious to the mean surface potential and only undergo elastic reflection in close encounters with the ion cores. Because of the large break-up probability of Ps (binding energy $= 6.8eV$), multiple scattering and other subsurface contributions to the elastically scattered Ps are expected to be negligible. Thus, Ps diffraction offers the possibility of being a valuable probe.[6]

The degree to which Ps scatters only from the outer surface layer is determined mainly by the interstitial density of valence or conduction electrons of the material. Because of the low mass of weakly-bound electrons, and hence

large recoil, collisions with the electrons destroy the coherence of the scattered Ps and thus must be regarded as a source of attenuation of the incident and diffracted Ps beam. Typical elastic cross sections in the $10eV$ region for Ps-free e^- collisions are on the order of $10^{-15}cm$.[7,8] Thus for solids having interstitial electron densities of $\approx 10^{23}cm^{-3}$,[9-12] a mean free path of ≈ 1Å for the Ps can be expected. Consequently, LEPSD from a solid surface would yield diffracted Ps intensities versus incident energy (i.e., "I(V)" curves) which would be dominated by the elastic scattering from only the outer layer atomic distribution. In the case of an ordered adsorbate overlayer, chemisorbed to a surface, however, the incident Ps could easily penetrate the relatively open spaces between the adsorbate atoms. This would lead to the interesting case of interference between Ps scattering from the adsorbate and from the outer surface with a high sensitivity to the structure of the adsorbate layer and outer surface.

In this paper we will first discuss the results we have already obtained,[13] present an interpretation of them, then provide a description of the method (gas cell) used to produce the Ps beam, and conclude with a description of a completely different method to obtain a Ps beam which is presently under construction.

Positronium Specular Reflection from LiF

Upon entering the experimental chamber the Ps beam divergence is limited by aperture to 5° full width of half maximum of the peak. It is reflected from the sample, S, shown in Fig. 1 and detected by its annihilation gamma rays by two bismuth germanate ($Bi_3Ge_4O_{12}$, titled BGO) detectors in coincidence. The incidence and reflected angles θ_i and θ_r are measured with respect to the normal to the sample; the total angle with respect to the Ps beam is $\psi = \theta_i + \theta_r$. The sample, S, can be rotated through an angle of $50° \leq \theta_i \leq 90°$. The intensity of the detected Ps beam from the gas cell is measured by removing the sample and placing the annihilation plate and BGO detectors at $\psi = 180°$. The distance

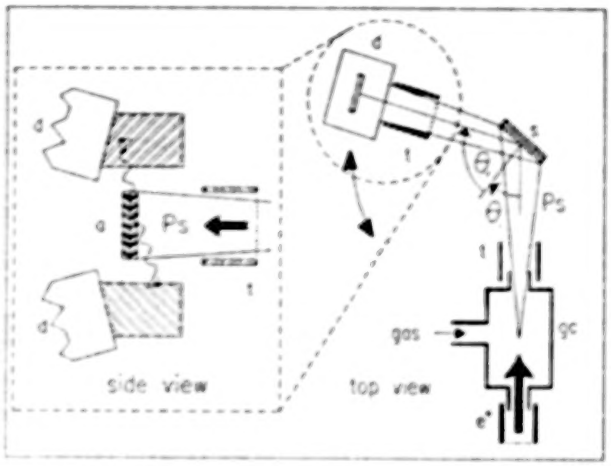

Figure 1 — The experimental arrangement: gc-gas cell, s-sample, t-tubes and grids, and a-annihilation plate.

from the center of the gas cell to the annihilation plate and BGO detectors is a constant, $40cm$, for $100° \leq \psi \leq 180°$. The efficiency for producing and detecting Ps is shown in Fig. 2.

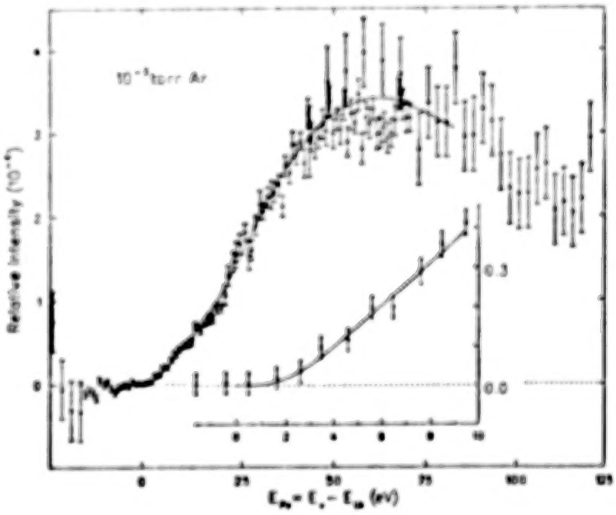

Figure 2 — The efficiency of detecting Ps at the annihilation plate versus the Ps energy. This efficiency was obtained with the gas cell filled with Ar at a pressure of $10^{-3}torr$. The Ps atoms were restricted to a 5° cone (FWHM). The efficiency includes the decay in flight and the Ps detection efficiency.

The efficiency is measured per incident positron versus the Ps energy. It reflects the efficiency of the gas cell filled with 10^{-3}*torr* Ar to form ortho Ps in a 5° cone, the decay in flight of the initial Ps beam, and the ratio of the efficiency to detect of the annihilation gamma rays from Ps to those from positrons. The inset in Fig. 2 is an expanded scale of the low energy Ps region. The absolute efficiency is not required for the measurement of the reflection coefficient because the efficiencies of Ps formation, reflection, and detection are the same (except for 2S Ps) for detecting Ps with the sample removed from the beamline ($\psi = 180°$). We calculate the ratio of the reflected Ps intensity to the intensity at $\psi = 180°$.

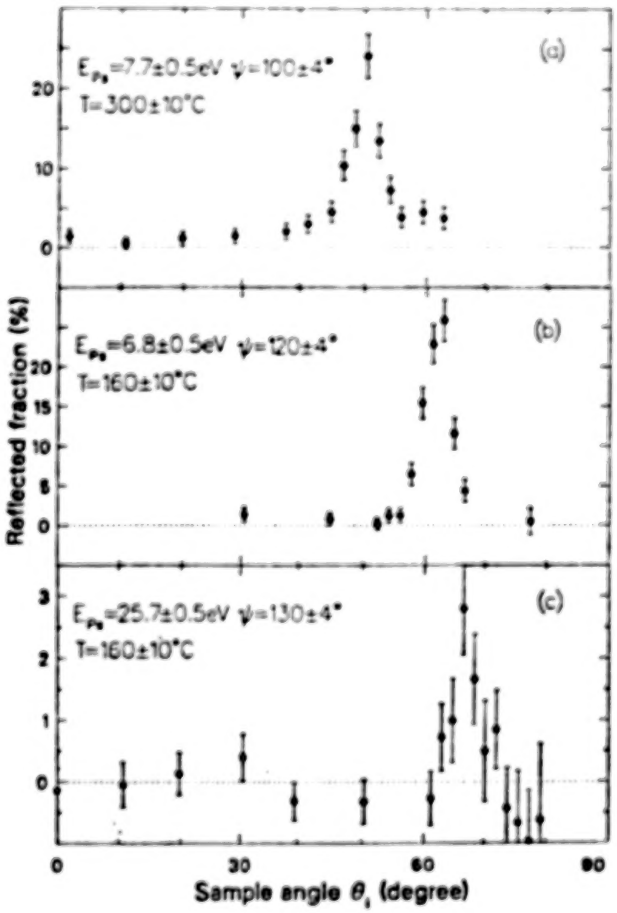

Figure 3 — Reflection probability of Ps at constant incident energy and total scattering angle $\psi = \theta_i + \theta_r$ vs the incident angle, θ_i.

Rocking curves were obtained of the specular reflection of Ps from LiF(100) by rotating the LiF crystal with respect to the Ps beam and holding the detectors fixed. Data was taken with the position of the Ps detector at $\psi = 100°$, $120°$, and $130°$. The results for three different Ps energies and three different specular angles are shown in Fig. 3.[13] It is evident the Ps specular reflection does occur and that the reflected fraction is surprisingly high $(30 \pm 5)\%$ at a Ps energy of $7eV$. We also measured the fraction of Ps reflected at a fixed specular angle as a function of the energy of the Ps (see Fig. 4). The fraction of Ps reflected for $\psi = 100 \pm 4°$ from LiF(100) was measured when the LiF was at a temperature of $160 \pm 10°C$ and at a temperature of $300 \pm 10°C$. The two measurements are in good agreement, although the reflection at $300°C$ is somewhat higher than that at $160°C$.

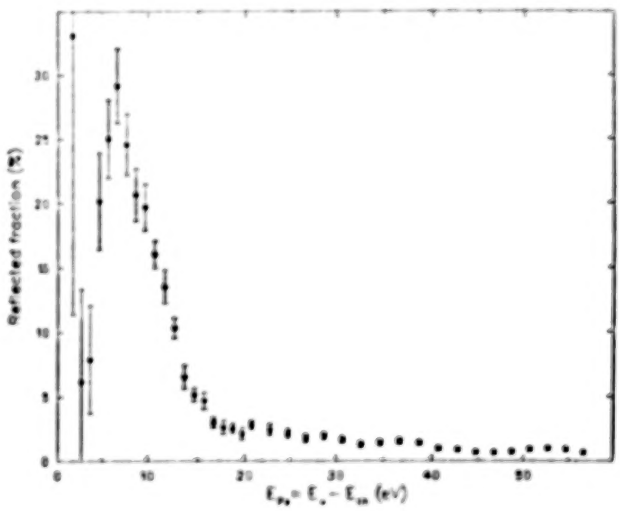

Figure 4 — Ps reflection coefficient as a function of the Ps energy for $\theta_i = \theta_r = 50.4°$.

A simple interpretation of the Ps reflection fraction and its energy dependence can be obtained by considering plane waves reflecting from a potential step. Letting z be the coordinate perpendicular to the crystal surface we consider the potential:
$V(z) = 0$ [illegible] 0, i.e., in the vacuum outside of the crystal; $V(z) = V_r + iV_{im}$ for $z > 0$,

i.e. inside the crystal there is a real and imaginary potential. Using the one dimensional Schrodinger equation in its time independent form we obtain the reflection probability:

$$R = R_o|\frac{k_o - k_{in}}{k_o + k_{in}}| \qquad (1)$$

where k_{in} and k_o are the perpendicular components of the Ps wave vectors inside and outside the crystal, and where the factor R_o is inserted to account for the reflection probability is less than unity at low energies. (This may be due to only a fraction of the surface being clean enough). We estimate $V_r = 4eV$, which is the difference between the binding energy of Ps in the vacuum state ($\approx 7eV$) and the binding energy of Ps inside LiF ($3eV$).[14] If we consider $V_{im} = 0$ and $V_r = 4eV$ we do not predict the observed energy dependence of the reflection probability. R equals R_o for energies less than $V_r/cos^2\theta_i$, but it falls off sharply for higher energies, and finally approaches approximately a $1/E_{p_z}^2$ dependence (see the dashed curve in Fig. 5). Choosing a different V_r only causes a translation of the dashed curve along the horizontal axis, it does not provide a better fit to the data. There is evidently much more apparent elastic scattering than can be accounted for by the real part of the inner potential alone. We can obtain a better fit to the data by adding an energy-dependent imaginary part, V_{im}, to the potential. The wave vector inside the crystal has two components $k_{in} = k_r + ik_{im}$. We can solve Eq. (1) for the value of k_{im} given a certain reflectivity R at a given energy E:

$$k_{im}^2 = \frac{2mE}{\hbar^2} \times \Big(\frac{1}{2}\zeta^2[1 + (\frac{1 - 2V_r}{E\zeta^2})^{1/2}] - 1 + \frac{V_r}{2E}\Big) \qquad (2)$$
$$\zeta = (R_o + R)/(R_o - R)$$

where $E = E_{p_z}cos^2\theta_i$. By using the data in Fig. 5, with $R = 0.30 \pm 0.05$ and letting

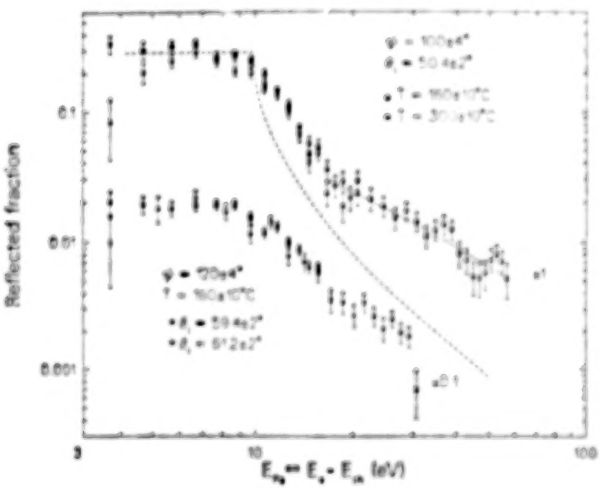

Figure 5 — Ps reflection probability vs the incident Ps energy. The solid line is calculated with the use of Eq. (2) with $V_r = 4eV$ and λ taken from the fitted line in Fig. 6. The dashed line is calculated with $V_r = 4eV$ and $\lambda = \infty$.

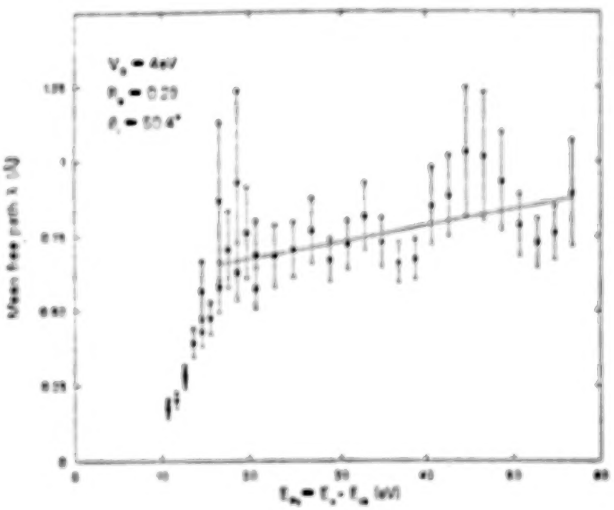

Figure 6 — Ps mean free path calculated from Eq. (2). The straight line is a least-square fit of $\lambda = \lambda_o + aE_{p_z}$ to the data in the interval $16.5eV < E_{p_z} < 56.7eV$. The fitted parameters are $\lambda = (0.57 \pm 0.06)$Å and $a = (4.4 \pm 1.7) \times 10^{-3}$Å$eV^{-1}$, with a χ^2 per degree of freedom $\chi^2/n = 15.26/26$.

$V_r = 4eV$ we can calculate k_{im}. The mean free path is:

$$\lambda = \frac{1}{cos\theta_i}\frac{\int_0^\infty z|\psi|^2 dz}{\int_0^\infty |\psi|^2 dz} = \frac{1}{2k_{im}cos\theta_i} \qquad (3)$$

where $\psi = Aexp(ik_{in}z) = Aexp\, i(k_r + ik_{im})z$. The result plotted in Fig. 6 is $\lambda = (0.75 \pm 0.15)$Å for $16.5eV < E_{P_s} < 56.7eV$. Below $16.5eV$ the mean free path by this analysis becomes unphysically small. The solid line in Fig. 6 is a two parameter fit to the data that suggests λ is slowly increasing with energy. The solid line in Fig. 5 is the corresponding reflectivity calculated with the use of Eq. 2; the dashed line was calculated with a real potential only, i.e. $\lambda = \infty$ and $V_r = 4eV$. The reasonably high-elastic Ps reflection probability observed even at high energies, in spite of the presence of the large absorptive potential is in retrospect not surprising in view of the requirements of unitarity.[15] The reason for the few percent reflection at energies much greater than V_r is principally the short λ. If V_r were to vanish there would still be a measurable reflection coefficient for small λ. In addition one should consider the region between $10eV$ and $16.5eV$ may exhibit a higher reflectivity due to a elastic scattering from the outer most ion cores. It is interesting to note that since the lattice parameter of LiF is 4.02Å, at an incident angle of 50° the first order Bragg diffraction would occur at a Ps energy of $21eV$; however due to the short mean free path at low energies it is hard to envision the high reflectivity would be due to Bragg diffraction at this energy.

It is evident from the above mentioned measurements and analysis that there is a high reflection coefficient and short mean free path for Ps in LiF, and that an intense, well collimated, and monoenergetic Ps beam holds promise as a unique probe of surfaces.

Positronium Beam–Gas Cell Production

Low energy positrons emitted from ^{64}Cu are magnetically transported through an $\vec{E} \times \vec{B}$ filter out of the shielding blockhouse[16] into an Ar gas chamber (see Fig. 7). The pressure of Ar in the gas cell was kept at $10^{-3}torr$. By the use of baffles and by differentially pumping the pressure in the experimental chamber was reduced to $10^{-5}torr$. This relatively high pressure may not have had much effect on the cleanliness of our sample because prior to introducing Ar, which had a purity of 99.995%, into the gas cell; the pressure in the experimental chamber was $10^{-10}torr$. Thus the gas in the experimental chamber was primarily due to Ar from the gas cell. Ps is formed in the gas cell by the positron picking up an electron from the Ar atom.[17–19] The ionization potential for Ar is $15.8eV$, however, the binding energy of Ps is $6.8eV$ thus the threshold energy for Ps production is a positron energy of $9.0eV$. The first excited state of the Ar atom is $11.5eV$ and the first excited state of Ps is $5.1eV$ above the ground state. Thus a positron beam which an energy between $9.0eV$ and $14.1eV$ will produce a monoenergetic beam of Ps in the energy range of $0 - 5.1eV$. The ratio of the cross section for e^+ to produce Ps in the 2S state to producing Ps in the 1S state reaches its maximum value of 13% for an e^+ energy of $50eV$ in He.[2] (We are unaware of any calculations for a similar ratio in Ar). Above $20.5eV$ it is energetically possible to produce Ps after exciting an Ar atom. However, the probability of a positron undergoing both collisions in the gas cell is exceedingly low. In summary, we estimate that the excited state contamination of our beam to average less than 5% and the energy purity due to Ar excitation to be less than 1%.

Positronium Beam–Foil Production

We are presently constructing a new high intensity positron beam in the Material Science Building across the street from the High Flux Beam Reactor (HFBR) Building. The new facility will have four advantages over the present one located at the reactor: the low energy positron beam will be more intense than the beam used for our first generation Ps experiment described here; we will not be subject to the increasingly more severe security regulations which exist on the operating level of the HFBR; the background radiation will be greatly reduced; and the area available for experiments will be increased. The new facility will have a blockhouse approximately twice the size of the one built in the reactor building. It is planned

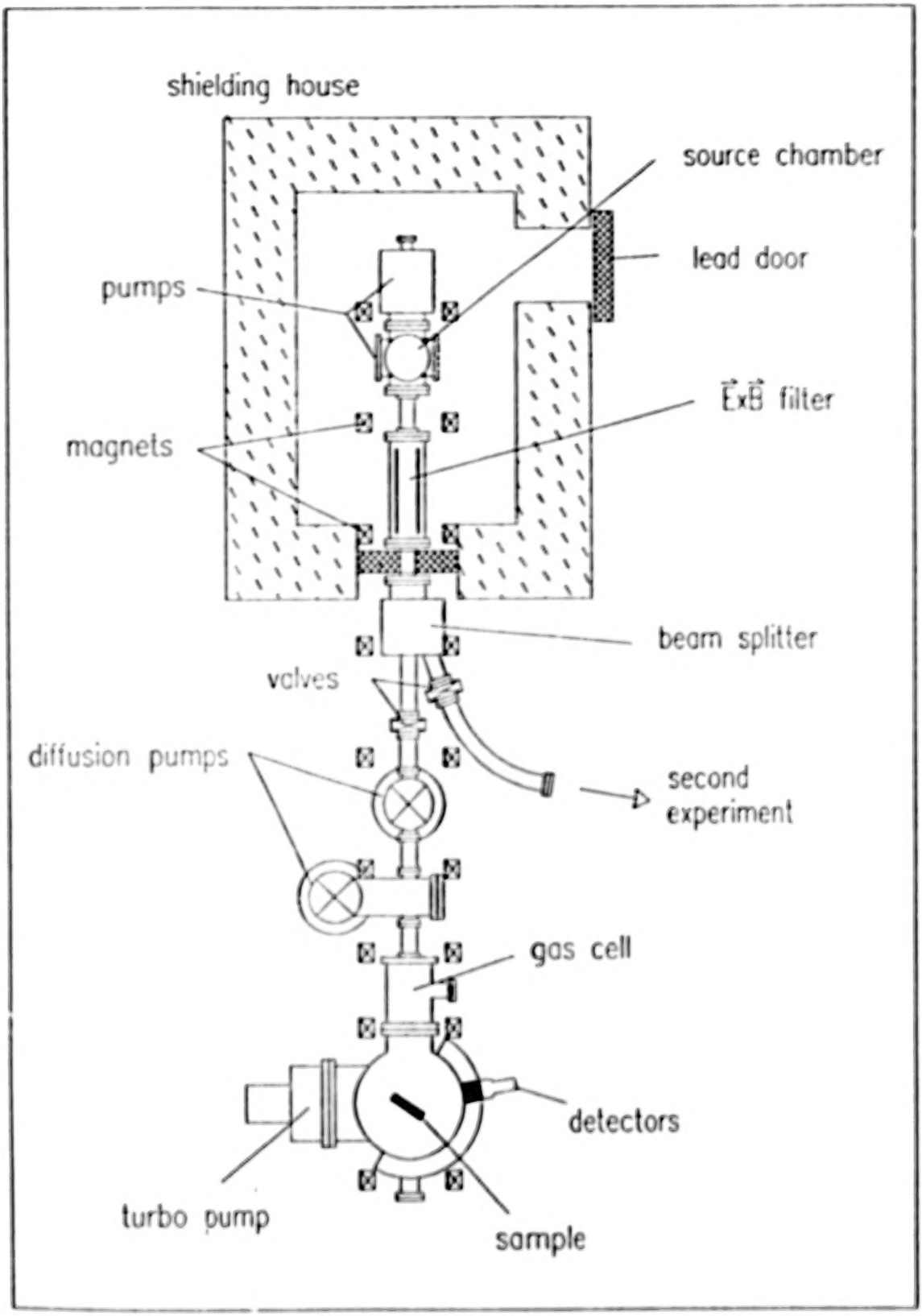

Figure 7 — Schematic view of the apparatus to produce a positron beam and a Ps beam by the gas cell method.

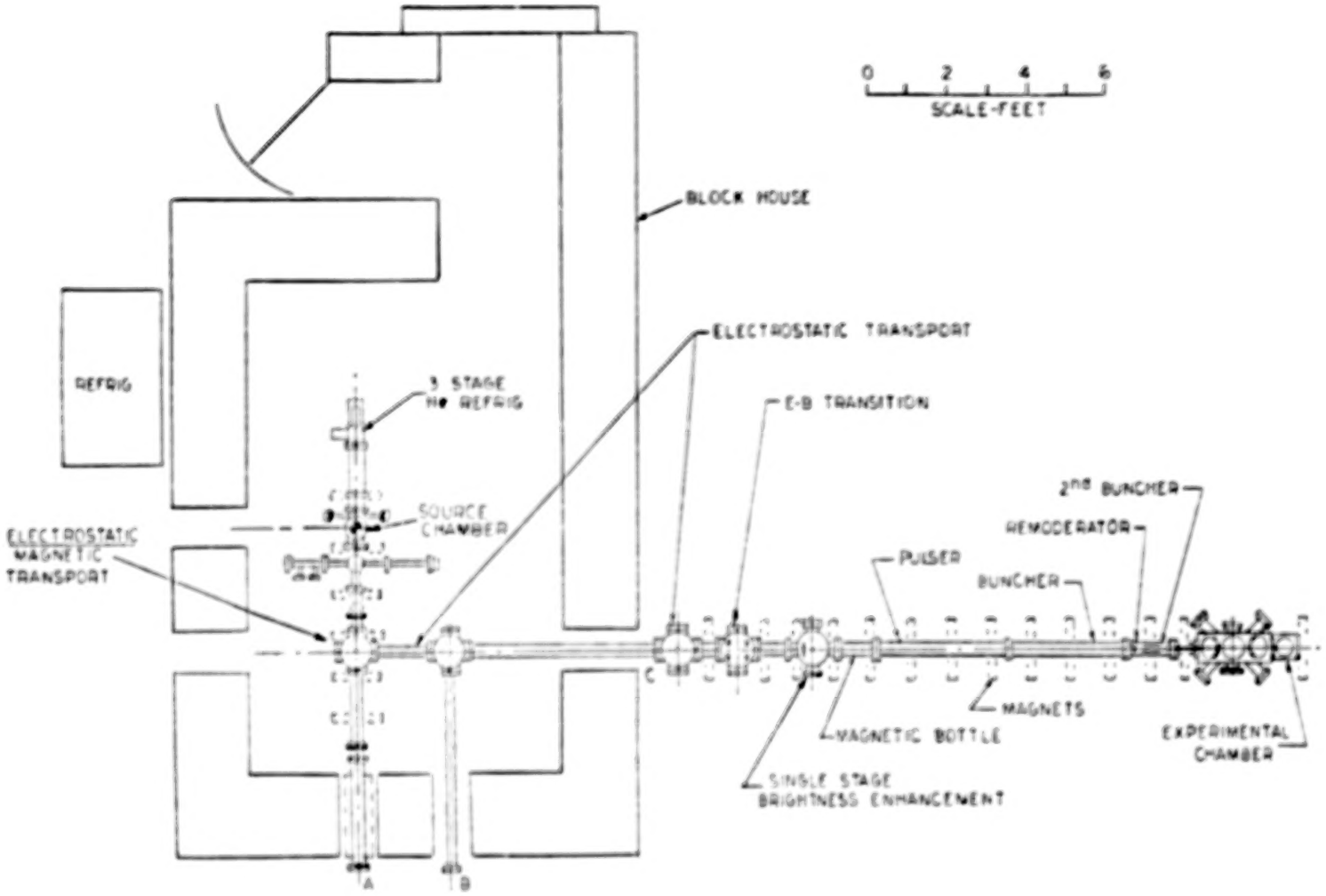

Figure 8 — Schematic view of the apparatus to produce a positron beam and a Ps beam by the foil method.

to have three low energy positron beam ports, the present blockhouse has one beam port. Two ports (ports B and C in Fig. 8) will have a electrostatic transport system and the third (port A) will be a magnetically guided transport system. A copper pellet will be irradiated in the core of the HFBR for 2 days, then removed from its capsule in a blockhouse located alongside of the reactor on the operations level of the HFBR and deposited into a lead and heavi-met container. It will then be transported by an electric truck to the Material Science Building, and inserted into a crucible in the new blockhouse. The copper pellet will be evaporated onto the inside of a cone which then will have deposited on it 10^4Å of solid Ne. Our past moderator was crystalline copper, but our future one will be solid neon because of its higher efficiency. We have measured an efficiency of $\approx 1\%$ for producing low energy positrons with solid neon in a cone configuration.[21-24]

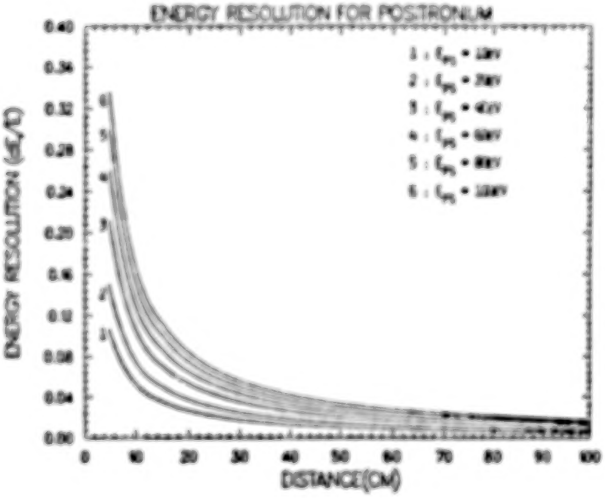

Figure 9 — The energy resolution for observing Ps in a pulse of 8ns width vs distance from the foil to the detector for various Ps energies.

Instead of using the charge transfer of an electron from an Ar atom to combine with a positron to produce Ps we will send positrons through a thin carbon foil to produce them.[25] The positron beam will be pulsed which allows us to perform time of flight measurements. This method has three distinct advantages in comparison to the gas cell method to produce Ps. The advantages are first the surface of the sample will not be as easily subject to contamination as it is from the gas cell since we will be able to operate in a $\approx 10^{-10} torr$ environment. The second advantage is that we will be able to have a direct measure of the energy of each Ps atom with better resolution. Third, although the Ps produced by the foil would not be as monoenergetic as can be obtained using a rare gas target the time of flight method would give us the advantage of being able to investigate many energies at once.

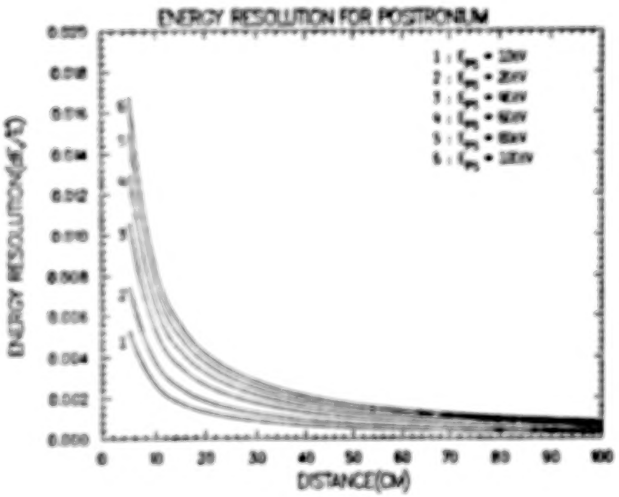

Figure 10 — The energy resolution for observing Ps in a pulse of 0.1ns width vs distance from the foil to the detector for various Ps energies.

The new Ps beam will be produced by the following method.[26,27] The positron beam will be transported out of the blockhouse electrostatically. It will then enter a magnetically guided section. It is then remoderated to minimize its transverse energy component and injected into a pinched magnetic field to enter a magnetic bottle. Upon entering the bottle the beam transverses a rf cavity which oscillates at 430MHz to give it transverse motion and to excite the positron cyclotron resonance. The positrons are then reflected by a positive potential on a grid, they again transverse the

rf cavity and they now have enough transverse motion to be reflected by the pinched magnetic field at the entrance of the bottle. The positrons now oscillate between the two ends of the trap for $100\mu s$. During this time positrons continue to stream into the trap from the radioactive source and accumulate in the trap. After a $100\mu s$, the grid which was at a positive potential is given a negative potential pulse by an oscillator operating at 10kHz and the positrons enter a section of 100 ring electrodes each having a bias such that the accumulated positrons experience a potential which varies harmonically with distance along the beamline and are bunched to a pulse of width $8ns$. The total length of the accumulator/pulser/buncher is $90inches$. This accumulator/pulser/buncher has been constructed, tested and measured to have an efficiency of 63%.[26] Upon leaving the buncher the positrons are again remoderated and enter a second buncher of length one inch which produces a harmonic potential due to a geometric distortion of the electric field at one end of the buncher. This second buncher will reduce the positron pulse width from $8ns$ to a subnanosecond bunched positron beam. The technical details of the first accumulator/pulser/buncher are given in Refs. 26 and 27 and the details of the second buncher are given in Ref. 28. Upon leaving the second buncher, the positrons traverse a carbon foil and produce a pulsed beam of Ps atoms which then enter the experimental chamber which was described above. The charged particles in the beam are removed by electric fields. The energy of the Ps atom is determined by measuring the time difference between the time the pulsed positron beam strikes the carbon foil and the time the positronium atoms travel a fixed distance to the Ps detection system. The pulse width of the positrons leaving the buncher very much affects the measured energy resolution of the Ps atom. This is shown in Figs. 9 and 10 which plot the Ps energy resolution versus Ps flight path for various energies of the Ps atom. Fig. 9 is for a positron pulse width of $8ns$ and Fig. 10 is for a positron pulse width of $0.1ns$. Although a longer flight path increases the energy resolution it also reduces the number of Ps atoms detected due to Ps decay. The effect of Ps decay in flight is given in Fig. 11 which plots the Ps attenuation coefficient as a function of Ps energy for various length of flight paths.

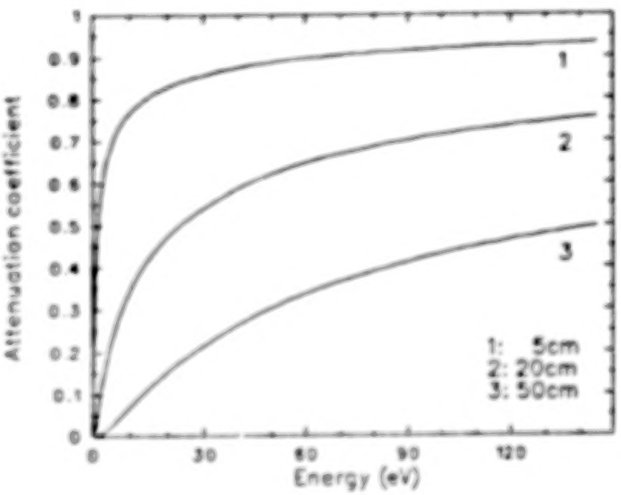

Figure 11 — The attenuation coefficient for Ps decay in flight vs the Ps energy for various flight path distances.

The table below shows the expected efficiencies of the various components of the pulsed Ps beam production. The average efficiency was calculated for the production of Ps in the energy range of $6eV$ to $100eV$ in a solid angle of 10^{-2} steradian after traveling a path length of $20cm$. The column at the right lists the number of particles to be expected at each stage of the beamline. These numbers are predicated on a spherical copper pellet of weight of $0.86g$ and diameter $0.57cm$ placed in the core of the HFBR for a period of 48 hours where the positron-emitting isotope ^{64}Cu is produced by the reaction ^{63}Cu(n,γ) ^{64}Cu. The activity of the pellet after 48 hours is $100.5Ci$ of positron emission.[16] Our past experience indicates that approximately one-third of this activity can be evaporated unto a surface because of losses due to decay during the time period from removing the source from the reactor to completing the evaporation of the Cu on a surface, and due to Cu vapor escaping and not being deposited on

the surface. We have obtained a moderating efficiency of 1.2% with a solid Ne moderator,[24] but for the purpose of these calculations we are estimating an efficiency of 0.7%. We expect the efficiency of the 90° bender in the blockhouse to be 90%. The number of low energy positrons entering the remoderator given in the table, $7.8 \times 10^9 sec$, results from these calculations. It is the number of particles during the beginning of a run, for ^{64}Cu decays with a half-life of 12.8 hours. At the end of a two day run the number will be reduced by a factor of ≈ 16.

Ps BEAM EFFICIENCY

Process	Efficiency in %	Number of Particles e^+/sec
Slow positrons into remoderator		7.8×10^9
Remoderator 1	30	2.3×10^9
Accumulator/pulser/buncher	63	1.4×10^9
Remoderator 2	30	4.2×10^8
Ps formation in foil *)	8.9×10^{-3}	3.7×10^4
Loss in three grids †)	72	2.7×10^4

*) energy range $6eV$ to $100eV$ in a solid angle of $10^{-2} ster$. after traveling a path length of $20cm$.[25]
†) 90% transmission grids

An extensive research program is planned to vary the parameters of the carbon foil to improve its efficiency to produce Ps (foil thickness, positron energy, coatings on foil, other foils etc.). Another consideration which will be examined is the effect of a $34Ci$ of positron emission source on the Ne moderator. Will it cause the surface to be charged? Will it produce a large number of defects in the solid Ne? Both effects could adversely effect its efficiency. In the event that Ne moderation is adversely affected by a strong radioactive source we plan to revert back to a transmission moderator to produce low energy positrons and to compensate for its lower efficiency by using a stronger ^{64}Cu source.

Summary

Positronium reflection from a surface shows promise to be an extremely sensitive surface probe. We have shown that the mean free path in LiF(100) of Ps atoms in the energy range $16.5eV < E < 56.7eV$ is 0.75 ± 0.15Å.[13] This assures us that analysis of Ps diffracted intensities will only have to take into account the outer most atomic layer, and thus avoids the complication encountered in LEED where the mean free path is typically an order of magnitude larger.[29]

A description is given of two different methods for producing a Ps beam. Each method has its own set of advantages. The gas cell method will produce a monoenergetic Ps beam at low energies, whereas the foil beam will allow the sample to be in an ultra high vacuum environment and the energy of each Ps atom can be measured by a time of flight technique. The work was supported in part by the National Science Foundation (Grant No. DMR-8620168), and in part by the Division of Material Sciences, U.S. Department of Energy, under contract No. DE-AC-76CH0016.

References:

1. K.H. Rieder and N. Garcia, *Phys. Rev. Lett.* **49**, 43 (1982).

2. See, for example, F. Jona, *J. Phys. C* **11**, 4271 (1978).

3. C.B. Duke, in *Surface Properties of Electronic Materials*, edited by D.A. King and D.P. Woodruff (Elsevier, New York, 1986), Chap. 3.

4. A. Kahn, *Surf. Sci. Rep.* 4/5, 193 (1983).

5. H. Hoinkens, *Rev. Mod. Phys.* **52**, 933 (1980).

6. K.F. Canter, in *Positron Scattering in Gases*, edited by J.W. Humberston and M.R.C. McDowell (Plenum, New York, 1984), p. 219.

7. S.J. Ward, J.W. Humberston, and M.R.C. McDowell, *J. Phys.* B: At. Mol. Phys. **18**, L525 (1985).

8. S.J. Ward, J.W. Humberston, and M.R.C. McDowell, *J. Phys.* B: At. Mol. Phys. **20**, 127 (1987).

9. P.J.E. Alfred and M. Hart, *Proc. R. Soc. Lond.* **A 332**, 239 (1973).

10. J.A. Golovchenko, D.E. Cox, and A.N. Goland, *Phys. Rev.* **B 26**, 2335 (1982).

11. B. Dawson, *Proc. R. Soc. Lond.* **A 298**, 395 (1967).

12. A.J. Freeman, in *Electron and Magnetization Densities in Molecules and Crystals*, edited by P. Becker (Plenum Press, New York and London, 1980) p. 83.

13. M. Weber, S. Tang, S. Berko, B.L. Brown, K.F. Canter, K.G. Lynn, A.P. Mills, Jr., L.O. Roellig, and A.J. Viescas, *Phys. Rev. Lett.* **61**, 2542 (1988).

14. A. Dupasquier, in *Positron Solid State Physics*, edited by W. Brandt, A. Dupasquier (North-Holland, Amsterdam, 1983), p. 510.

15. Unitarity requires inelastic scattering to be accompanied by elastic scattering: see, for example, P. Roman, *Advanced Quantum Theory* (Addison-Wesley, Reading, MA, 1965), p. 198.

16. K.G. Lynn, A.P. Mills, Jr., L.O. Roellig, and M. Weber, in *Electronic and Atomic Collisions* , edited by D.C. Lorents, W.E. Meyerhof, and J.R. Peterson (North-Holland, Amsterdam, 1986) p. 227.

17. L.O. Roellig, M. Weber, S. Berko, B.L. Brown, K.F. Canter, K.G. Lynn, A.P. Mills, Jr., S. Tang, and A. Viescas, in *Atomic Physics with Positrons*, edited by J.W. Humberston and E.A.G. Armour (Plenum, New York, 1987), p. 233.

18. G. Laricchia, S.A. Davies, M. Charlton, and T.C. Griffith, *J. Phys.* E: Sci. Instrum. 21, 886 (1988).

19. B.L. Brown, in *Positron (Electron)-Gas Scattering*, edited by W.E. Kauppila, T.S. Stein, and J.M. Wadehra (World Scientific Publishing Co. Pte Ltd., Singapore, 1986) p. 212.

20. P. Khan, P.S. Mazumdar, A.S. Ghosh, *J. Phys.* B: At. Mol. Phys. **17**, 4785 (1984).

21. K.G. Lynn, E. Gramsch, S.G. Usmar, and P. Sferlazzo, *Appl. Phys. Lett.* **55**, 87 (1989).

22. A.P. Mills, Jr., and E.M. Gullikson, *Appl. Phys. Lett.* **49**, 1121 (1986).

23. E.M. Gullikson and A.P. Mills, Jr., *Phys. Rev. Lett.* **57**, 376 (1986).

24. R. Khatri, M. Charlton, P. Sferlazzo, K.G. Lynn, and A.P. Mills, Jr., (unpublished) 1988.

25. A.P. Mills, Jr. and W.S. Crane, *Phys. Rev.* **A 31**, 593 (1985).

26. A.P. Mills, Jr., E.D. Shaw, R.J. Chichester, and D.M. Zuckerman, *Rev. Sci. Instrum.* **60**, 825 (1989).

27. A.P. Mills, Jr., *Appl. Phys.* **22**, 273 (1980).

28. W.S. Crane, and A.P. Mills, Jr., *Rev. Sci. Instrum.* **56**, 1723 (1985).

29. M.G. Lagally, in *Methods of Experimental Physics*, Vol. 22, edited by R.L. Park and M.G. Lagally (Academic Press, Inc., Orlando 1985) p. 237.

LOW-ENERGY SCATTERING OF ELECTRONS AND POSITRONS IN LIQUIDS

D.M. Schrader
Chemistry Department, Marquette University
Milwaukee, WI 53233, USA

ABSTRACT

The scattering of low-energy electrons and positrons is described for the liquid phase and compared and contrasted with that for the gas phase. Similarities as well as differences are noted. The loci of scattering sites, called "spurs" in the liquid phase, are considered in detail. In particular, their temporal and spatial evolution is considered from the point of view of scattering. Two emphases are made: one upon the stochastic calculation of the distribution of distances required for slowing down to thermal velocities, and the other upon the calculation of cross sections for energy loss by means of quantum mechanics. In these we follow early work by Mozumder and Magee, and by Lekner, respectively.

INTRODUCTION

A fast electron or positron passing through a liquid is known to deposit its energy piecewise, in a large number of discrete locations. Thus the concept of free flight between collisions, which arises so naturally when studying the motions of electrons and positrons in gases, also occurs in liquids despite the great difference in the physical nature of the two scattering milieus, and provides us with an interesting stage for comparison of the two situations. There are similarities as well as differences.

Perhaps the most obvious difference is that the structure of liquids is far more complicated, and correspondingly less well understood, than that of gases. It is only in the past decade that experimental and theoretical results have converged for low incident energy in the case of positron scattering in gases. Therefore we should not expect to understand positron scattering in liquids at a comparable level. For example, we do not know how to calculate cross sections for energy loss at the lowest incident energies for liquids, even for electrons. For gases, the processes responsible for energy loss at lowest energy are simple elastic scattering and (molecules only) rotational excitation for which many high quality calculations and experiments have been performed. In liquids, the lowest energy process is the transfer of kinetic energy from the primary particle into intermolecular vibrational modes of the liquid (i.e., librational excitation, or phonon creation), which is thought to be much more efficient than either elastic scattering or rotational excitation. In any case, the latter is hindered in liquids.

Ionization in the Liquid Phase

For both liquids and gases, most of the energy deposited by the primary particle goes into ionization, electronic excitation, and fragmentation of the absorbing entities. For gases this entity is just one molecule, but for liquids several are normally involved. In either case, secondary electrons are produced. Multiple ionization of a single molecule is much less likely than single ionization, so for the gas phase usually only one secondary electron is produced per collision, but for liquids, several are produced. This is a consequence of the uncertainty principle (see below).

Ionization in the gas phase is a well defined event, and it possesses a definite threshold which can be measured with great accuracy. In liquids, however, there are several effects not present in gases; some of these contribute to a reduction in clarity of the concept of ionization. Besides the production of more than one secondary electron in a typical ionization event, these effects include: (1) The ionized electron enters an energy-absorbing medium upon leaving its molecule; therefore the work required to remove the electron to infinity at rest includes not only the Coulomb energy of

attraction for its parent ion, but also the energy transmitted to the medium in transit. The process responsible for this transfer is stochastic and hence is different for each electron. (2) Many media, especially polar media, trap the ionized electron while it is still in its outbound trajectory. These traps (which can be naturally occurring voids, voids of solvation, or chemical species which bind a primary particle with or without dissociation, etc.) can, in principle, be anywhere in a given medium. (3) All condensed media have dielectric constants greater that unity, which thus reduces the ionization potential compared to the gas phase. Finally, (4) the electron need not be removed to infinity but only to that critical distance r_c where its Coulomb attraction to its parent molecular cation, $e^2/\varepsilon r_c$, is equal to the thermal background kT. At this separation, $e^2/\varepsilon kT$, the attraction of the electron for its parent ion is indistinguishable from the thermal background. The distance r_c, called the Onsager radius, amounts to about 300 Å for typical organic liquids at room temperature.

Very few secondary electrons actually escape over this thermal horizon. Most have the opposite history, namely, immediate recombination with a molecular cation. This can be understood qualitatively with the aid of the uncertainty principle. Suppose the primary electron deposits 100 eV in a collision. This is typical. The time required for this to happen must be at least 3×10^{-18} sec, by which time the primary particle travels about 10 Å. This establishes the minimum size of the collision region, and gives a rough lower limit on the number of molecules ionized: $10^7\ \mathrm{cm}/(M/\rho A)^{1/3}$, where M is the molecular weight of the medium molecules, ρ the density of the medium, and A is Avagadro's number. For hexane this smallest number of molecules is about two. Actually, it is known independently that above five ionizations are produced in n-hexane for each 100 eV of energy loss by the primary particle; or each secondary electron possesses an average energy of 20 eV initially. They are moving much less rapidly than the primary particle, which we can ignore as a consequence, and much more rapidly than the massive molecular cations. Each of the five outgoing secondary electrons therefore looks back on a small entity carrying a total charge of (typically) +5. The slowest of the five electrons immediately falls back into this vast Coulomb hole. The second slowest then sees a charge of +4 and also falls back. And so the process continues until (usually) only one secondary electron is still uncombined. It is interesting that this sequence of recombination proceeds with memory: the electrons recombine geminately; i.e., each with its own parent ion. This is known from the observed scarcity of triplet products.

Focus of this Article

This complicated scenario leads us to a simplification: We need consider only the one surviving secondary electron. The average initial energy of the original five is 20 eV, and the last survivor is the most energetic of the five, so perhaps its energy is 40 eV. If the initial energy of the primary particle is 200 keV and the average energy per deposition is 100 eV (both typical quantities), it follows that for each primary particle there are about two thousand of these surviving secondary electrons, each residing in its own discrete region. These regions or entities are strung out randomly along the trajectory of the secondary particle, and the whole object is called a "track." In a given experiment there may be millions or more of these tracks, one for each primary particle, so the number of entities is billions or more.

Radiation chemists study this microensemble of entities and calculate and measure quantities which represent averages over the microensembles. For positron chemists, the primary particle is the positron itself, and there is no other positron present, so all the attention is given to the very last entity in the track of each primary particle. This entity is unique in the microensemble because it contains the only positron in the system, and because the primary particle forms it at the end of its track when it is slowest. Hence it cannot be argued that it is a typical entity. It is highly arguable that it even resembles a typical entity. The question arises: why do positron chemists study the microensemble? Because if we understand the microensemble (more to the point, a typical entity in the microensemble), then we have a chance of understanding the terminal positron entity. If we don't understand the microensemble as a whole, then we cannot understand the last entity in it.

In this article, we focus our attention on this microensemble of secondary electrons, and

consider their final degradation, starting from a distribution which has a maximum in the neighborhood of 40 eV, and continuing down to thermal equilibrium.

At 40 eV the dominant mechanism for slowing down is ionization and electronic excitation of medium molecules. These dominate other processes down to the threshold for excitation, typically 5 eV. This segment of the degradation process is regarded as being reasonably well understood on the basis of established electronic stopping power laws which yield both the time required and distance travelled by the slowing secondary electron. From 5 eV down to about 0.5 eV, intramolecular vibrational excitation is thought to provide the most important slowing down mechanism. This also is fairly well understood, from the viewpoints of both calculating and measuring cross sections and of computing ranges and times in the segment. Below 0.5 eV down to kT, the story is quite different: although it is believed that we have identified the degradation processes (excitation of intermolecular vibrations), we do not know how to calculate cross sections for them. Times and distances in this last segment are less certain, but can be inferred from sweeping electric field measurements and from microwave conductivity measurements.

In the remainder of this article, we consider mainly this last segment, which has been called the subvibrational region, from two viewpoints: Purely phenomenological descriptions of the degradation process using assumed cross sections, and considerations of ways to determine the cross sections themselves from first-principles quantal calculations.

PHENOMENOLOGICAL DESCRIPTION OF THERMALIZATION

The calculation of track structure of the primary particle has recently become an active area of research. The ever decreasing cost of computation has made large scale Monte Carlo calculations feasible. These calculations use cross sections from experiment and from other calculations. Calculations of the spatial, temporal, and ergodic development of the entities along the tracks are not as numerous or successful because the required cross sections are not all known, as we have already pointed out. However, the qualitative nature of the physical and chemical processes operating in the developing entities is fairly well known. It is inviting to conduct model calculations based on the known qualitative features, using assumed cross sections, and to try to reproduce relevant experimental observations.

The development of entities can be divided into two parts which we call the prethermal or physical regime and the postthermal or chemical regime. At the end of the prethermal regime, the secondary electron becomes thermalized. This takes one to ten picoseconds. In the postthermal regime, the secondary electron moves around by diffusion and engages in chemical reactions. This region terminates by recombination or some other reaction, and is essentially complete in a microsecond. Even though the boundary between these two regions is not perfectly distinct, the two-region concept is nevertheless useful.

We have already discussed three subregions or segments of the prethermal regime: ionization and electronic excitation (40 to 5 eV), intramolecular vibrational excitation (5 to 0.5 eV), and intermolecular vibrational excitation (0.5 to kT). At this point the secondary electrons in the microensemble are thermalized and have established a distribution f of thermalization distances r_n (as measured from the cation). The functional form of $f(r_n)$ is important and can be inferred from sweeping field measurements, but there is a good deal of uncertainty and controversy regarding its shape. [1,2] It is this function which provides the point of contact between theory (calculations of the prethermal regime) and experiment. We now describe this connection.

If an electron comes to rest a distance r_n from its parent cation, it is attracted to it by the Coulomb potential $V(r_n)$. The probability that it will diffuse away, beyond the Onsager radius r_c, is given by a Boltzmann factor:

$$g(r_n) = \exp(-V(r_n)/kT) = \exp(-r_c/r_n) \qquad (1)$$

This result is not at all obvious but rather is a seminal contribution by Onsager, [3] who demonstrated that g(r) is the long time solution of the Smoluchowski equation which describes diffusion of a particle in a Coulomb field. It follows from eq. (1) and the physical meaning of the distribution function f that P_{calc}, the calculated probability for the whole microensemble for diffusion of secondary electrons out of the entity and into the bulk liquid, is given by

$$P_{calc} = \int f(\vec{r})\, g(r)\, d\vec{r}. \qquad (2)$$

This quantity can be measured and is tabulated for many liquids. [4,5] It is the ratio of the yield of free electrons in the bulk of the liquid (ie., beyond the Onsager radius) in the absence of an external field to the limit yield for high electric fields. Its value depends upon temperature, solute concentration, etc., and the correlation of the calculated and the measured value for various trial distribution functions f constitutes the connection between theory and experiment, and tells us what we know about the functional form of f.

Historically, much more attention has been paid to the postthermal regime. Starting from thermalization, one calculates subsequent development of the entity by solving a diffusion equation using $f(\vec{r}_m)$ as the distribution of secondary electrons at t = 0. Thus $f(\vec{r}_m)$ has come to be known as the "initial" distribution, even though it describes where the electrons are at the conclusion of the prethermal regime.

We now turn to the calculation of the initial distribution function $f(\vec{r})$ and the theoretical deduction of the escape probability for the microensemble, P_{calc}. A procedure for the calculation of f was given a long time ago by Mozumder and Magee. [6] Some other workers have attempted to calculate f also, [7-11] but we like the prescription of Mozumder and Magee because it is instructive, it replicates well the actual physical events, and is easy to understand. It requires considerable calculations, however, and has not yet been put to an exhaustive numerical test to our knowledge.

First one chooses ΔE, the initial energy of the secondary electron. This determines R_v, the distance travelled in the first two segments of the prethermal regime, that is, from an energy of ΔE down to E_v, the threshold of the subvibrational segment. (See fig. 1.) For ΔE = 40 eV and E_v = 0.5 eV (our example values), this distance is known to be about 25 Å for most nonpolar liquids. From that point to thermalization one assumes the secondary electron proceeds by a random walk. The number of steps N in the random walk can be deduced in terms of p, the probability of exciting an intermolecular vibrational mode in a given mean free path (which are mostly for elastic scattering), and ω, the vibrational quantum lost per inelastic collision, by an energy balance argument: At the point R_v, the energy of the partical is $E_v - e^2/\varepsilon R_v$; after thermalization it has travelled to a new point R_T from the cation and has lost the energy $Np\omega$ to the medium. Hence

$$E_v - \frac{e^2}{\varepsilon R_v} = 3/2kT - \frac{e^2}{\varepsilon R_T} + Np\omega. \qquad (3)$$

By assuming a value for the product $p\omega$, one can calculate N for any given R_T. R_T is fixed by the variables of integration in eq. (2): We choose r and θ, the coordinates of the point of thermalization measured from R_v (see fig. 1). The law of cosines give R_T, and eq. (3) gives N. Clearly the bulk of the work lies in calculating $p\omega$, for therein lies the cross section for intermolecular vibrational excitation. This quantity, which depends upon the energy of the incident secondary electron, is to be gotten from a quantum mechanical calculation, but we do not know how to carry it out. By trial and error, Mozumder and Magee arrived at a value of 5.5×10^{-4} eV per collision, elastic or inelastic. [6] Using this value along with ΔE = 40 eV, E_v = 0.5 eV, R_v = 25 Å, T = 298 K, and ε = 1.9, we find N to be 460 for R_T = 80 Å (a representative value of the thermalization distance for nonpolar liquids). Such a large number of steps suggests that a Gaussian distribution is accurate:

$$f(\vec{r}) = \left(\frac{1}{2\pi NL^2}\right)^{3/2} \exp(-3r^2/2NL^2). \qquad (4)$$

L is the mean free path for elastic collisions. Mozumder and Magee somewhat arbitrarily take it to be the mean molecular separation of molecules in the liquid. Equation (4) is slightly misleading, for N depends upon R_1 and hence on r and θ, and the N-dependence of the preexponential factor must be included in the integrand in eq. (3). Another consequence of the R_1-dependence of N is that f as written above is not normalized; one must divide the right hand side of eq. (2) by $\int f\, d\vec{r}$.

The integration in eq. (2) is performed numerically and yields the escape probability of all entities with $\Delta E \approx 40$ eV. However, there is a distribution of ΔE values for a given value of E, [12] the energy of the primary particle when it enters the medium. This distribution is known, more or less. There is also a distribution of E values, and this depends on the nature of the source of primary particles. P_{esc} depends upon ΔE and must be averaged over it with the appropriate distribution function. The whole numerical process is shown schematically in fig. 2. The result of all this work will be the yield of bulk secondary electrons appropriate for the experiment.

This procedure amounts to a poor man's Monte Carlo calculation. There are a number of approximations: The use of a Gaussian (eq. (4)) implies we are ignoring the Coulomb influence of the cation during the random walk. The parameters L and p_{10} clearly should depend on the energy of the secondary electron; the dividing line between the segments of the prethermal regime are not as sharp as we have portrayed; the procedure as prescribed above is limited to one electron-cation pair per entity; and it ignores trapping by density fluctuations and scavenger solutes. Perhaps more significant is that time is not a part of the procedure, as it must be in order to include the influence of an externally applied electric field. The latter extension can be made, either with an after-the-fact modification of the procedure just described, or by integrating the Fokker-Planck equation in some appropriate approximation. [13]

New data indicates that straight chain saturated hydrocarbons are very effective traps for positrons with energies near 0.3 eV. [14] The mechanism is apparently the formation of vibrational resonances. For hexane, the cross section for this is quite considerable, about 1.5 $Å^2$, which corresponds to a mean free path of about 140 Å. A random walk of 460 steps, each 5 Å, will almost always be terminated by capture into such a resonance, and this result must be accomodated in an application of this procedure to positron thermalization for such liquids.

CALCULATION OF THE CROSS SECTIONS FOR SCATTERING IN LIQUIDS

The process under consideration in this section, the excitation of intermolecular vibrational modes, is difficult to study experimentally, because the energy quanta involved, about 0.001 eV, are in the far infrared. The Raman shift is observable for many liquids, and gives us the best information we have for the process. In principle, a knowledge of the oscillator strength distribution yields the cross section. Thermal diffusion data also yields some information, the idea being that energies of the subvibrational region are so low that the processes for energy loss (and gain) must be similar to those operating in the posttthermal regime. Thus the mobility or the diffusion constant, or, equivalentally, the momentum relaxation time for free Brownian motion, become crucial quantities.

Rather than proceed in this direction , we consider another system, closer to the interests and expertise of most of the conferees: argon. Liquid argon is at once simpler and more complicated than liquid hexane. Atoms are much simpler to treat quantum mechanically than molecules, but the absence of intermolecular vibrations eliminates one of the segments from the prethermal regime, and cooling below the threshold for electronic excitation relies on intermolecular vibrational excitation and on elastic scattering from atoms and from density fluctuations. These are inefficient cooling mechanisms, and the cooling electron has so much energy in the bulk of the segment where they are operating that the random walk assumption which fueled our phenomenological discussion above

is not valid.

In the remainder of this concluding section we consider the influence of the liquid medium on the calculation of elastic scattering cross sections for atomic argon. Specifically, we want to know what polarization potential to put into the scattering equation (using atomic units now and in the remainder),

$$(-1/2\ \nabla^2 + V_{stat} + V_{pol} - 1/2\ k^2)\ \psi\ (\vec{r}) = 0 \tag{5}$$

where V_{stat} is the static potential provided the incident electron or positron by the nucleus and the target electrons, and V_{pol} is the polarization potential. The latter has the welll known form $-\alpha/2r^4$ for an isolated atomic target at lcng range. At short range it is customary to multiply this by a function w(r), commonly known as the cut-off function, which moderates the strongly diverging short range behavior and hopefully includes some of the effects of short range correlation. For the liquid phase, we know that the polarization potential is screened at long range by the intervening atoms. We follow the important work of Lekner [15] in describing the calculation of this screening. The experimental quantity for comparison is the drift velocity of electrons in the liquid as a function of electric field strength. The comparison requires cross sections for elastic scattering and for momentum transfer.

Consider fig. 3, which is taken from ref. [15] The polarization potential experienced by the atom at $\vec{R}$ due to the electron has the direct contribution $-\alpha\ w(r)/2r^4$, and the indirect contribution due to the induced dipoles in all the atoms, one of which is shown at t. Lekner defines a function h(R) so that the total field at R is

$$\frac{1}{R^3}\ h(R)\ \vec{R} \tag{6}$$

This has the direct part $1/R^2$ and an indirect part. To deduce the latter, consider the field at $\vec{R}$ due to a dipole $\vec{\mu}$ at $\vec{t}$:

$$\vec{E}(\vec{s}) = \frac{3\ \vec{s}\ (\vec{\mu}\cdot\vec{s}) - s^2\ \vec{\mu}}{s^5} \tag{7}$$

We must sum this field over all atoms except the one at $\vec{R}$, but in doing so we may take advantage of the fact that the result will be in the direction of $\vec{R}$, so we need only include the component of $\vec{E}(\vec{R})$ along $\vec{R}$ in the average:

$$\frac{1}{R^3}\ h(\vec{R})\ \vec{R} = \frac{1}{R^3}\ \vec{R} - \frac{\vec{R}}{R^3} \int n g_{pr}(s)\ \vec{R}\cdot\vec{E}(\vec{s})\ d\vec{s} \tag{8}$$

The sum over atoms is accomplished by use of $g_{pr}(s)$, the pair-correlation function of the liquid, and n, the average number density of the atoms. The dipole $\vec{\mu}$ is clearly

$$\vec{\mu} = \frac{\alpha}{t^3}\ h(t)\ \vec{t} \tag{9}$$

which displays the essential role of self-consistency in the determination of the function h by solving the integral equation (8). The pair-correlation function is known, and straightforward iteration leads one directly to a realization of h.

The potential seen by the electron due to the polarization, direct and indirect, of the atom at

R is evidently

$$-\alpha\, w(r)\, h(r)/r^4. \tag{10}$$

Unfortunately this result cannot be used to calculate phase shifts by using it as V_{pol} in eq. (5), because the scattering electron (or positron) is never interacting with one atom across free space, but rather is always interacting with intervening atoms as well. Lekner responds to this quandary with the following construction: First we average $V_{tot} = V_{mol} + V_{pol}$ (the latter being given by eq. (10)) over the ensemble:

$$\langle V_{tot}(r)\rangle = V_{tot}(r) + \int n\, g_{pp}(s)\, V_{tot}(s)\, d\vec{s} \tag{11}$$

Now, since the scattering particle responds only to changes in the potential and not to its magnitude, we can subtract off a constant value and truncate. Lekner defines the effective scattering potential to be

$$V_{eff}(r) = \langle V_{tot}(r)\rangle - \langle V_{tot}(r_0)\rangle \qquad \text{for } r < r_0 \tag{12}$$

and zero beyond, where r_0 is the location of the first maximum in $\langle V_{tot}(r)\rangle$. The calculated cross section for the liquid and gas are compared in fig. 4, and the comparison between theory and experiment for the drift velocity is shown in fig. 5.

The limited question of how the gas phase polarization potential should be modified in order to accomodate scattering in liquids has been addressed. The approximations made are that fluctuations in the number density do not effect the scattering process, and that multiple scattering effects are negligible. The former approximation has been called into question by Basak and Cohen, [16] who believe that the scattering of thermal electrons in liquid argon is dominated by a deformation potential produced by long-wavelength density fluctuations.

ACKNOWLEDGEMENT

This article was written while the author was the guest of Prof. P. K. Tseng, Department of Physics, National Taiwan University. The author is grateful to Prof. Tseng for his hospitality and to the National Science Council, R. O. China, for support. The author is also grateful for K.-Q. Gan for technical assistance.

REFERENCES

1. J. M. Warman, in "The Study of Fast Processes and Transient Species by Electron Pulse Radiolysis," edited by J. H. Baxendale and F. Busi (D. Reidel, Dordrecht, 1982), p. 433.

2. G. R. Freeman, Ann. Rev. Phys. Chem. 34, 463 (1983).

3. L. Onsager, Phys. Rev. 54, 554 (1938).

4. "Kinetics of Nonhomogeneous Processes," edited by G. R. Freeman (John Wiley & Sons, New York, 1987).

5. A. O. Allen, "Yields of Free Ions Formed in Liquids by Radiation," National Bureau of Standards document NSRDS-NBS 57 (U.S. Dept. of Commerce, 1976).

6. A. Mozumder and J. L. Magee, J. Chem. Phys. 47, 939 (1967).

7. L. G. Christophorou and J. A. Stockdale, J. Chem. Phys. 48, 1956 (1968).

8. L. G. Christophorou, in "Progress and Problems in Contemporary Radiation Chemistry" (Prague, 1971), v. 1, p. 95.

9. V. M. Byakov and V. L. Grishkin, preprint ITEF-41 (Institute for Theoretical and Experimental Physics, Moscow, 1977).

10. J. L. Magee and W. P. Helman, J. Chem. Phys. 66, 310 (1977).

11. B. Grosswendt, in "Seventh Symposium on Microdosimetry," edited by J. Booz, H. G. Ebert, and H. D. Hartfield (Harwood Academic Publishers, Chur, Switzerland, 1981), p. 319.

12. I. Santar and J. Bednar, Int. J. Radiat. Phys. Chem. 1, 133 (1969).

13. H. Sano and A. Mozumder, J. Chem. Phys. 66, 689 (1977).

14. C. M. Surko, A. Passner, M. Leventhal, and J. F. Wysocki, Phys. Rev. Let. 61, 1831 (1988).

15. J. Lekner, Phys. Rev. 158, 130 (1967).

16. S. Basak and M. H. Cohen, Phys. Rev. B 20, 3404 (1979).

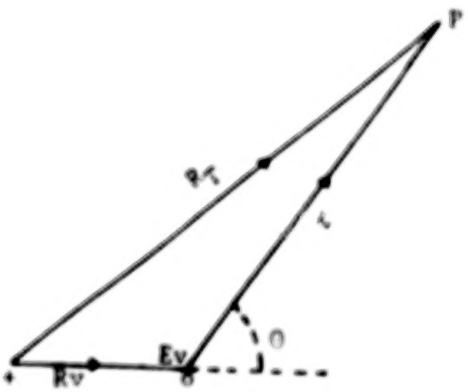

Fig.1. The coordinates involved in the random walk calculation

From reference 6

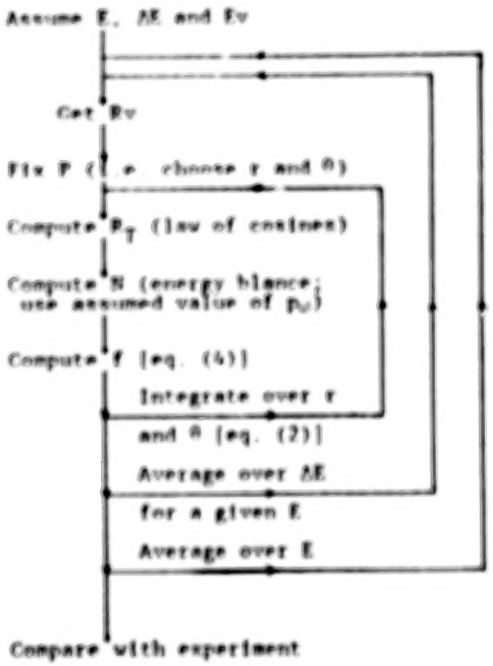

Fig.2. Schematic of the calculation of the field of bulk secondary electrons.

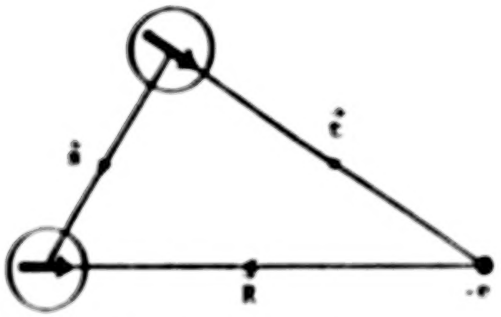

Fig.3 Local fields in liquids. The field on the atom at $\vec{R}$ is the sum of the direct field plus the dipole fields of atoms at all other points $\vec{r}$.

From reference 15

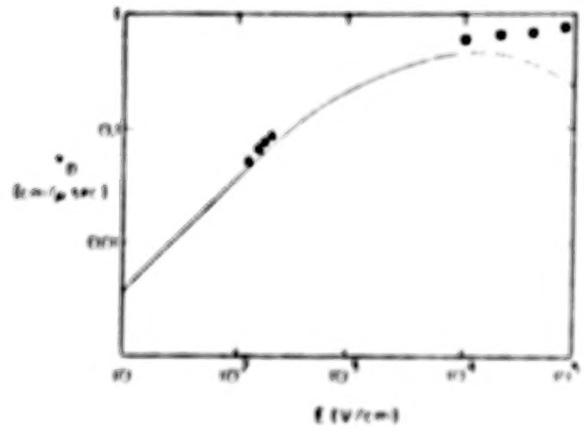

Fig.5 Calculated drift velocity in liquid argon (line) compared with experiment. Cross sections at high field are not accurate.

From reference 15

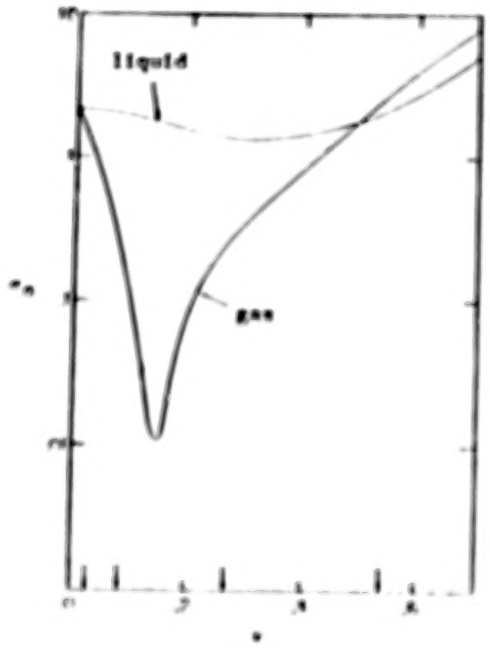

Fig.4 Elastic cross section σ_D (in units of $4\pi a_0^2$) calculated for the gas and liquid as functions of momentum k (in units of a_0^{-1}).

From reference 15

GRIS OBSERVATIONS OF THE GALACTIC CENTER

N. Gehrels, S. Barthelmy, B. J. Teegarden, J. Tueller
NASA/Goddard Space Flight Center

M. Leventhal
AT&T Bell Laboratories

C. J. MacCallum
Sandia National Laboratories

The 511 keV positron annihilation line source in the Galactic Center (GC) region has reappeared after being in a quiescent state since the early 1980's. We report observations by the GRIS balloon instrument showing that the 511 keV line has returned to an intensity level similar to that seen in the 1970's. We have resolved the line width for the first time and made a measurement of the spatial extent of the emission along the galactic plane. GRIS is a high-resolution germanium (Ge) spectrometer with a 17° field-of-view. Eleven hours of data were obtained from GC pointings on balloon flights over Australia on 1 May 1988 and again on 29 October 1988. An additional seven hours were obtained on 30 October 1988 from a point in the galactic plane (GP) 25° west of the center (l = 335°, b = 0°). Preliminary results for the line fluxes (in units of 10^{-4} ph cm^{-2} s^{-1}) from the GC are 9.8±1.9 in May and 12.3±1.6 in October, and from the GP are 2.4 ± 1.6 (1 sigma statistical errors). The flux for the off-center pointing is significantly lower than that for the GC pointings and indicates that the dominant emission is narrowly concentrated at the center. The line width for the GC pointing in October is 3.6±0.5 keV, which implies a temperature for the annihilation medium of $\leq 10^5$ K. A step in the continuum emission at 511 keV is found in both the GC and GP data. The step may be due to orthopositronium three-photon annihilation for the GC, but is too large relative to the 511 keV line for the GP to be simply explained by positronium.

INTRODUCTION

Positron annihilation radiation from the the GC region was first observed by Haymes et al. (1975) in 1970 with low-resolution NaI detectors. The first unequivocal identification of the 511 keV line was made in 1977 by Leventhal et al. (1978) using high-resolution Ge detectors. A summary of all 511 keV GC line measurements is plotted in Figure 1, with references given in reviews by Ramaty and Lingenfelter (1987) and Leventhal (1987). The Bell/Sandia (Leventhal et al. 1980, 1982, 1986), JPL (Riegler et al. 1981, 1985) and Goddard (Paciesas 1982) observations with relatively narrow (≤35°) fields of view show that the GC source turned off in 1980 and did not reappear until after 1984. The positive measurements (Share et al. 1988) during the 1980's by the wider field-of-view gamma-ray instrument on the Solar Maximum Mission (SMM) are evidence for an additional diffuse component to the emission.

We present in this paper results from new observations of the GC showing that the 511 keV line has reappeared. The data were obtained during the first two flights of a new-generation Ge balloon instrument called the Gamma-Ray Imaging Spectrometer (GRIS). Preliminary results are given by Leventhal et al. (1989).

INSTRUMENT

The GRIS instrument (Teegarden et al. 1985; Tueller et al. 1988), shown schematically in Figure 2, is a balloon-borne high-resolution spectrometer operating in the 20 keV to 8 MeV energy range. It consists of an array of seven Ge detectors (total volume = 1560 cm^3) cooled to ~90 K by liquid nitrogen. The detectors are surrounded by 396 kg of NaI in active anticoincidence. Aperture holes in the shield above each Ge detector define a 17° FWHM field of view at 511 keV. The detector effective area at 511 keV is ~85 cm^2 and the resolution is 1.8 keV FWHM. The payload launch weight is 1680 kg.

The flight gondola shown in Figure 2 provides a pointed platform for the instrument. An azimuth-over-altitude digitally controlled pointing system orients the instrument using a magnetic reference to an absolute accuracy of 0.3°. Star camera and sun sensor systems are used to confirm pointing performance in flight. The pointing and spectroscopic performance of the instrument were verified during each flight by observations of the Crab. The measured Crab spectra are consistent with previous observations.

OBSERVATIONS

GRIS was flown twice from Alice Springs, Australia in 1988. The first flight was on 1 May 1988 during which the Galactic Center ($\alpha = 17^h\ 42^m$, δ = -29° 0') was observed for 11 hours and SN 1987A for 12 hours. The second flight was a classic 2-day (44 hours at float) flight on 28-30 October 1988. The observations were as follows: the GC for 10 hours, a point in the GP 25° west of the GC ($\alpha = 16^h\ 22^m$, δ = -48° 42'; l = 335°, b = 0°) for 7 hours, and SN 1987A for 24 hours (2 passes). Spectral lines from ^{56}Co decay were detected during the SN 1987A observations as reported by Teegarden et al. (1989) and Tueller et al. (1989). The average float depth, d, and slant range, s, (in g cm^{-2}) for the GC and GP observations were: 1 May GC d=4.8, s=7.0; 29 October GC d=5.7, s=7.6; 30 October GP d=4.3, s=5.5.

Data were accumulated in alternating 20 minute target-background segments, with some background segments taken before and some after the target segments. For background the telescope was maintained at the same zenith angle but rotated in azimuth so as to minimize the extent of the GP in the field of view. Azimuth offset angles varied from 200° to 240°. Background fields were examined to make certain that no gamma-ray sources were contained in them.

DATA ANALYSIS

Counts in each detector were accumulated during each observing segment in channels 0.25 keV wide. Spectra from each detector were then gain corrected using lines at 198, 511 and 1461 keV and compressed by a factor of ~4 into 1 keV bins. The gain corrected spectra from the seven detectors were summed together. After division by segment accumulation time, background spectra were subtracted from target spectra. The 511 keV line in the background spectrum had an intensity of 0.17 cnts s^{-1} (compared with

0.06 cnts s^{-1} for the astrophysical line) and a width of 2.9 keV. The line is broader than the instrument resolution (and the width of other adjacent background lines) of 1.8 keV at 511 keV. The target-background differences were divided by livetime fraction (~0.9), atmospheric transmission and total effective area, to form flux estimates. Different target-background pairs were weighted inversely according to variance and averaged to obtain a final flux estimate and variance.

For model fitting of the spectra, the May and October data were treated differently in this preliminary data analysis. For the May flight, unanticipated difficulties related to very-high-energy cosmic-ray events degraded the energy resolution to ~5 keV at 511 keV and distorted the line shape, thus frustrating attempts to determine the line profile. Nevertheless, the net flux spectrum formed as described above contains a highly significant feature at 511 keV. To evaluate the flux in the feature, the continuum net flux values determined in the intervals 464-503 keV and 517-556 keV were interpolated inwards to 511 keV and subtracted from the net flux in the interval 504-515 keV.

For the October flight the resolution problem was fixed. We have analyzed these data in the vicinity of the 511 keV line by fitting with various models. The energy window used was 470-550 keV, and the models used included a flat continuum with and without a step at 511 keV to allow a positronium-like continuum below the line and with one and two Gaussian lines to allow for a two-component line shape. Fits were derived by transforming the model photon spectrum through a matrix which contains the detector resolution and off-diagonal terms. The off-diagonal response is due to Compton-scattered events in the detectors which are not rejected by the shield, and to scattering in the atmosphere. The terms are small and have only minor effects on the fits. Nonlinear fitting to the line parameters was performed using the CURFIT program from Bevington (1969). One sigma errors were calculated by finding the deviation of a parameter which increases the minimum value of chi-square by 1, with all other parameters free to vary (Avni 1976).

RESULTS

The spectra between 350 and 700 keV for the May and October GC observations and for the October GP observation are shown in Figure 3. An intense positron annihilation line at 511 keV is seen in both GC spectra, but is virtually absent from the GP spectrum. Our best fits to the October data sets in the 511 keV vicinity are shown in Figure 4. Both October spectra are well fit by a single Gaussian line plus a flat continuum with a step at 511 keV. For the GP spectrum the line statistics are poor so we reduced the number of parameters in the fit by constraining the line centroid at 511.0 keV. Chi-square for the two fits are 74 for 75 degrees of freedom for the GC data and 73 for 76 degrees of freedom for the GP data.

The results of the May 511 keV line flux integration and the October fits are listed in Table I. The line flux for the May and October GC observations are statistically consistent with each other, giving an average line flux for this period of $(11.3\pm1.2)\times10^{-4}$ ph cm^{-2} s^{-1}. This is similar to the flux levels seen in the 1970's and shows that the positron annihilation source in the GC region has re-emerged after disappearing in 1980 (see Figure 2). The line intensity is much reduced in the GP pointing, which at l=25° just excluded the GC from the 17° GRIS field of view. This implies that the dominant emission from the GC at the time of the GRIS observation was not the diffuse component measured by SMM (Share et al. 1988), but rather a narrowly distributed emission or point source in the GC region.

TABLE I

GRIS GALACTIC CENTER AND PLANE RESULTS

1 MAY 1988

511 keV LINE FLUX	$(9.8\pm1.9) \times 10^{-4}$ ph cm^{-2} s^{-1}

29 OCTOBER 1988 - GALACTIC CENTER

511 keV LINE FLUX	$(12.3\pm1.6) \times 10^{-4}$ ph cm^{-2} s^{-1}
LINE CENTROID	511.22±0.28 keV
LINE WIDTH (FWHM)	3.6±0.5 keV
3-γ Ps CONTINUUM FLUX *	$(4.4\pm1.7) \times 10^{-3}$ ph cm^{-2} s^{-1}
Ps FRACTION *	95±11 %

30 OCTOBER 1988 - GALACTIC PLANE

511 keV LINE FLUX	$(2.4\pm1.7) \times 10^{-4}$ ph cm^{-2} s^{-1}
LINE WIDTH (FWHM)	5.2 (+4.2,-3.9) keV
3-γ Ps CONTINUUM FLUX *	$(3.2\pm1.6) \times 10^{-3}$ ph cm^{-2} s^{-1}

* Assuming continuum step at 511 keV is due to positronium three-photon decay

We have resolved the GC 511 keV line for the first time. The width of 3.6±0.5 keV FWHM (compared with an instrument resolution of 1.8 keV at 511 keV) is broader than the value 1.6 (+0.9,-1.6) keV obtained by HEAO 3 (Riegler et al. 1981) in Fall 1979. The GRIS measurement corresponds to thermal broadening in an annihilation medium of 10^5 K or a velocity distribution of the emitting region of 2×10^8 cm s^{-1} FWHM.

Interpreting the step in the continuum at 511 keV as due to three-photon emission from orthopositronium annihilation, we have calculated the integral flux in the three-photon component as listed in Table I. The positronium fraction (see, e.g., Brown and Leventhal 1987) is given by $f = 4\, I_{3\gamma} / (4.5\, I_{2\gamma} + 3\, I_{3\gamma})$ where $I_{3\gamma}$ is the three-photon flux and $I_{2\gamma}$ is the 511 keV line flux. The GC observation gives a 95±11% positronium fraction. For the GP observation however, the flux in the three-photon continuum is too high to be explained by even 100% Ps annihilation. Assuming the step in the GP continuum is due to three-photon annihilation, the three-photon flux is more than an order of magnitude larger than the 511 keV line flux, compared with a maximum of a factor of 4.5 for 100% Ps annihilation. Note, however, that both the GP line flux and three-photon continuum are each $\leq 2\sigma$ measurements. Also, the fit to the three-photon continuum is sensitive to the assumed shape of the underlying continuum. We have assumed a flat continuum spectrum for this analysis, but a better assumption would be a continuum shape based on the data above and below the line region. Analysis is in progress to fit the entire spectrum and determine more accurate three-photon continuum fluxes.

DISCUSSION

The GRIS data, when coupled with previous observations of the GC 511 keV line, strongly suggest that a time-variable source of positrons is located near the GC. Our observation of the re-emergence the line after >4 years absence may be the first evidence for a periodic source. The 511 keV emission is intense. For an isotropic source at a distance of 8 kpc, the line flux corresponds to a luminosity of $\sim 7 \times 10^{36}$ erg s^{-1} (2000 $L_{\odot}$ in a single spectral line) and requires $\sim 4 \times 10^{42}$ annihilations per second. If all of these annihilations occur via the bound Ps state then these numbers are four times larger, with the additional luminosity appearing in a Ps continuum.

An interesting aspect of the GRIS data is the similarity between the GC and GP three-photon continuum fluxes while the line fluxes are so different. This suggests a common origin for the continuum. Ramaty and Lingenfelter (1989, see also Lingenfelter and Ramaty 1989) have recently proposed a two-component model of the GC and GP positron annihilation radiation that may provide an insight into this aspect of the GRIS data. One component is a distributed source of positrons (probably from supernovae) that annihilate in the warm component of the interstellar medium producing a flux of $\sim 1.5 \times 10^{-3}$ photons cm^{-2} s^{-1} rad^{-1} in the direction of the GC (derived from SMM) with a longitude distribution along the GP similar to that of the observed >70 MeV gamma rays. Annihilation occurs predominantly via Ps for this component producing a three-photon continuum flux of $(7.3 \pm 1.8) \times 10^{-3}$ ph cm^{-2} s^{-1} rad^{-1} (weighted mean of all previous orthopositronium measurements). The 511 keV line has a width of <2 keV based on the $\sim 10^4$ K temperature of the warm interstellar medium. The second component is a time-variable point source of positrons at or near the dynamical center of the galaxy. The source is likely to be a $<10^3$ $M_{\odot}$ black hole producing positrons by photon-photon interactions in a hot accretion disk. The three-photon continuum is absent for this component due to annihilation on dust or the photoionization of orthopositronium by UV radiation. The three-photon continuum is therefore due solely to the distributed source. The 511 keV line for the black hole may be narrow if the annihilation is on dust or may be broadened by thermal or bulk motion of the annihilating medium for the photoionized orthopositronium.

The GRIS data are consistent with the Ramaty and Lingenfelter model, although the agreement is at the limits of the statistics. The distributed source would give a 511 keV line flux at 25° west of the GC in the GRIS 17° FWHM aperture of $\sim 4.1 \times 10^{-4}$ ph cm^{-2} s^{-1} (Ramaty and Lingenfelter 1989) and a three-photon continuum flux of $(2.0 \pm 0.5) \times 10^{-3}$ ph cm^{-2} s^{-1}. This is to be compared with our measurement of $(2.4 \pm 1.7) \times 10^{-4}$ ph cm^{-2} s^{-1} for the line and $(3.2 \pm 1.6) \times 10^{-3}$ ph cm^{-2} s^{-1} for the continuum. The measured line is low and the three-photon continuum is high, but both are within statistics. The strongest disagreement is between the predicted three-photon continuum flux for the GC pointing of $(2.2 \pm 0.5) \times 10^{-3}$ ph cm^{-2} s^{-1} compared with the measurement of $(4.4 \pm 1.7) \times 10^{-3}$ ph cm^{-2} s^{-1}.

The Ramaty and Lingenfelter model would imply that the step in the continuum for the GRIS GP data is in fact due to the orthopositronium three-photon continuum, and that the unphysical ratio of continuum to line flux is caused by statistical fluctuations. Another possibility is that the step in the continuum is due to Compton scattering of line photons emerging from an embedded source (Forrest 1982, Bildsten and Zurek 1988). There are also non-black hole models for the GC point source. Recently, a tentative identification of the positron source with the X-ray pulsar GX1+4 was suggested by McClintock and Leventhal (1989), based on the similarity of the X-ray and gamma-ray light curves over 18 years, the positional agreement of the sources and the unusual properties of GX1+4.

CRITICAL OBSERVATIONS FOR GRO

The new GRIS observations of positron annihilation radiation from the GC suggest several critical observations for GRO. The intense 511 keV line observed during the 1970's that disappeared in 1980 is now known to be episodic. A long term study of the time variability of the source is required for which the extended GRO mission is ideally suited. The important determination of the source location and possible identification with a known X-ray source can be done early in the GRO mission by both the OSSE and COMPTEL instruments.

The nature of the distributed source can be studied by the planned GRO GP scan. If the low value for the GP 511 keV line flux measured by GRIS is accurate and applies to other regions of the GP, then the fraction of this emission due to ^{26}Al decay is larger than previously thought. Based on the the HEAO-3 value for the 1809 keV line flux of 4.8×10^{-4} ph cm^{-2} s^{-1} rad^{-1} (Mahoney et al. 1984), the predicted 511 keV flux from ^{26}Al decay for the GRIS GP observation is $(0.5\text{-}2.1) \times 10^{-4}$ ph cm^{-2} s^{-1} depending on the positronium fraction, compared with the measured $(2.4 \pm 1.7) \times 10^{-4}$ ph cm^{-2} s^{-1}. The distributed 511 keV line emission may be due almost entirely to ^{26}Al decay. GRO will be able to measure the 511 keV line to 1809 keV line ratios along the GP and study this question in detail.

REFERENCES

Avni, Y. 1976, Ap. J. 210, 642.

Bevington, P. R. 1969, Data Reduction and Error Analysis for the Physical Sciences, McGraw Hill, New York.

Bildsten, L. and Zurek, W. H. 1988, Ap. J. 329, 212.

Brown B. L. and Leventhal, M. 1987, Ap. J. 319, 637.

Forrest, D. J. 1982, AIP Conf. Proc. 83, 160.

Haymes, R. C. et al. 1975, Ap. J. 201, 593.

Leventhal, M. 1987, 13th Texas Symp. on Relativistic Astrophys., 382.

Leventhal, M. et al. 1978, Ap. J. 225, L11.

_____. et al. 1980, Ap. J. 240, 338.

_____. et al. 1982, Ap. J. 260, L1.

_____. et al. 1986, Ap. J. 302, 459.

_____. et al. 1989, Nature 339, 36.

Lingenfelter, R. E. and Ramaty, R. 1989, Ap. J., submitted.

Mahoney, W. A. 1984, Ap. J. 286, 578.

McClintock, J. E. and Leventhal, M. 1989, Ap. J., in press.

Paciesas, W. S. et al. 1982, Ap. J. 260, L7.

Ramaty, R. and Lingenfelter, R. E. 1987, in The Galactic Center, ed. G. R. Riegler (AIP), 51.

_____. 1989, Annals of the NY Acad. of Sci., in press

Riegler, G. R. et al. 1981, Ap. J. 248, L13.

_____. et al. 1985, Ap. J. 294, L13.

Share, G. H. et al. 1988, Ap. J. 326, 717.

Teegarden, B. J. et al. 1985, Proc. 19th Int. Cosmic Ray Conf. 3, 307.

_____. et al. 1989, Nature, in press.

Tueller, J. et al. 1988, AIP Conf. Proc. 170, 439.

_____. et al. 1989, these proceedings.

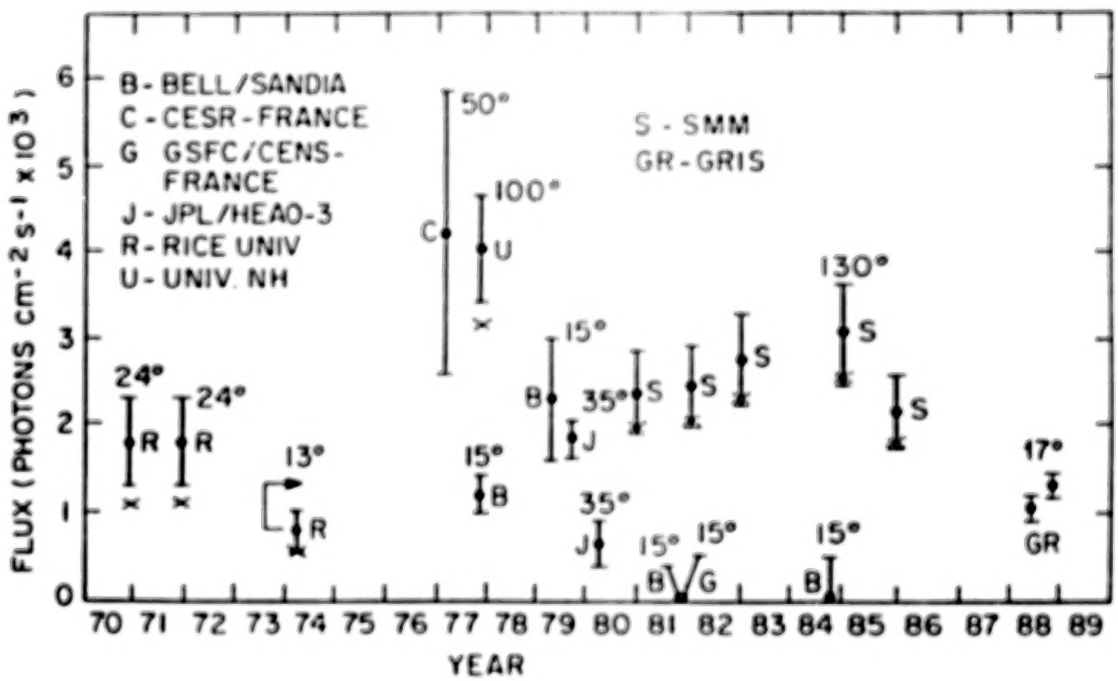

FIGURE 1

Observations of 511 keV line emission from the direction of the GC. The field of view of each instrument is indicated. The X's represent line flux corrections made for an assumed Ps fraction of 0.9. The NaI instruments unavoidably include some three-photon Ps continuum in the line. The 1974 Rice measurement was made in a direction −5° off the GC and needs to be corrected as indicated for a point source at the GC.. The B, C, G, J and GR observations were made with high-resolution Ge detectors. (From Leventhal et al. 1989).

GRIS

SUPERNOVA CONFIGURATION

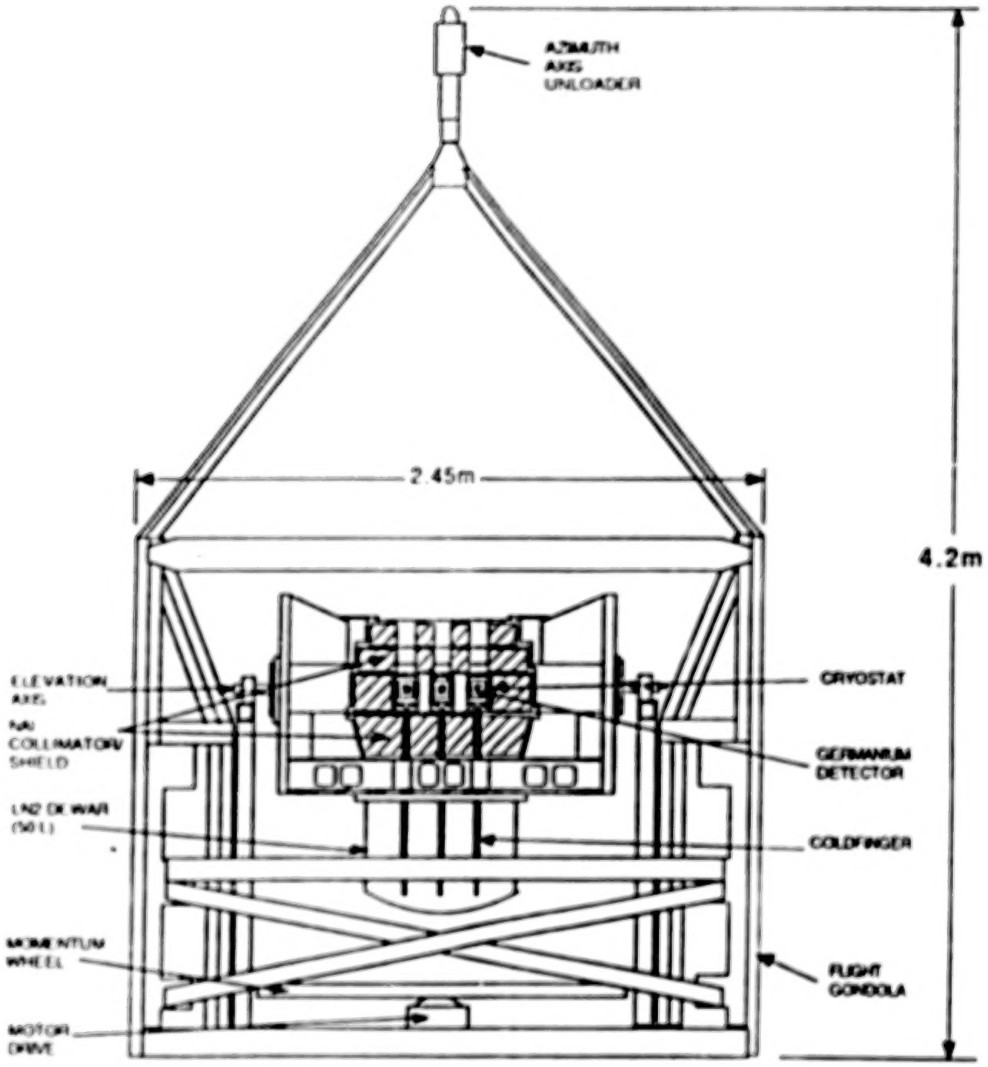

FIGURE 2

Cross-section of the GRIS payload as flown in May and October 1988.

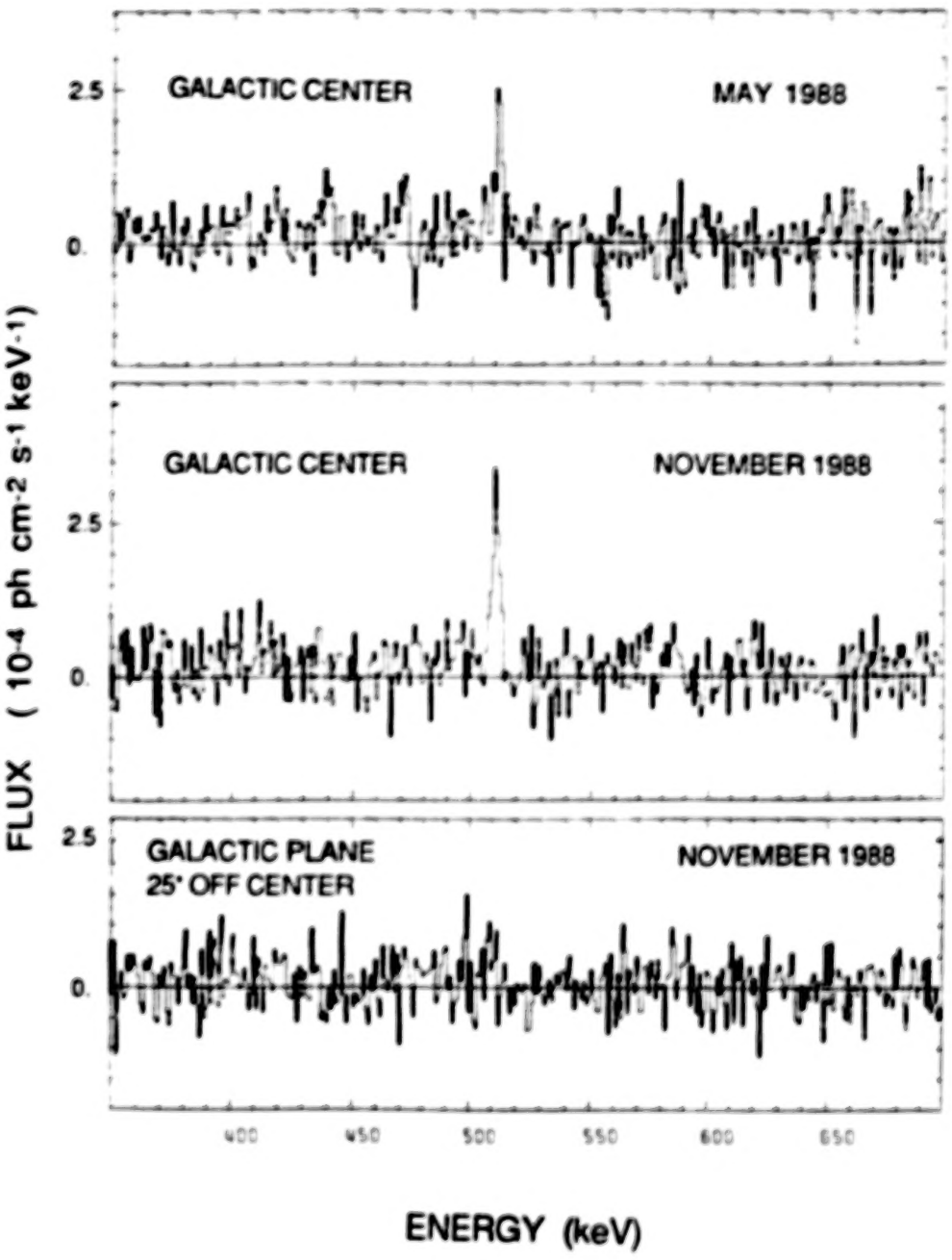

FIGURE 3

Spectra of the GC and GP near 511 keV measured by GRIS in May and October 1988. The data are background-subtracted fluxes that have been corrected for livetime, atmospheric attenuation and detector response to give source spectra.

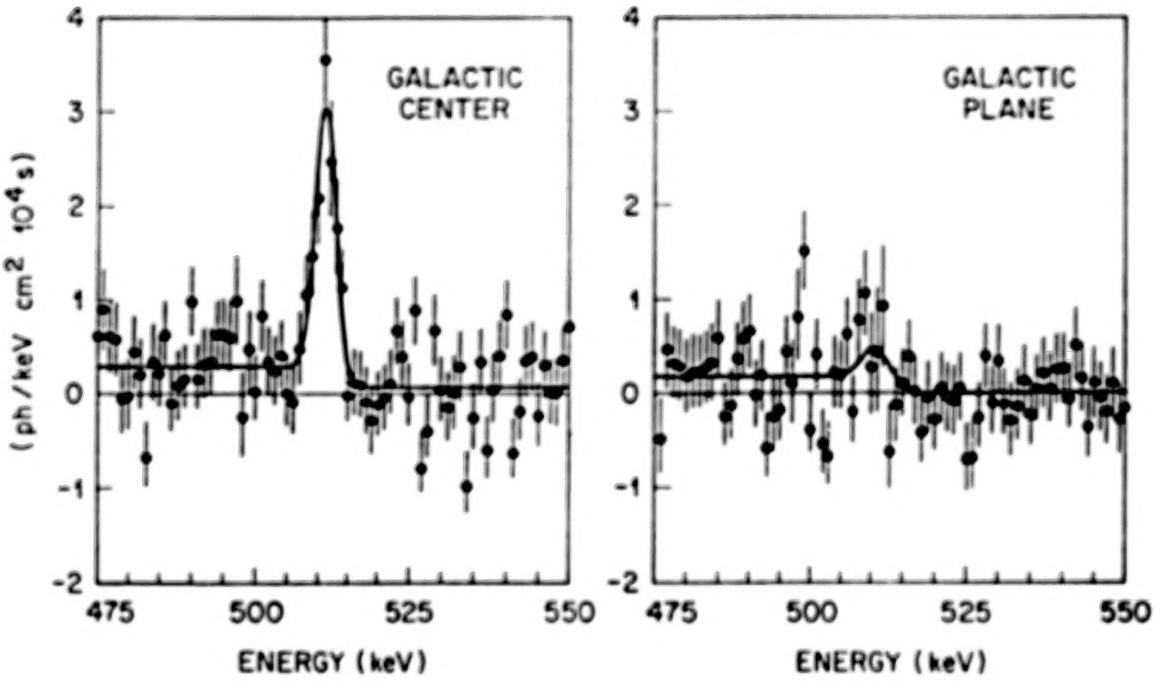

FIGURE 4

Source spectra of the GC and GP near 511 keV measured by GRIS in October 1988. The lines represent best fit models with a flat continuum, a step in the continuum at 511 keV and a Gaussian line. For the GP fit the line centroid is constrained to be at 511.0 keV.

POSITRON ANNIHILATION IN GAMMA-RAY BURSTS

Alice K. Harding
Laboratory for High Energy Astrophysics
NASA/Goddard Space Flight Center
Greenbelt, MD

ABSTRACT

Emission features appear at energies of 350 - 450 keV in the spectra of a number of gamma-ray burst sources. These features have been interpreted as electron-positron annihilation lines, redshifted by the gravitational field near the surface of a neutron star. Evidence that gamma-ray bursts originate at neutron stars with magnetic field strengths of $\approx 10^{12}$ Gauss has come from recent observations of cyclotron scattering harmonics in the spectra of two bursts. Positrons could be produced in gamma-ray burst sources either by photon-photon pair production or by one-photon pair production in a strong magnetic field. The annihilation of positrons is affected by the presence of a strong neutron star magnetic field in several ways. The relaxation of transverse momentum conservation causes an intrinsic broadening of the two-photon annihilation line and there is a decrease in the annihilation cross section below the free-space value. An additional channel for one-photon annihilation also becomes possible in high magnetic fields. The physics of pair production and annihilation near strongly magnetized neutron stars will be reviewed. Results from a self-consistent model for non-thermal synchrotron radiation and pair annihilation are beginning to identify the conditions required to produce observable annihilation features from strongly magnetized plasmas.

INTRODUCTION

Gamma-ray bursts (GRBs) are transient sources of gamma rays having remarkably little ($\approx 1\%$) of their emission below 1 keV (for complete review see Ref. 1). They were discovered by the Vela satellite in 1969, though not recognized as events of cosmic origin until 1973, during a search for gamma-ray transients correlated with supernovae[2]. Early spectra showed smooth shapes which resembled the emission of tenuous, hot plasmas with temperatures of a few hundred keV. Since then, each new generation of gamma-ray detectors has discovered more bursts, revealing new and unanticipated characteristics of these sources. The Soviet KONUS experiments on the Venera satellites observed a large number of bursts, many of which showed evidence of absorption and emission lines[3]. The absorption dips occur around 20 - 40 keV and were interpreted as cyclotron absorption or scattering in magnetic fields of $2 - 5 \times 10^{12}$ Gauss. The reality of these features has been recently confirmed by detectors with higher resolution on the GINGA satellite[4]. Emission features at energies around 350 - 450 keV appear in about $10\% - 20\%$ of the GRBs observed by KONUS and may be electron-positron annihilation radiation, redshifted in the gravitational field of a neutron star.

Although gamma-ray burst sources have been studied by astrophysicists for over fifteen years, their origin is still a mystery. One outstanding problem which has impeded theoretical progress is the lack of information on GRB distances. The energy of a typical burst as derived from the observed fluence, $E_B \approx 10^{38}\,\mathrm{erg\,(d/1kpc)^2}$, could reasonably be anywhere in the range, $10^{34} - 10^{44}$ erg. Fortunately, the situation is not completely unresolved, as there now exist several strong lines

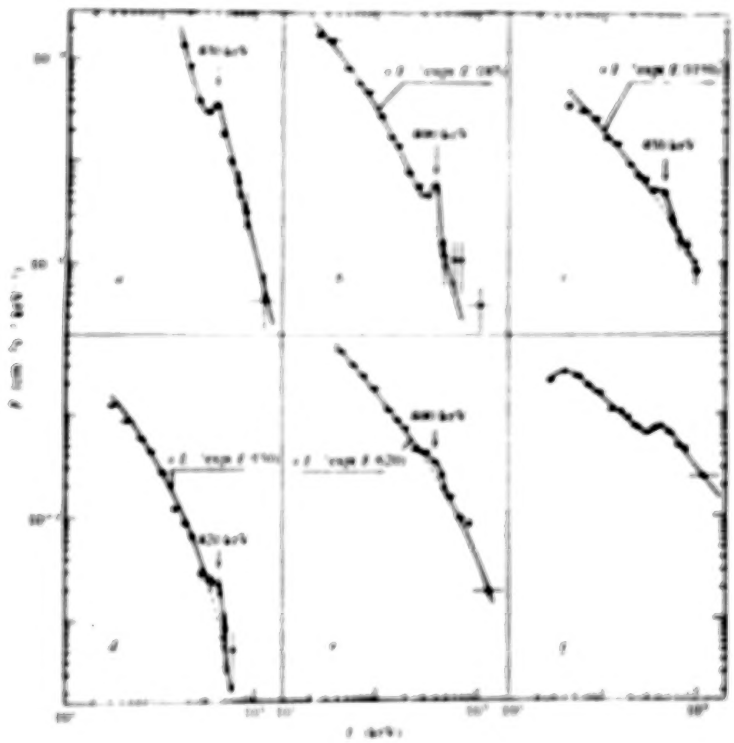

Fig. 1 - Photon spectra from the KONUS gamma-ray burst data base, fitted with narrow emission features (from Ref. 3).

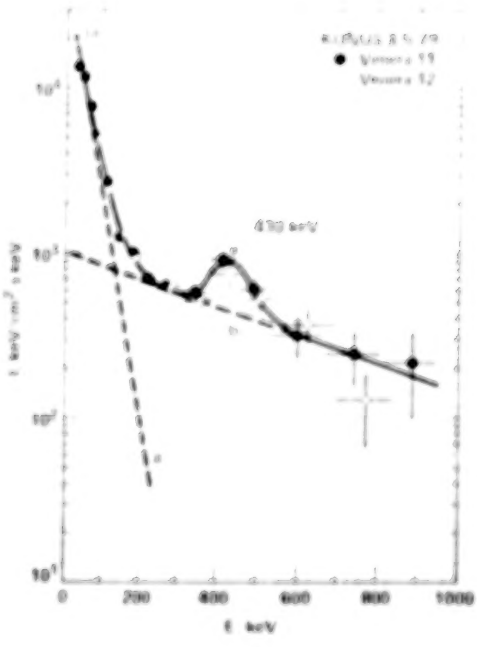

Fig. 2 - Spectrum of 1979 Mar. 5 burst from KONUS, showing annihilation feature at 430 keV (from Refs. 9 and 14).

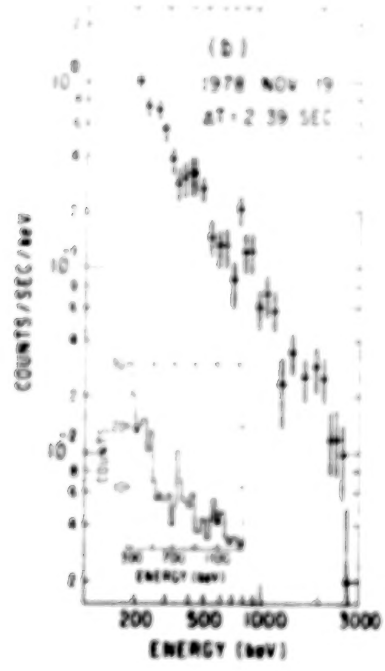

Fig. 3 - Count spectrum of 1978 Nov. 19 burst from the ISEE-3 Ge spectrometer, showing possible annihilation feature at 420 keV (from Ref. 8).

of evidence linking GRBs to neutron stars. The observed emission features, if identified as positron annihilation at rest, have redshifts in the range expected for a neutron star surface gravitational potential. The discovery of a very intense burst on March 5, 1979 had a rise time less than 0.2 ms, restricting the source size to less than 60 km, and also showed 8 second pulsations during the burst decay phase. The spectrum of this source also showed the strongest annihilation feature observed to date. Finally, the GINGA satellite has observed strong absorption features at 20 and 40 keV in the spectra of two bursts[4]. The most natural interpretation of the features is that they are harmonics of resonant cyclotron scattering in a field of 1.7×10^{12} Gauss[5-7], further indication of a neutron star origin.

The evidence that GRBs originate near strongly magnetized neutron stars allows us to model the emission processes, even if we do not know the ultimate source of the burst energy. It is likely that the strong magnetic field will profoundly influence the physical processes which produce the observed emission. In particular, the physics governing positron production and annihilation is so different from the corresponding free-space physics that new models for positron annihilation lines must be developed for GRBs. Ultimately, these kinds of emission models may lead to limits on the total burst energy required to produce observable annihilation features, thus imposing limits on GRB distances.

OBSERVATIONAL EVIDENCE FOR ANNIHILATION FEATURES

Evidence for positron annihilation in GRBs first appeared in data from the Ge spectrometer on the ISEE-3 satellite and from the KONUS detector on the Venera satellites. Figure 1 shows several examples of spectra obtained by KONUS with suggestions of features around 400 keV. The most convincing evidence for an annihilation line in a GRB spectrum was seen in the burst of Mar 5, 1979 (GB790305). Although this exceptionally strong burst was actually detected by nine different satellites, the best spectrum was obtained by KONUS (Figures 1a and 2) and shows a symmetric feature at 430 ± 30 keV which clearly stands out above the continuum. The feature has a relatively high statistical significance of 4.9σ. Observations of GB790305 by the French-Soviet SIGNE detector revealed that a large fraction of the excess at 430 keV came during the first 24 ms of the burst[10], providing some confirmation of the reality of the feature. Figure 3 shows the ISEE-3 spectrum of a burst with an emission feature at 420 keV and another possible feature at 738 keV. The higher energy feature is consistent with ^{56}Fe line emission at 847 keV, with the same redshift required for an annihilation line interpretation of the 420 keV feature.

There are, however, several problems connected with these observed emission features which require caution in interpreting them as annihilation lines. First of all, many of the lines are of low statistical significance (around 3σ) and the problem is compounded by the nature of the response functions of gamma-ray detectors. Since these instruments actually detect the energy loss rather than the energy of the gamma rays, the count rate spectra cannot be unfolded to yield a unique photon spectrum of the burst. The traditional technique has been to assume a spectral shape (in the case of the KONUS spectra, a thermal bremsstrahlung continuum plus a Gaussian line) and unfold the count spectrum, varying a set of adjustable parameters until an acceptable fit is achieved. Thus, the appearance of a line feature in the photon spectrum (especially one which is statistically marginal) can depend on the assumed continuum shape and the derived photon spectrum even tends to conform to the assumed input spectrum. This "obliging" nature of the data which can actually cause artificial amplification of a line feature in the photon spectrum, has raised doubts about many

of the reported features[11]. However, a number of these features also appear in the raw count spectra and some of the reported lines, especially the strong feature appearing in the spectrum of the Mar. 5, 1979 burst, *are* statistically significant.

The second problem is that other instruments, notably the Gamma-Ray Spectrometer on the Solar Maximum Mission (SMM), did not detect line features in *any* of their GRB spectra[12], including several of the same bursts showing emission features in the KONUS spectra. A possible resolution to this discrepancy is that the various detectors integrate over different time intervals to obtain burst spectra. If the lines are in fact time variable, then a detector with a shorter integration time could detect a line which would be averaged out over longer times. Actually, the emission features *do* appear to be variable over very short timescales. The SIGNE detector[13] reported an annihilation "flash" as short as their time resolution of 250 ms in the same burst from which SMM reported no line feature in a 16 s integration.

To summarize, there is convincing evidence from several instruments for annihilation lines in GRB spectra with the following general properties: 1) All of the reported features have redshifts in the range $\Delta E/E \simeq 0.2 - 0.5$, which are consistent with the softer neutron star equations of state[14]. This implies that positrons annihilate near a neutron star surface and probably in a strong magnetic field. 2) In most cases, the lines are so narrow (≤ 250 keV) that the required pair temperatures are much lower than the continuum temperatures[15]. In other cases, the features can be fit with broad line profiles ($\sim 0.5 - 1$ MeV) which may contribute significantly to the continuum above the line[16]. 3) The energy in the line represents typically around 10% and up to as much as 30% of the burst energy. 4) The annihilation features appear to be variable on timescales short compared to the total burst duration and are strongest near the peak of the burst.

POSITRON PRODUCTION AND ANNIHILATION PHYSICS

If the annihilation lines in GRBs originate at the neutron star surface, the theory of their formation must include the effects of the strong magnetic field on the physics of positron production and annihilation. Magnetic fields affect physical processes in several fundamental ways. Momentum perpendicular to the field direction is quantized, so that electrons and positrons must occupy discrete Landau states with energy

$$E_n = (m^2 + p^2 + 2nmB')^{1/2} \qquad (1)$$

where $n = l + \frac{1}{2}(s+1) = 0, 1, 2, \ldots$ with $l = 0, 1, 2, \ldots$. Particles may have either spin-up ($s = 1$) or spin-down ($s = -1$) along the field direction, except in the ground state $n = 0$, where only the spin-down state is allowed. The momentum component parallel to the field, p, is continuous and $B' = B/B_q$ is the magnetic field in units of the critical field, $B_q \equiv m^2c^3/eh = 4.414 \times 10^{13}$ Gauss, in which the cyclotron energy equals the electron rest mass. Transverse momentum is not strictly conserved in interactions, because the magnetic field can absorb or supply momentum (parallel momentum and total energy *are* strictly conserved). Thus, a number of first order processes are allowed that are forbidden in free space. Among these are cyclotron radiation and absorption, familiar as classical electromagnetic processes in weak fields, as well as one-photon pair production and annihilation, which become important only in strong fields approaching B_q. In very strong fields, processes depend on the spin of the electrons and positrons, with the most important effect being the suppression of spin-flip channels.

In addition to the possibility of first-order processes, second-order processes may be strongly influenced by all of the above effects in a strong magnetic field. Therefore, the behavior of the cross sections for two-photon pair production and annihilation in the presence of a field must also be understood in order to correctly model GRB annihilation lines.

Positron Production Processes

Pair production is probably the most important positron production process in GRBs and in a strong magnetic field, pairs can be produced by one photon as well as by two photons. The attenuation rate for conversion of a single photon into an electron-positron pair in the presence of an external magnetic field (also referred to as magnetic pair production) was first calculated in the early fifties[17,18], but since this process is not possibly observable in laboratory fields, it did not receive much attention until the discovery of pulsars in the late sixties. In both processes, the electron and positron can be produced only in the discrete Landau states which are kinematically available. When the photon energy is near threshold, there may only be one or two of these states, and the cross sections will be resonant at each of the pair state thresholds.

Figure 4 shows the attenuation coefficient for one-photon pair production as a function of photon energy for $\theta = 90^\circ$, where θ is the angle of the photon direction with respect to the magnetic field. The threshold for producing a pair in the ground state is $2m/\sin\theta$. Although this resonance structure is important very near threshold, the increasing density of resonances with photon energy allows the use of a more convenient asymptotic expression when the number of available pair states becomes large ($\sim 10^3$). In this limit, the polarization-averaged attenuation coefficient for a photon of energy E_γ is[20]:

$$R_{1\gamma} = \begin{cases} 0.23\frac{\alpha}{\lambda_c} B' \sin\theta \exp\left(-\frac{4}{3\chi}\right) & \chi << 1 \\ 0.6\chi^{-1/3} & \chi >> 1 \end{cases} \qquad (2)$$

where $\chi \equiv (E_\gamma/2m)B'\sin\theta$, α is the fine structure constant and λ_c is the electron Compton wavelength. The probability of one-photon pair production thus rises exponentially with increasing photon energy and transverse field strength. This strong angular dependence has important consequences for photon transport in GRB models. A quick rule-of-thumb is that magnetic pair production will be important when the argument of the exponential in Eqn (2) approaches unity, or when $(E_\gamma/2m)B'\sin\theta \geq 0.1$. Consequently, near-threshold pair production becomes important when $B \sim 4 \times 10^{12}$ Gauss, so that in neutron star fields Eqn (2) must be corrected for threshold effects[19].

The two-photon pair production cross section in a strong magnetic field also has resonances near threshold due to the discreteness of the pair states[21]. The threshold depends on photon polarization direction with respect the field, with the lowest threshold condition taking the form[22]:

$$(E_1\sin\theta_1 + E_2\sin\theta_2)^2 + 2E_1E_2[1-\cos(\theta_1-\theta_2)] \geq 4m^2, \qquad (3)$$

where E_1 and E_2 refer to the energies of the photons and θ_1 and θ_2 are their angles with respect to the field. The second term is the same as the free-space threshold condition and the first term appears as a result of nonconservation of perpendicular momentum. Thus it is possible for photons traveling parallel to each other ($\theta_1 = \theta_2 \neq 0^\circ$) to produce a pair, an event not permitted in free space.

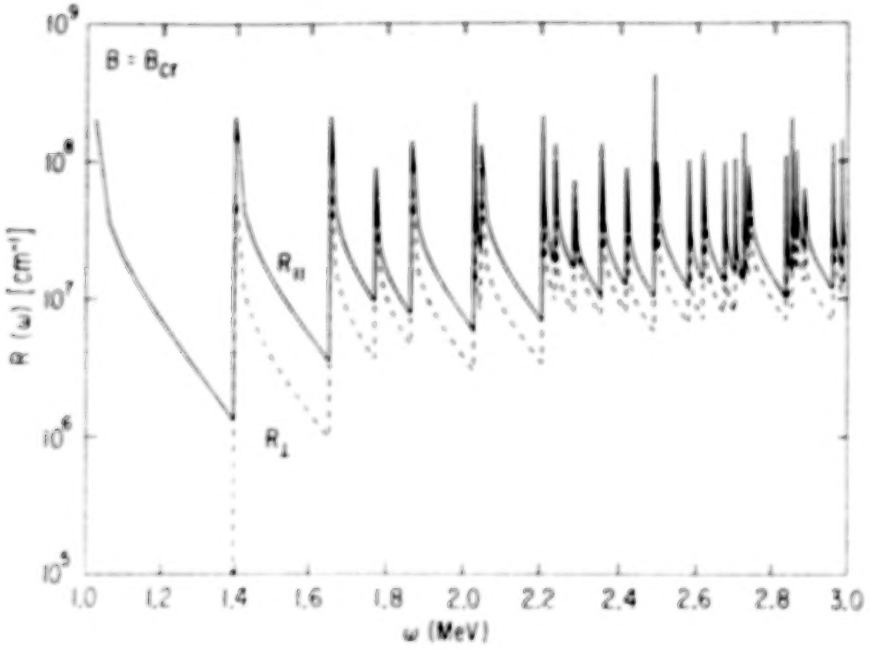

Fig. 4 - One-photon pair production attenuation coefficient as a function of photon energy, for photons propagating perpendicular to the field direction and with polarizations parallel and perpendicular to the field (from Ref. 19).

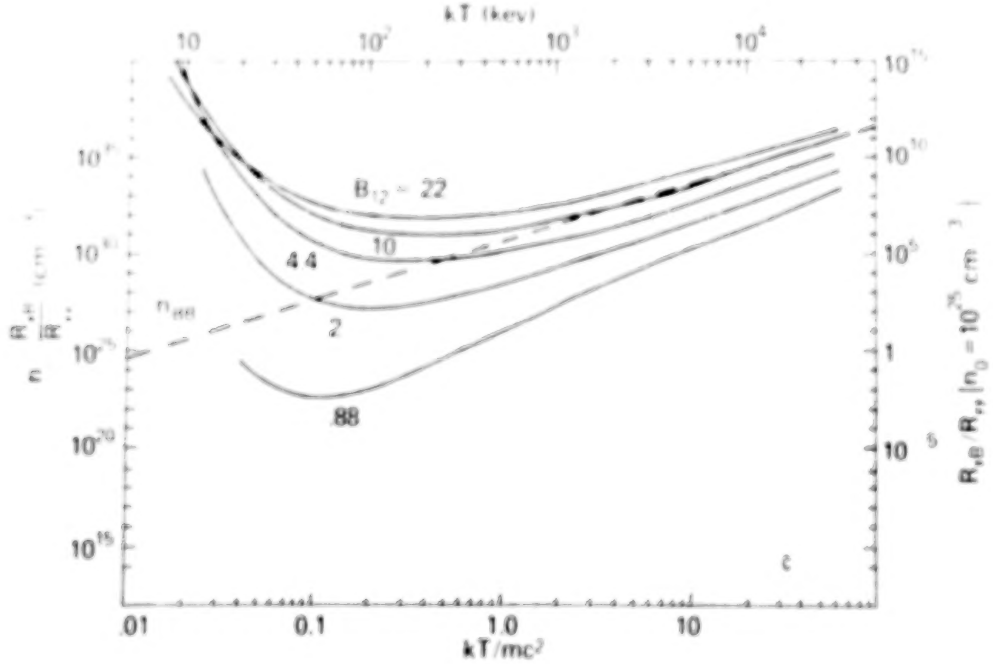

Fig. 5 - Ratio of one-photon to two-photon pair production rate vs. temperature for thermal synchrotron spectra. The curves are labeled with value of magnetic field strength in units of 10^{12} G (from Ref. 23).

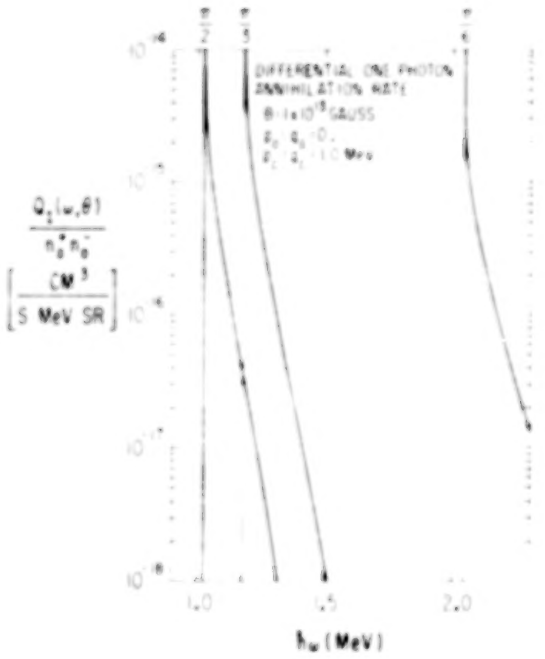

Fig. 6 - Differential one-photon annihilation spectrum emitted by ground state pairs with Gaussian parallel momentum distributions, here with widths of 1 MeV (from Ref. 22).

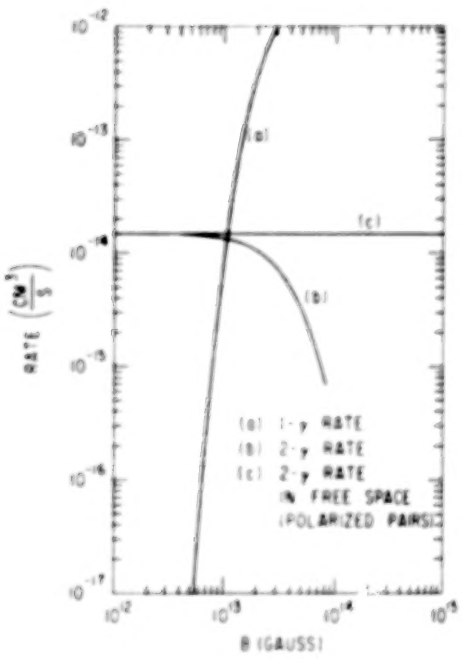

Fig. 7 - Comparison of the total rates for one and two photon annihilation at rest in the ground state, as a function of field strength. (from Ref. 22).

Because of the high photon densities and magnetic fields expected in GRB emission regions, one-photon and two-photon pair production will compete, and both will dominate over other positron production processes (e.g. radioactive decay). Figure 5 shows that in the case of a thermal synchrotron spectrum of photons with a density consistent with a GRB luminosity of 10^{38} erg s^{-1}, the one-photon process will generally dominate in magnetic fields above $\approx 10^{12}$ Gauss. It is probable then that, unless GRBs are more distant than 1 kpc, positrons will be created by one-photon pair production.

Positron Annihilation Processes

In a strong magnetic field, positrons may annihilate into one or two photons through the inverse of the pair production processes discussed above. Virtually all pairs annihilate directly rather than forming positronium at the temperatures and densities expected in GRB sources. Furthermore, because the synchrotron emission rates in fields $\approx 10^{12}$ Gauss ($\sim 10^{16}$ s^{-1}) are much larger than either collisional or annihilation rates, pairs are expected to cool to the ground state before annihilating.

One-photon annihilation from the ground state results in a line at $2m$, broadened asymmetrically by the parallel momenta of the pairs (cf. Figure 6). Unlike two-photon annihilation, Doppler broadening results only in a blueshift here, because the photon must take all of the kinetic energy of the pair in addition to the rest mass. The annihilation photons are emitted in a fan beam transverse to the field, which is broadened if the pairs have nonzero parallel momenta. Pairs annihilating from excited states would produce additional lines above 1 MeV which at high energies blend together into a continuum[21]. Figure 7 shows the one-photon and two-photon annihilation rates for pairs at rest in the ground Landau state. The one-photon rate increases exponentially with field strength, becoming comparable to the two-photon rate at around 10^{13} Gauss. The two-photon rate begins to decrease below the free-space rate at this same field strength, due to the smaller phase space of final pair states.

Two-photon annihilation results in a line at 511 keV as in free space, but the relaxation of transverse momentum conservation causes an additional broadening of the line at higher field strengths. For the case of annihilation of pairs at rest, the line is broadened by roughly $\Delta E \sim 4(B/10^{12}\ \mathrm{G})$ keV for emission parallel to **B** and $\Delta E \sim 54(B/10^{12}\ \mathrm{G})^{1/2} \sin\theta$ keV, $(\sin\theta > B'/2)$ for emission at angle θ to **B** (Ref. 22). In fact, there is an increasing tendency in very high fields for one of the photons to be produced with almost all of the pair energy, so that two-photon annihilation behaves more like one-photon annihilation. Widths of observed two-photon annihilation lines could in principle put limits on the magnetic field strength in GRBs. However, the widths of even the narrowest emission features observed in GRB spectra are too large (probably due to thermal broadening) to seriously constrain the magnetic fields by the above relations. The angular distribution of the photons from annihilation at rest also becomes more anisotropic with increasing field strength, with the peak of emission perpendicular to **B**, again similar to one-photon annihilation.

NON-THERMAL PAIR ANNIHILATION MODEL

Given the evidence for annihilation line emission in observed GRB spectra, it seems natural to investigate under what conditions we would theoretically expect such line emission to be observable from a strongly magnetized neutron star. Thermal emission models (ie. bremsstrahlung or thermal

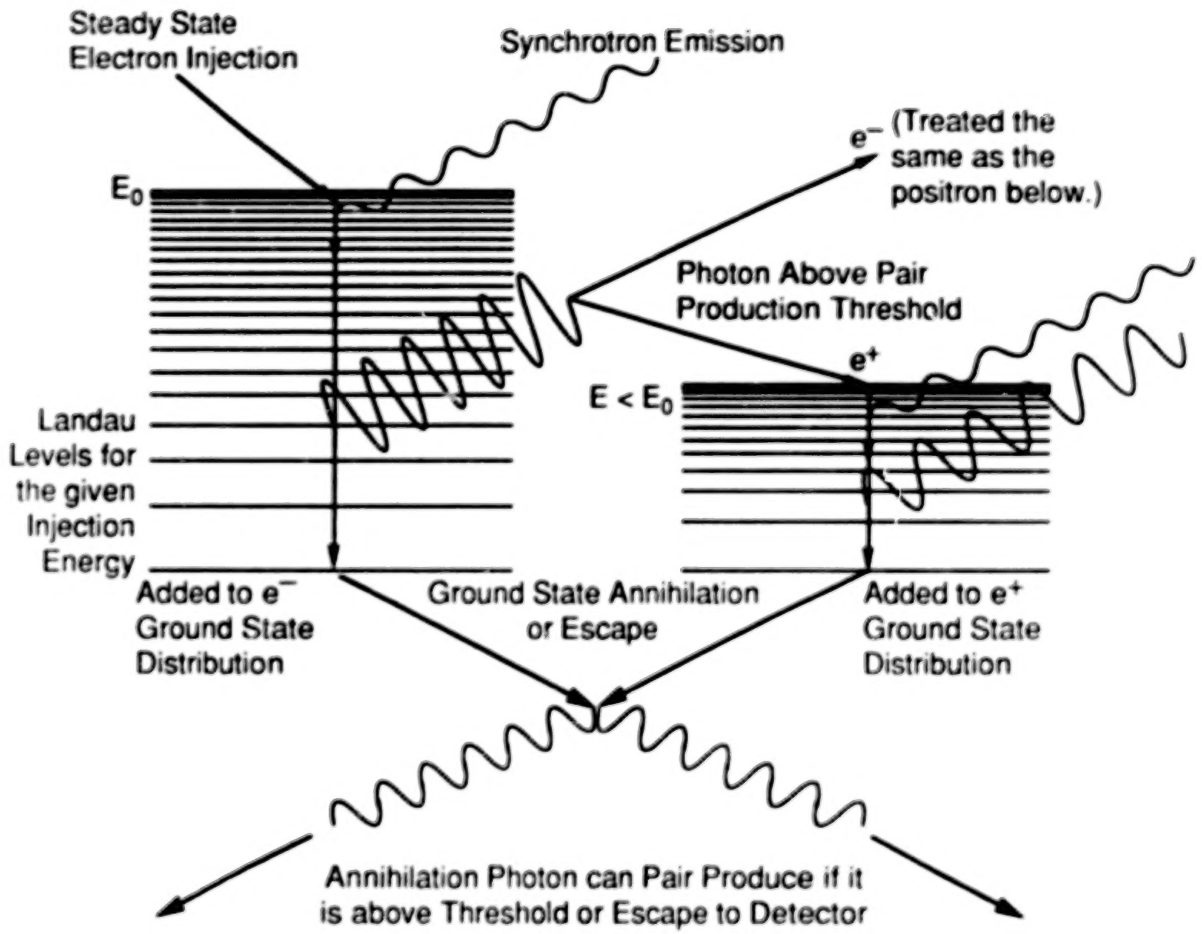

Fig. 8 - Schematic representation of nonthermal injection of energetic electrons in a strong magnetic field.

synchrotron) originally provided good fits to the early GRB continuum spectra. However, when the SMM detector obtained a number of GRB spectra showing hard power-law emission extending well above 1 MeV (Ref. 25), thermal models were questioned. A number of theoretical problems have also caused thermal models to fall out of favor: the inconsistency of annihilation line widths with continuum "temperatures" mentioned earlier, the difficulty of maintaining a thermal distribution of radiating particles in a strong magnetic field, and studies indicating that thermal pair-equilibrium plasmas do not yield observable annihilation features[26,27]. Thus, nonthermal emission models for GRBs seem more attractive.

The question of whether nonthermal injection of energetic electrons into a strong magnetic field can result in observable annihilation lines through the production of a dense electron-positron pair plasma is currently being investigated[28]. The photon emission spectrum is calculated by means of a Monte Carlo simulation. Figure 8 shows schematically the different processes involved in such a calculation. Electrons are injected with an assumed distribution of energy and pitch angle into a homogeneous, strong field. The polar angle, energy and spin of the injected electron determine its initial Landau state, characterized by (n, s, p). Since synchrotron radiation rates are very high, the electron quickly cascades down a series of Landau states to the ground state. Spin-dependent, quantum synchrotron transition rates, interpolated from tables, are used to determine the series of radiative transitions. The synchrotron photons above magnetic pair production threshold may create pairs in excited states. These particles are treated the same as the injected electrons and their synchrotron photons contribute both to the observed spectrum and to the production of additional pairs. As injection continues, particles accumulate in the ground state and either annihilate or escape. The free-space two-photon annihilation rate (valid as long as $B < 10^{13}$ G) is calculated from the annihilation cross section averaged over the ground state distribution. The differential cross section is used to determine the angle of one of the annihilation photons with respect to the field direction. The angle of the second photon and both photon energies follow from three-dimensional kinematics.

To obtain self-consistent electron and positron distribution functions in the ground state, the lifetime of each annihilating or escaping particle is used to calculate the density in the momentum bin of the particle. The newly calculated density replaces the current density value for that momentum and the process is repeated until convergence of the entire spectrum of particles is achieved. Compton scattering of pairs in the ground state with synchrotron photons prior to annihilation or escape may also be important in determining the steady-state particle spectrum, but is not yet included in the calculation.

Examples of the steady-state photon and pair spectra resulting from simulations with varying input parameters are shown in Figures 9 - 11. Each figure represents a large number ($\sim$ 30,000) of injected primary electrons and the photon distributions are differential spectra per primary. In each spectrum, photons from primary synchrotron emission (light solid line), pair synchrotron emission (dot-dashed line) and annihilation radiation (dashed line) are shown separately. The heavy solid line is the sum of the three contributions to the total spectrum. Self-consistent pair density distributions included with each spectrum are normalized to a density, $n_o \equiv (q_o/\sigma_T c)^{1/2}$, where q_o is the rate of injection per second per unit volume of primary electrons and σ_T is the Thomson cross section. In the case of monoenergetic injection of electrons with energy E_o, q_o is related to the total luminosity L and source size R by $q_o = L/(E_o R^3)$. In the simulations shown in Figs. 9 - 11, the value of R determines the relative importance of escape and annihilation and was assumed to be 10^6 cm.

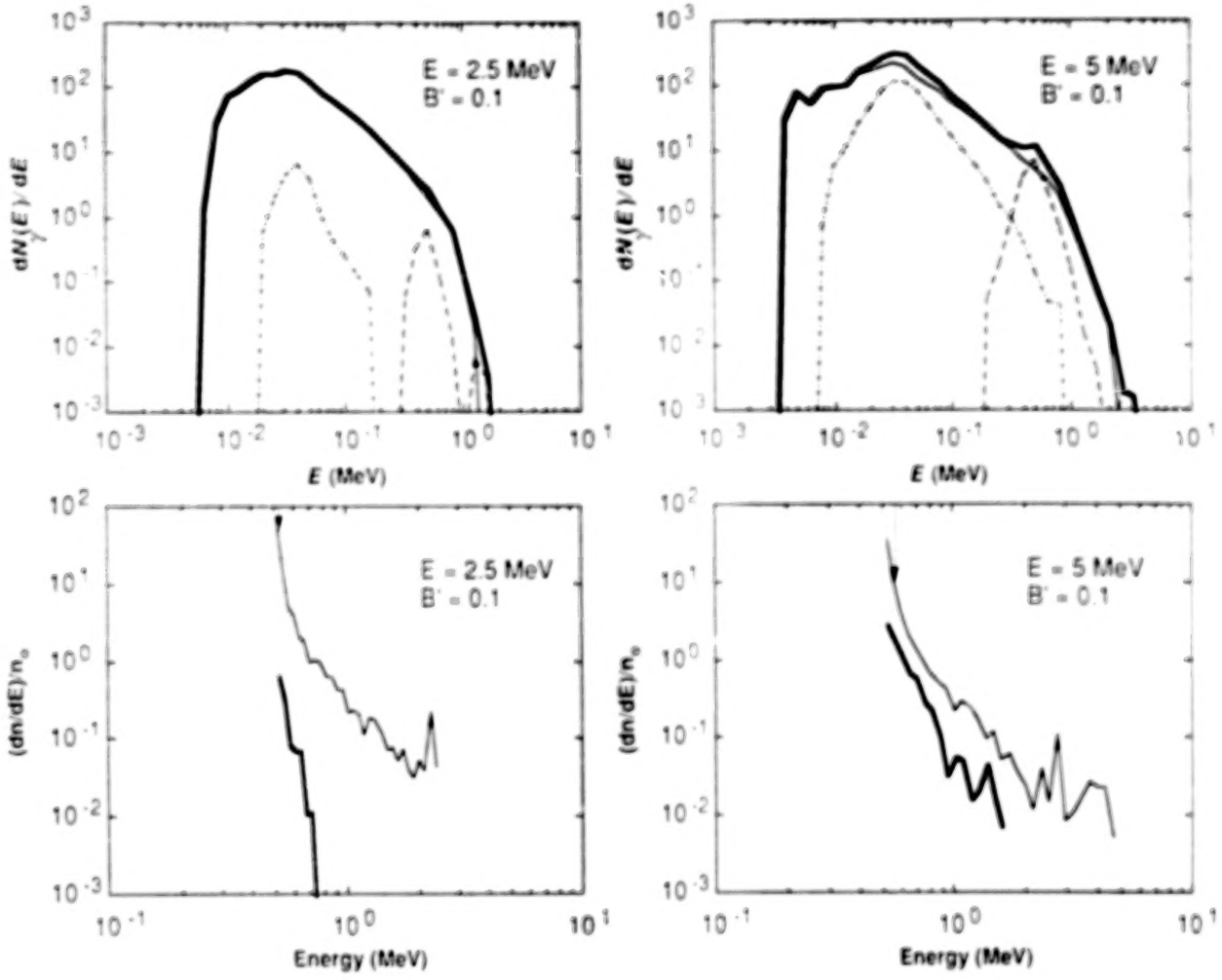

Fig. 9 - (Top) Angle-averaged photon number spectra for isotropic, monoenergetic injection in a 0.1 B_{cr} field. The light solid line is the synchrotron emission from primaries only, the dot-dashed line is synchrotron emission from created pairs, the dashed line is annihilation radiation and the dark solid line is the total spectrum. (Bottom) Self-consistent pair density distribution functions vs. energy for the same case as above. The light solid line corresponds to the electrons and the dark solid line corresponds to the positrons. The arrow indicates the point which divides the electrons that annihilate (to the left) from those that escape (to the right) (From Ref. 28).

As can be seen from these examples, an annihilation feature is visible above the continuum for a variety of parameters. Figure 9 shows the steady-state photon and pair spectra which result from a monoenergetic, isotropic injection of unpolarized primary electrons. The continuum spectra display the -3/2 power law shape of synchrotron cooling emission above the cyclotron energy $E_c = mB'$, with cutoffs above 1 MeV due to pair production. Harmonic structure due to transitions between very high, closely-spaced Landau states can be seen at the low energy end of the spectra. Synchrotron cooling emission from the pairs produced in excited states contributes most strongly around the cyclotron energy, because more pairs are produced in lower Landau states. The annihilation lines are roughly symmetric about the 511 keV peak (gravitational redshift has not been included), with power-law wings. Annihilation photons also undergo pair production attenuation, but since most of these photons are beamed along field lines, the threshold lies well above 1 MeV. As the field strength increases, so does the width of the annihilation line for a given injection energy. The widths of the lines range from a few hundred keV to roughly 1 MeV. At a given field strength, increasing the injection energy increases the strength of the annihilation feature.

The steady-state pair distributions have a power law shape at high energies with steep increase in density near rest. Since only electrons are being injected in these simulations and positrons come only from pair production, some of the electrons must escape rather than annihilating. The arrows mark the energy above which most electrons escape. The steepening of the pair spectra at low energies are thus caused by the energy dependence of the annihilation rate. As the magnetic field strength increases, the higher pair production rates cause the positron spectra to approach that of the electrons, both in shape and amplitude.

In these simulations, the annihilation features are fairly narrow. Synchrotron radiation cools primarily transverse to the field, but the pairs still have sufficient parallel momenta in the ground state to produce much broader annihilation lines. However, when the annihilation rate is compared with the escape rate for electrons as a function of energy, one sees that annihilation occurs preferentially near rest, with the rate dropping very fast with increasing parallel momentum. Therefore, the lines are narrow when the higher energy electrons escape and do not contribute to the Doppler broadening of the annihilation. This situation occurs when the average number of pairs produced per primary is less than unity (*i.e.* the plasma is not pair dominated).

Beamed injection of primaries in a cone along the magnetic field or in a fan beam across the field has also been investigated. The cone beam results in a decrease of pair production and the fan beam in an increase in pair production over isotropic injection. Cone-beamed injection (Figure 10) produces pair distributions not only with lower density but having peaks above rest energy, causing the annihilation feature to be considerably weaker. On the other hand, fan-beamed injection (Figure 11) produces exceptionally strong, narrow annihilation features, not only because of the increase in pairs, but because of the steepening of the steady-state pair spectra (*i.e.* more pairs can annihilate near rest). The continuum spectra in these cases have very sharp pair production cutoffs at 1 MeV.

From the results of these simulations, observable annihilation lines can result from steady-state, nonthermal injection of electrons in a strong magnetic field. It requires field strengths of at least $B' \sim .05$, injection energy of at least 5 MeV and a large fraction of primaries with high transverse momentum. The escape of higher energy electrons along the magnetic field is important and can result in narrow annihilation lines. The simultaneous production of strong, narrow annihilation features and hard power-law emission above 1 MeV seems to be difficult in this model. However,

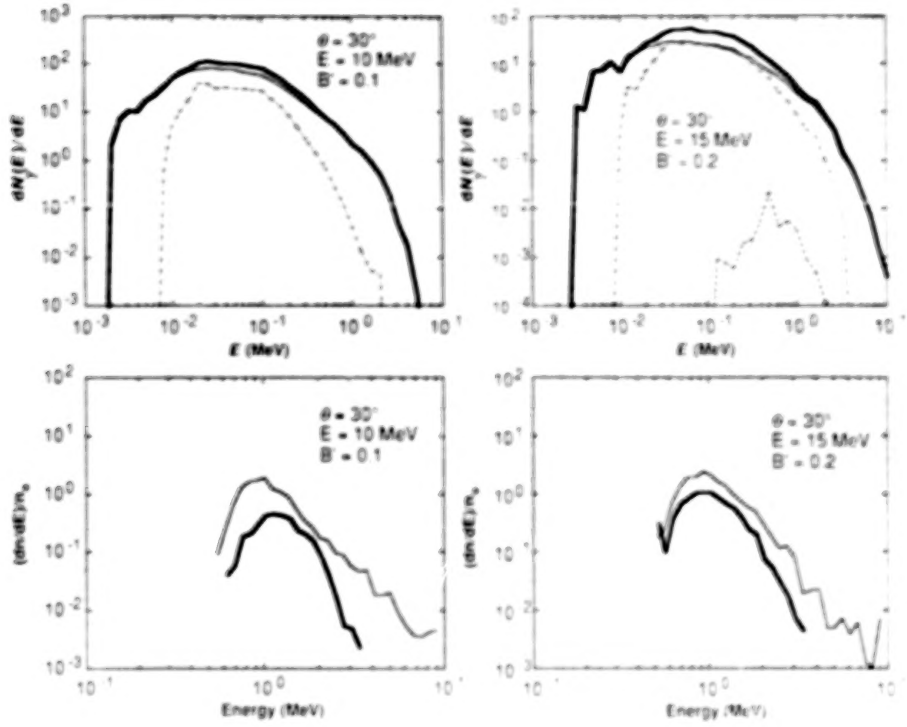

Fig. 10 - Same as Fig. 9, for cone-beamed, monoenergetic injection. Escape dominates annihilation at all energies in the electron distribution function.

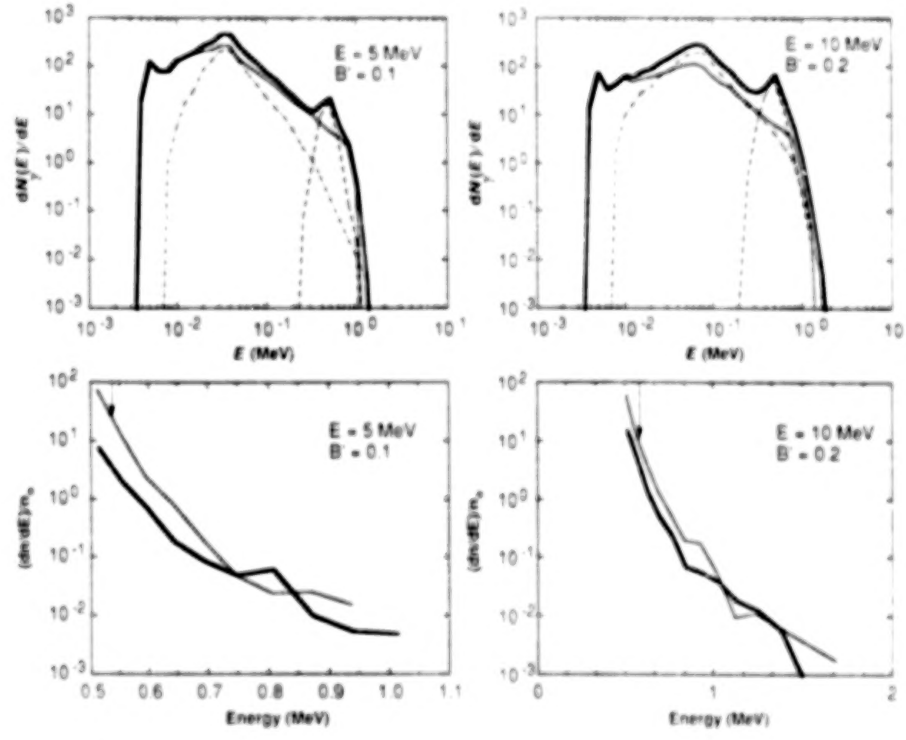

Fig. 11 - Same as Fig. 9, for fan-beamed, monoenergetic injection.

time variability of both the line and high-energy continuum could arise from changes in either the energy or the angular distribution of the injected electrons.

SUMMARY

Although the models for pair annihilation in GRBs are now including more of the physics of high magnetic fields, they are still in a fairly primitive state of sophistication. Inhomogeneity and spatial dependence have not been considered; and the inclusion of additional processes such as two-photon pair production and Compton scattering introduce new levels of complexity in the simulation codes. For example, the resonant nature of Compton scattering in a strong magnetic field is difficult to include in full detail, though the essential physics may be possible to include approximately. Nevertheless, the results of even the simplest models are beginning to identify the conditions under which observable pair annihilation can occur.

The experimental situation is expected to improve in the near future with the launch of new instruments on the Gamma-Ray Observatory. The Burst and Transient Source Experiment (BATSE) will have unprecedented sensitivity for performing spectral observations and temporal variability studies of GRBs. With time resolution as short as $10\mu s$, BATSE will be able to study the time variability of annihilation features during a burst and make a 5σ detection of a line feature with 20% equivalent width from a strong burst in less than a second[29]. Most importantly, the issue of whether positron annihilation is actually occuring in GRBs may finally be resolved.

ACKNOWLEDGEMENTS

I am grateful to my collaborators J. K. Daugherty and R. D. Preece for hard work and many fruitful discussions. I also thank R. W. Bussard, M. G. Baring, and D. Q. Lamb for helpful comments and insights.

REFERENCES

1. Liang, E. P. and Petrosian, V. 1986, *Gamma-Ray Bursts* (AIP: New York).
2. Klebesadel, R., Strong, I. and Olson, R. 1973, *Ap. J. Letters*, **182**, L85.
3. Mazets, E. P. *et al.* 1981, *Nature*, **290**, 378.
4. Murakami, T. *et al.* 1988, *Nature*, **335**, 234.
5. Lamb, D. Q. *et al.* 1989, *Proc. 14th Texas Symposium on Relativistic Astrophysics*, ed. E. Fenyves, in press.
6. Fenimore, E. E. *et al.*, 1988, *Ap. J. Letters*, **335**, L71.
7. Harding, A. K. and Preece, R. D. 1989, *Ap. J. Letters*, **338**, L21.
8. Teegarden, B. J. and Cline, T. L. 1980, *Ap. J. Letters*, **236**, L67.
9. Mazets, E. P. *et al.* 1979, *Nature*, **282**, 589.
10. Cline T. L. 1984, *High Energy Transients in Astrophysics*, ed. S. E. Woosley, (AIP: New York), p. 333.
11. Fenimore, E. E. *et al.* 1982, *Gamma-Ray Transients and Related Astrophysical Phenomena*, ed. R. E. Lingenfelter, (AIP: NewYork), p. 201.
12. Nolan, P. L. *et al.* 1983, *Electron-Positron Pairs in Astrophsyics*, ed. M. L. Burns, A. K. Harding

and R. Ramaty, (AIP: New York), p. 59.
13. Barat, C., Hurley, K. Niel, M. and Vedrenne, G. 1984, *Ap. J. Letters*, **286**, L11.
14. Liang, E. P. 1986, *Ap. J.*, **304**, 682.
15. Ramaty, R. and Meszaros, P. 1981, *Ap. J.*, **250**, 384.
16. Golenetskii, S. V. *et al.* 1986, *Astrophys. Space Sci.*, **124**, 243.
17. Toll, J. S. 1952, Ph. D. Thesis, Princeton Univ., unpublished.
18. Klepikov, N. P. 1954, *Zh. Eksp. Teor. Fiz.*, **26**, 19.
19. Daugherty, J. K. and Harding, A. K. 1983, *Ap. J.*, **273**, 761.
20. Erber, T. 1966, *Rev. Mod. Phys.*, **38**, 626.
21. Kozlenkov, A. A. and Mitrofanov, I. G. 1987, *Sov. Phys. JETP*, **64**, 1173.
22. Daugherty, J. K. and Bussard, R. W. 1980, *Ap. J.*, **238**, 296.
23. Burns, M. L. and Harding, A. K. 1984, *Ap. J.*, **285**, 747.
24. Harding, A. K. 1986, *Ap. J.*, **300**, 167.
25. Matz, S. M. *et al.* 1985, *Ap. J. Letters*, **288**, L37.
26. Zdziarski, A. A. 1984, *Ap. J.*, **283**, 842.
27. Harding, A. K. 1984, *Proc. of Varenna Workshop on Plasma Astrophysics*, (ESA SP-207), p. 205.
28. Preece, R. D. and Harding, A. K. 1989, *Ap. J.*, (Dec. 15) in press.
29. Fishman, G. J. *et al.* 1989, *Proc. of GRO Science Workshop*, in press.

ANNIHILATION PHYSICS OF EXOTIC GALACTIC DARK MATTER PARTICLES

F. W. Stecker
Laboratory for High Energy Astrophysics
NASA Goddard Space Flight Center
Greenbelt, MD 20771, U.S.A.

ABSTRACT

Various theoretical arguments make exotic heavy neutral weakly interacting fermions, particlularly those predicted by supersymmetry theory, attractive candidates for making up the large amount of unseen gravitating mass in galactic halos. Such particles can annihilate with each other, producing secondary particles of cosmic-ray energies, among which are antiprotons, positrons, neutrinos and γ-rays. Spectra and fluxes of these annihilation products can be calculated, partly by making use of e^+e^- collider data and QCD models of particle production derived therefrom. These spectra may provide detectable signatures of exotic particle remnants of the big bang.

INTRODUCTION

Astronomers have learned that there is much more to the universe than meets the eye[1]. The discovery that the rotation curves of spiral galaxies are quite flat to radii as far out as can be observed indicates the presence of dark matter comprising most of the mass in galactic halos and which could also dominate the mass of the universe[2]. This dark matter is most likely of non-baryonic form[3]. It may be made up of exotic new particles, perhaps such as those predicted by supersymmetry theory. The large body of literature on various aspects of the dark matter problem[4] and dark matter detection[5] have recently been reviewed.

Possible candidates for dark matter are exotic, stable, weakly interacting particles, which we hereafter call χ particles. Among these, the "neutralinos" predicted by supersymmetry theory should be left over as relics of the early big-bang in cosmologically significant densities[6,7]. Such particles can annihilate to produce baryons of cosmic-ray energies as well as other familiar particles whose decays will produce cosmic-ray leptons (electrons, positrons and neutrinos) and also cosmic γ-rays. The fluxes and energy spectra of these "ordinary particles" resulting from the annihilation of various χ particles can be calculated. The annihilation process will produce a characteristic high energy cutoff in these spectra at the rest mass energy of the χ particle, typically ~5 to ~30 GeV. The Lund Monte Carlo[8] simulation technique used by particle physicists in comparing with e^+e^- collider data provides a powerful tool for predicting $\chi\chi$ annihilation spectra[9-13], since the process of quark-antiquark pair production is involved in both cases. We will present and discuss detailed energy spectra from the annihilation of χ particles in the Galaxy and show how the features of these spectra may help lead to indirect evidence of exotic dark matter particles.

The lightest of the neutral supersymmetric particles, designated the LSP, would be stable by virtue of a new neutral conservation law called R-parity conservation, since it is the lightest state with odd R-parity. The mass eigenstate "neutralino" can be a pure state, but is more generally a superposition of the "higgsino" ($\tilde{h}$), "photino" ($\tilde{\gamma}$) and "zino", which are mixed by gauge and supersymmetry breaking. There is also the possibility that the χ particle could be a heavy Dirac neutrino. However, unlike the case with the LSP, there is no natural way of forbidding the decay of a "conventional" heavy neutrino. There is also experimental evidence

against dark matter heavy Dirac neutrinos.[14]

DARK MATTER ANNIHILATION

The basic physical processes involved in the $\chi\chi$ annihilation process are portrayed schematically in Fig 1. In the first stage of the annihilation (Stage "a" in Fig. 1), χ particles annihilate via a propagator Δ (e.g., a scalar fermion in the case of photinos and a Z particle in the case of higgsinos). These supersymmetric neutralinos are Majorana fermions, i.e., they are self annihilating. Then, (b) the annihilation usually produces a quark antiquark pair ($\chi\chi \rightarrow q\bar{q}$). This is followed by (c) a cascade of the quarks down to the mass shell by successive gluon emission, producing a quark-gluon shower and (d) conversion of the shower gluons into other quark antiquark pairs which (e) produce hadrons, followed by (f) the decay of the unstable hadrons. The hadronic showers carry the momentum of the original quark pair and so come out as two collimated "jets". Sometimes a hard gluon is also emitted in the process $\chi\chi \rightarrow q\bar{q}g$, which results in three jets. (More rarely two or more gluons can be produced.) The quark cascading and fragmentation processes must be described by quantum chromodynamics (QCD) models. The Lund simulation is based on a string fragmentation model of QCD interactions, with parameters determined from the e^+e^- collider data. However, it enables one to take account of the different fragmentation effects associated with various quark species. It thus provides a framework for extrapolating from e^+e^- collider data to determine $\chi\chi$ annihilation spectra from differing mixtures of final state quark jets.

Simulation of a $\chi\chi$ annihilation begins by selecting a fermion-antifermion final state according to the branching ratios (B.R.) appropriate for a given type of χ particle which depend on the mass (m_f) and charge (Q_f) of the fermion (quark or lepton) involved (B.R. $\sim \beta_f m_f^2 Q_f^4$ for photino ($\tilde{\gamma}$) annihilation; B.R. $\sim \beta_f m_f^2$ for higgsino and Majorana neutrino (ν_M) annihilations (Ref. 15, hereafter called RS).

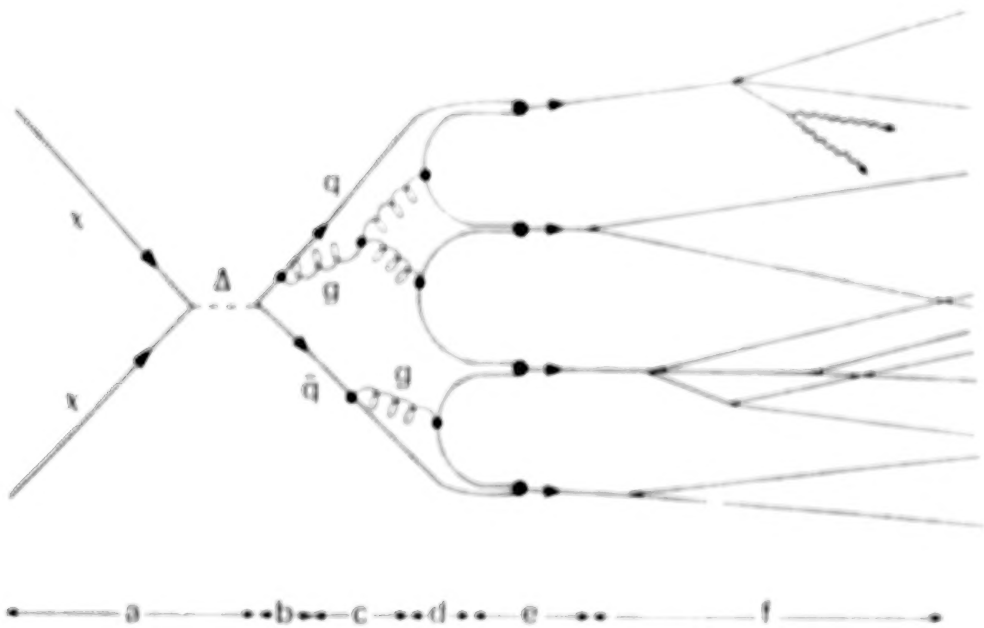

Fig. 1. Schematic diagram of the physics of χ particle annihilation with the various stages of the secondary particle production described in the text.

ANTIPROTON PRODUCTION

The energy spectrum of cosmic-ray antiprotons from photino annihilation was first calculated by Stecker, Rudaz and Walsh[16] (SRW), using $\bar{p}$ data obtained in e^+e^- collider experiments. They deduced from their results the fascinating possibility of explaining the entire observed spectrum of cosmic-ray $\bar{p}$'s as arising from the annihilation of 15 GeV χ particles. RS extended the spectral calculations to antiprotons, γ-rays and positrons, considering photinos, higgsinos and Majorana neutrinos as dark matter. Using the basic approach and formalism first given by SRW and RS, Stecker and Tylka[11] (ST1) extended the study of the antiproton spectrum with Lund Monte Carlo simulations, also taking account of recent upper limits on the low energy (< 0.5 GeV) cosmic-ray antiproton flux[17,18].

SRW and RS argued that the spectra of antiprotons and γ-rays would be quite similar to those observed for these products in e^+e^- collider experiments, owing to the universality of quark jet hadronization. However, e^+e^- annihilations produce a different mixture of heavy and light quark jets than that from $\chi\chi$ annihilations (e.g., higgsino annihilation produces final states with a very rich mixture of b quark jets). Collider data show that b and c quark jets carry off only 80% and 60% of the cms energy respectively. Thus, the results presented by SRW and RS should be considered to be a strict upper limit to the hardness of the $\chi\chi$ annihilation spectra.

As expected, the Lund simulation gives a significantly softer spectrum for final states weighted by heavy quark channels than that observed in e^+e^- experiments. Fig. 2 shows the inclusive antiproton production function in terms of the scaling variable $x = E/M_\chi$ for higgsinos (and Majorana neutrinos) or photinos of mass M_χ obtained from the Lund simulation.[11] E and β are the total $\bar{p}$ energy and velocity respectively. It should be noted that the cases of generic higgsinos and Majorana neutrinos of equal mass give identical results, as discussed by RS. Note that for χ annihilations at rest the cms energy is $2M_\chi$.

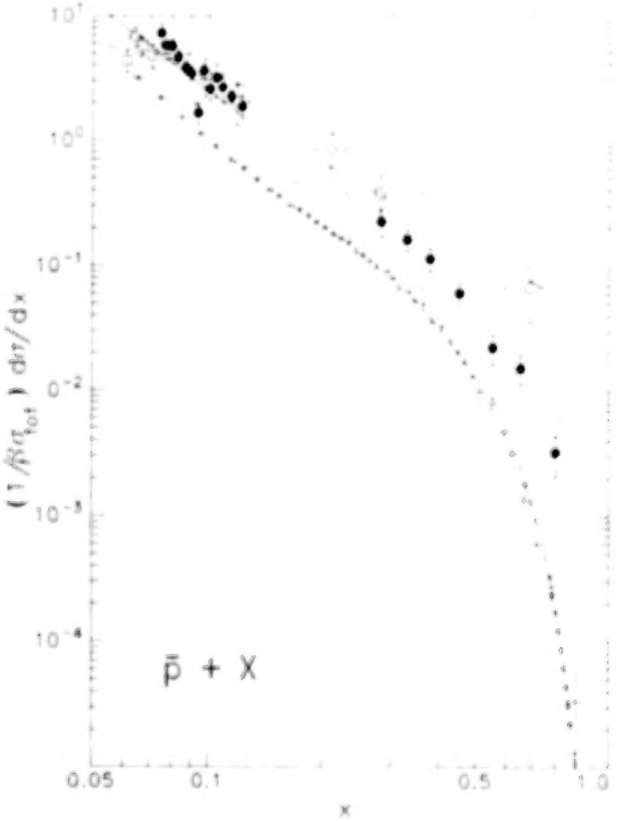

Fig. 2. Antiproton production spectra. Collider data are shown and compared with Lund prediction for e^+e^- annihilation (solid curve). Lund predictions for 15 GeV $\bar{n}n$ (middle dashed curve) and $\bar{\gamma}\gamma$ (lower dashed curve) annihilation are also shown. The crosses show the Lund data points.

The χ annihilation spectra are compared with the spectral function obtained from the Lund simulation of e^+e^- annihilations at a collider cms energy of 35 GeV (ST1). The e^+e^- collider data are also shown. Fig. 2 also shows the spectral source function used by RS to fit the TASSO data (upper dashed curve). The e^+e^- data do not include the antiprotons from $\bar{n}$ decay, however $\bar{n}$ decay was included in the $\chi\chi$ annihilation calculations. For comparison with the e^+e^- and $\chi\chi$ annihilation spectra in Fig. 2, the $\chi\chi$ spectra were

multiplied by a factor of 0.5. STI fit the results from the Lund Monte Carlo runs to simple analytic functions of the form

$$\zeta_{\bar{p}} f(x)/B \equiv (1/B\sigma)(d\sigma/dx) = A \exp(-\alpha x) + B(1-x)^{\delta}/x \qquad (1)$$

where $\zeta_{\bar{p}}$ is the number of $\bar{p}$'s per annihilation and f(x) normalized so that its integral is 1. This functional form reproduces the exponential dependence of the spectrum on x for low values of x. The second term dominates for $x > 0.15$ and goes smoothly to 0 at $x = 1$. The following source function fits to the parameter sets (A,α,B,δ) in eq. (1) were found: (a) for the e^+e^- collider simulation, (82, 46, 0.21, 2.13), (b) for 15 GeV higgsinos or Majorana neutrinos, (148, 50, 0.34, 4.39), and for 15 GeV photinos, (101, 50, 0.20, 3.99).

Photinos produce only ~2/3 as many antiprotons as generic higgsinos or Majorana neutrinos (0.2 per annihilation as opposed to 0.3). Much of this difference is due to the τ production channel, which is unimportant in higgsino annihilation but which accounts for 56% of photino annihilations and produces no baryons. (It should be noted that baryon-antibaryon production through quark jets is not as well understood as meson production (see discussion in STI and references therein.))

The production rate of antiprotons from $\chi\chi$ annihilation in the halo is

$$Q_{\bar{p}}(E) = n_{\chi}^2 \langle \sigma_{\chi} v \rangle_A f_{\bar{p}}(E) \qquad (2)$$

where $f_{\bar{p}}(E) = dN_{\bar{p}}/dE$, normalized to the number of antiprotons per annihilation. For example, in the case of $\tilde{h}$'s, the annihilation cross-section $\langle \sigma v \rangle_A$ is overwhelmingly dominated by the contributions of τ leptons and c and b quarks in the final state and is

$$\langle \sigma_{\chi} v \rangle_A = \frac{G_F^2}{4\pi} (m_{\tau}^2 + 3m_c^2 + 3m_b^2) = 1.3 \times 10^{-26} \ cm^3 s^{-1}. \qquad (3)$$

The antiprotons come from the hadronic $c\bar{c}$ and $b\bar{b}$ final states, but these account for a fraction $\delta_{\tilde{h}} = 30/31 = 1$ of the total. The ratio of $\bar{p}$ yields from photino and generic higgsino annihilation is

$$Q_{\bar{p}}^{\tilde{\gamma}} / Q_{\bar{p}}^{\tilde{h}} = | \delta_{\tilde{\gamma}}^{\tilde{\gamma}} \langle \sigma_{\tilde{\gamma}} v \rangle_A / \delta_{\tilde{h}}^{\tilde{h}} \langle \sigma_{\tilde{h}} v \rangle_A | = 9.4 \times 10^{-2} (m_W/m_{\tilde{q}})^4 \leq 0.1 \qquad (4)$$

where $m_W = 81$ GeV is the W boson mass and $m_{\tilde{q}}$ is the mass of the squark (scalar quark) that mediates the $\tilde{\gamma}$ annihilation (RS).

The interstellar antiproton spectrum is of the form (from eq.(1))

$$I(E) = (4\pi)^{-1} (\rho_{\chi}^2 / M_{\chi}^3) \langle \sigma_A v \rangle_{\chi} c \tau B^2 \{ A \exp[-\alpha E/M_{\chi}] + B M_{\chi} [1-(E/M_{\chi})]^{\gamma}/E \} \qquad (5)$$

where ρ_{χ} is the mass density of dark matter and τ is the effective residence time of cosmic-ray antiprotons in the Galaxy. As pointed out by SRW and RS, eq. (5) for the interstellar spectrum must be modulated to take account of the effects of the solar wind on the spectrum observed at Earth. To do this, STI used a numerical integration of the spherically symmetric solution of the Fokker-Planck equation.

Fig. 3 shows the resultant $\bar{p}/p$ ratio as a function of energy for higgsino and photino annihilation as compared with the present antiproton data, the calculated spectrum of antiprotons from cosmic-ray collisions and the possible spectrum of extragalactic primary antiprotons in the baryon symmetric cosmology, also modulated[11] (STI). For the higgsino case, the results are shown for both solar

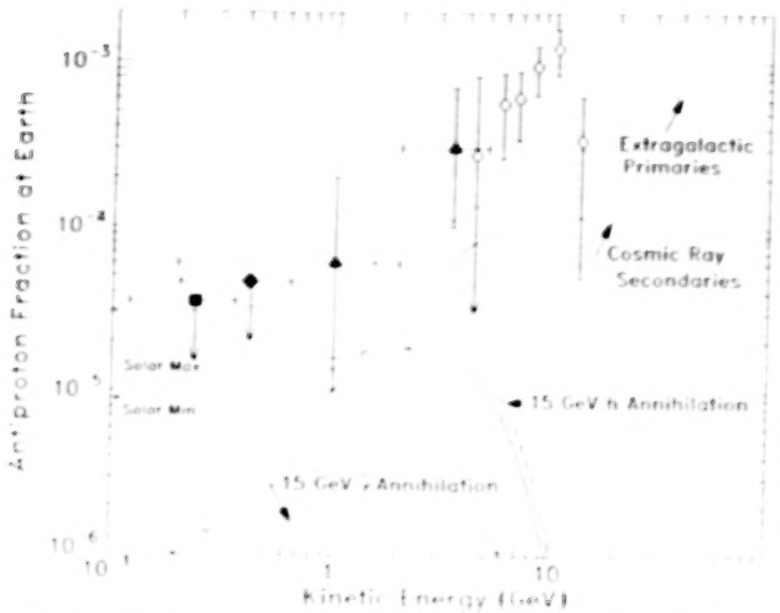

Fig. 3. The ratio $\bar{p}/p$ as a function of kinetic energy given for the different theoretical models (ST1). The data are as follows: (Ref. 17) - black square; (Ref. 18) - black diamond; (Ref. 19) - black triangles; (Ref. 20).

maximum and solar minimum. The annihilation spectra are shown for $\tau = 10^8$ y and $\rho = 0.3$ GeV cm^{-3}. For generic higgsinos, $\langle\sigma_A v\rangle = 1.26 \times 10^{-26}$ cm^{3}s^{-1}. In the photino case, ST took a minimal squark mass of 80 GeV, giving $\langle\sigma v\rangle = 0.22 \times 10^{-26}$ cm^{3}s^{-1}. It is clear from the figure that fluxes which are consistent with the upper limits[18,19] on the low energy antiprotons cannot account for the reported fluxes of antiprotons in the energy range around 10 GeV.

These results can be used to test for constraints on χ particles. The residence time τ is $\sim 10^8$ y for halo propagation[21] and $\sim 2\times10^7$ y for disk propagation models[22]. Studies of cosmic-ray electrons and secondary nuclei[23,24] appear to indicate that τ cannot be too much less than 2×10^7 y or too much more than 10^8 y. The density ρ_χ is probably in the range $\sim$0.2 to $\sim$0.4 GeV cm^{-3}.[25] The generic higgsino value for the cross section from eq. (3) is probably an upper limit to what one would expect for a χ annihilation cross section and significant values for the χ masses lie in the range of $\sim$5 to $\sim$30 GeV (RS). For photinos the cross sections can be much smaller than for higgsinos (see eq. (4)). Thus, $r_5 \equiv 10^5\,(\bar{p}/p)_5$ is at most $\sim$10 (for 15 generic GeV higgsinos) but can easily be as low as $\sim 4\times10^{24}\langle\sigma v\rangle << 1$. The experimental upper limit $r_5 \leq 3.5$ is consistent with an acceptable range of astrophysical parameters for all χ particles of interest. The relevant supersymmetric parameters can be adjusted to give cosmological densities of interest for values of M_χ between $\sim$5 and $\sim$30 GeV. Generic higgsinos or Majorana neutrinos with $M_\chi = 15$ GeV will give $\Omega_\chi h_{50}^2 = 0.2$. It is possible to generalize the values for the vacuum expectation values of the Higgs fields (see eq. (3) of RS) if one wishes to obtain $\Omega_\chi h_{50}^2 = 1$ (the inflation cosmology prediction) with 15 GeV higgsinos. Note that one requires $\Omega_\chi h_{50}^2$ of at least $\sim$0.1 to obtain dark matter halos. (As usual, Ω_χ is the fraction of the critical density in χ particles and h_{50} is the Hubble constant in units of 50 km s^{-1} Mpc^{-1}.)

The present upper limits on low energy $\bar{p}$'s do not constrain dark matter models. However, with the possible range of values for r_5 given above, it is possible to hunt for evidence of χ's with low energy $\bar{p}$ experiments, perhaps at a level not too far below the present limits. Upper limits on the order of $r_5 \leq 0.1$ would place significant constraints on dark matter models.

THE COSMIC-RAY NEUTRINO SPECTRUM FROM $\chi\chi$ ANNIHILATION

There are four main sources of neutrinos and positrons from $\chi\chi$ annihilation to consider, viz., first generation prompt leptons, second generation prompt leptons and charged π and K meson decay leptons (RS). Charmed and bottom quarks and τ leptons are efficient sources of prompt, high energy leptons and antileptons from their weak decays. E.g., for neutrino-positron production, the relevant decay chains are as follows (W^{+*} is a virtual W boson):

$$\tau^+ \to \bar{\nu}_\tau + W^{+*}$$

$$\bar{b} \to \bar{c} + W^{+*} \qquad (6)$$

and $c \to s + W^{+*}$

with W^{+*} decaying to $\ell^+\nu_\ell$, where $\ell^+ = e^+$ or μ^+ (for b decays, $\ell = \tau$ is considerably suppressed by phase space and will be neglected here). B.R.'s for these decays are 18% for τ and 13% for both b and c. Leptons also come from second generation prompt processes given by the decay chains $\tau \to \mu \to e$, $c \to \mu \to e$, $b \to \mu \to e$ and $b \to c \to e$. The B.R. for the first chain is 18%; that of the last three is 13%.

The neutrino flux from the decay of π mesons produced in heavy fermion annihilations can be determined by using the e^+e^- collider data. Within experimental error, the data for the pion production spectrum from e^+e^- annihilations with cms energies above 14 GeV can be fitted to a single spectral function having the form (RS).

$$\zeta_\pi f(E_\pi) = \beta_\pi (11.6\, e^{-1.13E_\pi} + 1.35\, e^{-0.46E_\pi}) \quad \text{GeV}^{-1}. \qquad (7)$$

where, $\beta = [1-(m_\pi/M_\chi)^2]^{1/2}$. ζ_π is the pion multiplicity per annihilation. The low energy pion-decay neutrinos, which peak at ~35 MeV, can be calculated using the well-known kinematical formulae. At energies >> 35 MeV, the π-decay neutrino spectrum may be approximated by noting that two pairs of ν_μ, $\bar{\nu}_\mu$ and one pair of ν_e, ν_e are produced for each e^+, e^- pair produced in the annihilations. All of these leptons take about 1/4 each of the pion energy. It follows from eq. (7) that

$$I_{(\pi)}(E) = \frac{Q_{(\pi)}(E)c\tau}{4\pi} = \frac{n_\chi^2 \langle\sigma v\rangle_A c\tau}{4\pi} (5.4e^{-1.84E}). \qquad (8)$$

The muon neutrinos from kaon decay have a harder spectrum than the pion-decay component so that it gives a significant contribution to the neutrino spectrum at about 2 GeV. The kaon-decay neutrino spectrum as a function of ν_μ energy can be approximated by the expression

$$I_{(K)}(E) = \frac{n_\chi^2 \langle\sigma v\rangle_A c\tau}{4\pi} (0.73e^{-0.76E}) \qquad (9)$$

The energies of all light leptons produced in each of the other processes respectively are similar. Neutrino spectra of ν_e's ($\bar{\nu}_e$'s) and ν_μ's ($\bar{\nu}_\mu$'s) may be calculated from the expression

$$I(E_\nu) = Q(E_\nu)\langle\ell\rangle/4\pi \qquad (10)$$

with $\langle\ell\rangle$ being the mean-path-length of the annihilation region (e.g. through the

galactic halo). The integral spectra for M_χ = 15 GeV are shown in Fig. 4 for a galactic center source. These spectra are normalized to the upper limit on the γ-ray flux from the galactic center[26] assuming that γ-rays at this level and neutrinos could be from $\chi\chi$ annihilation.

The differential ν_e production spectrum has been calculated for 15 GeV higgsinos (or Majorana neutrinos) using a Lund model Monte Carlo program with the results given in Fig. 5.[27] These results give a spectral shape which agrees well with the spectrum obtained from the analytic calculations given in Fig. 4.

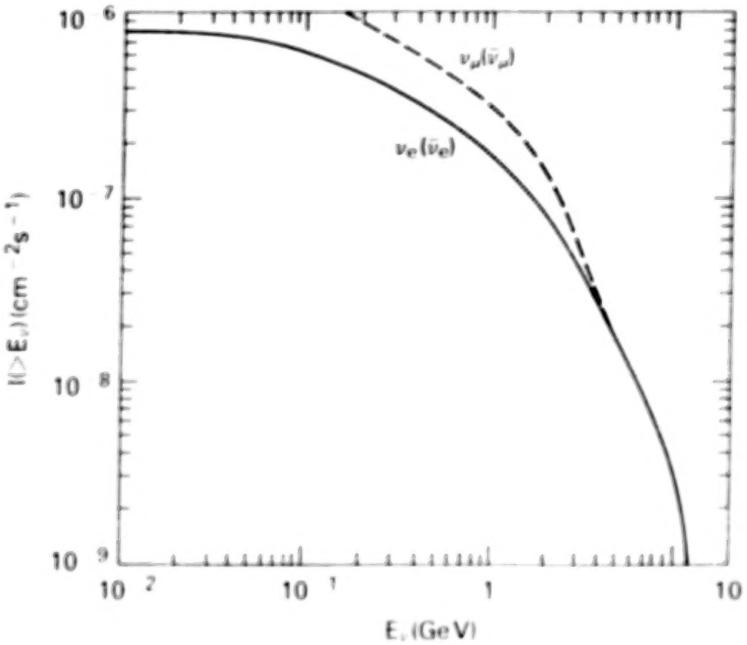

Fig. 4. The integral neutrino spectra from the galactic center normalized to the γ-ray upper limit as discussed in the text.

ANNIHILATION POSITRONS

The positron source spectrum is similar to that for neutrinos. However, the cosmic-ray positron spectrum is changed in propagating to Earth (RS) because of of energy degredation of the positrons by Compton scattering and synchrotron radiation. A detailed discussion of this is given by Rudaz and Stecker (RS). The upper limits on the low energy $\bar{p}$'s imply that positrons from $\chi\chi$ annihilation will have a flux which is expected to be significantly below that produced by cosmic ray interactions (STI). This spectrum has been calculated using the Lund program by Tylka[13] and is shown in Fig. 6. This result is generally in good agreement with the spectral shape calculated semi-analytically by RS. However, the magnitude of the flux has been normalized taking account of the upper limits on low energy $\bar{p}$'s so that it is considerably smaller than that of RS, as well as the cosmic-ray induced flux.

THE FLUX AND SPECTRUM OF NEUTRINOS FROM SOLAR CAPTURE AND ANNIHILATION

Galactic χ particles can be captured by the gravitational field of the Sun[28] and come together in the solar interior to annihilate, with the resulting flux of solar neutrinos potentially obervable by neutrino detectors on the Earth.[29] The spectrum of solar annihilation neutrinos, which has been discussed by many authors[30]

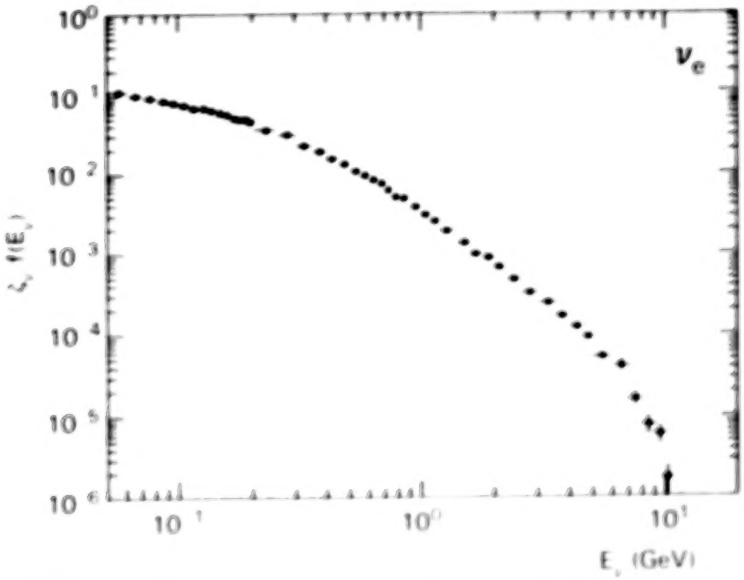

Fig. 5. The differential electron neutrino production spectrum from 15 GeV dark matter annihilation using the Lund Monte Carlo model[27]

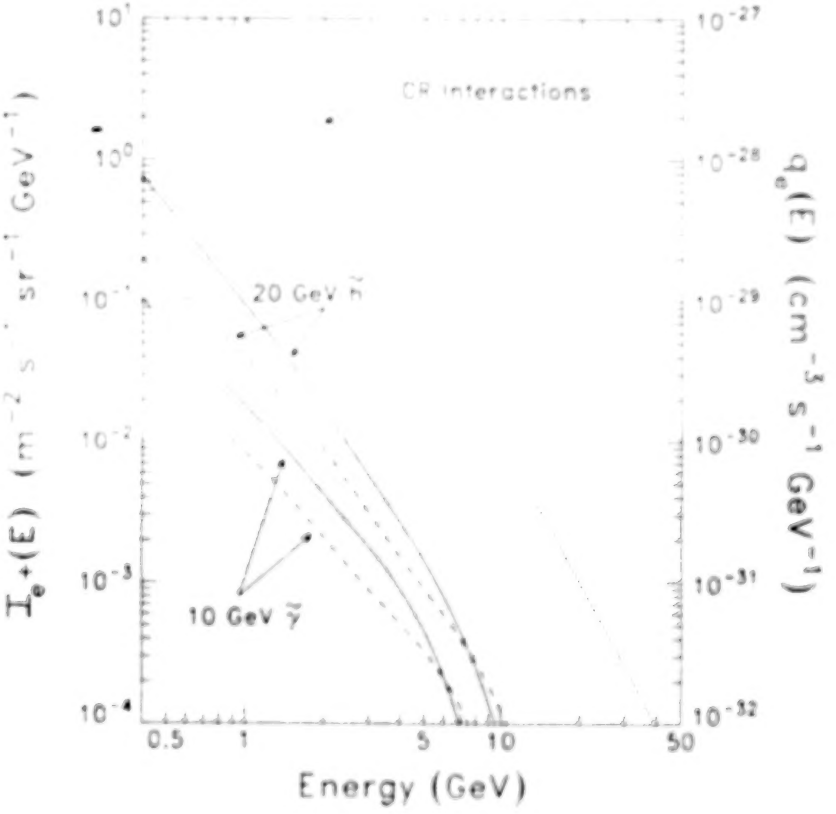

Fig. 6. The cosmic ray positron spectrum from $\chi\chi$ annihilation compared with that produced by cosmic ray interactions[13]. Source spectrum - dashed line and right hand scale; spectrum with propagation over a mean lifetime of 3×10^7 y - solid line and left hand scale.

will be significantly different from the one shown in Fig. 4, owing to the fact that muons and π's stop or interact in the solar interior before they decay. The resulting loss of ν flux or energy eliminates the π and K meson decay components and most of the second generation components from the observable spectrum. Calculations with the Lund model give a softer spectrum than most of those found previously, lowering the expected solar neutrino event rate by a factor of ~3.[9,27]

Galactic χ particles are captured and trapped by the Sun at a rate

$$\Gamma_{tr} = (3\pi/2)^{1/2}(2GM_{\odot}R_{\odot})\frac{n_{\chi}}{v_{\chi}} f_{sc} \qquad (11)$$

where f_{sc} is the probability that a χ particle loses enough energy by elastic scattering to be captured[28,31]. Although lower mass χ particles can evaporate from the Sun before annihilating, those of mass > 5 GeV, with which we are concerned, will not evaporate. Then, in equilibrium, the annihilation rate will be equal to half of the trapping rate and the neutrino flux at Earth will be given by

$$I(E_{\nu}) = (\Gamma_{tr}/2)(4\pi d^2)^{-1} \zeta_{\nu} f(E_{\nu}) \qquad (12)$$

where $d = 1$ A.U. $= 1.5 \times 10^{13}$cm.

For typical dark matter halo parameters $n_{\chi} = 0.4/M_{\chi}(\mathrm{GeV})$ and $v = 300$ km s^{-1}, the trapping rate is

$$\Gamma_{tr} \sim 10^{65}[M_{\chi}(\mathrm{GeV})]^{-1} \sigma_{p_{\chi}\text{-}p_{\odot}}(\mathrm{cm}^2) \quad \mathrm{s}^{-1}. \qquad (13)$$

For higgsinos and Majorana neutrinos, the elastic scattering cross section in eq. (13), is $\sigma \sim 1.5 \times 10^{-38}$cm^2. Taking $M_{\chi} = 15$ GeV, we find $\Gamma_{tr} \sim 10^{26}$ s^{-1} and the neutrino flux from solar $\chi\chi$ annihilation will be

$$I^{(\chi)}(E_{\nu}) \sim 2 \times 10^{-2} \zeta_{\nu} f(E_{\nu}). \qquad (14)$$

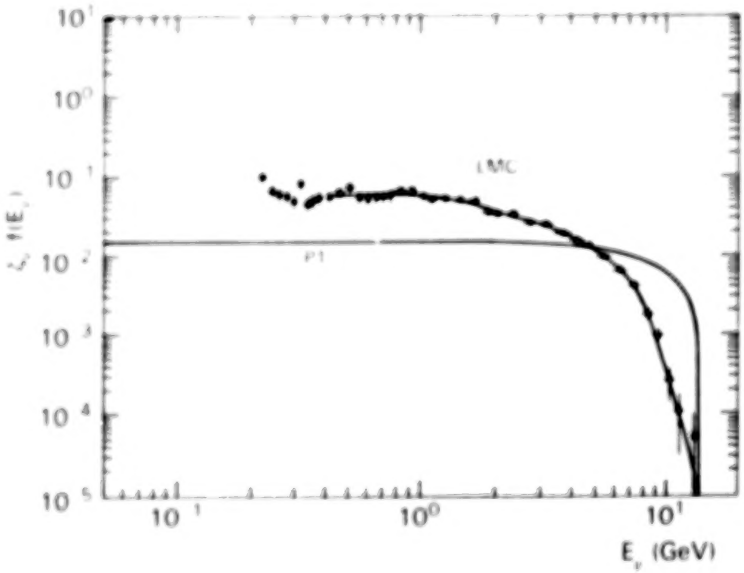

Fig. 7. The differential electron neutrino production function from 15 GeV $\chi\chi$ annihilation in the solar interior. The curve marked LMC is from the Lund Monte Carlo calculations.[27]

The total neutrino production function $\zeta_\nu f(E_\nu)$ relevant to eq. (14) is shown in Fig. 7. Fig. 7 shows both the first generation prompt (P1) approximation, similar to used in Refs. 32 and 33 and that obtained using the Lund Monte Carlo program[27], which gives a softer spectrum. Given the fluxes calculated using eq. (14), the event rate observed in a neutrino detector will be given by

$$\Gamma_{ev} = n_N \int dE\ V_{eff}(E)\ [\sigma_\nu(E_\nu) I_\nu(E_\nu) + \sigma_{\bar{\nu}}(E_{\bar{\nu}}) I(E_{\bar{\nu}})] \ , \qquad (15)$$

where V_{eff} is the effective detection volume, equal to the detector volume itself for the contained events from lower energy neutrinos (typically 0.5 to 2 GeV) and is proportional to E_ν for through going detector events of higher energy[34]. The neutrino-nucleon cross sections σ_ν and $\sigma_{\bar{\nu}}$ are linearly dependent on energy. Using eqs. (14) and (15), we can estimate the ratio of solar annihilation to atmospheric events for the IMB neutrino detector, following the discussion of Ng, et al.[30]. For contained events, this ratio is just

$$R_C = (4\pi/\Omega_\theta)_C \int_{0.5}^{2} dE\ E\ I_\nu^{(x)}(E)] \ / \ \int_{0.5}^{2} dE\ E\ I_\nu^{ATM}(E) = 0.03 \qquad (16)$$

where Ω_θ is the solid angle around the Sun, determined by the detector resolution, while for through going events it is

$$R_T = (4\pi/\Omega_\theta)_T \int_{2}^{M_x} dE\ E^2\ I_\nu^{(x)}(E)] \ / \ \int_{2}^{\infty} dE\ E^2\ I_\nu^{ATM}(E)] = 1.5 \qquad (17)$$

using the production function from the Lund model. Fig. 8 shows this production function along with the P1 approximation and a typical E^{-3} atmospheric spectrum (all

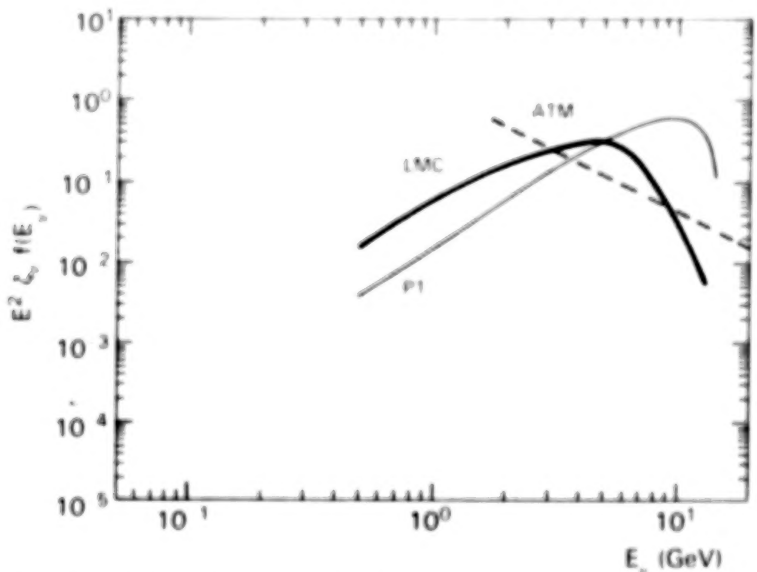

Fig. 8. Relative event rate predictions as a function of energy for solar dark matter annihilation and typical atmospheric neutrino fluxes[27]. Curve P1 and LMC are as in Fig. 6. The atmospheric spectrum is typically an E^{-3} power law[35].

weighted by E^2 as relevant to the throughgoing event rate,). This figure illustrates (1) that the event rate is overestimated by a factor of ~3 by the simple first generation approximation, and (2) that the best "window" for observing solar annihilation neutrinos is the 2-10 GeV energy range.

ANNIHILATION GAMMA RADIATION

The spectrum of γ-ray background radiation from $\chi\chi$ annihilation in the halo may be calculated by noting that the continuum flux is overwhelmingly due to the decay of neutral pions produced in the $\chi\chi$ annihilations. One can then make use of the pion production spectrum (7) in order to determine the γ-ray spectrum.[36]

The γ-ray spectrum resulting from the decay of the neutral pions is given by[37]

$$\zeta_\gamma f(E_\gamma) = 2\int_{E_\ell(E_\gamma)}^{M_\chi} dE_\pi \, (E_\pi^2 - m_\pi^2)^{-1/2} \zeta_\pi f(E_\pi) \qquad (18)$$

where $E_\ell(E_\gamma) = E_\gamma + m_\pi^2/4E_\gamma$ and ζ_γ is the γ-ray multiplicity.

A more exact calculation can be made again using the Lund Monte Carlo program[12] (ST2). For χ particles below the b quark threshhold ($M_\chi \sim 5$ GeV), ~90% of the resulting γ-rays are from π^0 decay. The remaining 10% come from the decay of other hadrons. For larger mass χ particles, a component from B* meson decay produces a distinctively hard spectral signature in the ~0.1 GeV energy range. This channel is

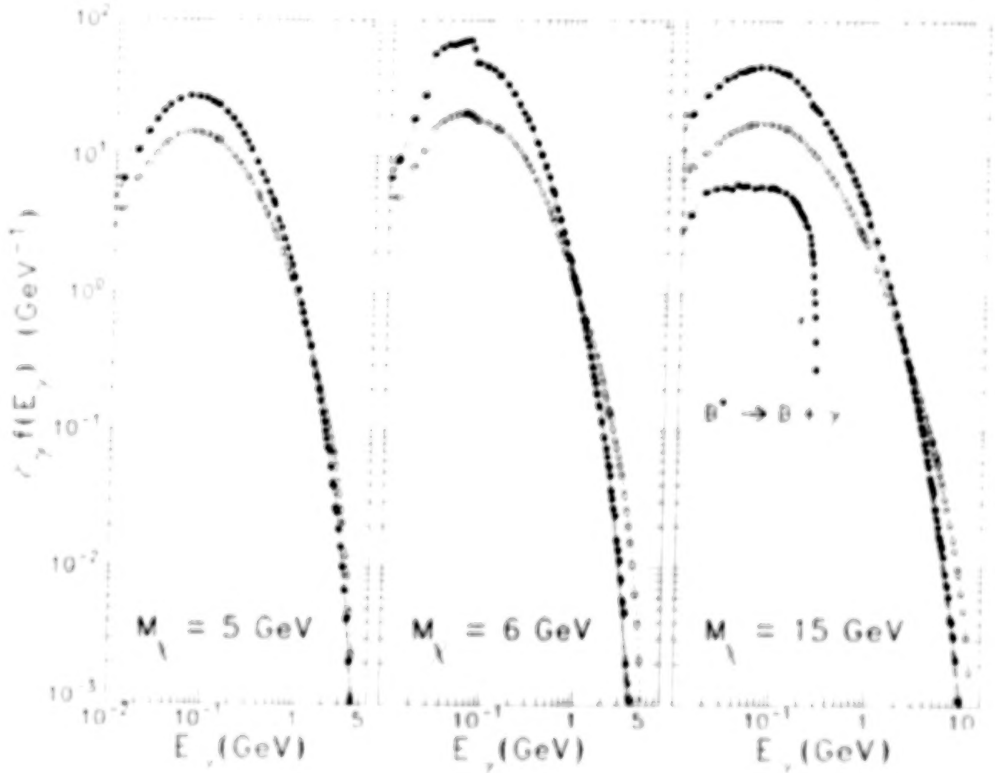

Fig. 9. Gamma-ray spectral production functions for photino (open circles) and higgsino (closed circes) annihilation. The dashed longer curves show the pion decay component only. The 15 GeV plot shows the B* decay component from $b\bar{b}$ annihilation separately.

especially important for $\tilde{h}$'s which annihilate into a $b\bar{b}$ pair ~85% of the time. In this case, γ-ray production occurs ~85% through pion decay, ~8% through B* decay and ~7% through other channels. Since $\tilde{\gamma}$'s have much smaller branching ratios for b production (~15%), B* decay accounts for only about 2% of the γ-ray production in their annihilations. Fig. 9 shows the results obtained by Stecker and Tylka[12] (ST2) for $\tilde{\gamma}$'s (closed circles) and $\tilde{h}$'s (or ν_M's)(open circles) with masses of 5, 6 and 15 GeV expressed as the quantity $\zeta f(E_\gamma)$, where ζ is the average γ-ray multiplicity per annihilation and $f(E_\gamma)$ is the normalized spectral distribution function. The π^0-decay component, is shown by a dashed line. The most striking feature is the contribution from $B^* \to B + \gamma$ decay, particulary for $\tilde{h}\tilde{h}$ annihilation. The decays $B^* \to B + \gamma$ produce a γ-ray line of energy $E^* = 51.7$ MeV in the B* rest frame. For isotropic decays, this line transforms to a square wave spectrum in the c.m. frame of the $\chi\chi$ annihilation with sharp drops at the cutoff energies[37]. For $M_\chi = 15$ GeV, the cutoff energies are 281.4 MeV and 9.5 MeV (see Fig 9).

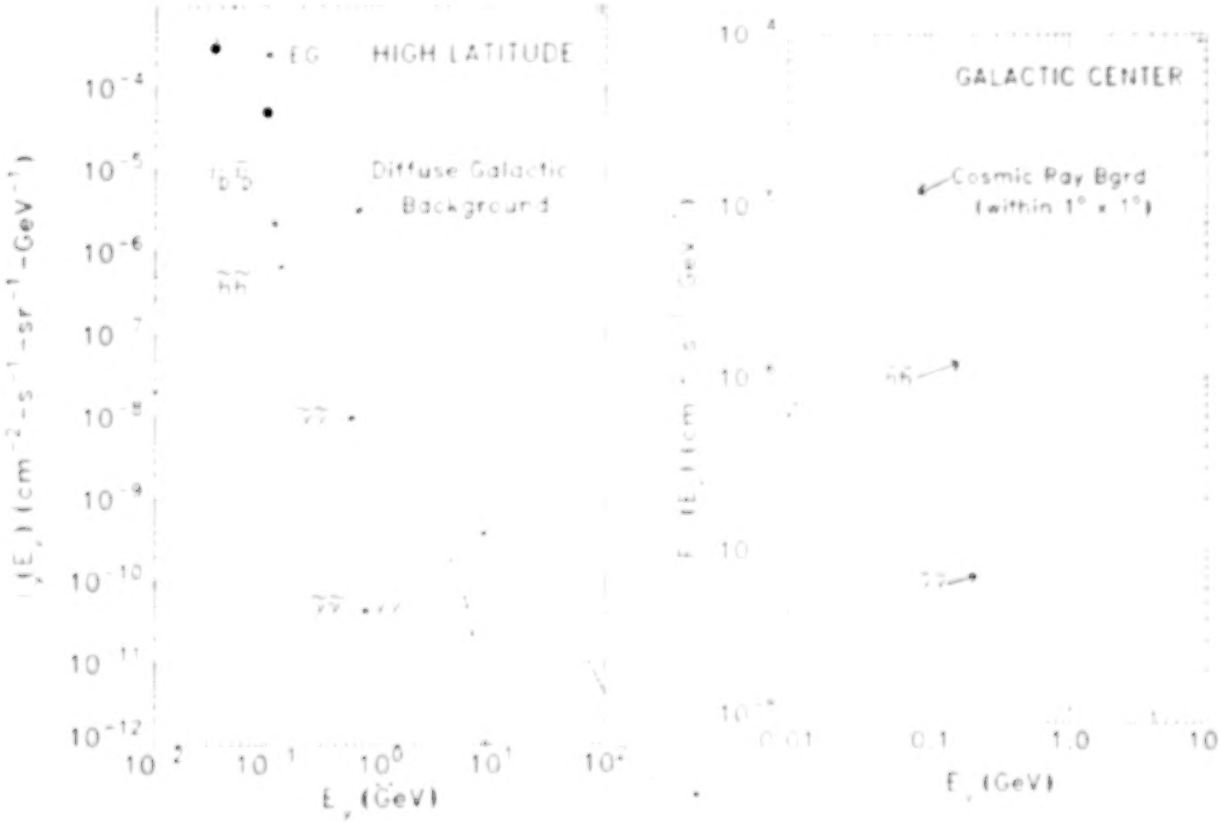

Fig. 10. The high latitude galactic γ-ray spectrum calculated for various 10 GeV χ particle annihilations compared with the extragalactic (EG) diffuse background and galactic disk radiation (see text).

Fig. 11. The annihilation spectrum from a hypothetical dark matter core at the galactic center consisting of either 15 GeV $\tilde{\gamma}$'s or $\tilde{h}$'s compared with the γ-ray flux at the galactic center from cosmic ray interactions.

The high latitude galactic γ-ray spectrum from $\chi\chi$ annihilation is (RS)

$$I(E_\gamma) = \frac{\langle \ell \rangle}{4\pi} n_\chi^2 \langle \sigma v \rangle_{ann} \zeta_\gamma f(E_\gamma)$$
$$= 1.8 \times 10^{-6} \langle \ell_8 \rangle \rho_{0.3}^2 M_\chi^{-2} \langle \sigma v \rangle_{26} \zeta_\gamma f(E_\gamma) \quad cm^{-2} s^{-1} sr^{-1} \qquad (19)$$

where $\langle \ell \rangle$ is the mean line-of-sight through the galactic halo in units of 8 kpc, $\rho_{0.3}$ is the χ density in units of 0.3 GeV cm^{-3}, and the annihilation cross section is in units of 10^{-26} $cm^3 s^{-1}$. The fluxes at high galactic latitudes from the annihilation of 10 GeV $\bar{n}$'s and 10 GeV $\tilde{\gamma}$'s are shown in Fig. 9 for $\rho_{0.3} = 1$ and $\langle \ell_8 \rangle = 1$. The generic $\bar{n}$ cross section is $\langle \sigma v \rangle_{26} = 1.26$. For $\tilde{\gamma}$'s, ST2 took a cross section corresponding to a lower limit on the squark mass of $M_W = 80$ GeV, which gives $\langle \sigma v \rangle_{26} = 0.22$.

The annihilation fluxes are compared in Fig. 10 with an estimate of the mean diffuse background flux expected from cosmic-ray interactions with interstellar gas in the galactic disk at high galactic latitudes (mean total column density of $\sim 4 \times 10^{20}$ cm^{-2})[12,38]. However, the high latitude interstellar medium is very patchy. Recent high resolution 21cm measurements, have shown that there are regions covering ~1% of the sky with neutral column densities $< 0.9 \times 10^{20}$ cm^{-2} (Ref. 39). In these regions, it may be possible to observe annihilation γ-radiation from a "naked" dark matter halo using a high angular resolution γ-ray telescope.[12,40]

There appears to be an extragalactic background of γ-radiation (curve EG in Fig. 10) which is softer than the galactic high latitude background[41,42]. The extragalactic flux may exceed the high latitude galactic background for energies below 0.4 GeV and may be comparable to the galactic component at higher energies provided that one can extrapolate from the observations. However, some theoretical models indicate that the extragalactic spectrum may steepen significantly above the observed energy range[43].

In addition to a γ-ray continuum, dark matter annihilation can produce line radiation in the GeV γ-ray region.[44] For photinos of mass greater than 4 GeV and taking a minimal squark mass, Rudaz[44] finds that the line flux in the direction of the galactic pole will be

$$F_{\gamma\gamma + \gamma Z} \simeq 1 \times 10^{-11} \rho_{0.3}^2 \langle \ell_8 \rangle \quad (cm^2 s \cdot sr)^{-1} \qquad (20)$$

independent of mass, with the line centered around M_χ and having a Doppler width given by $\Delta E_\gamma / E_\gamma = \beta_\chi \sim 10^{-3}$. It follows that if an energy resolution of 10^{-3} could be obtained, the line-to-continuum ratio in a bin centered around the line would be

$$F_{line}/F_g \simeq 0.7 \, (E_\gamma / 10 \text{ GeV})^{1.7}. \qquad (21)$$

Even with a 1% energy resolution, such lines should be detectable.

It is possible for dark matter χ particles to be concentrated in a core at the galactic center by the drag of ordinary baryonic matter through collapse in the early stages of galaxy formation[45]. Annihilations from such a source at a distance r_s consisting of χ's in a volume V_s with mean-square density $\langle \rho_\chi^2 \rangle$ will give a flux

$$F(E_\gamma) \simeq (4\pi r_s^2)^{-1} \langle \rho_\chi^2 \rangle M_\chi^{-2} \langle \sigma v \rangle V_s \zeta_\gamma f(E_\gamma) \quad (cm^2 s)^{-1}. \qquad (22)$$

Using the isothermal core model of Ipser and Sikivie[46], we find

$$(4\pi r_s^2)^{-1} V_s \langle \rho_\chi^2 \rangle \simeq 6.9 \times 10^{20} \quad GeV^2 cm^{-5}. \qquad (23)$$

For such a core of 15 GeV $\bar{n}$'s, the γ-ray flux is given by

$$F_{GC}(0.15) \approx 1.5 \times 10^{-6} \quad (cm^2 s \cdot GeV)^{-1} \qquad (24)$$

with a relatively flat spectrum between 0.1 and 0.2 GeV owing to B^* decay. This spectrum is much harder than the γ-ray spectrum from cosmic-ray interactions in the Galaxy, which acts as a foreground source. Both cosmic-ray (CR) induced and 15 GeV χ annihilation spectra are shown in Fig. 11 for a γ-ray telescope with a 1° beam size. The (CR) spectrum for the inner galaxy has been calculated theoretically for the inner galaxy and agrees well with the observational data[47]. Let us consider the observablity of such a source with the EGRET γ-ray telescope to be launched on the Gamma Ray Observatory (GRO). This telescope has (1) an angular resolution of the order of 1° in the 0.1-0.2 GeV energy range, (2) an effective area of ~1500 cm^2 in this energy range, and (3) an energy resolution of ~15%[48]. Dividing up its 80-200 MeV data into 3 energy bins of ~40 MeV each, with a 1 month exposure time, even the lowest energy bin would produce a signal of ~7σ. Using an on-off subtraction technique would further define the galactic center source. A detailed discussion of this work may be found ST2.

The extragalactic and cosmological γ-ray background spectrum from neutral heavy fermion annihilation can be calculated following the methods given by the author[49]. and can be shown to be negligible compared to the observed extragalactic background.

CONCLUSIONS

We have discussed the annihilation physics of exotic dark matter particles, in particular, those predicted by supersymmetry theory. This physics leads to the production of calculable, and potentially observable fluxes of cosmic-ray and cosmic γ-ray annihilation products. We conclude that a study of cosmic-ray antiprotons may give information about the nature of the dark matter, assuming that it is made up of χ particles. In addition, studies of galactic γ-radiation may also shed light on the dark matter problem. A characteristically hard spectrum in the 100 MeV region from a source at the galactic center or at high galactic latitudes could serve as a signature of χ particle annihilation. With significantly more sensitive γ-ray telescopes, the discovery of monochromatic radiation in the several GeV range would provide the most conclusive evidence. Solar neutrinos of several GeV energy may also give an observable signature for galactic χ particle dark matter. However, the positron flux from dark matter annihilation would be buried below that from cosmic-ray produced secondaries.

Acknowledgment: The author would like to thank Dr. A. J. Tylka for helpful discussions regarding the manuscript and for providing Fig. 6.

REFERENCES

1. Zwicky, F., 1933, Helv. Phys. Acta **6**, 110.
2. Rubin, V., et al., 1985, Astrophys. J. **289**, 81.
3. Hegyi, D. J and K. A. Olive, 1983, Phys. Lett. **126B** 28.
4. Trimble, V., 1987, Ann. Rev. Astron. Astrophys. **25**, 425.
5. Primack, J. R., et al., 1988, Ann. Rev. Nucl. Part. Sci. **38**, 751.
6. Ellis, J., et al., 1984, Nucl. Phys. **B238**, 453.
7. Greist, K., 1988, Phys. Rev. **D38**, 2357.
8. Sjöstrand, T., 1986, Comp. Phys. Comm., **39**, 347.
9. Ritz, S. and Seckel, D., 1988, Nucl. Phys. **B304**, 877.
10. Ellis, J., et al., 1988, Phys. Lett. **B214**, 403.
11. Stecker, F. W. and Tylka, A. J., 1989 Astrophys. J. Lett. **336**, L51 (ST1).
12. Stecker, F. W. and Tylka, A. J., 1989, Astrophys. J. **343**, 169 (ST2).
13. Tylka, A. J., 1989, Phys. Rev. Lett. **63**, 840.

14. Ahlen, S. P., et al., 1987, Phys. Lett. **B195**, 603.
15. Rudaz, S. and F. W. Stecker, 1988, Astrophys. J., **325**, 16.
16. Stecker, F. W., Rudaz, S. and Walsh, T. F., 1985, Phys. Rev. Letters **55**, 2622.
17. Streitmatter, R. E., et al., 1988, Adv. Space Sci., in press.
18. Ahlen, S. P. et al., 1988, Phys. Rev. Letters **61**, 145.
19. Bogomolov, E. A., et al., 1987, Proc. 20th Intl. Cos. Ray Conf. (Moscow) **2**, 72.
20. Golden, R. L., et al., 1984, Astrophys. Lett. **24**, 75.
21. Ginzburg, V. L. and V. S. Ptuskin, 1976, Rev. Mod. Phys. **48**, 161.
22. Garcia-Munoz, M., Mason, G. M., and Simpson, J. A., 1977, Ap. J. **217**, 859.
23. Webber, W. R., 1983, in Composition and Origin of Cosmic Rays, ed. M. M. Shapiro (Dordrecht: Reidel) p.25.
24. Møller, D., 1988, Adv. Space Sci., in press.
25. Flores, R. A., 1988, Phys. Lett. **B215**, 73.
26. Blitz, L., et al., 1985, Astron. Astrophys. **143**, 267.
27. Stecker, F. W. and Tylka, A. J., 1989, in preparation.
28. Press W. H., and Spergel, D. H., 1985, Astrophys. J. **296**, 679.
29. Srednicki, M., Olive, K. A., and Silk, J., 1987, Nucl. Phys. **B279**, 804.
30. Ng, K.-W., et al., 1987, Phys. Lett B **188**, 138 and refs. therein.
31. Krauss, L. M., et al., 1986, Phys. Rev. **D33**, 2079.
32. Gaisser, T. K., et al., 1986, Phys. Rev. **D34**, 2206.
33. Hagelin, J. S., et al., 1986, Phys. Lett. **B180**, 375.
34. Gaisser, T. K. and Stanev, T., 1984, Phys. Rev. **D30**, 985.
35. Perkins, D. H., 1984, Ann. Rev. Nucl. Particle Sci. **34**, 1.
36. Stecker, F. W., 1988, Phys. Lett B, **201**, 529.
37. Stecker, F. W., 1971, Cosmic Gamma Rays, Mono Book Co., Baltimore.
38. Stecker, F. W., 1989, Proc. GRO Workshop, in press.
39. Elvis, M., Lockman, F. J. and Wilkes, B. J. 1989, Astron. J., **97**, 777.
40. Silk, J., 1989, Nucl. Phys. B, in press.
41. Fichtel, C. E., et al., 1977, Astrophys. J. **217**, L9.
42. Thompson, D. J. and Fichtel, C. E., 1982, Astron. Ap., **109**, 352.
43. Stecker, F. W., 1989, Nucl. Phys. B, in press.
44. Rudaz, S., 1989, Phys. Rev. **D39**, 3549.
45. Zel'dovich, Ya. B., et al., 1980, Sov. J. Nucl. Phys. **31**, 664.
46. Ipser, J. R. and Sikivie, P., 1987, Phys. Rev. **D35**, 3695.
47. Stecker, F. W., 1989, in Cosmic Gamma Rays, Neutrinos and Related Astrophysics, ed. M. M. Shapiro and J. P. Wefel, (Dordrecht: Kluwer Academic Pub.), p. 85.
48. Thompson, D. J., 1986, Nucl. Instr. Methods, **A251**, 390.
49. Stecker, F. W., 1978, Astrophys. J. **223**, 1032.

OPTICALLY EXCITED STATES IN POSITRONIUM

R.H. Howell, K.P. Ziock, F. Magnotta, C.D. Dermer, and R.A. Failor
Physics Department
Lawrence Livermore National Laboratory
Livermore, CA 94550
and
K.M. Jones
Williams College
Williamstown, MA 01267

ABSTRACT

We report optical excitation of the 1^3S-2^3P transition in positronium, and a second excitation from n=2 to higher n states. The experiment used light from two pulsed dye lasers. Changes in the positronium annihilation rate during and after the laser pulse were used to deduce the excited state populations. We found that we could saturate the n=2 level and excite a substantial fraction of n=2 positronium to higher levels. Preliminary spectroscopic measurements were performed on n=14 and n=15 positronium.

INTRODUCTION

Although positronium (Ps) has been known for many years, few experiments have created and maintained a population of Ps in other than the ground state. In previous experiments, a small fraction of Ps has been formed in the n=2 state by bombarding metallic targets with a low energy positron beam [1], or by exciting Ps from the ground to the n=2 state with an incoherent, broadband light source [2]. Two photon excitation of the 1^3S-2^3S transition [3] has also been used, but leads to prompt photo-ionization. At Livermore, we have created significant populations of n=2 Ps through optical saturation of the 1^3S-2^3P transition using a frequency-doubled, pulsed dye laser [4,5]. We have also excited higher n states with a second dye laser tuned to red wavelengths [5]. We find that we are able to repeatedly excite the Ps atoms in our laser beam to the n=2 levels, and subsequently excite n=2 Ps to higher n states where it is long-lived. Moreover, we have optically saturated the n=2 level using a broad bandwidth laser resonant with a large fraction of the Doppler profile of the Ps. These conditions are required for the recently suggested technique of broadband laser cooling [6].

BACKGROUND

The Ps ground state is split into a singlet state which undergoes 2γ annihilation with a 125 ps lifetime, and a triplet state which undergoes 3γ annihilation with a 142 ns lifetime (figure 1). The annihilation lifetimes of

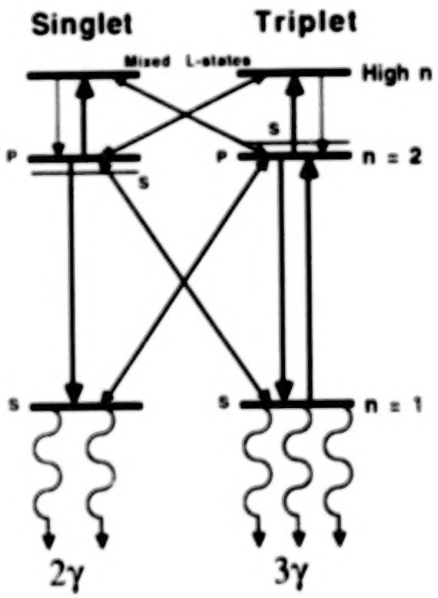

Figure 1. Schematic energy level diagram of Ps showing transitions between states mixed by magnetic and electric fields typical of this experiment. The laser bandwidths cover the entire n=2 and high n multiplets.

the singlet and triplet 2P levels are > 100 ls, which are significantly greater than the 3.2 ns radiative lifetime. In a field free region, singlet-triplet electric-dipole transitions are not permitted. However, in the presence of a magnetic field, the Zeeman effect mixes singlet and triplet levels with the same magnetic quantum number [7,9]. In the ground state, this leads to magnetic quenching [10], i.e., a reduction in the triplet lifetime due to the small admixture of the singlet state. In first order perturbation theory, mixing of the singlet and triplet levels is inversely proportional to the energy difference between the levels. Due to the smaller energy separation for larger n values, mixing fractions increase with increasing n state. Hence, a 200 G field, which does not significantly mix the ground state, induces a several percent admixture of the amplitudes of the singlet state in the n=2 triplet levels [11]. At high values of n (>10), this field will cause the spin states to be completely mixed.

In our experiment, we observe the excitation of Ps through changes in the annihilation rate. The initial population of excited state Ps is negligible at production, and the singlet Ps atoms rapidly annihilate, leaving a population of ground state triplet Ps. Since the annihilation lifetimes of the 2P and higher states are long compared with their radiative decay lifetimes, essentially all annihilation occurs in the ground state. When no magnetic field is present, exciting Ps to the n=2 levels reduces the observed annihilation rate during the laser pulse. However, when a magnetic field is present, an enhancement in the annihilation rate can occur during the laser pulse since transitions between singlet and triplet levels are possible between Zeeman-mixed levels. Thus, each excitation of the Ps to n=2 levels can result in an enhanced annihilation rate by allowing de-excitation to the singlet ground state. At high transition rates, i.e. high laser intensities, a significant fraction of the illuminated Ps may be made to annihilate in a short time compared to the triplet ground state lifetime. Moreover, due to the Δm selection rules for different photon polarizations, the annihilation rate is also influenced by the laser light polarization. Thus, for fixed magnetic field and laser polarization, the number of enhanced annihilations is directly proportional to the n=2 singlet population.

The loss of Ps from enhanced annihilation during the laser pulse will lead to a reduction in the number of annihilations after the laser pulse. This reduction is due to the decrease in the triplet ground state Ps population caused by enhanced annihilation. The Ps ground state population can also be reduced by excitation to higher n states. Thus, there are two time intervals that are separately identified with annihilation changes proportional to the singlet n=2 population and changes in the triplet ground state population. Excitation to higher n states will affect both these populations by reducing the triplet ground state population and changing the singlet n=2 state population.

The number of excess annihilations of Ps resulting from excitation to the n=2 level can be calculated using a rate equation model for the 1S-2P transitions, and using perturbation theory to calculate the Zeeman mixing [9]. The magnitudes of electric-dipole transitions to states with $\Delta m = 0, \pm 1$ depend on both photon polarization and direction of photon propagation with respect to the magnetic field. Mixing into singlet Ps follows the Zeeman selection rules [7,8], and all 2^1P_1 Ps are assumed to decay to 1^1S_0 and annihilate. The results of the calculation are presented as a function of the laser pulse energy in figure 2, where we plot the change in annihilations induced in a 40 ns window by a 10 ns FWHM Gaussian laser pulse. The same detection probability was assumed for both singlet and triplet decays. The results are presented for several values of magnetic field. For low values of B, where little mixing occurs, the number of annihilations decreases due to the time spent in the n=2 level. At large values of magnetic field (~ 200 G), the annihilation rate from mixing into the singlet state becomes large causing an enhancement in the annihilation rate.

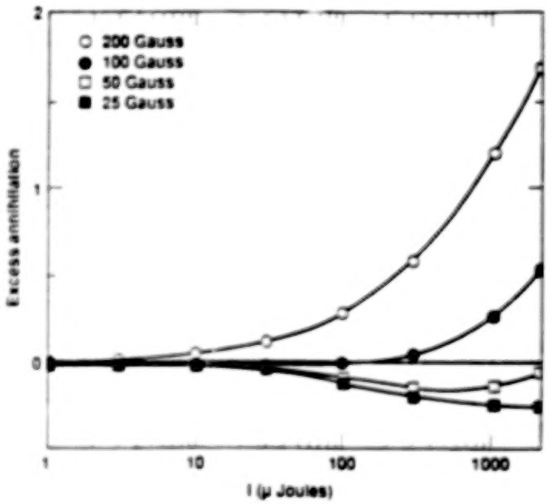

Figure 2. Calculated fractional change in the number of annihilations observed in a 40 ns window due to a 10 ns FWHM laser pulse (centered in the window) as a function of energy per laser pulse.

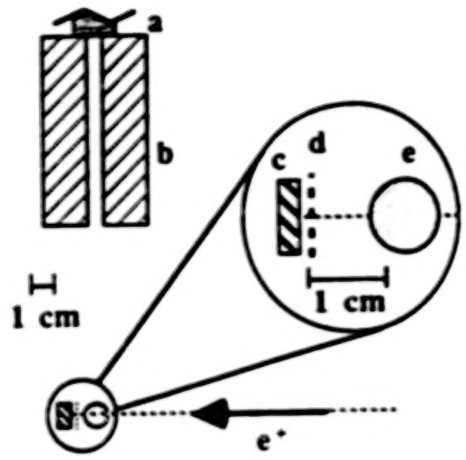

Figure 3. Schematic diagram of the apparatus showing the annihilation gamma detector (a) and its collimator (b) in relation to the target (c), grid (d), and laser profiles (e) (inset drawing). The incoming positron beam is centered on the dotted line.

EXPERIMENT

A schematic of the experimental geometry is shown in figure 3. Positronium is produced by focusing the Livermore intense, low energy (1 keV), positron beam [12] in an ultrahigh vacuum chamber on a clean, heated (1000 K) Cu target. An electrically biased grid, mounted in front of the target, returns any bare positrons to the target. The heated sample emits both energetic (kinetic energy ~ 2.6 eV) and thermally desorbed Ps (kinetic energy ~ 0.1 eV) [13] which then drifts through the grid into the laser interaction region. Several plastic scintillator detectors were used to detect annihilation gamma rays. Uncollimated detectors observe the Ps annihilation throughout the chamber, while collimated detectors are used to separate Ps by energy through time-of-flight techniques [14]. The laser interaction region, directly in front of the Cu target, is viewed by a collimated scintillator paddle with a field of view 1.4 cm wide along the path of the laser beam.

To achieve resonant n= 2 excitation over a significant fraction of the Doppler profile of the thermal Ps, we have frequency-doubled the 485.906 nm output of our excimer pumped, Lambda Physik FI 2002 dye laser. The light is focused in a β-Barium Borate doubling crystal to obtain 242.953 nm light with a typical 0.07 nm FWHM bandwidth. This covers a significant fraction of the estimated 0.15 nm FWHM Doppler profile of the transition and allows excitation of all of the 2P levels. The output of the doubling crystal is passed through a prism to separate the fundamental from the first harmonic. The resulting ultraviolet beam is passed through a second prism, expanded to an ~ 1 cm diameter, and then passed in front of the Cu target. Calibration of the laser is performed to 0.005 nm with a monochromator, cross-calibrated to the 242.795 nm line of an Au, hollow cathode, discharge lamp.

To excite higher n states from the n=2 population, we split the pump beam of our excimer laser to pump a second dye laser which was tuned to wavelengths in the 720 to 750 nm region and calibrated to 0.005 nm by comparison to an Ne discharge lamp. The red laser had a band width of 0.4 nm and a beam profile of 1 cm^2. The two laser beams covered equal path lengths and merged to coincidently enter the Ps interaction region.

The laser was timed to the linac positron pulse with a variable delay. Timing between the laser light and the positrons was monitored by a photomultiplier tube mounted with both a plastic scintillator and a fiber optic. We establish timing of the 10 ns laser pulse relative to the 15 ns positron pulse to ± 2.5 ns.

RESULTS

Time distributions of annihilation gamma rays viewed with the collimated detector were separately collected for positron pulses with the laser on and off. The laser pulsed every eleventh positron burst. A typical result is shown in figure 4a (see next page) with B=200 Gauss, the ultraviolet light delayed 90 ns after the positron pulse, and 460 μ-joules per laser pulse. The normalized laser-off data is subtracted from the laser-on data to obtain the difference distributions shown in figures 4b-4d. Figure 4b is the difference plot obtained from figure 4a. In figure 4c, the peak in the annihilation rate is seen during the laser pulse, now delayed by 70 ns. In figure 4d, the laser has been detuned by 1.0 nm, producing a random distribution.

Measurements were made for the n=2 excitation for several values of laser pulse energy, with B=200 G. In figure 5b we see the excess counts during the laser pulse normalized to counts in a time interval including all annihilations except the prompt burst. Data taken with the laser detuned by 1.0 nm in a 200 G magnetic field and with the laser on resonance in a 50 G magnetic field are represented by the open triangle and the open circle,

respectively. Both of these points show no enhanced annihilation during the laser pulse, as expected from our rate calculations.

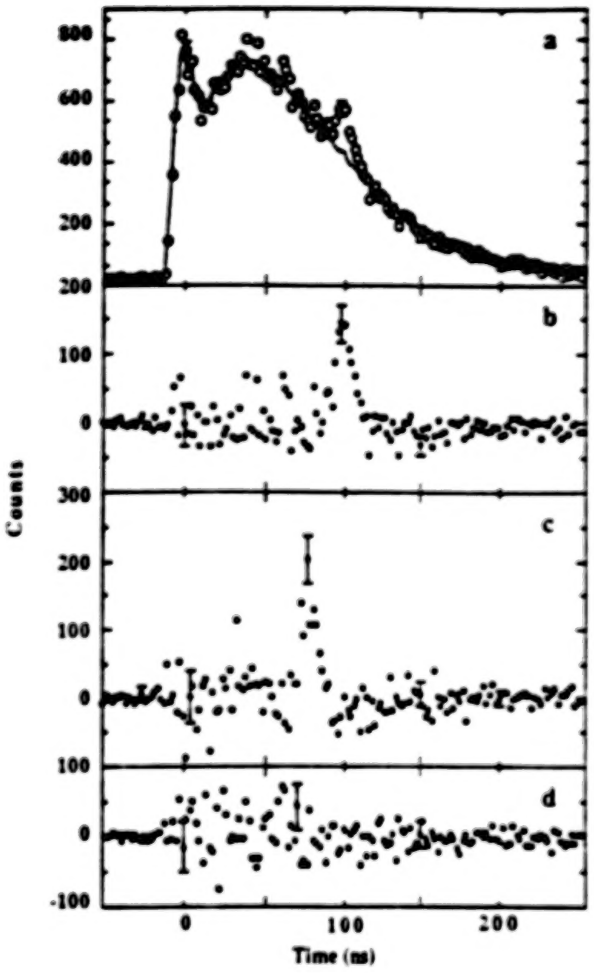

Figure 4. a) Typical annihilation time distributions collected by the collimated detector for ultraviolet illumination with the laser off (solid curve), and laser pulsed at 90 ns (open circles) taken with a 200 G magnetic field. b) Laser-on minus laser-off difference spectrum obtained from the data of 4a. c) Difference spectrum as in 4b, but with the laser pulsed 20 ns earlier. d) Difference spectrum as in 4c, but with the laser detuned 1.0 nm to the red of the transition.

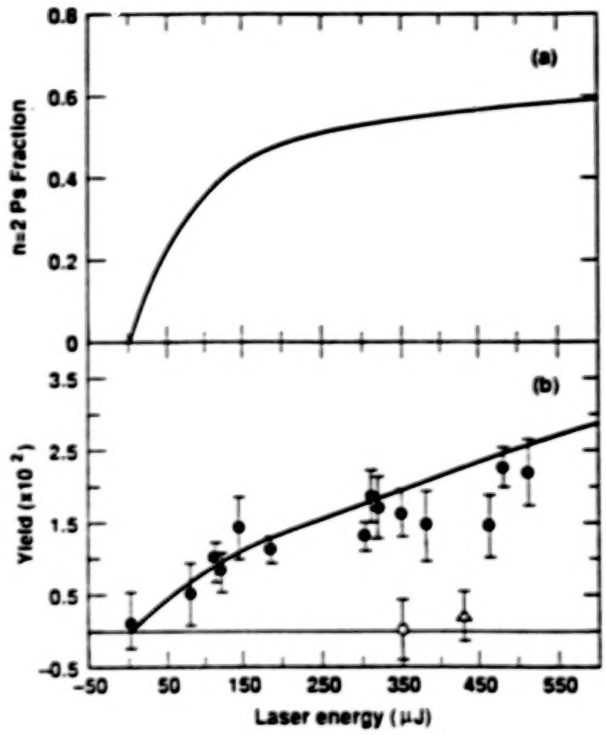

Figure 5. a) Results of the rate equation model showing the fraction of illuminated Ps in the n = 2 state. The calculation is performed for a 200 Gauss magnetic field and laser parameters typical of our measurement. b) Excess annihilations during laser illumination normalized to the total Ps production for several laser powers. The solid curve is the calculated excess annihilations. The open circle is taken with the laser detuned 1.0 nm and B = 200 G. The open triangle is taken with the laser on resonance and B = 50 G.

We also measured the excess annihilations for linearly and circularly polarized ultraviolet light. In both cases the direction of photon propagation was normal to the magnetic field. The linear polarization plane was parallel to the magnetic field. With circularly polarized light, the annihilation rate was found to be 0.42 ± 0.21 of that observed with the plane polarized light (~100 μJ per laser pulse) in agreement with the calculated ratio of 0.36 obtained in the rate equation model for those polarizations [9].

By comparing the excess annihilation data with our rate equation calculation, we see that we have reached optical saturation. The results of the calculation, normal-

ized to the data using a Monte Carlo simulation, are plotted as the solid line in Fig. 5b. The model accurately describes the laser energy-dependence of the transition rates. We view the numerical agreement between the calculated and measured excess annihilations as fortuitous due to the strong sensitivity of the Ps population in the laser beam on small variations in experimental parameters. The calculated fraction of the Ps in the n=2 state for illuminated Ps is plotted as a function of laser energy in figure 5a. This curve shows the characteristic shape of a saturation spectrum. There is a linear dependence on laser power at low energy per pulse, with an asymptotic approach to the limit of 0.67 at high laser energy.

Typical data for the excitation of higher n states are shown in figure 6. The data in figure 6a were taken with only ultraviolet light illuminating the Ps, leading to resonant excitation of n=2 state. The data in figure 6b were taken with both ultraviolet and red light illuminating the Ps. This data shows the effects of resonant excitation of both the n=2 and n=15 states. Here we find that excitation of the n=15 level reduces the ground state Ps population. This causes a larger deficit in the late time annihilations. The annihilation rate during the laser pulse is also reduced, implying that the n=2 state population is also depleted by excitation to higher n states.

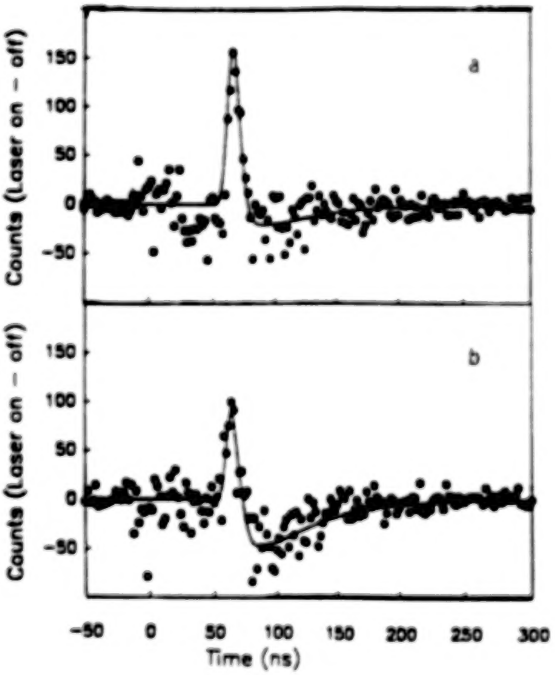

Figure 6. Difference spectra for a) ultraviolet illumination only and b) resonant two photon excitation to the n=15 state. Curves are calculated using a rate equation model with strong mixing in the n=15 state.

The decrease in excess annihilations during the laser pulse when the red laser is on resonance implies a decrease in the singlet n=2 state population. Ps remaining in long-lived, high n states after the laser turns off is a source of depletion of the Ps ground state population. However depletion of the n=2 state population will not occur unless the total number of de-excitations from the high n state is less than the number of excitations. Losses to photoionization are negligible. We calculate that the photoionization rate is less than 0.001 of the high n excitation rate at our laser energies. Large differences in the population of the n=2 and high n states can be obtained if there are corresponding differences in the number of sublevels.

We have numerically solved time-dependent rate equations describing this experiment for several possible cases. The dipole selection rule for the n=2 to high n transition limits the number of high n state sublevels to too low a value to explain the observed decrease in the n=2 state population during the laser pulse. Zeeman mixing will cause the high n singlet and triplet spin states to be statistically populated for our experimental parameters. Our calculations show that de-excitation from a statistically populated singlet high n state would result in an increase in annihilations during the laser pulse rather than the decrease we observe. However, including strong Stark mixing can break down the $\Delta l=+/-1$ dipole selection rule and allow population of all of the l sublevels of the high n state accessible with $\Delta m=0,+/-1$. Such mixing can occur due to static and motionally induced electric fields of ~40 V/cm found in the chamber.

The computed results of the rate equation model are shown in figure 6a and b, normalized to the level of annihilation enhancement seen in figure 6a. The calculations were performed using measured values for laser power and pulse characteristics. The curve in Figure 6b includes transitions from all populated n=2 sublevels, to all accessible l-sublevels of the n=15 state. These calculations reproduce the observed change in enhanced annihilations and even the change enhanced annihilation time profile seen in comparing on and off resonance spectra. Calculations containing many fewer sublevels

in n=15 state, which might result from weaker Stark mixing, cannot reproduce both the change in annihilations during the laser pulse and the decrease in the ground state population observed with the red light on resonance. Thus, we conclude that the high n states are completely mixed. Our calculated results also show that a significant fraction, ~0.3, of the n=2 state population is promoted to higher n states where it remains after the laser pulse has ended.

Shown in figure 7 are data for wavelengths on and off resonance between n=13 and n=19. Data were taken at more closely spaced wavelengths around the n=14 and 15 resonances in order to determine experimental centroid wavelengths and widths. A ratio, formed from counts in two time intervals as a function of wavelength, is shown here. The first interval is a narrow time window including the duration of the laser pulse and subsequent radiative decay from the n=2 level. The second interval extends from the end of the first interval until the data reached background values. The absolute value of the counts lost during the second interval were decided by the counts in the first interval to form the ratio. Thus, this ratio is the decrease in ground state Ps normalized to the singlet n=2 population and is insensitive to systematic differences in the geometry and target condition. Positronium lost to excess annihilations in the n=2 state alone results in a baseline value of 0.62 . Excitation of Ps into higher n states gives a larger ratio due to a larger depletion of the ground state Ps.

In the data in figure 7 we see a convincing demonstration to resonantly excite high n states from the n=2 population. There is a large increase in the yield at wavelengths resonant with excitation to the n=13, 14 and 15 levels. Calculated excitation profiles for the resonant peaks are also shown in figure 7. The peak wavelengths were calculated from the Balmer formula, and the widths of the curves included the 0.4 nm laser line width and the 0.4 nm Doppler broadening width for these transitions. The relative areas of the calculated peak shapes were determined using the rate equation model with the transition rates scaled by n^{-3}. The absolute normalization was set to the sum of the areas of the n=14 and 15 data. From these calculations we see that values of n greater than 15 are more difficult to excite and are not easily observed with the statistics now available in the experiment.

Values for the centroids and widths for the n=14 and n=15 peaks were calculated from the data in figure 7 after background subtraction. We obtained values of 744.049 +/- 0.035 nm and 741.993 +/- 0.040 nm for the n=14 and n=15 centroids, respectively, and 0.37 nm and 0.44 nm for the full widths at half maximum, respectively. The centroid values compare favorably with the reference values of 743.988 nm and 741.995 nm obtained by calculating the energy difference between the unshifted energy of the 2^3P_1 and the energy of the high-n state. Hyperfine splitting in the high-n state is negligible in this comparison, but spliting of the 2P levels adds .02 nm to the width of the excitation-line profile. The

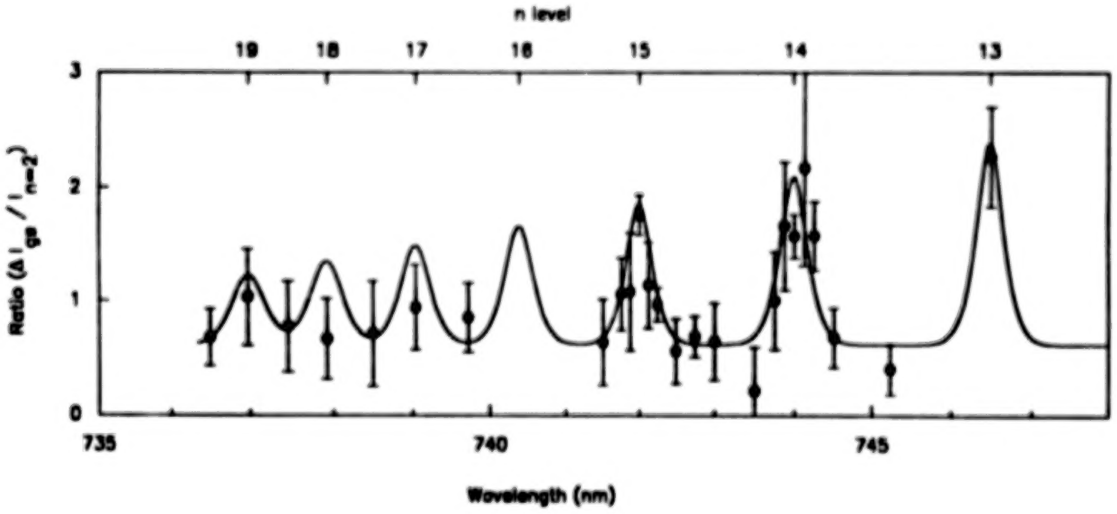

Figure 7. Ratio of loss in the ground state population normalized to the n=2 population. The solid line is the expected response calculated from known parameters of the experiment.

large measured widths for the n=14 and 15 excitation are consistent with the Doppler spread in the Ps and line profile of the two laser beams. The good reproduction of the energies and widths within the experimental errors demonstrates the potential to perform higher precision spectroscopy by using narrower laser line widths and lower velocity Ps.

These results represent a first step towards laser-cooling Ps. They show that transition rates, photon bandwidths and excitation of spectator transitions required to achieve and measure cooling are possible. As pointed out by Liang and Dermer [6], one must use a broadband laser to cool Ps since the lifetime is too short to sweep the laser frequency. The 0.07 nm bandwidth of our laser is ideally suited to cool the Ps but the pulse duration is currently too short. The agreement between calculation and experiment for excitation to the n=2 and higher n states indicates that sufficient Ps atoms survive to perform cooling experiments.

The observation of high n state excitations provides a useful diagnostic for the velocity of cooled Ps, and a basis for new spectroscopic investigations. Detecting the ionization products of excited Ps resulting from photon or static electric field ionization can be used to develop a higher efficiency detector for high n state Ps. With this detector we use narrow laser lines to tune over the velocity profile. This same system would form the bases for spectroscopic studies on the cooled Ps.

In summary, we have demonstrated optical saturation of the resonant transition of Ps from the ground to the first excited state. We have also observed the first resonant excitation of high n states of Ps using two resonantly excited transitions, from 1S to 2P and 2P to nL. The population of the excited states was deduced from observation of annihilation rates during and after the laser pulse. Magnetic mixing in the n=2 state increased the annihilation rate during the laser pulse, and loss of Ps in the ground state population reduced the annihilation rate after the laser pulse. Changes in the enhanced annihilation rate with laser power, photon polarization and magnetic field show that the n=2 state was in optical saturation. Magnetic and electric fields in the chamber mixed the high n states so that all l sublevels were populated in the high n state. Values for the line centroid and widths agreed with calculations. Qualitative reproduction of the n^3 scaling of the relative transition rates was also observed.

ACKNOWLEDGMENTS

We thank E. P. Liang, J. C. Weisheit, and P. O. Egan for helpful discussions.

This work was performed under the auspices of the U. S. Dept. of Energy by Lawrence Livermore National Laboratory under Contract No. W-7405-ENG-48.

REFERENCES

1. K. F. Canter, A. P. mills and S. Berko, Phys. Rev. Lett. 33 7 (1975).
2. S. L. Varghese, E. S. Ensberg, V. W. Hughes and I. Lindgren, Phys. Lett. 49A 415 (1974).
3. S. Chu, A. P. Mills, and J. L. Hall, Phys. Rev. Lett. 48 1689 (1984).
4. K. P. Ziock, C. D. Dermer, R. H. Howell, F. Magnotta and K. M. Jones, J. Phys. B, in press.
5. C. D. Dermer, R. H. Howell, K. M. Jones, E. P. Liang, F. Magnotta and K. P. Ziock, Positron Annihilation, p292, L Dorikens-Vanpraet, M. Dorikens and D. Segers, eds. World Scientific, Singapore (1989).
6. K. P. Ziock, R. H. Howell, F. Magnotta, R. A. Failor and K. M. Jones, to be published.
7. E. P. Liang and C. D. Dermer, Opt. Comm. 65 419; and C.D. Dermer in this volume (1988).
8. S. M. Curry, Phys. Rev. A 7 447.
9. M. L. Lewis and V. W. Hughes, 1973 Phys. Rev. A 8 625 (1973).
10. C. D. Dermer and J. C. Weisheit, Phys. Rev. A, in press.
11. M. Deutsch and E. Dulit, Phys. Rev. 84 601 (1951).
12. R. H. Howell, M. J. Fluss, I. J. Rosenburg, and P. Meyer, Nucl. Inst. Meth. in Phys. Res. B10/11 373 (1985).
13. A. P. Mills and L. Pfeiffer, Phys. Rev. B 32 53.
14. R. H. Howell, I. J. Rosenburg and M. J. Fluss, 1987 Appl. Phys. A 43 247 (1985).

STARK AND ZEEMAN EFFECTS ON LASER COOLING OF POSITRONIUM

Charles D. Dermer
Physics Department, L-297, Lawrence Livermore National Laboratory
Livermore, CA 94550

ABSTRACT

Theoretical work on laser cooling of Positronium (Ps), including effects of external magnetic and electric fields, is reviewed and extended.

INTRODUCTION

Laser cooling of Positronium (Ps) was proposed in Ref. [1]. Cold Ps would benefit precision spectroscopy, production of a Bose-Einstein condensate of Ps, and the development of an annihilation gamma-ray laser. It could also be important in forming antihydrogen through the reaction $\bar{p} + Ps \rightarrow \bar{H} + e^-$ [2].

Saturation of the 1s-2p transition is a necessary condition for producing cold Ps through the technique of laser cooling. Optical saturation of this transition was recently demonstrated through observations of enhanced annihilation radiation during resonant laser excitation [3]. The enhancement of annihilation radiation results from Zeeman mixing in n=2 states of Ps [4]. External fields could, however, counteract laser cooling by trapping and/or mixing Ps into other substates. Here, detailed numerical simulations of Ps laser cooling in one-dimension are used to obtain limits on the strength of external fields for which laser cooling of Ps can be achieved.

n=1 ↔ n=2 RADIATIVE TRANSITIONS IN POSITRONIUM

Fig. 1 shows an energy level diagram for the n=1 and n=2 levels of Ps. In the absence of external fields, the energy difference ΔE_{nl} between fine structure states ~ (α^2/n^3) Ryd ~ 200 GHz/n^3. Because of the presence of ΔE_{nl} in the denominator of Stark- and Zeeman-effect corrections to the Ps wave functions in first-order perturbation theory, the magnitude of the correction is greater for states with larger values of n. Hence magnetic mixing is appreciable in n=2 Ps when B ~ 100 Gauss, whereas it is important in n=1 Ps only when B >> 1 kGauss.

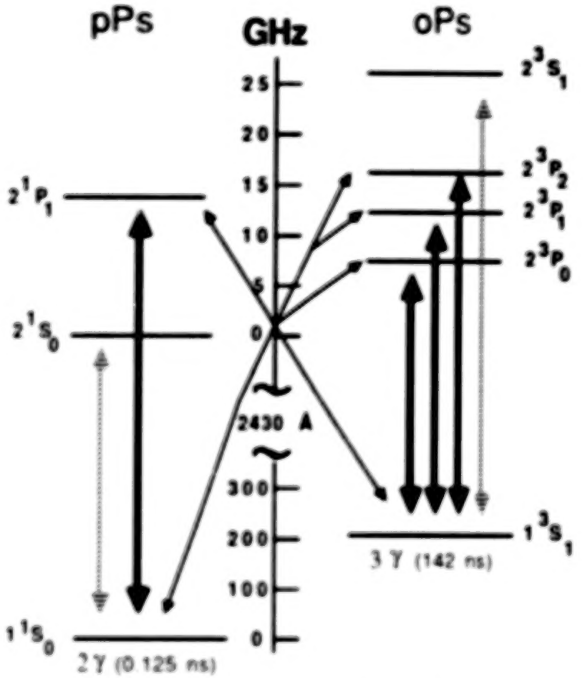

Fig. 1. Fine structure energy-level diagram of n=1 and n=2 positronium. Heavy solid lines show allowed electric dipole transitions; light solid lines and shaded lines show radiative transitions permitted in the presence of external magnetic and electric fields, respectively.

The heavy solid lines in Fig. 1 show allowed electric dipole transitions in the absence of external fields. Light solid lines show n=1↔n=2 transitions permitted in the presence of a magnetic field. A pathway between the 1^3S_1 and 1^1S_0 levels therefore exists via radiative transitions to and from the 2^1P and 2^3P levels when a magnetic field is present [4]. Because of the short annihilation lifetime of Ps in the 1^1S_0 state, an increase in the annihilation rate, depending on magnetic field strength, laser power and polarization, can be produced from resonant excitation of Ps. This signal was used to monitor optical saturation of the 1^3S-2^3P transition in Ps [3]. Also shown in Fig. 1 by the shaded lines are radiative transitions possible in the presence of an external electric field, in which case transitions between states with the same value of orbital angular momentum are possible.

LASER COOLING OF POSITRONIUM

Laser cooling of Ps to temperatures below 1 K is possible using a broadband laser negatively detuned to the 1^3S-2^3P transition [1]. For Ps, the minimum achievable temperature is determined by the photon recoil energy $R = \hbar^2/2m_{Ps}\lambda^2$, so that $T_{min} \sim R/k_B \approx 150$ mK for the $1s \leftrightarrow 2p$ transition. Laser cooling depends on spontaneous emission to rid the atom of one unit of photon momentum. The fastest cooling allowed by this technique thus corresponds to a recoil velocity $v_R = \hbar/m_{Ps}\lambda \equiv 1.5\times10^5$ cm s^{-1} per spontaneous lifetime $\tau_{1s\leftrightarrow2p} \equiv 3.2$ ns. Successful cooling of a substantial fraction of the Ps made at high temperatures must compete with the $t_{oPs} = 142$ ns annihilation lifetime of ortho-Positronium (oPs). Approximately 50 spontaneous emissions occur during the average lifetime of an oPs atom, implying that laser cooling will be successful if Ps are produced with characteristic temperatures no greater than ~ 700 K.

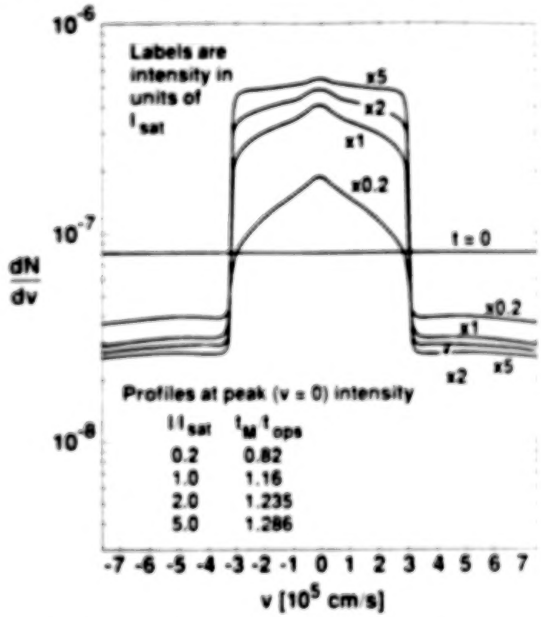

Fig. 2 (above). Positronium velocity distribution resulting from laser cooling by broadband laser light negatively detuned to the 1s→2p transition frequency of Ps. Distributions for different laser intensities are shown at the time of the maximum Ps population at zero velocity. Initial Ps velocity distribution is shown by the t=0 curve.

Fig. 3 (right). Time dependences of $N_{tot}(t)$, the total number of positronium atoms remaining at time t, and $N_c(t)$, the number of Ps with velocities within one recoil velocity ($v_R \equiv 1.5\times10^5$ cm s^{-1}) of zero velocity, for saturation laser intensity of the Ps 1s→2p transition.

A rate equation treatment of laser cooling of Ps was used to investigate the various processes in detail. Fig. 2 shows the oPs velocity distribution dN/dv as a function of laser intensity I in units of I_{sat}, the saturation laser intensity. (I_{sat} is here defined such that the induced rate is $\pi/4$ times the spontaneous rate; cf. Ref.[4]). A laser profile with uniform intensity redward of the $1s \leftrightarrow 2p$ transition frequency was used in this simulation, and the original oPs velocity distribution was assumed to be a one-dimensional Maxwellian at room temperature. The oPs velocity profiles are plotted when $dN(v=0)/dv$ reaches its maximum value, representing the point at which further cooling of the remaining warm oPs no longer compensates for losses due to annihilation. The peaks of the velocity profiles have roughly similar shapes irrespective of I/I_{sat}, corresponding to an effective temperature $T_{eff} \sim 0.6$ K. The amplitudes of the peak profiles approach an asymptotic value with increasing laser intensity; this again reflects the fact that only spontaneous emissions are effective in cooling.

The dependences on time t of the fraction $N_{tot}(t)$ of oPs that have not annihilated, and the fraction $N_c(t)$ of oPs with $-v_R \le v \le +v_R$, are plotted in Fig. 3 for $I = I_{sat}$. Because the oPs spend an appreciable amount of time in n=2 states with a long annihilation lifetime (≥ 0.1 ms), the average lifetime of an oPs atom is greater than t_{oPs} in the absence of fields. This is not necessarily the case when external fields are present, as we discuss in the next section.

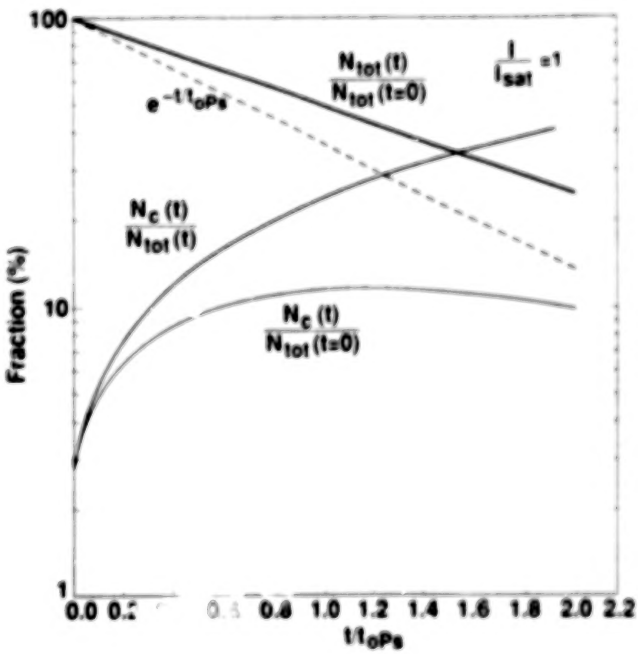

STARK AND ZEEMAN EFFECTS ON LASER COOLING OF POSITRONIUM

External magnetic and electric fields counteract laser cooling. Magnetic fields cause mixing into S=0 para-Positronium (pPs) states from which annihilation of Ps occurs on a time scale short compared to t_{oPs}. Electric fields permit Ps to make transitions to states whose long radiative lifetimes slow the cooling rate.

Fig. 4 shows the effects of a magnetic field on laser cooling of Ps. The rate equations describing cooling were supplemented with a loss term $\propto B^2/\delta E$, representing Zeeman mixing from oPs to pPs. The term δE is an average over the energy differences between the various Zeeman-mixed states in the n=2 level, and corresponds in this simulation to linearly polarized laser light with photon propagation vector $\mathbf{k} \perp \mathbf{B}$.

Define the cooling efficiency as the ratio of the number of Ps with velocities in the range $-v_R \leq v \leq +v_R$ at time $t = t_{oPs}$, to the number of Ps in this same velocity interval at t=0. Both the cooling efficiency and the fraction of total Ps remaining at $t = t_{oPs}$ decrease rapidly with increasing magnetic field when B > 100-200 G, for $I \approx I_{sat}$ [Fig. 4(a)]. If B = 200 G, the cooling efficiency is greatest when $I \cong I_{sat}$, as shown in Fig. 2(b). The cooling efficiency decreases at larger values of I because faster transition rates lead to increased Zeeman mixing and loss of oPs from the system which is not compensated for by the marginally increased cooling rate.

An external electric field interferes with cooling by providing a pathway between the 1^3S_1 and the 2^3S_1 states which, having a slower radiative lifetime, therefore slows cooling. The magnitude $\mathcal{E}$ of the electric field above which this effect is important can be estimated by recalling that ~ 50 absorptions and spontaneous emissions are required for cooling. If each radiative cycle is accompanied by a loss to the 2^3S_1 state of magnitude η^2, then the electric field will affect cooling when $(1-\eta^2)^{50} \approx 1/2$. In the perturbation limit $\eta \approx 6ea_o\mathcal{E}_{\|} / \delta E_S$ [4], where $\delta E_S \approx 12$ GHz (Fig. 1). Thus when the parallel electric field $\mathcal{E}_{\|} \gtrsim$ 200 V/cm, laser cooling of Ps is impeded. Detailed numerical simulations, including spontaneous emission from 2^3S_1 to 1^3S_1, are required to assess the Stark effect on laser cooling of Ps in detail.

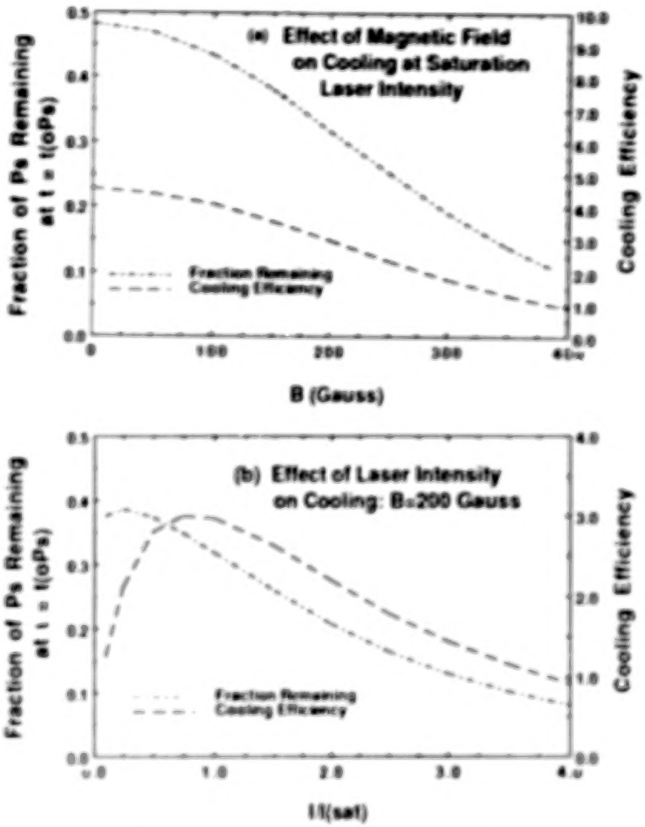

Fig. 4. Effects of an external magnetic field on laser cooling of positronium. The cooling efficiency and the fraction of Ps remaining after one oPs lifetime are shown as a function of the magnetic field at saturation laser intensity in Fig. 4(a), and as a function the laser intensity for a 200 Gauss magnetic field in Fig. 4(b).

In summary, laser cooling of Positronium can be achieved if the strengths of external magnetic and electric fields are < 100-200 Gauss and $\lesssim$ 200 V/cm, respectively.

I thank R.H. Howell, E. P. Liang, F. Magnotta, J.C. Weisheit, and K.P. Ziock for continued interest in this work, which was performed under the auspices of the U.S. Department of Energy by the Lawrence Livermore National Laboratory under contract number W-7405-ENG-48.

[1] Liang, E.P., and C.D. Dermer, *Optics Comm.*, **65**, 419 (1988).
[2] Humberston, J.W., M. Charlton, F.M. Jacobsen, and B.I. Deutch, *J. Phys. B*, **20**, L25 (1987).
[3] Ziock, K.P., C.D. Dermer, R.H. Howell, F. Magnotta, and K. Jones, *J. Phys. B*, submitted (1989).
[4] Dermer, C.D., and J.C. Weisheit, *Phys. Rev. A*, submitted (1989).

Decay Rate and Other Properties of the Positronium Negative Ion

A. P. Mills, Jr., P. G. Friedman, and D. M. Zuckerman

AT&T Bell Laboratories
Murray Hill, New Jersey 07974

ABSTRACT

A new method for detecting the positronium minus ion is described, and the possibility of a long positronium mean free path in a solid is discussed.

1. INTRODUCTION

I am going to talk about the decay rate and other properties of the positronium minus ion. This is a workshop, so I don't have to apologize for the fact that you're catching our experiment in mid air: we don't have an answer yet, unfortunately, for Y. K. Ho's table. The reason I put "other properties" into the title is that in the process of trying to do the experiment we found out a little bit more than what we wanted to know about how positrons and positronium interact with a foil. I will be asking my theoretician friends to help out in figuring what a positronium atom does going through a foil. How does it break up? By way of introduction, I'll remind you about John Wheeler's famous paper, in which he invented the polyelectron at the same time as a couple of other people invented positronium; I'll describe the slow positron source that is used to do these experiments with positrons; I'll show you the ancient method for the production of positronium minus by beam foil and the old lifetime measurement; I'll tell you briefly about our new effort to detect positronium minus by double charge exchange; Finally I'll be asking what's wrong. This will be the meat of the talk where you can help me out. I will show you our one pitiful lifetime curve which unfortunately needs to be extrapolated to infinite energy to get the answer: we're still working on it. At the end I'll say just a couple of words about what's next.

2. POLYELECTRONS

Lest we forget the inventor of the polyelectron, John Wheeler, I will remind you that his 1946 article asked the question, "Can you get clusters of various of various sizes of electrons?"[1] Wheeler predicted that positronium and the positronium minus ion would be bound, but he was unable to get binding for positronium molecules with his simple wave function. You have heard from Y. K. Ho that lots of work has been done since that time.[2] In particular, the lifetime of Ps^- has been calculated and would be interesting to measure accurately because of the current interest in the the triplet lifetime being measured by the Michigan group for the last 10 or 15 years.[3] There is a descrepancy, and we do not know whether the theory is really going to be right. As an additional test it would be interesting to measure the singlet lifetime, but its eighth of a nanosecond lifetime makes it pretty hard to do. An alternate would be to measure the lifetime of positronium minus ions which contains in it a large factor that is due to the singlet lifetime. We would need to achieve parts in ten to the three or four accuracy in order to make a useful contribution towards the solution of the controversy. Unfortunately, I can only tell you about why we haven't gotten that accuracy yet.

3. EXPERIMENT

The whole experiment starts with the usual slow positron beam,[4] where slow

positrons are made by moderating them in a layer of some material, either an insulator or a metal. For this particular experiment we're using a solid neon moderator.[5] We obtain a beam of roughly a quarter of a million positrons a second using a 5 mCi source of Na^{22}. Positronium minus ions can be made by putting relatively slow positrons through a thin foil.[6] In the first experiment the ions were accelerated with a grid into a field free region where they annihilated, giving Doppler shifted photons that were counted by a germanium detector. In the spectrum shown in Fig 1 we see a line from positrons that annihilated somewhere in the foil, and a Doppler shifted line that moves when you apply more electric field to shift the positronium minus velocity in the direction of the detector.

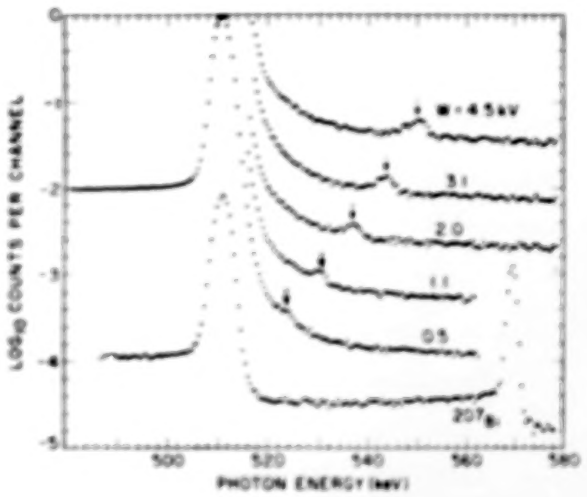

Fig. 1 Annihilation γ-ray energy spectra obtained for five different Ps^- acceleration voltages W. [From Ref 6]

Especially relevant to our problems today is Fig 2 which shows (large error bars) the yield of positronium minus as a function of the energy with which the positrons are implanted into the foil. The small dots are the the transmission of the positrons through the foil as a function of energy. My interpretation at the time was that you get the most positronium minus when you have the greatest density of straggling particles near the surface of the foil. The six or seven measured data points agree with what you would expect: the derivative of the stopping curve does have a peak roughly coinciding with the maximum yield of Ps^-. It looks like the yield has a single broad peak, but more precise data suggest that things are more complicated.

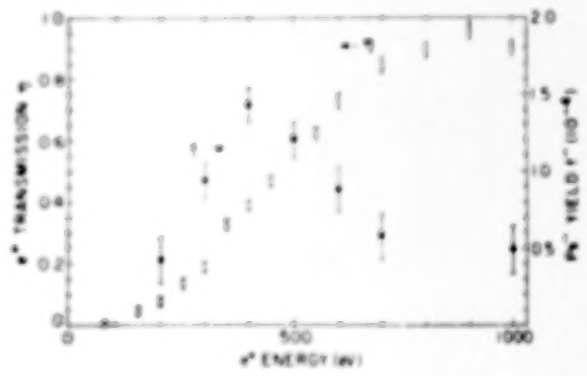

Fig. 2 Positron transmission probability η and Ps^- formatioin fraction f^- plotted vs positron incident energy E. To account for grid losses, F^- should be multiplied by 2.0±0.2. [From Ref 6]

The lifetime was measured some years ago by carefully determining the amplitude of the Doppler shifted peak again with the germanium detector.[7] As you change the distance between the formation foil and the acceleration foil, the proper time that the positronium minus spends is proportional to the distance. By plotting amplitude versus calculated time, you can get the lifetime, as shown in Fig 3. Unfortunately, the positronium minus is coming out of the foil with velocities comparable to atomic velocities, so you have to extrapolate to infinite acceleration in order to get the right answer. The extrapolation to infinite energy is right on top of Y. K. Ho's prediction.[8]

To do a better experiment, we would like to get rid of the germanium detector, which is inefficient, and we have to go to higher voltages to reduce the size of the extrapolation needed. There has to be an improved way of moving the foil because, in the previous experiment, the foil was on the end of a manipulator about one foot away, and I had to measure the distance with a traveling microscope. The present attempt has a much better moving mechanism: three synchronous linear motion vacuum feedthroughs define the foil position to 10^{-2} mm precision.

Our new effort uses a tandem acceleration method depicted in Fig 4. A positronium formation foil is bombarded by a quarter of a million positrons a second. Any positronium minus formed is accelerated by what we call "the analysis grid", which has a potential W across it for measuring the lifetime. As before, the distance d between the analysis grid and the formation foil is variable. By varying d while measuring the count rate, you determine the lifetime. Following the analysis grid is another electrode that accelerates the positronium minus to some large voltage on the order of fifty kilovolts. At this point, there is a thick carbon film that is supposed to strip the positronium minus and turn it back into two electrons and a positron. On the other side is a grounded electrode that repels the electrons, but accelerates the positrons. The positrons emerge with four-thirds times the acceleration potential on the stripping foil, which would be about 67 kilovolts if the stripping potential is 50 kV. We thus have a definite Ps^- signature of rather high energy positrons which cannot be produced any other way except by having taken a torturous route of making positronium minus and getting stripped. About two and a half meters away, to get rid of gamma rays, we have a charged particle detector (a silicon detector) which detects the energy spectrum of the positrons to distinguish them from any background that might be there from ions.

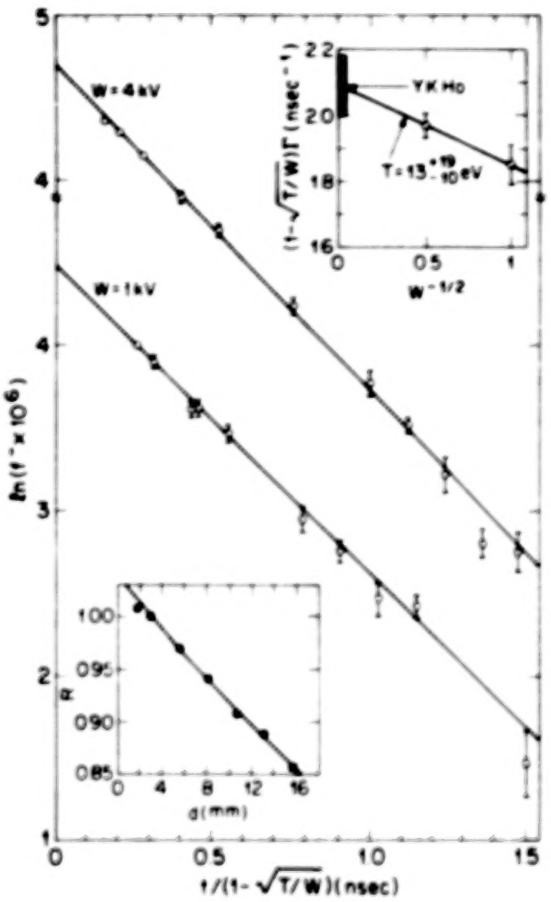

Fig. 3 Log of the relative amount of Ps^- surviving for a time t corrected for the initial Ps^- kinetic energy T. The inset shows the extrapolation of the decay rate to infinite acceleration potential W. [From Ref 7]

An ion shield, one tenth mil of mylar, covers the detector. Unfortunately, there were so many ions that we had to use a plastic scintillator in coincidence to cut the background rate.

Fig 5 shows spectra taken with the silicon detector at three different acceleration voltages. The potential applied to the stripping foil is 20, 34, or 45 kilovolts. The peak due to the positrons that make it through the whole apparatus is evident, and

there is a sloping background due to ions which looks like it's not important, at least at the higher acceleration potentials. There is a plateau below the peak, and I don't know what that could possibly be, since the fraction of particles that scatter [9] is supposed to be only about 15%. If you spread that fraction over a large energy range, it should not give a 10% amplitude. That is problem number one; but at least we are producing tandem generated positrons.

Using our double charge exchange Ps^- signal, we have remeasured the yield of positrons as a function of energy in Fig 6. As in Fig 2, we get a blob as a function of energy, peaking at slightly higher energy because the film is a little thicker. The film is nominally 15 angstroms thick, a cloudy carbon film on top of a glass slide that is slid off onto water, to be picked up with a grid. The thicknesses are nominal, since there are obviously layers of grease and water. Notice in the new data at the low energies, there seems to be a plateau and a real threshold at a ridiculously low energy of 25 volts. I have no idea what this structure means. If the film is really only 15 angstroms thick, I suppose that is an average thickness, and once in a while there could be a flake that's only one crystal layer thick that might be 5 angstroms. However, I would think that there would be a series of plateaus for different thicknesses and that they shouldn't occur down at 50 volts. If anybody has a suggestion, I would be happy to hear it. It will go right into the book if you have anything to say.

Another mystery is why is the yield so small, about five times smaller than we saw in 1981 and 1983. We have mapped out the count rate as the detector is moved around. As far as I can tell, all the fast positrons seem to be hitting the detector. The grids that the foil is on and the acceleration grids have 90% transmission. Putting in all the grid correction factors does not account for the apparent losses. The grid corrections are just about the same as they were in 1981.

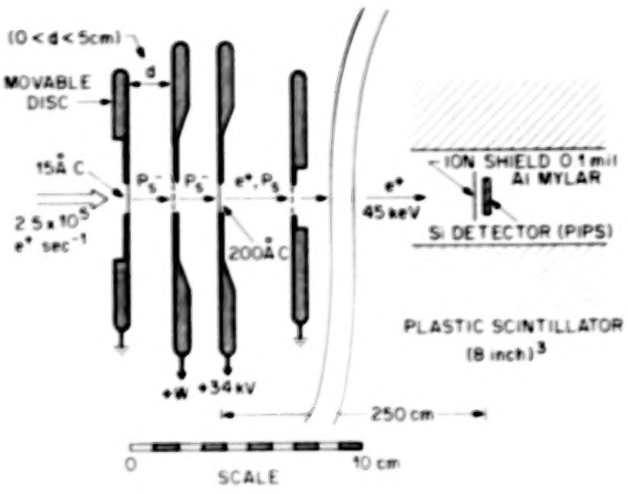

Fig. 4 Tandem acceleration method of detecting Ps^-.

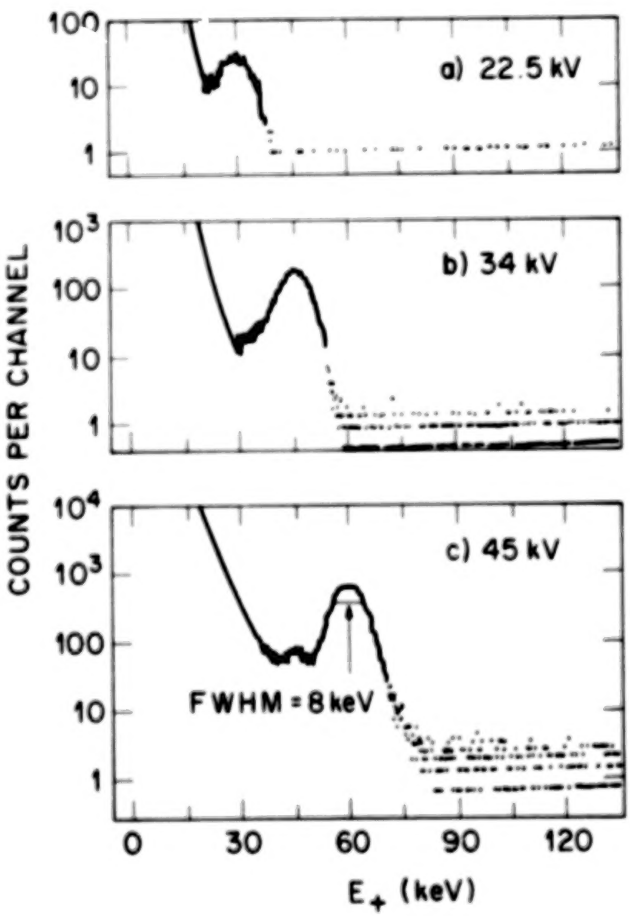

Fig. 5 Energy spectra of the fast positrons detected by the surface barrier detector.

Table I shows the yield of positronium minus measured at 20, 34, and 45 kilovolts. The coincidence rate is corrected for decay loss in various places where the positronium minus is being accelerated. There's a negligible loss in the mylar foil.[10] The positron beam rate is what you divide by in order to get the total fractional yield of positronium minus. There's a constant grid transmission coincidence efficiency, and a little bit of back-scatter loss. The net result is a positronium minus yield of about 7×10^{-5} independent of the energy. That is a surprise to me because the only way that I can think of to make the yield smaller than the $2-3\times10^{-4}$ found previously is to have the stripping foil be less efficient.

4. *DISCUSSION*

Now we come to the central point of the talk where I ask you what happens to positronium and positronium minus when it gets stripped. There are several convenient theories. The simplest theory, which turns out to be the same as Surko's Theory that he told me about at breakfast, is that you simply use multiple scattering calculations and an independent particle approximation. Let's just talk about positronium going through the foil. In the time scale over which the particles are in the solid the positron and an electron don't orbit at all. They just go straight through the solid without moving relative to each other. In this approximation, you would say each particle gets an independent kick from scattering off the potential which, in this case, would be a frozen potential of the solid because the electrons don't have time to move either. It's very easy to calculate the perpendicular kick that each particle gets: it will be the perpendicular electric field integrated times dt. The amplitude for making a transition turns out to be the perpendicular momentum kick times the dipole matrix element. Summing all the dipole moments that lead to the continuum gives a transition probability that is perpendicular kick squared over 2m

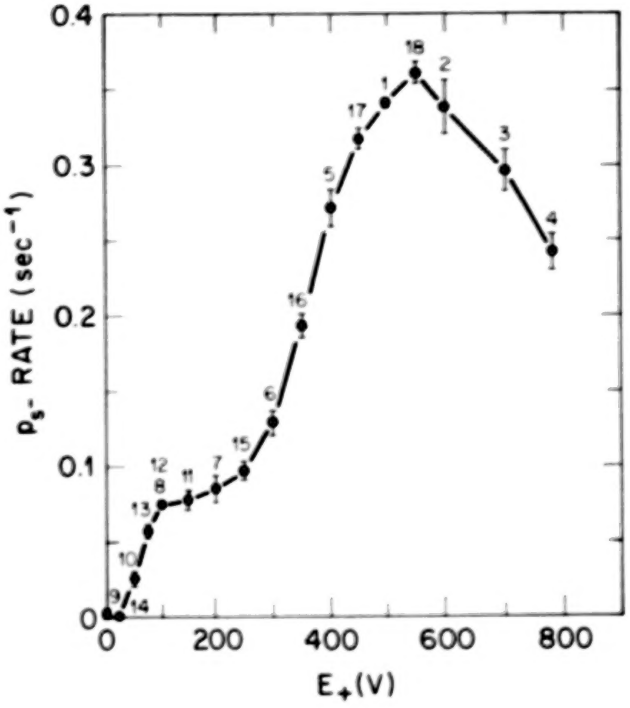

Fig. 6 Yield of Ps^- versus positron energy uncorrected for transverse beam motion.

Table I

Accel. Pot. [keV]	22.5	33.75	45
coinc. rate [sec^{-1}]	0.225(6)	0.341(3)	0.385(2)
decay loss $e^{-\Delta t/\tau}$	0.113	0.135	0.140
loss in mylar [%]	14[a]	6.5[a]	3.5[a]
beam rate [e^+ sec^{-1}]		2.5×10^5	
grid transmission		0.45 ± 0.1	
coinc. efficiency		0.4 ± 0.1	
backscatter loss [%] from Si detector		15[b]	
Γ^- $[10^{-5}]$	6.1 ± 2	7.1 ± 2	7.5 ± 2

a) R. D. Evans, *The Atomic Nucleus*

b) V. E. Cosslett & R. N. Thomas, Brit. J. Appl. Phys. *16*, 779 (1965)

divided by an energy, a couple of Rydbergs, times a factor 0.849 given by Bethe and Salpeter.[11] The multiple scattering tables[12] tell us that the perpendicular momentum picked up is 14MeV/c over the velocity times the square root of the distance travelled through the foil in units of radiation lengths. The result is 2Å times the ratio of the positronium energy to 14 kilovolts. The higher the energy, the farther the positronium goes before breaking up, which is reasonable. But 2Å is a very short distance! We're talking about roughly 14 kilovolt positronium and this formula says just the slightest amount of carbon foil should be enough to break it up. If that were the case, then I have no explanation for our low yield.

Surko's approximation, an equivalent theory, is to find the Fourier components of the frozen potential of the solid, and calculate the "photo emission" probability. In the dipole approximation, Surko's theory is the same as the multiple scattering theory. Including higher order non-dipole transitions will make the length even shorter. Maybe there's something wrong with these theories. Phil Platzman would say that the scattering is all in the forward direction, and the impact parameters are therefore large. The first order Born term is going to vanish and it is the gradient of the electric field that acts to break up the positronium. It appears that the break up probability is related to the energy loss in going through the foil. I am not sure if you can actually make a calculation that you can look up in the handbook yet, but there is a recent [2nd order?] Born approximation calculation[13] for positronium scattering. He finds that the mean free path for positronium breakup in solid carbon is 65 angstroms times the ratio of the energy to 14 kilovolts. Now that's more like it except that our carbon foil is 200 angstroms thick. Just as a footnote, another theory[14] claims that as soon as the positronium has gone a few mean free paths, the residual positronium will have an enormous super-penetrability which goes like

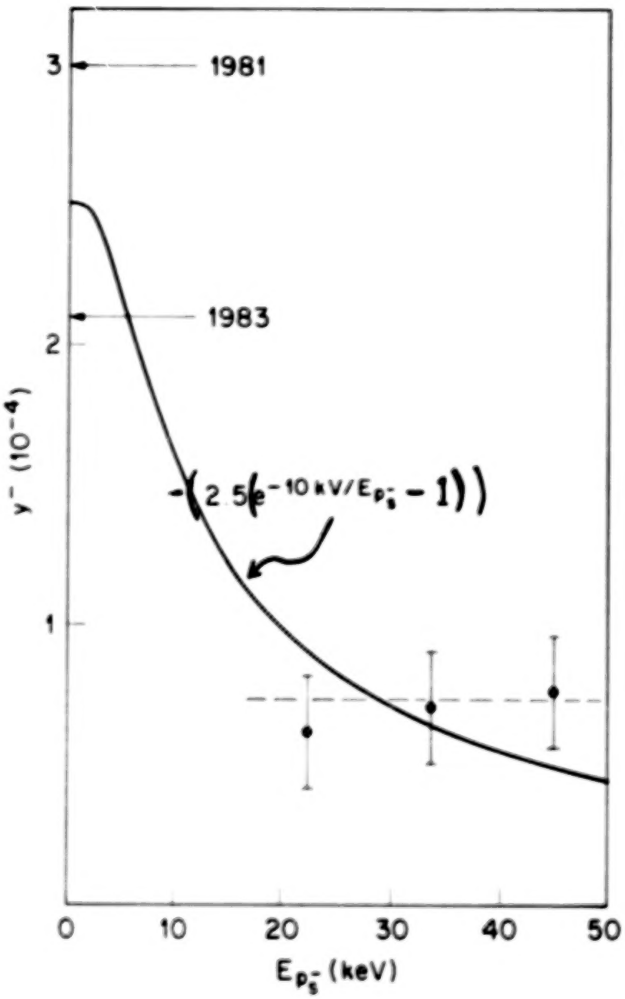

Fig. 7 Ps^- signal vs stripping voltage.

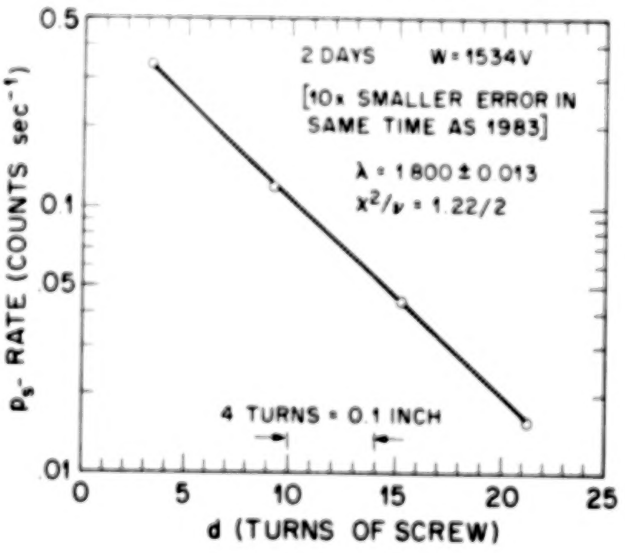

Fig. 8 Typical lifetime curve.

one over the length instead of exponentially!

Now I will show you the only piece of information we have. I already told you what it was, but will plot it now in Fig 7. If we are seeing an effect due to positronium resistance to breakup, then there ought to be more breakup at lower energies, so the yield ought to go up at lower energies. From Fig 7 it is evident that the yield is more consistent with constant rather than going like one over the energy. If we want the yield to go up to the 1981 and 1983 measurements, we can try to fit the measurements with an exponential dependence on a mean free path that goes like one over the energy. An eyeball fit implies that the mean free path is about 500Å, and that the ionization cross section for positronium is really quite small. Unfortunately, that's as far as we've gotten. I'll be happy to hear anybody's opinion. But since we're talking about the Born approximation and that is all anybody can do, maybe nobody has anything to say, although Jack Stratton[15] talked about doing a calculation where the positronium was actually one of the particles.

Fig 8 shows a representative lifetime curve; the data points are nearly obscured by the fitted line. The fitted decay rate is 1.80±0.01 per nanosecond, roughly half a percent statistical accuracy in two days. We get ten times smaller error in the same time as in 1983 even though the positronium minus yield seems to be down by a factor of five.

As for "what's next," there are lots of things you can do. Marv Leventhal and I are maybe thinking about accelerating a positronium minus beam to rather high energies, and stripping it with a laser to make a fast positronium beam with which to do several interesting experiments.[16] But if we're having a stripping problem for measuring the lifetime then we'll actually be benefiting in this next experiment because we won't need the ionizing laser. At least there may be a silver lining to the present cloud.

5. *QUESTIONS*

Peter Schultz: Isn't the factor of five yield loss maybe due to the formation foil having a different density? (My name is Karl Canter!)

Mills: The sample foil was prepared in about the same way as before.

Alex Weiss: Have you measured the Ps^- yield in the same way as before?

Mills: That is a good suggestion and we are setting up to do that.

Alex Weiss: Wasn't it Bob Wilson who made the carbon films?

Mills: Wilson was making films at the time, but the one I used may have been from a commercial supplier.

Lester Hulett: Can one use a neon moderator as a thin film transmission remoderator?

Mills: It might work, but you must take into consideration the large energy spread of a neon remoderator. It would also be hard to make a thin film of neon because the radiation baffles would be tricky to construct.

Mike Charlton: Do the positrons lose energy on the way out of the stripper foil?

Mills: Yes, maybe about 10 eV; the film is only 200Å thick. I'm only guessing 10 eV, but we use a tenth mil mylar film to reject ions, and the positrons lose only a few keV.

Arthur Rich: Are these the same foils as used previously?

Mills: They are simliarly prepared by evaporating carbon onto glass slides. The present supplier, Arizona Carbon Foil Company, was not used previously.

Mohamed Abdel-Raouf: Do you also have Ps^+ ions in your apparatus?

Mills: Its not too likely - we mostly have only one positron at a time presently.

Y. K. Ho: You showed a slide with a laser interacting with the Ps^- beam; can you measure the photoionization cross section and the electron affinity?

Mills: Yes, Marv Leventhal and I are working on it, and Lewis Rothberg has given us a laser. We'll have the answer for you in ten years.

Y. K. Ho: So you can measure the binding energy of Ps^-?

Mills: Maybe, but its pretty hard to find the binding energy from the photoionization threshold because the cross section vanishes at threshold.

Marv Leventhal: We can find the binding energy quite accurately from the location of the Feshbach resonances.

Alex Weiss: What are the wigglers that you showed? [See Fig 23 of Ref 16]

Mills: The wigglers are to excite the triplet-singlet hyperfine resonance in a fast monoenergetic positronium beam. By moving two identical wigglers one can obtain Ramsey fringes in the triplet positronium abundance, and so measure the hyperfine interval accurately.

Richard Drachman: Is there a preliminary lifetime result from the new data?

Mills: Unfortunately, no.

Alex Weiss: Have you thought about making a tuneable gamma-ray source?

Mills: Not very hard. The gamma rays are emitted isotropically in the center of mass, so its not like having a laser. If you had a very intense relativistic beam of Ps^-, the photons would be foreward directed, and it would be a good idea.

6. *POSTSCRIPT*

In a subsequent experiment using a Ge detector in a geometry similar to that of Ref 7, we found that the Ps^- yield of the 0.3 μgcm^{-2} foil (15 Å thick) is in fact about an order of magnitude less than a 0.6 μgcm^{-2} foil, and the yield of the latter is in agreement with the measurements of 1981 and 1983. The stripping foil was observed to be damaged over a significant portion of its area. We conclude that

1) very thin carbon films are perhaps multiply connected like lace;

2) more care is required to prevent high voltage damage to the stripper foil;

and 3) there is no evidence to suggest that energetic positronium has a particularly long mean free path.

REFERENCES

[1] J. A. Wheeler, *Annals of The New York Academy of Sciences* **XLVIII,** 219 (1946).

[2] Y. K. Ho,"Positronium Ions and Molecules", contribution to this volume. See also M. A. Abdel-Raouf, *Fortschr. Phys.* **36,** 521 (1988).

[3] D. W. Gidley, P. W. Zitzewitz, K. A. Marko, and A. Rich, *Phys. Rev. Lett.* **37,** 729 (1976); C. I. Westbrook, D. W. Gidley, R. S. Conti, and A. Rich, *Phys. Rev. Lett.* **58,** 1328 (1987).

[4] A. P. Mills, Jr., in *Positron Solid State Physics*, edited by W. Brandt and A. Dupasquier (North-Holland, Amsterdam, 1983) p. 432; P. J. Schultz and K. G. Lynn, *Rev. Mod. Phys.* **60,** 701 (1988).

[5] A. P. Mills, Jr. and E. M. Gullikson, *Appl. Phys. Lett.* **49,** 1121 (1986).

[6] A. P. Mills, Jr., *Phys. Rev. Lett.* **46,** 717 (1981).

[7] A. P. Mills, Jr., *Phys. Rev. Lett.* **50,** 671 (1983).

[8] Y. K. Ho, *J. Phys. B: At. Mol. Phys.* **16,** 1503 (1983).

[9] V. E. Cosslett and R. N. Thomas, *Brit. J. Appl. Phys.* **16,** 779 (1965).

[10] R. D. Evans, *The Atomic Nucleus*, (McGraw-Hill, New York, 1955) chap. 21.

[11] H. A. Bethe and E. E. Salpeter, *Quantum Mechanics of One- and Two-Electron Atoms* (Springer-Verlag, Berlin, 1957), p. 264.

[12] V. L. Highland, *Nucl. Instrum. Meth.* **161,** 171 (1979); **128,** 497 (1975); Particle Data Group, C. G. Wohl, et al., *Rev. Mod. Phys.* **56,** No. 2, Part II, pp. S51-S53.

[13] S. Mrówczyński, *Phys. Rev. A* **33,** 1549 (1986); *Phys. Rev. D* **36,** 1520,1529 (1987).

[14] L. L. Nemenov *Yad. Fiz.* **34,** 1306 (1981); V. L. Lyuboshits and M. I. Podgoretsky, *ZETF*, **81,** 1556 (1977).

[15] Jack Stratton, "Positronium Formation in e^+ - H^- Collisions", contribution to this volume.

[16] A. P. Mills, Jr., *Hyperfine Interactions* **44,** 107 (1988).

ANTIHYDROGEN FORMATION IN COLLISIONS OF POSITRONIUM WITH ANTIPROTONS

J.W. Humberston
Department of Physics and Astronomy
University College London, Gower Street, London WC1E 6BT, U.K.

INTRODUCTION

Antihydrogen, consisting of a positron orbiting around an antiproton, is the simplest few body system consisting entirely of antimatter and as such is of considerable importance in providing additional tests of the validity of charge conjugation invariance. In addition, the nature of the gravitational interaction between matter and antimatter might more readily be investigated for an electrically neutral system than one which is charged.

Before such studies can be undertaken the antihydrogen must, of course, be produced by attachment of a positron to an antiproton. Unfortunately, both constituents can only be produced in very small quantities and the viability of a particular method of antihydrogen production therefore depends critically on the efficiency of the attachment process.

Several production mechanisms have been proposed, the two most favoured of which are radiative capture (spontaneous or stimulated)

$$e^+ + \bar{p} \rightarrow \overline{H} + \gamma, \qquad (1)$$

$$e^+ + \bar{p} + n\gamma \rightarrow \overline{H} + \gamma + n\gamma, \qquad (2)$$

and charge exchange in positronium-antiproton collisions

$$Ps + \bar{p} \rightarrow \overline{H} + e^-. \qquad (3)$$

Both methods are being actively investigated.[1-3]

The cross section for radiative capture is very much less than that for charge exchange, so that it might be thought that the latter process is greatly to be preferred. However, in the proposed experiment using the radiative capture process the positrons will be confined in a storage ring (as also will be the antiprotons in both methods) and, therefore, those positrons which do not undergo capture by antiprotons on the first occasion will be recycled until capture occurs. In this way nearly all the antiprotons can be converted into antihydrogen.

The charge exchange process (equation (3)) is a single pass method because positronium is neutral, but the somewhat simpler nature of the proposed apparatus (see figure 1) and the much larger antihydrogen formation cross section are advantages which may, nevertheless, make this an effective method of production also. We shall, therefore, now consider various calculations of the cross section for the charge exchange process.

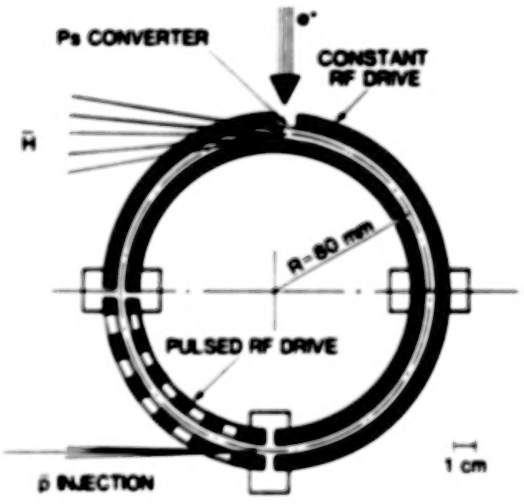

Figure 1. Proposed experimental arrangement for the formation of antihydrogen[3].

CALCULATIONS OF THE CHARGE EXCHANGE CROSS-SECTION

Until very recently the prospect of forming antihydrogen in positronium-antiproton collisions seemed so remote that no calculations of the cross-section had been considered. However, the required cross-section is rather simply related by charge conjugation and time reversal invariance to the cross-section for positronium formation in positron-hydrogen collisions, a process which has received extensive theoretical attention for several years.[4-6]

Starting with the process of interest

$$Ps + \bar{p} \rightarrow \overline{H} + e^- \qquad (\text{cross-section } \sigma_{\overline{H}}), \qquad (4)$$

the charge conjugate system is

$$Ps + p \rightarrow H + e^+ \qquad (\text{cross-section } \sigma_H), \qquad (5)$$

and charge conjugation invariance requires $\sigma_H = \sigma_{\overline{H}}$. The time reversed process is then

$$H + e^+ \rightarrow Ps + p \qquad (\text{cross-section } \sigma_{Ps}). \qquad (6)$$

Time reversal invariance implies the symmetry of the S-matrix which provides the following connection between the cross-sections $\sigma_{\overline{H}}$ and σ_{P_s}. Consider a positron colliding with a hydrogen atom in a state with energy and orbital angular momentum quantum numbers n_1 and ℓ_1 respectively, to produce positronium with corresponding quantum numbers n_2 and ℓ_2. If the cross-section for this process is $\sigma_{P_s}(n_2,\ell_2;n_1,\ell_1)$ then the cross-section for the time reversed process is $\sigma_{\overline{H}}(n_1,\ell_1;n_2,\ell_2)$, and

$$\sigma_{\overline{H}}(n_1,\ell_1;n_2,\ell_2) = \sigma_H(n_1,\ell_1;n_2,\ell_2) \tag{7}$$

$$= \frac{k^2}{\kappa^2}\frac{(2\ell_1+1)}{(2\ell_2+1)}\sigma_{P_s}(n_2,\ell_2;n_1,\ell_1), \tag{8}$$

where k and κ are the wave numbers of the positron and positronium respectively. They are related by energy conservation such that (in atomic units)

$$E_{H+e^+} = E_{P_s+p} = \frac{k^2}{2} - \frac{1}{n_1^2} = \frac{\kappa^2}{4} - \frac{1}{2n_2^2}. \tag{9}$$

If the initial positronium and residual antihydrogen are both in their ground states

$$\sigma_{\overline{H}} = \sigma_H = \frac{k^2}{\kappa^2}\sigma_{P_s}, \tag{10}$$

where

$$k^2 - 1 = \frac{1}{2}\kappa^2 - \frac{1}{2}. \tag{11}$$

This simple rescaling formula may be applied to the various positronium formation cross sections already calculated.

As we shall see, the peak in $\sigma_{\overline{H}}$ occurs at low kinetic energies of the positronium relative to the antiproton, corresponding to positronium formation in, and just above, the Ore gap (6.8 - 10.2 eV for hydrogen). In the Ore gap, where the only two open channels are elastic scattering and positronium formation, the most accurate results are probably those of Humberston[4], and Brown and Humberston[5]. They used a two channel version of the Kohn variational method of the form

$$\begin{bmatrix} K_{11} & K_{12} \\ K_{21} & K_{22} \end{bmatrix} = \begin{bmatrix} K_{11}^t & K_{12}^t \\ K_{21}^t & K_{22}^t \end{bmatrix} - \begin{bmatrix} (\Psi_1,\mathcal{L}\Psi_1) & (\Psi_1,\mathcal{L}\Psi_2) \\ (\Psi_2,\mathcal{L}\Psi_1) & (\Psi_2,\mathcal{L}\Psi_2) \end{bmatrix} \tag{12}$$

where $\mathcal{L} = 2(H-E)$.

The two components of the trial wave function, Ψ_1 and Ψ_2, represent positron elastic scattering plus positronium formation and positronium elastic scattering plus hydrogen formation respectively. Each component contains many short range correlation terms with associated variational parameters to allow adequately for the strong electron-positron correlations. Investigations of the variations of the values of the K-matrix elements with respect to systematic improvements in the trial functions suggest that the most accurate results obtained in this manner have converged to within a few per cent of the exact values.

The partial wave cross-section for positronium formation is then (in units of πa_0^2)

$$\sigma_{P_s} = \frac{4(2\ell+1)}{k^2}\left|\left(\frac{K}{1-iK}\right)_{12}\right|^2 \tag{13}$$

Results were obtained for s-, p- and d-wave scattering and compared with results from other simpler methods of calculation. The accurate variational values are several orders of magnitude smaller than the results of the Born approximation for s-wave scattering but only a factor of three smaller for p-wave scattering, and for the d-wave the difference between the two methods is rather small. It is therefore reasonable to suppose that the Born approximation provides quite accurate values for the positronium formation cross-section for all higher partial waves. With this assumption, the total positronium formation cross section in the Ore gap is as given in figure 2. The Born results were first calculated by Omidvar (unpublished).

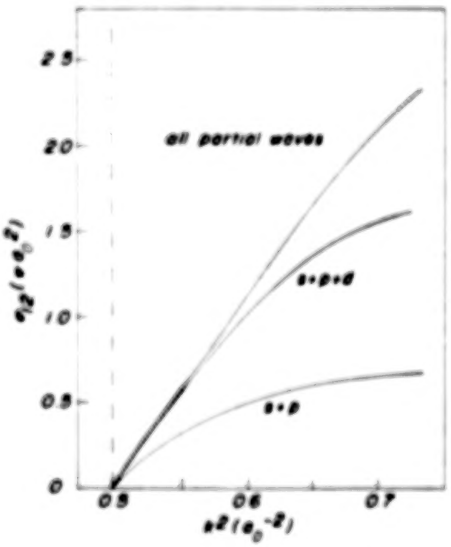

Figure 2. Partial wave cross sections for ground state positronium formation in positron collisions with atomic hydrogen[4,5]. The s-wave contribution is too small to be shown on this scale.

At positron energies somewhat above the top of the Ore gap, where the Born approximation is still not sufficiently accurate for the low partial waves, the most reliable calculations of the positronium formation cross section are probably those of Shakeshaft and Wadehra[6], who used a distorted wave Born approximation and obtained results in the positron energy range 13.6 - 200eV. These results match on reasonably well at the lower end of the range to the more accurate variational results.

Beyond 200eV the Born results of Omidvar may be used.

These three sets of positronium formation cross sections produce, upon rescaling according to equation (10), the hydrogen (antihydrogen) formation cross-section in collisions of positronium with protons (antiprotons) shown in figure 3[7]. The peak value of the cross-section is approximately $3.5 \times 10^{-16} cm^2$ at a positronium energy of $\sim$ 3.5eV relative to the antiproton, corresponding to an antiproton energy relative to the positronium of $\sim$ 3keV.

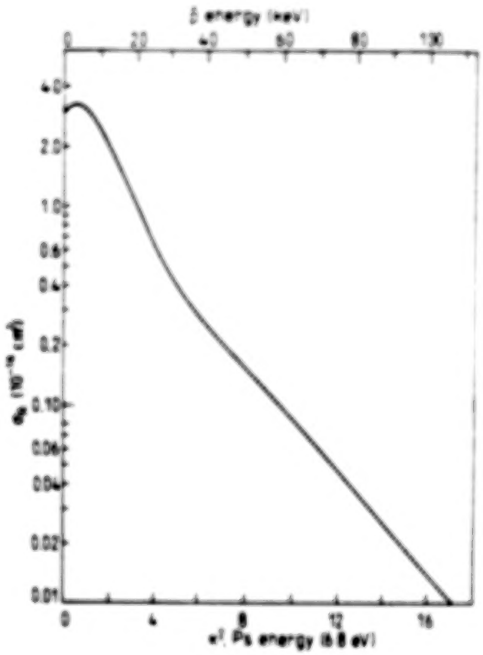

Figure 3. Theoretical estimates by Humberston et al[7]. of the ground state antihydrogen formation cross section from ground state positronium.

There is an interesting feature of the antihydrogen formation cross section at very low positronium energies, as is shown on the expanded scale in figure 4, with the cross section tending to infinity as $\kappa^2 \to 0$. The zero orbital angular momentum contribution to $\sigma_{\overline{H}}$ is, from equation (13),

$$\sigma_{\overline{H}}^{(0)} = \frac{4}{\kappa^2}\left[\frac{K_{12}^2}{(1-K_{11}K_{22}+K_{12}^2)^2+(K_{11}+K_{22})^2}\right] \tag{14}$$

and the K-matrix elements have the following behaviour as the positronium threshold is approached from above:

$$\left.\begin{aligned} K_{11} &\to \text{ const.} \\ K_{12} &\to \kappa^{\frac{1}{2}} \\ K_{22} &\to \kappa \end{aligned}\right\} \quad \kappa \to 0 \tag{15}$$

so that

$$\sigma_{\overline{H}}^{(0)} \propto \frac{1}{\kappa} \quad \text{as } \kappa \to 0, \tag{16}$$

as is to be expected for an exothermic reaction such as this. However, the rate of production of $\overline{H}$ is $v\sigma_{\overline{H}} \propto \kappa\sigma_{\overline{H}} \to$ finite const. as $\kappa \to 0$.

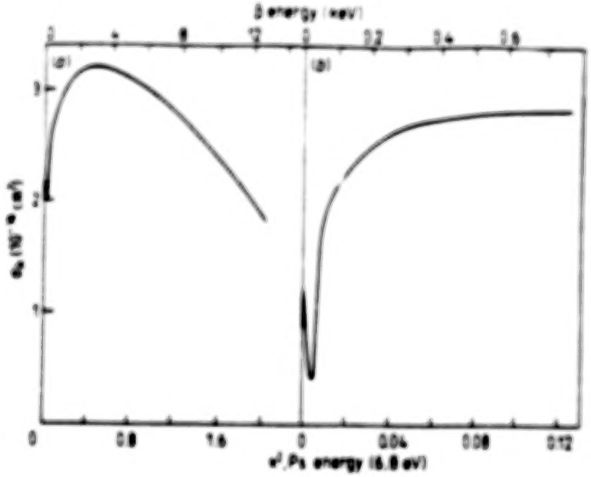

Figure 4. Low energy portions of figure 3 on expanded scales.

Thus far we have considered the formation of antihydrogen in its ground state, using positronium also in its ground state. It would be equally acceptable to form antihydrogen in one of its excited states, and several authors have recently considered this process. Darewych[8] used the first Born approximation to calculate the cross sections for antihydrogen formation into the $1s, 2s, 2p$ and $3s$ states and his results are shown in figure 5. As can be seen, these excited state formation cross sections

are comparable to the ground state formation cross section at low positronium energies and, therefore, make a very significant contribution to the total formation cross section. Almost certainly the Born approximation significantly overestimates the s-wave contributions to each of these cross-sections, as it does for the ground state, but even if this partial wave contribution is totally supressed the excited formation cross sections remain significant, as shown in figure 5.

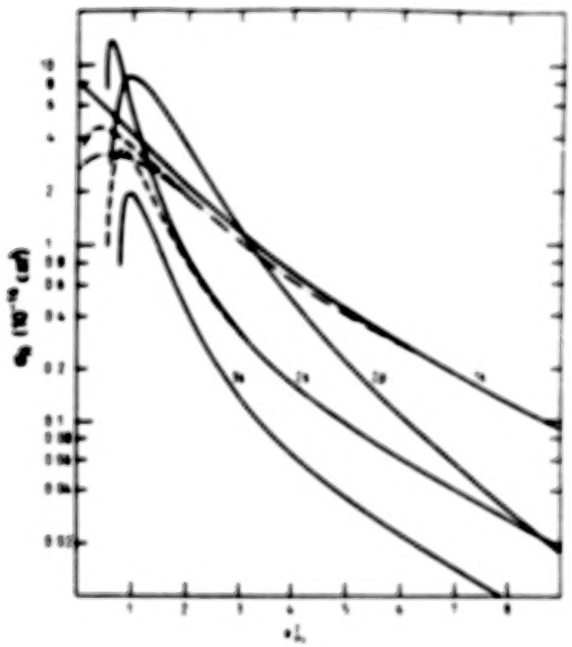

Figure 5. Cross sections for antihydrogen formation in various states from ground state positronium according to Darewych[8]. Full curves; Born approximation: broken curves; s-wave subtracted Born approximation: chain curve; 'exact' results of Humberston *et al*.[7]

Similar investigations, also using the first Born approximation, have recently been conducted by Nahar and Wadehra[9] and are shown in figure 6. They obtained good agreement with Darewych for the s-state but not quite so good for the p-state, where Darewych had used an approximate method to evaluate some of the angular integrals. These authors attempted to include the contribution to the total antihydrogen formation cross section from even higher energy states by making use of the fact that, at sufficiently high energy, the Born cross section for antihydrogen formation into a state with quantum numbers n, ℓ is

$$\sigma_{\overline{H}}(n,\ell) \propto \frac{1}{n^3}. \tag{17}$$

However, such a scaling formula is almost certainly not valid in the low energy range of interest here.

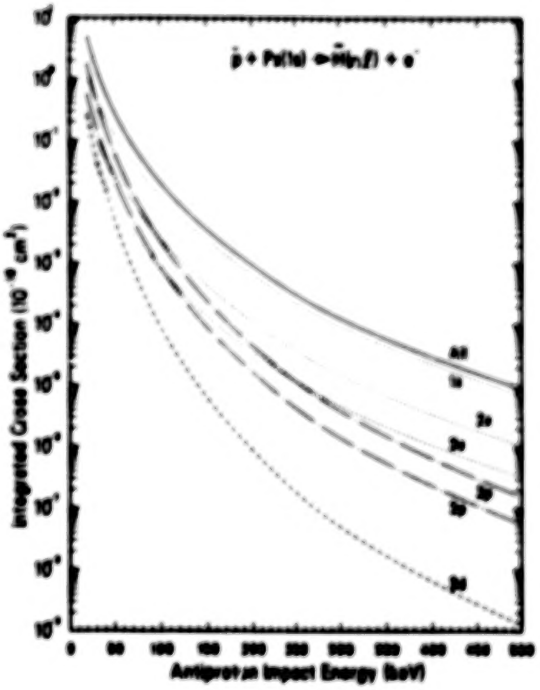

Figure 6. Cross sections for antihydrogen formation in various states from ground state positronium according to the Born calculations of Nahar and Wadehra.[9]

Ermolaev *et al*.[10] used classical and semiclassical methods to investigate the same formation cross sections, and their total results for formation of antihydrogen into all states with $n \leq 3$ are shown in figure 7. Although the low mass of the incident positronium must cast some doubt on the validity of such methods for this system, the results are, nevertheless, in tolerably good agreement with the quantum mechanical results.

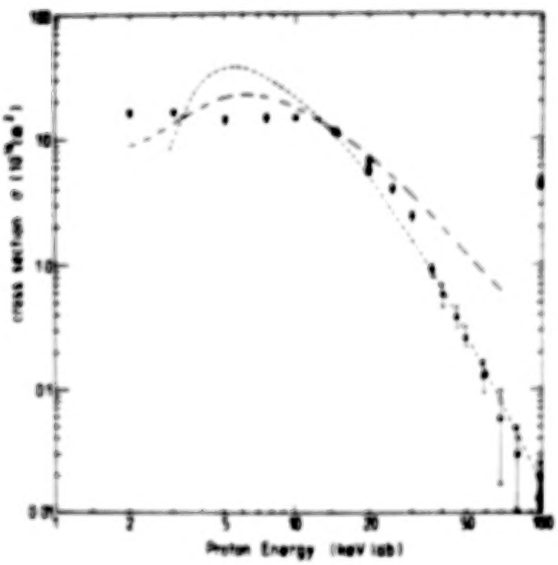

Figure 7. Total antihydrogen formation cross-sections from ground state positronium according to Ermolaev[10] ——; impact parameter method: •; classical trajectory Monte-Carlo: – – –; Born approximation (Darewych[8]).

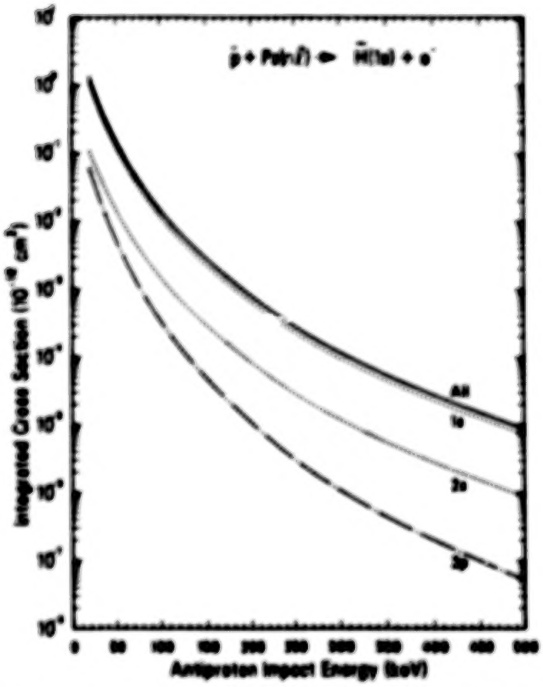

Figure 8. Cross sections for ground state antihydrogen formation from various states of positronium according to the Born calculations of Nahar and Wadehra.[9]

In all the investigations described so far, the incident positronium has been assumed to be in its ground state, but antihydrogen formation from positronium in excited states should also be considered.

Nahar and Wadehra[9] have used the Born approximation to investigate the formation of ground state antihydrogen in collisions of excited state positronium with antiprotons. They included the positronium states with n= 1 and 2 explicitly and again used the scaling law given in equation (17) to estimate the effect of all other states. Their results are given in figure 8. .

These Born calculations were not conducted at very low energies around the peak in the antihydrogen formation cross section and, even had they been, they would probably have suffered again from a similar overestimation of the low partial wave contributions to that mentioned previously. Nevertheless, it is very likely that antihydrogen formation from positronium in excited states will make a further very significant contribution to the total antihydrogen formation cross section.

Taking all these contributions into account, it would not seem unduely optimistic to predict a total antihydrogen formation cross section of at least $20\pi a_0^2$. With the expected currents of positronium and antiproton, this cross section suggests a possible rate of production of antihydrogen atoms of a few per second.

I should like to thank Prof. R.P. McEachran and his colleagues, Profs. J.W. Darewych and A.D. Stauffer for their hospitality at York University, Toronto during the writing of this article.

REFERENCES

1. H. Poth, "Atomic Physics with Positrons", edited by J.W. Humberston and E.A.G. Armour (Plenum, New York, 1987) p. 307.
2. A. Rich, R. Conti, W. Friese, D.W. Gidley, H. Griffin, M. Skalsey, T. Steiger, J. Van House, W. Zheng and P.W. Zitzewitz, ibid, p. 321.
3. F.M. Jacobsen, L.H. Andersen, B.I. Deutsch, P. Hvelplund, H. Knudsen, M. Charlton, G. Laricchia and M. Holzscheiter, ibid, p. 333.
4. J.W. Humberston, Can. J. Phys. **60**, 591 (1982).
   ———, J. Phys. B. **17**, 2355 (1984).
   ———, Adv. At. Mol. Phys. **22**, 1 (1986).
5. C.J. Brown and J.W. Humberston, J. Phys. B. **17**, L423 (1984).
   ———, J. Phys. B. **18**, L401 (1985).
6. R. Shakeshaft and J.M. Wadehra, Phys. Rev. **A22**, 968 (1980).
7. J.W. Humberston, M. Charlton, F.M. Jacobsen and B.I. Deutch, J. Phys. **B20**, L25 (1987).
8. J.W. Darewych, J. Phys. **B20**, 5917 (1987).
9. S.N. Nahar and J.M. Wadehra, Phys. Rev. **A37**, 4118 (1988).
10. A.M. Ermolaev, B.H. Bransden and C.R. Mandal, Phys. Lett. **A125**, 44 (1987).

ANTIPROTON-MATTER INTERACTIONS IN ANTIPROTON APPLICATIONS

David L. Morgan, Jr.*
728 Polaris Way
Livermore, California 94550

ABSTRACT

By virtue of the highly energetic particles released when they annihilate in matter, antiprotons have a variety of potentially important applications. Among others, these include remote 3-D density and composition imaging of the human body and also of thick, dense materials, cancer therapy, and spacecraft propulsion. Except for spacecraft propulsion, the required numbers of low-energy antiprotons can be produced, stored, and transported through reliance on current or near-term technology.

Paramount to these applications and to fundamental research involving antiprotons is knowledge of how antiprotons interact with matter. The basic annihilation process is fairly well understood, but the antiproton annihilation and energy loss rates in matter depend in complex ways on a number of atomic processes. The rates, and the corresponding cross sections, have been measured or are accurately predictable only for limited combinations of antiproton kinetic energy and material species. However, our knowledge has been improving in two areas: in energy loss and annihilation rates at low KeV energies and below, where adiabatic ionization, elastic scattering, and nuclear capture are important, and in differences between antiproton and proton atomic interactions with matter at high KeV and MeV energies. At present, estimates of annihilation and stopping rates adequate for planning purposes can be made in most aspects of the applications.

I INTRODUCTION

Over the past several years it has been recognized that antiprotons, like positrons, have potentially important practical applications.[1] In each of these applications, some of which may be instituted within the next few years, the manner in which antiprotons interact with matter while moving through it, in terms of energy loss during slowing and energy production when they annihilate, is of considerable significance. Of particular significance is the fact that the slowing and annihilation rates are wholly determined or strongly influenced by atomic interactions.[2]

A description of the interaction between antiprotons and matter is the main purpose of this paper; it is discussed specifically in Sections III,V, and VI. The possible applications, and the means of achieving them, are briefly described in Section IV. The nature, significance, and properties of the various forms of antimatter, with emphasis on antiprotons, are summarized in the following section along with some historical notes.

II BACKGROUND

The concept of antimatter, albeit in a gravitional context, goes back to the last century.[3] Antimatter in its modern form was first postulated by Dirac in 1931.[4] Anderson discovered the positron (antielectron) in 1933,[5]

and Chamberlain et al. discovered the antiproton in 1955.[6] Around this time it was accepted that the already-discovered positive pion and positive muon were the antiparticles of their negative counterparts, and subsequently an increasing number of antiparticles were discovered, including the antineutron.

We now know that for every fundamental particle there is a corresponding antiparticle whose strong and electroweak internal quantum numbers (e.g. electric charge) are opposite in sign to those of the particle. Some antiparticles, like those of the photon and neutral pion, in a given state are each identical to their particle in another state, so particle and antiparticle are not distinguished. All antiparticles have the same lifetimes as the particles and, apparently, inertial masses, but there is reason to believe that some may have different gravitational masses.[7]

It is possible, at least in principle, to construct antinuclei, antiatoms, antimolecules, and even antisubstance from antiprotons, antineutrons, and positrons. Light antinuclei are observed in high energy accelerator experiments and in cosmic rays. The simplest antiatom, the antiprotium isotope of antihydrogen, is yet to be made although there are motivations[8] and plans[9] to do so.[10] Theoretical work concerning antihydrogen and other antiatoms began about 20 years ago.[11,12,13] Since antimatter, from particle through substantive form, is the mirror image of matter in a number of respects, it is also termed "mirror matter", a term promoted by Forward.[14]

The cosmological significance of antimatter was recognized in the 1950's and 1960's by Alfven, Klein, Harrison, Omnes, and others.[15] Models of the early universe include its presence at the initial or a very early stage, but definitive observations of cosmological antimatter or its consequences include only that which may have been or is being produced in later stages by matter interactions.[16] There is, however, a feature in the cosmic gamma ray background that suggests antiproton annihilation in the universe at a red shift of about 100, but this evidence of primordial antimatter is not conclusive.[17]

In addition to their role in improving our knowledge of physics and astrophysics, antiprotons may, as positrons do, have practical applications. Some years after Sänger suggested using positron-electron annihilation to propel interstellar spacecraft in 1953,[18] NASA reconsidered the issue of annihilation propulsion in the 1970's,[19] and Morgan developed the basic concepts that might allow use of antiproton annihilation for both interplanetary and interstellar propulsion.[20] That application may have to wait decades for the required amounts of antiprotons to be available (e.g. roughly one gram for a high performance interplanetary mission). More recently a number of individuals (in particular Kalogeropoulos[21]) and organizations have discovered and investigated practical applications for antiprotons that are more readily attainable. These include remote 3-D density and elemental composition mapping of the interior of materials[22] including the human body,[21] cancer therapy,[21] equation-of-state and opacity measurements,[23] and others mentioned in Section IV. Most of the applications require no more antiprotons than could be produced, captured, and transported with current and near-term attainable technology.[1]

III BASIC ANNIHILATION PROCESSES

Most of the antiproton applications depend strongly on the energy and other characteristics of the annihilation products. These particles and gamma rays can deposit substantial amounts of energy in the matter around the point of annihilation, yet retain enough of their large energy to pass through substantial distances to exit the matter and be readily detected.

In contrast to the annihilation of a positron with an electron, which proceeds almost entirely through an electromagnetic interaction and produces two or more gamma rays, an antiproton annihilates predominantely through a strong interaction and initially produces other hadrons, mainly pions. When a

slow antiproton (p^-), with an energy around a few MeV or less, annihilates with an individual proton (p^+) at rest, the result is

$$p^- + p^+ \rightarrow 1.5\,\pi^+ + 1.5\,\pi^- + 2.0\,\pi^0 + \text{kaons} + \text{others}, \quad (1)$$

$$\pi^0 \rightarrow 2\gamma, \quad (2)$$

$$\pi^\pm \rightarrow \mu^\pm + \nu_\mu, \quad (3)$$

$$\mu^\pm \rightarrow e^\pm + \nu_e + \nu_\mu, \quad (4)$$

$$e^+ + e^- \rightarrow 2\gamma, \quad (5)$$

where π denotes a pion, γ denotes a gamma ray, μ denotes a muon, e denotes electrons and positrons, and ν denotes both neutrinos and antineutrinos.

In reaction 1 the average numbers of pions produced are given, there being a great number of possible outcomes to the reaction. About 4% of the annihilation energy goes into kaons (mainly) and other particles (including rarely two or more gammas). In reaction 2 the π^0 lifetime is so short that the π^0 travels only microns before decaying. In reaction 4 with the lower sign, the product electron will remain in the environment, and in reaction 5 the electron annihilating with the positron is a different (very likely) electron from that environment. Thus the end products of the annihilation are gamma rays and neutrinos. The energies and lifetimes of the pions and subsequent gammas and muons from the annihilation of $p^- + p^+$ are given in Table 1. The annihilation energy for reaction 1 is 1876.51 Mev, the mass energy of the proton plus the equal mass energy of the antiproton.

The relavent processes in most applications occur at a time after the neutral pions have decayed but before the charged pions (or in some cases, before the muons) have decayed. Because the relevant properties of kaons do not differ extremely from those of pions and because the neutral pions travel such a short distance before decaying, it is therefore usually adequate to assume

$$p^- + p^+ \rightarrow 1.6\,\pi^+ + 1.6\,\pi^- + 4.0\,\gamma, \quad (6)$$

where, using the same mean energies as in Table 1, the artificial increase in the mean numbers of charged pions accounts for the 4% of energy going to other particles.

Table1 The energies and lifetimes of the pions and subsequent gammas and muons from the annihilation of $p^- + p^+$ at low relative speed with the center of mass at rest. It is assumed that the pions undergo no energy or number loss before decaying. Based on informayion from a variety of sources.

Par-ticle	Mean Num-ber/An-nihilation	Mass Energy /MeV	Mean Kin-etic Energy /MeV	Life-time / s
π^+	1.5	139.58	235	2.60×10^{-8}
π^0	2.0	134.98	203	$9.\times10^{-16}$
π^-	1.5	139.58	235	2.60×10^{-8}
γ	4.0	0	169	∞
μ^+	1.5	105.66	189	2.20×10^{-6}
μ^-	1.5	105.66	189	2.20×10^{-6}

The annihilation of an antiproton with a neutron is about the same as annihilation with a proton, except that the mean number of negative pions is one greater than the mean number of positive pions and the number ratio of charged to neutral pions is somewhat greater. Depending on the nuclear environments of the neutron and proton, the cross section for annihilation with a neutron is about 0.75 times the cross section for annihilation with a proton.

When an antiproton annihilates with a proton or neutron in a nucleus other than that of protium (^1H), the above desrciption of the annihilation is altered. Some of the annihilation products interact with the remainder of the nucleus giving rise to additional products that, depending on the atomic number of the nucleus, may include light nuclear fragments consisting

of individual neutrons and protons as well as deuterons, tritons, helions, alpha particles, etc. Details are given in Ref. 24 and 25 and in the references quoted there. The results of a slow antiproton annihilating in a uranium nucleus are given in Table 2. Likewise the details of the annihilation are altered when the antiproton has an appreciable kinetic energy (several MeV or greater). Besides the additional energy, the antiproton may annihilate within the nucleus, as opposed to on the surface, and the distribution of initial annihilation products is tilted toward the nucleus. These factors lead to more and more energetic secondary products. For uranium, the fraction of annihilation energy going into the kinetic energy of the charged nuclear fragments increases by roughly 35% as the incident kinetic energy increases from zero to 100 MeV.[25]

Table 2. Annihilation Energy Partition when a slow antiproton annihilates in a uranium nucleus at rest, compared to annihilation with a proton. The fission energy includes the energies of fission Gamma rays (0.4 %) and the kinetic energies of the fission neutrons (0.5 %) and the daughter nuclei. Based mainly on information in Ref. 24.

Partition Category	Percent of Proton-Antiproton Annihilation Energy	
	In Uranium Nucleus	With Proton
Fission Energy	10	0
Neutrons (Non-Fission) (Kinetic Energy)	18	0
Charged Fragments (Kinetic Energy)	16	0
Charged Pions (Kinetic Energy)	28	38
Neutral Pions (Kinetic Energy)	10	22
All Pions (Mass Energy)	26	36
Other (Kinetic and Mass Energy)	2	4
Total	110	100

The direct annihilation cross section for antiprotons on protons is the cross section for annihilation when there is no intervening state between the antiproton's state of free motion and its annihilation. It is known experimentally for antiproton kinetic energies from about 20 MeV to about 10 GeV.[26] At the lower end of this range, the scattering is predominately s-wave, so it may be extrapolated to lower energies with the 1/v law, where v is the speed of the antiproton relative to the nucleus. Below 10 MeV it is necessary to include the coulomb correction factor, which represents the enhancement of the cross section due to the attraction between the antiproton and proton. The result is[11]

$$\sigma = 0.19\,(c/v)\pi r_0^2 \gamma/(1-e^{-\gamma}) \ , \qquad (7)$$

$$\text{with} \quad \gamma = 2\pi\alpha c/v \ ,$$

where $\gamma/(1-e^{-\gamma})$ is the coulomb correction factor, c is the speed of light (2.998×10^{10} cm/s), r_0 is the classical electron radius (2.82×10^{-13} cm), and α is the fine structure constant (1/137.0). The cross section is shown in Figure 1. Eq. 7 does not apply for energies around 20 eV and below where p^- capture in the $p^- + H$ (hydrogen atom) rearrangement reaction (Section VI) becomes important. Radiative capture is unimportant at essentially all energies.[11]

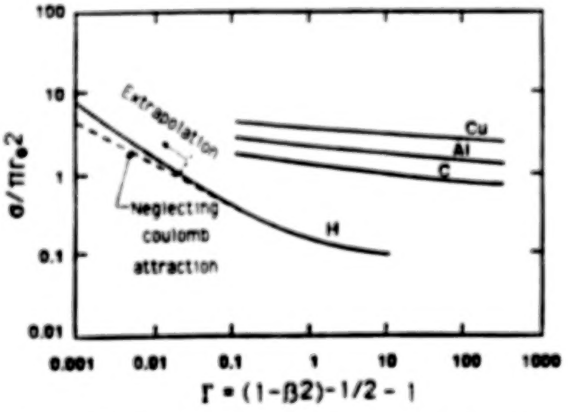

Fig. 1. Cross section (σ) for annihilation of antiprotons in hydrogen, carbon, aluminium, and copper. r_e is the classical electron radius, Γ is the ratio of antiproton kinetic energy to rest mass energy, and $\beta = v/c$.

Cross sections for direct antiproton annihilation in carbon, aluminum, and copper nuclei have been measured for energies from about 100 MeV to about 200 GeV.[27] They are also shown in Fig. 1. A formula that fits these data below about 10 GeV and may allow extrapolation to heavier nuclei is:[25]

$$\sigma = \pi(1.35\,A^{1/3} + 0.83)^2 \times (p/\,600\,\mathrm{MeV/c})^{-B} \times 10^{-26}\ \mathrm{cm}^2\,, \qquad (8)$$

$$\text{with } B = 0.5A^{-0.4}\,,$$

where A is the atomic weight of the nucleus and p is the antiproton momentum. Data are needed for a wider variety of nuclei and energies.

IV APPLICATIONS

The number of antiprotons required in each application event in the applications mentioned below varies from roughly 10^6 to 10^{12}. The larger of these figures is also the approximate, current upper limit on the number that probably can be transported in a storage device on a truck.[28] That device might be a storage ring, a Penning-like trap, or another kind of ion trap. For currently achievable vacuums, the lifetime of the antiprotons could be a few weeks to several months.

Antiprotons are currently produced in particle accelerators by bombarding nuclei with protons with energies of a few tens of GeV to a few hundred GeV. The potential production rate of storable antiprotons (i.e. slowed to KeV energies) for each of a few current or planned accelerators, as they are or with well understood modifications, is about 10^{16} per year.[29] With current and foreseeable technology, it may be possible to construct an accelerator specifically for antiproton production giving 1 mg (6×10^{20}) per year.[30] Reasonable speculations exist on means to produce gram or even kilogram amounts per year.[31]

Antiprotons can be used to obtain three dimensional "x-rays" of materials,[22] including the human body,[21] by directing a narrow beam of them into the material. The annihilation products can pass through a meter of condensed materials of light elements or at least a few centimeters of those of heavy elements and remain detectable. Reconstruction of their paths allows the coordinates of annihilation points to be determined as functions of beam direction and energy. The depth of penetration up to the anihilation point is a function of the energy and integrated density of the material, with some dependence on elemental composition. Thus one may obtain a density map of the interior of the material. Resolutions of about 1 mm or less appear obtainable. The radiation dosage is about one tenth the value resulting from procedures using x-rays that accomplish the same quality of density map. By combining this technique with measurements of the x-ray spectrum given off by the antiprotons captured by nuclei prior to annihilation, one might also obtain a 3-D map of the elemental composition.[21]

Antiprotons may be valuable in cancer therapy[21,32] and in healing defects within a material[22,33] because, in a condensed material, a significant portion of their combined kinetic and annihilation energy is released close to the point of annihilation. The Bragg peak in the energy loss as a function of distance travelled is narrow, most annihilations occur only after the antiprotons have stopped, and the flux of annihilation products decreases as the inverse square of the distance from the annihilation point. Additionally, for most relevant materials, a significant fraction of the annihilation products are protons that usually stop within a few centimeters. For an antiproton beam in water, roughly 100 MeV per particle is deposited within about 5 mm of the aim point. The remainder is spread thinly over the surroundings or escapes.

For equation-of-state and opacity measurements in a small laboratory, transportable antiprotons may allow pressures and temperatures comparable to those available in a large facility.[22] The antiprotons are used to

induce fissions in fissile material placed next to the material sample under investigation. Essentially one fission results per annihilation,[24,34] and the exploding fissile material (a very small amount) compresses and heats the sample. To assess feasability it is important to know how short in duration the pulse of antiprotons could be made and how the fractions of stopped antiprotons and deposited fragment energy depend on fissile material size.

Roughly speaking, antiproton annihilation propulsion of spacecraft could make exploration of the solar system like exploration of the earth by steamship, and its near-light-speed capability over longer distances could make travel to nearby stars a reality. Reasonable concepts exist for annihilation rocket engines,[35-38] for means of producing solid antihydrogen (required storage form of antiprotons),[39] for antihydrogen storage,[36,37] for extracting antiprotons from solid hydrogen,[36] and for other necessary processes and hardware. However, the amounts of antiprotons required per mission, milligrams (earth to orbit) through tonnes (interstellar), are well beyond current means to produce. Nevertheless, available amounts of antiprotons allow many worthwhile experiments that can explore and validate these concepts.[35,40]

For most annihilation engine concepts, the basic problem is to get the antiprotons well into the annihilation/propellant medium without annihilations occuring elsewhere, while containing (e.g. with magnetic fields) a large fraction of the annihilation products as they transfer their energy to the medium. Hence the importance to propulsion of the slowing and annihilation rates of antiprotons in matter. Knowledge of antiproton interactions with matter are likewise important in other aspects of annihilation propulsion.

Two means have been suggested in which antiproton annihilation is coupled to nuclear fusion processes. In one, antiproton annihilation initiates a deuterium/tritium fusion reaction in a bomb configuration.[41] The minimum number of antiprotons required is probably on the order of 10^{17} or 10^{18}, which will be very expensive to produce, at the least, for some time to come. In the other, deuterium and tritium are introduced into the combustion chamber of an annihilation engine in which the annihilation/propellant medium is in a gas or plasma state.[42] The muons from pion decay then induce fusion of the deuterium and tritium nuclei through the muon-catalyzed-fusion process.[43] The extra energy might double or triple the energy output of the engine for little additional mass.[35] In the "plasma-core" engine,[36] the temperature and density are sufficiently high that deuterium-tritium fusion would occur without the presence of muons. Whether such an engine could sustain a fusion reaction if the antiprotons were turned off is not known.

V SLOWING AND ANNIHILATION RATES

In most applications and many physics experiments, it is important to know how antiproton kinetic energy and annihilation probability depend on initial energy, distance traveled through a material, and composition of the material.

For antiprotons in hydrogen at energies above 20 eV, Eq. 1 may be multiplied by the atomic number density, n, to give an approximation for the annihilation probability per increment of the distance, x, traveled (the annihilation rate)

$$dP/dx = 0.19\, n(c/v)\pi r_0^2 \gamma/(1-e^{-\gamma}) , \qquad (9)$$

$$\text{with} \quad \gamma = 2\pi\alpha c/v$$

For substances with atomic numbers equal to carbon and above and antiproton energies from 100 MeV to 10 GeV, dP/dx may be obtained similarly from Eq. 8. The result cannot be extrapolated to lower energies without knowledge of how higher angular momentum waves and the coulomb correction factor are involved in the data used in Eq. 8. A very rough approximation at low energies for other materials may be obtained by multiplying the right side of Eq. 9 by the two thirds power of

the mean atomic number, a rough measure of the ratio of an effective nuclear cross sectional area to that of the proton. Annihilation and slowing rates below 20 eV in unionized or partially ionized media are dealt with in the following section.

For antiprotons in the low KeV range and above, the slowing rate ($-dE/dx$, where E is the antiproton kinetic energy in the rest frame of the medium) is almost entirely due to transfer of energy to atomic electrons in binary collisions. A good approximation is provided by the "Bethe formula"[44] which is based on the Born approximation and applies to charged particles in an unionized medium. For antiprotons it is

$$-dE/dx = 8\pi e^4 (Nn/fE) \ln(fE/I_m) \quad , \quad (10)$$

$$\text{with} \quad f = 4 m_e m /(m+m_e)^2 \equiv 4 m_e/m,$$

where e ($= 4.8 \times 10^{-10}$ esu) is the electron charge, N and I_m are the mean atomic number and ionization energy of the medium, and m_e ($= 9.11 \times 10^{-28}$g) and m ($= 1.673 \times 10^{-24}$ g) are the electron and antiproton masses. For most elements, $I_m/N \equiv 13$ eV. Some exceptions are helium, beryllium, nitrogen, and calcium for which I_m/N is 24, 16, 11, and 11 eV respectively. More accurate versions of Eq. 10 exist that include relativistic corrections, important around 1 GeV and above, shell corrections, Barkas-effect corrections, which lead to different slowing rates for particles of equal mass but opposite sign, and the block correction.[45] There is recent experimental confirmation of the Barkas effect for antiprotons (vs. protons) at low MeV energies, and it has been confirmed that at least some single and multiple ionization cross sections are different for protons and antiprotons.[46]

Eq. 10 is probably accurate to within a few tens of percent or better for $E \gg I_m/f$ ($\equiv 5$ to 500 KeV for hydrogen to uranium) but less than 1 GeV. Such accuracy is consistent with the magnitudes of the above theoretical corrections. In addition, calculations of ionization and excitation cross sections for antiprotons in hydrogen[47,48] at such energies are in good agreement for these energies with the cross sections which, along with the final energies of the ionized electrons, give Eq. 10.

For $E \equiv 2.7\ I_m/f$, $-dE/dx$ has a maximum (the "Bragg peak"), similar to that seen experimentally for other charged particles. In lieu of experimental information on antiprotons at such energies, the accuracy, if not the form, of Eq. 10 and the more accurate versions is questionable, however, for a number of reasons. First, the perturbative nature of the calculation may not be valid. Second, the electrons may not be treatable as free particles for energy transferral, as is assumed. Last, the equations are certainly inaccurate for $E \equiv I_m/f$, since the fact that they give $-dE/dx = 0$ at $E = I_m/f$ is not true. That energy is the cutoff below which the antiproton (or any other particle with the same mass) cannot transfer an energy equal to I_m to a free electron in a binary collision. An alternate formula for Eq. 10 employs a more realistic, distributed ionization energy.[2] It may obviate the need for shell corrections, and within the Born approximation it gives a lower, more realist cutoff energy since that cutoff can be based on the minimum ionization (or excitation) energy.

Eq. 10 is used to give the rightmost, nearly straight portion of the curve in Fig. 2 of $-dE/d(\rho x)$ for antiprotons slowing in hydrogen, where ρ is the mass density of the hydrogen. In spite of the incorporation of ρ, $-dE/d(\rho x)$ is still dependent on the properties of the slowing medium. Both the factor, N/A (A = medium's mean atomic mass), which appears in Eq. 10 after division by ρ, and I_m^{-1}, which appears in the argument of the logarithm, decrease (on the average) as N and A increase. Thus materials composed of heavier elements usualy have lower values of $-dE/d(\rho x)$ than materials composed of lighter elements.

Under most circumstances, knowledge of slowing below the Bethe formula cutoff is inconsequential. In condensed media or gasses at normal pressures, charged particles are then moving so slowly that even small subsequent energy loss leads them to thermal energies in a

very short distance (a few mm or less) if they have not already decayed (if unstable) or been captured (if negative). However, if slowing is purposely used as a means to produce antiprotons at low and sub KeV energies or if rocket engines with very low density annihilation media should seem worth considering, then knowledge of slowing mechanisms around and below the cutoff can be necessary.

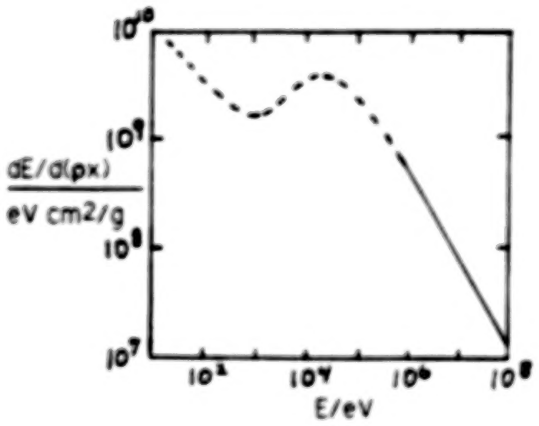

Fig. 2. Energy loss rate (per unit distance-times-density) for antiprotons slowing in unionized hydrogen. ρ is the mass density of hydrogen and E is the antiproton kinetic energy in the lab frame.

There are at least two mechanisms that lead to energy loss around and below the cutoff but still above about 20 eV where antiproton capture begins to become likely: adiabatic excitation and ionization of atomic electrons by the antiprotons and elastic scattering of the antiprotons by whole atoms (or molecules). In the former, the presence of the antiproton near a nucleus lowers its effective charge, so an electron may move to a higher state, or be ionized, and remain in the altered configuration when the antiproton, having therefore lost energy, leaves. In the latter, the antiproton loses energy in the lab frame, on the average, as long as its kinetic energy is above the mean thermal energy of the medium.

An approximate, but complicated formula for energy loss by heavy negative particles due to elastic scattering by atoms is given in Ref. 2 and 35. It assumes the atoms are free and separated by at least a few Bohr radii, so it applies to gas media and with less accuracy to some condensed media. For antiprotons in hydrogen this formula gives the leftmost, fairly straight portion of the curve of -dE/d(ρx) in Fig. 2. A consequence of the model employed there for the particle-atom potential energy, V, (a raised coulomb potential, cutoff when V=0) is that the scattering (classical) is exactly backwards for a particular particle energy in the center-of-mass system for all impact parameters for which V≠0. If a negative particle at this energy encounters an atom of equal mass it stops dead in its tracks in the rest frame of the atom (lab frame approximately), if it encounters a more massive atom it reverses direction in that same frame. Hence the term, "brick wall" scattering, for this process. The particular energy is about 10 eV for antiprotons in hydrogen, so the capture process may dominate, but for media with heavier atoms it occurs at higher energies (60 eV in carbon) for which capture may be less important. There are apparently no experiments or more accurate calculations that bear on the reality of this possible phenomenon.

A rough consideration of adiabatic excitation/ionization[35] indicates that it may be important for antiprotons in hydrogen at energies around 1 KeV but that energy loss by elastic collisions is more important around and below a few hundred eV. Other loss mechanisms at these energies may be vibrational and rotational excitation of molecules and the creation of phonons and similar entities.

Division of the energy loss process into particular mechanisms operating over particular energy ranges is in part a consequence of a need to find relatively simple, pictureable, and tractable means of describing and calculating the process. The particle-electron collision mechanism, that leads to the Bethe formula for the slowing rate, and adiabatic excitation/ionization are perhaps better described as high and low energy approximate views of a single

process. This is borne out by Ermolaev's recent calculation of excitation and ionization cross sections for antiprotons on hydrogen atoms.[47] The total excitation/ionization cross section is smooth and roughly constant from 2 to 50 KeV (2.3 to 1.5 $\times 10^{-16}$ cm^2). This range includes the Bethe formula cutoff at about 6 KeV and the Bragg peak at about 16 KeV. If it assumed that the mean energy loss per collision in that range varies from 10 eV at the low end to 30 eV at the high end, then the portion of the curve of $-dE/d(\rho x)$ in Fig. 2 around the local maximum results. Portions of the curve around 1 KeV and around 200 KeV are interpolations between the elastic scattering result on the left, the Ermolaev-based results in the middle, and the simple-Bethe-formula results on the right.

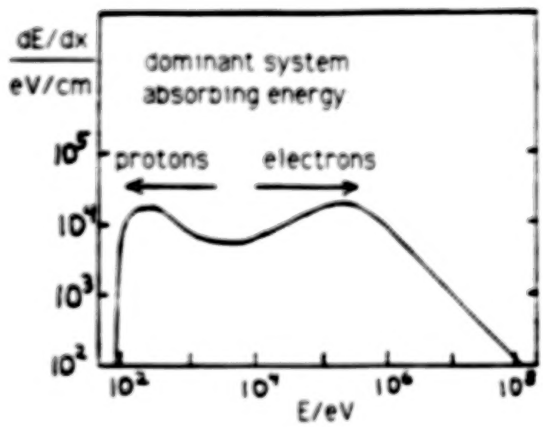

Fig. 3. Energy loss rate (per unit distance) for antiprotons slowing in a fully ionized hydrogen plasma at a temperature of 10^6K and an atomic number density of 3.6 $\times 10^{18}$ / cm^3. E is the antiproton kinetic energy in the lab frame.

For antiproton slowing in fully ionized plasmas one may use Langmire's formula.[49] Application to a hydrogen medium with a temperature of 10^6 K and an atomic number density of 3.6 $\times 10^{18}$ (conceivable conditions within a plasma-core annihilation engine) yields the result for $-dE/dx$ shown in Fig. 3. Here the slowing rate is not exactly proportional to the density so ρ cannot be factored out, results must be given for particular densities. Such factorization is approximately correct at high energies for which, interestingly, the slowing rates in Fig. 2 and 3 are about the same.

Once an antiproton reaches thermal energy in a plasma (usually doing so before annihilating), it diffuses and eventually annihilates. For the above plasma, annihilation will occur within a few millimeters and within several microseconds of the point and time at which it thermalizes.[50]

VI REARRANGEMENT AND CAPTURE

At low- and sub-eV energies in media that are not largely ionized, antiproton slowing and annihilation rates are thoroughly dominated by a rearrangement reaction in which the antiproton loses energy and becomes bound to (captured by) a nucleus, while the electrons absorb that energy, most likely through ionization.[2,11,12,51-53] Once captured, the antiproton cascades to lower energy levels, while emitting x-rays, and eventually annihilates in the nucleus.[54] For antiprotons that have not annihilated before slowing to energies around 1 eV and below (normally most of them), the cross section for this process is so high ($> 20\pi a_0^2$, a_0 = Bohr radius = 5.29 $\times 10^{-9}$cm) that final stopping and annihilation occur within lengths that can be measured in interatomic distances in all media but dilute gasses.

For antiproton energies around or below 20 eV relative to the medium, the antiproton's speed will be less than 0.03 of the mean speed of the least bound electrons (slowest) of an atom of the medium. Thus the adiabatic approximation applies to the response of all of the atomic electrons to the influence of an incoming antiproton as long as the mean speed of any electron does not decrease considerably. In this approximation, also called the Born-Oppenheimer approximation, the wave function

of the electrons at any instant is taken to be the wave function the electrons would have if the antiproton were stationary at its location at that instant. In addition, an antiproton at 20 eV or less can transfer no more than a small amount (0.04 eV) of its energy to an electron in a binary encounter. Thus, any significant transferral of energy will occur adiabatically.

As the antiproton passes by or within the atom, the electrons will adiabatically reconfigure themselves into a state of higher energy, since they are repelled by the antiproton. That extra energy is taken from the kinetic energy of the antiproton. There are then three possibilities: (1) the antiproton leaves, gaining back the energy from the electrons as they return to their initial configuration, (2) the antiproton leaves, having lost energy to to the electrons, which are left in a higher energy state (adiabatic excitation/ionization spoken of above at higher energies), or (3) the antiproton becomes permanently bound to the nucleus with the electrons left in a negative-ion state (possibly excited) of an atom with atomic number one less, or one or more electrons ionize while the remainder are in a neutral or positive-ion state of that new atom (possibly excited).

The first possibility is always possible, it will certainly occur for sufficiently high angular momentum waves of the incoming antiproton (i.e. large impact parameters classically). Indeed, if the adiabatic condition were perfectly satisfied, it is the only possibility that could occur. The second possibility can occur, in particular at the higher antiproton energies (and therefore speeds) considered earlier, because at least one of the electrons will slow down to a speed more comparable to that of the antiproton as it moves to a less bound or an unbound state. Under that condition, its portion of the wave function can no longer change rapidly enough to follow the changing influence of the antiproton to satisfy adiabaticity. It is this latter fact that allows the excitation or ionization to be permanent. The third possibility, of main concern here, similarly requires a breakdown in the adiabatic approximation.

In the second and third possibilities, the low energy of the antiproton for the range under consideration requires that at least one electron slow down considerably and/or the antiproton speed up considerably for the adiabatic approximation to break down. The former can occur if an electron moves to a state of nearly zero energy, either highly excited or ionized. The latter can occur if the antiproton gets close enough to the nucleus for its attraction to increase its kinetic energy considerably.

For an antiproton to excite or ionize a hydrogen atom (essentially same mass as the antiproton) without being captured requires that there be at least 10.2 eV (minimum excitation energy) of kinetic energy in the center-of-mass (c.m.) frame, so the antiproton must have an energy of at least 20.4 eV in the rest frame of the atom (lab frame approximately). This is consistent with earlier statements that adiabatic excitation/ionization (without capture) becomes unimportant toward the lower end of the eV energy range. Capture of the antiproton with the electron remaining in a negative ion is impossible for hydrogen. Capture into a state of protonium (bound p^+-p^-) that is just barely bound, with ionization of the electron to a state of zero energy, requires that the antiproton energy (lab frame) be no more than 27.2 eV (kinetic energy in c.m. frame = 13.6 eV = ionization energy). If the antiproton had any additional energy, it would would have to be carried off by the electron, but with reference to statements above, it appears unlikely that this additional energy could be more than a relatively small amount. Capture into protonium states of greater binding energy requires that the antiproton energy not exceed progressively smaller amounts.

For hydrogen, therefore, rearrangement (i.e. capture and ionization) is unlikely for energies above about 20 eV, but as will be seen, it is very likely at lower energies. This dividing line is probably roughly the same for other atoms and for molecules because it is the outer electrons that will respond most strongly to the antiproton.

Using a semiclassical method, Morgan and Hughes calculated the cross section for antiproton - hydrogen atom rearrangement for energies from a few eV down to about 1 meV.[11,12] An approximation that may be applicable for any neutral atom, accurate below about 2 eV for hydrogen, is

$$\sigma = \pi(2(1+m/M)e^2\alpha/E)^{1/2} \quad , \qquad (11)$$

where σ is the rearrangement cross section and thence the annihilation cross section, M is the mass of the atom, and α is its polarizability (4.502 a_0^3 for hydrogen). They assumed, as had others in reference to negative pions and muons,[55] that the rearrangement takes place whenever the antiproton passes closer than a certain distance, R_c, to the proton. R_c is called the critical radius, it is the maximum distance ($0.639a_0$ [55]) between the proton and antiproton for which there are no bound states for the electron in the adiabatic approximation.

A feature of the interaction that helps with the accuracy of their results is that the inner turning point of the antiproton orbit relative to the proton is a discontinuous function of the impact parameter. For energies below a few eV, the inner turning point is well outside of R_c (no rearrangement) or it is well inside it (100% rearrangement probability assumed). Their more acurate calculation is based on the exact antiproton - hydrogen atom interatomic potential, while Eq. 11 is based on the long range, induced dipole part of that potential energy, $-e^2\alpha/(2R^4)$, where R is the proton-antiproton separation. It is the long range part of the potential energy that principally determines the value of impact parameter at which the discontinuity occurs. Since the energy-dependent impact parameter at which the discontinuity occurs is typically several Bohr radii, the rearrangement cross section is quite large.

As the antiproton approaches to within a short distance of R_c, the adiabatic approximation breaks down as the antiproton speeds up and the electron, whose wave function has expanded considerably as its energy approaches zero from below, is slowing down. At this time the electron motion becomes decoupled from the motion of the antiproton. Considering this process in detail, Morgan has made an estimate of the probability that the electron will reattach itself to the proton as the antiproton returns to the vicinity of R_c.[52] The probability is 20% for $E \leq 1$ eV that reattachment will occur with the antiproton proceeding away from the atom and the electron returning to its initial state, so Eq. 11 and the "more accurate" results might be more correct if the cross section were multiplied by 0.80. For energies of a few eV and less the rearrangement cross sections can be so high that the separate cross sections overlap within each layer of molecules in a solid or liquid.[56] This means that antiprotons at these energies will be captured and will annihilate within the first few molecular layers of the substance, with the actual values of the cross sections under these circumstances being less than given by Eq. 11.

VII ROCKET ENGINE INJECTION ENERGIES

Information on the annihilation and energy loss rates of antiprotons in hydrogen is adequate to determine the antiproton injection energy required to center the annihilation region within the engine when the annihilation/propellant medium is hydrogen. Additionally one may determine the fraction of annihilations that occur away from the center.[50] Results for two engine types will be sumarized.

In a gas-core engine the hydrogen medium is heated by the charged pions and subsequent muons and electrons which are confined by a magnetic field as they lose their energy. By design the antiproton injection rate and consequent heating rate relative to the mass flow rate of hydrogen is insufficient to produce significant ionization. A typical density within such an engine is about 10^{-3} g/cm^3 and a typical combustion chamber radius is roughly 1 m. Under these conditions the approximate nature of -dE/dx (as shown in Fig. 1) below about 500

KeV is inconsequential since any reasonable values of $-dE/dx$ will make distance traveled from 500 KeV to stopping be a very small fraction of engine size. Additionally the rearrangement-capture process is so strong and the subsequent annihilation process so fast that when the antiprotons come close to a stop they annihilate before moving any significant distance. Thus one may employ Eq. 9 and 10 for annihilation and slowing rates and assume that reaching 500 KeV is tantamount to stopping. Thereby the required injection energy that leads to the antiprotons stopping at the center of the engine is 1.4 MeV, and the fraction of annihilations that occur before the antiprotons reach the center is only 0.025.

In a particular concept for a plasma-core engine, the medium is fully ionized hydrogen at a temperature of 10^6K and a number density of 3.6×10^{18} ionized atoms per cm^3. The results shown in Fig. 2 and Eq. 9 combine to give 1.3 MeV for the injection energy if the engine radius is 1 m, and the fraction of annihilations occurring before the antiprotons thermalize is only 0.003. Once they thermalize, they undergo direct annihilation before moving but a small fraction of the size of the engine.

VIII. CONCLUSIONS AND COMMENTS

There a number of potentially important and feasible practical applications of antiprotons. In these, knowledge of the interactions of antiprotons with matter is necessary, and in particular, formulae for the annihilation and slowing rates of antiprotons in matter are required.

The annihilation rate in hydrogen appears to be known with fair accuracy for all important antiproton energies, but the values for energies in the low MeV range and throughout the KeV and eV ranges need experimental confirmation. The annihilation rates in other substances are known experimentally for only a limited number of cases and only for energies of a few hundred MeV and above. Experiments and/or experimentally confirmed formulae are needed for other substances and for lower energies for all substances.

Formulae for the slowing rate are accurate around and above an energy that is in the high KeV range for hydrogen up to the low or mid MeV range for substances with higher atomic number. Experiments and/or experimental confirmation of these or other formulae are needed at lower energies.

Present information on the interactions is often adequate for estimates in planning the applications, but improved knowledge is required for the actual design of procedures and equiptment and for the interpretation of the resultant information coming from each application.

ACKNOWLEDGEMENTS

Support for the author's work summarized here has been received from the Jet Propulsion Laboratory under NASA contract NAS 7-100, from the Air Force Astronautics Laboratory (MIPR RPL 59004), from The Rand Corporation, and has been conducted in part under the auspices of the U.S. Department of Energy at Lawrence Livermore National Laboratory under Contract W-7405-Eng-48. I am greatful for Matthew Morgan's advice in regard to the manuscript.

---

*The author is employed at Lawrence Livermore National Laboratory. This paper is not work for hire for that organization.

[1] B.W. Augenstein, B.E. Bo[illegible] E. Mills, and M.M. Nieto, Ed., *Proceedings of the [illegible]hop on Antiproton Science and Technology*, the Ren[illegible]ection, U.S.A., October 6-9, 1987 (World Scientific, Singa[illegible], 1988), 759 p.

[2] D.L. Morgan, Jr., Ref. 10, p 399, (In the argument of the squared logarithm factor in Eq. 3 there, lm should be $lmin$, and in Table I there, the symbols V and El should be reversed).

3A. Schuster, Nature (Lond.) **58**, 367 (1898); Nature (Lond.) **58**, 618 (1898).

4P.A.M. Dirac, April 1931 letter to J.H. Van Vleck, quoted on p. 1060 in D.F. Moyer, Am. J. Phys. **49**, 1055 (1981).

5C.D. Anderson, Science **76**,238 (1932).

6O. Chamberlain, E. Segre, C. Wiegand, and T. Ypsilantis, Phys. Rev. **100**, 947 (1955).

7M.M. Nieto and B.E. Bonner, Ref. 1, p 328.

8T. Goldman, M.V. Hynes, and M.M. Nieto, Gen. Rel. and Gravitation **18**, 67 (1986); G. Gabrielse, Ref. 10, p 349; N. Beverini, V. Lagomarsino, G. Manuzio, F. Scuri, and G. Torelli, Ref. 10, p 357; A. Rich, R. Conti, W. Frieze, D.W. Gidley, M. Skalsey, T. Steiger, J. Van House, H. Griffin, W. Zheng, and P.W. Zitzewitz, *Proceedings of the NATO Advanced Research Workshop on Atomic Physics with Positrons*, University College, London, July 15-18, 1987; R. Neumann, Ref. 10, p 305; V.V. Parkhomchuk, Ref. 10, p 315; B.E. Bonner and M.M. Nieto, Ref. 1, p 249.

9H. Poth, B. Seligman, W. Schwab, M. Wörtge, A. Wolf, R. Conti, W. Frieze, D. Gidley, A. Rich, M. Skalsey, J. Van House, P. Zitzewitz, J. Berger, P. Blatt, R. Neumann, and G. Zu Putlitz, Ref. 10, p 259; B.I. Deutch, L.H. Anderson, P. Hvelplund, F.M. Jacobsen, H. Knudsen, M.H. Holzscheiter, M. Charlton, and G. Laricchia, Ref. 10, p 271-286; G. Gabrielse, S.L. Rolston, L. Haarsma, and W. Kells, Ref. 10, p 287-294.

10H. Poth and A. Wolf, Ed., *Production and Investigation of Atomic Antimatter*, proceedings of "Antimatter '87" symposium, Karlsruhe, 30 Nov. - 2 Dec., 1987 (J.C. Baltzer, Basel, 1988) 425 p., reprinted from Hyperfine Interactions, **44** (1988).

11D.L. Morgan, Jr. and V.W. Hughes, Phys. Rev. D **2**, 1389 (1970).

12D.L. Morgan, Jr. and V.W. Hughes, Phys. Rev. A **7**, 1811 (1973).

13G. Steigman, Nature (Lond.) **224**, 477 (1969); Ph.D. dissertation (New York University, 1968); K. Omidvar, Abstracts of the Third International Conference on Atomic Physics, Boulder, 1972, p 202.

14R.L. Forward and J. Davis, *Mirror Matter, Pioneering Antimatter Physics* (John Wiley & Sons, New York, 1988) 262 p.

15Ref. 2,3,4,5,8, and 9 in Ref. 12 here, also A.D. Sakharov, JETP Lett. **55**, 24 (1967); Ya.B. Zel'dovich, Sov. Phys. JETP **9**, 603 (1967); G. Steigman, Nature (Lond.) **224**,477 (1969). (See first listing in Ref. 17 here for modern references).

16S.P. Ahlen, S. Barwick, J.J. Beatty, C.R. Bower, G. Barbier, R.M. Heinz, D. Lowder, S. McKee, S. Mufson, J.A. Musser, P.B. Price, M.H. Salmon, G. Tarle, A. Tomasch, and B. Zhou, Ref. 10, p 97; V. Schönfelder, Ref. 10, p 85.

17F.W. Stecker, Ref. 10, p 73-84; F.W. Stecker, D.L. Morgan, Jr., and J. Bredekamp, Phys. Rev. Lett. **27**, 1469 (1971).

18E. Sänger, Ingenieur-Archiv V. **21**, 213 (1953) (in German).

19D.F. Dipprey, in Frontiers in Propulsion Research, JPL TM-33-722, Ed. D.D. Papailiou (Jet Propulsion Laboratory, Pasadena, 15 March 1975).

20D.L. Morgan, Jr., *Rocket Thrust from Antimatter Annihilation*, JPL Contract Report CC-571769 (Jet Propulsion Laboratory, Pasadena, 1975) unavailable; *Coupling of Annihilation Energy to a High Momentum Exhaust in a Matter-Antimatter Annihilation Rocket*, JPL Contract Report JS-651111 (Jet Propulsion Laboratory, Pasadena, 1976) unavailable; information in these is included in Ref. 36.

21T. Kalogeropoulos, J. Archambeau, D. Bassano, G. Bennett, B. Gottchalk, L. Grey, A. Koehler, R. Muratore, and M. Urie, Ref. 1, p 640.

22L.B. Greszczuk, Ref. 1, p 679.

23J.C. Solem, Ref. 1, p 502; S. Polikanov, in *Physics at LEAR with Low-Energy Cooled Antiprotons*, Ed. U. Gastaldi and R. Klapisch (Plenum Press, New York, 1984) p 851.

24G.A. Smith, Ref. 1, p 296.

25D.L. Morgan, Jr., *Annihilation of Antiprotons in Heavy Nuclei*, AFRPL-TR-86-011 (Air Force Astronautics Laboratory, Edwards AFB, April 1986) 29 p.

26T. Armstrong, C. Chiu, J. Clement, C. Elinon, M. Furic, K. Hartman, A. Hicks, E. Hungerford, T. Kishimoto, J. Kruk, R. Lewis, D. Lowenstein, W. Lochstet, B. Mayes, R. Moss, G.S. Muchler, L. Pinsky, G.A. Smith, L. Tang, W. von Witsch, and Y. Xue, Phys. Rev. D **36**, 659 (1987).

27K. Nakamura, J. Chiba, T. Fujii, H. Iwasaki, T. Kageyama, S. Kurabayashi, T. Sumiyoshi, T. Takeda, H. Ikeda, and Y. Takeda, Phys. Rev. Lett. **52** (1984) 731.

28D. Cline, Ref. 1, p 45; S.D. Howe, M. Hynes,and A. Picklesimer, Ref. 1, p 481.

29D.C. Peaslee, Ref. 1, p 16, Ref. 10, p 37; Y.Y. Lee and D.I. Lowenstein, Ref. 1, p 26, p 39; T. Goldman, Ref. 1, p 123; E. Blackmore, Ref. 1, p 155; C.D. Johnson, Ref. 10, p 21; F.E. Mills, Ref. 10, p 31.

30F.E. Mills, Ref. 1, p 169; D.J. Larson, Ref. 1, p 202.

31G. Chapline, J. Brit. Interplan. Soc. **35**, 423 (1982); B.C. Maglich, Nuc. Instr. and Meth. in Phys. Res. **A271**, 167 (1988); H. Takahashi and J. Powell, Ref. 1, p 620; A.S. Christopoulos, H. Hora, R.J. Stening, H. Loeb, and W. Scheid, Nuc. Instr. and Meth. in Phys. Res. **A271**, 178 (1988).

32L. Grey and T.E. Kalogeropoulos, Radiation Research **97**, 246 (1984); Ref. 1, p 662.

33G. Nordley, private communication, Oct. 1987.

34S. Polikanov, letter to author, 28 Nov. 1985.

35D.L. Morgan, Jr., Ref. 1, p 530.

36D.L. Morgan, Jr., J. Brit. Interplan. Soc. **35**, 405 (1982).

37R.L. Forward, J. Brit. Interplan. Soc. **35**, 391 (1982); R.L. Forward, *Antiproton Annihilation Propulsion*, AFRPL TR-85-0334 (Air Force Astronautics Laboratory, Edwards AFB, Sept. 1985) 189 p.

[38]B.N. Cassenti, Ref. 1 p 574; AIAA/SAE/ASME/ASEE 23rd Joint Propulsion Conference, San Diego, 29 June - 2 July 1987; AIAA paper 84-1485, 20th Joint Propulsion Conference, Cincinnati, June 1984; G. Vulpetti and E. Pieragostini, paper IAF-86-178, 37th Congress of the International Austronautical Federation, Innsbruch, 4-11 October 1986 (Pergamon Press, New York, 1986); G. Vulpetti, paper IAF-83-397, 34th Congress of the International Astronautical Federation, Budapest, 9-15 Oct. 1983; B.W. Augenstein, *Some Examples of Propulsion Systems Using Antimatter* (The Rand Corporation, Santa Monica, July 1985); G.D. Nordley, paper IAA-87-609, 38th Congress of the International Astronautical Federation, Brighton, 10-17 Oct. 1987.

[39]J.B.A. Mitchell, Ref. 1, p 359; W.C. Stwalley, Ref. 1, p 373; R.L. Forward, Ref. 1, p 434.

[40]J.L. Calles, Ref. 1, p 566.

[41]A. Gsponer and J.-P. Hurni, Atomkernenergie - Kerntechnik **49**, No. 4, 198 (1987).

[42]H. Takahashi, Ref. 1, p 603; J. Rafelski, unpublished presentation at conference of Ref. 1.

[43]*Proceeding of the International Symposium on Muon Catalyzed Fusion (μCF-86)*, Ed. K. Nagamine, Tokyo, 1-3 Sept. 1986, (J.C. Baltzer,Basel,1987), 409 p., reprinted from Muon Catalyzed Fusion **1** (1987).

[44]B.G. Harvey, *Introduction to Nuclear Physics and Chemistry* (Prentice Hall, Englewood Cliffs, New Jersey, 1969) p 310.

[45]L.E. Porter and S.R. Bryan, Nucl. Instr. and Meth. **178**, 227 (1980); Radiat. Res. (USA) **97**, 25 (1984); L.E. Porter, Phys. Rev. B **22**,2221 (1980); G. Basbas, Nucl. Instr. and Meth. in Phys. Res. B **4**, 227 (1984); L.E. Porter and R.G. Jeppsen, Nucl. Instr. and Meth. **204**, 605 (1983); W. Brandt and G. Basbas, Phys. Rev. A **27**, 578 (1983); J. Lindhard, Nucl. Instr. and Meth. **132**, 1 (1976).

[46]Barkas effect: G. Gabrielse, X. Fei, L.A. Orozco, S.L. Rolston, R.L. Tjoelker, T.A. Trainer, J. Haas, H. Kalinowsky, W. Kells, Phys. Rev. A, Rapid Communications, in publication (1989). Multiple ionization cross sections: L.H. Andersen, P. Hvelplund, H. Knudsen, S.P. Møller, A.H. Sørensen, K. Elssener, K.-G. Rensfelt, and E. Uggerhøj, Phys. Rev. A **36**, 3612 (1987); L.H. Andersen, P. Hvelplund, H. Knudsen, S.P. Møller, A.H. Sørensen, K. Elssener, K.-G. Rensfelt, and E. Uggerhøj, Phys. Rev. Lett. **57**, 2147 (1986).

[47]A.M. Ermolaev, Ref. 10, p 375.

[48]M.H. Mørtir, A.L. Ford, J.F. Reading, and R.L. Becker, J. Phys. B: At. Mol. Phys. **15**, 1729 (1982).

[49]C.L. Longmire, *Elementary Plasma Physics* (Interscience Publishers, New York,1963) p 166, 174-175, 202-203.

[50]D.L. Morgan, Jr., paper IAA-88-554, 39th Congress of the International Astronautical Federation, Bangalore, 8-15 Oct. 1988, talk delivered by G. Vulpetti, to be published.

[51]L. Bracci, G. Fiorentini, and G. Pitzurra, Phys. Letts. **85B**, 280 (1979).

[52]D.L. Morgan, Jr., *Antiproton - Hydrogen Atom Annihilation*, AFRPL-TR-86-019, (Air Force Astronautics Laboratory, Edwards AFB, CA, May 1986) 17 p.

[53]M. Kimura and Mitio Inokuti, Phys. Rev. A **38**, 3801 (1988).

[54]G. Beckenstoss, in *Atomic Physics 10*, Ed. H. Narumi and I. Shimamura (North Holland, Amsterdam, 1987) p 147.

[55]E. Fermi and E. Teller, Phys. Rev. **72**, 399 (1947); A.S. Wightman, Phys. Rev. **77**, 521 (1950).

[56]J. Rafelski, private communication, 1987.

Positronium Ions and Molecules

Y. K. Ho

Department of Physics and Astronomy
Louisiana State University
Baton Rouge, Louisiana 70803 U.S.A.

ABSTRACT

Recent theoretical studies on positronium ions and molecules will be discussed. A positronium ion is a three-particle system consisting of two electrons in singlet spin state, and a positron. Recent studies include calculations of its binding energy, positron annihilation rate, and investigations of its doubly excited resonant states. A positronium molecule is a four-body system consisting of two positrons and two electrons in an overall singlet spin state. We will discuss the recent calculations of its binding energy against the dissociation into two positronium atoms, and studies of auto-detaching states in positronium molecules. These auto-dissociating states, which are believed to be part of the Rydberg series as a result of a positron attaching to a negatively charged positronium ion, Ps^-, would appear as resonances in Ps-Ps scattering.

POSITRONIUM IONS

In this talk I will describe two atomic systems involving positrons. They are positronium ions and molecules. For Ps^-, I will concentrate the discussions on the recent theoretical calculations of binding energy, annihilation rate, and autoionizing resonant states. In positronium molecules, I will discuss calculations of the ground state energy and the studies of auto-dissociating states.

A positronium negative ion (Ps^-) is a bound three-particle system consisting of two electrons and one positron which interact via Coulomb forces. The calculation of the binding energy of this system has a long history that can be traced back to the early work of Wheeler.[1] This system was observed for the first time in the laboratory by Mills.[2] Later he also measured[3] the positron annihilatin rate for Ps^-. The production of these positronium negative ions have stimulated intense theoretical investigations. In the last decade, several progress reports and review articles on Ps^- have appeared in the literature.[4–7] So here I will discuss mostly the recent advances since publication of these reviews. In many aspects the positronium negative ions have properties similar to those of hydrogen negative ions, H^-, a system which has been intensively studied by both theorists and experimentalists. Recently, the muonium ions, Mu^-, have also been observed.[8] These three systems differ in the mass of the positively charged particles. There are, however, many properties which are unique in Ps^- and have no counterparts in H^- and Mu^-. These properties involve the annihilation of the positrons in the positronium negative ions. On the practical side, the role that the positronium negative ions play in astrophysics and space physics has been suggested by Sivaram and Krishan.[9]

Let me first talk about the calculations of ground state energy for Ps^- and its annihilation rate. For a highly correlated atomic system such as Ps^-, it is essential for the wave functions to have accurate representation of the correlation effects. There are two types of wave functions used in recent years that are proven to be quite effective to describe Ps^-. One type is of the Hylleraas wave functions, as used by Bhatia and Drachman[10] (with two non-linear parameters),

and by Ho (with one non-linear parameter),[11]

$$\Psi = \sum_{k,\ell,m_{>0}} C_{k\ell m} exp\{-\alpha_1 r_{1p} - \alpha_2 r_{2p}\} r_{12}^k \left(r_{1p}^\ell r_{2p}^m + r_{1p}^m r_{2p}^\ell \right) . \tag{1}$$

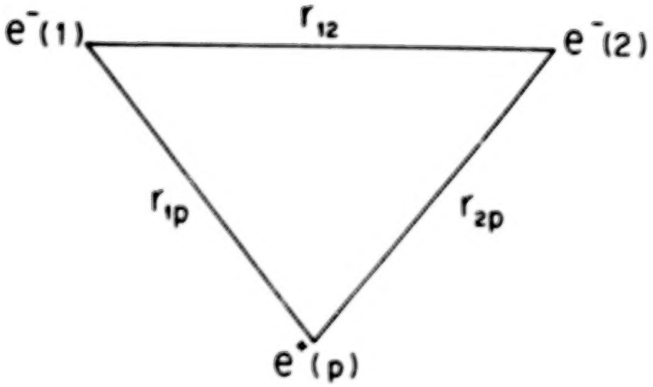

Fig. 1. Coordinate System for Ps^-.

The coordinate system is shown here in Fig. 1. The other type is the exponential variational expansion for the basis set with the form, as used by Petelenz and Smith,[12] and by Frolov and Yeremi[13],

$$\Psi = \frac{1}{\sqrt{2}}(1 + P_{12}) \sum_{i=1}^{N} C_i exp(-\alpha_1^{(i)} r_{2p} - \alpha_2^{(i)} r_{1p} - \alpha_3^{(i)} r_{12}) , \tag{2}$$

where P_{12} is the permutation operator for electrons 1 and 2. C_i are linear combination coefficients, and $\alpha_j^{(i)} (j = 1,2,3)$ were generated in a quasirandomly form from three intervals. Results calculated by using these functions are shown here in Table 1. The Ho (1989)[14] result is the extension of the Ho (1983) calculation with the basis set now extended to N = 715 terms ($\omega = k + \ell + m \leq 18$).

One of the experimentally interesting parameters is the annihilation rate, Γ, given in units of ns^{-1}

$$\Gamma = 2\pi\alpha^4 \left(\frac{c}{a_o}\right) \left[1 - \alpha\left(\frac{17}{\pi} - \frac{19\pi}{12}\right)\right] \frac{< \Psi|\delta(r_e - r_p)|\Psi >}{< \Psi|\Psi >} = 100.617 < \delta_{ep} > . \tag{3}$$

Table 1. Ground state energy of Ps^- (in Ry).

Ho (1983), Ref. 11 (125 term Hylleraas function, one non-linear parameter)	-0.524009790
Bhatia and Drachman (1983), Ref. 10 (220 term Hylleraas function, two non-linear parameters)	-0.5240101300
Frolov (1987), Ref. 14	-0.5240101404
Petelenz and Smith (1988), Ref. 12 (150 term exponential variational expansion)	-0.524010140
Ho (1989), Ref. 15 (715 term Hylleraas function)	-0.524010140
Frolov and Yeremin (1989), Ref. 13 (700 term exponential variation expansion)	-0.5240101404656 $\pm 1 \times 10^{-12}$

The lifetime of Ps^- against annihilation is

$$\tau = \frac{1}{\Gamma}. \tag{4}$$

In Eq. (3), the correction term proportional to α is due to the triplet lifetime[16] and the leading radiative correction to the singlet lifetime.[17] Once the energy-minimized wavefunctions are obtained, they can be used to calculate Γ by the use of equation (3). Some recent results are shown in Table 2. It is seen that they are compared quite well with the experimental measurement of $\Gamma = 2.09 \pm 0.09 ns^{-1}$ (Ref. 3). Furthermore, some progress for an improved measurement of the annihilation rate has recently been made.[18] This would stimulate further theoretical studies.

Table 2. Positron annihilation rate in Ps^-.

	Γ (nsec^{-1})	ν_{ep}	Ref.
Bhatia and Drachman 1983 (220 term Hylleraas function)	2.0861	0.50000	10
Ho 1983 (125 term Hylleraas function)	2.0850	0.4991	11
Ho 1989 (715 term Hylleraas function)	2.08613	0.50001	15
Mills (1983) experiment	2.09 ± 0.09		3

The qualities of the wavefunctions can be tested by calculating the electron-electron and electron-positron cusp values. For a system interacting through Coulomb forces, the average value of the cusp condition beween particles i and j is given by[19]

$$\nu_{ij} = \langle \Psi | \delta(r_{ij}) \frac{\partial}{\partial r_{ij}} | \Psi \rangle (< \Psi | \delta(r_{ij}) | \Psi >)^{-1} , \tag{5}$$

and the exact value for ν_{ij} is

$$\nu_{ij} = q_i q_j \mu_{ij} . \tag{6}$$

where q_i is the charge for the particle i and μ_{ij} is the reduced mass for particles i and j. The exact values for electron-electron and electron-positron conditions are hence +0.5 and -0.5 respectively. The positron-electron cusp values calculated in the recent calculations are also shown here in Table 2. It is seen that the cusp results are very close to the exact one. It also indicates that the positron-electron cusp values would give indications of the accuracy for annihilation rate calculations.

In addition to the lifetimes and annihilation rates, another experimentally interesting parameter for the positronium negative ion is the two-photon angular correlation function $P(\theta)$. In most of the angular correlation measurements only one component of the momentum distribution is measured. The angle between the two photons, measured in the laboratory frame, has a value of $\pi - \theta$. The relation between θ and q_3, the third component of the momentum, is $q_3 = mc\theta$, or $\theta = 7.3 \times 10^{-3}\, q_3$. The one-dimensional angular correlation function will have a form

$$P(q_3) = \int_{-\infty}^{\infty} \int_{-\infty}^{\infty} dq_1 dp_z S(q) \tag{7}$$

where

$$S(q) = | \int dr_{1p} e^{\,} exp(-iq \cdot r_{1p}) \Psi(r_{1p}, r_{2p}, r_{12}) |^2_{\substack{r_{12} = r_{1p} \\ r_{2p} = 0}} . \tag{8}$$

The angular correlations functions were calculated in Ref. 11. The full width at the half maximum, denoted by 2Δ, was $1.3994 \times 10^{-3} rad$. The smaller width of the angular correlation function for Ps^- is due to the following. Since the Ps^- ion is a loosely bound system, the momentum distribution of the Ps atom in Ps^- is smaller than the more tightly bound atomic counterparts. The angular correlation function for Ps^- is hence smaller. Furthermore, when the positron annihilates with one of the electrons in Ps^- to become two photons, a portion of the momentum of the two photons will be absorbed by the remaining electron because the mass of the electron is small.

We also reported a calculation on the two-photon-annihilation rates for the doubly excited resonant states in Ref. 20. The resonance positions were calculated by using the stabilization method.[21] A positronium negative ion in its ground state will, of course, eventually undergo the annihilation process. The annihilation of positrons in a doubly excited state of Ps^- presents an interesting question. The autoionization process is now also possible, as is the radiative cascade to a lower autoionizing state or to the ground state. The radiative lifetimes are related to the oscillator strengths for transitions between the upper and lower states. They are usually small for low Z systems. The lifetimes of these various processes are of obvious interest, since such information would play an important role for experimental observations of the doubly excited states.

Calculations of annihilation rates for doubly excited states in Ps^- were done in Ref. 20. Results are summarized here in Table 3. The autoionization lifetimes were obtained by using the method of complex-coordinate rotation.[22]

Table 3. Autoionization lifetimes and annihilation lifetimes for $^1S^e$ doubly excited states of Ps^- .

State	Autionization lifetimes (nsec)	Annihilation lifetimes (nsec)	Annihilation rate ($nsec^{-1}$)
2s2s	0.0005625	5.0277	0.1989
2s3s	0.002419	6.9204	0.1445
3s3s	0.0003225	23.474	0.0426
3s4s	0.0004398	32.895	0.0304
4s4s	0.0002016	80.000	0.0125

It is seen that for all the resonant states the system will have a greater probability to autoionize than to annihilate. Furthermore, when the quantum numbers of the outer electrons are the same, the annihilation rates decrease as $1/n^3$, as n represents the quantum numbers of the inner electrons. For example, the ratio of the annihilation rates for the 2s3s and $3s3s\,^1S^e$ states is $0.1445/0.0426 = 3.392$. The ratio of $(\frac{1}{2})^3/(\frac{1}{3})^3$ is 3.375. Similarly, the ratio of the annihilation rates for the 3s4s and $4s4s\,^1S^e$ states is $0.0304/0.0125 = 2.43$. The ratio of $(\frac{1}{3})^3/(\frac{1}{4})^3$ is 2.37. These results indicate that the annihilation of the positron in a doubly excited Ps^- takes place mostly with the inner electron since the overlap of the positronium S states also decreases as $1/n^3$. The findings in Ref. 20 were consistent with the earlier studies of the ground state of Ps^- that the positronium negative ion is a system of an electron loosely bound to a positronium atom.[23]

Autoionizing resonance states in Ps^- are very similar to those of H^-. They are both the result of dipole degeneracy of the excited states of target systems. The first theoretical study[24] of doubly excited resonance phenomena in Ps^- were carried out by using the method of complex coordinate rotation.[25] Several resonances associated with the $N = 2$ and $N = 3$ Ps thresholds were reported. Since then, resonances associated with the $N = 5$ Ps threshold have been calculated.[26] They are now summarized in Table 4.

In addition to the calculations of the S-wave doubly excited states using the method of complex coordinate rotation, other methods have also been used to study resonance phenomena in Ps^-. For states with $L > 0$, results are summarized in Table 5. They were obtained by using the hyperspherical coordinates[27] and by scattering calculations.[28] However, in the hyperspherical coordinate, no widths were calculated. Also, in Ref. 28, a resonance structure was obtained in the $^1P^o$ scattering calculation. None of the doubly excited resonant states has however been observed experimentally.

Table 4. **Doubly excited resonances of Ps^- associated with positronium excitation threshold N. Resonance energies and widths are expressed in Rydbergs.**

N	$^1S^e$			$^3S^e$		
	state	$-E_r$	Γ	state	$-E_r$	Γ
2	2s2s	0.1520608	0.000086	2s3s	0.12706	0.00001
	2s3s	0.12730	0.00002			
3	3s3s	0.070683	0.00015	3s4s	0.05873	0.00002
	3s4s	0.05969	0.00011			
4	4s4s	0.04045	0.00024	4s5s	0.03415	0.00002
	4p4p	0.0350	0.0003			
	4s5s	0.03463	0.00034			
5	5s5s	0.0258	0.00045			
	5p5p	0.02343	0.00014			

Table 5. **Doubly excited autoionizing states (with L > 0) of Ps^- below the N = 2 Ps threshold.**

	Botero (1988)[27] (Hyperspherical coordinate)	Ward, Humberston, and McDowell (1987)[28] (scattering calculation)	
	E(Ry)	E(Ry)	Γ(eV)
$^3P^o(1)$	-0.1456	-0.14662	0.0035
(2)		-0.12509	0.001
$^1D^e$	-0.13486		
$^1P^o$	-0.125174		

Figure 2 shows the current understanding of the energy levels for Ps^-. I should also point out that very recently, a resonance lying just above the Ps (N = 1) threshold was predicted by Melezhik and Vakajlovic.[29] However, Bhatia and Drachman[30] reported in this workshop that they did not find such a resonance. It seems the existence for this resonance has yet to be established.

One implication from the current understanding of doubly excited Ps^- states as shown in Fig. 2 is that more studies on highly excited (associated with high N of Ps thresholds) are called for. In atomic physics one of the latest theoretical discoveries is the underlying symmetry of the doubly excited resonances in H^- and in helium. The striking similarity between the doubly excited spectrum of a two-electron atom and that of a linear triatomic molecule (XYX) has been investigated by Kellman and Herrick.[31] In positronium negative ions, the study of the doubly excited resonances has just begun. Whether such highly symmetrical spectra will also be found in Ps^- is an open and interesting question.

It seems that a positronium ion does not have a $^3P^e$ state below the $Ps(N = 2)$ threshold, in contrast to the counterpart of H^-. Here, I am not going to talk about these studies in detail. Interested readers are referred to the original papers[10,32,33] and the recent reviews. Other theoretical studies on Ps^- include calculatins of photodetachment cross sections.[34,35]

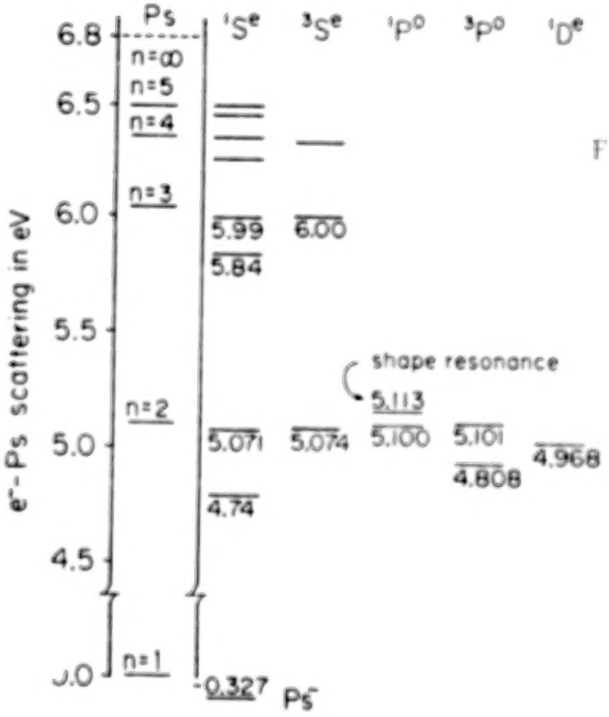

Fig. 2. Bound state and autoionizing states of Ps^-.

POSITRONIUM MOLECULES

Positronium molecules, Ps_2, is a system consisting of two positronium atoms (or a four-particle system consisting of two electrons and two positrons, and interacted via Coulomb forces). The first calculation that showed such a system does form a bound system was by Hylleraas and Ore.[36] They showed that the binding energy for Ps_2 is 0.116 eV. Over the years, several theoretical studies have appeared in the literature for this system.[36–41] Results are summarized in Table 6. Possible experimental studies of positronium molecules have been discussed by Mills.[42]

Table 6. Calculations of binding energies of positronium molecules.

Authors	Binding energy (Ry)	(eV)
Hylleraas and Ore 1947 (Ref. 36)	0.0085	0.116
Ore 1947 (Ref. 37)	0.009	0.122
Akimoto and Hanamura 1972 (Ref. 38)	0.0135	0.184
Brinkman, Rice, and Bell 1973 (Ref. 39)	0.0145	0.197
Lee, Vashista, and Kalia 1983 (Ref. 40)	0.03 ± 0.002	0.408 ± 0.027
Lee 1985 (Ref. 40)	0.0303 ± 0.0005	0.412 ± 0.007
Ho 1986 (Ref. 41)	0.0302	0.411

A variational calculation was carried out by myself.[41] I now discuss the work in the following. The Hamiltonian for this system was expressed as

$$H = \sum_{(i<j)} \left[-\left(\frac{1}{m_i} + \frac{1}{m_j}\right)\left(\frac{\partial^2}{\partial r_{ij}^2} + \frac{2}{r_{ij}}\frac{\partial}{\partial r_{ij}}\right) + \frac{2Z_iZ_j}{r_{ij}} \right] - \sum_{\substack{(i,j,k) \\ (j<k)}} \frac{2}{m_i}\cos(\theta_{ij,ik})\frac{\partial^2}{\partial r_{ij}\partial r_{ik}} , \quad (9)$$

with

$$\cos(\theta_{ij,ik}) = \frac{r_{ij}^2 + r_{ik}^2 - r_{jk}^2}{2r_{ij}r_{ik}}$$

where m_i and Z_i are the mass and charge of the particle i, respectively. Atomic units were used with energy expressed in Rydbergs. Figure 3 shows the coordinate system where a and b denote the positrons, and 1 and 2 the electrons. The interparticle coordinate r_{1a} represents the distance between the electron 1 and the positron a.

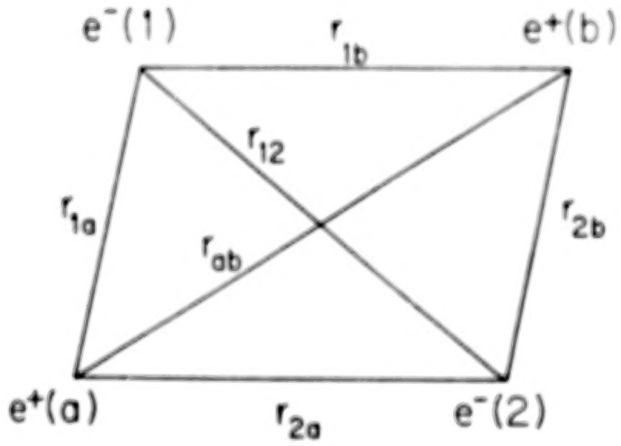

Fig. 3. Coordinate system for Ps_2.

A general form of wave function for positronium molecules is

$$\Psi = \sum C_{kmnsjl}\Big[r_{1a}^{k}r_{2a}^{m}r_{ab}^{n}r_{2b}^{s}r_{1b}^{j}r_{12}^{l}\,exp\Big(-c_1r_{1a}-c_2r_{2a}-c_3r_{ab}-c_4r_{2b}-c_5r_{1b}-c_6r_{12}\Big)$$

$$+\,r_{1a}^{m}r_{2a}^{k}r_{ab}^{n}r_{2b}^{j}r_{1b}^{s}r_{12}^{l}\,exp\Big(-c_2r_{1a}-c_1r_{2a}-c_3r_{ab}-c_5r_{2b}-c_4r_{1b}-c_6r_{12}\Big)$$

$$+\,r_{1b}^{k}r_{2b}^{m}r_{ab}^{n}r_{2a}^{s}r_{1a}^{j}r_{12}^{l}\,exp\Big(-c_1r_{1b}-c_2r_{2b}-c_3r_{ab}-c_4r_{2a}-c_5r_{1a}-c_6r_{12}\Big)$$

$$+\,r_{1b}^{m}r_{2b}^{k}r_{ab}^{n}r_{2a}^{j}r_{1a}^{s}r_{12}^{l}\,exp\Big(-c_2r_{1b}-c_1r_{2b}-c_3r_{ab}-c_5r_{2a}-c_4r_{1a}-c_6r_{12}\Big)\Big]$$

$$\times\frac{1}{\sqrt{2}}(\alpha_1\beta_2-\beta_1\alpha_2)\,\frac{1}{\sqrt{2}}(\alpha_a\beta_b-\beta_a\alpha_b)\,, \tag{10}$$

where α and β are the spin-up and -down wave functions, respectively. The wave function in the form of Eq. (2) is antisymmetric with respect to interchange of the two electrons or of the two positrons. To solve the necessary integrals involved in this extensive form of wave functions is not an easy task. Some simplications were hence made in Ref. 41. First, we omitted the symmetry of the two positrons, i.e., the last two terms in Eq. (2) were dropped. Secondly, we let $C_4 = C_5 = C_6 = 0$. The omission of the explicit exponential factors involving r_{1p}, r_{2p}, and r_{12} will be compensated by the use of extensive terms involving power series of such interparticle coordinates. Under these approximations, the wave function becomes

$$\Psi = \sum C_{kmnsjl}\Big[r_{1a}^{k}r_{2a}^{m}r_{ab}^{n}r_{2b}^{s}r_{1b}^{j}r_{12}^{l}\,exp\Big(-c_1r_{1a}-c_2r_{2a}-c_3r_{ab}\Big)$$

$$+\,r_{1a}^{m}r_{2a}^{k}r_{ab}^{n}r_{2b}^{j}r_{1b}^{s}r_{12}^{l}\,exp\Big(-c_1r_{2a}-c_2r_{1a}-c_3r_{ab}\Big)\Big]$$

$$\times\frac{1}{\sqrt{2}}(\alpha_1\beta_2-\beta_1\alpha_2). \tag{11}$$

Up to $N = 400$ terms were used in Ref. 41. The ground state energy is shown here in Table 7, together with cusp values for different pairs of charged particles. It is seen that the cusp values are quite close to the exact ones. Table 6 lists different calculations of binding energy of Ps_2 in the literature. Ref. 41 is a variational bound calculation and the result in Ref. 40 was obtained by using the Green's Function Monte Carlo method. This method, however, is not a bound calculation and has statistical errors. I should also point out that calculations of binding energy with considerable larger values (0.978 eV and 0.846 eV) also exist in the literature.[43,44] It appears that these calculations should be repeated. As for the variational calculation in Ref. 41, although the binding energy is reliable, the book is by no means closed. For example, wave functions that take into account of the proper symmetry for the two poistrons should be used (i.e., Eq. 10) in the future.

Table 7. Energy and cusp values for positronium molecules: $\omega = k + m + n + i + j$, with $m = 0$ (see Ref. 41)

	E (Ry)	ν_{1a}	ν_{12}	ν_{ab}	ν_{1b}
$\omega = 6, \ell \leq 4, N = 400$	-1.03021	-0.498	0.485	0.509	-0.479
Exact		-0.5	0.5	0.5	-0.5

Table 8 shows the average distances between various pairs of charged particles. One of the interesting results shown in Table 8 is that all the six interparticle distances seem to have the same value of $5.9a_o$ (if we assign a 10% uncertainty to $< r_{1b} >$). This suggests that on average, the four paticles form a triangular pyramid, with the two electrons occupying any two of the four vertices, and the two positrons occupying the other two. All the six edges have the same length of $5.9a_o$. In this arrangement the system is symmetric with respect to the interchange of the two electrons, or of the two positrons, as well as to the interchange of the two positronium atoms.

Table 8. Average distances (in a_o) between various pairs of charged particles (see Ref. 41)

$< r_{1a} > = < r_{2a} >$	$< r_{12} >$	$< r_{ab} >$	$< r_{1b} > = < r_{2b} >$
5.98	5.93	5.88	5.50

We have also recently begun a theoretical study of higher-lying resonant states of positronium molecules.[45,46] In some aspects, these high-lying states are similar to those in a positronium hydride, PsH. In PsH, it has been shown that Rydberg series do exist as a result of the positron attaching to the H^- ion.[47] Such Rydberg states, with the exception of the lowest S-wave state which lies below the $Ps + H$ threshold and becomes the ground state of PsH, would appear as resonances in $Ps - H$ scattering. We would, therefore, expect such Rydberg series to also exist in the Ps_2 molecules as a result of the positron attaching to Ps^- ions. Figure 4 shows the Coulomb potential between the positronium negative ion and the positron, and the resulting Rydberg series. The lowest state of the S-wave series also lies below the $Ps - Ps$ scattering threshold and becomes the ground state of the positronium molecules.[41] Higher members of the Rydberg states would lie in the $Ps - Ps$ scattering continuum and appear as resonances in $Ps - Ps$ scattering.

There is, however, a difference between resonances in $Ps - H$ scattering and $Ps - Ps$ scattering. In the latter case there are two Rydberg series since the total spin of the two positrons would form singlet or triplet spin state. In the former case there is one series for a given partial wave since the positron and proton are not identical. We located six members of resonances below the Ps^- threshold. Results are summarized in Table 9. It was suggested that three of them belong to a Rydberg series in which the two positrons form a singlet spin state and the other three members belong to a series in which the two positrons form a triplet spin state. In the former case the complex eigenvalues would appear as resonances in scattering between two orthopositronium (o-Ps) atoms or two parapositronium (p-Ps) atoms. In the latter case, the complex eigenvalues correspond to resonances between a p-Ps atom and an o-Ps atom. Figure 5 shows the resonance positions for these autodissociating states. It should be mentioned that the

classification of different spin states for the resonances in Table 9 is just tentative. For the wave functions we used in Ref. 46, it was not straightforward to identify the positron spin state to which a resonance belongs. Interestingly enough, the use of wave functions of Eq. (11) enabled us to obtain resonance parameters for the two series with different spin symmetries simultaneously.

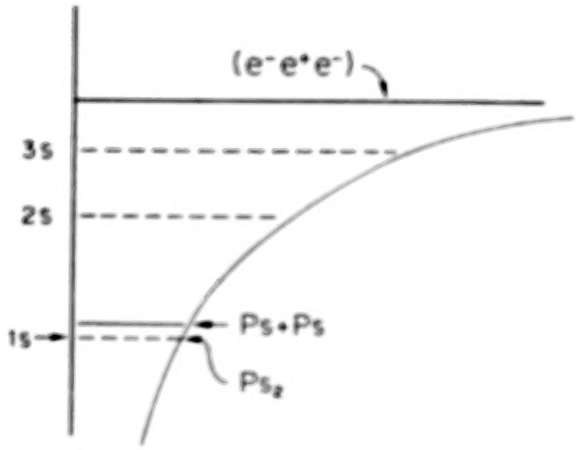

Fig. 4. Coulomb potential and Rydberg states between a positron and a positronium ion. Ignore the spins of the positrons for the time being.

Table 9. Autodissociating resonant states in Ps_2. (see Ref. 46)

Resonant state	E(Ry)	Γ(Ry)	E(eV)[a]	Γ(eV)
		Triplet series		
2S	-0.6588	0.0056	4.642	0.0762
3S	-0.592	0.0080	5.551	0.109
4S	-0.5625	0.0030	5.946	0.041
Series limit	-0.5240[b]		6.476	
		Singlet series		
2S	-0.626	0.016	5.089	0.216
3S	-0.580	0.012	5.714	0.163
4S	-0.553	0.016	6.082	0.216
Series limit	-0.5240[b]		6.476	

[a]Relative to $Ps - Ps$ scattering threshold.
[b]See Ref. 11 for example.

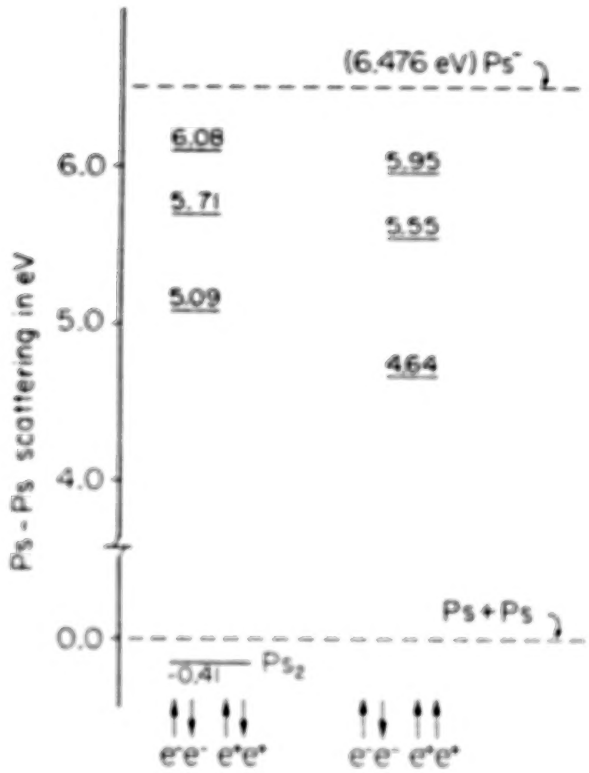

Fig. 5. Bound state and autoionizing states in Ps_2.

CONCLUDING REMARKS

In this talk, I have discussed the recent advances of theoretical studies for two atomic systems involving positrons. In closing, let me speculate what might happen in future workshops. Ever since the discovery of positrons, increasingly complicated atomic systems involving positrons have been studied. Various properties for positronium atoms (1 electron, 1 positron) and positronium ions (2 electron, 1 positron) were studied both experimentally and theoretically. The next complicated system is positronium molecules (2 electrons, 2 positrons), Ps_2. As I have mentioned in this talk that theoretical studies on this system have a long history, the observation for such species has yet to be done. The next complicated system would be "positronium molecular ions" (3 electrons, 2 positrons), Ps_2^-. Of course, we don't even know this five-body system would form a stable bound state. But in any case, the dissociative attachment process ($e^- + Ps_2 \rightarrow Ps + Ps^-$) would be of interest. Next, if we add one more positron to this system, this six-particle system (3 electrons, 3 positrons) may form a tri-atomic positronium molecule, Ps_3. Again, whether they would form a stable system is an interesting question. Furthermore, if we extend our imagination, we would ask what happens to a system consisting of n positronium atoms (n electrons, n positrons). Would they form positronium clusters? Perhaps in future positron workshops, some of these questions about such exotic species would be answered.

ACKNOWLEDGEMENTS

This work was supported in part by the U. S. National Science Foundation.

REFERENCES

1. J. A. Wheeler, Ann. N. Y. Acad. Sci. 48, 219 (1946).
2. A. P. Mills, Jr., Phys. Rev. Lett. 46, 717 (1981).
3. A. P. Mills, Jr., Phys. Rev. Lett. 50, 671 (1983).
4. For references up to 1982, see D. M. Schrader, in *Positron Annihilation*, edited by P. G. Coleman, S. C. Sharma, and L. M. Diana (North-Holland, Amsterdam, 1982), P. 71.
5. M. R. C. McDowell in *Positron (Electron)-Gas Scattering*, edited by W. E. Kauppila, T. S. Stein, and J. M. Wadehra (World Scientific, Singapore, 1985), p. 11.
6. J. W. Humberston, Adv. in Atomic and Mole. Phys. 22, 1 (1986).
7. R. J. Drachman in *Atomic Physics with Positrons*, edited by J. W. Humberston and E. A. G. Armour (Plenum, New York, 1987), p. 203.
8. Y. Kuang et al., Phys. Rev. A 35, 3172 (1987).
9. C. Sivaram and V. Krishan, Astron. Space Sci. 85, 31 (1946).
10. A. K. Bhatia and R. J. Drachman, Phys. Rev. A 28, 2523 (1983).
11. Y. K. Ho, J. Phys. B 16, 1530 (1983).
12. P. Petelenz and V. H. Smith, Jr., Phys. Rev. A 36, 5125 (1987).
13. A. M. Frolov and A. Yu Yeremin, J. Phys. B 22, 1263 (1989).
14. A. M. Frolov, Zh. Eksp. Teor. Fiz. 92, 1959 (1987).
15. Y. K. Ho, to be published (1989).
16. A. Ore and J. L. Powell, Phys. Rev. 57, 1696 (1949).
17. I. Harris and L. M. Brown, Phys. Rev. 105, 1656 (1957).
18. A. P. Mills, Jr. 1989, see this proceeding.
19. T. Kato, Commun. Pure Appl. Math. 10, 151 (1957); D. P. Chong and D. M. Schrader, Mol. Phys. 16, 137 (1969).
20. Y. K. Ho, Phys. Rev. A 32, 2501 (1985).
21. H. S. Taylar, Adv. Chem. Phys. 18, 91 (1970).
22. Y. K. Ho, Phys. Lett. 102A, 348 (1984).
23. R. J. Drachman, Can. J. Phys. 60, 494 (1982).
24. Y. K. Ho, Phys. Rev. A 19, 2347 (1979).
25. Y. K. Ho, Phys. Rep. 99, 1 (1983).
26. Y. K. Ho, Phys. Letts. 102A, 348 (1984).
27. J. Botero, A. Phys. D 8, 177 (1988); Phys. Rev. A 35, 36 (1987).
28. S. J. Ward, J. W. Humbertson, and M. R. C. McDowell, J. Phys. B 20, 127 (1987).
29. Y. S. Melezhik and F. R. Vukajlovic, Phys. Rev. A 38, 6426 (1988).
30. A. K. Bhatia and D. J. Drachman, 1989, see this proceeding.
31. M. E. Kellman and D. R. J.Herrick, Phys. Rev. A 22, 1536 (1980).

32. A. P. Mills, Jr., Phys. Rev. A 24, 3242 (1981).

33. A. K. Bhatia and R. J. Drachman, Phys. Rev. A 35, 4051 (1987).

34. A. K. Bhatia and R. J. Drachman, Phys. Rev. A 32, 3745 (1985).

35. J. Botero and C. H. Greene, Phys. Rev. Lett. 56, 1366 (1986).

36. E. A. Hylleraas and A. Ore, Phys. Rev. **71**, 493 (1947).

37. A. Ore, Phys. Rev. **71**, 913 (1947).

38. O. Akimoto and E. Hanamura, Solid State Commun. **10**, 253 (1972).

39. W. F. Brinkman, T. M. Rice, and B. Bell, Phys. Rev. B **8**, 1570 (1973).

40. M. A. Lee, P. Vashista, and R. K. Kalia, Phys. Rev. Lett. **51**, 2422 (1983); M. A. Lee (private communications).

41. Y. K. Ho, Phys. Rev. A 33, 3584 (1986).

42. A. P. Mills, Jr., in *Positron Scattering in Gases*, edited by J. W. Humberston and M. R. C. McDowell (Plenum, New York, 1984), p. 121.

43. E. R. Sharma, Phys. Rev. 171, 36 (1968).

44. W. T. Huang, Phys. Stat. Sol. (b) 60, 309 (1973).

45. Y. K. Ho, Phys. Rev. A 34, 1768 (1986).

46. Y. K. Ho, Phys. Rev. A 39, 2709 (1989).

47. R. J. Drachman, Phys. Rev. A 19, 1900 (1979).

SEARCH FOR RESONANCES IN POSITRON-ATOM SYSTEMS

A. K. Bhatia and Richard J. Drachman
Laboratory for Astronomy and Solar Physics
Goddard Space Flight Center
Greenbelt, MD 20771

ABSTRACT

No one likes to see a scattering cross-section curve that is too smooth; it is much more interesting to find bumps and wiggles and most interesting if it is possible to understand their cause. Several types of resonances have been clearly established in positron-containing systems: those lying just below a degenerate threshold[1] (like 2s-2p in hydrogenic atoms or ions) and those representing Coulomb bound states in a re-arranged channel[2] (like Ps + H $\rightarrow$ e^++H^-.) Recently, two new sorts of resonances have been reported for which the resonant mechanism is not clear. The first[3] is a very low-lying resonance in the e-Ps system (obtained by an adiabatic expansion method), and the second[4] is a similarly low-lying two-channel resonance in the e^+-H system (obtained by a close-coupling technique.) These developments encouraged us to examine such systems using the standard methods of stabilization and complex rotation. Most of our results are negative; we do not verify the low-lying resonances in either system. Some indication of new resonances in the e^+-He^+ system is found; this may be caused by the attraction between Ps in the n=2 state and the He^{++} nucleus.

METHOD

The Hamiltonian for the three-body systems of interest is the following

$$-\sum_{i=1}^{3} \frac{1}{m_i} \nabla_i^2 + \sum_{i<j=1}^{3} \frac{2Z_{ij}}{r_{ij}} ,$$

where the three particles are indicated in an obvious way by subscripts. We then proceed to obtain approximate eigenvalues of this Hamiltonian by the usual variational technique, using a standard Hylleraas type of trial function.

If we were looking for bound states this would be the end of the story. We are, however, interested here in resonances; this changes the situation considerably. There are two ways to use the variational method in a search for resonances, and we use both. These are the stabilization and complex rotation methods. The first of these is the simpler one, and it is usual to apply it first; if an indication of possible resonant structure is found the second may then be applied.

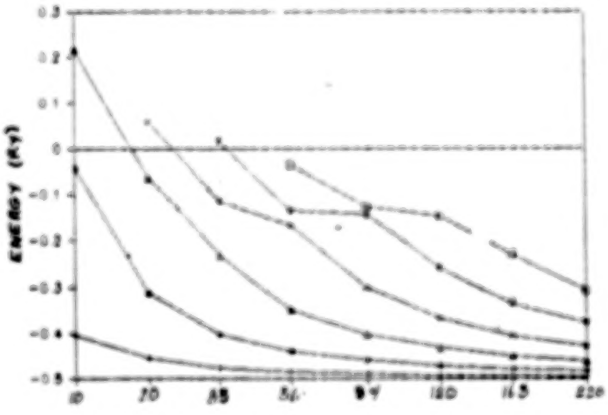

Figure 1

In the stabilization method one proceeds just as if one were looking for bound states but tries to find energy levels that are not very sensitive to the number of terms retained in the Hylleraas expansion. If there is a resonance at an energy where only a single channel is open, then a good indication would be an avoided crossing of two energy levels. A stabilized or

slowly decreasing eigenvalue would be successively passed by rapidly decreasing energy levels. This is illustrated in Fig.1, which is the case of electron-positronium S-wave scattering in the electronic singlet state (m_1=1, Z_{12}=1, Z_{13}=Z_{23}=-1.) The clear avoided crossings just below the n=2 level of Ps at E=-0.125 Ry is the first of an infinite series of Feshbach resonances that are well understood to be due to the degeneracy of that level. In Ref.3 the existence of a resonance just above the elastic threshold is suggested; there is clearly no support for this in the present work.

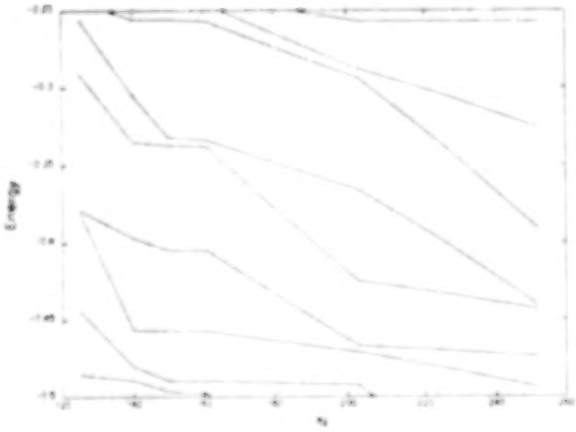

Figure 2

In Fig.2 we show the same sort of diagram for the case of S-wave positron-hydrogen scattering (m_1=m_2=1, m_3=∞, Z_{12}=Z_{23}=-1, Z_{13}=1.); Again it is clear that there is a stabilized eigenvalue just below the n=2 threshold in hydrogen corresponding to the first of an infinite series of Feshbach resonances[5] produced by the degeneracy of the n=2 levels. Although this resonance lies in a region where two channels are open (e^+-H and Ps-H^+) there is no possibility of confusing the stabilized energy with an open threshold. Notice, however, that there is an indication of a second resonance just <u>above</u> the Ps threshold at E=-0.5 Rydberg. Is it possible that this corresponds to one of the resonances reported in Ref.4? Experience has taught us that it is most likely for an apparently stabilized energy lying above an open threshold to represent an ordinary elastic scattering state predominantly involving that particular channel; this is especially likely when there is no apparent mechanism for forming a resonance at that energy. (In this case only a shape resonance would be possible, and for S-wave scattering it is hard to see where an effective barrier in the potential could originate.) To be more certain of the situation we turn to the complex rotation method.

This method is based on carrying out the <u>dilatation transformation</u>

$$\mathbf{r}_i \rightarrow \mathbf{r}_i e^{i\theta}$$

which is equivalent to multiplying the potential energy part of Eq.1 by $e^{-1\theta}$ and the kinetic energy part by $e^{-2i\theta}$. This analytically continued Hamiltonian is then diagonalized as before to obtain complex eigenenergies; since we use real basis functions the expansion coefficients must now be complex. If these energies are now plotted on the complex energy plane, they should behave as follows. True bound states are represented by points on the real axis, and ordinary scattering states are points that lie (in principle) along "rotated cuts" beginning at each target threshold on the real axis and making an angle -2θ with that axis. Most importantly, points representing resonances, usually hidden on the second Riemann sheet, are revealed by the transformation; they should be independent of the angle θ and are complex. It is clear that true resonances should be well differentiated from ordinary scattering states, but in practice this requires quite large basis sets.

In Fig.3 we show the energy plane for the e^+-H system discussed above where θ=10.3° and N=161. The cuts (rotated through an angle -2θ)

corresponding to the first two thresholds in H and the ground state of Ps have been plotted, and one can see the points that approximately lie along them; the higher cuts are better represented in this case because of our particular choice of non-linear parameters in the trial function. There is no clear sign of an isolated point above the Ps threshold that might be a resonance although Doolen's resonance[5] is visible just below the n=2 threshold. Probably the "stabilized" energy that appeared in Fig.2 is in reality one of the points lying on the Ps cut; such points slide down the cut as N is increased but slow down as they approach the threshold. This is the reason for doubting the reality of apparent resonances lying close above a target threshold.

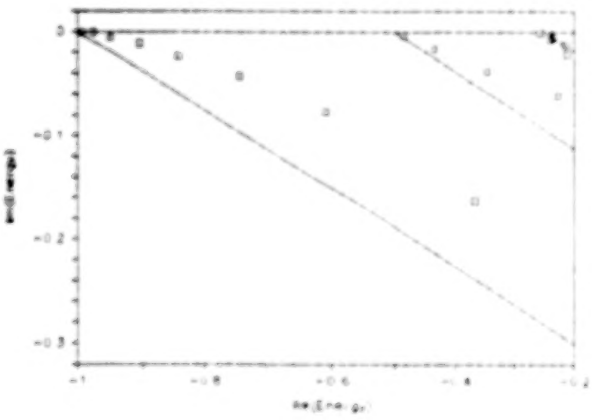

Figure 3

We made one final attempt to find simple new resonances by examining the e^+-He^+ system. Although the same degeneracies exist as in the e^+-H case, the repulsive Coulomb force is so dominant for large separations that the Feshbach resonances below target atom thresholds are unlikely to appear. But such resonances are probable below the degenerate thresholds in the Ps-He^{++} channel; because of the increased charge these should be lower lying than in the Ps-H^+ case. So far, we have found indications of two such resonances at E=-.73 and E=-.39 Ry. These lie very far below their apparent "parent" threshold at E=-.125 Ry; the first is below the Ps ground state but above the two lowest states of He^+. Our next attack on this problem will involve the Feshbach projection operator technique[6] which should be definitive.

---

1. Y. K. Ho, Phys. Lett. **120A**, 348 (1984).

2. R. J. Drachman and S. K. Houston, Phys. Rev. A **12**, 885 (1975); Y. K. Ho, Phys. Rev. A **17**, 1675 (1978).

3. V. S. Melezhik and F. R. Vukajlovic, Phys. Rev. A **38**, 6426 (1988).

4. M. Basu, M. Mukherjee, and A. S. Ghosh, J. Phys. B **22**, 2195 (1989).

5. G. D. Doolen, J. Nuttall, and C. Wherry, Phys. Rev. Lett. **40**, 313 (1978); L. T. Choo, M. C. Crocker, and J. Nuttall, J. Phys. B **11**, 1313 (1978).

6. H. Feshbach, Ann. Phys. (N.Y.) **19**, 287 (1962)

RESONANCES IN LOW-ENERGY POSITRON–ALKALI SCATTERING

M. Horbatsch, S. J. Ward†, R. P. McEachran and A. D. Stauffer
Department of Physics, York University, Toronto, Canada, M3J 1P3

ABSTRACT

We have performed close-coupling calculations with up to five target states at energies in the excitation threshold region for positron scattering from Li, Na and K. We have discovered resonances in the $L = 0$, 1 and 2 channels in the vicinity of the atomic excitation thresholds. The widths of these resonances vary between 0.2 and 130 meV. As well we have found evidence for the existence of positron–alkali bound states in all cases.

INTRODUCTION

Our previous calculations of the total and excitation cross sections[1–3] for e^+– alkali scattering are in reasonable agreement with experiment[4–7] and similar to electron scattering calculations. We have concentrated recently on the detailed study of phase shifts and eigenphase sums in the region of very low energies.[8]

One interesting observation is that for all three alkali atoms under study, namely Li, Na and K, the s-wave phase shifts start at a positive multiple of π rad. This is to be contrasted with similar electron scattering calculations where the phase shift approaches zero at zero energy.[9] The behaviour, just below the first excitation theshold, of our s-wave phase shifts for Na and K is, however, similar to that observed in relativistic R matrix calculations of e^-–Cs scattering.[10] If Levinson's theorem holds for these systems (it is not valid for electron scattering due to exchange) then this implies that there are stable (e^+–alkali) bound states. However, since positronium formation is energetically allowed at zero energy, these states may be embedded in the continuum of the Ps–alkali$^+$ system.

RESULTS

The $L = 0$, 1 and 2 resonances found in our calculations are summarized in table 1. It is not clear how these resonances will be affected by the inclusion of positronium channels in the close-coupling expansion. A study of the possibility of e^+–alkali bound states ideally would be performed using either the complex coordinate method[11] or the hyperspherical coordinate method.[12,13] It is expected that, due to the ns–np level degeneracy of positronium, additional resonances associated with excited positronium configurations will appear.[14]

TABLE 1. Resonance parameters for positron scattering from Li, Na and K in the close-coupling approximation. Resonance positions are given in eV, full widths in meV.

	Li		Na		K	
	E_{res}	Γ	E_{res}	Γ	E_{res}	Γ
S(1)	1.86 *	35	1.985	0.4	1.5	1.7
S(2)	3.01	40	3.195	0.2	2.45	0.54
S(3)	3.365	1	3.62	4		
P(1)	3.11	130	2.065	6	1.57	1.8
P(2)			3.124	32		
D(1)	3.19	110	3.2	30		

* This resonance features a variation in the eigenphase sum of only 2 rad.

Below the ns–np threshold we observe s-wave and p-wave resonances in both Na and K with widths in the meV range. The inclusion of the 3d as well as the $(n+1)$s states is crucial in order to obtain these resonances. Since the e^+–alkali system has not been studied in detail for bound states, it is difficult to classify the resonances. The necessity of including the above mentioned states in the close-coupling expansion indicates that the dipole polarization potential alone is not sufficient but that contributions from the quadrupole polarization potential are also important in order to obtain resonances. Since more than one state in the close-coupling expansion contributes to the development of these resonances it is also evident that the electronic wavefunction for these quasi-bound Ps–alkali$^+$ states consists of a superposition of several target states. Similarly the positronic wavefunction is expected to be complicated.

In figure 1 we show the contributions to the elastic cross section for e^+–Na scattering from the lowest four partial waves below the "resonant" 3s–3p excitation threshold. It is clear that the s-wave resonance which is situated over 0.1 eV below this threshold will be hard to measure due to its small width and the small overall contribution of that partial wave to the total cross section at this energy. The p-wave resonance, however, with its relatively broad width should be detectable once positron scattering measurements achieve energy resolutions which are comparable to those of electron scattering.

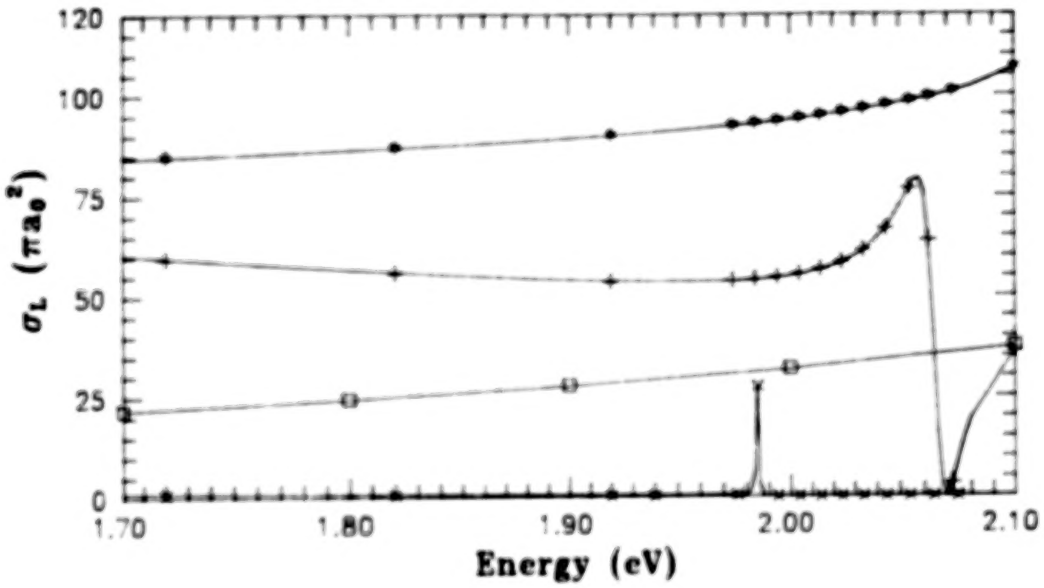

FIG. 1. Partial wave elastic cross sections (in πa_0^2) for $L = 0$, ×; $L = 1$, +; $L = 2$, • and $L = 3$, □, e^+–Na scattering in the (3s–3p–4s–3d–4p) model potential close-coupling approximation.

The shape of this resonance is somewhat different from the corresponding one in the e^+–K system; there the p-wave resonance appeared as a fully destructive resonance due to the fact that in the vicinity of the resonance the contribution of the p-wave to the cross section was close to its maximum possible value.

ACKNOWLEDGMENTS

We wish to thank Professors T. S. Stein, W. E. Kauppila and Dr. C. K. Kwan for valuable discussions. This work was supported by the Natural Sciences and Engineering Research Council of Canada.

† Present address: Department of Physics and Astronomy, University of Tennessee, Knoxville, TN 37996-1501, U.S.A.

[1] S. J. Ward, M. Horbatsch, R. P. McEachran and A. D. Stauffer, J. Phys. B. **21**, L611, (1988).

[2] ——, J. Phys. B. **22**, 1845, (1989).

[3] ——, Nucl. Instrum. Methods (1989), in press.

[4] T. S. Stein, R. D. Gomez, Y.-F. Hsieh, W. E. Kauppila, C. K. Kwan and Y. J. Wan, Phys. Rev. Lett. **55**, 488, (1985).

[5] T. S. Stein, M. S. Dababneh, W. E. Kauppila, C. K. Kwan and Y. J. Wan, *Atomic Physics with Positrons*, ed. J. W. Humberston and E. A. G. Armour (New York: Plenum) p. 251, (1988).

[6] C. K. Kwan, W. E. Kauppila, R. A. Likaszew, S. P. Parikh, T. S. Stein, Y. J. Wan and M. S. Dababneh, Phys. Rev. A, (1989), submitted.

[7] T. S. Stein, C. K. Kwan, W. E. Kauppila, R. A. Likaszew, S. P. Parikh, Y. J. Wan and M. S. Dababneh, *Proc. of the Workshop on Annihilation in Gases and Galaxies*, to be published.

[8] S. J. Ward, M. Horbatsch, R. P. McEachran and A. D. Stauffer, J. Phys. B. **22**, (1989), submitted.

[9] D. W. Norcross, J. Phys. B. **4**, 1458, (1971).

[10] N. S. Scott, K. Bartschat, P. G. Burke, O. Nagy and W. B. Eissner, J. Phys. B. **17**, 3775, (1984).

[11] Y. K. Ho, Phys. Rep. **99**, 1, (1983).

[12] E. Pelikan and H. Klar, Z. Phys. A **310**, 153, (1983).

[13] Y. K. Ho and C. H. Greene, Phys. Rev. A **35**, 3169, (1987).

[14] M. Mittleman, Phys. Rev. **152**, 76, (1966).

Positronium Formation in $e^+ + H^-$ Collisions

Jack C. Straton
Department of Physics
Cardwell Hall
Kansas State University
Manhattan, KS 66506

Richard J. Drachman
Code 681
Goddard Space Flight Center
Greenbelt, MD 20771

I. ABSTRACT

Cross sections for positronium formation by capture from the negative hydrogen ion are given. Orthogonalization corrections to the Coulomb (First) Born Approximation (CBA) differential and total cross sections are calculated using approximate H^- wave functions of both Löwdin[1] and Chandrasekhar.[2]

The present calculation of the CBA cross sections using the post interaction for Löwdin's wave function (LCBAPS) disagree with the calculation of Choudhury, Mukherjee, and Sural (CMS), whereas our results using the prior interaction agree. Thus, where CMS found an order of magnitude post-prior discrepancy in the differential cross sections except at forward angles, and a markedly different shape to the minima, the present post and prior results differ by 1% to 10% at 100 eV, and the minima have the same shape and occur within one degree of each other. Chandrasekhar's "open-shell" wave function, which is superior to Löwdin's in bound-state problems since it gives a negative binding energy, gives post and prior cross sections that are almost indistinguishable at this energy and 1/2 to 2/3 as large as the LCBA.

Various methods of orthogonalizing the unbound projectile to the possible bound states are considered. It is found that treating the atomic nuclei as if they were isotopic spin projections[4] of a single type of "nucleon" gives cross sections that are an improvement over the CBA.

II. INTRODUCTION

Reliable cross sections for the various positronium (Ps) formation processes are essential for an accurate calculation of the width of the .511 MeV annihilation line that has been observed in the region of the galactic center,[5] in solar flares,[6] and in planetary nebulae.[7] In the transition regions of planetary nebulae the concentration of the negative hydrogen ion[8] should be large enough for the reaction

$$e^+ + H^- \rightarrow Ps(nl) + H(1s) \tag{1}$$

to make an important contribution to the line width.[9] Furthermore, because this reaction is exothermic, it appears to be the dominant mechanism for positronium formation at energies below the 6.8 eV positron kinetic energy threshold for electron capture from neutral hydrogen even in regions where the H^- density is low.

The present calculation relies on the exact treatment of the three species of bound states inherent in Fock-Tani representation. Also included is the further presumption,[4] which produced remarkable agreement between the orthogonalized first order calculation[11] of charge transfer from hydrogen and the (presumably exact) variational result,[12] of treating the proton and positron as isospin-like projections (of different mass) of a single species of "nucleon."

III. ORTHOGONALIZATION

In scattering processes involving bound states, one must subtract the projection of the translational states of free particles onto the corresponding bound states if the contribution of these particles to the amplitude is not to be counted twice. Fock-Tani representation[13] has been a powerful tool for generating these orthogonalization corrections. In this representation the reactants, intermediate states, and products are treated symmetrically,and composites are treated exactly within a single second-quantized Hamiltonian. Unbound particles are *exactly* orthogonal to bound states, and all interactions contain the proper orthogonalization subtractions so that free particles do not have sufficient energy to bind (this binding energy is accounted for in the asymptotic Hamiltonian), and assuring that there is no double counting.

Because the Lippmann-Schwinger series for the Fock-Tani T-matrix contains higher order contributions at each

order than does the standard Born series, one has the hope of improved results at each order. Ojha *et al.*[14] have calculated the first-order Fock-Tani cross sections for the reaction

$$H^* + H \rightarrow H + H^* \tag{2}$$

and have obtained good agreement with experiment[15] for differential angles within 1 mrad of the forward direction at 25, 60, and 125 keV and for total cross sections at energies greater than 10 keV. They noted that the orthogonalization correction substantially cancels the internuclear potential. Straton[16] has shown that excluding these p-p terms yields Fock-Tani cross sections that are 18% smaller than when these terms are included. In contrast, the Brinkman-Kramers result,[17] which excludes the p-p term, is 1000% larger than the first Born total cross section that includes this term.[18] Thus the Fock-Tani Hamiltonian produces substantial agreement *at first order* between experiment and Wick's observation[18] that the internuclear potential should play a negligible role in *exact* calculations of this process.

Finally, it may be seen that the *first-order* Fock-Tani differential cross section is virtually identical to that of the *second-order* boundary-corrected Born approximation[19] (B2B) at 125 keV. This correspondence both affirms the appropriateness of testing the lowest-order Fock-Tani theory in problems in which generic first-order theories would not be expected to be reliable, and requires a deeper study of the question of why it should do so well. In particular, is there a fundamental relation between the orthogonalization process that produces free-particle (continuum) states by subtracting off their Coulomb projections onto the bound states, and cancels the internuclear interaction in the scattering region, and the Coulomb boundary correction process that gives the correct asymptotic states?

IV. ISO-ORTHOGONALIZATION

The obvious region in which a first-order theory might not be expected to be reliable is at low energies. Straton[16] has calculated the Fock-Tani total cross section for the reaction

$$e^* + H \rightarrow Ps(1s) + H(1s) \tag{3}$$

and obtained a result that was larger than the first Born approximation (FBA), whereas the (presumably exact) variational result of Brown and Humberston[12] was smaller than the FBA.

This failure was due to an anomaly of the product form of the Fock-Tani transformation, which does not produce orthogonalizations with respect to all species of bound states. This was immaterial in the reaction (2) since the initial and final bound-state species were identical.

Straton and Girardeau[4] were able to generalize the Fock-Tani transformation on the two-nucleon, one-electron Hilbert space to produce a T-matrix for either (2) or (3) that was post-prior symmetrical. This was accomplished by thinking of the two atomic nuclei as isospin-like projections of a single species of "nucleon," just as in nuclear physics it is useful to think of the proton and the neutron as isospin projections of a single species of nucleon. The consequence of this way of viewing the system is an upleveling of the nucleon-exchange contribution to the scattering (elastic and inelastic) amplitude, as in Fig. 1.

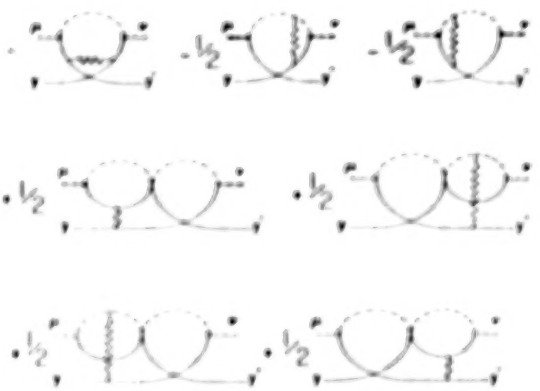

FIG. 1. Proton exchange terms in the Coulomb and orthogonalization interactions in proton-hydrogen scattering. The solid lines are proton propagators, the dashed line is the electron propagator, and the doubled line is the hydrogen atom (composite elementary particle) propagator. Time flows right to left so that the first term represents breakup of a bound-state with quantum numbers ν followed by formation of bound-state μ due to interaction with the exchanged proton. The last two terms contain the post and prior orthogonalization projectors $\mathcal{C}$.

to a reactive amplitude. Since exchange essentially amounts to a reactive process, it is not surprising that Fig. 1 may be promoted to a reactive matrix element by promoting an "effective" difference between incoming and outgoing free particles to a true difference through the use of an isotopic spin formalism.

Girardeau and Lo[11] applied this iso-orthogonalized matrix element to reaction (3) with superb agreement with the variational result of Brown and Humberston[12], reproduced in Table I.

Note that Fig. 1 is the average of the post and prior interaction amplitudes, but that neither the post or prior Fock-Tani probabilities, nor the average of the probabilities without interference gives a good result in Table I.

V. THE FOCK-TANI HAMILTONIAN FOR TWO NUCLEONS AND TWO ELECTRONS

One may develop a Fock-Tani Hamiltonian for a system that contains two nucleons and two electrons using the product form of the transformations that orthogonalize to the three bound species in (1). By working in a coordinate system in which one atomic nucleus is fixed at the origin, and therefore ceases to be a dynamic particle,[16] the unitary operator that transforms the Fock Hamiltonian into the subspace in which the three bound states may be treated as elementary particles may be compounded by the product

$$\hat{U} = \hat{U}_A \hat{U}_B \hat{U}_E \ , \tag{4}$$

where $A = Ps$, B is the state with two electrons bound to the origin, and E is the state with one electron bound to the origin, as in Fig. 2.

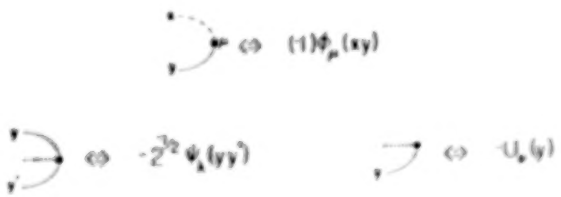

FIG. 2. Diagram correspondences for the positronium wave function, the states in which two electrons are bound to the origin, and the state in which one electron is bound to the origin. The solid lines represent electron propagators, the dashed line represents a positron propagator, and the nondynamical nucleus fixed at the origin is represented by the dotted line.

Then by interchanging the meanings of the electron and proton propagators in the Hamiltonian given by Straton and Girardeau[4], the first and most difficult transformation is at hand. Under the second transformation, the electron propagator transforms as in Fig. 3.

FIG. 3. Transformation orthogonalizing the electron propagator to the states in which two electrons are bound to the origin. The triple line represents the (composite elementary particle) 2-electron bound state propagator.

Under the third transformation, the electron propagator transforms as in Fig. 4

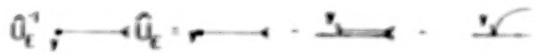

FIG. 4. Transformation orthogonalizing the electron propagator to the states in which one electron is bound to the origin. The double line represents the (composite elementary particle) 1-electron bound state propagator.

Then the (product form) Fock-Tani Hamiltonian on the 2-nucleon, 2-electron Hilbert space is given in Fig. 5 and Fig. 6.

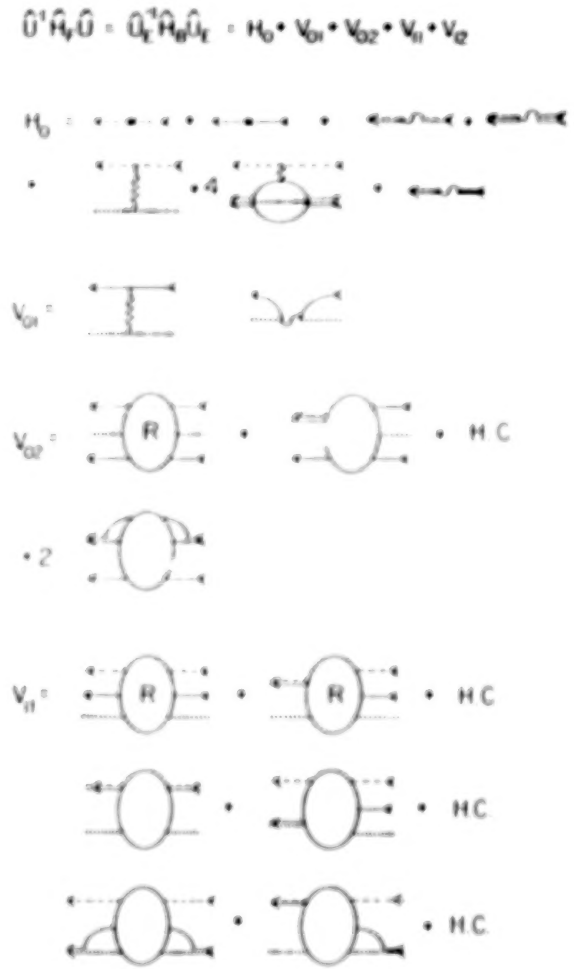

FIG. 5. The Fock-Tani Hamiltonian on the 2-nucleon, 2-electron Hilbert space. All free propagators are integrated over and all bound state propagators are summed over. The bound state energy is indicated by the ~.

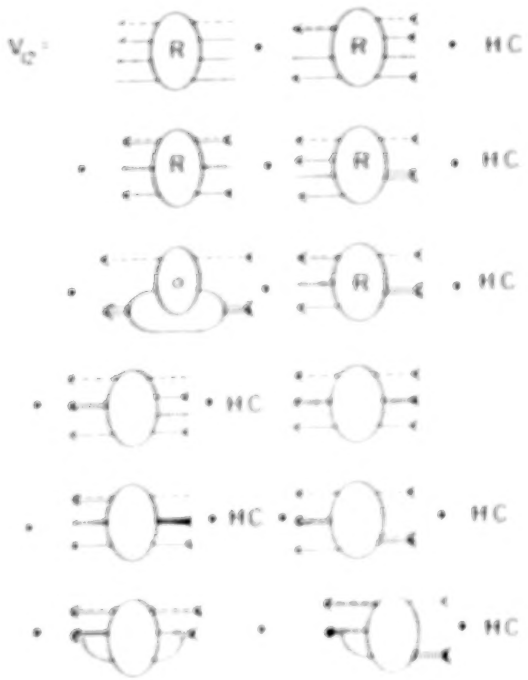

FIG. 6. The 2-nucleon, 2-electron Foch-Tani interaction terms.

The oval in the last term in Fig. 6, which is the interaction potential for (1), is given explicitly in Fig. 7. The second oval in Fig. 7 is given by Fig. 8. The first oval in Fig. 6 is given by the first four terms of Fig. 8 with the y' propagator replaced by the dotted line representing the nucleon fixed at the origin.

Thus the algebraic translation of Fig. 8 in Fig. 7, after the asymptotic states select the bound state quantum numbers from the sums, is[4,20]

$$\int dX dX' dX'' \{\delta(X' - X'')[V(XX') + V(X'x)]\phi_\rho(Xx) - \delta(X' - X'') \int dY dy \phi_\rho^*(Yy)[V(X'Y) + V(X'y)] \times \Delta(Yy, Xx) + \int dy \phi_\rho^*(X'y)[H(X'y)\Delta(X''y, Xx) + \frac{1}{2}\Delta(X''y, Xx)H(Xx)] + \int dy \phi_\rho^*(X'y)\left[\frac{1}{2}V(X'x) + V(X'X'') + \frac{1}{2}V(XX') + V(X''y)\right]\Delta(X''y, Xx)\Big) \times \psi_\alpha(XX')\Psi_\Lambda(X') \quad (5)$$

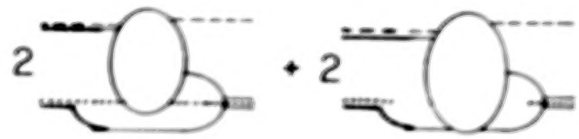

FIG. 7. The last term in 6 in more detail.

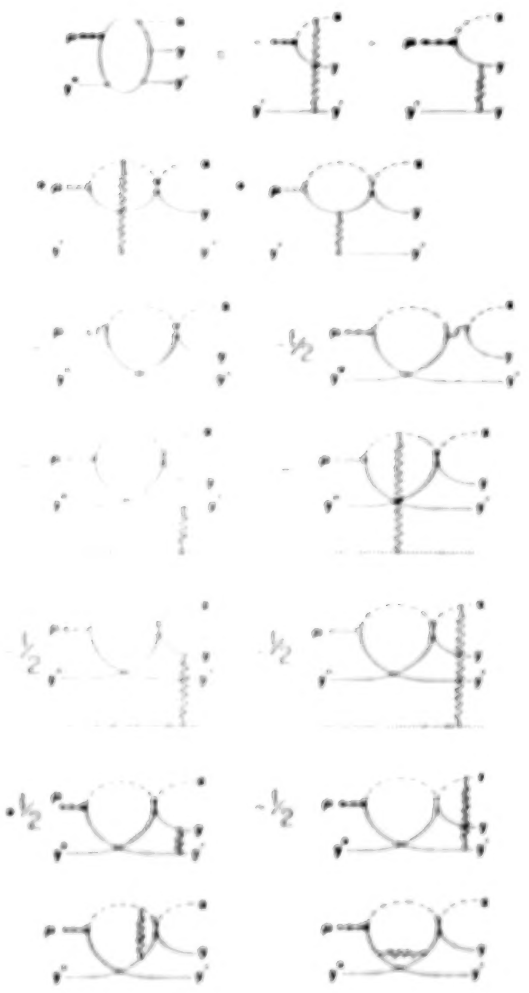

FIG. 8. The second oval in Fig. 7. The zigzag line represents both the sum of Coulomb interactions and the inertial potentials[21] (sometimes called "mass-polarization" terms) experienced by all other particles due to the accelerated reference frame in which one nucleon is constrained to remain at the origin. Crossed fermion lines yield a factor of -1.

The analytic reduction of the Coulomb terms, in which the two electron wave function has been approximated by Löwdin's wave function[1] (with parameters $\alpha = .4228$, $A = .30025$, $\beta = .9794$, and $B = 1.0001$), has been outlined in CMS[3]. The derivation for Chandrasekhar's wave

function[2] (with parameters a=.28309, b=1.03925, and normalization N=.39513) is identical except that only the cross terms AB are nonzero.

The reduction of the direct-orthogonalization terms, the third and fourth terms in Fig. 8 is much more difficult because of the extra three-dimensional integral. The X' integral may be done directly giving four terms in the pairings of $V_f V''_{f'}$

$$T_{V_f V'_{f'}} = \sum_{\nu} \left[T^{\nu 1\nu}_{V_f V'_{f'}} - (-1)^{\ell'} T^{\nu 0\nu}_{V_f V'_{f'}} \right] \tag{6}$$

where a is the ratio of the nucleon to electron masses in the final bound state, and the sum is over all possible final bound states. In positronium this ratio is one so that only the odd-parity terms in the sum are nonzero, as was found[16] for the orthogonalization corrections in reaction (3). In the results below, only the 2p contributions are included since the 3p contributions for the similar terms in (3) were negligible. The T's are

$$\begin{aligned} T^{\nu 1\nu}_{V_f V'_{f'}} = & -\frac{2\sqrt{2}\lambda^{7/2}(a+b)^3\lambda^{3/2}}{(2\pi)^3\sqrt{\pi}(\lambda+\varepsilon)^3} \\ & \times \int d\mathbf{x} d\rho ds\, e^{-i\mathbf{k}_f\cdot(\mathbf{s}+(\eta+\zeta)\mathbf{x})} u^{\rho}_{1,\nu}(\mathbf{r}) \\ & \times exp\left[-\frac{\lambda+\varepsilon}{\eta(a+b)} |\mathbf{s}+(\eta+\zeta)\mathbf{x} - \eta\beta\mathbf{r}| \right] \\ & \times \left[\frac{\eta(a+b)}{|\mathbf{s}+(\eta+\zeta)\mathbf{x}-\eta\beta\mathbf{r}|} + \frac{\varepsilon+\lambda}{2} \right] \\ & \times u^{\rho}_{\nu}(\mathbf{r}) u^{\rho*}_{\nu}(\mathbf{s},\eta) e^{-i\mathbf{k}_i\cdot(\mathbf{s}+\eta\mathbf{x})} \psi^*_{\nu}(\mathbf{k}_i,\mathbf{x}) \end{aligned} \tag{7}$$

where $\zeta = m_p/(m_p+m_e)$, $\eta = 1-\zeta$, $\mu = \zeta m_e$, $\lambda = m_e m_e/(m_e+m_e)$, and ψ is the Coulomb wave function.

Introducing the Fourier (three dimensional integral) representation of the exponential function and the Yukawa potential allows the $\mathbf{r}$ integral to be evaluated.[21] One may then introduce a (one dimensional integral) Gaussian transform[22] to evaluate the $\mathbf{s}$ and $\mathbf{x}$ integrals, leaving a final expression requiring numerical evaluation of a four-dimensional integral. At low energies and small angles the (momentum) radial, θ, ϕ, and (gaussian) ρ integrals required 32, 16, 24, and 16 Gaussian points, respectively, which used 11 hours of cpu time per data point on a VAX 750.

The exchange-orthogonalization terms in Fig. 8 involve a mixing of coordinates, seen in the last three lines of (5), that further complicates the analytical reduction of these terms. The minimum number of dimensions to be integrated appears to be five for these terms, which would involve a prohibitive amount of time on conventional computers. However, since these terms are exchange corrections to the direct-orthogonalization corrections, they are expected to be small and will be neglected in what follows.

VI. ISOSPIN SYMMETRY

Because (1) is similar to, and more complicated than, (3), one would expect that the problems associated with a Fock-Tani Hamiltonian derived using a product transformation for the one-electron case would also arise in using a product transformation for the two-electron case. Indeed, the cancellation of the even-parity orthogonalization terms appears in both cases, and if the positron is replaced by a proton the internuclear Coulomb term is cancelled by the corresponding orthogonalization term. It is hoped that the ideas behind the correction of these problems in (3), which lead to excellent agreement with the variational result, will likewise give a reliable result for (1).

Girardeau and Straton[20] have been able to formally generalize the Fock-Tani transformation to include any number of nucleons, electrons, and bound-state species, but the exacting process of applying Wick's theorem to produce the Hamiltonian on the 2-nucleon, 2-electron Hilbert space has not been completed. Until this process is completed one must use physical ideas to intuit the result.

One might look at the amplitude, Fig. 1, for reaction (1) and postulate that the desired amplitude for (1) should be the average of the amplitudes derived by the post and prior product transformations. Indeed the prior product form corresponding to (4)

$$U = U_B U_A U_E \tag{8}$$

is also allowed (though E before A or B is not because its constituents are a proper subset of the constituents of both A and B).[23] The amplitude for this transition is particularly simple because all of the electron-electron interaction energy is included in the bound states and the internuclear potential does not appear (or one might say that the Coulomb term is exactly cancelled by the orthogonalization term for all masses). It is given in Fig. 9.

FIG. 9. The prior amplitude for (1).

Evaluation of this amplitude follows that of the CBA closely.

But the fundamental idea that lead to the excellent results for (3) was not post-prior averaging—that was the consequence. The fundamental idea was the treatment of particles of different mass and same charge as if they were isospin projections of a single species of nucleon. Consider Fig. 10.

FIG. 10. Direct and (nucleon) exchange Coulomb terms for the electron-nucleon transition amplitude for reaction (1).

If one draws the electron-nucleon interaction diagrams corresponding to the direct and (nucleon) exchange (in a coordinate system in which all four particles are dynamical), it can be seen that the latter may be transformed into the former by a vertical stretching process (multiplying by -1 for each fermion line that is crossed or uncrossed in the process), so that they represent the same physical process. The corresponding direct and exchange orthogonalization projector onto the prior bound states are also equivalent. See Fig. 11.

FIG. 11. Direct and (nucleon) exchange prior orthogonalization corrections for the electron-nucleon transition amplitude for reaction (1).

Thus, *isospin symmetry does not imply post-prior symmetry* in reaction (1).

The corresponding direct and exchange orthogonalization projectors onto the upper post bound state are shown in Fig. 12.

FIG. 12. Direct and (nucleon) exchange corrections orthogonalizing the free nucleon with respect to the upper post bound state, for the electron-nucleon transition amplitude for reaction (1).

These are topologically different and must be treated as two distinct physical processes. Deforming the latter diagram so that the post bound state propagators interchange positions reveals the interpretation of this diagram as the direct orthogonalization projector onto the lower post bound state. Thus the prescription for promoting the exchange amplitude to a reactive amplitude, by promoting the "effective" difference between upper and lower nucleons to a true difference through use of an isotopic spin formalism, leads to an amplitude in which the projectile is orthogonalized using the average of the direct projectors onto the two post bound states.

Reverting to the coordinate system in which the proton is fixed at the origin, one may show that the direct orthogonalization to the state in which one electron is bound to the origin may be analytically reduced in the same manner as the CBA.

VII. RESULTS

The differential cross section for reaction (1) is given in Fig. 13 for a positron energy of 100 eV.

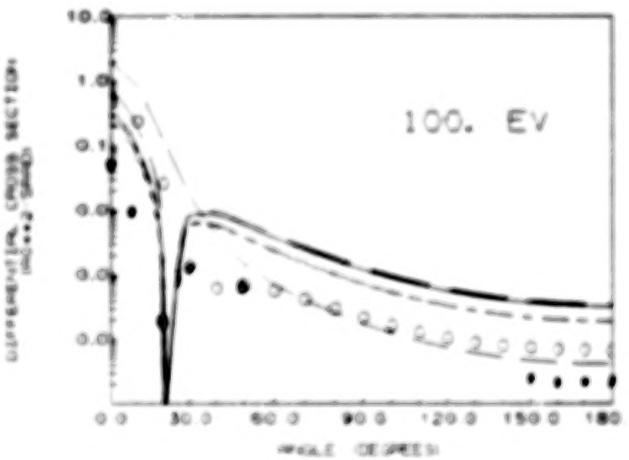

FIG. 13. Electron capture from H^- into the ground state of positronium. The solid line is the present calculation of the post CBA using Löwdin's wave function (LCBAPS), the open circles are the LCBAPS of CMS[7], the dashed lines are, in order of decreasing length, the prior LCBA (LCBAPR), the prior direct-orthogonalization result (CDOPR), the CBAPR using Chandrasekhar's wave function (CCBAPR), and the CCBAPS. The solid points are the ion-orthogonalization correction.

Although the present LCBAPR and the calculation of Choudhury, Mukherjee, and Sural[3] agree, the present calculation of the post CBA cross sections using the post interaction for Löwdin's wave function[1] (LCBAPS) disagree with the calculation of CMS. Where they found an order of magnitude post-prior discrepancy in the differential cross sections except at forward angles, and a markedly different shape to the minima, the present post and prior results differ by 1% to 10% at 100 eV, and the minima have the same shape and occur within one degree of each other.

A cross-check of the present analytic result and their result (which they kindly sent) produced agreement at this stage, so the disagreement is in the computer codes. Four independent reprogrammings, two using an alternate reduction of the integrals giving a different but equivalent analytical result, have reproduced the present results. Ad-

ditionally, there is a "phase space" argument in favor of the present result: that it is less likely that an error would produce nearly identical post and prior curves if they were truly dissimilar than that an error would produce dissimilar curves if they were truly nearly identical.

The CBA results using Chandrasekhar's "open-shell" wave function[2] function gives a binding energy of -.522592 atomic units for H^-, which is within .4% of the correct value, but Löwdin's wave function does not give a negative binding energy. One would suspect that the former would also yield better results in a scattering problem. It may be seen in Fig. 13 that the post and prior results are are almost indistinguishable for the former. Also the magnitude of the CCBA results are 1/2 to 2/3 as large as the LCBA results, which is expected to exceed the exact result.

The differential cross sections at energies .1, .5, and 1. eV are given in Fig. 14 and the total cross sections are given in Table II. The latter was obtained by a simple extended Simpson's rule from the differential cross sections so the error may be of order 10%, as seen by comparing LCBAPR at 100 eV to the result, .255(-1), of CMS. As noted below, the error due to the approximate H^- wave function is certainly larger.

Note that the CDIOPS and CDOPS results show some oscillations characteristic of a lack of convergence in the energy region around 90 degrees, but are well converged in at small and large angles, the regions with the greatest contributions to the total cross sections. The LDIOPS is smoother because of the averaging inherent in the larger number of nonzero terms in Löwdin's wave function. It may be posible to redistribute the number of Gaussian integration points among the four integrals to improve the convergence in the central region. But the difference between the LDIOPS and CDIOPS results gives a bound on the accuracy of the approximate wave function that lead to the CDIOPS result and the oscillations are much smaller than this estimate.

It may be seen that all orthogonalization corrections tend to remove the minimum that appears in the CBA results, a minimum that was shown to be spurious in the reaction (2). However, the CDOPR and CDOPS cross sections (and the result obtained by averaging these amplitudes) are larger than both the CCBAPR and CCBAPS cross sections. Since the Coulomb Born approximation for the exact H^- wave function appears to be larger than the unitarity limit near zero incident energy, one would want cross sections less than the CBA result in this region. The iso-orthogonalization correction gives a result that is less than the CBA in this region.

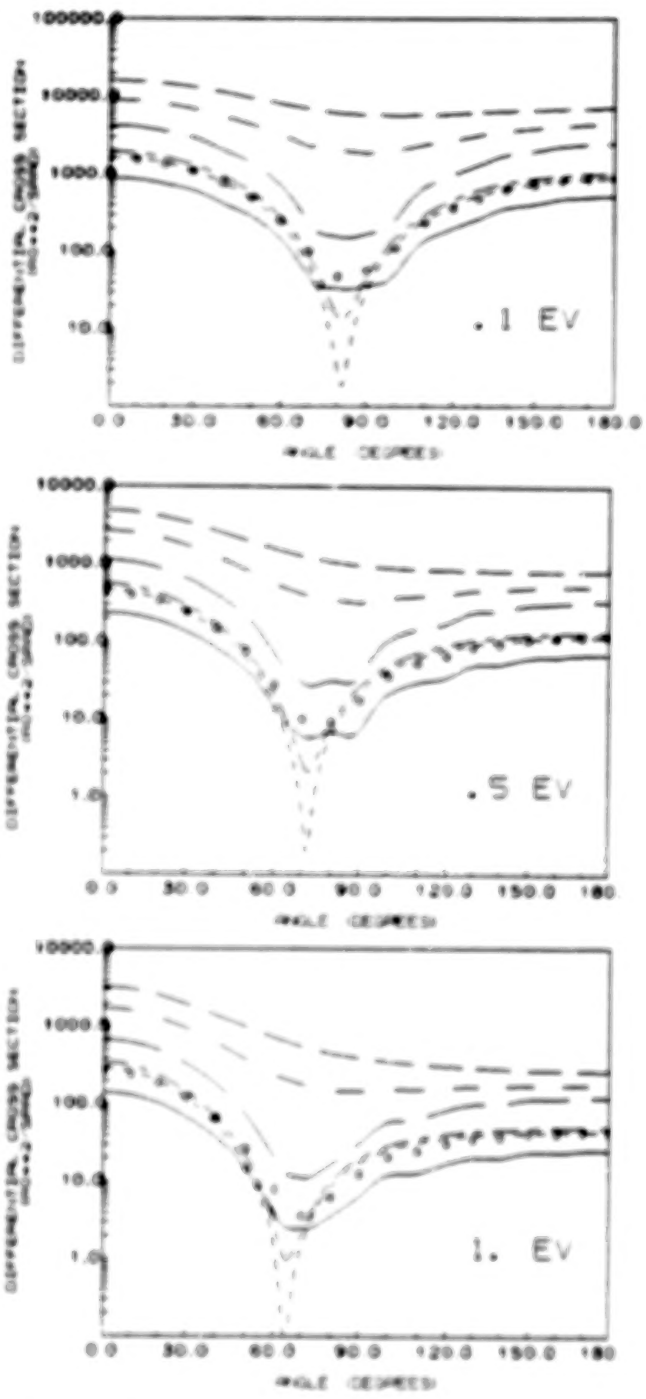

FIG. 14. Electron capture from H^- into the ground state of positronium using the "open-shell" wave function. The solid line is the present calculation including the (post direct) iso-orthogonalization (CDIOPS) (the open circles are the same result using Löwdin's wave function (LDIOPS)), the dashed lines are, in order of decreasing length, the post direct-orthogonalization result (CDOPS), the prior direct-orthogonalization result (CDOPR), the CCBAPR, and the CCBAPS.

TABLE I. Fock-Tani cross sections for reaction (3) in units of πa_0^2.[11]

Energy (eV)	FBA	Post FT	Prior FT	Average without interference	Symmetric FT	Humberston
6.8	0.032	0.00094	0.011	0.0061	0.0046	0.0032
7.65	1.869	1.454	0.458	0.956	0.74	0.7
8.7	3.344	3.247	0.426	1.836	1.259	1.3
9.2	3.835	3.868	0.457	2.162	1.443	
9.826	4.287	4.447	0.499	2.473	1.653	1.67
10.0	4.385	4.573	0.511	2.542	1.709	
13.6	4.788	5.187	0.979	3.083	2.541	
20.0	3.349	3.631	1.352	2.491	2.278	
30.0	1.651	1.773	1.078	1.425	1.359	
40.0	0.848	0.902	0.681	0.791	0.761	
50.0	0.465	0.489	0.417	0.453	0.436	
60.0	0.269	0.281	0.260	0.271	0.260	
70.0	0.164	0.170	0.166	0.168	0.162	
80.0	0.104	0.107	0.110	0.108	0.104	
90.0	0.068	0.070	0.074	0.072	0.069	
100.0	0.046	0.047	0.052	0.049	0.047	

TABLE II. Total cross sections for electron capture from H^- into the ground state of positronium, in units of πa_0^2.

E (eV)	LCBAPR	LCBAPS	CCBAPR	CCBAPS	CDOPR	CDOPS	LDIOPS	CDIOPS
.1	.167(4)	.237(4)	.201(4)	.170(4)	.304(5)	.458(4)	.904(3)	.947(3)
.5	.634(3)	.456(3)	.384(3)	.327(3)	.576(4)	.865(3)	.321(3)	.179(3)
1.	.303(3)	.217(3)	.181(3)	.155(3)	.269(4)	.402(3)	.149(3)	.825(2)
100.	.232(-1)	.151(-1)	.112(-1)	.986(-2)	.791(-1)			

VIII. CONCLUSION

Cross sections for positronium formation by electron capture from the negative hydrogen ion have been calculated in the energy region below the 6.8 eV threshold for capture from hydrogen. The lowest order Born approximation has been augmented by orthogonalization corrections. The present treatment has utilized the perspective of treating the atomic nuclei (of like charge and vastly different mass) as if they were isospin projections of a single species of "nucleon," and has examined the consequences of this perspective. In capture from hydrogen this iso-orthogonalized Fock-Tani result yielded excellent agreement with the variational result. To date there is no variational result for capture from H^-, due difficult integrals involving Coulomb waves, but the iso-orthogonalized result show promise of yielding a reliable result.

A. Acknowledgements

Part of this work was done while JCS was a guest scientist conducting research through the National Research Council-NASA Research Associateship Program. He would like to thank Drs. Anand Bhatia and Aaron Temkin for fruitful discussions during this tenure. Part of this work was supported by the Division of Chemical Sciences, Office of Energy Research, U.S. Department of Energy.

[1] P.O. Löwdin, Phys. Rev. 90, 123 (1953).
[2] S. Chandrasekhar, Astrophys. J. 100, 176 (1944).
[3] K.B. Choudhury, A. Mukherjee, and D.P. Sural, Phys. Rev. A33, 2358 (1986).
[4] J.C. Straton and M.P. Girardeau, Phys. Rev. A (September 1989).
[5] M. Leventhal et al., Astrophys. J. 225, L11 (1978).
[6] E.L. Chupp et al., Nature 241, 333 (1973).
[7] M. Leventhal et al., Nature 266, 696 (1977).
[8] J.H. Black, Astrophys. J. 222, 125 (1978).
[9] R.J. Drachman, in *Positron Scattering in Gases*, Ed. J.W. Humberstein and M.R.C. McDowell (Plenum Press, New York, 1983) p. 206.
[10] M. D. Girardeau and J. C. Straton (unpublished).
[11] M.D. Girardeau and C. Lo (submitted).
[12] C.J. Brown and J.W. Humberston, J. Phys. B17, L423 (198).
[13] M. D. Girardeau, J. Math Phys. 16, 1901 (1975).
[14] P. C. Ojha, M. D. Girardeau, J. D. Gilbert, and J. C. Straton, Phys. Rev. A 33, 112 (1986).
[15] P. J. Martin, *et al.* Phys. Rev. A 23, 3357 (1981), and G. W. McClure Phys. Rev. 148, 47 (1966).
[16] J. C. Straton, Phys. Rev. A 35, 3725 (1987).
[17] Acad. Sci. Amsterdam 33, 973 (1930).
[18] J. D. Jackson and H. Schiff, Phys. Rev. 89, 359 (1953).
[19] D. P. Dewangan and B. H. Bransden, J. Phys. B 21, L353 (1988).
[20] *Atomic Physics with Positrons*, edited by J. W. Humberston and E. A. G. Armour (Plenum, New York, 1987), p442.
[21] J. C. Straton, Phys. Rev. A 35, 2729 (1987); 37, 4531 (1988).
[22] Phys. Rev. A 39, 1676 (1989), equations (68) through (75);Phys. Rev. A (September 1989).
[23] Phys. Rev. A 26, 217 (1982).

Positron-Molecule Bound States and Positive Ion Production

M. Leventhal and A. Passner
AT&T Bell Laboratories
Murray Hill, NJ 07974

and

C. M. Surko
Physics Department, University of California, San Diego
La Jolla, CA 92093

ABSTRACT

We have studied the interaction of low-energy positrons with large molecules such as alkanes ($C_n H_{2n+2}$).[1] These data provide evidence for the existence of long-lived resonances and bound states of positrons with neutral molecules. The formation process and the nature of these resonances are discussed. We have observed the positive ions produced when a positron annihilates with an electron in one of these resonances,[2] and this positive-ion formation process is discussed. This paper is a review of the current state of our understanding of these positron-molecule resonances and the resulting positive ion formation.[3] We also discuss a number of outstanding issues in this area.

INTRODUCTION

We have conducted experiments to accumulate and store large numbers of positrons in an electrostatic trap.[4] This has allowed us to study, in a sensitive way, the low-energy inelastic processes occurring between positrons and neutral atoms and molecules. In the course of these experiments, we have found that the addition of large organic molecules to the trap increases the annihilation rate of the positrons to the extent that this annihilation process cannot be explained by direct collision phenomena alone. From a systematic study of the interaction of positrons with alkane molecules as a function of molecular size, we have demonstrated the existence of long-lived resonances and bound states of the positrons and these neutral molecules. A model of the formation of these resonances is discussed. Annihilation rate data are presented for a variety of chemical species in order to test various aspects of the model. At present, there are discrepancies between the model and the experiments, and we do not have a complete picture of the bound-state formation process. One consequence of the bound states is that they naturally provide an efficient mechanism for the production of positive ions when the positrons annihilate with an electron on the molecule. We have directly observed the ions produced in this manner, and we discuss this phenomenon.[2]

THE POSITRON TRAP[4]

The experimental arrangement is shown schematically in Fig. 1. Positrons from a ^{22}Na radioactive source are moderated to 2 eV by a single-crystal, tungsten, transmission moderator. They are incident from the right onto the configuration of potentials and neutral-gas pressure shown. The background gas used to trap the positrons is molecular nitrogen. The gas pressure is adjusted so that, in one transit through the trap, the positrons make inelastic, electronic-excitation or ionizing collisions with the N_2 and are trapped in regions I, II, and III. The potentials are adjusted so that subsequent vibrational excitation of the N_2 traps the positrons, first in regions II and III in about 1 ms (transition *B* in Fig. 1), and then in region III in less than 0.1 s (transition *B'*). The N_2 pressure in region III (the confinement volume) is typically 1-5 x

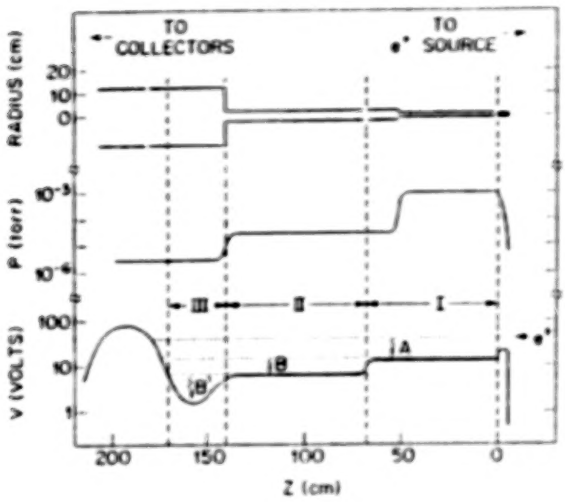

FIG. 1. A schematic diagram of the three-stage positron trap, including the electrode structure, nitrogen gas pressure, and the electrostatic potential profile. There is an axial magnetic field in the Z direction. The positrons lose energy by electronic excitation and/or ionization of the N_2 (labeled A) or by vibrational excitation of the N_2^- (B and B').

10^{-6} Torr, and the base pressure of the vacuum system is less than 3×10^{-8} Torr. The magnetic field in region III is in the range from 250 to 800 G. For the work presented here, the total number of trapped positrons is always less than 1×10^4.

After variable fill and storage times, the contents of the trap are dumped onto an arrangement of annular collectors located at Z = 265 cm in Fig. 1, and the resulting 511-keV γ-ray annihilation radiation is monitored with a NaI detector and pulse-counting electronics. By suitable biasing of the collector plates, either the total number of positrons in the trap or the radial distribution of the positrons can be measured. We have also studied the confinement of electrons in the same geometry.

We have measured the time dependence of the cooling of the positrons in the trap. When the potential difference between regions II and III is set at 8.3V, the characteristic time that the positrons remain in regions II plus III, before being trapped in region III, is 20 ms. The positrons entering region III are found to cool to energies ~1eV in less than 0.1 s. It is likely that, in this range of energies, the positrons cool via vibrational excitation of N_2. The subsequent cooling of the positron gas occurs at a slower rate, and it is either due to rotational excitation of N_2 molecules or to elastic scattering with N_2. The temperature of the positron gas in this range of energies is measured by a "magnetic beach" energy analyzer.[5] This technique involves measuring the number of positrons reaching the collector as a function of a retarding potential with and without an increased magnetic field between region III and the collector. This added magnetic field acts as a magnetic mirror to reflect positrons with energies, $\langle E_\perp \rangle$, perpendicular to the field. The shift in the retarding potential curves is a measure of $\langle E_\perp \rangle$. Since the positrons make frequent collisions with N_2 molecules, they are expected to have an isotropic velocity distribution in region III. Thus, we can infer the average energy $\langle E \rangle \equiv (3/2) \langle E_\perp \rangle$.

Shown in Fig. 2 are data for $\langle E \rangle$ as a function of storage time for short filling times (~50-100 ms), at a magnetic field B_0 of 430 G. The N_2 gas pressure for this data was 1.5×10^{-6} torr. For these data, the corresponding positron confinement time in the trap was greater than 20 sec. The characteristic time for cooling in the range of energies shown in Fig. 4 is 0.6 s. The data are plotted by subtracting the kinetic energy of 0.038 eV expected for positrons at room temperature. The fact that the data can be fitted by a single straight line confirms that the positrons are cooling to room temperature. The observed cooling rate is found to be proportional to the N_2 pressure.

In order to study the ions formed in the trap, a two-stage channel plate, electron multiplier was placed 100 cm away from the center of region III (i.e., at Z = 260 cm in Fig. 1), and the electrodes surrounding region III were biased at +5 V to accelerate the ions toward the channel plate. After suitable fill and storage times, the potential barrier located near 195 cm in Fig. 1 is lowered, and the contents of the trap are dumped onto the channel plate. The channel plate is biased at -2400 V, providing near-unity detection efficiency for ions with masses in the range studied (i.e., 10-150 amu). When this ion signal is measured as a function of time delay after the trap is dumped, we have a simple, time-of-flight mass spectrometer.

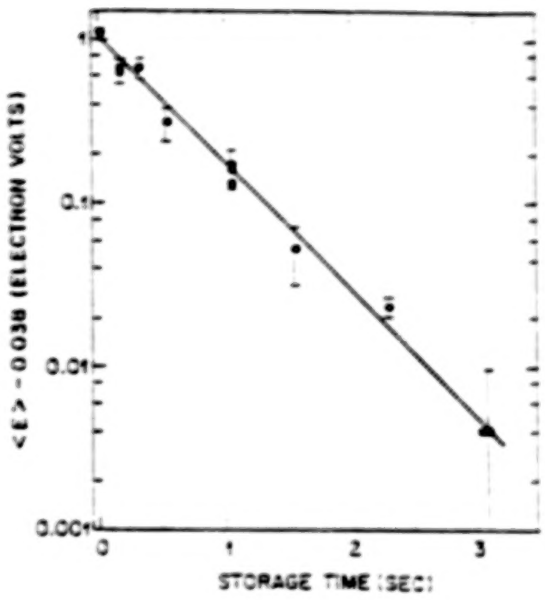

FIG. 2. The total, average energy of the positrons ⟨E⟩ minus their energy at room temperature as a function of storage time. The straight line corresponds to a characteristic cooling time of 0.6 s. The positrons cool to nearly room temperature n about 3 s.

POSITRON ANNIHILATION IN THE PRESENCE OF LARGE MOLECULES[1]

When no special precautions were taken in the treatment of the vacuum chamber, the characteristic confinement time, τ, of positrons stored in the trap was found to be of the order of 1 s, as compared to confinement times of 100 s for electrons, even when the total number of stored electrons was of the order of 1×10^9, where space-charge effects tend to enhance the radial diffusion. It was the surprisingly short positron confinement time which led to the discovery of the positron-molecule resonances described here. Measurement of the radial distribution of the positrons indicates that, under these circumstances, they do not diffuse appreciably on time scales of the order of 1 s but are confined in the central region of the trap. Thus, we concluded that they annihilate before diffusing to the walls. The positron confinement time, τ, is *insensitive* to the N_2 gas pressure, so that the annihilation does not appear to involve the N_2. The key observation was that the positron confinement is extremely sensitive to the history of the vacuum chamber. For example, mild heating of the chamber wall decreases τ, while the introduction of a liquid-nitrogen-cooled surface near region III increases τ from 1 to 150 s. This led us to the conclusion that impurity molecules in the vacuum system were involved.

Previous studies indicate that positron annihilation is well understood for a number of gases, including nitrogen and hydrogen, but is not understood in other gases such as methyl chloride and butane.[6] We therefore introduced specific impurities into the vacuum system to investigate this effect. We found that water molecules had no effect on τ, but that τ was, for example, extremely sensitive to the oil from our pumps, to the extent that 1×10^{-9} Torr of oil could explain the observed containment time.

We chose to study this effect systematically with linear, hydrocarbon molecules (alkanes) of the form $C_n H_{2n+2}$, for several values of n ranging from 4 to 16.[7] Shown in Fig. 3 are data for the positron confinement as a function of time when small amounts of butane ($C_4 H_{10}$) and heptane ($C_7 H_{16}$) are introduced into the vacuum chamber.[7] The number of trapped positrons, $N(t)$, as a function of the storage time, t, can be described by a simple exponential, $N(t) = N(0) \exp(-t/\tau)$, with τ a strong function of the pressure of the alkane species added. As shown in Fig. 3, heptane has a much greater effect on τ, per molecule added, than does butane. Similar results were obtained for all of the alkane molecules studied -- the larger the molecule, the shorter the observed annihilation time per unit pressure of the added alkane species.

In order to analyze the data quantitatively, we assume that the increase in the annihilation rate is proportional to the increase in pressure, ΔP, of the added gas species. Thus,

$$\tau^{-1} = \tau_0^{-1} + A\,\Delta P, \qquad (1)$$

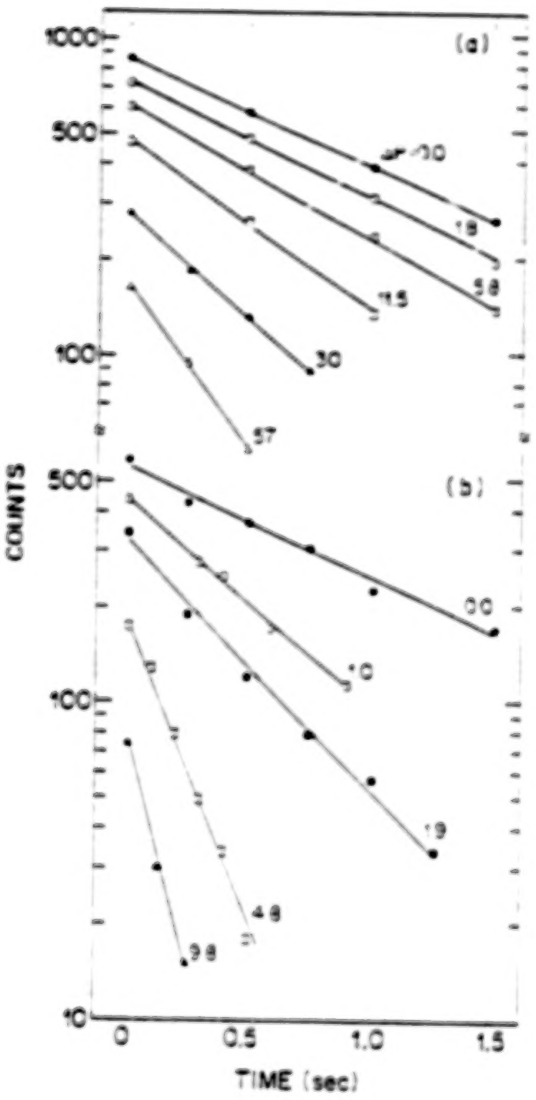

FIG. 3. Positron confinement as a function of storage time when (a) butane (C_4H_{10}), and (b) heptane (C_7H_{16}), are introduced into the containment volume (region III) in the presence of 4.4×10^{-6} Torr of N_2 gas. The pressure, ΔP, of the added alkanes is in units of 1×10^{-8} Torr.

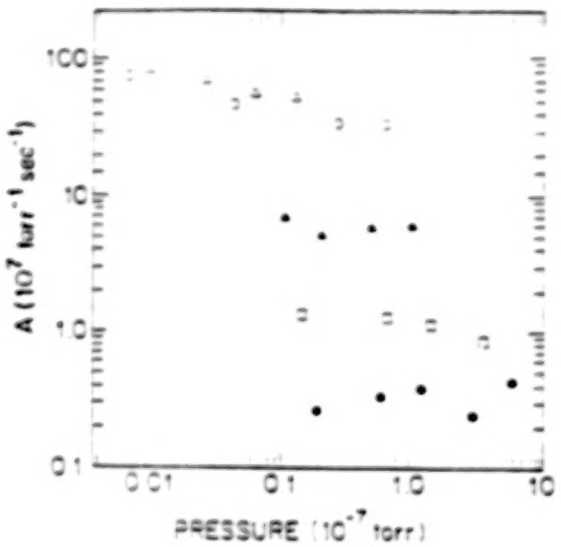

FIG. 4. The annihilation rate per unit pressure, A, of the positrons as a function of the added pressure of alkane molecules: filled circles, butane (C_4H_{10}); open squares, pentane (C_5H_{12}); filled triangles, heptane (C_7H_{16}); open circles, dodecane ($C_{12}H_{26}$); and open triangles, hexadecane ($C_{16}H_{34}$).

where τ_0 is the lifetime of the trapped positrons with no alkanes added, and A is a constant. Shown in Fig. 4 are data for several of the alkane molecules. In each case, A is approximately independent of gas pressure, as assumed. The most striking feature of the data is the large increase in A when the size of the alkane molecule is increased.

The annihilation rate, Γ, of positrons in collision with atoms or molecules is historically written in terms of the Dirac annihilation rate for positrons in a free-electron gas:[6] $\Gamma = Z_{eff}\rho\pi c r_0^2$, where c is the speed of light, r_0 is the classical radius of the electron, ρ is the number density of the gas, and Z_{eff}, which is the effective number of electrons per molecule, takes into account details of the electronic structure. In Fig. 5, we use our measured data for A to infer Z_{eff}/Z as a function of the number of electrons, Z, in the alkane molecule. The data indicate that Z_{eff} for dodecane and hexadecane is approximately 2×10^6. Also shown in Fig. 4 are data for Z_{eff} for the smaller alkane molecules measured in dense gases.[6]

Figure 5 shows an increase in the annihilation rate of over three orders of magnitude when the size of the molecule is increased, and it also shows that this effect is not due simply to an increase in the number of electrons.

This large enhancement in the annihilation rate is not likely to be due to an enhancement of the collision cross section, which might be expected to scale with molecular size (i.e., ~ Z). Thus, we were led to consider other possibilities, such as a resonance or a bound state of the positron and the molecules. The spin-averaged lifetime of a positronium atom is $\tau_{ps} \sim 0.5$ ns. Thus, we expect that if the resonance lifetime is of the order of τ_{ps}, the positron has unit probability of annihilation. Since the alkane studies were conducted at an N_2 gas pressue of 4.4×10^{-6}torr, we expect, based on the positron cooling studies described above, a characteristic cooling rate of less than 0.2 sec. Thus the positrons are quite cool--nearly at room temperature--during much of the time when the positron population is decaying exponentially.

MODEL OF THE POSITRON-MOLECULE RESONANCES[1]

Since τ is found to be insensitive to the background N_2 pressure, the binding appears to be due to a two-body process. Such processes have been discussed in the context of the binding of electrons to neutral molecules,[8,9] and we are led to a similar picture. The positrons have enough energy to directly excite low-energy vibrational modes in the large molecule, but they are not likely to excite electronic excitations in the molecule or to dissociate it. If we *assume* that the positron has an energy affinity, ε_A, for the molecule, then the incident positron energy plus some fraction or all of ε_A can be used to excite vibrational modes, in which case the positron will be attached to the molecule.

A reasonable explanation of the observed plateau in Z_{eff}/Z, shown in Fig. 4, when Z is increased beyond Z = 74, is that, with increasing size, the lifetime τ_m of the complex has become comparable to the annihilation time ($\tau_m \approx \tau_{ps}$). If we make this assumption, then we find a cross section of $\sigma \approx 4 \times 10^{-16}$ cm^2 for the binding of the positron and a molecule with Z = 74 (i.e., nonane, C_9H_{20}). Our measurements of the cooling of the positrons by the N_2 indicate that the inelastic, e^+-N_2 vibrational cross section is of the order of 0.5×10^{-17} cm^2. Thus, a value of 4×10^{-16} cm^2 for C_9H_{20} does not seem unreasonable.

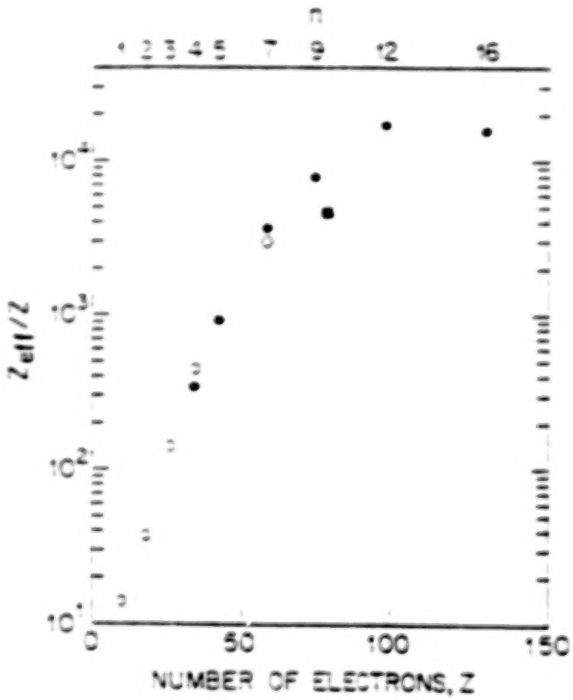

FIG. 5. The quantity Z_{eff}/Z for alkane molecules plotted as a function of the number of electrons, Z, in the molecule; Z_{eff}/Z is the annihilation rate per electron normalized by the Dirac annihilation rate expected in a free-electron gas. Filled circles are alkane data from the present work; open circles are from Ref. 3. The number of carbon atoms, *n*, in the alkane molecules studied is indicated by the upper scale. The solid square corresponds to decahydronapthalene ($C_{10}H_{18}$), and the open diamond to deuterated heptane (C_7D_{16}).

With the use of detailed-balance arguments[8] (commonly referred to as RRKM theory)[9], an expression for τ_m has been derived for the case of electrons bound to molecules. Adapted to the case of positrons, it can be written in terms of the positron affinity, ε_A, the incident positron energy, ε_i, the number, ℓ, of vibrational modes of the molecule, and their total zero-point vibrational energy, ε_z. In particular,

$$\tau_m^{-1} = (m_e/\pi^2 \hbar^3)\, \varepsilon_i^{1/2} \tilde{\varepsilon}_z^{3/2} [\tilde{\varepsilon}_z/(\varepsilon_A + \tilde{\varepsilon}_z)]^{\ell} \times \sigma(\varepsilon_i)\, I\,(\varepsilon_i, \varepsilon_z), \qquad (2)$$

where $I(\varepsilon_i, \varepsilon_z)$ is a definite integral[8]; $\varepsilon = b\varepsilon_z$, with b a correction factor differing from unity by a few tens of percent;[9,10] and $\sigma(\varepsilon_i)$ is the excitation cross section discussed above.

There are two features of Fig. 5 which can be compared with Eq. (2) to yield estimates of the positron affinity ε_A— the plateau beginning at Z = 74 and the slope of ln (τ_m) vs Z at small Z. Using Eq. (2) for our positron data at Z = 74 with ε_i =0.04 eV, and assuming $\sigma(\varepsilon_i) = 4 \times 10^{-16}$ cm^2, ℓ = 81 (corresponding to Z = 74), and $\tau_m = 0.5 \times 10^{-9}$ s, we find $\varepsilon_A/\bar{\varepsilon}_z = 0.15$. We now compare the slope of the curve in Fig. 5 at small values of Z to d ln (τ_m)/$d\ell$. Changes in Z are linearly proportional to changes in ℓ (i.e., $\Delta\ell = (9/8)\,\Delta Z$). Thus, the dominant dependence of ln (τ_m) on Z will come from the $[\bar{\varepsilon}_z/(\varepsilon_A + \bar{\varepsilon}_z)]^\ell$ factor in Eq. (2), even if $\sigma(\varepsilon_i)$ and $I(\varepsilon_i,\varepsilon_z)$ have some ℓ dependence. The observed linear slope in Fig. 5 will occur only if $\varepsilon_A \propto \bar{\varepsilon}_z$, indicating that ε_A increases linearly with the size of the alkane molecule. On comparing the data to Eq. (2), we find $\varepsilon_A/\bar{\varepsilon}_z = 0.12$. For nonane with Z = 74, we estimate $\bar{\varepsilon}_z$ = 6.8 eV and assume b = 0.7 (c.f., Ref. 10) to find that $\varepsilon_A = 0.6 \pm 0.1$ eV.[11]

The sign of ε_A is assumed to be such that the positrons can form bound states with the molecules. However, energy is conserved in the two-body collisions studied here. Thus, the positrons are not bound, since this would require subsequent collisions to drain off the energy. Instead, they form resonances in which the positrons annihilate with increasing probability as the lifetime of the resonance increases. The data are consistent with the model presented here; however, it is clear that further work is necessary. In particular, it would be useful to have calculations of both the magnitude of ε_A and its dependence on molecular size for the case of positrons bound to alkane molecules.

In the model presented above, both the nature of the molecular vibrations, the vibrational density of states, and the positron affinity, ε_A, play an important role. We have now conducted a number of experiments to study the effect of different molecular species on the annihilation rate, A. In Table I, we present a summary of these results.

One test of the model is to change the nature of the molecular vibrations keeping the chemical species the same. We did this by measuring the value of A for a deuterated alkane and comparing this result with that for a protonated version of the same molecule. We expected that deuteration would lower the frequencies of a sizable fraction of the vibrational modes, thereby appreciably lowering ε_z, while keeping ε_A approximately the same. The result for heptane is A = 5.2± .5 torr^{-1} sec^{-1} for C_7D_{16} (shown as the open diamond in Fig. 5) as compared with A = 6.4 for C_7H_{16}. In contrast, Eq. (2) would predict that, for heptane, a 10% decrease in the frequencies of only 10% of the modes would *increase* A by a factor of 2.6. Thus the annihilation rate does not appear to be as sensitive as we would expect to the vibrational modes affected by the substitution of D for H. Neither the sign nor the magnitude of the effect is that which was expected.

Another possibility is that the low frequency modes are important in the binding process. With this in mind, the quantity A was measured for toluene (C_7H_8), a ring compound, and compared with that for heptane, the corresponding alkane, with the same number of carbons. The result was that A is the same for both molecules to within 20%. We also measured A for decahydronapthalene, $C_{10}H_{18}$, which is similar in chemical structure to the alkanes but has a "bridge" between two parts of the molecule, which we expected would eliminate some of the low frequency modes. As shown in Table I, the measured annihilation rate for $C_{10}H_{18}$ is a factor of 1.7 smaller than the 9-carbon alkane, nonane, and therefore even smaller with respect to the value expected for the corresponding 10-carbon alkane. The quantity Z_{eff}/Z for $C_{10}H_{18}$ is shown by the solid square in Fig. 5, and it appears to lie considerably below the alkane data.

In summary, the results of our tests of the effect on τ_m of changing the vibrational modes are mixed. We had expected deuteration to increase τ_m, and it did not. On the other hand, decahydronapthalene has fewer low-frequency vibrational modes than the corresponding 10-carbon alkane; and, from the physical picture presented, we might expect this to lower the probability of attachment. The data are consistent with this idea. It is clear that further work is necessary before we can claim to understand the formation of the positron-molecule resonances.

TABLE I

Annihilation Rate A (in $torr^{-1}$ sec^{-1})
of Various Organic Molecules

		Z	A
butane	C_4H_{10}	34	0.33
pentane	C_5H_{12}	42	1.1
heptane	C_7H_{16}	58	6.4
heptane (deuterated)	C_7D_{16}	58	5.2
nonane	C_9H_{20}	74	17
dodecane	$C_{12}H_{26}$	98	47
hexadecane	$C_{16}H_{34}$	130	59
glycerol	$C_3H_8O_3$	74	18
toluene	C_7H_8	50	5.3
decahydronapthalene	$C_{10}H_{18}$	78	10
pump oil	–	–	90
sebacic acid methyl ester	$C_{12}O_4H_{20}$	156	210

We have also measured the annihilation rate for glycerol ($C_3H_8O_3$), which, in contrast to the alkanes, has electron orbitals not involved in chemical bonding with appreciable electron density isolated from the nuclei. This molecule was measured to have a high value of A when compared to the alkane with a comparable number of carbon atoms. However, the value Z_{eff} for fixed Z is approximately that which we would expect from the alkane data.

Finally, we measured A for both "pump oil" and sebacic acid methyl ester; the latter is expected to be a chemically similar molecule to the oil. In both cases, A was larger than the largest alkane studied. It is likely that oil molecules are the source of the rapid positron annihilation rates observed in our early experiments which led to the study of the interaction of positrons and large molecules described here.

POSITIVE ION FORMATION

The existence of the long-lived resonances described above greatly enhances the probability that a positron will annihilate with an electron on the molecule. When this occurs, a positive ion of the same molecular species will result. We have directly observed the ions produced in this manner using the simple channel-plate electron multiplier as a detector in a time-of-flight mass spectrometer as described above.

Shown in Fig. 6 is the channel-plate signal as a function of time, t, after the contents of the trap are dumped when butane (C_4H_{10}) is added to region III.[7] The signal at zero storage time, which is typical of that when no butane is added, shows a prompt peak at $t = 0$, corresponding to the trapped positrons, and a peak at 185 μs which corresponds to N_2^+. The N_2^+ ions are believed to be formed in region I, when the positrons ionize the N_2. This signal decreases monotonically as a function of storage time. Based on the simplest calculation using the applied potentials, the expected arrival time of the N_2^+ would be 170 μs, which is 9% lower than that measured. When CO_2 was introduced into the system, the expected arrival time was also 9% lower, and so the expected arrival times for all of the ions were scaled by this factor in order to identify the ion species detected.

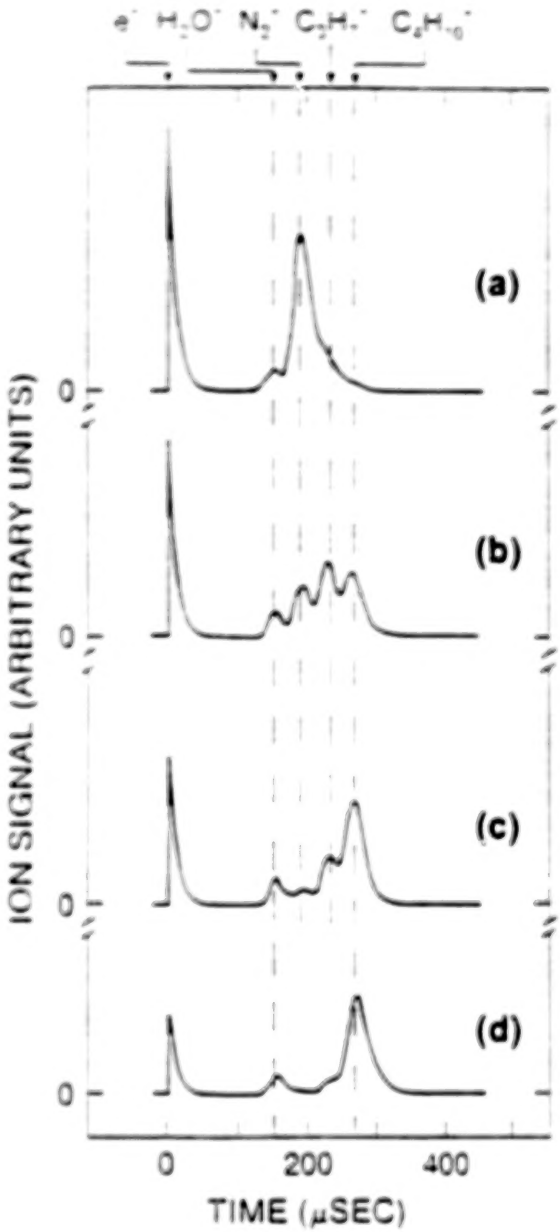

FIG. 6. Time-of-flight spectra of the ions observed when the positron trap is dumped, for the case where butane is added to region III. The traces correspond to storage times of (a) 0 s, (b) 0.5 s, (c) 1 s, and (d) 2 s. The filling time was 0.5 s, the N_2 pressure in region III was 0.5×10^{-7} Torr, and the butane pressure was 2.5×10^{-7} Torr. The identification of the peaks and their expected positions are indicated.

In addition to the e^+ and N_2^+ signals, three other ion peaks are evident in Fig. 6. Our identification of these signals is indicated above the Figure. The decay time of the ion signals is strongly dependent on the applied magnetic field. This is consistent with estimates of the radial diffusion of these species out of the region where they are detected by the channel plate. In contrast, direct measurements of the radial distribution of the e^+ show that they do not diffuse appreciably on the time scale of the experiment.[4]

After about 1 s, the dominant ion peak occurs at 265 μs and corresponds to butane ions, $C_4H_{10}^+$. We have previously shown that the annihilation rate of the positrons is directly proportional to the C_4H_{10} density.[1] Thus, we would expect that the time dependence of the $C_4H_{10}^+$ could be described by the solution of the rate equations for the e^+ and $C_4H_{10}^+$, assuming that the population of each decays exponentially in time, with the first feeding the second (i.e., "parent-daughter decay" common in nuclear physics).[12] We have conducted such an analysis,[2] and we find that this model does explain the data.

The two other identifiable peaks in Fig. 6 appear to be H_2O^+ (150 μs) and $C_3H_7^+$ (235 μs).[13] Water is a likely impurity in our vacuum system and appears to play little or no role in the dynamics of the other species. The rise time and the amplitude of the $C_3H_7^+$ signal are consistent with it being generated by charge exchange between the N_2^+ and the butane, producing $C_3H_7^+$ and other products. We have carried out an analysis of the N_2^+ - $C_3H_7^+$ data similar to that described above for the e^+ - $C_4H_{10}^+$ data which supports this hypothesis.

Shown in Fig. 7 are data for the ions produced when heptane (C_7H_{16}) is added to region III. In this case, heptane ions are observed, but never as the dominant peak which appears to correspond to $C_4H_9^+$.[13] The previously observed N_2^+, H_2O^+, and $C_3H_7^+$ peaks are also evident. The $C_4H_9^+$ and $C_7H_{16}^+$ signals are approximately proportional to each other. They increase at early times as the positrons disappear in a manner similar to that described above for $C_4H_{10}^+$. These data indicate that the positrons can breakup large molecules into fragments. The details of this process remain to be studied.

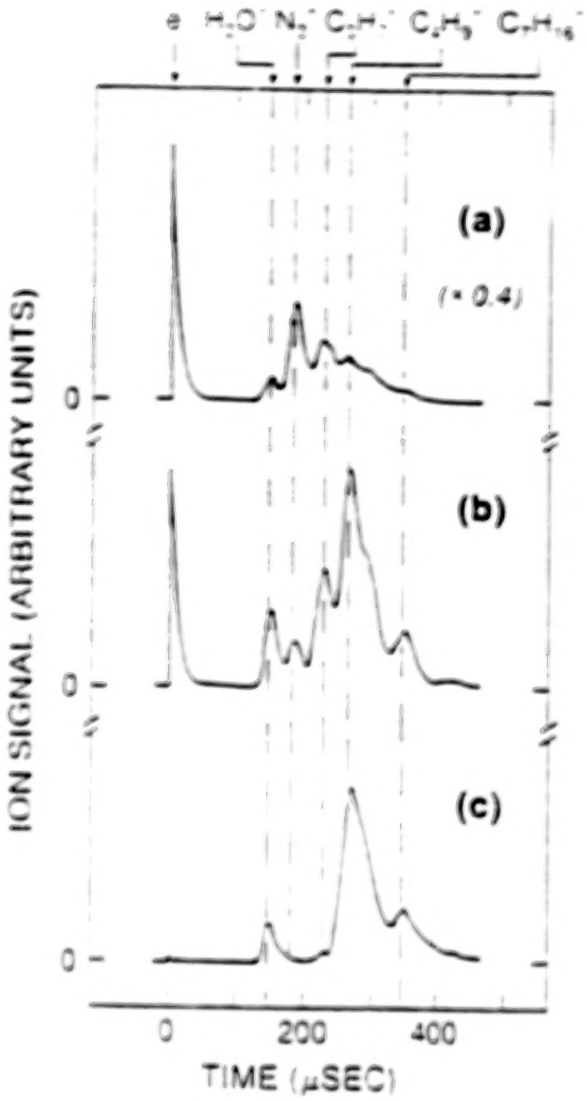

FIG. 7. Time-of-flight spectra of the ions observed when the trap is dumped, for the case where heptane (C_7H_{16}) is added to the trap. The storage times are (a) 0.5 s, (b) 2 s, and (c) 4 s. The filling time was 0.2 s in (a) and 1 s in (b) and (c). The identification of the peaks and their expected positions are indicated.

The results presented here show that positrons can be used to form positive ions from large neutral molecules. Because of the formation of long-lived e^+ -molecule resonances, the cross sections for these processes are much larger than previously anticipated. Since the ion formation process is qualitatively different than conventional techniques for forming positive ions, it may be useful in obtaining additional information about unknown molecular species when these molecules are studied using mass spectrometry. It is also possible that more detailed studies of the specific ions formed from a given molecule after positron annihilation may give insight into the nature of the e^+ -molecule resonances themselves.

SUMMARY

We have presented data for the annihilation rate of room-temperature positrons in the presence of a combination of N_2 and large organic molecules. The large annihilation rates which we observed have led us to conclude tha the positrons form long-lived resonances with the organic molecules. These resonances are formed in two-body collisions. If there were a third body to carry away the excess energy, true bound states would be formed. In any case, however, the lifetime of the complex is limited to about 1 nsec, due to annihilation of the positron with an electron on the molecule.

We have discussed a model for the formation and the lifetime, τ_m, of these resonances. The model indicates that, for the alkanes, the positron-molecule affinity ϵ_A is proportional to the size of the molecule, and that, for nonane, $\epsilon_A \approx$ 0.6 eV. Specific tests of the model using different chemical species and comparing deuterated and protonated alkanes produced mixed results. It is clear that more work in this area is warranted.

Finally, we have observed the positive ions produced when a positron annihilates in one of these resonances. This is a qualitatively new and different method of positive ion production. Details of this process and its potential applications to mass spectrometry warrant further study.

ACKNOWLEDGEMENTS

We would like to thank T. J. Murphy for help with the positron temperature measurements, and K. Fagerquist, K. Jordan, K. Raghavachari, and D. Schrader for helpful conversations. The work at the University of California, San Diego is supported by the Office of Naval Research.

REFERENCES

1. C. M. Surko, A. Passner, M. Leventhal and F. J. Wysocki, Phys. Rev. Lett. 61, 1831 (1988).

2. A. Passner, C. M. Surko, M. Leventhal and A. P. Mills, Jr., Phys. Rev., Rapid Comm., A39, 3706 (1989).

3. Much of the first part of this paper is taken more or less directly from Refs. 1 and 2.

4. C. M. Surko, M. Leventhal and A. Passner, Phys. Rev. Lett. 62, 901 (1989).

5. A. W. Hyatt, C. F. Driscoll and J. H. Malmberg, Phys. Rev. Lett. 59, 2975 (1987), and references therein.

6. G. R. Heyland, M. Charlton, T. C. Griffith, and G. L. Wright, Can. J. Phys. 60, 503 (1982). This study of positron annihilation in dense gases reports annihilation rates per molecule for butane which are in good agreement with our measurements. The authors suggest that the large rates which are observed might be due to bound-state formation, which is also the conclusion of our work.

7. Pressures were measured with a Varian, Bayard-Alpert gauge. Calibrations for alkane molecules were taken from J. E. Bartness and R. M. Georgiadias, Vacuum 33, 149 (1983).

8. L. G. Christophorou, A. Hadjiantoniou, and J. G. Carter, J. Chem. Soc. Faraday Trans. 2 69, 1713 (1973); L. G. Christophorou, D. L. Mccorkle, and A. A. Christodoulides, *Electron-Molecule Interactions and Their Applications* (Academic, New York, 1984), Vol. 1, pp.478-618.

9. See, for example, W. Forst, *Theory of Unimolecular Reactions* (Academic Press, New York, 1973); and W. Forst, Chemical Reviews 71, 339 (1971).

10. G. Z. Whitten and B. S. Rabinovitch, J. Chem. Phys. 38, 2466 (1963).

11. This value of ϵ_A is in the lower end of the range of values quoted in Ref. 1. The difference is due to the correction of a numerical error in the plateau calculation and to improved estimates of both ϵ_z and b, which are now taken to be smaller than the values previously assumed.

12. See, for example, W. R. Leo, *Techniques for Nuclear and Particle Physics Experiments* (Springer-Verlag, New York, 1987).

13. The data are not of sufficient resolution to determine the precise numbers of hydrogen atoms in these ions, so the numbers of hydrogen were chosen based on what are likely to be stable ions [K. Raghavachari (private communication)].

INITIAL RESULTS OF POSITRON IONIZATION MASS SPECTROMETRY

D. L. Donohue, L. D. Hulett, Jr., S. A. McLuckey
G. L. Glish and B. A. Eckenrode

Analytical Chemistry Division
Oak Ridge National Laboratory
Oak Ridge, TN

ABSTRACT

The use of monoenergetic positrons for the ionization of organic molecules in the gas phase is described. The ionic products are analyzed with a time-of-flight mass spectrometer and detected to produce a mass spectrum. The ionization mechanisms which can be studied in this way include positron impact at energies above the ionization limit of the target molecules, positronium formation in the "Ore gap" energy range, and positron attachment at energies less than 1 eV. The technique of positron ionization mass spectrometry (PIMS)[1] may have analytical utility in that chemical selectivity is observed for one or more of these processes.

INTRODUCTION

Theoretical predictions by Schrader[2,3] based on molecular orbital calculations indicate that certain organic molecules will exhibit a positive affinity for low-energy (<1 eV) positrons. Higher-energy processes such as positronium formation and positron impact ionization are expected to involve a nearly vertical Franck-Condon transition from the ground state of the neutral molecule to the ionic state, resulting in a highly excited ionic state and fragmentation of the molecular ion.

Work by Surko, et al.[4] indicated that the trapping time of positrons in a Penning trap was strongly correlated with the size (molecular weight) of simple alkanes from butane to hexadecane at a pressure of 10^{-7} to 10^{-6} Torr. Later experiments[5] involving time-of-flight mass analysis indicated that low-energy positron resonances were taking place, along with other processes.

We have designed and constructed a high-quality mass spectrometer to study these processes more systematically and to demonstrate the analytical utility of positron-induced ionization.

EXPERIMENTAL

The positron source for this work is based on the Oak Ridge Electron Linear Accelerator[6-8] and makes use of excess gamma-ray bremsstrahlung which induces pair production in tungsten metal plates. The tungsten also serves as a moderator for the positrons which are re-emitted at approximately 2.5 eV with a narrow energy spread. The positrons are then accelerated to 3000 eV and transported to an experimental room 11 meters away by means of solenoids. The 3000 eV positrons are

then electrostatically deflected by 60 degrees into the ion source chamber of the time-of-flight mass spectrometer (TOFMS).

In our initial studies[1], this 3000 eV beam was allowed to traverse the ionization volume of the TOFMS ion source and strike a tungsten moderator operated in the reflection mode. Numerous spectra were obtained in this way which resulted from positron impact ionization by the 3000 eV beam.

A change in geometry allowed us to eliminate this impact ionization background and concentrate on the low-energy attachment process. This was accomplished by allowing the 3000 eV beam to strike a 1000 Angstrom thick tungsten film which acts as a transmission moderator[2]. A fraction of the positrons (10-30%) emerge on the other side of this film at 2.5 eV. These are then injected into a miniature Penning trap through a molybdenum grid which allowed us to select the energy of the positrons in the trap in the range of 0.1 to 3 eV.

The positron trapping ion source consists of a metal block with two end grids biased +5 V and an axial magnetic field of 10-60 Gauss to confine the low-energy positrons. Ions which are formed in the trap are extracted after 10 to 30 microseconds of positron trapping and are accelerated into the TOFMS flight tube which is 1 meter long. The ions are detected with a channelplate and the anode signal acts as a stop signal for a bank of 8 time-to-digital converters operated in ripple fashion.

RESULTS AND DISCUSSION

Figure 1 shows the spectrum of toluene obtained with the trapping ion source, where the positron energy was estimated to be less than 1 eV. The spectrum consists of only one peak corresponding to the molecular ion (but possibly at m/z = M-1) and virtually no fragment ions. This is strong evidence for a "soft ionization" process in which the intermediate state (before annihilation) resembles the ionic state. The positron impact spectrum of toluene using 3000 eV positrons resembles the conventional electron impact spectrum in which fragment ions are seen at lower masses.

CONCLUSIONS

The initial results with our PIMS system are encouraging. We have successfully demonstrated positron impact ionization and have seen strong evidence for low-energy positron attachment. Future studies will center on measuring the crossections for a number of organic molecules as a function of positron energy.

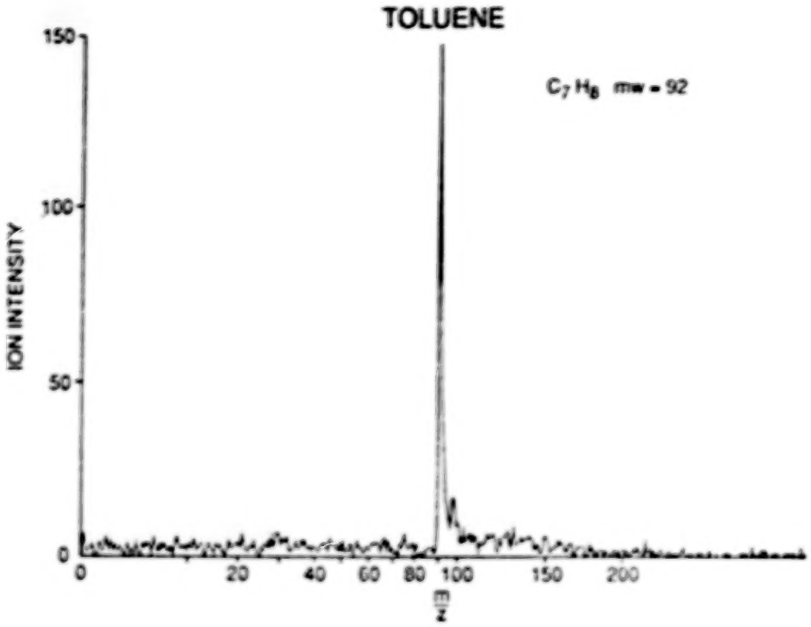

Figure 1. Low-energy positron ionization spectrum of toluene.

ACKNOWLEDGEMENT

This work is sponsored by the U.S.Department of Energy, Office of Energy Research, under contract DE-AC05-840R21400 with Martin Marietta Energy Systems Inc.

REFERENCES

1. D. L.Donohue, G. L. Glish, S. A. McLuckey, L. D. Hulett, Jr., and H. S. McKown, in Positron Annihilation, edited by L. Dorikens-Vanpraet, M. Dorikens, and D. Seegers, World Scientific, Singapore, 1989, p.612.
2. D. M. Schrader and C. M. Wang, J. Phys. Chem., 80, 2507 (1976).
3. D. M. Schrader in Positron and Positronium Chemistry, edited by D. M. Schrader and Y. C. Jean, Elsevier Science Publishers, Amsterdam, 1988.
4. C. M. Surko, A. Passner, M. Leventhal, and F. J. Wysocki, Phys. Rev. Lett., 61, 1831 (1988).
5. A. Passner, C. M. Surko, M. Leventhal, and A. P. Mills, in preparation.
6. L. D. Hulett, Jr., T. A. Lewis, R. G. Alsmiller, Jr., R. Peelle, S. Pendyala, J. M. Dale, and T. M. Rosseel, Nuclear Inst. Methods in Phys. Res., B24/25, 905 (1987).
7. L. D. Hulett, Jr., T. A. Lewis, D. L. Donohue, and S. Pendyala, in Positron Annihilation, edited by L. Dorikens-Vanpraet, M. Dorikens, and D. Seegers, World Scientific, Singapore, 1989, p.586.
8. T. A. Lewis, L. D. Hulett, Jr., and D. L. Donohue, in Positron Annihilation, edited by L. Dorikens-Vanpraet, M. Dorikens, and D. Seeger, World Scientific, Singapore, 1989, p.589.
9. M. R. Poulsen, M. Charlton, J. Chevalier, B. I. Deutch, F. M. Jacobsen, and G. Laricchia, in Positron Annihilation, edited by L. Dorikens-Vanpraet, M. Dorikens, and D. Seeger, World Scientific, Singapore, 1989, p.597.

Positron Annihilation Induced Auger Electron Spectroscopy

Alex Weiss, A.R. Koymen, David Mehl, K.O. Jensen[a], Chun Lei and K. H. Lee

Physics Department, The University of Texas at Arlington, Arlington Texas 76019

Recently, Weiss et al. have demonstrated that it is possible to excite Auger transitions by annihilating core electrons using a low energy (less than 30eV) beam of positrons. This mechanism makes possible a new electron spectroscopy, Positron annihilation induced Auger Electron Spectroscopy (PAES). The probability of exciting an Auger transition is proportional to the overlap of the positron wavefunction with atomic core levels. Since the Auger electron energy provides a signature of the atomic species making the transition, PAES makes it possible to determine the overlap of the positron wavefunction with a particular element. PAES may therefore provide a means of detecting positron-atom complexes. Measurements of PAES intensities from clean and adsorbate covered Cu surfaces are presented which indicate that ~5% of positrons injected into Cu at 25eV produce core annihilations that result in Auger transitions.

I. Introduction

The Auger process is a nonradiative transition in which an atom with a inner shell hole relaxes by filling this hole with an less tightly bound electron while simultaneously emitting another electron (the Auger electron) which carries off the excess energy. The energy of the Auger electron is given by the equation, $E_{XYZ} = E_X - E_Y^* - E_Z^*$ where E_X is the binding energy of the electron removed to form the original inner shell hole, and E_Y^*, E_Z^* are the binding energies associated with the two hole final state. Because the energy levels of different elements are in general unique, the elemental identity of an atom may be deduced from the energies of the Auger electrons emitted as a result of core hole excitations. This fact along with the short escape depth of low energy electrons has been exploited in the widely used surface analysis tool, Auger Electron Spectroscopy (AES).

Conventional Electron induced Auger Electron Spectroscopy (EAES) makes use of high energy electrons to collisionally ionized the atom. However in many instances the utility of EAES is limited by problems associated with the large secondary electron background and the lack of surface specificity inherent in the EAES excitation process. Recently, Weiss et al.[1] have demonstrated that Auger electrons can be excited with high efficiency by using low energy positrons to produce the core hole excitations necessary for Auger electron emission by matter - antimatter annihilation. This process makes possible a new surface spectroscopy, Positron annihilation induced Auger Electron Spectroscopy (PAES) which has significant advantages over conventional EAES in some systems. In the remainder of the paper we will describe experiments which demonstrate the potential advantages of the PAES technique. We the describe theoretical calculations from which we estimate the efficiency with which positrons induce Auger transitions. This estimate is then compared to experimental values. The paper concludes with a discussion of the possible use of PAES to detect positron -atom or positron - molecule bound states

Elimination of Secondary Electron Background

The PAES technique can be used to eliminate the large secondary electron background that limits the sensitivity and accuracy of conventional methods of Auger Electron Spectroscopy (AES).[1-3] In PAES, the core hole excitations necessary for AES are generated by matter-antimatter annihilation and not by collisional processes. It is therefore possible to use an incident beam energy well below the Auger electron energy thus precluding the creation of secondary electrons in the energy range of the Auger signal. In contrast, in conventional electron

stimulated Auger electron spectroscopy, (EAES), the incident beam energy must be in excess of the Auger electron energy which makes it impossible to avoid creating a large secondary electron background. The large improvement in signal to background that can be obtained using PAES is demonstrated in Figure 1. which compares Auger spectra obtained using positron excitation to that using conventional EAES. Both spectra were obtained using the UTA positron Auger system. Signal to background levels of greater than 40:1 were obtained (more than a factor of 80 improvement over conventional methods of AES). The improved signal-to -background allows PAES data to be taken with beam currents several orders of magnitude less than in conventional electron excited Auger (EAES). The low currents and low beam energies used in PAES allow the energy dose require to obtain data to be reduced four to six orders of magnitude as compared to EAES. This will permit the use of PAES in fragile systems where conventional methods of AES are severely limited.

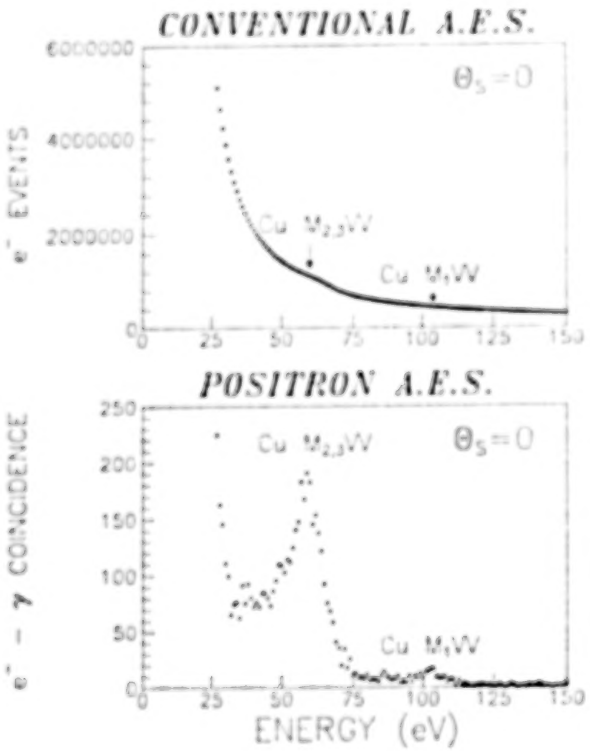

Fig. 1. Comparison of Conventional EAES and PAES spectra. Note the large increase in signal to background for the Cu $M_{2,3}VV$ peak obtained using PAES.

Surface Selectivity: Positron annihilation induced Auger spectroscopy displays enhanced surface selectivity.[3,4] This selectivity is due to the restriction of the excitation volume to the top atomic layer due to localization of the positron. This is in contrast to conventional Auger in which the excitation volume extends hundreds of atomic layer below the surface. EAES acquires its surface sensitivity solely from the 4-20Å escape depth of the Auger electron. The intensity of the Cu $M_{2,3}VV$ PAES signal decrease by a factor of 4 with the addition of a 1/2 monolayer of S on the surface (see figure 2). This is contrasted with only a 25% decrease in the EAES signal caused by the overlayer. These results were accounted for by theoretical calculations which show that the positron wavefunction is pushed away from the Cu surface causing the decrease in PAES intensity. These same calculations demonstrate that as much as 97% of the Auger signal will originate in the top atomic layer using PAES as compared to about 50% using conventional AES techniques.

Theoretical Calculations: Theoretical calculations were carried out[5] to determine the expected magnitude of PAES intensities. In addition, detailed surface calculations were carried out in support of our experimental measurements of the surface selectivity for PAES results to determine the spatial extent of the positron wavefunction and the degree of surface selectivity that could be attained with PAES.[3,4] Calculations using a corrugated mirror model for the positron surface potential were performed on clean metal and overlayer on metal surfaces producing good agreement with experimental results.[3]

Nearly all Cu 3p holes decay via emission of an $M_{2,3}$ VV Auger electron (energy ≈ 60eV) since the radiative transition probability is extremely small.[5] For clean Cu(100) and Cu(110) the annihilation probabilities for the 3s and 3p electrons are calculated to be p_{3s} = 0.83% and p_{3p} = 3.0%, respectively. Putting in the relevant Auger transiton rates we estimate that, σ_{M23VV}, the probability of a positron trapped in a surface state causing the a $M_{2,3}VV$ Auger transition is ~3.6%. The annihilation probabilities for the deeper lying 2s and 2p levels are two orders of magnitude lower. The calculations also indicate that core annihilations take

place primarily in the top surface layer, with about 5% and 20% of the total rate arising from second or deeper layers for Cu(100) and Cu(110), respectively.

For the purpose of making a comparison with theoretical calculations, we estimate σ_{M23VV} as follows[6]: an integral over the energy spectrum of the PAES Cu $M_{2,3}$ VV Auger peak was compared to an integral over the positron induced secondary electron peak. The secondary electron peak was obtained with the sample at -60V, so the electrons pass through the spectrometer at approximately the same energy as the Auger electrons. The positrons were incident with a kinetic energy of 80eV. Measurements of positron induced secondary electron emission from Ni at an angle of 50° to normal incidence allowed an estimate of the ratio of secondary electrons per incident positron, δ, in this experiment. The measured ratio of the Auger yield to the secondary yield was then substituted into a formula[6] which takes into account detector solid angle and efficiencies to give: $\sigma_{m_{2,3}} = 5.6\%$. Part of the discrepancy between this value and the theoretically calculated value of 3.6% may be due to neglect of the many-body enhancement factor.

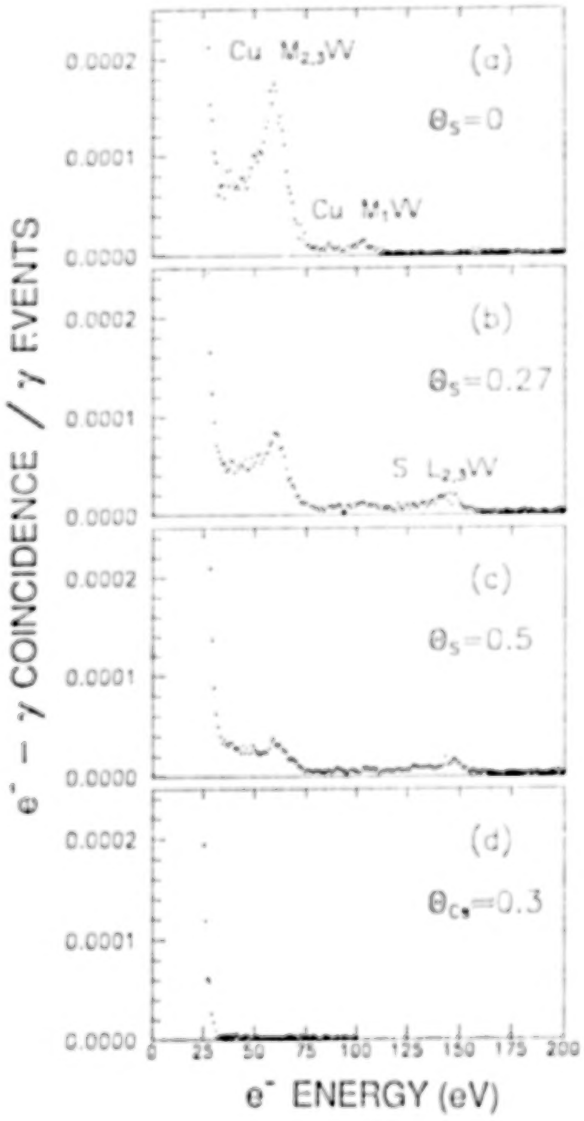

Figure 2. PAES spectra obtained from clean and adsorbate covered Cu. The large decrease in the Cu signal with overlayer coverage demonstrates the top layer selectivity of PAES.

It is interesting to speculate on the possibility using PAES as a means of signaling the existence of a positron-atom or positron-molecule bound state. Since the overlap of the positron wavefunction with the core levels of an atom should be enhanced if the positron were bound to that atom, the existence of a bound state would be signaled by an increase in the PAES intensity. It may be possible to test this hypothesis by using a very low energy beam of positrons incident on atoms or molecules physisorbed on a metallic substrate.

This research was supported in part by the Texas Advanced Research Program and the Robert A. Welch Foundation.

a. Permanent address: Physics Department, The University East Anglia, Norwhich, UK

References

1. Weiss, Mayer, Mehl,Jibaly, Lei, and Lynn, Phys. Rev. Lett. 61, 2245(1988).
2. Weiss, Mehl, Lei, Jibaly, Mayer and Lynn, accepted for publication in *Positron Annihilation*, World Scientific Press, Singapore (1989).
3. Mehl, Koymen, Jensen, Gotwald and Weiss, submitted to Phys. Rev. Lett.
4. Lei, Mehl, Koymen, Jibaly, Gotwald and Weiss, UTA preprint.
5. Jensen and Weiss, UTA preprint.
6. David Mehl, Thesis (unpublished)

Report Documentation Page

1. Report No.	2. Government Accession No.	3. Recipient's Catalog No.
NASA CP-3058		

4. Title and Subtitle	5. Report Date
Annihilation in Gases and Galaxies	January 1990
	6. Performing Organization Code: 681.0

7. Author(s)	8. Performing Organization Report No.
Richard J. Drachman, Editor	90B00019
	10. Work Unit No.: 681-170-10-01-08

9. Performing Organization Name and Address	11. Contract or Grant No.
Goddard Space Flight Center Greenbelt, Maryland 20771	
	13. Type of Report and Period Covered: Conference Publication July 19-21, 1989
12. Sponsoring Agency Name and Address	14. Sponsoring Agency Code
National Aeronautics and Space Administration Washington, DC 20546-0001	

15. Supplementary Notes

Richard J. Drachman: Goddard Space Flight Center; Greenbelt, Maryland

16. Abstract

This publication contains most of the papers, both invited and contributed, that were presented at the Workshop of Annihilation in Gases and Galaxies held at NASA/Goddard Space Flight Center on July 19-21, 1989. This was the fifth in a biennial series associated with the International Conference on the Physics of Electronic and Atomic Collisions. Subjects covered included the scattering and annihilation of positrons and positronium atoms in various media, including those of astrophysical interest. In addition, the topics of antimatter and dark matter were covered.

17. Key Words (Suggested by Author(s))	18. Distribution Statement
Annihilation, positron, positronium, antimatter, scattering, gamma rays, Galactic Center, dark matter, resonances	Unclassified - Unlimited Subject category - 70

19. Security Classif. (of this report)	20. Security Classif. (of this page)	21. No. of pages	22. Price
Unclassified	Unclassified	299	A14

NASA FORM 1626 OCT 86

NASA Langley, 1990

National Aeronautics and
Space Administration
Code NTT-4

Washington, D.C.
20546-0001

Official Business
Penalty for Private Use, $300

SPECIAL FOURTH-CLASS RATE
POSTAGE & FEES PAID
NASA
Permit No. G-27

NASA

POSTMASTER: If Undeliverable (Section 158
Postal Manual) Do Not Return